Montag, 14. März 2011		
10:00	13:00	**Registrierung im Tagungsbüro Raum 88H**
13:00	13:50	**Eröffnung im Hörsaal HS2** Prof. Dr. Ursula Nelles, Rektorin der WWU Münster Prof. Dr. Hans Kerp, Dekan Geowissenschaften Dr. Guido Lüniger, Deutsche Forschungsgemeinschaft Prof. Dr. Harald Strauß, WWU Münster
Berichte / Entwicklungen		
13:50	14:10	J. Erbacher / R. Stein IODP Rückblick auf 2010 - Wie geht es weiter? R. Oberhänsli / R. Emmermann ICDP Deutschland – Wie geht es weiter?
14:10	14:25	Harms, U., Conze, R., Klump, J., Erbacher, J., Wallrabe-Adams, H.J., Wefer, G. **Development of GESEPs new National Drillcore Data Repository**
14:25	14:40	Neugebauer, I., Frank, U., Schwab, M.J., Dulski, P., Brauer, A. **Holocene Dust Storms and Flood Events in the Dead Sea Region – Establishing a New Methodological Approach of High-Resolution Dead Sea Sediments Analyses for the ICDP Dead Sea Deep Drilling Project (DSDDP**)
14:40	14:55	Pross, J., Röhl, U. and IODP Expedition 318 Science Party **Main Results of IODP Expedition 318 – Wilkes Land**
14:55	15:10	Rausch, S., Deschamps, F, Dorais, M., Bach, W., Klügel, A., IODP Expedition 330 Science Party **Preliminary results from IODP Expedition 330 (Louisville Seamount Trail)**
15:10	15:25	Bauersachs, T., Strasser, M. and the IODP Expedition 333 Science Party **Preliminary results from IODP Expedition 333 (Nankai Through, Japan)**
15:25	15:40	Kopf, A., Araki. E., Toczko, S., Hammerschmidt, S. and Expedition 332 Science Party **IODP Expedition 332: NanTroSEIZE Stage 2: Riserless Observatory**
15:40	17:00	**Posterpräsentation** der Themen: Berichte und Entwicklungen, Seismogene Zone, Hangstabilitäten, Impaktstrukturen, Gashydrate, Gase, Fluide **Kaffeepause**
Seismogene Zone / Hangstabilitäten		
17:00	17:20	Hüpers, A., Kopf, A.J. **Preliminary results of modeling drainage efficiency of sand layers in underthrust sediments of the Nankai subduction zone, Japan.**
Stoffkreisläufe / Tiefe Biosphäre		
17:20	17:40	Ockert, C., Wehrmann, L.M., Ferdelmann, T.G., Kaufhold, S., Teichert, B.M.A., Gussone, N. **Calcium adsorption and ion exchange in marine sediments**
17:40	18:00	Glombitza, C., Kallmeyer, J. **Microbial activity and abundance in sediments Lake Van (Turkey), first results from ICDP Project PALEOVAN**
18:00	18:20	Breuker, A., Schippers, A. **Real-time PCR quantification of *Bacteria* and *Archaea* in subsurface marine sediments**
18:20	18:40	Engelhardt, T., Cypionka, H., Engelen, B. **Viruses in the deep biosphere**
ab 18:45		**Transfer mit Bussen**
ab 19:30		**Icebreaker** - Gemeinsames Abendessen im Mühlenhof-Freilichtmuseum Theo-Breider-Weg 1

Dienstag, 15. März 2011		
Stoffkreisläufe / Tiefe Biosphäre		
09:00	09:20	Meister, P.H., Liu, B., Contreras Quintana, S., Khalili, A., Ferdelman, T.G., Kuypers, M., Barker **A dynamic sulphate/methane transition zone at Peru Margin Site 1229 (ODP Leg 201) reproduced by reactive transport modelling**
Magmatische Petrologie / Metamorphismus		
09:20	09:40	Gärtner, C., Martin, A.P., Bahlburg, H., Lepland, A., Prave, A.R., Condon, D.J., Melezhik, V., Berndt, J., Kooijman, E. and the FAR-DEEP Scientists **The Archaean to Palaeoproterozoic transition: U-Pb geochronology of detrital zircons and accompanying provenance analysis of siliciclastic sedimentary rocks from FAR-DEEP**
09:40	11:00	**Posterpräsentation** der Themen: Stoffkreisläufe, Tiefe Biosphäre, Magmatische Petrologie, Metamorphismus **Kaffeepause**
11:00	11:20	Morgavi, D., Perugini, D., De Campos, C., Lavallée, Y., Morgan, L., Dingwell, D.B. **The role of magma mixing between rhyolitic and basaltic magmas in the Bruneau-Jarbidge eruptive center, Snake River Plain (USA): an experimental study**
11:20	11:40	Shishkina, T., Almeev, R., Botcharnikov, R., Holtz, F. **Magma storage conditions and degassing processes of low-K and high-Al island-arc tholeiites: Experimental constraints for Mutnovsky volcano, Kamchatka**
11:40	12:00	Heydolph, K., Geldmacher, J., Hoernle, K. **The early stage of Shatsky Rise plateau formation: Isotope-geochemical characterization (Srr, Nd, Pb and Hf) of volcanic rocks from IODP site U1347 (Shatsky Rise, Northwest Pacific)**
12:00	12:20	Schmädicke, E., Gose, J., Will, T.M. **Heterogeneous mantle underneath the North Atlantic: Evidence from water in spinel peridotite from different locations at the Mid-Atlantic Ridge**
12:20	12:40	Höfig, T., Hoernle, K., Duggen, S., Hauff, F. **The trace element and Sr-Nd-Pb isotopic record of IODP/ODP – Site 1256 sedimentary overburden and its implications for the Neogene paleo-oceanographic evolution of the eastern equatorial Pacific**
12:40	14:00	**Mittagspause + Poster**
Paläozeanographie / Paläoklima		
14:00	14:20	Litt, T., Anselmetti, F.S., Cagatay, N., Kipfer, R., Krastel, S., Öcen, S., Sturm, M. and the 'PaleoVan' Scientific Drilling Party **Lake Van Drilling Project 'PaleoVan', a long continental record of Eastern Anatolia: Report of the ICDP drilling operation in 2010**
14:20	14:40	Mayr, C., Oehlerich, M., Lücke, A., Ohlendorf, C., Zolitschka, B., Schäbitz, F., Wille, M., Haberzettl, T. and the PASADO Science Team **Methodology and paleoenvironmental significance of carbonate isotope records from the ICDP-site Laguna Potrok Aike**
14:40	16:30	**Posterpräsentation** der Themen: Paläozeanographie, Paläoklima **Kaffeepause**
16:30	16:50	Vogel, H., Wagner, B., Albrecht, C., Finsinger, W., Leng, M.J., Lotter, A.F., Reed, J., Schouten, S., Sulpizio, R., Valsecchi, V, Zanchetta, G. and the Scopsco Science Team **The sediment record of Lake Ohrid (Albania/Macedonia) – a valuable archive of past climate and ecosystem dynamics**
16:50	17:10	Gischler, E., Bourillot, R., Droxler, A.W., Kan, H., Seard, C., Webster, J.M., Yokoyama, Y. and Expedition 325 Scientists **Sedimentology of late Quaternary coral reefs, Great Barrier Reef, Australia (IODP 325)**
17:10	18:30	**Imbiss**
19:00	21:00	**Fürstenberg Haus, F5 (2. OG), Domplatz 20-22** **Öffentlicher Abendvortrag:** Prof. Dr. Harald Strauß, WWU Münster: **Auf der Suche nach dem Sauerstoff in russisch Karelien**

Mittwoch, 16. März 2011		
Paläozeanographie / Paläoklima		
08:30	8:50	Naafs, B.D.A., Hefter, J., Pancost, R., Stein, R., Haug, G.H. **Warm North Atlantic waters allow for Heinrich events but prevent major deglaciations**
08:50	09:10	Sarnthein, M. **Onset of Quaternary glaciations near 3 Ma induced by final closure of Panama *and* reduction of atmospheric CO_2**
09:10	09:30	März, C., Vogt, C., Schnetger, B. , Brumsack, H.-J. **Complex sedimentation processes and bottom water redox conditions across the Eocene-Miocene "hiatus" in the Central Arctic Ocean (IODP Expedition 302)**
09:30	09:50	Bornemann, A., Norris, R.D., Lyman, J.A., D'Haenens, S, Groeneveld, J., Röhl, U., Farley, K.A., Speijer, R.P. **A complex history of the Paleocene–Eocene Thermal Maximum in the NE Atlantic**
Neue Projekte / Projektvorschläge		
09:50	10:10	Daut, G., Haberzettl, T., Doberschütz, S., Kasper, T., Gleixner, G., Frenzel, P., Hetzel, R., Reicherter, K., Schwalb, A., Schwenk, T., Spieß, V., Wang, J., Zhu, L., Mäusbacher, R. **Nam Co - a potential ICDP drilling site on the Tibetan Plateau?**
10:10	11:30	**Posterpräsentation** der Themen: Neue Projekte, Projektvorschläge, Paläozeanographie, Paläoklima **Kaffeepause**
11:30	11:50	Koepke, J., Kelemen, P., Al Rajhi, A., Arai, S., Bach, W., Blackman, D., Ceuleneer, G., Coogan, L., Godard, M., Goldstein, S., Gouze, P., Hirth, G., Hofmann, A., Jamtveit, B., Langmuir, C., Macleod, C., Manning, C., Matter, J., Michibayashi, K., Miller, J., Nasir, S., Sherwood Lollar, B., Shock, E., Sonnenthal, E., Teagle, D., Umino, S., Warren, J., Zhu, W., Boudier, F., Gillis, K.M., Klein, F., Ildefonse, B., Miyashita, S, Nicolas, A., Pézard, P., Singh, S., Takazawa, E. **The Oman Ophiolite Drilling Project – a new ICDP drilling proposal**
11:50	12:10	Oberhänsli, H., Molnar, P. **Issyk Kul: ein Klimaarchiv für Zentralasien**
12:10	12:30	Vogel, H., Russell, J.M., Bijaksana, S., Cahyarini, S.Y., Fowle, D., Haffner, D., Huang, Y., Idriyanti, S., King, J., Melles, M., Noren, A., Oppo, D., von Rintelen, T, Wattrus, N. **Paleoenvironments, Evolution, and Geomicrobiology in a Tropical Pacific Lake: The Lake Towuti Drilling Project (TOWUTI)**
12:30	13:00	**Posterprämierung und Schlussworte**
13:00		**Tagungsende**

Mittwoch, 16. März 2011	
Im **Anschluß** an das IODP/ICDP Kolloquium	
14:00	**GESEP School 2011: "Planning and Applying for Scientific Drilling Projects"**
Der modulare Kurs, organisiert von GESEP, dem Deutschen Forschungsbohrkonsortium, wird von Ingenieuren und Wissenschaftlern mit langjährigen Erfahrungen in nationalen und internationalen Bohrprogrammen gehalten und soll jungen Wissenschaftlern praktisches Wissen zu Forschungsbohrungen vermitteln. Der diesjährige Trainingsschwerpunkt liegt auf der Vorerkundung und Antragstellung von Forschungsbohrungen.	
ENDE: **Donnerstag, 17. März 2011, ca. 17.00 Uhr**	

Teilnehmerliste

Name	Vorname	Institution und Ort
Albrecht	Christian	Universität Gießen
Almeev	Renat	Universität Hannover
Arroyo	Ivonne G.	IFM-GEOMAR, Kiel
Aulbach	Sonja	Universität Frankfurt
Bach	Wolfgang	Universität Bremen
Bahlburg	Heinrich	Universität Münster
Baldermann	Andre	Universität Greifswald
Bartetzko	Anne	Wellbore Integrity and Pressure Management, Baker Hughes INTEQ GmbH, Celle
Bauersachs	Thorsten	Universität Kiel
Baumgarten	Henrike	LIAG Hannover
Behrens	Harald	Universität Hannover
Böhm	Evelyn	Heidelberger Akademie der Wissenschaften
Böhm	Florian	IFM-GEOMAR, Kiel
Bolte	Torsten	Universität Hannover
Bornemann	Andre	Universität Leipzig
Bosch	Frank	RWTH Aachen
Botcharnikov	Roman	Universität Hannover
Böttcher	Michael	Leibnitz Institut für Ostseeforschung, Warnemünde
Brandl	Philipp	Universität Erlangen
Breuker	Anja	Bundesanstalt für Geowissenschaften und Rohstoffe, Hannover
Buske	Stefan	TU Bergakademie Freiberg
Chun	Cecily	Universität Frankfurt
Conze	Ronald	Scientific Drilling ICDP, Deutsches GeoForschungsZentrum Potsdam
Cukur	Deniz	IFM-GEOMAR, Kiel
Cypionka	Heribert	Universität Oldenburg
Daut	Gerhard	Universität Jena
Dersch-Hansmann	Michaela	Hessisches Ministerium der Justiz, für Integration und Europa, Wiesbaden
De Schepper	Stijn	Universität Bremen
Diester-Haass	Liselotte	Universität des Saarlandes, Saarbrücken
Dietze	Frank	KIT, Karlsruher Institut für Technologie
Drath	Gabriela	IODP, Bundesanstalt für Geowissenschaften und Rohstoffe, Hannover
Dultz	Stefan	Universität Hannover
Dupont	Lydie	MARUM, Universität Bremen
Dziony	Wanja	Universität Hannover
Eckert	Sebastian	Universität Oldenburg
Ehmann	Sebastian	TU Braunschweig
Engelen	Bert	Universität Oldenburg
Engelhardt	Tim	Universität Oldenburg
Erbacher	Jochen	IODP, Bundesanstalt für Geowissenschaften und Rohstoffe, Hannover
Erzinger	Jörg	Deutsches GeoForschungsZentrum, Potsdam
Fallahi	Mohammad	Universität Leipzig
Fehr	Annick	RWTH Aachen
Ferdelman	Timothy	MPI für Marine Mikrobiologie, Bremen
Flaws	Asher	Universität München
Fohlmeister	Jens	Heidelberger Akademie der Wissenschaften
Förster	Verena	Universität Köln
Frank	Ute	Deutsches GeoForschungsZentrum Potsdam
Friedrich	Oliver	Universität Frankfurt
Gärtner	Claudia	Universität Münster
Gebhardt	Catalina	Alfred-Wegener-Institut für Polar- und Meeresforschung, Bremerhaven
Gischler	Eberhard	Universität Frankfurt
Götze	Hans-Jürgen	Universität Kiel
Gussone	Nikolaus	Universität Münster
Haase	Karsten	GeoZentrum Nordbayern, Universität Erlangen
Haberzettl	Torsten	Universität Jena
Hahn	Annette	Universität Bremen
Hammerschmidt	Sebastian	Universität Bremen
Handiani	Dian	Universität Bremen
Harms	Ulrich	Scientific Drilling ICDP, Deutsches GeoForschungsZentrum Potsdam
Hauffe	Torsten	Universität Gießen
Heistek	Rosanne	Universität München
Heldt	Matthias	IODP, Bundesanstalt für Geowissenschaften und Rohstoffe, Hannover
Hepp	Daniel A.	MARUM, Universität Bremen
Herrle	Jens	Universität Frankfurt
Hesse	Reinhard	Universität München
Heßler	Ines	MARUM, Universität Bremen
Heydolph	Ken	IFM-GEOMAR, Kiel
Hoffmann	Nadine	RWTH Aachen
Höfig	Tobias	IFM-GEOMAR, Kiel
Hofmann	Peter	Universität Köln
Holbourn	Ann	Universität Kiel
Holtz	François	Universität Hannover

Hunze	Sabine	LIAG Hannover
Hüpers	Andre	MARUM, Universität Bremen
Husen	Anika	Universität Hannover
Illing	Christian	Universität Münster
Janssen	Christoph	Deutsches GeoForschungsZentrum Potsdam
Joachim	Christian	Universität Bochum
Jöns	Niels	Universität Bremen
Jung	Claudia	Universität Frankfurt
Kallmeyer	Jens	Universität Potsdam
Karas	Cyrus	Universität Frankfurt
Khélifi	Nabil	IFM-GEOMAR, Kiel
Kirchner	Clemens	Universität Hannover
Kliem	Pierre	Universität Bremen
Klügel	Andreas	Universität Bremen
Koch	Mirjam	Universität Frankfurt
Koepke	Jürgen	Universität Hannover
Kontny	Agnes	KIT Karlsruher Institut für Technologie
Korn	Michael	Universität Leipzig
Kotthoff	Ulrich	Universität Hamburg
Krastel	Sebastian	IFM-GEOMAR, Kiel
Kuhnt	Wolfgang	Universität Kiel
Kukkonen	Maaret	Universität Köln
Kukowski	Nina	Universität Jena
Langkamp	Oliver	Universität Köln
Lavallée	Yan	Universität München
Lazarus	David	Museum für Naturkunde, Berlin
Leuschner	Dirk	Universität Leipzig
Lezius	Jeannette	ESSAC, Alfred-Wegener-Institut für Polar- und Meeresforschung, Bremerhaven
Linnert	Christian	Universität Bochum
Lipp	Julius	MARUM, Universität Bremen
Litt	Thomas	Universität Bonn
Lorenschat	Julia	TU Braunschweig
Lücke	Andreas	FZ Jülich
Lückge	Andreas	Bundesanstalt für Geowissenschaften und Rohstoffe, Hannover
Lüniger	Guido	DFG, Bonn
Mackensen	Andreas	Alfred-Wegener-Institut für Polar- und Meeresforschung, Bremerhaven
Mang	Christoph	KIT Karlsruher Institut für Technologie
Maronde	Dietrich	Universität Bonn
März	Christian	Newcastle University, Newcastle upon Tyne, United Kingdom
Matthiessen	Jens	Alfred-Wegener-Institut für Polar- und Meeresforschung, Bremerhaven
Mayr	Christoph	Universität Erlangen
Mayr	Sibylle	Freie Universität Berlin
McAnena	Alison	Universität Köln
Meister	Denise	Universität Münster
Meister	Patrick	MPI für Marine Mikrobiologie, Bremen
Melles	Martin	Universität Köln
Meyer	Christian	Freie Universität Berlin
Meyers	Phil	University of Michigan, Ann Arbor, U.S.A.
Montinaro	Alice	Universität Münster
Morgavi	Daniele	Universität München
Mueller-Michaelis	Antje	Alfred-Wegener-Institut für Polar- und Meeresforschung, Bremerhaven
Mullick	Nirjhar	TU Bergakademie Freiberg
Mutterlose	Joerg	Universität Bochum
Naafs	David	Alfred-Wegener-Institut für Polar- und Meeresforschung, Bremerhaven
Neugebauer	Ina	Deutsches GeoForschungsZentrum Potsdam
Niedermann	Samuel	Deutsches GeoForschungsZentrum Potsdam
Numberger-Thuy	Lea	Universität Göttingen
Nürnberg	Dirk	IFM-GEOMAR, Kiel
Oberhänsli	Roland	ICDP, Universität Potsdam
Ockert	Charlotte	Universität Münster
Oehlerich	Markus	Universität Erlangen
Ohlendorf	Christian	GEOPOLAR, Universität Bremen
Osborne	Anne	IFM-GEOMAR, Kiel
Pabich	Stephanie	Universität Münster
Palamengi	Luisa	Universität Bremen
Pälike	Heiko	National Oceanography Centre, Southampton, United Kingdom
Pickarski	Nadine	Universität Bonn
Piribauer	Christoph	RWTH Aachen
Pross	Joerg	Universität Frankfurt
Raddatz	Jacek	IFM-GEOMAR, Kiel
Raschke	Ulli	Museum für Naturkunde, Berlin
Rausch	Svenja	Universität Bremen
Reich	Mike	Universität Göttingen
Reicherter	Klaus	RWTH Aachen
Reimold	W. Uwe	Museum für Naturkunde, Berlin
Reischmann	Thomas	Hessisches Landesamt für Umwelt und Geologie, Wiesbaden
Renaudie	Johan	Museum für Naturkunde, Berlin

Reuschel	Marlene	Universität Münster
Röhl	Ursula	MARUM, Universität Bremen
Rullkötter	Jürgen	Universität Oldenburg
Sarnthein	Michael	Universität Kiel
Schäbitz	Frank	Universität Köln
Schippers	Axel	Bundesanstalt für Geowissenschaften und Rohstoffe, Hannover
Schmädicke	Esther	GeoZentrum Nordbayern, Universität Erlangen
Schmincke	Hans-Ulrich	IFM-GEOMAR, Kiel
Schnieders	Luzie	MARUM, Universität Bremen
Scholonek	Kornelia	Universität Münster
Schreiber	Kirstin	Universität Gießen
Schulte	Peter	GeoZentrum Nordbayern, Universität Erlangen
Schulz	Hartmut	Universität Tübingen
Schumann	Kai	IFM-GEOMAR, Kiel
Schwalb	Antje	TU Braunschweig
Schwamborn	Georg	Alfred-Wegener-Institut für Polar- und Meeresforschung, Potsdam
Schwenk	Tilmann	Universität Bremen
Shishkina	Tatiana	Universität Hannover
Shu	Liping	Universität Bremen
Sieverding	Marieke	Universität Oldenburg
Simonyan	Anna	Universität Hannover
Sindern	Sven	RWTH Aachen
Smolka	Peter P.	Universität Münster
Stadler	Susanne	Bundesanstalt für Geowissenschaften und Rohstoffe, Hannover
Stein	Rüdiger	ESSAC, Alfred-Wegener-Institut für Polar- und Meeresforschung, Bremerhaven
Stipp	Michael	IFM-GEOMAR, Kiel
Strack	Dieter	International Oil & Gas Consultant, Ratingen
Strasser	Michael	MARUM, Universität Bremen
Strauss	Harald	Universität Münster
Strube	Nicole	Universität Hannover
Sumita	Mari	IFM-GEOMAR, Kiel
Teichert	Barbara	Universität Münster
Teschner	Claudia	IFM-GEOMAR, Kiel
Thuy	Ben	Universität Göttingen
Timmerman	Martin	ICDP, Universität Potsdam
Uenzelmann-Neben	Gabriele	Alfred-Wegener-Institut für Polar- und Meeresforschung, Bremerhaven
Virgil	Christopher	TU Braunschweig
Vogel	Hendrik	Universität Köln
Voigt	Silke	Universität Frankfurt
van de Schootbrugge	Bas	Universität Frankfurt
von der Handt	Anette	Universität Freiburg
Wagner	Bernd	Universität Köln
Wagner	Dirk	Alfred-Wegener-Institut für Polar- und Meeresforschung, Potsdam
Wagner	Thomas	Newcastle University, Newcastle upon Tyne, United Kingdom
Wallrabe-Adams	Hans-Joachim	MARUM, Universität Bremen
Weber	Michael E.	Universität Köln
Wefer	Gerold	MARUM, Universität Bremen
Wehrmann	Laura	MPI Bremen
Wennrich	Volker	Universität Köln
Westerhold	Thomas	MARUM, Universität Bremen
Weyer	Stefan	Universität Hannover
Wiersberg	Thomas	Scientific Drilling ICDP, Deutsches GeoForschungsZentrum Potsdam
Wigger	Peter	Freie Universität Berlin
Wille	Michael	Universität Köln
Winkelmann	Daniel	IFM-GEOMAR, Kiel
Wonik	Thomas	LIAG Hannover
Zhu	Jiayun	FZ Jülich

Sarnthein, M.	Onset of Quaternary glaciations near 3 Ma induced by final closure of Panama and reduction of atmospheric CO2	IODP	150
Schefuß, E., Dupont, L., Rommerskirchen, F.	African climate changes during C4 plant evolution and expansion	IODP	150
Schmädicke, E., Gose, J., Will, T.M.	Heterogeneous mantle underneath the North Atlantic: Evidence from water in spinel peridotite from different locations at the Mid-Atlantic Ridge	IODP	152
Scholonek, K., Bahlburg, H., Gärtner, C., Lepland, A., Melezhik, V. and the FAR-DEEP Scientists	Heavy mineral analysis of Archaean-Palaeoproterozoic rocks of the Fennoscandian Shield	ICDP	153
Schreck, M., Matthiessen, J.	Mid-Miocene to Pliocene Dinoflagellate Cyst Datums in ODP Hole 907A (Iceland Sea)	IODP	154
Schreiber, K., Hauffe, T., Albrecht, C., Wilke, T.	Do major evolutionary events in ancient Lake Ohrid indicate its origin?	ICDP	154
Schulte, P., Bornemann, A., Westerhold, T., Mutterlose, J.	Earliest Paleogene climate events – A multiproxy study from the Demerara Rise, western equatorial Atlantic	IODP	157
Schumann, K., Stipp, M., Klaeschen, D., Behrmann, J.H.	Ultrasonic wave velocity changes during experimental deformation of water-rich sediments from the Nankai accretionary prism (offshore SW Japan)	IODP	158
Schwamborn, G., Willenbring, J., Meyer, H., Andreev, A., Fedorov, G.B., Ostanin, N., Schirrmeister, L. and El`Gygytgyn Scientific Party	Tracing NE-Siberian palaeo-permafrost with multi-proxy core data	ICDP	159
Schwenk, T., Krastel, S., Bickert, T., Fricke, S., Meyer, M.	Potential drill sites offshore NW-Africa to study the Neogene climate and related sediment dynamics – results of the pre-site survey MSM 11/2	IODP	160
Shishkina, T., Almeev, R., Botcharnikov, R., Holtz, F.	Magma storage conditions and degassing processes of low-K and high-Al island-arc tholeiites: Experimental constraints for Mutnovsky volcano, Kamchatka	ICDP	161
Shu, L., Bach, W., Klügel, A., Jöns, N.	Compositions of phyllosilicates from the TAG hydrothermal system at 26°N on the Mid-Atlantic Ridge as guide to subseafloor entrainment of seawater: Results from ODP Leg 158	IODP	164
Sieverding, M., Engelen, B., Sass, H., Scholz-Böttcher, B., Cypionka, H., Rullkötter, J.	Estimation of endospore numbers in marine sediment samples by quantification of dipicolinic acid	IODP	166
Simonyan, A., Dultz, S., Behrens, H., Fiebig, J., Voges, K.	Carbonation of porous rocks by interaction with magmatic and hydrothermal fluids - a case study on Unzen volcano, Japan	ICDP	167
Smolka, P.P.	Cold Aspects of past neogene warm Climates – interim Results	IODP	170
Stadler, S., Holländer, H., Hayashi, T., Mottl, M. and the Exp313 Science Party	A SEAWAT-2000 approach for modeling the fresh and salt water genesis in the New Jersey Shallow Shelf, Exp. 313	IODP	170
Stipp, M., Rolfs, M., Kitamura, Y., Behrmann, J.H.	Structurally weak sediments indicate a high tsunami risk for the Megasplay fault of the Nankai accretionary prism (Japan)	IODP	171
Sumita, M., Schmincke, H.-U.	Structural, volcanic, temporal, compositional and environmental evolution of explosive volcanism of Nemrut and Süphan volcanic systems, sources for the tephra framework of Lake Van sediments (Anatolia)	ICDP	174
Talbot, H.M., Handley, L., De Lange, G., Wagner, T.	Biomarker evidence for intense aerobic methane oxidation during sapropel transitions	IODP	176
Teschner, C., Frank, M., Haley, B.A.	Plio-Pleistocene evolution of Arctic-Atlantic water mass exchange and erosional input in the Fram Strait	IODP	176
Teschner, C., Frank, M., Haley, B.A.	Reconstructing water mass exchange and climate variability in the northernmost Atlantic and Arctic oceans during the beginning of the Quaternary	IODP	177

Fahrtberichte

Preliminary results from IODP Expedition 333 (Nankai Through, Japan)

T. BAUERSACHS[1], M. STRASSER[2], IODP EXPEDITION 333 SCIENCE PARTY

1 Department of Organic Geochemistry, Kiel University, Ludewig-Meyn-Str. 10, 24118 Kiel, Germany
2 MARUM - Centre for Marine Environmental Sciences, University of Bremen, 28334 Bremen, Germany

IODP Expedition 333 (NanTroSEIZE Stage 2: subduction Inputs) is part of the multi-expedition drilling project Nankai Trough Seismogenic Zone Experiment (NanTroSEIZE) program, which is designed to investigate fault mechanics and seismogenesis along subduction megathrusts southeast of Japan. The overall aim of IODP Expedition 333 was to provide a reference for the sediments and basement of the subduction zone by characterizing the incoming sedimentary strata and igneous basement of the Shikoku Basin prior to their arrival in the Nankai Trough. In addition, the distal part of a mass transport deposits (MTD) was analyzed for its rheological behaviour to constrain sliding dynamics and tsunamigenic potential of submarine landslides as part of the Nankai Trough Submarine Landslide History (NanTroSLIDE) program.

Three drill sites located on a margin-perpendicular transect close to the Kii Peninsula were cored during Expedition 333 (SE Japan, Fig.1). Site NST-1A was located on the continental slope close to the up-dip terminus of the local mega splay fault. Seismic surveying indicated the presence of stacked mass transport deposits at this site, which were the primary subjects of interest for the NanTroSLIDE program. A total of 313 m were drilled at Site NST-1A with excellent recovery. Depositional units were based on variations in grain size, mineralogy, composition, presence and thickness of sand as well as ash layers. Lithological subunits mainly comprised silty clay with variable quantities of volcanoclastic sand and silt. Six intervals with evidence for mass-transport deposition were observed in the cored succession. The most pronounced MTD occurred at a depth of ca. 128 m and expressed a thickness of ca. 62 m. Further shore based analysis that will address the mechanical properties of these MTDs will enhance our understanding of the processes influencing magnitude and occurrence of submarine landslides and their potential for triggering catastrophic events in terms of both hazards (tsunamigenic landslides) and sediment mass-transfer within the context of margin evolution.

Drilling at Sites C0011 and C0012 aimed on the characterization of the uppermost stratigraphic unit of the Shikoku Basin facies, which was not recovered during previous NanTroSEIZE Expedition 322, and to determine *in situ* temperatures within the surficial sediments. For this reason, drilling was performed using the advanced piston corer temperature tool (APTC3) connected to the hydraulic piston coring system (HPCS).

Site C0011 is located on the northwest flank of the Kashinosaki Knoll in a water depth of ca. 4000 m (Fig. 1). This bathymetric high lay in the eastward prolongation of the Zenisu ridge intra-oceanic thrust, which brings back-arc basin crust to outcrop at the seafloor (Henry et al., 1997). Coring at Site C0011 recovered a sedimentary sequence with a thickness of ca. 380 m. The uppermost 251 m of this succession consisted of organic-poor pelagic mudstones that contained high abundances of intercalated ash layers. The underlying sediments, up to a depth of 348 m, were characterized by a sudden drop in the abundance of volcanic clastics and a concomitant increase in

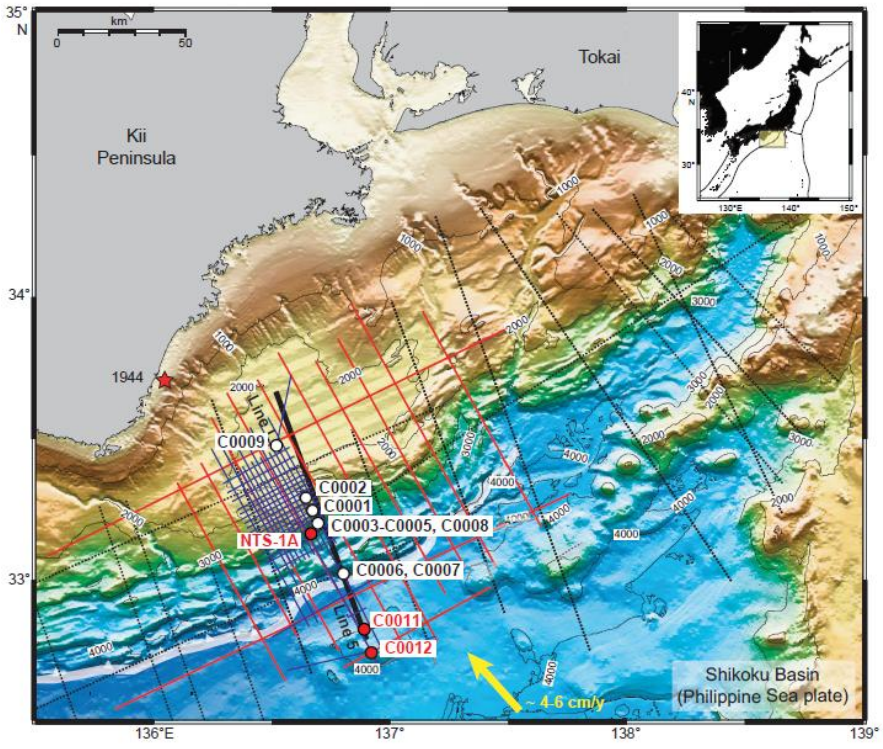

Figure 1

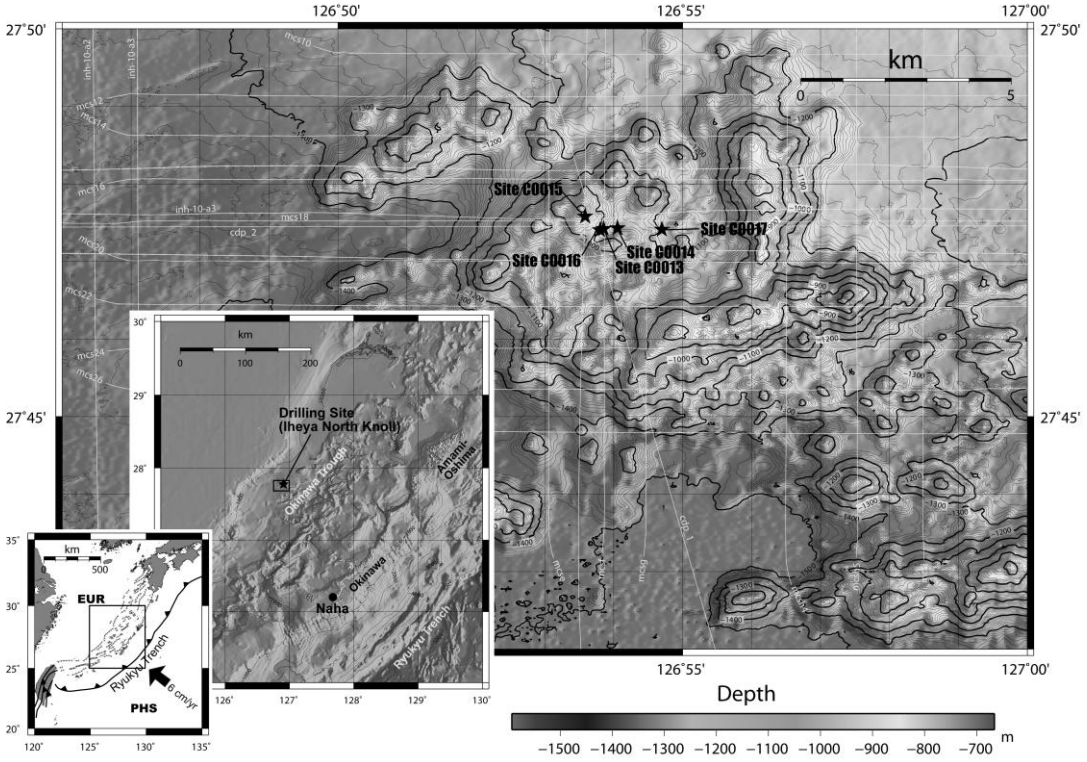

Figure 1: Bathymetric map of the Iheya North Knoll (Okinawa Trough) showing Expedition 331 drilled sites (black stars). White lines represent seismic profile locations.

bioturbation. In its entirety this succession comprises the uppermost stratigraphic unit of the Shikoku Basin facies, which was underlain by coarser-grained tuffaceous sandstones and heterolithic gravels of the middle Shikoku Basin facies.

Site C0012 was located near the crest of the Kashinosaki Knoll in a water depth of ca. 3500 m (Fig. 1). The cored sequence consisted of 180 m of hemipelagic mud and mustones comprising the upper Shikoku Basin facies as well as coarse-grained sediments of the upper part of the middle Shikoku Basin facies. Based on logging and core-log-seismic integration, these sediments had an estimated Holocene to Late Miocene age (~0-8.3 Ma). Temperature measurements using the advanced piston corer temperature tool indicated significantly increased surface heat flow around the Kashinosaki Knoll than the theoretical estimated from the age of the Shikoku Basin. In addition to the surficial sediments, the transition from pelagic sedimentation to the igneous basement was cored at Site C0012. The sediment/basalt interface was penetrated at 526 m CSF and the cored basement, consisting of pillow lava basalts and basaltic-hyaloclastite breccia that underlay a red and green calcareous claystones, showed very good recovery rates.

References:

Henry, S. Mazzotti, R. Maury, C. Robert, S.J. Lallemant (1997) Uplifted oceanic crust outcrops on Zenisu Ridge, JAMSTEC J. Deep Sea Research 13: 509- 520.

Preliminary results of IODP Expedition 331 „Deep Hot Biosphere“ (Okinawa Trough)

S. ECKERT[1], A. BREUKER[2], IODP EXPEDITION 331 SHIPBOARD SCIENCE PARTY

[1] Institut für Chemie und Biologie des Meeres (ICBM), Universität von Oldenburg, Postfach 2503, D 26111 Oldenburg (sebastian.eckert@uni-oldenburg.de)
[2] Bundesanstalt für Geowissenschaften und Rohstoffe (BGR), Stillweg 2, D-30655 Hannover (Anja.Breuker@bgr.de)

The main goal of IODP Expedition 331, Deep Hot Biosphere, was to determine directly the existence of a functionally active, metabolically diverse subvent biosphere in its physical, geochemical, and hydrogeologic context within the Iheya North field in the mid-Okinawa Trough. This work addresses one of the primary themes of the IODP Initial Science Plan, the Deep Biosphere and the Subseafloor Ocean. This expedition provided the first opportunity to drill into an active hydrothermal system and associated deposits within a backarc basin in a continental margin setting.

The “subvent biosphere” is the subseafloor biosphere that is predicted to exist just beneath active hydrothermal vents and fluid discharge zones. Subseafloor environments within active hydrothermal systems are the most promising locations for functionally active, metabolically diverse subseafloor microbial ecosystems. The existence of a subvent biosphere has been inferred from many microbiological and geochemical investigations of vent chimney structures and diffuse hydrothermal fluids. In the Iheya North field, it has been suggested that a variety of

microbial communities sustained by different chemolithoautotrophic primary producers are present in subseafloor habitats.

The major scientific objectives of Expedition 331 drilling were to prove the existence of a functionally active, metabolically diverse subvent biosphere associated with subseafloor hydrothermal activity in the Iheya North field. To clarify the architecture, function, and impact of subseafloor microbial ecosystems and their relationship to physical, geochemical, and hydrogeologic variations within the hydrothermal mixing zones around the discharge area was the second aim. For future research, artificial hydrothermal vents in cased holes have been established to prepare research platforms for later studies of fluids tapped from various parts of the hydrothermal system and their associated microbial and macrofaunal communities. Understanding the geochemistry especially of hydrothermal fluids, wich are controlled by phase separation and phase partition (e.g. carbon dioxide and methane) is essential for evaluating its influence on microbial communities and therefore for biogeochemical cylings on earth.

In this Expedition a total of 24 holes at five sites (C0013, C0014, C0015, C0016 "North Big Chimney", and C0017) were drilled. From these holes 300 m of core from 605 m of penetration was recovered, yielding an overall recovery of 49.6% with a maximal drilled depth of 151 mbsf. The onboard measurements of total cell counts was carried out for all microbial samples up to a dephts to 110 m.

Downhole temperature measurements yielded an increase of the temperature with depth from 3 °C at the sediment surface to values of >210 °C at 50 mbsf (Site C0014). Interstitial water was sampled in very high resolution to get a picture of geochemical processes in conjunction with microbial activity and hydrothermal alteration. Also four artificial vents were created to monitor fluid composition and in situ microbial colonization in long-term post-cruise studies. The emissions of these vents were confirmed to be >240 °C.

The deepest lithostratigraphic unit of all sites consists of hydrothermally altered and thus silicified volcaniclastic rocks. On top of these rocks lies pumice clast interbedded with anhydrite veins and hemipelagic mud. These pumice horizons have been hydrothermally changed in parts to mud and clay layers. Massive sulfide-rich sediment was found at sites C0013 and C0016. These sulfide horizons, which are enriched in sphalerite, represent an evolving system, with early sphalerite mineralization overprinted by pyrite and then chalcopyrite, as temperature increased. Afterwards, a second sphalerite mineralizing event occurred when temperatures decreased, and finally seawater influx is indicated by late coarsely crystalline anhydrite. Native sulfur is also abundant near-surface at site C0013, which, together with the abundance of kaolinite, suggested acidic fluids, interpreted to be caused by oxidation of H_2S dissolved in the hydrothermal fluid or released from the fluid during decompression. A transition from kaolinite-muscovite-rich sediment to Mg chlorite-rich rocks was observed with increasing depth at Site C0013. The Mg chlorite and anhydrite sections are additionally scattered with quarz. In general, the mineralogy of the Iheya North field is depleted in iron and abundant in potassium, compared to the Mid-Atlantic Ridge.

The biostratigraphy varies from site to site, thus the sites C0013, C0015, and C0016 do not have microfossils in any cores. At site C0014 microfossils are found only in the uppermost 6.5 mbsf. Microfossils occur at 9-28 mbsf and at 112 mbsf, respectively, at site C0017, which acts as a recharge zone. In all cases, the majority of microfossils are modern assemblages of planktonic foraminifers and rarely found coccoliths, which are badly corroded.

Geochemical analyses show an input of hydrothermal fluid with an unusual high concentration of microbially produced CH_4. The logarithmic increase in H_2 with depth suggested a deep source for this gas, as well as a relatively shallow sink at about 10 mbsf at site C0013, that is probably due to microbial consumption. The generally low contents of total organic carbon and total nitrogen let suggest, that hydrothermal alteration and possibly also microbial activity remineralized the sedimentary organic material relatively quickly. At site C0014 the interstitial water of the uppermost 10 m of sediment resembles sea water, except for sulfate, alkalinity, and the nutrient species, which are affected by microbial activity. Below 10 mbsf sulfate, Mg, and Na/Cl are decreasing and Ca, K and Si are increasing, thereby sulfate is inversely correlated with methane. A similar inversly correlated methane sulfate profile was previously found for Peru margin sediments (ODP Leg 201). Nevertheless, this correlation and its microbial participation is not understood in detail (Parkes et al., 2005). Chloride concentration decreases here from sea water value in the upper layers to a more vapor enriched layer at 27-40 mbsf and after this it increases again beyond sea water values, indicating a brine layer at 40-114 mbsf. This Cl depleted vapor-rich layer has also elevated methane concentrations. This points to a lateral and vertical flow of hydrothermally influenced fluids through more or less permeable layers (e.g. coarse sediments containing pumice and anhydrite) and microbially driven methane production. Interstitial waters at site C0017 shows also the effect of lateral flow of fluid through permeable layer, but here it is unaltered sea water, which change the concentrations of the bacteria aligned cations and anions back to sea water values. In general, an uptake of Na into altered minerals was observed and also the exchange of Ca for K and Mg in clay minerals.

The abundance of microbial cells in the sediments was evaluated by epifluorescence microscopy (Weinbauer et al., 1998). The microbial cells were enumerated with a fluorescence microscope equipped with the fluorescence filter set of 470/20 nm (center wavelength/bandwidth) for excitation and 515 nm for emission. The results did not obtain immediate evidence of an active deep hot biosphere during Expedition 331. Nevertheless, the hydrogeologic basis was firmly established for a variety of subseafloor microbial habitats associated with a high-temperature hydrothermal system. To tests for contamination by drilling fluid PFC was used as tracer in all drilling and coring systems. The results of PFC measurements show that the sample collection on D/V Chikyu is almost free of contamination and therefore useful for microbial studies.

The sites C0015 and C0017 hosted relatively abundant subseafloor microbial populations, but these depended on buried sedimentary organic matter. Even at these two sites, the microbial cell abundance was much lower than those found previously at ODP/IODP sites along continental margins (Parkes et al., 1994; D'Hondt et al., 2004;

Schippers et al., 2005), even though the Iheya North hydrothermal field is located in a backarc basin along a continental margin. The low cell abundances presumably result from the relatively low total organic carbon in the sediments, generally <0.1 wt% at Site C0015 and <0.5 wt% at Site C0017. The abundant occurrence of very permeable layers of pumice and volcaniclastic sediments and the consequent recharge of seawater into the hydrothermal system at Site C0017 generates a locally highly oxic subseafloor environment. This environment promotes the formation of oxidative oligotrophic and chemolithoautotrophic microbial communities, rather than fermentative, heterotrophic, and methanogenic communities. Methane concentrations at Sites C0015 and C0017 are generally low, and microbial methanogenesis is quite unlikely. Instead, we found layers enriched in iron oxide minerals at these two sites, which were probably produced by aerobic to microaerobic subseafloor microbial communities sustained by oligotrophic and chemolithoautotrophic iron oxidizers such as members of the class of *Zetaproteobacteria* (Emerson et al., 2007).

The results of this drilling cruise provide a more detailed view into the large-scale hydrogeology, geochemistry and microbiology of the Iheya North Knoll hydrothermal system. These results could sketch the interaction of primary deposition, hydrothermal alteration, and fluid migration, which characterize this hydrothermal system. But to get a clear view of all reactions and interactions in such a complex system, further research in an interdisciplinary context is needed.

References:

Expedition 331 Scientists, 2010. Deep Hot Biosphere. IODP Prel. Rept., 331. doi:10.2204/iodp.pr.331.210

D'Hondt, et al. (2004), Distributions of microbial activities in deep subseafloor sediments, Science, Vol. 306, p. 2216-2221.

Emerson et al. (2007), A novel lineage of proteobacteria involved in formation of marine Fe-oxidizing microbial mat communities. PLoS ONE 2(8): e667. doi:10.1371/journal.pone.0000667

Parkes et al. (1994), Deep bacterial biosphere in pacific ocean sediments, Nature, Vol. 371, p. 410-413.

Parkes et al. (2005), Deep sub-seafloor prokaryotes stimulated at interfaces over geological time, Nature, Vol. 436, p. 390–394.

Schippers, et al. (2005), Prokaryotic cells of the deep sub-seafloor biosphere identified as living bacteria, Nature, Vol. 433, p. 861-864.

Weinbauer et al. (1998), Utility of green fluorescent nucleic acid dyes and aluminum oxide membrane filters for rapid epifluorescence enumeration of soil and sediment bacteria, Applied and Environmental Microbiology, Vol. 64, p. 5000-5003.

IODP Expedition 329, South Pacific Gyre Sub-seafloor Life – Preliminary Results

T. ENGELHARDT[1], T.G. FERDELMAN[2], J. KALLMEYER[3], S. D'HONDT[4], F. INAGAKI[5], C. ALVAREZ ZARIKIAN[6], IODP EXPEDITION 329 SCIENCE PARTY

[1] Institut für Chemie und Biologie des Meeres, Oldenburg
[2] Max-Planck-Institut für marine Mikrobiologie, Bremen
[3] Institut für Erd- und Umweltwissenschaften, University of Potsdam,
[4] Graduate School of Oceanography, University of Rhode Island, USA
[5] Kochi Institute for Core Sample Research, JAMSTEC, Japan
[6] IODP, Texas A&M University, College Station, Texas, USA

The ultra-oligotrophic South Pacific Gyre is the Earth's largest oceanic province and lies over one of the largest scientifically unexplored regions of the seafloor. The South Pacific Gyre is farther from the continents than any other ocean gyre. Surface chlorophyll concentrations and primary productivity are lower than any of the other regions of the world ocean. It contains the world's clearest seawater (Morel et al., 2007). The sediments underlying this gyre represent extreme lows in sedimentation rates and surface cell abundances; oxygen penetration depths to several meters indicate that microbial activities are persistently low and suggest that a flux of oxygen may be controlled by crustal processes (D'Hondt et al. 2009; Fischer et al. 2009). Although the heterotrophic microbial activities tend to decline greatly with increasing depth in most deeply buried sediments, microbial abundances appear be robust in the deeper sediments. This observation has led to the hypothesis that non-photosynthetic sources of energy may play a role in maintaining these deeply-buried populations (e.g. by water radiolysis, D'Hondt et al. 2009). Whereas most drilling sites where sub-seafloor life studies have been made are at the continental margins or in equatorial upwelling regions, the just completed drilling of the South Pacific Gyre sub-seafloor ecosystem provided the opportunity to begin to test these and other hypotheses, and to fill a large gap in our knowledge of this vast sub-seafloor microbial habitat. Overall, IODP Expedition 329

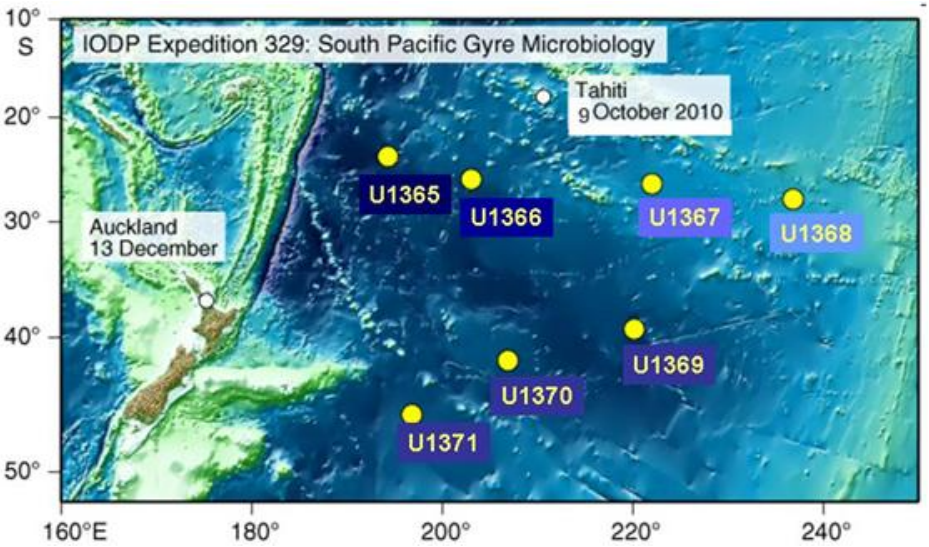

Figure 1: Sites drilled during IODP Expedition 329 South Pacific Gyre Subseafloor Life

had the four following main objectives:

1. To document the habitats, metabolic activities, genetic composition and biomasses of microbial communities in sub-seafloor sediment with very low activity.
2. To test how oceanographic factors, such as ocean productivity, control variation in sedimentar habitats, activities and communities from gyre center to gyre margin.
3. To quantify the extent to which sub-seafloor microbial communities of this region may be supplied with electron donors by water radiolysis, a process independent of the surface photosynthetic world.
4. To determine how basaltic basement habitats, potential activities and, if measurable, microbial communities vary with crust age and hydrologic regime (from ridge crest to abyssal plain).

To address these objectives during IODP Expedition 329 (start in Papeete, French Polynesia on Oct. 9th and ending on Dec. 13th in Auckland, New Zealand), we conducted operations in 42 holes at seven sites (U1365 to U1371). The sites followed two transects from the edge to the center of the gyre, with the easternmost hingepoint in the center of the ultra-oligotrophic gyre. (See Figure 1). Water depths ranged from 3749 to 5707 meters below sea level. At all sites except U1371, the entire sediment column down to the sediment-basalt interface was drilled and cored. At three sites (U1365, U1367, U1368) attempts were made to drill deeper in order to retrieve samples from the unaltered basement. Whereas the recovery rates and the quality of sediment cores were generally very good, recovery and quality of the basement rocks were highly variable. A total of 1322 meters of sediment from seven sites were cored, as well as 206 meters (36.7% recovery) of basalt at three sites along the northern transect.

The dominant lithology along the deep water sites (U1365 – U1367) is a zeolitic metalliferous clay. Manganese nodules are common on and near the surface at these sites. Chert and porcellinite layers were found in the deeper layers at Sites U1365 and U1366. These were also the sediments lying in the oldest crust (> 100 Ma). A shift to carbonate lithology was observed at the easternmost, shallowest water depths (Site U1368). The southernmost and last Site (U1371), just outside the South Pacific Gyre was dominated by siliceous ooze, although deeper sediment was composed of zeolitic metalliferous deep-sea clay.

High resolution interstitial water chemical analyses - with unprecedented emphasis on precision and sensitivity - formed a major activity onboard the JOIDES Resolution during Expedition 329. Deep penetration of dissolved oxygen and nitrate as primary electron acceptors was observed at most sites. Controls on these fluxes, as well as other interstial water properties such as phosphate and dissolved inorganic carbon, are proposed to include heterotrophic bacterial processes, crustal reactions, and past glacial deep-water conditions. Organic carbon and nitrogen concentrations are low and decrease with increasing sediment depth to non-detectable concentrations.

Microbiological sampling activities also constituted a major activity onboard during the expedition. Consistent with the site survey results, cell abundances are orders of magnitude lower than in continental margin settings, and decrease with depth. Further refined counting will take place in shore-based laboratories (Potsdam). Estimates of viral abundances and activities were also an important component of the expedition shipboard research and will continue onshore (Oldenburg). Activities of deep sub-surface communities are being addressed by ship-board and shore-based radio-isotope and stable isotope experiments (Bremen).

Overall, IODP Expedion 329 has already made major strides toward fulfilling the principal objectives of documenting this vast, unexplored habitat; exploring the role of oceanography in controlling the variation in sub-seafloor habitats; testing non-photosynthetic models for the maintenance of life; and in constraining habitability in basement and ultra-low activity sediments.

References:

D'Hondt S, Spivack A, Polckalny R, Ferdelman TG, Fischer JP, Kallmeyer J, Abrams L, Smith D, Graham D, Hasiuk F, Schrum H, Stancin A, 2009, Subseafloor sedimentary life in the South Pacific Gyre. Proc. Nat. Acad. Sci.,106, 11651-11656 doi:10.1073/pnas.o811793106.

Fischer JP, Ferdelman TG, D'Hondt S, Røy H, Wenzhöfer F, 2009, Oxygen penetration deep into the sediment of the South Pacific gyre. Biogeosciences 6, 1467-1478. www.biogeosciences.net/6/1467/2009

Morel, A., Gentili, B., Claustre, H., Babin, M., Bricaud, A., Ras, J., and Tieche, F., 2007. Optical properties of the "clearest" natural waters. Limnol. Oceanogr., 52: 217-229.

IODP Expedition 325 to the Great Barrier Reef: climate and sea level changes since the Last Glacial Maximum

T. FELIS[1], E. GISCHLER[2], EXPEDITION 325 SCIENTISTS

[1] MARUM – Zentrum für Marine Umweltwissenschaften, Universität Bremen, 28359 Bremen, Germany
[2] Institut für Geowissenschaften, Goethe-Universität, 60438 Frankfurt am Main, Germany

The timing and courses of deglaciations are considered an essential component for understanding the dynamics of large ice sheets and their effects on Earth's isostasy. Moreover, the disappearance of glacial ice sheets was responsible for dramatic changes in the freshwater fluxes to the oceans, which disturbed the thermohaline circulation and hence global climate. Coral reefs are excellent sea level indicators, and their accurate dating by mass spectrometry is of prime importance for determining the timing of deglaciation events, and, thus for understanding the mechanisms driving the glacial–interglacial as well as millennial scale cycles. Furthermore, scleractinian coral colonies can monitor sea-surface temperatures and other oceanographic parameters (e.g., salinity and sediment run-off), and fossil corals can be used as recorders of past variations in these parameters. Finally, assessing the impact of sea-level and climate changes on fossil coral reefs may represent an important advance in understanding how coral reef systems, in particular the Great Barrier Reef, respond to environmental stress.

Integrated Ocean Drilling Program (IODP) Expedition 325 "Great Barrier Reef Environmental Changes", designed to investigate the fossil reefs on the shelf edge of the Great Barrier Reef in the western tropical South Pacific, was the fourth expedition to utilize a mission-specific platform and was conducted by the European Consortium for Ocean Research Drilling (ECORD) Science Operator (ESO) (Webster, Yokoyama, and Cotterill, 2009; Expedition 325 Scientists, 2010). The objectives of Expedition 325 are to establish the course of sea level change, to define sea-surface temperature variations, and to analyze the impact of these environmental changes on reef growth and geometry for the region over the period of 20–10 ka. Expedition 325 complements Expedition 310 "Tahiti Sea Level" (Camoin et al., 2007) that in 2005 recovered postglacial coral reef material from the flanks of the island of Tahiti in the central tropical South Pacific in depths ranging from 41 to 117 meters below sea level and ages spanning from ~16 to ca. 8 ka, but also from intervals of the penultimate deglaciation.

To meet the Expedition 325 objectives, a succession of fossil reef structures preserved on the shelf edge seaward of the modern Great Barrier Reef were cored at three geographic locations from the dynamically positioned vessel *Greatship Maya* in February–April 2010 (Expedition 325 Scientists, 2010). A total of 34 boreholes across 17 sites were cored in depths ranging from 42 to 167 meters below sea level. Borehole logging operations in four boreholes provided continuous geophysical information about the drilled strata. The cores were described by a group of 28 scientists from 9 countries during the Onshore Science Party (OSP) at the IODP Bremen Core Repository (Germany) in July 2010, where minimum and some standard measurements were made (Expedition 325 Scientists, 2010). Preliminary dating of core catcher samples and initial observations of the cores made during the OSP confirm that coral reef material ranging in age from >30 to 9 ka was recovered during Expedition 325. High-quality fossil coralgal frameworks are found in a number of horizons of different cores thus recording high energy reef settings, which is crucial for precise reconstructions of sea-level and sea-surface environmental change. The late Pleistocene sections appear diagenetically unaltered and comprise coralgal boundstone, coralgal-microbial boundstone, skeletal grainstone and rudstone, and unconsolidated sand. In five cores taken in depths of 40 to 85 meters water depths at three traverses, older Pleistocene (>25 ka) reefal deposits were recovered in lower core sections. Lithologies include skeletal grainstone to rudstone, some packstone, coralgal boundstone, and few occurrences of coral-microbial boundstone. Usually, they exhibit clear evidence of diagenetic modification in the meteoric realm, such as caliche phenomena, neomorphism, dissolution vugs, and low magnesium calcite cement growth. The preliminary chronology, combined with the recovered depths of the core catcher samples, is particularly exciting as it clearly demonstrates that Expedition 325 recovered coral reef material from key periods of interest for sea level change and environmental reconstruction, including the Younger Dryas, the Bølling-Allerød, meltwater pulse 1A (MWP-1A), the 19 ka-MWP, the Last Glacial Maximum and Heinrich stadials 1 and 2. Given that there are so few fossil coral records spanning these intervals, and even fewer from stable, passive margin settings far from the confounding influence of ice sheets, highlights further the importance of the new Expedition 325 cores. Further postcruise research on samples taken during the OSP is expected to fulfil the objectives of the expedition.

References:

Camoin, G.F., Iryu, Y., McInroy, D.B., and the Expedition 310 Scientists, 2007. Proceedings IODP, 310: Washington, DC (Integrated Ocean Drilling Program Management International, Inc.). doi:10.2204/iodp.proc.310.2007.

Expedition 325 Scientists, 2010. Great Barrier Reef environmental changes: the last deglacial sea level rise in the South Pacific: offshore drilling northeast Australia. IODP Preliminary Report, 325. doi:10.2204/iodp.pr.325.2010.

Webster, J.M., Yokoyama, Y., and Cotterill, C., 2009. Great Barrier Reef environmental changes: the last deglacial sea level rise in the South Pacific: offshore drilling northeast Australia. IODP Scientific Prospectus, 325. doi:10.2204/iodp.sp.325.2009.

IODP Expedition 332:NanTroSEIZE Stage 2: Riserless Observatory

A. KOPF, E. ARAKI, S. TOCZKO, EXPEDITION 332 SCIENCE PARTY

One primary objective of the NanTroSEIZE (Nankai Trough Seismogenic Zone Experiment) complex drilling project (CDP) is to drill and instrument a series of holes across the seismogenic subduction system offshore the Kii Peninsula, Japan. IODP Expedition 332 "Riserless Observatory" followed up on initial observatory operations begun during IODP Expedition 319 in Summer 2009. The cruise focused mainly on engineering work, including (1) retrieval of a temporary observatory instrument installed during Expedition 319 at Site C0010, which penetrates the shallow "megasplay" fault in the mid-forearc, and installation of a new suite of temporary sensors, (2) deploy an upgraded temporary observatory at Site C0010, and (3) permanent observatory installation at Site C0002 in the outer Kumano Basin, at the location of planned future deep riser drilling.

The expedition began on 25 October and ended on 11 December 2010. During the first few weeks, the focus was on exchanging the SmartPlug temporary "mini-CORK" with an upgraded GeniusPlug, both attached to a retrievable casing packer above the screened megasplay fault zone at Site C0010. SmartPlug recovery was successful despite the strong Kuroshio current, which can be attributed to an efficient reduction of vortex-induced vibration (VIV) on the drill string by attaching ropes. Times series data recovered from the self-contained instrument include seafloor and formation pressure as well as 4 independent temperature records from the fault zone and the overlying seafloor reference. Tentative analysis of those data proves the effective seal of the bridge plug, dampened pressure amplitudes in the tight, slightly overpressured formation, and identification of prominent earthquake and tsunami events in the 15-month record (23 August 2009 – 7 November 2010). The SmartPlug was then replaced with a GeniusPlug, similar in geometry and equally self-contained, but with an addendum that hosts an Osmo-Sampler for collecting fluids for geochemical analysis and a FLOCS (FLow-through Osmotic Colonization System) for microbiological study. The system was installed at a depth that placed the addendum in the center of the 22 m-wider screened cased section across the "megasplay" fault.

At Site C0002, somewhat upslope of Site C0010, a new hole was drilled with LWD (Logging-While-Drilling) and cased for placement of a Long-term borehole monitoring system (LTBMS). It comprises a CORK assembly with a hydrogeological unit measuring pressure at four depth levels as well as a broadband seismometer, volumetric strainmeter, tiltmeter, geophones, and a thermistor string. The key goals include pore pressure monitoring in the upper accretionary prism (Unit IV), a series of measurements in the homogeneous sediments of Unit III (strain, tilt, seismicity, pressure) in the transition zone, and temperature and pressure in the overlying Kumano Basin sediments of Unit II. The string of the CORK assembly had a total length of 965 m and was carefully secured during deployment with centralizers, bands and straps to withstand the strong current. VIV was minimized using ropes, and acceleration was monitored during deployment. The lower portion of the assembly is isolated against the overlying ocean body by a swellable packer at 746 mbsf. Part of the instrument string below was cemented (appx. 780-935 mbsf) to couple strainmeter and seismometer to the formation/casing. The CORK head was revisited prior and after cementing for system tests of the borehole instruments using the ROV, and all of these experiments were successful. The CORK is working in a self-contained (battery-driven) mode for some of the instruments, while others will be connected to external batteries in spring 2011. The long-term perspective is a connection of the system to the real-time seafloor cabled network DONET.

Main Results of IODP Expedition 318 – Wilkes Land

J. PROSS, U. RÖHL, IODP EXPEDITION 318 SCIENCE PARTY

The overall objective of Expedition 318 was to obtain a long-term record of Antarctic glaciation and its relationships with global paleoclimate, paleoceanography and eustatic sea-level change by drilling the Antarctic margin along an inshore-offshore transect (Figure 1).

The principal goals were to

- determine the timing, nature and consequences of the first major phase of East Antarctic Ice Sheet (EAIS) growth and the arrival of ice at the Wilkes Land margin (onset of glaciation), which presumably occurred during the earliest Oligocene. In marine records elsewhere, this event is thought to correlate with a steep increase in oceanic $\delta^{18}O$ values widely referred to as the Oligocene isotope Event 1 (Miller et al., 1985);
- recover a high-resolution record of Antarctic climate variability during the Oligocene, Neogene, and Quaternary, and an unprecedented ultrahigh-resolution (i.e., seasonal to decadal) Holocene record of climate variability;
- decipher the nature and ages of changes in the geometries of the progradational wedges. These changes are interpreted to correspond to large fluctuations in the extent of the EAIS and possibly coincide with the transition from a wet-based to a cold-based glacial regime.

Expedition 318, January–March 2010 (Wellington to Hobart), occupied seven sites that produced ~2000 m of high-quality upper Eocene to Quaternary sediments at Sites U1355, U1356, U1359, and U1361 on the Wilkes Land rise and Sites U1358, U1360 and U1357 on the Wilkes Land shelf at water depths between ~400 and 4000 mbsl (Figures 1 and 2). Together, the cores represent ~53 m.y. of Antarctic history (Figure 3). The cores document the evolution of the Wilkes Land Antarctic margin from an ice-free "greenhouse Antarctica" to the present-day icehouse conditions, including the onset and erosional consequences of the first glaciation and the subsequent dynamics of the waxing and waning ice sheets, and unique "tree ring style" records with seasonal resolution of the last deglaciation that began ~10,000 y ago. They also allow to reconstruct the tectonic history of the so-called Australo-Antarctic Gulf (from 53 Ma onwards), the onset of the second phase of rifting between Australia and Antarctica (Close et al., 2009), and the process of margin subsidence and deepening

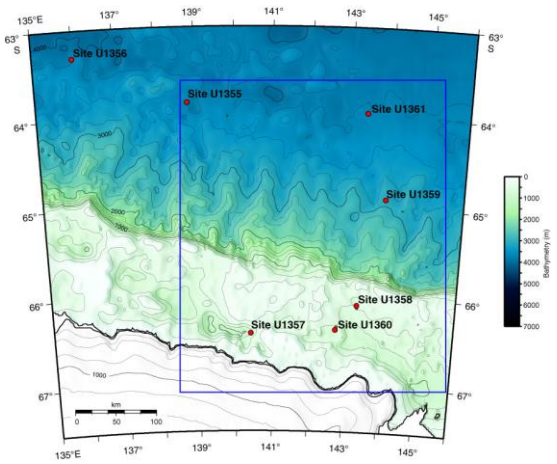

Figure 1: Bathymetric map showing locations of the seven sites drilled during Expedition 318. From Expedition 318 Scientists (2010).

all the way to the present ocean/continent configuration. Tectonic and climatic change turned the initially shallow, broad subtropical Wilkes Land offshore shelf into a deeply subsided basin with a narrow ice-covered margin. Thick Oligocene and notably Neogene deposits, including turbidites, contourites, and larger- and smaller-scaled debris mass flows, document the erosional force of the waxing and waning ice sheets and deep-ocean currents. The recovered clastic sediments (clays, silts and sands) and their microfossil content also reveal the transition of subtropical ecosystems and a densely vegetated Antarctic continent into sea ice–dominated ecosystems bordered by calving glaciers.

1. Timing, nature, and consequences of the first major phase of East Antarctic Ice Sheet (EAIS) growth

The "preglacial" regional Unconformity WL-U3 (Figure 2) represents a major erosion event related to the onset of glaciation at ~34 Ma (early Oligocene), with immediately overlying deposits dated at 33.3 Ma. Strata overlying the unconformity at the inshore shelf Site U1360 are of early Early Oligocene age (~33.3 Ma). Below Unconformity WL-U3, a late Early to early Middle Eocene record from peak greenhouse conditions, likely including some of the early Eocene hyperthermals, was recovered at Site U1356. A hiatus spanning 2 m.y. separates the Lower Eocene from the Middle Eocene record. This hiatus may be in tandem to tectonic activity related to the onset of rapid sea-floor spreading in the Australian Antarctic Basin (AAB), reported to initiate around the same time (~50 Ma) (Close et al., 2009). The upper Middle Eocene to the basal Oligocene is conspicuously missing in a ~19 m.y.-long hiatus at ~890 mbsf (~47.9-33.3 Ma) (Figure 3).

Above Unconformity WL-U3, Oligocene sediments from Site U1356 unequivocally reflect icehouse environments with evidence of iceberg activity (dropstones) and at least seasonal sea-ice cover. The sediments, which are dominated by hemipelagic sedimentation with bottom-current and gravity-flow influence, as well as the microfossil evidence biota indicate a deeper-water setting as compared to that of the underlying Middle Eocene.

2. Antarctic climate variability during the Oligocene, Neogene and Quaternary, and nature and ages of the changes in progradational wedge geometries

Drilling at the continental rise Site U1356 also recovered a thick section of Oligocene to upper Miocene sediments indicative of a relatively deep-water, sea-ice-influenced setting (Figure 3). Oligocene to upper Miocene sediments imply episodically reduced oxygen conditions either at the seafloor or within the upper sediments prior to ~17 Ma. From the late Early Miocene (~17 Ma) onward, progressive deepening and possible intensification of deep-water flow and circulation lead to a transition from a poorly oxygenated low-silica system (present from the Early to early Middle Eocene to late Early Miocene) to a well-ventilated silica-enriched system akin to the modern Southern Ocean. This change coincides with one of the major regional unconformities at the Wilkes Land margin, Unconformity WL-U5, which represents a ~3 m.y.-long hiatus in the Early Miocene. This unconformity marks a change in the dominant sedimentary processes at this site, which are characterized by mass-transport processes below the unconformity and by hemipelagic turbidity-flow and bottom-current deposition above.

A complete record with good recovery of late Miocene

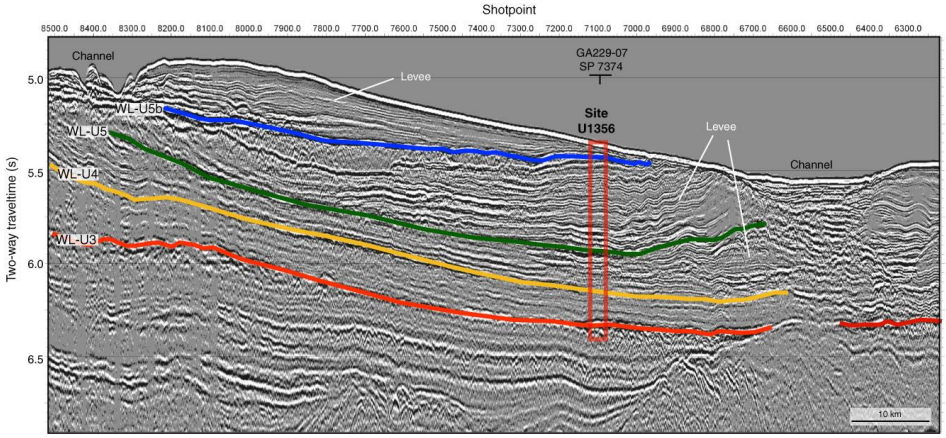

Figure 2: Multichannel seismic reflection profile across **Site U1356** showing regional Unconformities WL-U3, WL-U4, and WL-U5. Red box = approximate penetration achieved at Site U1356. Unconformity WL-U3 is interpreted to mark the first preserved grounding of an ice sheet across Wilkes Land, eroding the continental shelf ~40 m.y. (Eittreim et al., 1995) to 33.5-30 Ma ago (Escutia et al., 2005). From Expedition 318 Scientists (2010).

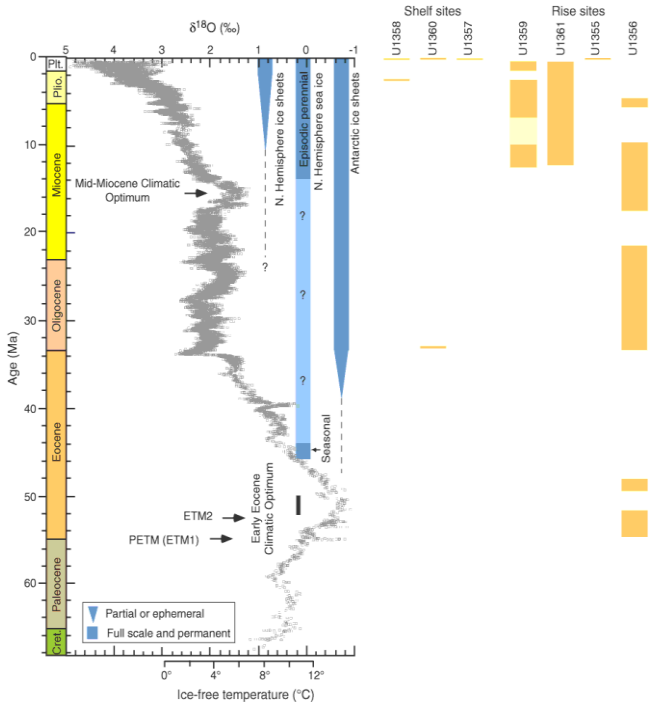

Figure 3: Updated Cenozoic pCO_2 and stacked deep-sea benthic foraminifer oxygen isotope curve for 0-65 Ma combined with chronostratigraphy of the sites drilled during Expedition 318. From Expedition 318 Scientists (2010).

to Pleistocene deposits was recovered at continental rise Sites U1359 and U1361 (Figure 3), drilled on levee deposits bounding turbidity channels. The cyclicity in the cores seems to reveal EAIS dynamics down to orbital timescales (100 and 40 k.y. cyclicity). This cyclicity likely documents the successive advances and retreats of the ice sheet and sea-ice cover, as well as the varying intensity of cold saline density flows related to bottom water production at the Wilkes Land margin (e.g., high-salinity shelf water flowing from the shelf into the deep ocean to form Antarctic Bottom Water, ABW). In general, typical Southern Ocean open- and cold-water taxa, with variable abundances of sea-ice-associated diatoms, indicate a high-nutrient, high-productivity sea-ice-influenced setting throughout the Neogene. Combined sedimentological and microfossil information indicates the ever-increasing influence of typical Antarctic Counter Current surface waters and ABW intensifying flow.

Continental shelf Site U1358 recovered a record from the early Pliocene to Pleistocene (with a small hiatus at ~2.5 Ma). Although the targeted Unconformity WL-U8 was not reached, glacial and glacial-marine sediments recovered at this site are dated as early Early Pliocene. Therefore, the change in the geometries of the progradational wedge from low-angle progradational strata above to very steep foresets is older than 4.5 Ma.

3. Ultrahigh-resolution Holocene record of climate variability

Coring at Site U1357 yielded a 186-m-long, triple-cored section of continuously laminated diatom ooze that will aid in the construction of a composite stratigraphy spanning at least the last 10,000 y as well as a portion of the underlying Last Glacial Maximum diamict. The Site U1357 sediments are unusual for Antarctic shelf deposits because of their high accumulation rate (2 cm/y), lack of bioturbation, and excellent preservation of organic matter as well as calcareous, opaline, phosphatic, and organic fossils. These sediments provide a unique sample set for geomicrobiology and sedimentary geochemistry studies.

The greatest achievement from a paleoclimatic standpoint was the retrieval of a continuously layered deposit. Initial shipboard investigations of laminae in Hole U1357A suggests that paired light-dark laminae sets range in thickness from ~1 to 3 cm, very likely that each laminae pair represents 1 y. This record has the potential to be the first varved sedimentary sequence extending through the Holocene recovered from the Southern Ocean, also allowing ultrahigh-resolution correlation to one of the most important Holocene ice cores in Antarctica (Law Dome Ice Core). Analysis at the annual timescale will allow to examine decadal to subdecadal variability in sea ice, temperature, and wind linked to the Southern Annular Mode (SAM), Pacific Decadal Variability, and possibly ENSO.

References:

Close, D.I., Watts, A.B., and Stagg, H.M.J., 2009. A marine geophysical study of the Wilkes Land rifted continental margin, Antarctica. Geophys. J. Int., 177(2):430–450. doi:10.1111/j.1365-246X.2008.04066.x

Eittreim, S.L., Cooper, A.K., and Wannesson, J., 1995. Seismic stratigraphic evidence of ice-sheet advances on the Wilkes Land margin of Antarctica. Sediment. Geol., 96(1–2):131–156. doi:10.1016/0037-0738(94)00130-M

Escutia C., De Santis, L., Donda, F., Dunbar, R.B., Cooper, A.K., Brancolini, G., and Eittreim, S.L., 2005. Cenozoic ice sheet history from East Antarctic Wilkes Land Continental Margin sediments. Global Planet. Change, 45(1–3):51–81. doi:10.1016/j.gloplacha.2004.09.010

Expedition 318 Scientists, 2010. Wilkes Land Glacial History: Cenozoic East Antarctic Ice Sheet evolution from Wilkes Land margin sediments. IODP Prel. Rept., 318. doi:10.2204/iodp.pr.318.2010

Miller, K.G., Aubry, M.-P., Kahn, M.J., Melillo, A.J., Kent, D.V., and Berggren, W.A., 1985. Oligocene–Miocene biostratigraphy, magnetostratigraphy, and isotopic stratigraphy of the western North Atlantic. Geology, 13(4):257–261. doi:10.1130/0091-7613(1985)13<257:OBMAIS>2.0.CO;2

IODP Expedition 326. NanTroSEIZE Stage 3 - Plate Boundary Deep Riser-1

H. TOBIN, M. KINOSHITA, N. EGUCHI, S. NIELSEN, A. KOPF

The NanTroSEIZE project is a multi-expedition, multistage IODP drilling program focused on understanding the mechanics of seismogenesis and rupture propagation along subduction plate boundary faults. The drilling program includes a coordinated effort to characterize, sample, and instrument the plate boundary system at several locations offshore the Kii Peninsula culminating in drilling, sampling, and instrumenting the plate boundary fault system near the updip limit of inferred coseismic slip, at 5~7 km below seafloor. The main objectives are to understand include the mechanisms controlling the updip aseismic–seismic transition along the megathrust fault system, processes of earthquake and tsunami generation and strain accumulation and release, the absolute mechanical strength of the plate boundary fault, and the potential role of a major upper plate fault system (termed the "megasplay" fault) in seismogenesis and tsunamigenesis.

Expedition 326 was the first stage of drilling and coring to the boundary zone between the Philippine Sea and Eurasian Plates, the ultimate target of the NanTroSEIZE Complex Drilling Program. In fact, it was the top hole operation in non-Riser mode required to set the stage for ultra-deep (>>5km) Riser drilling across the subduction thrust in the Nankai Trough subduction system. The main focus of this expedition was Site C0002, a well-studied location since previous NanTroSEIZE drilling Expeditions (Exp. 314, 315) conducted LWD/MWD and coring at Holes C0002A-D. It was therefore possible to carefully choose the hole location for future deep Riser drilling based on 3Dseismic reflection data and previous hole locations.

Expedition 326 was purely engineering and aimed at (i) installation of the wellhead, and (ii) drilling and casing the top ~800 m of the potentially 7 km deep hole. As a result, there was no science party on board apart from representatives from CDEX and the two NanTroSEIZE project chief scientists. The expedition ran from July 19 to August 20, 2010. A seafloor survey was conducted early on July 20, finding no obstructions around the location. The 36" conductor pipe and jetting BHA were made up and run, and by July 21 the guide horn was installed and the vessel started drifting to site. However, ROV winch trouble on July 22 held up the operation until spare parts could be loaded. This happened on the night of July 24, and repair of the ROV winch continued until July 25. Hole C0002F was finally spudded at 38° 18.0507'N, 136° 38.2029'E on July 25, jetting the 36" conductor pipe in to 54 mbsf. Releasing the Drill Ahead Tool (DAT) went smoothly, followed by drilling with 26" bit to target depth of 856.5 mbsf on July 27. After a wiper trip, 20" casing installations started on July 31, and by August 1 *Chikyu* could drift back towards Hole C0002F with 72 joints of 20" casing trailing underneath. However, during the afternoon of August 1, probably due to a sudden increase of the current speed, the string sheared off just above the Casing Running Tool (CART) and most of the casings were lost on the sea floor. After a short port call where more casing was loaded, Chikyu reamed down another 4 m (to 872.5 mbsf) and continued wiper trips until August 14, then returned upstream to a low current area to prepare for setting casing. On August 15, the new casing was lowered, with four ropes attached to the drill pipe in order to reduce the Vortex-Induced Vibration (VIV). Drifing downstream begain in the early morning of August 16. By midday August 17, the casing was stabbed into Hole C0002F under the current speed of more than 4 knots. On August 18, the casing was successfully set and cemented, and the drill pipe could be tripped back up. In the evening of August 19 the ROV dove with the corrosion cap and set it by midnight.

At the end of expedtion 326, Site C0002F had been drilled to 868.5 mbsf and the hole lined with successfully cemented 20-inch casing. A corrosion cap was set in preparation for future returns to continue drilling. Hole C0002F is now ready for deep Riser drilling, currently planned in 2012-2013.

Abstracts

IODP

Experimental investigation of gabbro partial melting in the presence of NaCl-rich water fluid - implications for the genesis of oceanic plagiogranites

R. ALMEEV[1], N.STRUBE[1], J. KOEPKE[1], S. SILANTIEV[2], F. HOLTZ[1]

[1]Institute of Mineralogy, Leibniz University of Hannover
[2]Vernadsky Insitute for Geochemistry and Analytical Chemistry, Moscow

Figure 1. Plagiogranitic vein in gabbro. Core 304-U1309-62R1.

Oceanic plagiogranites: project objectives

Oceanic plagiogranites (e.g. diorites, tonalites, trondjhemites) are intermediate to felsic plutonic rocks, widely reported in ophiolite complexes and from recently formed oceanic crust (Coleman, 1977). The mechanisms proposed for their genesis include late-stage differentiation of a parental MORB melt and partial melting of gabbroic rocks triggered by water-rich fluids. Recently the last mechanism has received realistic experimental confirmation (Koepke et al., 2004). It was demonstrated that at temperatures in excess of 900 °C and at low pressures (200 MPa) the hydrous partial melting of different typical oceanic gabbros and gabbro-norites can lead to melt compositions close to natural plagiogranites. The key result of these experiments is the requirement of H_2O-bearing fluid phase to produce melts silicic in composition, however the nature of these water-rich fluids (magmatic or seawater-derived) is still under debate (Koepke et al., 2007). There is a number of geological and geochemical observations suggesting the involvement of deep, seawater-derived fluids in anatexis of the lower crust that results in formation of oceanic plagiogranites. These are: (1) close spatial relationships of oceanic plagiogranites and active high-temperature hydrothermal systems (e.g. Mid-Atlantic Ridge (MAR), 12-17°N, (Silantyev et al., 2008)); (2) data on halite-rich fluid inclusions in the MAR gabbro with entrapment temperature exceeding 700°C (Kelley & Delaney, 1987); (3) the presence of high-temperature amphibole with high Cl contents (up to 2 wt%) which are probably seawater-derived (Koepke et al., 2008); (4) geochemical evidence for enrichment in LREE as well as high (compared to the host rocks) $^{87}Sr/^{86}Sr$ characteristics of oceanic plagiogranites (Silantyev et al., 2005); (5) First in-situ analyses of Sr isotopes in those interstitial minerals assumed to be residual phases after a hydrous anatexis event (Koepke et al., 2008).

It is well known that Cl strongly affects the solid/fluid partitioning behavior of many elements (e.g. LILE, REE, Zn, Cu, Mo, Au, Ag, PGE, U, Th). The addition of Cl to a fluid can noticeably change the phase equilibria and especially the melt composition coexisting with solid phases (Botcharnikov et al., 2004). In addition, it was demonstrated recently that the Na_2O content of melts coexisting with a fluid phase is strongly dependent on the Cl content of the system (granitic composition in equilibrium with HCl-NaCl-KCl-enriched H_2O-bearing fluid; Frank et al., 2002; Simon and Pettke, 2009). However, there is a lack of appropriate experimental information on (1) the role and behaviour of a NaCl-rich fluid during partial melting of gabbro and on (2) the partitioning of major and trace elements between melt, fluid and saline liquid.

Our project started in 2010 was aimed to perform partial melting experiments in the presence of NaCl-rich water fluid (modeled seawater-derived fluid) to (1) investigate the specifics of generating SiO_2-rich melts by partial melting of oceanic gabbros and (2) to study the effect of NaCl in the fluid on major and trace element partitioning.

Implication to the problem of formation of early crust on Earth

The understanding of the role of hydrothermal driven anatexis in the genesis of the felsic rocks in modern oceanic settings may have an important implication to the problem of formation of the early crust on the Earth. It has been shown recently (Rollinson, 2008) that compositions of modern oceanic plagiogranites are reminiscent of the archaen TTG rocks (Condie, 1981) to some extent. It was suggested for example, that the high Na_2O content and LREE-enrichment of oceanic plagiogranites and some of the archaen tonalites and trondjhemites can be explained by the involvement of the sodium-rich sea-water derived fluids in the processes of partial melting (Rollinson, 2008). Thus, the experimental investigation of deep anatexis within the ocean crust driven by water- and Cl-rich fluids has also the potential to shed light on the formation of the first continental crust in the early Earth history within a period of exclusively basaltic magmatism.

Experiments

In the course of our study we performed two sets of melting experiments which mainly differ in sample preparation, rock and fluid compositions as well as thermodynamic conditions of melting-crystallization (P-T-fO_2). The first set of experiments was done on gabbro-norite FR12-08 (Table 1) collected during Expedition FARANAUT on the slopes of MAR at 15.37°N and 46,31°W. All experiments have been performed using rock powder (grain size 100-150 μm) and fluids of various compositions: pure H_2O, pure H_2O-CO_2 and NaCl-bearing (with initial 3.3 and 6 wt% NaCl in the fluid) hydrous fluid. The melting experiments were performed in an internally heated pressure vessel (IHPV) pressured with argon at 200 MPa and in the temperature interval between 800 and 1000°C. The redox conditions (fO_2) of this series of experiments were corresponded to the QFM+3.3 oxygen buffer (QFM – quartz-magnetite-fayalite) at H_2O-saturated conditions and were slightly reduced in all runs in the presence of NaCl in the fluid. The second experimental series was consisted of melting experiments where solid rock cylinders (sliced along vertical axes) were used

	SiO_2	TiO_2	Al_2O_3	FeO*	MnO	MgO	CaO	Na_2O	K_2O	Total
F12-08	52.71	0.29	18.63	5.61	0.14	8.18	11.88	2.56	0.08	100.08
1309 D218-R4-55-63	50.3	0.30	16.4	4.62	0.10	11.0	15.1	1.71	0.017	99.52

Table 1. Chemical compositions of the starting gabbros

instead of rock powder as a starting material. This approach was assumed to serve as a better experimental setup to collect larger pools of partial melts (e.g. at the interface of two parts of cylinder) which are necessary for more reliable analytical measurements (e.g. LA-ICPMS). In addition, the effect of NaCl on partial melting was investigated in a larger scale of initial fluid salinity with 3.3, 20 and 50 wt% of NaCl. This set of experiments was conducted at 100 MPa in the temperature interval between 900 and 1040°C using olivine gabbro (1309 D218-R4, 16-20cm) collected during IODP Expedition 304/305 (MAR 30°10.12′N, 42°07.11′W) as a starting material (Table 1). Oxygen fugacity fO_2 in this series of experiments was varied along QFM buffer by setting a distinct partial pressure of hydrogen, which was controlled with the help of a ‘‘Shaw membrane’’ (see details of IHPV with hydrogen sensor in Berndt et al., 2002). The run duration for two sets of experiments was 5-6 days.

The analyses of the experimental phases were performed with a Cameca SX100 electron microprobe. All data were obtained using 15 kV acceleration potential, a static (fixed) beam, Ka emission from all elements, and a matrix correction according to Pouchou and Pichoir (1991). The crystals were analysed with a beam current of 15 nA using a focused beam and a counting time of 10 s on peak and background. For glass analyses, in order to minimize the migration and volatilization of the alkali elements, the beam current was set to 4 nA. The counting time was 4 s for Na and K and 8 s for the other major elements (Si, Ti, Al, Fe, Mn, Mg, Ca). Chlorine and sulfur concentrations were obtained with a beam current of 40 nA and a counting time 60 s. Whenever possible, a defocused beam with a spot size of 10 μm was used. For small melt pools, a beam diameter of 1–5 μm was used.

Experimental problems

The first experimental setup and conditions chosen for melting experiments are routinely used in IHPV in many research projects running in the Lab of Hannover (http://www.mineralogie.uni-hannover.de/mineralogie.html) and no particular problems related to the experimental facilities were expected for the successful realization of the planed experiments. However, the size of the quenched glass pools in our run products, especially at low temperatures, never exceeded 5-10 μm, thus limiting the application of the modern analytical methods to measure trace elements in partial melts. The second setup with sliced rocks cylinders also failed in producing larger pools of partial melts at the semi-cylinder interface and another novel experimental technique have to be developed in future.

The second problem is related to achievement of global equilibrium in melting experiments. Coarse-grained starting material (e.g., <50 μm) results in relatively large experimental crystals, well suited for electron microprobe analyses, but often with cores of unreacted starting material leading to an attainment of only local equilibrium. In opposite, very fine-grained starting material (e.g., <10 μm) achieves global equilibrium conditions, but leads to the development of only very tiny crystals, making the microprobe work more difficult, and preventing reliable LA-ICPMS analyses of phases (see discussion in Koepke et al. 2004). We suggest that an approach to at least local equilibrium (due to the presence of relict phases) was attained in our experiments since: (1) the newly formed crystal phases are homogeneous and euhedral; (2) rims of newly formed phases around relic phases show the same composition as newly formed euhedral crystals (e.g., olivines); (3) the glass shows relatively constant compositions within the counting statistics of the microprobe analyses, irrespective of location within the sample; (4) all compositions of the newly formed phases vary systematically with temperature.

Experimental Results

Experimental products consist of unmodified relic phases of the starting gabbros as well as relic phases with reaction rims and zones of re-equilibrated minerals, newly formed crystals (olivine, amphibole, low- and high-Ca pyroxenes, sodic plagioclase) and partial melts. So far only melt compositions have been analyzed by microprobe and only few measurements of crystal phases have been performed.

In general, our new data are in a very good agreement with previous experimental studies focused on formation of silicic melts during hydrous partial melting of gabbro (e.g. Koepke et al., 2004, 2007; France et al., 2010). At temperatures below 900°C, hydrous melting of gabbro-norite in the presence of fluids even of low salinity (0, 3.3 and 6 wt% NaCl in initial fluid) resulted in formation of silica-rich melts (70-80 wt% SiO_2), similar in composition to natural plagiogranites. The effect of presence of NaCl in the fluid is negligible at high temperatures and is noticeable at low temperatures (below 850°C) and can not be attributed to analytical problems. Figure 2 (left) demonstrates that the presence of NaCl tends to promote partial melting. This effect of NaCl on degree of melting also influences the melt composition resulting in silica depletion from 78 wt% of SiO_2 in NaCl-free system to 73 wt% of SiO2 in the presence of 6% NaCl in the fluid at 800°C, and from 73 to 64 wt% SiO_2 at 850°C. This effect however can be explained by the excess of sodium in the partially molten system which as other alkalis serves as a flux component. This conclusion is further confirmed by the study of olivine gabbro partial melting where fluid composition was varied in a larger scale from 0 to 50 wt% NaCl in initial fluid (Fig. 2 right). The addition of 20 and 50 wt % of NaCl into a fluid (irrespective of the presence or absence of a NaCl-rich liquid phase at experimental conditions) results in a remarkable increase of partial melting of the system even at high temperatures (1000 and 1040°C). This observation allows us to conclude that the presence of NaCl in the fluid at investigated conditions (QFM- QFM+3.3, 100-200 MPa, 800-1040°C) promote partial melting of the system, and does not tend to produce

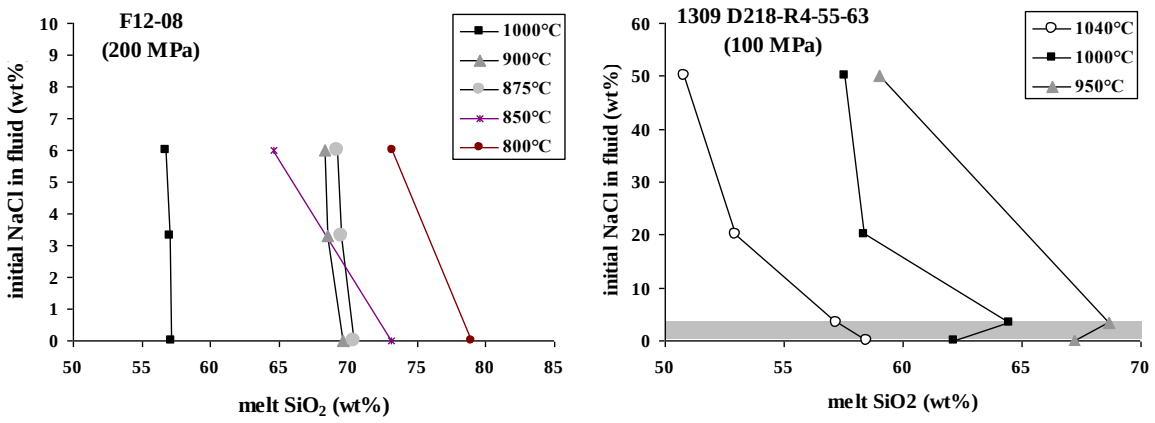

Figure 2. Evolution of melt compositions (SiO2) during partial melting of gabbro-norite F12-08 (left) and olivine gabbro 1309 D218-R4-55-63 (right) at different temperatures and in the presence of fluid phase of different salinity expressed in the form of added NaCl (initial NaCl in fluid). The shadow area on right plot corresponds to the range of initial NaCl in the fluid used in experiments with gabbro-norite (left plot). Right plot demonstrates the profound effect of NaCl (excess of alkalis) on degree of partial melting resulted in silica depletion up to 8-10 wt% in comparison with NaCl-free hydrous partial melting. This effect can be also seen at low salinities, however if only very low temperatures are considered (left plot).

silica-rich melts. However the presence of NaCl may have played an important role at much lower temperatures below the hydrous (only H_2O-bearing fluid) solidus of the system. Therefore new experiments at lower temperatures (below hydrous solidus) can be useful to understand low-T partial melting induced by NaCl-rich fluids in gabbros.

References:
Berndt, J. et al., (2002): Am. Mineral., 87(11-12), 1717-1726.
Botcharnikov, R. E. et al., (2004): Chem. Geol. 213(1-3), 207-225.
Condie, K. C. (1981): Archean Greenstone Belts. Amsterdam: Elsevier.
Coleman, R. G. (1977) Ophiolites. Ancient Oceanic Lithosphere?
France, L. et al., (2010): CMP, 160(5), 683-704.
Frank, M.R. et al., (2002): GCA, 66(21), 3719-3732.
Kelley, D. S. & Delaney, J. R. (1987): EPSL, 83, 53-66.
Koepke, J. et al., (2004): CMP, 146, 414-432.
Koepke, J. et al., (2007): CMP, 153, 67-84.
Koepke, J. et al. (2008): G3, 9, 1-29.
Pouchou, J.L. & Pichoir, F. (1991) 31–75. In: Heinrich, K.F.J. & Newbury, D.E. (eds) Electron probe quantification. New York.
Simon, A.C.& Pettke, T. (2009): GCA, 73(2), 438-454.
Silantyev, S. A. et al., (2005): InterRidge News, 14, 1-4.
Silantyev, S. A. et al., (2008): Petrology, 16, 73-100.
Simon, A.C.& Pettke, T. (2009): GCA, 73(2), 438-454.
Rollinson, H. (2008): Terra Nova, 20(5), 364-369.

IODP

Magma Differentiation processes in Shatsky Rise oceanic Plateau basalts: constraints from mineral, glass and melt inclusion compositions

R. ALMEEV[1], A.HUSEN[1], J.KOEPKE[1], F.HOLTZ[1]

1Institute of Mineralogy, Leibniz University of Hannover, Callinstrasse 3, D-30167 Hannover, Germany

Shatsky Rise and IODP Expedition 324

Oceanic plateaus are giant volcanic constructs whose formation and existence is related to the enormous magma flux from mantle to lithosphere. These Large Igneous Provinces (LIPs) can be important indicators of fundamental processes of mantle convection and geodynamics, as well as major environmental changes and are crucial for understanding of the whole Earth system. It is widely accepted that oceanic plateaus arise from massive eruptions resulting from the arrival of a deep mantle plume head at the lithosphere. An alternative hypothesis invokes decompression melting of unusually fusible mantle beneath fast-spreading ridges. Shatsky Rise is a unique oceanic plateau, formed during the Late Jurassic and Early Cretaceous at a rapidly spreading triple junction, with characteristics that could be attributed to either model of formation (plume head versus ridge-controlled). The goal of Integrated Oceanic Drilling Program Expedition 324 conducted in 2009 was to core the igneous rocks of Shatsky Rise and the sediments above to examine the age, physical volcanology, geochemistry, and tectonic evolution of the rise.

Drilling results: preliminary assessments

In the course of the Expedition 324 five sites were cored and four were logged, with one site (U1346) on the summit of Shirshov Massif and two sites each on Ori (Sites U1349 and U1350) and Tamu (Sites U1347 and U1348) Massifs. Basaltic lava flows were recovered at four of these sites and the samples complement the previous Ocean Drilling Program Site 1213 (south flank of Tamu Massif). Cores from Site U1348 recovered a thick sequence (~120 m) of volcaniclastic sediments topped with shallow-water carbonaceous sandstones. Lavas recovered at Sites U1347 and U1350 are fresh enough (even fresh glass rinds in pillow units exist) to be suitable for age dating and geochemical/isotopic studies. Although lavas from Site U1346 and U1349 were moderately to highly altered, it is expected that they will also provide important age information and may be useful for most geochemical studies.

The initial results from drilling, which are descriptions of cores and shipboard analyses of core samples, give several important results (Expedition 324 Scientists, 2010). Core lithologies show that the initial eruptions (Tamu Massif) were characterized by massive sheet flows and that sites farther northeast on the plateau (younger, smaller Ori and Shirsov Massifs) show progressively lesser

contribution from massive flows. This is consistent with hypotheses of a massive, initial volcanic event and waning magmatic output with time. Shipboard geochemical data show that the lava flows consist of variably evolved tholeiitic basalt. Site U1347 and U1350 lavas, least affected by alteration, have broad similarities with Site 1213 basalts (ODP Leg 198 (Mahoney et al., 2005)) and display compositional ranges overlapping those of Ontong Java Plateau basalts and mid-ocean-ridge basalt (MORB), although more with the latter. Samples from Site U1347 and many samples from Site U1350 probably resemble enriched- type ocean ridge basalts. A broad generalization is that Shatsky Rise basalts are slightly enriched in incompatible elements compared to normal MORB (N-MORB). Site U1349 basaltic flows appear to represent significantly less differentiated magmas than those recovered from other sites and have similarities to picritic Ontong Java Plateau basalts (Fitton and Godard, 2004). Multiple lines of evidence indicate that Shatsky Rise volcanoes had summits at or above sea level, implying that during Jurassic and Cretaceous times, Shatsky Rise was an archipelago of large volcanic islands.

Research project at Hannover

The determination of magma evolution and magma chamber processes at Shatsky Rise is amongst the major scientific objectives of the Expedition 324 and subsequent onshore research projects. Geochemical studies of oceanic plateaus suggest that many compositional variations in extrusive lavas are controlled by magma evolution processes (fractional crystallization, magma mixing, assimilation, and reaction with cumulates) in large-scale magma chambers. Understanding magma evolution processes in large magma chambers will also help to understand the formation of the cumulative part of the lower oceanic crust. Current geochemical data from Shatsky Rise suggest that basement rocks experienced significant fractionation before their eruption (Mahoney et al., 2005; Expedition 324 Scientists, 2010). However, the magma chamber scale and evolution mechanism of oceanic plateaus are not clear compared to well-studied MORB. Systematic basement sampling during Expedition 324 could provide information about the magma evolution process from chemical variations of whole rocks. Examination of chemical zoning profiles of phenocryst phases, recording physiochemical properties (temperature, pressure, and magma compositions) during their growth, can further contribute to reconstruct the history of magma evolution. In the research project recently supported by DFG we would like to focus on the determination of magma storage conditions and to the simulation of magma differentiation processes in Shatsky Rise oceanic plateau. This information will be gained from the study of mineral, glass and melt inclusion compositions, from crystallization experiments and thermodynamic modeling. Our preliminary microprobe measurements of coexisting plagioclase-clinopyroxene cotectic compositions provide first estimates of temperatures and degrees of magma evolution in Shatsky Rise magma chambers.

References:

Expedition 324 Scientists, 2010. Testing plume and plate models of ocean plateau formation at Shatsky Rise, northwest Pacific Ocean. IODP Prel. Rept., 324. doi:10.2204/iodp.pr.324.2010.

Fitton, J.G. and Godard, M., 2004. Origin and evolution of magmas on the Ontong Java Plateau. Geological Society, London, Special Publications, 229(1): 151-178.

Mahoney, J.J., Duncan, R.A., Tejada, M.L.G., Sager, W.W. and Bralower, T.J., 2005. Jurassic-Cretaceous boundary age and mid-ocean-ridge type mantle source for Shatsky Rise. Geology, 33(3): 185-188.

IODP

CRISP-EQ: Costa Rican Seismogenic potential outlined by IODP drilling and the 2002 Osa earthquake sequence

I.G. ARROYO[1,2], I. GREVEMEYER[1,2], J. BEHRMANN[2], C.R. RANERO[3], R. VON HUENE[4], E.R. FLÜH[1,2]

[1]SFB 574, University of Kiel, Kiel, 24148 Germany
[2]Leibniz Institute for Marine Sciences, Wischhofstr. 1-3, Kiel, 24148 Germany
[3]ICREA, Institute of Marine Sciences, CSIC, Barcelona, Spain
[4]Department of Geology, University of California, Davis, CA, USA

Interplate earthquakes in subduction zones are generated in the seismogenic zone, i.e. the segment of the plate boundary where unstable slip occurs. Understanding the mechanisms that control the updip and downdip limits of this zone, as well as the nature and role of asperities within it, provide significant insights into the rupture size and dynamics of the world's largest earthquakes. The Costa Rica Seismogenesis Project (CRISP) is designed to understand the processes that control nucleation and seismic rupture propagation of large earthquakes at erosive subduction zones (Ranero et al. 2007). In 2002 a magnitude Mw=6.4 earthquake may have nucleated at the subduction thrust to be penetrated and sampled by CRISP, 40 km west of Osa Peninsula (Figure 1). However, global event localization is associated with too large errors to prove that the event actually occurred at a location and depth to be reachable by riser drilling.

We have compiled a database including foreshocks, the main shock, and ~400 aftershocks, with readings from all the seismological networks that recorded the 2002 Osa sequence locally (Figure 1). This includes a temporal network of ocean-bottom hydrophones (OBH) that happened to be installed close to the area (Arroyo et al. 2009). The greatly improved coverage provided by the OBH enable us to better constrain the event relocations that we are presently undertaking. Within the frame of a proposal recently submitted to DFG with IODP emphasis, detailed inspection of the data and 3-D data modelling will be carried out to yield source parameters that can be rated against structural information from seismic and drilling constraints. Moreover, teleseismic waveform inversion will provide additional constraints for the centroid depth of the 2002 Osa earthquake, allowing further study of the focal mechanism.

This sequence is the latest at the Costa Rican seismogenic zone to date, in a segment of the erosional margin where seamount-covered oceanic floor is presently subducting (Figure 1). It took place trenchward from a 1999 Mw=6.9 earthquake sequence, that it is thought to have been nucleated by a seamount acting like an asperity (Bilek et al. 2003).

The work proposed here aims to provide definite evidence that the planned Phase B of CRISP will be successful in drilling the seismogenic coupling zone. Furthermore, the seismological data will be interpreted jointly with thermal and drilling data from IODP

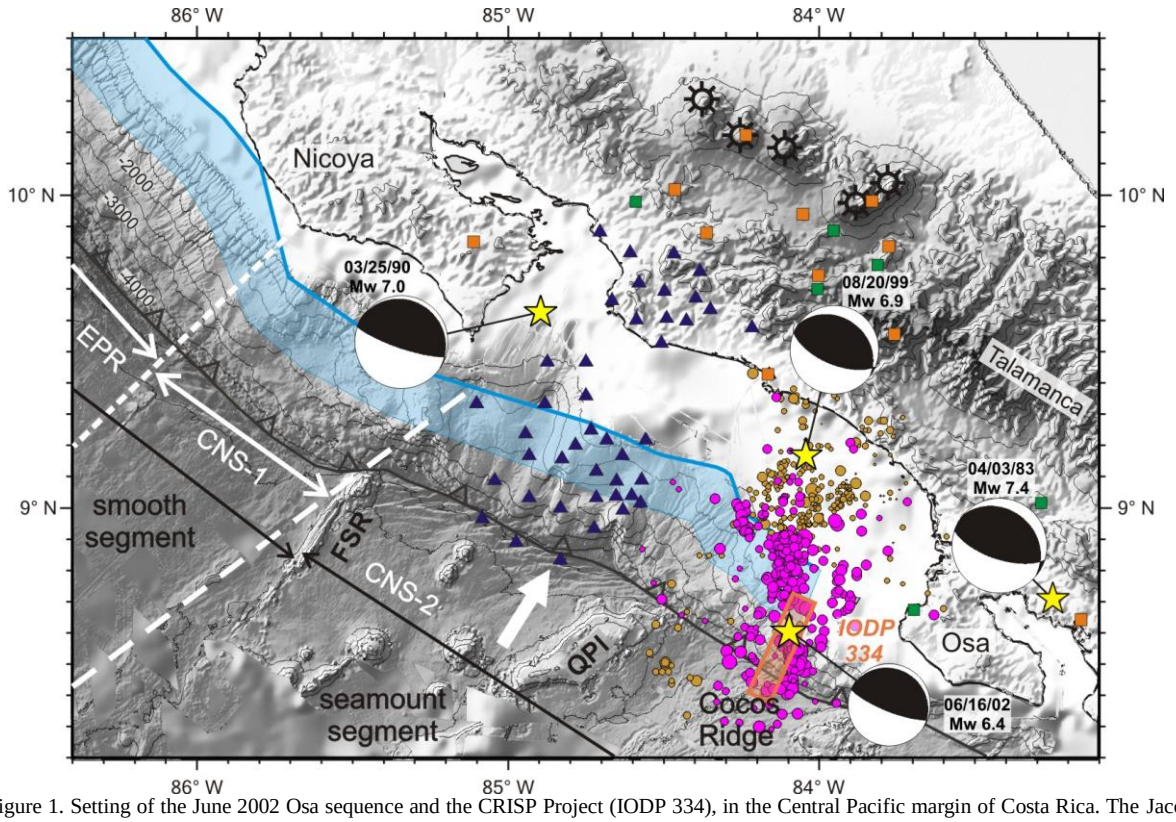

Figure 1. Setting of the June 2002 Osa sequence and the CRISP Project (IODP 334), in the Central Pacific margin of Costa Rica. The Jaco network (triangles) consisted of land and ocean-bottom stations that operated from April to October 2002; additional readings from land stations of the permanents networks RSN (orange squares) and Ovsicori (green squares) complete the coverage. Total recorded seismicity during the sequence is shown (magenta circles), superimposed to the aftershocks of 1999 Mw=6.9 Quepos earthquake (DeShon et al. 2003). Bathymetry (exaggerated), including contours every 500 m, and main tectonic segments after von Huene et al. (2000) and Barckhausen et al. (2001), respectively. Cocos Plate oceanic crust was formed at the East Pacific Rise (EPR) and at the Cocos-Nazca Spreading Center (CNS). The blue line is the 100° C isotherm at the plate interface and the blue shade its seaward displacement considering modest frictional heating, by Harris et al. (2010). Yellow stars represent the epicenters of recent large earthquakes associated to subduction of bathymetric highs: 1983 Mw=7.4, 1990 Mw=7.0 (Husen et al. 2002), 1999 Mw=6.9, and 2002 Mw=6.4 Osa (preliminary location from Jacó and permanent networks combined). FSR: Fisher Seamount and Ridge, QPl: Quepos Plateau.

Expedition 334 to refine the link between temperature and seismogenesis at erosive convergent margins.

References:

Arroyo, I.G., S. Husen, E.R. Flueh, J. Gossler, E. Kissling, G.E. Alvarado, Three-dimensional P-wave velocity structure on the shallow part of the Central Costa Rican Pacific margin from local earthquake tomography using off- and onshore networks, Geophys. J. Int., 179, 827-849, 2009.

Barckhausen, U., C. Ranero, R. von Huene, S.C. Cande, and H.A. Roeser, Revised tectonics boundaries in the Cocos Plate off Costa Rica: Implications for the segmentation of the convergent margin and for plate tectonic models, J. Geophys. Res., 106, 19,207-19,220, 2001.

Bilek, S.L., S.Y. Schwartz, and H.R. DeShon, Control of seafloor roughness on earthquake rupture behaviour, Geology, 31, 455-458, 2003.

DeShon, H.R., S.Y. Schwartz, S.L. Bilek, L.M. Dorman, V. González, J.M. Protti, E.R. Flueh, and T.H. Dixon, Seismogenic zone structure of the southern Middle America Trench, Costa Rica, J. Geophys. Res., 108, doi:10.1029/2002JB002294, 2003.

Harris, R.N., G. Spinelli, C.R. Ranero, I. Grevemeyer, H. Villinger, U. Barckhausen, The thermal regime of the Costa Rican convergent margin 2: Thermal models of the shallow Middle America Subduction Zone offshore Costa Rica, Geochem. Geophys. Geosyst.,11, Q12S28, doi:1029/2010G003273, 2010.

Husen, S., R. Quintero, and E. Kissling, Tomographic evidence for a subducted seamount beneath the Gulf of Nicoya, Costa Rica: the cause of the 1990 Mw = 7.0 Gulf of Nicoya earthquake, Geophys. Res. Lett., 29, doi:10.1029/2001GL014045, 2002.

Ranero, C.R., P. Vannucchi, R. von Huene, and the CRISP proponents, Drilling the Seismogenic Zone of an Erosional Convergent Margin: IODP Costa Rica Seismogenesis Project CRISP, Scientific Drilling, Special Issue, 1, 51-54, doi:10.2204/iodp.sd.s01.29.2007, 2007.

von Huene, R., C. Ranero, W. Weinrebe, and K. Hinz, Quaternary convergent margin tectonics of Costa Rica, segmentation of the Cocos Plate, and Central American volcanism, Tectonics, 19, 314-334, 2000.ICDP

IODP

Glauconitization process in Mesozoic green marine sediments from Central Germany - A glauconitization model for IODP Site 959 (Ivory Coast, Ghana)?

A. BALDERMANN[1], G.H. GRATHOFF[1], L. HOFMANN[1]

[1]Department of Geography and Geology, University of Greifswald, Friedrich-Ludwig-Jahn-Straße 17A, 17487 Greifswald, Germany

Although numerous models for the formation of glauconite have been presented (e.g. Hower, 1961; Odin & Fullagar, 1988), the development of this marine, authigenic, green 2:1 clay mineral is still poorly understood. Based on the work of Wiewióra et al. (2001) at IODP Site 959 on the Ivory Coast, Ghana Marginal Ridge, glauconitization was interpreted as neo-formation reaction of Al-Fe-smectite or nontronite, followed by a partial dissolution and recrystallization into Fe-illite and glauconite. Their formation depends on the rates of sedimentation and pore water geochemistry. In contrast, Meunier & Albani (2006) favour a solid-state transformation model for glauconite formation. Hence, the precise process and timing of glauconitization is still under discussion.

We focussed on the micromilieu and growth mechanism of glauconitic minerals in agglutinated and calcareous benthic foraminifers and fecal pellets from two localities in Central Germany: The Eastern Subhercynic Cretaceous Basin containing Cenomanian shallow marine units (Langenstein) and the Western Harznordrand thrust containing Kimmeridgian intertidal units (Oker). The glauconitization process in Central Germany is comparable to the Pleistocene sediments of the Ivory Coast, Ghana, and was characterized using X-ray diffraction, electron microscopy (including SEM-EDX, TEM-EDX, and electron diffraction), X-ray fluorescence, and optical microscopy. These investigated sedimentary units were used due to their well known depositional setting and burial history.

Our results indicate that glauconitization in the marine sediments from Central Germany occurs in two stages:

1. Smectite growth: Fe-Al-smectites, precursor phases of glauconite, are neo-formed either at the periphery of fecal pellets, at the marginal areas of foraminifer chambers, and in the cracks of detrital quartz grains. The neo-formed, white to light green K- and Fe-poor smectitic crystallites grow mainly parallel both to the interior of the biogenic and siliziclastic grains, whereby the size of individual smectitic crystallites is oftentimes less than 0.5 µm. Outgoing from these smectitic clays, beige to light green, lath-like, or crystallites with flake morphology start to grow towards the open pore space. Commonly, these K- and Fe-bearing mixed-layer clays have a size between 0.5-1.0 µm. Intergrowths between these slowly evolved illite-smectites, framboidal pyrite, and apatite nodules are oftentimes observable at this stage of glauconitization.

2. Solid-state transformation into glauconite: With ongoing glauconitization, the smectitic 2:1 clays continuously transform into Fe-rich illite-smectite, Fe-rich illite and finally into highly evolved, medium to dark green glauconite. During this mineral transformation, an increase in crystallite size up to 1.0-3.0 µm is observable. The most frequent nano-structures at this evolution stage are honeycomb structures, which successively pass over to caterpillar and rosette structures, whereby the packing density of the neo-formed glauconitic crystallites increases steadily. This genetically related mineral reaction series induces the presence of a specific micromilieu during early diagenesis, where glauconitization takes place. The semi-confined micromilieu favours a slow but continuous cation exchange with the pore water, the sea water, and the substrate, because especially the presence of K^+ and Fe^{2+} (but also Mg^{2+}, Al^{3+}, and Si^{4+}) is essential for the glauconitization process to ensure that the smectite-illitization does not stop.

Glauconite formation can be followed using charge distribution diagrams, due to the decrease either in tetrahedral and octahedral charge, while the interlayer charge continuously increases during glauconitization. The progressive development of the glauconites charge distribution from Central Germany and from the Ivory Coast all show comparable glauconitization trends; complete for both Mesozoic localities from Central Germany, and only incomplete for the Pleistocene glauconitic clays from Ghana, therefore, further investigations are needed. Hence, glauconite formation is interpreted as solid-state transformation reaction from neo-formed Al-Fe-smectite into glauconite. This process is limited by the amount of available cations provided during early diagenesis.

We conclude that glauconitization in marine sediments is dependent on the presence of a semi-confined micromilieu, either inside the chambers of benthic foraminifers, within fecal pellets, or inside the cracks of detrital minerals. However, the geochemical conditions inside these semi-confined micromilieus and the precise mineralogical and geochemical changes, which occur during glauconitization, need to be constrained. Therefore, the IODP Site 959 at the Ivory Coast, Ghana Marginal Ridge, could serve as a case study for recent glauconite formation. Hence, this locality might be perfect to characterize the semi-confined micromilieu by SEM studies and identify the mineralogical and geochemical changes during glauconitization using XRD and TEM, combined with polytype and age determinations.

References:

Hower, J. (1961): Some factors concerning the nature and origin of glauconite.- Amer. Mineral., 46, 313-334.

Meunier, A. & Albani, A.E. (2007): The glauconite-Fe-illite-Fe-smectite problem: a critical review.- Terra Nova, 19, 95-104.

Odin, G.S & Fullagar, P.D. (1988): Geological significance of the glaucony facies.- In: Odin, G.S. (eds.): Green Marine Clays.- Elsevier, 295-332, Amsterdam.

Wiewióra, A., Giresse, P., Petit, S. & Wilamowski, A. (2001): A deep-water glauconitization process on the Ivory Coast-Ghana Marginal Ridge (ODP Site 959): Determinations of Fe3+-rich montmorillonite in green grains.- Clays and Clay Minerals, 49, 540-558.

IODP

Preliminary sedimentology and bulk geochemical results of IODP Expedition 333 (NanTroSEIZE Stage 2: subduction Inputs)

T. BAUERSACHS[1], M. STRASSER[2], P. HENRY[3],. T. KANAMATSU[4], IODP EXPEDITION 333 SCIENCE PARTY

[1]Department of Organic Geochemistry, Christian-Albrechts-University, Germany
[2]MARUM, Center for Marine Environmental Sciences, University Bremen, Germany
[3]CRNS, CEREGE – College de France, France
[4]Institute for Research on Earth Evolution (IFREE), Japan Agency for Marine-Earth Science and Technology (JAMSTEC), Japan

The Nankai Trough Seismogenic Zone Experiment (NanTroSEIZE) program represents a multi-expedition drilling project that investigates fault mechanics and seismogenesis along subduction megathrusts. Within this framework, IODP Expedition 333 aimed to (i) provide a reference for the sediments and basement of the subduction zone by characterizing the incoming sedimentary strata and igneous basement of the Shikoku Basin prior to their arrival in the Nankai Trough and (ii) to study sediment remobilization by landsliding along the accretionary prism. For this, a total of three drill sites (C0018, C0011 and C0012) located on a margin-perpendicular transect close to the Kii peninsula were cored. Drilling at Site C0018, located in a accretionary-prism slope basin near the up-dip terminus of the megasplay fault, recovered a 314 m thick sequence of hemipelagic mud with varibale quantities of volcaniclastic sands and ash. Six intervals with evidence for mass-transport deposition and of variable thickness, ranging from 50 cm to ca. 60 m, were observed within this succession. The most prominent of these mass-tranport deposits (MTDs) occurred in the lowermost part of the

sedimentray succession and mediated between a facies rich in sandy turbidites and one of ash bearing hemipelagic mudstones. The MTD comprised a mixture of mud-rich debrites, remnant hemipelagic strata and covoluted banded deposits denoting considerable deformation in their interior. A thick sandy ash layer attributed to a cataclysmic eruption on Kyushu Island dated 1.05 Ma was found immediately below this MTD, which leads us to speculate that excess pore pressure and subsequent liquidization within these layers is one mechanism by which submarine landslides could be triggered in subduction zones.

The Kashinosaki Knoll, a bathymetric high southeast of the Kii peninsula, was investigated for the composition of the upper Shikoku Basin facies. Drill site C0011 is located at the northwest flank of the knoll and during Exp 333 the upper sedimentary sequence of ca. 380 m was recovered. The uppermost part of this succession primarily consisted of hemipelagic mud with high abundances of interbedded ash layers, which were underlain by a 90 m thick interval of heavily bioturbated mudstones. Interestingly, the transition between both units is accompanied by an abrupt increase in total sulfur concentrations. X-ray diffraction suggests that sulfur is primarily bound to sedimentary pyrite, which is present in form of small-sized nodules or layers. Authigenic pyrite minerals develop only under strictly anoxic conditions and their presence in sediments of Site C0011 may suggest that the environmental conditions became unfavorable for growth of endobenthic scavangers, which eventually led to the termination of the extensive bioturbation. However, more detailed analysis on the geochemical composition of the sedimentary sequence at Site C0011 are needed to constrain possible changes in the depositional environment. The upper Shikoku facies at Site C0012, located on the crest of the Kashinisaki Knoll, showed similar lithological characterstics as found at the previous site. However, the individual lithological units expressed significant differences in thickness and lacked the heavily bioturbated interval. Differences in the lithological composition thus suggest that sedimentary processess acted differently at the crest and further down the slope.

ICDP

Pre-eruptive conditions of the Campanian Ignimbrite eruption: Experimental constraints from phase equilibria and volatile solubility studies and its implication for the Campi Flegrei drilling project

H. BEHRENS, R.E. BOTCHARNIKOV, A. HUSEN

Institut of Mineralogy, Leibniz University of Hannover, Callinstr. 3, 30167 Hannover, Germany, (h.behrens@mineralogie.uni-hannover.de)

The planned deep drilling project at Campi Flegrei (CFDDP) will be a milestone in the improvement of our knowledge of the collapse of calderas associated with giant ignimbritic eruptions. It can provide insight into the structural features of the caldera, mechanisms of unrest episodes, magma chemistry and the mechanisms of magma-water interaction. A prerequisite for the understanding and modeling of volcanic and degassing processes at Campi Flegrei is (1) the determination of magma storage conditions, (2) the understanding of magma replenishment processes, especially the composition, temperature, volatile contents of the new magmas injected in magmatic chamber and (3) the simulation of degassing and crystallization processes during magma ascent. So far experimental data and thermodynamic models at elevated pressures and temperatures, allowing us to gain this information, are scarce and can not be directly applied for the phonolitic and trachytic systems of Campi Flegrei. Such information is crucial for the interpretation of drilling products and of observations at the planned drilling site at Campi Flegrei (CFDDP).

Different experimental approaches (i.e. phase equilibria, kinetic experiments, solubility of mixed H_2O-CO_2-Cl-S-bearing volatiles in silicate melts) using trachytic and phonolitic rocks from the Campanian Ignimbrite will be used to investigate magma storage conditions, the properties of end-member magmas before replenishment, as well as the composition of fluids coexisting with melts in the magma chamber. The knowledge of these parameters is crucial to understand and model the evolution of rheological magma properties, fragmentation, eruptive style, which are recorded in the textural patterns of the Campanian Ignimbrite and of the volcanic ashes. The experimental data will provide useful constraints for volcanic hazard assessment at the high risk Campi Flegrei volcanic area.

The project was officially started in December 2010, but a couple of pre-investigations were performed already since summer of last year. A field trip to different locations relevant to the Campei Flegrei volcanism, inlcuding the crater of Solfatara and the island of Procida, was organized together with the Italian cooperation partner Prof. Danilo Palladino. Five bachelor theses and two diploma theses related to Campei Flegrei were submitted in 2010 at the University of Hannover. Three of the bachelor theses described outcraps and rocks on Procida Island (Imke Kroll, Janina Mozar, Eileen Guettler). In two bachelor theses, focused on experimental studies, the solubility of H_2O and CO_2 in trachytic and tracho-phonolytic melts relevant to Campei Flegrei was studied (Sonja Brauer, Stefanie Gaide).

The differentiation of a trachytic melt towards phono-trachytic melt was experimentally investigated in the diploma thesis of Anika Husen. Low temperature experiments were performed in cold seal pressure vessels (CSPV) and high temperature experiments in internally heated gas pressure vessels (IHPV). Run products were analysed by microscope, electron microprobe and spectroscopic techniques. The evolution of the Fe^{2+}/Fe^{3+} ratio during the experiments was recorded by a colorimetric method. The phase relationships at 200 MPa pressure under relatively oxidizing conditions are shown in Fig. 1. It is demonstrated that a simple differentiation path cannot explain the complexity of magma compositions of the Campagnian Ingrimbrite, consistent with the hypothesis in previous studies that the variety of magmas is due to mixing between magma reservoirs and accumulation of host rock material.

The solubility of volatiles (H_2O and CO_2) in the parental trachybasaltic magma was studied in the diploma thesis of Julia Buddensieck. Experiments were performed at 1100°C and pressures from 50 MPa to 500 MPa in an internally heated gas pressure vessel. It could be shown,

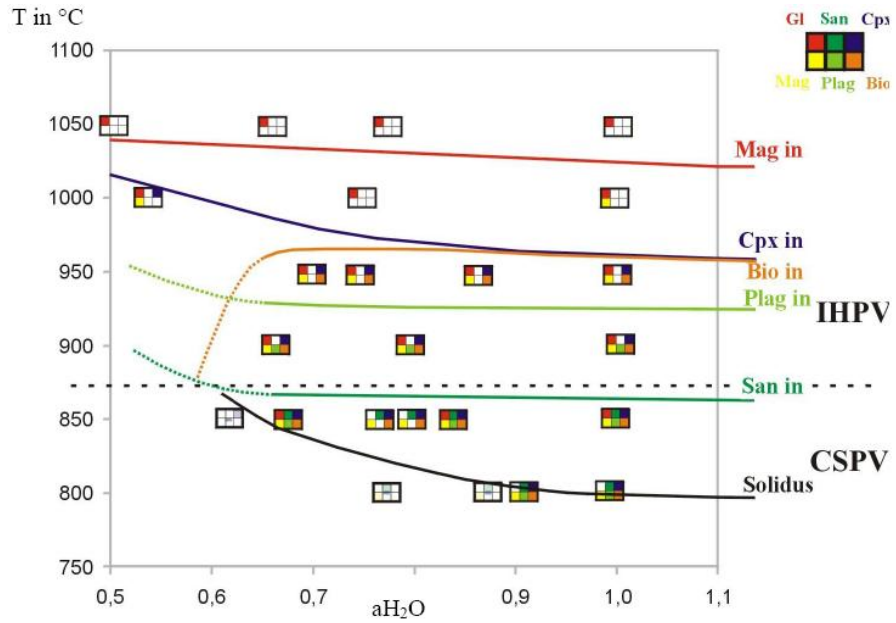

Fig. 1. Phase relationships for phonotrachytic melts at 200 MPa. Gl=glass, San=sanidine, Cpx = clinopyroxene, Mag = magnetite, Plag = plagioclase, Bio = Biotite.

that the solubility behavior of volatiles in trachybasaltic magma resembles that of tholeitic basalt (Shishkina et al. 2010), but the CO_2 solubility is much lower than found for phonotephritic melts (Behrens et al. 2009). At constant pressure, the maximum H_2O solubility is by a factor 30 - 60 higher than the maximum CO_2 solubility in trachybasaltic melts.

References:

Behrens, H., Misiti V., Freda C., Vetere F., Botcharnikov, R.E., Scarlato, P., 2009. Solubility of H2O and CO2 in ultrapotassic melts at 1200 and 1250°C and pressure from 50 to 500 MPa. American Mineralogist 94, 105-120.

Shishkina, T., Botcharnikov, R.E., Holtz, F., Almeev, R.R. and Portnyagin, M.V. Solubility of H2O and CO2-bearing fluids in tholeiitic basalts at pressures up to 500 MPa. Chemical Geology 277, 115-125.

IODP

Strontium and Calcium Isotope Fractionation of Inorganic Calcite

F. BÖHM[1], A. EISENHAUER[1], A. KRABBENHÖFT[1], S. RAUSCH[2], W. BACH[2], A. KLÜGEL[2], J. TANG[3], M. DIETZEL[4]

[1]IFM-GEOMAR, Kiel, German; email: fboehm@ifm-geomar.de
[2]Geoscience Department, University of Bremen, Germany
[3]Department of Earth & Environmental Sciences, Tulane University, New Orleans, USA
[4]Institute of Applied Geosciences, Graz University of Technology, Graz, Austria

In the modern oceans inorganic calcite forms in different diagenetic settings, predominantly at low temperatures or from modified porewaters in deep burial. Calcite frequently occurs in veins and vesicles of ocean crust basalts, where it forms during low temperature alteration (LTA). It was recently shown that these calcites can provide a long-term record of seawater chemistry, covering more than the last 150 million years (Coggon et al. 2010). The latter study showed that in calcite precipitated at bottom water temperatures both Sr/Ca and Mg/Ca ratios of the seawater are recorded.

If this is true, LTA calcite also has the potential to provide records of the isotopic composition of seawater through time. As a basis for using LTA calcites as recorders of Sr ($\delta^{88/86}$Sr) and Ca ($\delta^{44/40}$Ca) isotopes we investigated the isotope fractionation of these elements in experimentally precipitated calcite. Both isotopes were measured with double spike techniques at the Finnigan Triton TIMS at IFM-GEOMAR (Heuser et al. 2002, Krabbenhöft et al. 2009). Calcite formed at defined constant precipitation rates and temperatures in a pH-stat system. Precipitation rate was controlled by the flux rate of CO_2 (Tang et al. 2008). We find that precipitation rate is the most important factor influencing isotope fractionation, while temperature has a secondary influence in Ca isotopes. Strontium and calcium isotopes show a well defined linear correlation. The slope of the regression line is compatible with kinetic fractionation during deyhdration of the cation-aquocomplexes before incorporation into the crystal lattice. At very low rates the fractionation of both calcium and strontium isotopes is close to zero. I. e. there is no isotopic difference between fluid and calcite in isotopic equilibrium. This hypothesis is confirmed by the analysis of some LTA calcite samples, showing $\delta^{88/86}$Sr and $\delta^{44/40}$Ca values very close to the composition of seawater.

Using samples from a suite of DSDP and ODP sites, mainly from the Atlantic Ocean, we try to reconstruct the $\delta^{44/40}$Ca history of the oceans. As Ca has a residence time that is an order of magnitude longer than the mixing time of the oceans, the oceans are homogeneous with respect to $\delta^{44/40}$Ca. Therefore sites from different oceans can be combined for the reconstruction and the resulting record can be assumed to be representative for the world oceans. Taking the observed rate effects into account we use the heaviest $\delta^{44/40}$Ca values from each site as the best approximation of the seawater $\delta^{44/40}$Ca value at the time the calcites formed. The time of formation is constrained by radiogenic strontium isotope values (^{87}Sr/^{86}Sr), applying the seawater strontium isotope stratigraphy of McArthur & Howarth (2004). The calcite precipitation directly from cold bottom water is confirmed by very high oxygen isotope values of the samples.

The resulting $\delta^{44/40}$Ca reconstruction shows similar trends as the Sr/Ca and Mg/Ca records of Coggon et al. (2010), i.e. almost constant values between 160 and 30 Myr and a strong increase during the Neogene. Jurassic-Cretaceous seawater $\delta^{44/40}$Ca was slightly lower than the value at 30 Myr. Between 30 Myr and the late Neogene $\delta^{44/40}$Ca increased by 0.4‰. The latter value is in agreement with the results from Heuser et al. (2005) who found a Neogene increase in $\delta^{44/40}$Ca of 0.5‰ in records of planktic foraminifera, albeit with a slightly different timing. Therefore the LTA calcites may indeed record seawater $\delta^{44/40}$Ca values.

The low Cretaceous $\delta^{44/40}$Ca value (-0.5‰ compared to Recent seawater) is in contradiction to the fossil based reconstruction of Farkas et al. (2007) who found only short $\delta^{44/40}$Ca excursions to such low values, while in general $\delta^{44/40}$Ca values during the Cretaceous were comparable to modern values. An alternative explanation for the low Mesozoic LTA calcite $\delta^{44/40}$Ca values could be given by a progressive recrystallization at increasing burial temperatures. This could have led to uptake of calcium with low $\delta^{44/40}$Ca from the basaltic host rocks and/or kinetic isotope fractionation during recrystallization (sensu Tang et al. 2008). If recrystallization and kinetic effects affected the calcium isotopes, it is likely that Sr and Mg concentrations of the LTA calcites may also have been altered by diagenesis. Additional information about kinetic and diagenetic processes could be gained by combining $\delta^{44/40}$Ca and $\delta^{88/86}$Sr measurements, as indicated by the experimental results. This may finally allow to reconstruct records of both isotope systems in the Mesozoic-Cenozoic oceans.

References:

Coggon, R.M., Teagle, D.A.H., Smith-Duque, C.E., Alt, J.C., Cooper, M.J. (2010), Reconstructing past seawater Mg/Ca and Sr/Ca from mid-ocean ridge flank calcium carbonate veins. Science, 327, 1114-1117.

Farkaš J, Böhm F, Wallmann K, Blenkinsop J, Eisenhauer A, van Geldern R, Munnecke A, Voigt S, Veizer J. (2007a) Calcium isotope record of Phanerozoic oceans: Implications for chemical evolution of seawater and its causative mechanisms. Geochimica et Cosmochimica Acta, 71: 5117-5134.

Heuser A, Eisenhauer A, Gussone N, Bock B, Hansen BT, Nägler TF (2002) Measurement of calcium isotopes (δ44Ca) using a multicollector TIMS technique. International Journal of Mass Spectrometry 220: 385-397.

Heuser A, Eisenhauer A, Böhm F, Wallmann K, Gussone N, Pearson PN, Nägler TF, Dullo W-C. (2005) Calcium isotope (δ44/40Ca) variations of Neogene planktonic foraminifera. Paleoceanography, 20, doi:10.1029/2004PA001048.

Krabbenhöft A., Fietzke J., Eisenhauer A., Liebetrau V., Böhm F., Vollstaedt H. (2009) Determination of radiogenic and stable strontium isotope ratios (87Sr/86Sr; δ88/86Sr) by thermal ionization mass spectrometry applying an 87Sr/84Sr double spike. Journal of Analytical Atomic Spectrometry, 24, 1267-1271.

McArthur J.M., Howarth R.J. (2004) Strontium isotope stratigraphy. In Gradstein F., Ogg J., Smith A. (eds.) A Geologic Time Scale 2004, 96-105, Cambridge University Press, Cambridge.

Tang J., Dietzel M., Böhm F., Köhler S. J., Eisenhauer A. (2008) Sr2+/Ca2+ and 44Ca/40Ca fractionation during inorganic calcite formation: II. Ca isotopes. Geochimica et Cosmochimica Acta 72: 3733-3745.

ICDP

Evolution of magma storage conditions along the track of Yellowstone Hotspot: investigation of the volcanic rocks from Snake River Plain (DFG project HO 1337/22)

T. BOLTE[1], B. NASH[2], R. ALMEEV[1], F. HOLTZ[1]

[1]Leibniz-Universität Hannover, Institute for Mineralogy, Hannover, Germany
[2]Department of Geology and Geophysics, University of Utah, Salt Lake City, USA

General aim of the study

It is widely accepted that during the last 15 Ma, North American plate moved more than 600 km in west-southwest direction over the Yellowstone hotspot and induced a bimodal (rhyolitic – basaltic) magmatism (Morgan and McIntosh, 2005). This volcanism partly produced large volume eruptions of high-silica rhyolites with ash fall tuffs and ignimbrites in a large geographic area. These well-preserved and stratigraphically good correlated outcrops provide unique information for continued studies on the magma dynamics and evolution of magma storage conditions in rhyolitic reservoirs prior to climatic eruptions. In addition, the characterization of the chemical and isotopic composition of the basalts through time at each drill site is useful to constrain the effects of fractionation, recharge, and assimilation, the effects of the underlying lithosphere on magma compositions, and the changes in these processes with time.

There are six large eruptive rhyolitic centers located in the Snake River Plane along the hotspot track: Owyhee Humboldt volcanic field (15.2 – 12. Ma): Bruneau Jarbidge volcanic field (12.7 – 10.5 Ma); Twin Falls volcanic field (10.5 – 8.5 Ma); Picabo volcanic field (8.5 – 7.0 Ma); Heise volcanic field (7.0 – 3.5 Ma) and Yellowstone Plateau volcanic field (2.5 - 0Ma) (Perkins and Nash, 2002). The major goal of our investigations is to estimate pre-eruptive conditions of the rhyolitic magmas from several well-documented eruptive centers. This information will be gained from the chemical analysis of natural minerals and glasses combined with high pressure experimental studies to determine phase equilibria and with thermodynamic modeling. In a first stage of this study, particular attention will be given to trace the evolution of the depth and temperature of the rhyolitic magma chambers using the Bruneau-Jarbidge and Heise volcanic centers as reference materials.

Report on the drilling progress: At the end of September 2010 the scientific drilling in the Snake River Plain started at Kimama, Idaho to deepen the first two of four wells. Both drillings have been completed and the rigging equipment has now been moved to Kimberly, Idaho, for the next well. Both first core runs have been done successfully and produced in sum 2030m of core with an average core recovery of ~ 96%. Only (partially altered) basalts have been cored at the Kimama drill hole with some small interbeddings of sediments or palaeo soil.

Report on the results from this proposal (Start, Dec. 2010): Samples for research have been collected from Bruneau Jarbidge, Heise and Yellowstone eruptive centers. The composition of the mineral phases (phenocrysts) were investigated by microprobe analysis. Using the available

geothermometers for pyroxenes and oxides, the temperature determined from mineral pairs yielded values in the range 820 to 830°C for Heise and 905 to 925°C for the Yellowstone volcanic field. Previous data for the Bruneau-Jarbidge rhyolites are in the range 905 to 980°C (Cathey et al., 2004).

Preliminary experiments were conducted to constrain the effect of fO_2 and P on the phase stabilities in the rhyolitic system of Bruneau-Jarbidge eruptive center. Experiments were conducted at 500MPa and 50MPa and in the fO2 range FMQ +1 to FMQ -6,5 and complement previous data obtained at 200 MPa (Project Ho 1337/17). Experiments had to be conducted at very low water activities and the run duration necessary to attain near equilibrium conditions were 7 to 14 days (even at temperatures as high as 900 °C).

Our new data demonstrate that water activities lower than at least 0,3 at 500 MPa and 0,5 at 50MPa are neccesary to reach the observed degree of crystallization in the natural samples (mostly 5 to 15 vol%) . The high temperatures determined from mineral pairs are confirmed by the experimental studies. First results also indicate that the pressure prevailing in the Bruneau-Jarbidge magma chamber is not higher than 200 MPa. The co-existence of ilmenite and titanomagnetite (observed in natural samples) indicates that fO_2 is close to FMQ. A similar experimental approach is planed for typical compositions of the Heise eruptive center. Particular attention will be given to check if the temperatures (determined from mineral pairs) are lower by nearly 100-150°C when compared to Bruneau Jarbidge.

Objectives:

Glass inclusion in different minerals (quartz, fayalite) from natural rhyolites will be investigated by microprobe to characterize melt compositions. The new experiments will be focused on the determination of pressure and water contents as well as on fO_2 prevailing in magma chambers to bracket magma storage conditions. Furthermore, investigations with basaltic systems will be conducted to understand the differentiation degree of the samples collected at the surface and in the drill holes (as soon as samples will be available). The determination of magma storage conditions of the basalts will provide boundary conditions to constrain the partial melting reactions in the crust leading to the formation of the rhyolites.

References:

Cathey, H. & Nash, B. (2004), The Cougar Point Tuff: Implications for Thermochemical Zonation and Longevity of High Temperature, Large Volume silicic Magmas of the Miocene Yellowstone Hotspot, Journal of Petrology, 45, 27 – 58.

Morgan, L.A. & McIntosh, W.C. (2005), Timing and development of the Heise volcanic field, Snake River Plain, Idaho, western USA. GSA Bulletin, 117 (3/4), 288-306.

Perkins, M. & Nash, B. (2002), Explosive silicic volcanism of the Yellowstone Hotspot: The ash fall tuff record. GSA Bulletin, 114 (3), 367-381.

Shervais, J.W., Vetter, S.K. & Hanan, B.B. (2006). Layered mafic sill complexes beneath the Eastern Snake River Plain: Evidence from cyclic geochemical variations in basalt. Geology 34, 365 – 368.

IODP

A complex history of the Paleocene–Eocene Thermal Maximum in the NE Atlantic

A.BORNEMANN[1], RICHARD D. NORRIS[2], JOHNNIE A. LYMAN[2], S. D'HAENENS[3], J. GROENEVELD[4], U. RÖHL[5], K.A. FARLEY[6], R..P. SPEIJER[3]

[1]Intitut für Geophysik und Geologie, Universität Leipzig,
[2] Scripps Institution of Oceanography, University of California – San Diego, USA,
[3]Department of Earth and Environmental Sciences, K.U. Leuven, Belgium,
[4]Alfred-Wegener Institut für Polarforschung, Bremerhaven,
[5] MARUM, Universität Bremen,
[6] Division of Geological and Planetary Sciences, California Institute of Technology, USA.

The Paleocene–Eocene Thermal Maximum (PETM or ETM-1; 55.8 Ma) is the most prominent of a number of global transient warming events during the Paleocene and Eocene epochs. This so-called hyperthermal has been studied in numerous deep and shallow marine sediments as well as in terrestrial archives. The event is generally characterized by (a) a short-lived 170 ky lasting, negative $\delta^{13}C$ excursion of 1 to 5‰ (e.g., Röhl et al., 2007; Sluijs et al., 2007), (b) a decrease of the $\delta^{18}O$ values of benthic foraminifera by >1‰ suggesting warming of bottom waters, (c) a decrease of calcium carbonate values in deep sea sediments and a shallowing of the lysocline/CCD, probably due to ocean acidification (Zachos et al., 2005), and (d) a major extinction of benthic foraminifera and a turnover of the calcareous plankton communities (e.g., Thomas, 2003; Kelly et al., 1996). The strong negative PETM carbon isotope excursion indicates that the amount of isotopically light carbon added to the global carbon cycle, probably at least partly derived from methane hydrates, is comparable to the present day input of carbon to the atmosphere through the combustion of fossil fuels and is considered as a deep-time analogue to rapid climate change (e.g., Jansen et al., 2007). However, only few detailed deep-sea records exist from the North Atlantic region yet.

Deep Sea Drilling Project (DSDP) Site 401 (47°25.65' N, 08° 48.62' W) is located on the Meriadzek Terrace, a tilted fault block on the northern margin of the Bay of Biscay, North–East Atlantic Ocean. In the early Paleogene this site was located at a paleo-latitude of ~45°N making it, next to DSDP Site 550, one of the most northern scientific drill sites to provide pelagic carbonates of Paleogene age. This site has been drilled in a water depth of 2495 m, while the paleo-water depth for the Eocene has been estimated at 1.8 to 2 km based on the benthic foraminiferal faunal composition (Schnitker, 1979; D'haenens et al., in prep.). The latest Paleocene to middle Eocene sedimentary succession consists of yellowish-brown to orange-brown nannofossil marls and marly chalks covering a very extended PETM succession with well preserved calcareous microfossils.

Geochemical studies of foraminiferal test carbonate reveal a complex history for the PETM in the NE Atlantic region, which characterized by a prominent drop in calcium carbonate content from 80 to 30 wt% at Site 401. All studied taxa (benthic *N. truempyi*, thermocline dwelling subbotinids and surface dwelling morozovellids) display a discrete negative $\delta^{13}C$ excursion (CIE) by up to 2.5‰

followed by a synchronous recovery phase. By contrast, the $\delta^{18}O$ data of planktic and benthic foraminifera show a synchronous decrease of about 1.5‰ at the onset of the PETM, but are decoupled during the recovery phase. This suggests different temperature histories for the different water-masses with a post-CIE cooling for bottom waters while surface waters remained warm, or alternatively changes in the deep-water source. Mg/Ca data of these taxa show a different picture. All three records show the PETM warming at the base of the CIE, but the benthic foraminiferal record does not recover as expected by the $\delta^{18}O$ data suggesting no major change in bottom water temperature. Planktic foraminifera show a slight decline in Mg/Ca indicating a decrease in water temperature, while $\delta^{18}O$ values stay low. This suggests that the $\delta^{18}O$ anomalies during the PETM recovery phase likely represent a geochemical change characterizing different water masses rather than a predominant temperature signal.

In addition, He isotope data suggest a major input of terrestrial material and an increase in sedimentation rate starting with the onset of the CIE. These changes are in agreement with the clay-rich, extended seccession representing the PETM at DSDP Site 401. An increase in terrestrial ^{3}He is subsequently followed by a pronounced pulse of kaolinite deposition, which persists for several hundred thousand years after the termination of the CIE. The prolonged period of clay deposition implies that the PETM fundamentally altered both weathering conditions and sediment supply long after the end of the climatic transient.

References:

D'haenens, S., Bornemann, A., Stassen, P., Speijer, R.P. (in prep.). Transient benthic foraminiferal assemblage fluctuations during the earliest Eocene at DSDP Site 401, Bay of Biscay, North East Atlantic. Marine Micropaleontol.

Jansen, E., et al., 2007. Paleoclimate. In: S. Solomon et al. (Eds.), Climate Change 2007: The Physical Basis. Contribution of Working Group I to the Fourth Assessment Report of the Intergovernmental Panel on Climate Change, Cambridge University Press, Cambridge, pp. 433-497.

Kelly, D. C., Bralower, T. J., Zachos, J. C., Silva, I. P., Thomas, E., 1996. Rapid diversification of planktonic foraminifera in the tropical Pacific (ODP Site 865) during the late Paleocene thermal maximum. Geology 24, 423-426.

Röhl, U., Westerhold, T., Bralower, T. J., Zachos, J. C., 2007. On the duration of the Paleocene-Eocene thermal maximum (PETM). Geochem. Geophys. Geosyst. 8, doi:10.1029/2007GC001784.

Schnitker, D., 1979. Cenozoic deep water benthic foraminifers, Bay of Biscay. Initial Rep. DSDP 48, 377-414.

Sluijs, A., Bowen, G. J., Brinkhuis, H., Lourens, L. J., Thomas, E., 2007. The Palaeocene-Eocene Thermal Maximum super greenhouse: Biotic and geochemical signatures, age models and mechanisms of global change. In: M. Williams, A.M. Haywood, F.J. Gregory, D.N. Schmidt (Eds.), Deep-time perspectives on climate change. The Micropaleontol. Soc., Spec. Publ., Geol. Soc., London, pp. 323-349.

Thomas, E., 2003. Extinction and food at the sea floor: A high-resolution benthic foraminiferal record across the Initial Eocene Thermal Maximum, Southern Ocean Site 690. Geol. Soc. Am. Spec. Pap. 369, pp. 319-332.

Zachos, J. C., Rohl, U., Schellenberg, S. A., Sluijs, A., Hodell, D. A., Kelly, D. C., Thomas, E., Nicolo, M., Raffi, I., Lourens, L. J., McCarren, H., Kroon, D., 2005. Rapid acidification of the ocean during the Paleocene-Eocene thermal maximum. Science 308, 1611-1615.

IODP

A new look on the barium cycle: Barium stable isotope signatures of ODP sediments and experimental calibrations

BÖTTCHER, M.E.[1], VON ALLMEN, K.[2], NEUBERT, N.[1,3], SAMANKASSOU, E.[2,4], BRUMSACK, H.-J.[5], PAYTAN, A.[6], NÄGLER, T.F.[3]

[1]Leibniz Institute for Baltic Sea Research (IOW), D-18119 Warnemünde, FRG
[2]Department of Geosciences, University of Fribourg, CH-1700 Fribourg, Switzerland
[3]Institute of Geological Science, University of Bern, CH-3012 Bern, Switzerland
[4]Section of Earth and Environmental Sciences, University of Geneva, CH-1205 Geneva, Switzerland
[5]ICBM, University of Oldenburg, D-26111 Oldenburg, FRG
[6]Earth & Planetary Sciences Department, UCSC, Santa Cruz, CA 95064, USA

We show by the analysis of the stable barium isotope composition ($^{137}Ba/^{134}Ba$) of natural marine barite ($BaSO_4$), that significant isotope fractionation takes place in the marine biogeochemical barium cycle. We have combined previous measurements of the S and O isotopic composition with new Ba isotope ratio determinations. We find that biogenic marine barites separated from sediments collected in different parts of the world´s Ocean with ages up to about 55 million years fall within a close range and have isotope ratios comparable to recently reported value for continental barium-bearing minerals (von Allmen et al., 2010). Whereas, cold seep barites, show isotope values close to modern biogenic barite, marine hydrothermal samples are enriched in the lighter isotope. Highest ^{134}Ba-enrichments are found in authigenic barite minerals formed above black shales in the deep sediments of ODP Leg 207 that are depleted in sulfate due to AOM-triggered microbial sulfate reduction.

Laboratory experiments were conducted to investigate the potential of different low-temperature reactions to result in barium isotope discrimination. These reactions include adsorption of dissolved Ba on MnO_2 and kaolinite and precipitation of anhydrous $BaCO_3$ and $BaSO_4$ under different conditions (reaction process and temperature).

As an important new finding, we conclude that diagenetic barites record coupled transport induced isotope discrimination, probably superimposed by desorption/adsorption processes in the sulfate-depleted part of the sediment column. Despite the relatively short residence time, the barium isotopic composition of primary barites seem to remain relatively constant through the past 55 m.y.

References:

von Allmen K., Böttcher M.E., Samankassou E. & Nägler T.F. (2010) Barium isotope fractionation in the global barium cycle: First evidence from barium minerals and precipitation experiments. Chem. Geol., 277, 70-77.

Böttcher M.E., Neubert N., von Allmen, K., Samankassou E., Dellwig, O. & Nägler T.F. (2011) Barium isotope fractionation during formation of anhydrous barium carbonate (witherite): Influence of experimental conditions. Geophys. Res. Abs. 13, #4982

IODP

The evolution of the Earth's mantle: new insights from old seafloor

P. A. BRANDL[1], M. REGELOUS[1], K. M. HAASE[1]

[1]Lehrstuhl für Endogene Geodynamik, GeoZentrum Nordbayern, Schlossgarten 5, D-91054 Erlangen

Formation of the oceanic crust at mid-ocean ridge spreading centres and its subsequent evolution has an important influence on sea-level, the carbon cycle and seawater chemistry over timescales of 50-100 My (e.g. Gaffin, 1987; Hardie, 1996; Berner and Kothavala, 2001). Several studies have suggested that changes in mantle temperature and/or ridge spreading rate over the Mesozoic-Cenozoic were at least partly responsible for the changes in global climate and eustatic sealevel over this period (e.g. Larson, 1991; Machetel and Humler, 2003; etc.).

Oceanic crust covers approximately 60% of the Earth's surface area, and preserves a valuable record of mantle melting processes at mid-ocean ridges, and possible changes in mantle composition and temperature since the Middle Jurassic. Oceanic crust older than about 20 Ma is generally covered by sediment and only accessible by drilling, but although many DSDP-ODP-IODP sites have penetrated more than 100 m into 'normal' oceanic basement up to 170 Ma in age, there has been no systematic geochemical study of these samples using modern analytical techniques. Previous geochemical studies of ancient MORB (Humler et al., 1999; Fisk and Kelley, 2002) reported an apparent difference between fractionation-corrected Fe and Na contents of Cretaceous mid-ocean ridge basalt (MORB) and young MORB from active spreading centres, and this difference was

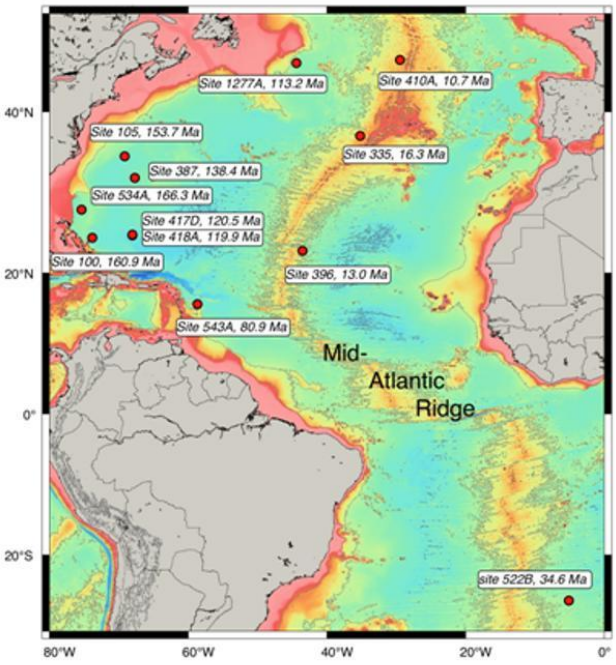

Figure 1. Location and age of DSDP-ODP Sites drilled into ancient oceanic crust in the Atlantic Ocean which were sampled in this study

interpreted as the result of a 50-60°C higher upper mantle temperature in the Jurassic-Cretaceous. A 50°C higher mantle temperature would result in oceanic crust that is 1-2 km thicker, ridge depths about 1 km shallower and global sealevel several hundred meters higher, and approximately 30% higher volcanic CO_2 output at mid ocean ridges, compared to the present day. However, the use of MORB compositions to infer mantle temperature has been questioned by Niu and O'Hara (2008), who proposed that variations in mantle composition are largely responsible for differences in fractionation-corrected MORB compositions. If so, a mantle overturning or 'superplume' event, perhaps linked to the formation of the widepread mid-Cretaceous oceanic plateaus (Larson, 1991; Janney and Castillo, 1997) and resulting in a change in upper mantle composition at that time may better explain the apparent temporal changes in MORB chemistry reported by Humler et al. (1999). Clearly it is important to distinguish between these alternatives.

Most existing analyses of ancient oceanic crust were carried out on whole-rock samples, which are variably chemically altered as a result of interaction with seawater. The existing database for ancient MORB is too sparse to identify the exact timescale over which the chemical variations reported by Humler et al. (1999) took place. We are therefore carrying out a systematic study of the chemistry of ancient ocean crust from DSDP-ODP sites in each of the major ocean basins, using microanalytical techniques (electron probe, laser-ablation ICPMS) and fresh volcanic glasses to avoid the effects of alteration.

Our prelimary data for the Atlantic (187 samples from 12 sites; Figure 1) show that there has been no systematic change in the major element composition of MORB erupted at the Mid-Atlantic Ridge since 166 Ma, and that all data for ancient Atlantic oceanic crust lie within the compositional range observed in lavas erupted along the active Mid-Atlantic Ridge (Figure 2). The apparent chemical changes reported by Humler et al. (1999) are therefore not present in the Atlantic, which rules out an origin due to secular cooling, but may be consistent with a basin-wide 'superplume' or mantle overturning event which was restricted to the Pacific. In this case, chemical changes in Pacific MORB are predicted to occur on short (<20 My) timescales, and major and trace element analysis of a suite of Pacific samples, ranging in age from 10 to 170 Ma is underway in order to test this.

Our new data for samples from an individual drillcore can also be used to examine the chemical stratigraphy of the extrusive section of the oceanic crust at a particular location, about which very little is currently known. Based on the width of the neovolcanic zone at active ridges, these lavas are likely erupted within a period of 10-100 ky. Geophysical studies (e.g. Hooft et al., 1996) have argued that the observed thickening of the crust can be reconciled with the narrow width of the feeder dyke-crust transition in ophiolites if the extrusive sction of the oceanic crust is generated partly by small volume flows erupted within the axial rift, and larger volume flows that are able to 'escape' the central rift and flow down the rift flanks and make up the upper part of the oceanic crust. On Iceland, there are significant differences in chemistry between small-volume lava flows erupted in the active rift zones, and larger-volume flows from the rift flanks (Hardarson and Fitton, 1997). This implies that the widespread practice of

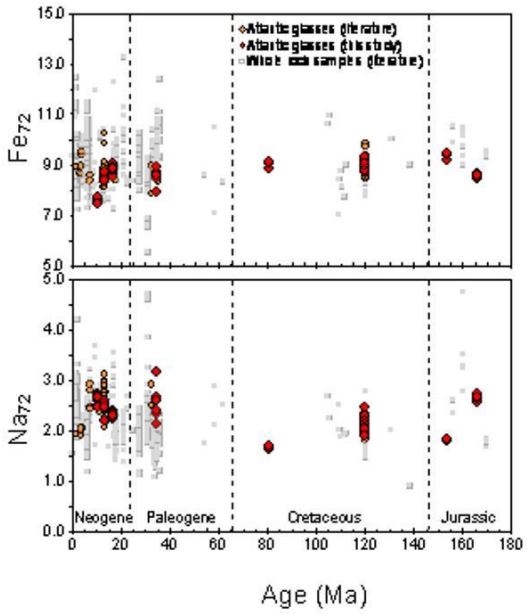

Figure 2. Na_2O and FeO concentrations of Atlantic MORB corrected for fractional crystallisation to Mg#=72.

dredging MORB from active spreading ridges may give a biased estimate of the composition of the average composition of the oceanic crust, because the small-volume flows which eventually build only the lower part of the extrusive section are preferentially sampled. At least some of the geochemical differences between lavas dredged from slow- and fast-spreading ridges (Rubin and Sinton, 2007) might be explained by this 'rift-filter' effect. We are carrying out a statistical comparison of the chemical variability within our Atlantic samples (which are from the upper 2 km of the crust) and young Atlantic MORB dredged from within the active rift, and plan to do the same for the Pacific samples (where an axial rift is less well developed) in order to test this hypothesis.

References:
Berner, R.A., Kothavala, Z. GEOCARB III: A revised model of atmospheric CO_2 over Phanerozoic time. Am. J. Sci. 301 (2001) 182-204.
Fisk, M., Kelley, K.A. Probing the Pacific's oldest MORB glass: mantle chemistry and melting conditions during the birth of the Pacific Plate. Earth Planet. Sci. Lett. 202 (2002) 741-752.
Gaffin, S. Ridge volume dependence on seafloor generation rate and inversion using long-term sealevel change. Am. J. Sci. 287 (1987) 596-611.
Hardarson, B.S., Fitton, J.G. Mechanisms of crustal accretion in Iceland. Geology 25 (1997) 1043-1046.
Hardie, L.A. Secular variation in seawater chemistry: an explanation for the coupled secular variation in the mineralogies of marine limestones and potash evaporites over the past 600 m.y. Geology 24 (1996) 279-283.
Hooft, E.E.E., Schouten, H., Detrick, R.S. Constraining crustal emplacement processes from the variation in seismic layer 2A thickness at the East Pacific Rise. Earth Planet. Sci. Lett. 142 (1996) 289-309.
Humler, E., Langmuir, C., Daux, V. Depth versus age: new perspectives from the chemical compositions of ancient crust. Earth Planet. Sce. Lett. 173 (1999) 7-23.
Janney, P.E., Castillo, P.R. Geochemistry of Mesozoic Pacific mid-ocean ridge basalt: constraints on melt generation and the evolution of the Pacific upper mantle. J. Geophys. Res. 102 (1997) 5207-5229.
Larson, R.L. Latest pulse of Earth: Evidence for a mid-Cretaceous superplume. Geology 19 (1991) 547-550.
Machetel, P., Humler, E. High mantle temperature during Cretaceous avalanche. Earth Planet. Sci. Lett. 208 (2003) 125-133.
Niu, Y., O'Hara, M.J. Global correlations of ocean ridge basalt chemistry with axial depth: a new perspective. J. Petrol. 49 (2008) 633-664.
Rubin, K.H., Sinton, J.M. Inferences on mid-ocean ridge thermal and magmatic structure from MORB compositions. Earth Planet. Sci. Lett. 260 (2007) 257-276.

IODP

Real-time PCR quantification of *Bacteria* and *Archaea* in subsurface marine sediments

A. BREUKER, A. SCHIPPERS

Bundesanstalt für Geowissenschaften und Rohstoffe (BGR), Stilleweg 2, 30655 Hannover

The proportions of *Bacteria* and *Archaea* in marine sediments have shown to be highly variable in different sediments and sediment layers. Based on real-time PCR (Q-PCR) analysis overall similar proportions of *Bacteria* and *Archaea* have been determined for sediments of the Porcupine Seabight (IODP Exp. 307; Webster et al. 2009), the northeast Pacific ridge-flank (IODP Exp. 301; Engelen et al. 2008), Sumatra forearc basins (Schippers et al. 2010), as well as for sediments off Namibia and the Black Sea (Meteor 72/5 and 76/1; Schippers, unpublished data). *Bacteria* dominated in sediments of the Sea of Okhotsk (Inagaki et al. 2003), the Gulf of Mexico (IODP Exp. 308; Nunoura et al. 2009), the Peru continental margin and the equatorial Pacific sediments (ODP Leg 201; Schippers et al. 2005; Schippers and Neretin 2006; Inagaki et al. 2006), as well as in gas-hydrate bearing sediments from the Cascadia margin (ODP Leg 204; Inagaki et al. 2006) according to Q-PCR data. The dominance of *Bacteria* for the Peru continental margin was confirmed by CARD-FISH (Schippers et al. 2005). In contrast to the nucleic acid based methods (CARD-FISH and Q-PCR) the analysis of intact polar lipids (IPL) of prokaryotic cell membranes determined *Archaea* as major prokaryotes in deeply-buried sediments (Biddle et al. 2006; Lipp et al. 2008). These conflicting results may be explained by a different preservation of DNA and IPL in deeply-buried sediments (e.g. stabilized on clay surfaces or organic matter; Coolen et al. 2006; Inagaki and Nealson 2006; Schippers and Neretin 2006). Recently, Schouten et al. (2010) reported about a preservation of archaeal IPL biomarkers in marine sediments indicating that IPL biomarkers do not necessarily detect living *Archaea* and putting their dominance in the deep biosphere into question. However, our recent Q-PCR analysis of sediments from the North Pond area in 7 Ma Western Flank of the Mid-Atlantic Ridge 23°N taken during the IODP Exp. 336 site survey cruise with R/V Maria S. Merian (MSM 11/1) in 2009 showed a much higher abundance of *Archaea* than of *Bacteria* in these oligotrophic sediments (Fig. 1). These data show that our Q-PCR method does not miss a high proportion of *Archaea* and therefore does not underestimate archaeal numbers as speculated (Teske and Sørensen 2008). Furthermore, taken all Q-PCR data together obtained so far it seems that *Bacteria* dominate in eutrophic sediments, *Archaea* dominate in oligotrophic sediments, and both domains are more or less equally abundant in mesotrophic sediments.

References:
Biddle J. F., J. S Lipp, M. Lever, K. G. Lloyd, K. B. Sørensen, R. Anderson, H. F. Fredricks, M. Elvert, T. J. Kelly, D. P. Schrag, M. L. Sogin, J. E. Brenchley, A. Teske, C. H. House, and K.-U. Hinrichs. 2006. Heterotrophic archaea dominate sedimentary subsurface ecosystems off Peru. Proc. Natl. Acad. Sci. 103: 3846–3851.
Coolen, M. J. L., G. Muyzer, S. Schouten, J. K. Volkman, and J. S. Sinninghe Damsté. 2006. Sulfur and methane cycling during the Holocene in Ace Lake (Antarctica) revealed by lipid and DNA stratigraphy. In Past and Present Water Column Anoxia. Neretin, L.N.

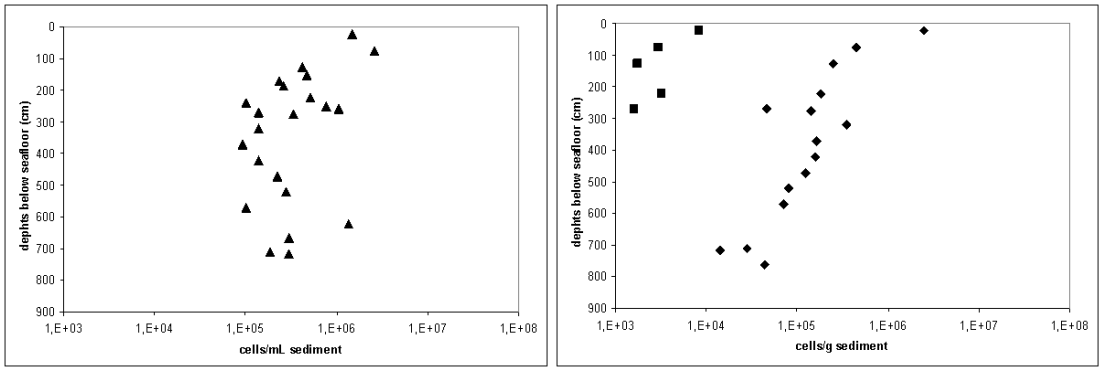

Site GeoB 13501

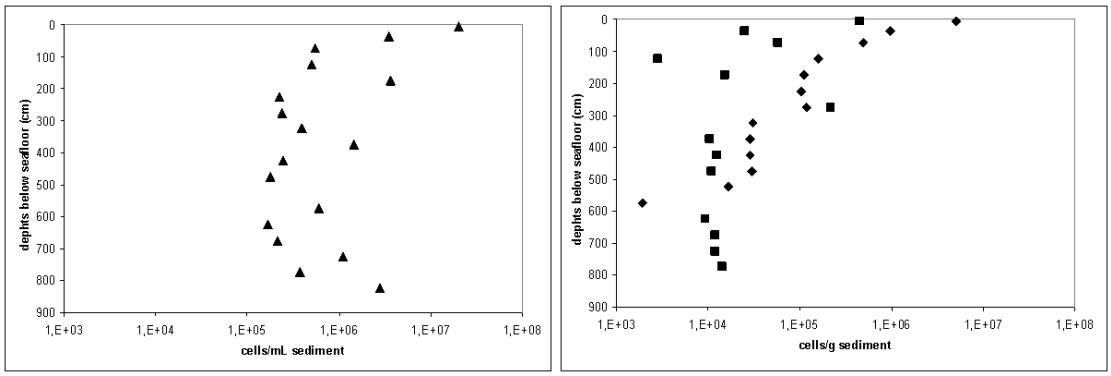

Site GeoB 13502

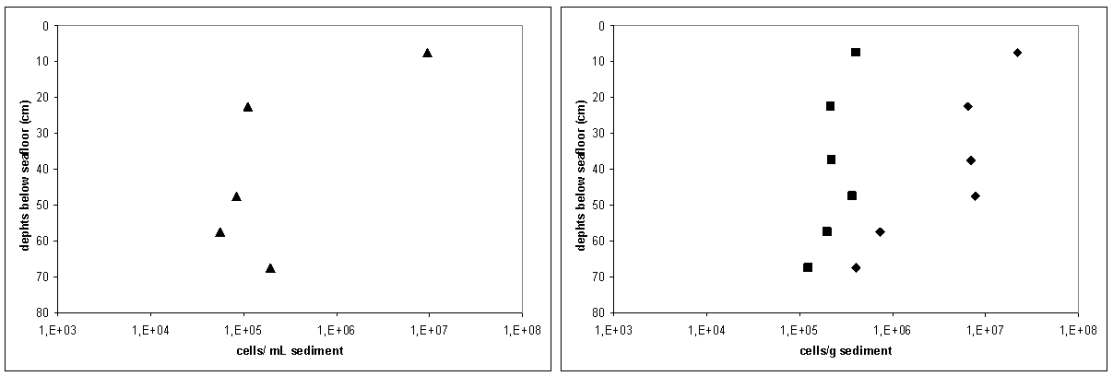

Site GeoB 13504

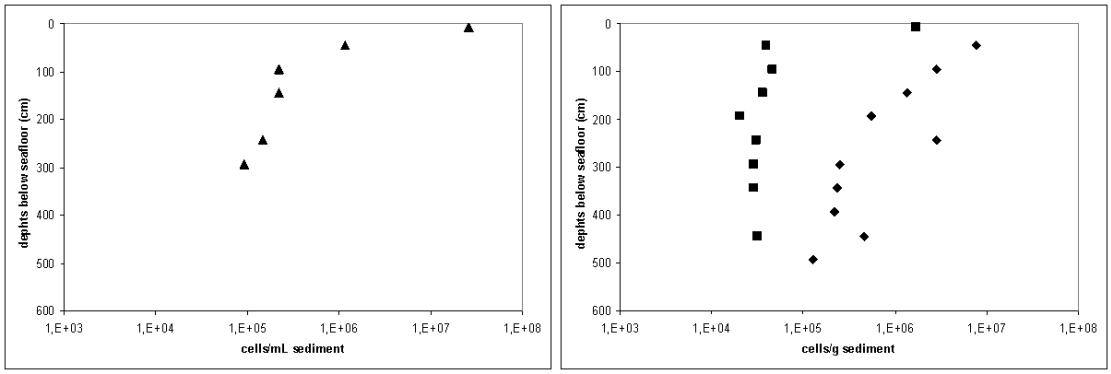

Site GeoB 13512

Figure 1. Total cell counts (triangles, left) and Q-PCR numbers (right) of *Archaea* (rhombuses) and *Bacteria* (squares) for four North Pond sediment sites. Total cell counts were determined after Weinbauer et al. (1998) with an additional HCl washing step. Q-PCR data were achieved with a preeceeding washing step with hydroiodic acid before DNA extraction as previously done (Schippers et al. 2005). Assumed mean 16S rDNA gene copies per cell were 4.1 for *Bacteria* and 1.5 for *Archaea*.

(ed.). NATO Science Series, IV. Earth and Environmental Sciences - Vol. 64, Springer, pp. 41-65.
Engelen, B., K. Ziegelmüller, L. Wolf, B. Köpke, A. Gittel, H. Cypionka, T. Treude, S. Nakagawa, F. Inagaki, M. A. Lever, and B. O. Steinsbu. 2008. Fluids from the oceanic crust support microbial activities within the deep biosphere. Geomicrobiol. J. 25: 55-66.
Inagaki, F., and K. H. Nealson. 2006. The Paleome: Letters from ancient earth. In Past and Present Water Column Anoxia. Neretin, L. N. (ed.). NATO Science Series, IV. Earth and Environmental Sciences - Vol. 64, Springer, pp. 21-39.
Inagaki, F., M. Suzuki, K. Takai, H. Oida, T. Sakamoto, K. Aoki, K. H. Nealson, and K. Horikoshi. 2003. Microbial communities associated with geological horizons in costal subseafloor sediments from the Sea of Okhotsk. Appl. Environ. Microbiol. 69: 7224-7235.
Inagaki, F., T. Nunoura, S. Nakagawa, A. Teske, M. Lever, A. Lauer, M. Suzuki, K. Takai, M. Delwiche, F. S. Colwell, K. H. Nealson, K. Horikoshi, S. L. D'Hondt, and B. B. Jørgensen. 2006. Biogeographical distribution and diversity of microbes in methane hydrate-bearing deep marine sediments on the Pacific Ocean Margin. Proc. Natl. Acad. Sci. 103: 2815–2820.
Lipp, J. S., Y. Morono, F. Inagaki, and K.-U. Hinrichs. 2008. Significant contribution of archaea to extent biomass in marine subsurface sediments. Nature 454: 991-994.
Nunoura, T., B. Soffientino, A. Blazejak, J. Kakuta, H. Oida, A. Schippers, and K. Takai. 2009. Subseafloor microbial communities associated with rapid turbidite deposition in the Gulf of Mexico continental slope (IODP Expedition 308). FEMS Microbiol. Ecol. 69: 410-424.
Schippers, A., and L. N. Neretin. 2006. Quantification of microbial communities in near-surface and deeply buried marine sediments on the Peru continental margin using real-time PCR. Environ. Microbiol. 8: 1251-1260.
Schippers, A., L. N. Neretin, J. Kallmeyer, T. G. Ferdelman, B. A. Cragg, R. J. Parkes and B. B. Jørgensen. 2005. Prokaryotic cells of the deep sub-seafloor biosphere identified as living bacteria. Nature 433: 861-864.
Schippers, A., G. Köweker, C. Höft, and B. Teichert. 2010. Quantification of microbial communities in three forearc sediment basins off Sumatra. Geomicrobiol. J. 27: 170-182.
Schouten, S., J. J. Middelburg, E. C. Hopmans, and J. S. Sinninghe Damsté. Fossilation and degradation of intact polar lipids in deep subsurface sediments: a theoretical approach. Geochim. Cosmochim. Acta 74: 3806-3814.
Teske, A. P., and K. B. Sørensen. 2008. Uncultured archaea in deep marine marine subsurface sediments: have we caught them all? The ISME Journal 2: 3-18.
Webster, G., A. Blazejak, B. A. Cragg, A. Schippers, H. Sass, J. Rinna, X..Tang, F. Mathes, T. G. Ferdelman, J. C. Fry, A. J. Weightman, and R. J. Parkes. 2009. Subsurface microbiology and biogeochemistry of a deep, cold-water carbonate mound from the Porcupine Seabight (IODP Expedition 307). Environ Microbiol 11: 239-257.
Weinbauer, M. G., C. Beckmann, and M. G. Höfle. 1998. Utility of green fluorescent nucleic acid dyes and aluminium oxide membrane filters for rapid epifluorescence enumeration of soil and sediment bacteria. Appl. Environ. Microbiol. 64: 5000-5003.

ICDP

Seismic and seismological features of the Vogtland-Bohemia earthquake swarms - in preparation for a high resolution seismic survey and scientific drilling

S. BUSKE[1], N. MULLICK[1,2], S. SHAPIRO[2], P. WIGGER[2], B. RŮŽEK[3], A. ŠPIČÁK[3], J. HORÁLEK[3], P. HRUBCOVÁ[3], T. FISCHER[4]

[1]TU Bergakademie Freiberg, Institute of Geophysics and Geoinformatics, 09596 Freiberg, buske@geophysik.tu-freiberg.de
[2]Freie Universität Berlin, Department of Geophysics, Malteserstrasse 74-100, 12249 Berlin
[3]Institute of Geophysics of the Academy of Sciences of the Czech Republic, Boční II/1401, 141 31 Prague 4, Czech Republic
[4]Institute of Hydrogeology, Engineering Geology and Applied Geophysics, Charles University, Albertov 6, 128 43 Praha 2, Czech Republic

Repeated earthquake swarms and exhalation of mantle-derived CO_2-enriched fluids are important expressions of presently ongoing magmatic processes in the intra-continental lithospheric mantle of the Western Eger rift region. The geodynamic nature and the implications of these processes are far from being understood. Neither the origin of magmatic activity (upper mantle or lower crust ?) nor the geodynamic role of fluids are well constrained. Within this recently started project we will address these issues by modern reprocessing of two deep reflection seismic profiles from neighbouring areas (German DEKORP MVE-90 and Czech 9HR profiles). We will try to establish correlations between deep microseismic and reflecting structures. The seismic imaging approaches will be universal for both profiles. The microseismic data and reflection structures will be obtained using common velocity models. This will improve possible correlations and enable a comparison of the Eger Rift features to reflection and microseismic features of the neighbouring KTB site, where a similar methodology has been already

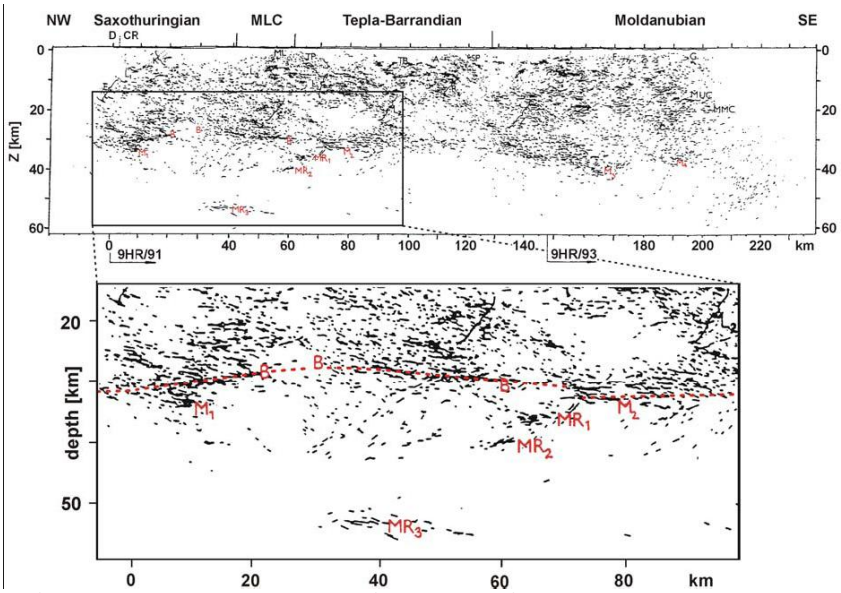

Fig. 1: Current state of seismic processing (and knowledge of the structure of the crust and upper mantle within the investigation area) for the seismic reflection profile 9HR (Tomek et al., 1997) which runs from the Czech-German border near Klingenthal south-eastwards. The area of the earthquake swarms is located west of the northernmost part of the profile (close-up at approx. 0 – 50 km). M_{1-4} are interpreted as Moho reflections; B possibly origin from basaltic intrusions; MR_{1-3} denote upper mantle reflections. A Moho antiform beneath the Saxothuringian zone is clearly visible, exactly where the Eger Graben is located at the surface (Sokolov Basin)

applied. In the near future the expected results will help to design a new high resolution seismic reflection profile crossing a persistent swarm area of the Cheb Basin. Such a profile, in turn, will be part of a pre-site study for scientific drilling.

This project is part of PIER-ICDP (Initiative Drilling Vogtland/Eger rift). For an overview of the related project structure see abstract by Korn et al.

References:
Tomek, C., Dvorakova, V., Vrana, S., Geological interpretation of the 9HR and 503M seismic profiles in Western Bohemia, J. Geol. Sciences, 47, Special Issue: Vrana and Stedra (eds.) Geological Model of Western Bohemia related to the KTB borehole in Germany, Czech Geological Survey, 1997.

ICDP

Sedimentary Processes in Lake Van: First results from a joint interpretation of seismic and drilling data

D. CUKUR[1], S. KRASTEL[1], T. WONIK[2], T. LITT[3]

[1]Leibniz Institute for Marine Sciences, IFM-GEOMAR, Wischhofstrasse 1-3, 24148 Kiel, Germany
[2]Leibniz Institute for Applied Geophysics, Stilleweg 2, 30655 Hannover, Germany
[3]Steinmann-Institut für Geologie, Mineralogie und Paläontologie, Rheinische Friedrich-Wilhems-Universität Bonn, Nußallee 8, 53115 Bonn,

Lake Van is located in a tectonically active zone in eastern Anatolia, Turkey (Fig. 1). It has a volume of 607 km^3 and a maximum depth of 450 meters. In summer 2010, Lake Van was target of a deep drilling campaign (PaleoVan) in the frame of ICDP (International Continental Drilling Program). Two sites (Northern Basin, NB, and Ahlat Ridge, AR) were drilled based on reflection seismic data collected during a seismic campaign in 2004 (Fig. 1). Here we present a first joint interpretation of the seismic and drilling data.

Interpretation of seismic reflection data from the lake reveals three physiographic provinces: a lacustrine shelf, a lacustrine slope, and a deep, relatively flat lake basin (Fig. 2). The most prominent features of the lacustrine shelf and slope are prograding deltaic sequences, numerous unconformities, submerged channels, as well as closely spaced U- and/or V-shaped depressions, reflecting the variable lake level history of Lake Van. The seismic units of the shelf are dominantly composed of low-to-good continuity, variable amplitude reflections interpreted as fluvial deposits.

The lake has three prominent basins (Tatvan, Deveboynu, and Northern Basins, see Fig. 2), separated by basement highs or ridges (e.g., Ahlat Ridge). The seismic units in these basins are characterized by low to very high amplitude, well-stratified reflection patterns. Chaotic reflections are seen in parts of these basins. The Deveboynu Basin consists mainly of chaotic reflections. The Tatvan and Northern Basins are characterized by an alternating succession of well-stratified and chaotic reflecting layers, which were drilled in the Northern Basin. The chaotic seismic facies are interpreted as slump and slide deposits, which are probably the result of quick lake level fluctuations and/or earthquakes. The moderate- to high amplitude, well-stratified facies seen in the deep parts of the basins away from the terrigenous sediment sources are interpreted as lacustrine deposits and tephra layers. This interpretation is still preliminarily as core to seismic correlation is not finished yet (core opening is ongoing).

Ahlat Ridge at the Northern edge of Tatvan Basin rises up to 80 m above the surrounding lake floor. As a consequence, mass flow deposits originating from the lacustrine slope and deposited in the basins have not reached the Ahlat Ridge. Based on seismic data it was proposed that a ~220m long undisturbed and continuous sedimentary succession could be drilled on Ahlat Ridge. Preliminary visual core inspections support this interpretation. Strong reflectors correlate well with abundant tephra layers.

The total sediment thickness reaches more than 400 m in the deep Tatvan Basin and ~300 m on Ahlat Ridge. Prominent clinoforms indicate the initial flooding of Lake Van about 500 ka ago. This event was identified at the Ahlat Ridge site in about 220m drilling depth, where transgressional sediments (coarse grains, shells) indicate the basal flooding upon volcanism-controlled birth of the lake.

The acoustic basement and the sediments lying on top of the basement in the southern part of the lake are disrupted by various intrusions and extrusions suggesting, which are most likely the result of volcanic activity.

Synthetic seismograms (Fig. 3) calculated based on core logging, wire-line logging, and check shot data will allow accurate correlation between seismic and drill data. This approach aims in extrapolating the stratigraphy from the wells to 3D-space by using the seismic data.

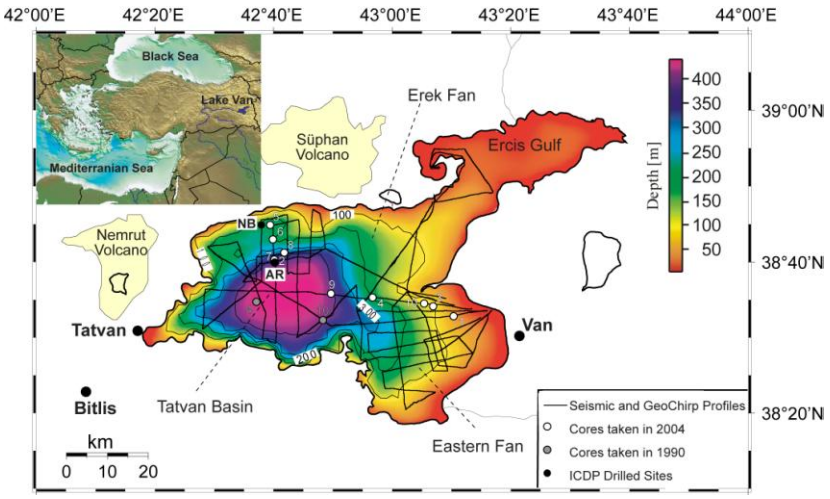

Fig. 1. Bathymetry of the Lake Van as well as locations of seismic reflection profiles and wells. The inset map shows the location of Lake Van.

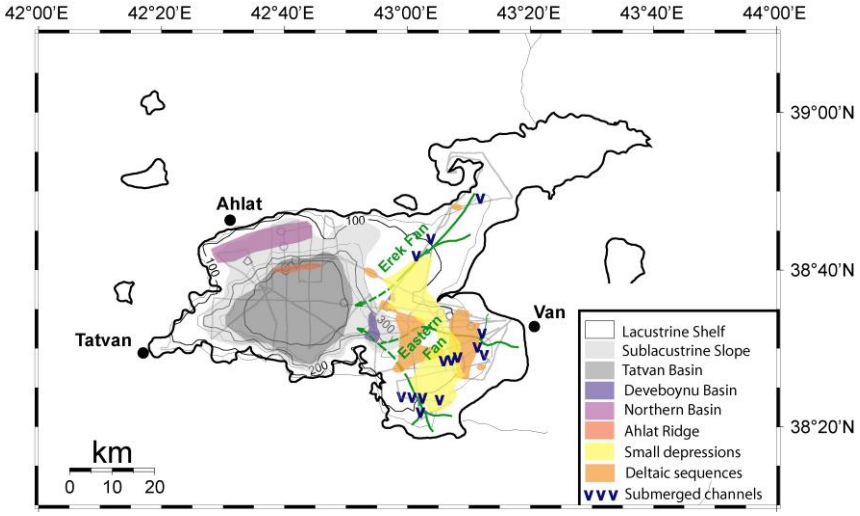

Fig. 2. Physiographic provinces of Lake Van interpreted from seismic data.

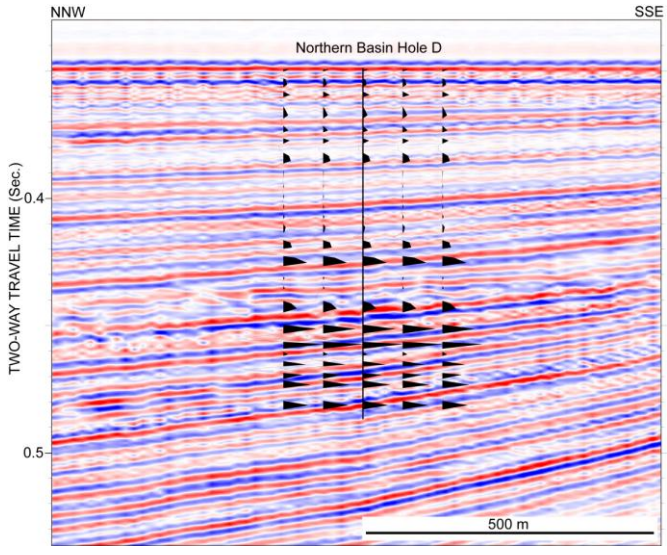

Fig. 3. Correlation of seismic reflection data and synthetic traces generated from core logging data.

ICDP

Nam Co - a potential ICDP drilling site on the Tibetan Plateau?

G. DAUT[1], T. HABERZETTL[1], S. DOBERSCHÜTZ[1], T. KASPER[1], G. GLEIXNER[2], P. FRENZEL[3], R. HETZEL[4], K. REICHERTER[5], A. SCHWALB[6], T. SCHWENK[7], V. SPIEß[7], J. WANG[8], L. ZHU[8], R. MÄUSBACHER[1]

[1] Physical Geography, Institute of Geography, Friedrich-Schiller-University Jena, Löbdergraben 32, 07743 Jena, Germany
[2] Max Planck Institute for Biogeochemistry, Hans-Knöll Str.10, 07745 Jena, Germany
[3] Institute of Geosciences, Friedrich-Schiller-University Jena, Burgweg 11, 07749 Jena, Germany
[4] Institut für Geologie und Paläontologie, Westfälische Wilhelms-Universität Münster, Corrensstr. 24, 48149 Münster, Germany
[5] Neotektonik und Georisiken, RWTH Aachen University, Lochnerstr. 4-20, 52056 Aachen, Germany
[6] Institute of Environmental Geology, Technische Universität Braunschweig, Pockelsstr. 3, 38106 Braunschweig, Germany
[7] Department of Geosciences, University of Bremen, P.O. Box 330440, 28334 Bremen, Germany
[8] Chinese Academy of Sciences, Institute for Tibetan Plateau Research, 18, Shuangqing Rd., P.O. Box 2871, Beijing, 100085, China

Lake Nam Co (4718 m a.s.l., 30°45'N and 90°30'E) is a terminal lake with a maximum water depth of 98m located on the Central Tibetan Plateau, China. We assume that this lake is a suitable archive for the reconstruction of monsoon history because paleoshorelines all arround the lake attest major lake level fluctuations in the past but the rather high water depth of this lake assures that it was not desiccating completely during dry phases (LGM). In this contribution we try to show that the lake sediments of Nam Co deliver high quality proxy data for paleoenvironmental reconstruction.

The subbottom profiling survey (10 kHz parametric system) shows a sequence of layered sediments with a minimum thickness of 35m. An acoustic basement could not be detected so far. The overall sequence can be subdivided into a lower part with high reflectivity and partly structures of folding. This is followed by a sequence with the same acoustic behaviour, but without any signs of folding. To the top layered sediments with lower reflectivity are recorded. In several parts of the lake clear signs for still active tectonic movements were detected within the sediments, following the general tectonic framework of this area. A drowned lake terraces in 10m water depth gives evidence for also lower lake levels than today.

Besides several gravity cores, one piston core (~10.4 m) was recovered at a water depth of 93 m in September 2008. A wide spectrum of sedimentological, geochemical and mineralogical investigations was carried out, including radiocarbon dating. The age depth model for the core is so far based on 36 ^{14}C AMS data and shows with 23 000 cal BP one of the longest continous records of lake sedimentation available on the Central Tibetan Plateau. Because of uncertainties for the correction of the reservoir effect, magnetostratigraphic analyses and 23 OSL measurements are currently underway to support the established chronology.

Based on the age depth model a high resolution sedimentological and geochemical data set (1cm res.) including XRF scanning (2mm res.), ICP-OES element analyses, CNS analysis and XRD measurements were carried out. Furthermore pollen data were used to trace changes in the vegetation history. By using modern sediments the scientific basis for example for the interpretation of compound-specific hydrogen isotope ratios in paleoclimatology and paleohydrology was improved. The isotope signal of the terrestrial biomarkers of Lake Nam Co is primarily a function of temperature, humidity controlled evapotranspiration and vapour pressure deficit. Consequently δD values of biomarkers can be used to reconstruct climate variability effecting ecosystem evapotranspiration, the water balance of lake systems and changes in monsoonal precipitation. In addition training sets with modern ostracode assemblages including their isotopic record (^{18}O, ^{13}C) were established. The compound specific biomarkers together with ostracode assemblages and stable oxygen and carbon isotopes from bulk sediment and ostracode shells of the core provide a continuous and exceptional record of lake level and climate history for the past 23 cal ka BP on the Tibetan Plateau.

The the good dataquality of the so far available core, that reaches only 1/3 of the sediments detected by the shallow seismic survey, shows that there is a high possibility, that Lake Nam Co covers a continues, long term, and high resolution archive that can be used to trace environmental changes on the Tibetan Plateau. The estimate how far we can get back in time and the question wether Lake Nam Co has the potential for an ICDP drilling site, has to be proofed by a deep seismic survey.

IODP

Unravelling the palaeoecology of dinoflagellate cysts

S. DE SCHEPPER[1], E. FISCHER[2], M. J. HEAD[2], J. GROENEVELD[3], J. MATTHIESSEN[3]

[1] Geosciences Department, University of Bremen, Bremen, Germany
[2] Department of Earth Sciences, Brock University, St. Catharines, ON, Canada
[3] Alfred Wegener Institute, Bremerhaven, Germany

In an attempt to unravel the (palaeo)autecological preferences of extant and extinct dinoflagellate cysts, we compared Late Pliocene and Early Pleistocene dinoflagellate cyst assemblage data with geochemical data from the same sample. Currently, the database contains more than 200 dinoflagellate cyst samples from four North Atlantic IODP/DSDP sites that are calibrated to Mg/Ca ratios of *Globigerina bulloides* as a measure of sea surface temperatures.

Comparing the fossil dataset with present-day dinoflagellate cyst distributions demonstrated good agreement between the sea surface temperature ranges of extant taxa today and in the past. This showed that our new approach and methods are also a valuable tool for inferring the sea surface temperature range of extinct taxa. For example, *Ataxiodinium confusum*, *Impagidinum solidum* and *Invertocysta lacrymosa* had a preference for warmer conditions, whereas *Habibacysta tectata* inhabited cooler environments. However, it is notable that the extant cold-indicatng *Impagidinium pallidum* showed important

differences between its present and past temperature range and spatial distribution.

IODP

Marine biological productivity, carbon cycling, and climate cooling during the Oligocene to Miocene transition in the Indo-Pacific Oceans

L.DIESTER-HAASS[1], K.BILLUPS[2], K.-C. EMEIS[3]

[1]Universität des Saarlandes, Zentrum für Umweltforschung, 66041 Saarbrücken.[l.haass@mx.uni-saarland.de]
[2]School of Marine Science and Policy ,University of Delaware ,700 Pilottown Road ,Lewes, DE 19958 , [kbillups@udel.edu]
[3]Institut fuer Biogeochemie und Meereschemie, Universitaet Hamburg , Bundesstr. 55, [kay.emeis@zmaw.de]

The Oligocene to Miocene boundary (the so-called Mi1 event) marks one of the major Cenozoic cooling steps. A corresponding but slightly out of phase $\delta^{13}C$ maximum has been attributed to increased organic matter burial associated with global climate cooling (e.g., Zachos et al., 2001). To test this idea we have constructed records of marine biological productivity (based on benthic foraminiferal accumulation rates, BFAR) to parallel the stable isotope records from 19-26 Ma at three sites from the Atlantic Ocean (shown at the IODP Kolloquium 2010; Diester-Haass et al., in press) and three ODP Sites from the Indo-Pacific oceans. Our new data confirm findings from the Atlantic Ocean in that the $\delta^{18}O$ and $\delta^{13}C$ maxima that characterize the Oligocene/Miocene boundary are accompanied by a pronounced maximum in BFAR-derived paleoproductivity at all sites, except at Site 747 from the Kerguelen Plateau. Here, productivity varies cyclically between 7 and 15 gC/cm²*ky with maxima corresponding to $\delta^{13}C$ maxima. But the productivity maximum at 23 Ma in the $\delta^{13}C$ spike is not greater than in earlier or later maxima. We assume that local upwelling along this submarine elevation contributes nutrients to the surface as suggested by van Haren and Gostiaux (2010) and as assumed for the Eocene (Faull et al., 2010).

Tropical Site 1237 off Peru shows lowest productivity and a gradual cyclic increase from 4 gC/cm²*ky at 26 Ma to a maximum of 10gC/cm²*ky at 23 Ma. At high latitude Tasman Sea Site 1170 the productivity increase in most pronounced and increases from 5 prior to 24 Ma to up to 27 gC/cm²* ky in the $\delta^{13}C$ and $\delta^{18}O$ maximum at 23 Ma.

Ongoing modeling work (Louis Francois and Ingrid Jacquemin in Liège) currently tests the hypothesis whether orbitally forced enhanced latitudinal temperature gradients and stronger vertical mixing in the oceans can explain the enhanced productivity at the Oligocene/Miocene transition and a reduction in atmospheric CO_2 levels and related global cooling.

References:

Diester-Haass,L., Billups, K., and Emeis, K.-C, in press. Enhanced Paleoproductivity across the Oligocene/Miocene boundary as evidenced by benthic foraminiferal accumulation rates.Palaeogeogr., Palaeoclimat., Palaeoecol.

Faul,K.L. and Delaney,M.L.,2010. A comparison of early Paleocene export productivity and organic carbon burial flux for Maud Rise, Weddell Sea, and Kerguelen Plateau, south Indian Ocean. Paleoceanography,vol. 25, PA 3214, doi:10.1029/2009PA001916.

Van Haren, H. and Gostiaux, L.A deep ocean Kelvin Helmholtz billow train, 2010.Geophys. Res. Lett., 37, L03605, doi:10.1029/2009GL041890.

ICDP

Rock magnetic properties and development of magnetic fabrics in metaperidotites of the Outokumpu area during the Svecofennian orogeny (1.95 – 1.85 Ga)

F. DIETZE, A. KONTNY

Institut für Angewandte Geowissenschaften, Karlsruher Institut für Technologie (KIT), Germany

The terrain boundary between the Archaic and Proterozoic shield in Eastern Finland is characterized by strong magnetic anomalies. The striped anomalies which occur in the Outokumpu (OKU) area (boundary region) are probably related to different strong magnetized, gently towards SE dipping rocks of the Outokumpu assemblage (Airo et al. 2007). From reflection seismic data, these SE dipping sequences are assumed to bend more horizontal at depth and cause a prominent seismic reflector and magnetic anomaly. The continuously cored 2516 m deep OKU Deep Drill Hole intersected this crustal-scale geophysical anomaly zone between 1314 and 1515 m depth. The depth interval comprises peridotite-derived altered ultramafic rocks, serpentinized mantle material, skarn and carbonates associated with black schists (Fig. 1), enclosed by paramagnetic mica schist units. The partially extremely high magnetic anomalies are related to these serpentinized mantleperidotite in the OKU assemblage. The main magnetic phases are secondary formed magnetite and pyrrhotite, which are abundant in the serpentinized rocks.

The OKU assemblage is also the host rock of the famous Outokumpu-type massive Cu-Zn-Co-Ni-(Au-Ag) sulfide deposits (e.g. Airo & Loukola-Ruskeeniemi 2004). The polygenetic Outokumpu type deposits is interpreted by Peltonen et al. (2008) to be the result of mixing of two genetically distinct end-member sulfide reservoirs. First, a pretectonic Cu-rich proto-ore formed within peridotitic sea floor at about 1.95 Ga. Second, syntectonic disseminated Ni-sulfides formed through chemical interaction between obducting ultramafic massifs and adjacent black schists some 40 Ma after deposition of the Cu-rich proto-ore. The locally occurring carbonate-silica alteration of the serpentinite post-dated the initial tectonic emplacement of the mantle fragments but predated the earliest regional deformation. Five stages (D1 - D5) of the tectonic-metamorphic evolution are described in Kontinen et al. (2006), which are interpreted as a result of a continuum process under a sustained NNE-SSW orogenic compression during the Svecofennian orogeny.

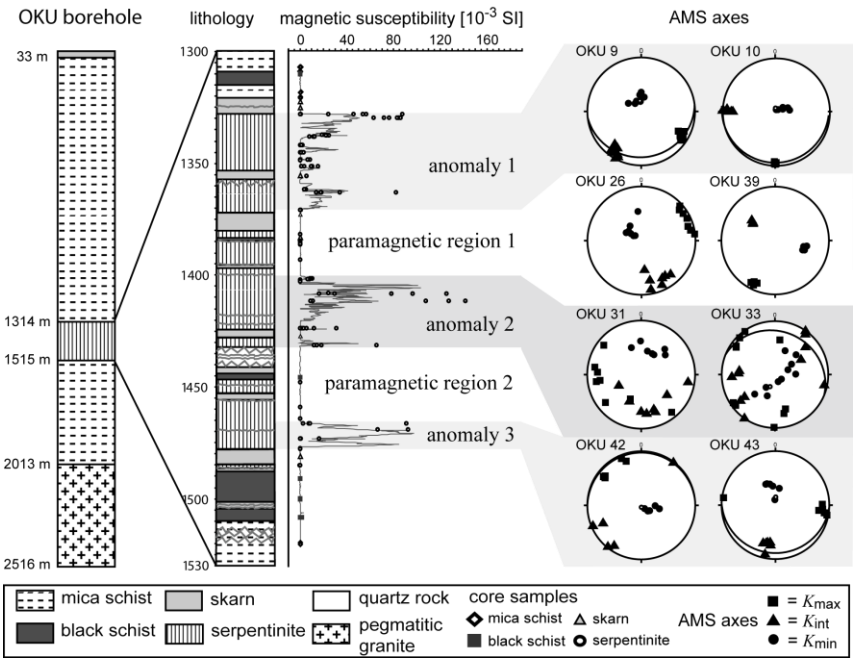

Figure 1: (left) Lithology of the Outokumpu borehole and the OKU assemblage with magnetic susceptibility from core data (measured with a handheld kappameter ZH30). Dots are data from core samples taken for detailed rock magnetic measurements; (right) Stereonets of directional AMS data (*K*max, *K*int, *K*min axes) for thre three magnetic anomalies and paramagnetic regions, great circles discribe the macroscopic foliation.

This study provide basic petrophysical, rock- and paleomagnetic data in combination with magnetic fabric analyses to understand the formation of magnetic minerals during serpentinization and carbonatization in a complex tectonic environment. We correlate the rock magnetic properties with the polygenetic Outokumpu ore formation. Furthermore our data offers an explanation and possible interpretation of magnetic logging measurements, Magnetic susceptibility (κ) measurements every 20 cm along the cores revealed that the rocks of the OKU assemblage vary significantly from dia- and paramagnetic values below 0.7*10-3 SI to ferrimagnetic ones above that value. Furthermore, 50 core samples including 241 single specimens (diameter of 2.5 cm and height of 2.1 cm), were investigated in the laboratory. The significant scattering of rock magnetic properties at the scale of a few centimetres indicates a heterogeneous distribution of ferrimagnetic minerals at that scale, which is also confirmed by microscopic observation. Three depth intervals with high magnetic anomalies with κ values up to $193*10^{-3}$ SI have been discriminated : at the top (1328 – 1364 m), in the centre (1408 – 1432 m), and at the bottom (1466 – 1473 m).These strong magnetic intervals are separated by paramagnetic rock units (Fig. 1, left).

X-ray diffraction analyses indicated variable mineralogy of the ultramafic rocks which can be correlated with the susceptibility intensity. In serpentinite with high magnetic susceptibility, lizardite is the dominating mineral. Chlorite (clinochlore), brucite and magnetite can also be identified. With decreasing magnetic susceptibility the magnetite and lizardite content decreases and dolomite and talc, partially associated with tremolite are the main mineral phases (Dietze and Kontny *in press*).

While temperature-dependent magnetic susceptibility measurements indicate magnetite as main carrier of κ, thermal demagnetization of the natural remanent magnetization (NRM) sometimes reveals a second remanence carrier beside magnetite, which is pyrrhotite. It seems that both magnetic minerals carry mostly a similar direction of magnetization, with a mostly moderate to steep inclination up to 64°.

Generally a positive correlation between κ and NRM

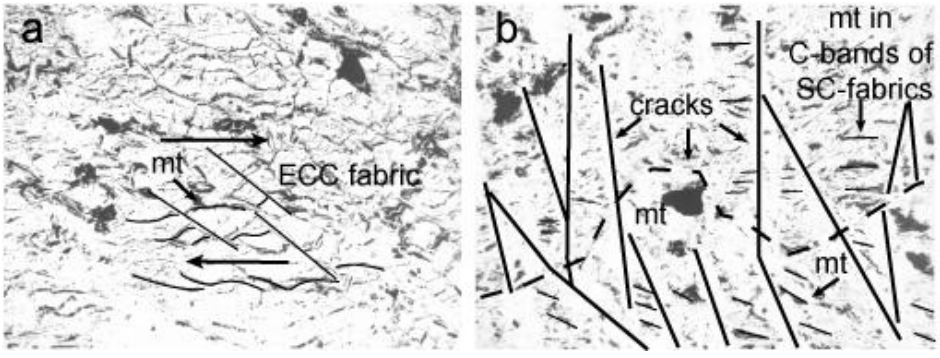

Figure 2: (a) Magnetite grains associated with serpentine minerals, ECC-fabric indicate shear stresses; (b) magnetite grains located in C-bands of SC-fabrics in serpentinized sample, strongly overprinted by brittle deformation.

intensity of the ferrimagnetic serpentinites exists, indicating that the amount of magnetic minerals is responsible for NRM variation. Königsberger (Q) ratios (ratio between remanent and induced magnetization) for serpentinite rocks show a large variation and only strongly serpentinized samples with NRM values above 0.01 A/m show a remanent magnetization (Q > 1). Therefore the remanently magnetized serpentine units cause the magnetic field anomalies (Dietze et al. 2009). Q ratios are above 1 for most of the black schist (remanent magnetization) and below 1 for the mica schist and most of the skarn rocks (induced magnetization). Nevertheless, the black schist units have no contribution to the magnetic field anomalies.

Magnetite as well as pyrrhotite shows corrugation lamellae, which have formed from an originally homogeneous individual during strong mechanical stresses. This observation indicates that these minerals have been formed previous to or in between of the regional deformation stages. Furthermore antiferrimagnetic pyrrhotite (po), associated with relictic pendlandite (pe) are abundant in the ultramafic rocks. Such sulfide aggregates (po-pe or po-niccolite) are mostly homogeneous and show sutured grain boundaries, which might indicate recrystallisation during the metamorphic events.

Microstructure analyses reveal SC- and ECC-fabrics formed by serpentine and talc minerals in the foliated serpentinite indicating shear zone formation under ductile conditions (Fig. 2a). This texture was overgrown by randomly orientated tremolite porphyroblasts, which implies a static crystallization during peak metamorphic conditions at temperatures of 550 – 600 °C (Säntti et al. 2006, Peltonen et. al 2008) probably due to a contact metamorphic overprint of the ~ 1.87 Ga old nearby granite intrusion. Finally these microstructures were strongly overprinted by brittle deformation at lower temperatures after the peak metamorphic stage (Fig. 2b).

Analyses of the anisotropy of magnetic susceptibility (AMS) reveal magnetic fabrics with mostly clear defined magnetic axes (*K*max, *K*int, *K*min) in the magnetic anomaly regions at the top and the bottom, as well as in the paramagnetic regions. A less clear alignment of the magnetic axes was observed in the center region (Fig. 1, right part). The magnetic foliation plane (containing *K*max and *K*int axes) is mostly horizontal to shallow inclined, and subparallel to the macroscopic foliation (great circles). Also in samples from the central zone the *K*min axes trends to a steep inclination, indicating a more or less horizontal magnetic foliation plane. The magnetic lineation (*K*max axis) of the AMS ellipsoid, is also mostly horizontal to shallow inclined. This well defined magnetic fabric indicates preferred orientation of magnetite along veins and serpentine minerals, which are parallel to the foliation.

The degree of anisotropy (P') in the anomaly regions are high and range between 1.3 and 2.4 at the top and between 1.4 – 3.6 at the bottom anomaly, while the shape factor (T) trends to more oblate shapes (T > 0) towards higher P' values. The central anomaly (which contain the highest κ values) shows extremely high P' values up to 5.6. The AMS ellipsoids vary strongly between prolate and oblate shapes in this area, but trend to oblate shapes towards higher k values. These results probably indicate high strain zones at the boundaries of the OKU body during the emplacement in the upper crust and therefore an alignment of magnetic minerals parallel to the structural foliation.

Compared to rock magnetic properties of serpentinites reported in the literature, serpentinites from the OKU drill core show a large variation but the mean values are in good agreement with those reported from other occurrences worldwide (e.g. Toft et al. 1990, Oufi et al. 2002). The large variation in the Outokumpu serpentinites can be correlated with a complex and inhomogeneous serpentinization and carbonatization alteration history, which seems to be mirrored in their rock magnetic properties. Säntti et al. (2006) and Peltonen et al. (2008) interpret that the formation of magnetite and pyrrhotite is related to a post peak metamorphic serpentinization process in the OKU assemblage, because lizardite is not stable above temperatures of 300 °C, and only the chromian spinell is a relictic phase of the Proterozoic ozean crust. In contrast, our results suggest that the magnetic fabric rather originated during a shearing event previous to peak-metamorphism, during the emplacement stage of the serpentine body in the upper crust (Dietze and Kontny 2010). The randomly orientated tremolite porphyroblasts, which were formed during the peak metamorphic stage, indicate the absence of shear stresses during the retrograde deformation. Furthermore there are some studies which describe the stability field of lizardite up to 600 °C (Caruso and Chernosky 1979, O'Hanley et al. 1989). While serpentinization (pre-tectonic) is related to magnetite formation, the carbonate-silica alteration of the serpentinites (during deformation stages D1 – D2) caused a decomposition of magnetite and a formation of (non-magnetic) pyrrhotite and pentlandite.

Our comparison between lithologies of the Outokumpu assemblage with rock magnetic properties, mineralogy and the γ-ray log (kindly provided by J. Kück, GFZ Potsdam) revealed a clear relationship with the low-temperature listwaenite-birbirite-type carbonate-quartz alteration of the peridotite body margins, which is most likely related to the Ni proto-ore formation of the obduction stage as suggested by Peltonen et al. (2008). This low-temperature alteration caused the decomposition of magnetite and is responsible for low magnetic susceptibilities within the serpentinite sequence (Kontny and Dietze 2009). No correlation between the AMS fabric (mostly horizontal to shallow inclined foliation plane and lineation, respectively) and the NRM vector (moderate to steep inclination) can be observed. This indicate that the syn to late orogenic granitoid emplacement (1.87-1.85 Ga) with accompanying hydrothermal fluid circulation and metamorphic peak temperatures of 550 - 600 °C in this area probably caused a remagnetization of the magnetic minerals and a partial destruction of the earlier acquired shear zone fabric.

References:

Airo M.-L. and Loukola-Ruskeeniemi K. (2004) Characterization of sulfide deposits by airborne magnetic and gamma-ray responses in eastern Finland. Ore geology reviews, 24, 67-84.

Airo M.-L., Elbra T., Kivekäs L., Laine T., Leino M., Mertanen S., Pesonen L., Vuoriainen S., Säävuori H. (2007) Petrophysical laboratory measurements of the Outokumpu deep drill core samples. In: Kukkonen I.T., (Editor), 2007. Outokumpu Deep Drilling Project, Sec. International Workshop, May 21-22, 2004, Espoo, Finland. Programme and Extended Abstracts. Geological Survey of Finland, Report Q10.2/2007/29, 35-40.

Caruso, L.J. & Chernosky, Jr. J.V. (1979) The stability of Lizardite. Canadian Mineralogist 17, 757-769.

Dietze F., Kontny A., Virgil C., Kück J., Hördt A., Airo M.-L. (2009a) Correlation of petrophysical logging data with core data for the depth

interval 1300 – 1530 mof the OKU drilling. Abstract. Outokumpu Deep Drilling Project, Third International Workshop, Espoo, 86-90.
Dietze F. and Kontny A. (2010) Magnetic fabric analysis of the Outokumpu serpentinite body in the upper crust of Eastern Finland. Abstract GP41A-1028 presented at 2010 Fall Meeting, AGU, San Francisco, Calif., 13-17 Dec.
Dietze F. and Kontny A. (in press) A study of rock magnetic properties of serpentinites from the Outokumpu Deep Drill Hole, Finland. 'Special Paper' series of the Geological Survey of Finland.
Kontinen A., Peltonen P., Huhma H. (2006) Description and genetic modelling of the Outokumpu-type rock assemblage and associated sulphide deposits. GTK report M10.4/2006/1.
Kontny A. and Dietze F. (2009) Rock magnetic properties of the Outokumpu rock type assemblage as function of mineralization process. Abstract. Outokumpu Deep Drilling Project, Third International Workshop, Espoo, 77-80.
O'Hanley, D.S., Chernosky, Jr. J.V. & Wicks, F.J. (1989) The Stability of Lizardite and Chrysotile. Canadian Mineralogist 27, 483-493.
Oufi O. and Cannat M. (2002) Magnetic properties of variably serpentinized abyssal peridotites. J. Geophys. Res., 107, No. B5, 2095, 10.1029/2001JB000549.
Peltonen P., Kontinen A., Huhma A. and Kuronen U. (2008) Outokumpu revisited: New mineral deposit model for the mantle peridotite-associated Cu-Co-Zn-Ni-Ag-Au sulphide deposits. Ore Geology Reviews, 33, 559-617.
Säntti J., Kontinen A., Sorjonen-Ward P., Johanson B. & Pakkanen L. (2006) Metamorphism and chromite in serpentinized and carbonate-silica-altered peridoties of the Paleoproterozoic Outokumpu-Jormua ophiolite belt, eastern Finland. International Geology Review 48, 494-546.
Toft P.B., Arkani-Hamed J., Haggerty S. (1990) The effects of serpentinization on density and magnetic susceptibility: a petrophysical model. Phys. Earth Planet. Inter., 65, 137-157.

IODP

The development of the Benguela Upwelling System triggered speciation in the Cape Flora

L. DUPONT[1], H.P. LINDER[2], F. ROMMERSKIRCHEN[1], E. SCHEFUß[1]

[1] MARUM – Center for Marine Environmental Sciences, University of Bremen, Leobener Str, DE-28359 Bremen, Germany
[2] Institute of Systematic Botany, University of Zurich, Zollikerstrasse 107, CH 8008 Zurich, Switzerland

The Cape Flora is exceptional in terms of endemism and species richness, which is the result of strong speciation in certain groups of plants. This radiation of the Cape Flora has been dated for the Late Miocene and is associated with the start of the Benguela Upwelling System. To test whether the radiation of the Cape Flora is correlated with marine-driven climate change, we studied the palynology of the thoroughly dated Middle to Late Miocene sediments of ODP Site 1085 retrieved from the Atlantic Ocean off the mouth of the Oranje River. Both marine upwelling and terrestrial contributions are recorded at this site, which allows a direct correlation between the changes in the terrestrial flora and the marine Benguela Upwelling System in the south-east Atlantic. Pollen types from plants of tropical affinity disappeared, and those from the Cape flora gradually increased between 10 and 6 Ma. Inferred vegetation changes for the Late Miocene south-western African coast are the disappearance of *Podocarpus*-dominated Afromontane forests, and a change in the vegetation of the coastal plain from tropical grassland and thicket to semi-arid succulent vegetation. These changes are indicative of increased summer drought, and are in step with the development of the southern Benguela Upwelling System. They pre-date the Pliocene uplift of the East African escarpment, suggesting that it did not play a role in stimulating vegetation change. Some Fynbos elements were present throughout the recorded period (from 11 Ma onwards), suggesting that at least some elements of this vegetation were already in place during the onset of the Benguela Upwelling System. This is consistent with a marine-driven climate change in south-western Africa triggering substantial speciation in the terrestrial flora, especially in the Aizoaceae.

Climate development and vegetation feedbacks in tropical Africa during Heinrich Stadials

L. DUPONT, A. PAUL, I. HESSLER, D. HANDIANI

MARUM – Center for Marine Environmental Sciences, University of Bremen. Leobener Str. DE-28359 Bremen

Large and abrupt shifts between extreme climatic conditions characterize the last glacial period. They are not restricted to the North Atlantic, but transmitted by the atmospheric and oceanic circulation. It has been suggested that the abrupt shifts associated with the North Atlantic Heinrich events (Heinrich stadials) are the effect of a reduction of the strength of the Atlantic meridional overturning circulation. According to the hypothesis of inter-hemispheric climate coupling a reduced overturning circulation leads to the accumulation of heat in the South Atlantic. Additionally, Heinrich stadials are thought to influence the vegetation composition on land due to the linkage between ocean and atmosphere. In order to investigate the connection between tropical African vegetation and oceanic conditions during Heinrich stadials, we reconstructed the vegetation development in Angola and the sea surface temperatures of the eastern South Atlantic using marine sediments of ODP Site 1078 (11°55'S, 13°24'E, 426 m water depth). Combining high-resolution palynological and Mg/Ca records from the same site we can directly study variations in the marine and terrestrial realm and their interactions. We compare our results to transient model simulation using a earth system model of intermediate complexity including a dynamic vegetation module.

Mg/Ca paleotemperature and oxygen isotope reconstructions on planktonic foraminifers of ODP Site 1078 reveal insight into the behavior of the Angola Current, the Angola-Benguela Front, and the Benguela Current during the last glacial (50-23.5 ka BP). North of the Angola-Benguela Front a warming of the surface waters during austral summer in association with Heinrich stadials is recorded in the Mg/Ca record of *Globigerinoides ruber* (pink) between 28.5 and 30 ka, between 36.5 and 39 ka, and between 39.5 and 46.5 ka. The timing of the warming of the tropical surface waters coincides with the onset of Heinrich stadials supporting the hypothesis of the bipolar seesaw. In contrast, the Mg/Ca temperatures and $\delta^{18}O$ values of *Globigerina bulloides*, representing the surface water conditions of the Benguela Current upwelling regime during austral winter, show no impact of Heinrich stadials in the study area during the investigated time interval (Fig. 1). We suggest that the expected warming during Heinrich stadials in the Benguela Current upwelling regime was mitigated by short periods of intensified upwelling and cooling coinciding with Heinrich stadials.

To address the issue of the connection between tropical African vegetation development and high-latitude climate change we present a high-resolution marine pollen record

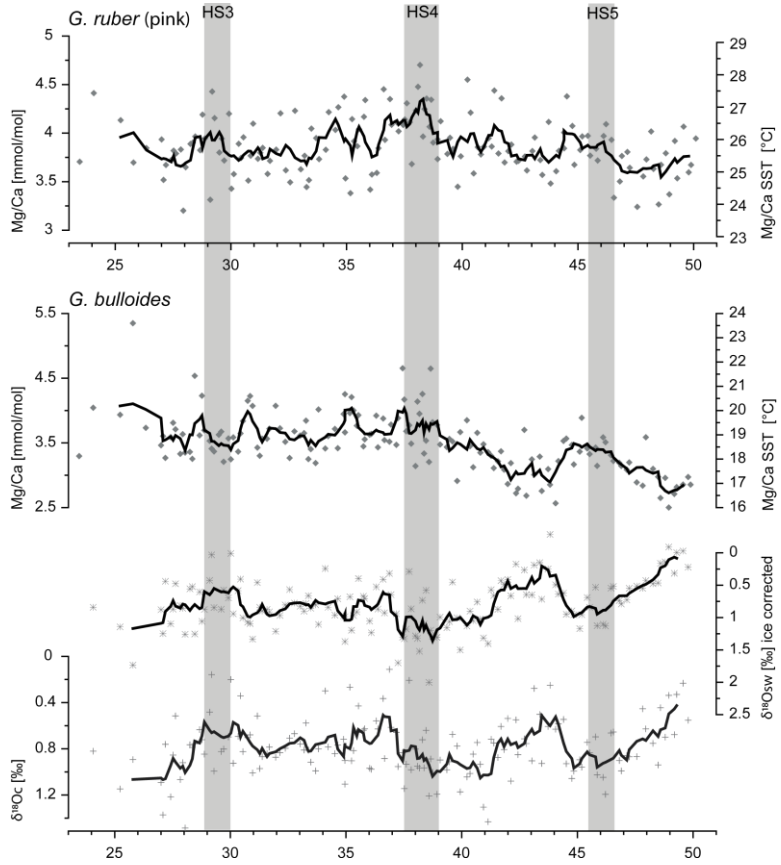

Figure 1, Mg/Ca ratios and stable oxygen isotopes of planktonic foraminifera against age in ka BP (1000 year calibrated before present). From top to bottom. Mg/Ca of *G. ruber* (pink) in mmol/mol (left axis) converted to sea surface temperatures (SST; right axis) after Anhand et al. (2003). Mg/Ca of *G. bulloides* in mmol/mol (left axis) converted to SST (right axis) after Mashiotta et al. (1999). δ^{18}Oc of *G. bulloides* calcite [‰ VPDB], converted to δ^{18}Osw of seawater after Shackleton (1974) and corrected for sea ice using sea level data of Waelbroeck et al. (2002). Crosses are the actual measurements; lines show a 5-point running average.

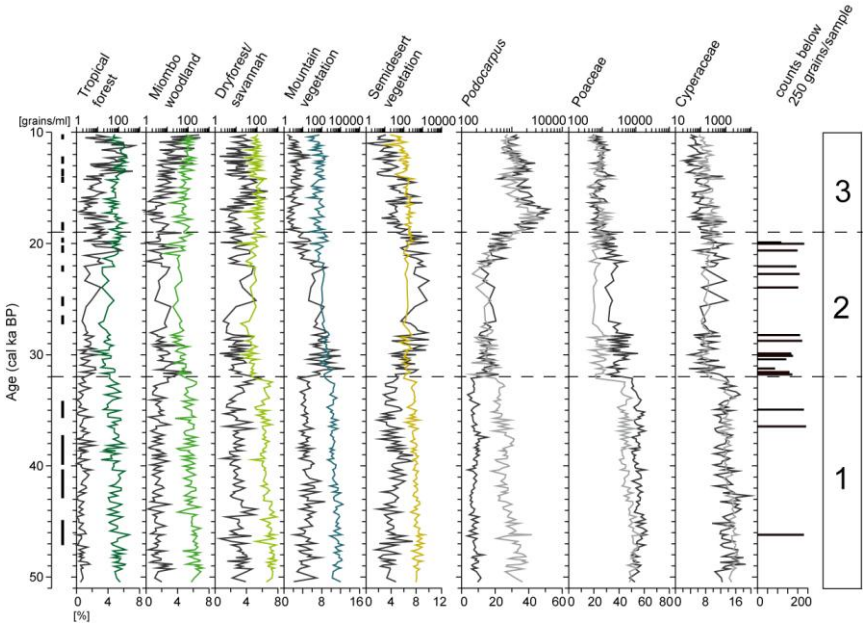

Figure 2: Pollen percentages (dark grey) and pollen concentrations of vegetation groups (coloured) and selected pollen taxa (light grey). Black vertical lines indicate calibrated radiocarbon age ranges (1 σ range). Samples with less than 250 pollen grains counted are indicated on right. Concentration are given in 10log grains/ml, note different scales. Pollen zones 1 to 3 (PZ) are separated by dashed lines.

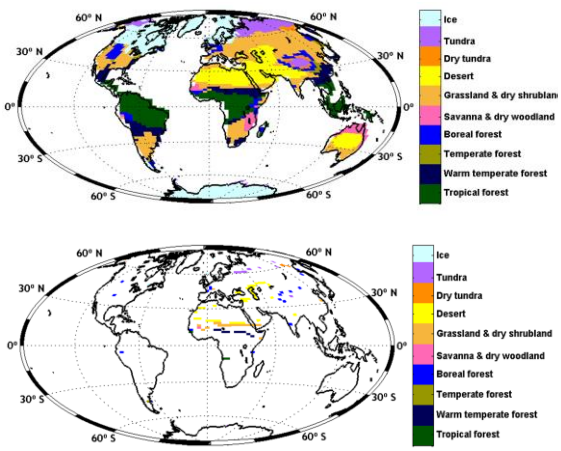

Figure 3: Model experiments of UVic ECSM with a dynamic vegetation component. Vegetation is grouped into mega-biomes according to Harrison and Prentice (2003). Scenario for HS1(top) and difference between HS1 and LGM conditions (bottom).

off Angola (ODP Site 1078) covering the interval 50-10 ka BP (Fig. 2). Surprisingly, the prevalent vegetation development on the African subcontinent reflects no changes during the Heinrich stadials. Indeed, it seems that the vegetation response during Heinrich stadials is disguised by mechanisms that cancel each other out.

To put the vegetation response during the last glacial in the perspective of a wider geographical area, we compiled pollen records from the circum-Atlantic tropics between 23°N and 23°S from both marine and terrestrial sediment cores (Hessler et al. 2010). Pollen data were grouped into mega-biomes to facilitate the comparison between the different records. There is a stronger signal of Dansgaard-Oeschger and Heinrich stadials variability in the South American records. Records close to the modern northern and southern limits of the Intertropical Convergence Zone show opposite trends in vegetation development during Heinrich stadials and Dansgaard-Oeschger cycles. The pollen data from tropical South America corroborate the hypothesis of a southward shift in the migration pattern of the Intertropical Convergence Zone and a reduction in the Atlantic Meridional Overturning Circulation during Heinrich stadials. However, tropical African records do not appear to register Dansgaard-Oeschger variability, although there are some vegetation changes during Heinrich stadials.

To understand the differential response in the terrestrial tropics, we studied the vegetation changes during Heinrich stadials by using a dynamic global vegetation model (TRIFFID in combination with MOSES; Cox 2001) as part of the University of Victoria Earth System-Climate Model (UVic-ESCM; Weaver et al. 2001). The model results show a bipolar seesaw pattern in temperature and precipitation during a near-collapse of the overturning circulation. The succession in plant-functional types showed changes from forest to shrubs to desert, including spreading desert in northwest Africa, retreating broadleaf trees in West Africa and northern South America, but advancing broadleaf trees in Brazil. The pattern is explained by a southward shift of the tropical rainbelt resulting in a strong decrease in precipitation over northwest and West Africa as well as in northern South America, but an increase in precipitation in eastern Brazil. To further analyze the UVic ESCM results, we compared them to those obtained with the NCAR Community Climate System Model version 3 (CCSM3). The CCSM3 experiments used three different boundary conditions: pre-industrial, Last Glacial Maximum (LGM) and Heinrich Stadial 1 (HS1). The pre-industrial vegetation distributions from both models showed similarities in the Sahel region, West Africa and eastern North America, while they revealed discrepancies in South America and Europe. In contrast to the UVic ESCM, the CCSM3 simulated grass rather than tree cover in South America, while in Europe the UVic ESCM failed to simulate tree cover (see Handiani et al. this volume).

To facilitate the comparison between modeled vegetation results with pollen data, we diagnosed the distribution of biomes from the plant-functional type coverage and the simulated model climate. The biomes diagnosed from the control-run were compared to the modern vegetation reconstruction of BIOME 4*. Consistent biome patterns were simulated for the tropical forests of western and south-western Africa and the grasslands of northern Africa. On the other hand, in southern Europe, where the BIOME 4 vegetation reconstruction is dominated by warm temperate and temperate forest, our model shows a strong bias towards grassland. The biome distribution was computed for HS1 and the LGM as well as for pre-industrial conditions (Fig. 3). We used a classification of biomes in terms of "mega-biomes", which were defined following a scheme originally proposed by BIOME 6000 (v 4.2). The biome distribution of the Sahel region changed from warm temperate forest during the LGM to grassland and dry shrubland, suggesting a drier climate during HS1. In south-western Africa the simulated vegetation change is minimal. Modeling experiments conducted with the earth system climate model including a dynamical vegetation component compare well with the results of the marine pollen record of ODP Site 1078.

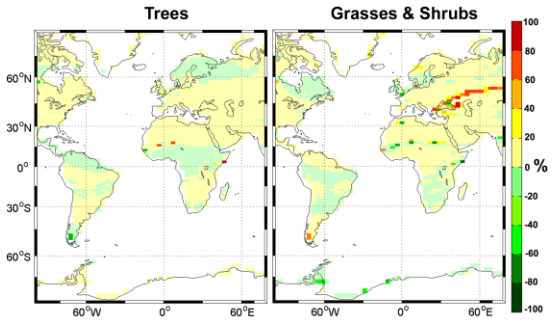

Figure 4: Tree and grass cover differences between the Southern Ocean freshwater forcing and HS1 simulations under pre-industrial boundary conditions.

A resumption of the Atlantic Meridional Overturning Circulation after the slowdown during HS1 is considered as a possible trigger for the onset of the Bølling-Allerød warm period. To gain a better understanding of its possible effect on the climate and vegetation distribution in the tropics, we carried out additional experiments using the UVic ESCM. Following Weaver et al. (2003) we perturbed the freshwater balance of the Southern Ocean by adding an amount of freshwater similar to Meltwater Pulse 1A (Clark

et al. 1996) in two locations where Antarctic Intermediate Water is formed. Under otherwise pre-industrial boundary conditions, we could indeed trigger a transition from a collapsed to an active Overturning Circulation. In response, the tree cover in the Sahel region tended to recover at the expense of grass and shrub cover (Fig. 4). Changes in the extra-tropics were generally larger than in the tropics. To maintain consistency with our previous HS1 simulations and available biome compilations (Hessler et al. 2010), we conducted an experiment under HS1 boundary conditions. However, in this case the Atlantic Meridional Overturning Circulation could not be reinitiated, which may be explained by the different density distributions simulated by the UVic ESCM under pre-industrial and glacial boundary conditions (e.g. Schmittner et al. 2002).

References:
*http://www.bridge.bris.ac.uk/ resources/Data-bases/ BIOMES_data
Anand, P., Elderfield, H., Conte, M.H., 2003. Calibration of Mg/Ca thermometry in planktonic foraminifera from a sediment trap time series. *Paleoceanography* 18, 1050, doi:10.1029/2002PA000846, 1-28.
Clark, P.U., Alley, R.B, Keigwin, L.D., Licciardi, J.M., Johnsen, S.J., Wang, H., 1996. Origin of the first global meltwater pulse following the Last Glacial Maximum. *Paleoceanography* 11, 5, doi:10.1029/96PA01419, 563-577.
Cox, P.M., 2001. Description of the TRIFFID dynamic global vegetation model. *Hadley Center technical note* 24, 1-17.
Harrison, S.P., Prentice, C.I., 2003. Climate and CO_2 controls on global vegetation distribution at the last glacial maximum: analysis based on palaeovegetation data, biome modeling and palaeoclimate simulations. *Global Change Biology* 9, 983-1004.
Hessler, I., Dupont, L., Bonnefille, R., Behling, H., González, C., Helmens, K.F., Hooghiemstra, H., Lebamba, J., Ledru, M-P., Lézine, A-M., Maley, J., Marret, F., Vincens A., 2010. Millennial-scale changes in vegetation records from tropical Africa and South America during the last glacial. *Quaternary Science Reviews*, 2882-2899.
Mashiotta, T. A., Lea, D. W., Spero, H. J., 1999. Glacial-Interglacial changes in Subantarctic sea surface temperature and δ^{18}O-water using foraminiferal Mg. *Earth and Planetary Science Letters* 170, 417-432.
Schmittner, A., Meissner, K. J., Eby, M., Weaver, A.J., 2002. Forcing of the deep ocean circulation in simulations of the Last Glacial Maximum. *Paleoceanography* 17, doi:10.1029/2001PA000633, 1-15.
Shackleton, N., 1974. Attainment of isotopic equilibrium between ocean water and the benthonic foraminifera genus Uvigerina: Isotopic changes in the ocean during the last glacial. *Colloquium International CNRS* 219, 203-209.
Waelbroeck, C., Labeyrie, L., Michel, E., Duplessy, J. C., McManus, J. F., Lambeck, K., Balbon, E., Labracherie, M., 2002. Sea-level and deep water temperature changes derived from benthic foraminifera isotopic records. *Quaternary Science Reviews* 21, 295-305.
Weaver, A.J., Eby, M., Wiebe, E.C., Bitz, C.M., Duffy, P.B., Ewen, T.L., Fanning, A.F., Holland, M.M., MacFadyen, A., Matthews, H.D., Meissner, K.J., Saenko, O., Schmittner, A., Wang, H., Yoshimori, M., 2001. The UVic earth system climate model: Model description, climatology, and applications to past, present and future climates. *Atmosphere-Ocean* 39, 361-428.
Weaver, A.J., Saenko, O.A., Clark, P.U., Mitrovica, J.X., 2003. Meltwater pulse 1A from Antarctica as a trigger of the Bølling-Allerød warm interval. *Science* 299, 1709-1713.

IODP

High Δ^{56}Fe in magnetite-ilmenite assemblages from IODP Hole 1256D rocks (ODP Leg206 and IODP Exp. 309 & 312, East Pacific Rise)

W. DZIONY[1], I. HORN[1], J. KOEPKE[1], F. HOLTZ[1]

[1] Institut für Mineralogie, Leibniz Universität Hannover

The formation of the oceanic crust is one of the main fundamental processes building our planet. IODP multi-cruise mission "Superfast Spreading Crust" successfully drilled a complete section of the upper oceanic crust into the underlying gabbros (Site 1256; eastern equatorial Pacific; 15 Ma crust formed at the East Pacific Rise). The recovered rocks, now representing the first reference profile through fast-spreading upper oceanic crust, provide us with the good opportunity to improve our understanding of the formation and evolution of the crust. Complex interplay between magmatic and metamorphic processes, such as Primary crystallization; low- and high-temperature alteration; contact-metamorphism; partial melting/assimilation; magma mixing can be observed. The petrographic record of the whole section reveals that all processes involve the formation of, or the reaction with, Fe-Ti oxides, which can consequently be used as suitable proxies for monitoring the different stages in the magmatic-metamorphic evolution of fast-spreading oceanic crust.

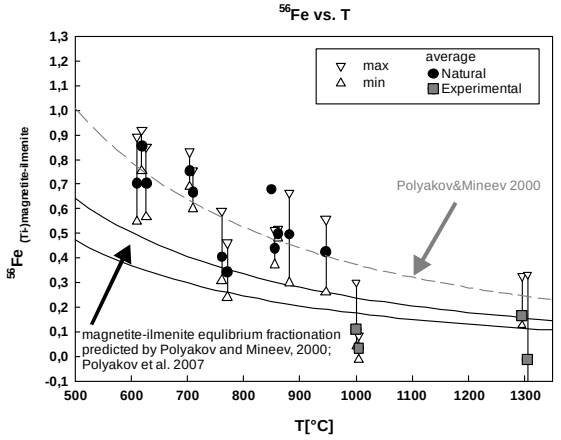

Fig. 1: Inter-mineral $^{56}Fe/^{54}Fe$ fractionation observed between coexisting pairs of ilmenite-magnetite. Minimum and maximum values of coexisting pairs are connected with vertical lines. The dashed curve shows the predicted values based on former data by Polyakov and Mineev 2000 that were revised by Polyakov et al. 2007 (solid curves).

In situ iron isotope determination

We have measured Fe isotope ratios of magnetite, ilmenite and pyrite of basalts and gabbros in order to gain basic knowledge of the Fe isotope cycle in the ocean crust, and to investigate if their isotopic signatures can be used as a proxy for hydrothermal alteration or as a geothermometer either.

In this approach we are using a deep UV-femtosecond laser ablation system coupled to a MC-ICP-MS (multiple-collector inductively coupled plasma mass spectrometer). This method allows us to determine iron isotope ratios *in-situ* with a precision of ±0.1 ‰ (2σ) for the δ^{56}Fe ($\delta^{56}Fe = (^{56}Fe/^{54}Fe_{sample}/^{56}Fe/^{54}Fe_{IRMM\text{-}14}\text{-}1)*1000$). It has been shown in several studies (Horn et al., (2006) and within this project) that the influence of the matrix on the calibration of the δ^{56}Fe values is negligible. Furthermore it provides a spatial resolution that can not be reached with conventional aqueous solution mass spectrometry. Analytical and methodical techniques are given by Horn et al. (2006).

Most igneous rocks normally have a very destricted range in δ^{56}Fe, except of some high silica granitoids (Poitrasson and Freydier, 2005; Schoenberg and von Blanckenburg, 2006), mantle xenoliths and carbonatites (e.g. Weyer et al, 2005, Johnson and Beard, 2006). In contrast, Fe isotope compositions of hot fluids (> 300 °C) from mid-ocean-ridge spreading centers define a narrow range that is shifted to lower δ^{56}Fe values by 0.2‰–0.5‰

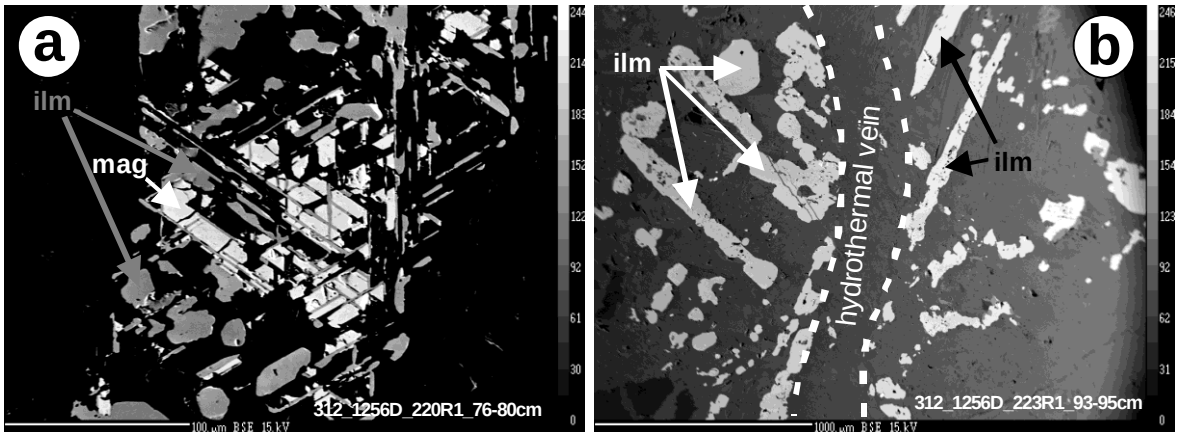

Fig. 2: Backscatter electron images of two primary crystallized magnetites which show the typical exsolution bodies of ilmenite. In (b) the magnetite host has been completely replaced by secondary amphiboles.(sample 1256-223R1_93-95cm).

as compared to igneous rocks (e.g. Beard et al., 2003; Rouxel et al., 2003; Beard and Johnson, 2004). Therefore, it is expected that mineral phases that contain large amounts of iron like magnetite and ilmenite are especially affected by the interaction with a fluid that fractionates iron isotopes during exsolution/ precipitation of those minerals.

We observe significant variations in the $\delta^{56}Fe$ in both, magnetite and ilmenite as well as in pyrite within the investigated samples, even at very small scale.So far, it is not clear whether this heterogeneities are primary effects or secondary. However, $\Delta^{56}Fe_{magnetite\text{-}ilmenite}$ values ($\delta^{56}Fe_{magnetite}$ - $\delta^{56}Fe_{ilmenite}$) of coexisting pairs of magnetite and ilmenite are in agreement with the general trend of temperature-dependent fractionation (Fig.1, Polyakov and Mineev, 2000, Polyakov et al., 2007), but are shifted towards higher $\Delta^{56}Fe$ values when compared to the predicted values. This could implie that they are isotopically out of equilibrium, while synthesized, well equilibrated magnetite-ilmenite pairs are compatible with the theoretical predictions. The difference between the natural and the experimental datasets could be explained by the influence of hydrothermal fluid, since all investigated samples show signs of typical hydrothermal alteration. It has been shown that Cl-bearing supercritical fluids can contain considerable amounts of bi-valent iron (Chou and Eugster, 1977). Such solutions tend to favor mobilization of isotopically light iron. Assuming that magnetite is more soluble than ilmenite in the presence of a Cl-bearing fluid, this would increase the $\delta^{56}Fe$ of magnetite and therefore the $\Delta^{56}Fe_{mag\text{-}ilm}$. Petrographical evidence for this assumption is shown in Fig. 2, which shows two steps of the dissolution of magnetite which has exsolved trellis lamellae of ilmenite. In the second step ilmenite is still present while magnetite has been completely replaced by secondary amphibole. Variations of up to 0.4‰ $\delta^{56}Fe$ within one single grain of magnetite also shows that isotopic alteration can be extremely localized.

Pyrites are with one exception generally isotopically light. In the gabbros and the basalts of the lava pond they show relatively low $\delta^{56}Fe$ values that lie between -1.1‰ and -0.6‰, identifying them as secondary precipitations from a hydrothermal fluid. In contrast, we observed a $\delta^{56}Fe$ for pyrite coexisting with ilmenite in a sample of the granoblastic dikes of about +0.3‰, which is close to the predicted fractionation with respect to the coexisting ilmenite (Polyakov and Mineev, 2000). Since actually all phases in the granoblastic dikes seem to be completely recrystallized, it is not clear so far, whether this pyrite is preserving its initial primary isotopic signature or has been formed by secondary precipitation and then isotopically re-equilibrated during the ongoing contactmetamorphic overprint, that the granoblastic dikes have suffered (see next paragraph).

Thermo-oxibarometry along Hole 1256D

The basalts recovered between the lava pond and the granoblastic dikes are not suitable for two-oxide thermometry due to the lack of ilmenite. They are not suitable for laser ablation either, since magnetites in those rocks are too tiny and have mostly skelettal shape.

Chemical data of the oxide minerals based on several thousands of microprobe analyses (Dziony et al., 2008, Koepke et al, 2007) from the lava pond and rocks collected below 1300 mbsf were applied to reconstruct the redox and temperature conditions during the evolution of the oceanic crust at Site 1256D. We applied the improved two-oxide geothermo-oxibarometer of Sauerzapf et al. (2008). Since most magnetites show more or less heavy exsolving, different methods to estimate the initial composition were used. In those cases where exsolutions were large enough to measure separately, the initial compositon was recalculated using image analysis. In the case of very fine exsolutions, a broad beam of 20 µm diameter was used. For fresh basalt and most gabbros we estimated more reducing redox conditions (Delta NNO ~ -1, with NNO corresponding to the Nickel-Nickeloxide oxygen buffer), as expected for the MOR petrogenesis. For the lowermost dikes (“granoblastic dikes”), which suffered a contactmetamorphic overprint due to the thermal imprint of an underlying magma chamber (Koepke et al., 2008) and for the gabbro directly at the dike/gabbro contact, a dramatic shift of the $f(O_2)$ (nearly 4 orders of magnitude) towards more oxidizing conditions (Fig. 3) was observed. The apparent higher temperatures recorded in the oxides of the uppermost gabbros could be explained by faster cooling rates at the contact to the sheeted dikes, causing an early closing for Fe-Ti exchange before re-equilibration at lower temperatures is possible. Such higher temperatures are not found at the contact between gabbro screen 2 and a ~20m thick “screen of granoblastic dikes”(see Fig. 3), which separates the two gabbro screens (located ~50m below the first sheeted dike/gabbro contact). This observation supports the model of France et al, 2009, who interpret this zone as granoblastic xenoliths, surrounded by gabbroic melt, and is in contrast with the model of Koepke et al.,

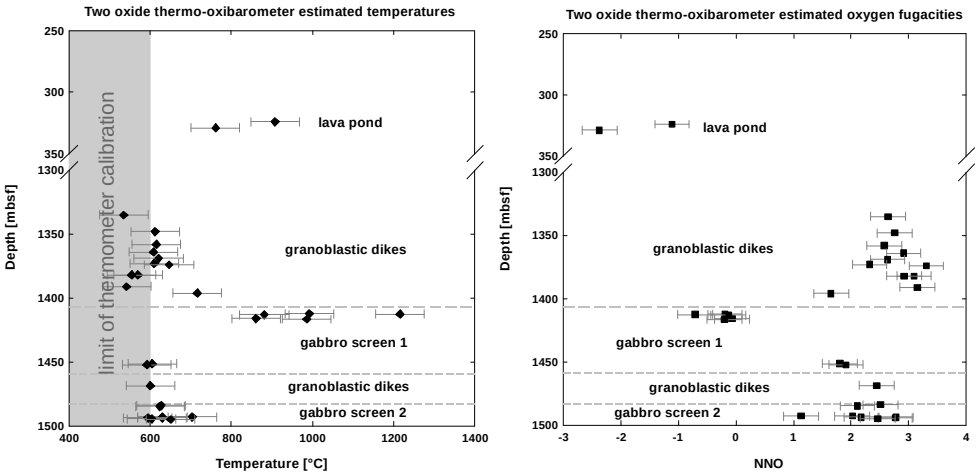

Fig. 3: Temperature and oxygen fugacity estimations by using the magnetite / ilmenite geothermo-oxibarometer by Sauerzapf et al. (2007). The dashed line corresponds to the dike/gabbro transition. mbsf=meters below sea floor; ΔNNO=f(O_2) in log units compared to the Ni/NiO oxygen buffer.

2008, who interpret the two gabbro screens as two separate intrusions into the sheeted dikes.

Summary

The general evolution of $\Delta^{56}Fe_{magnetite\text{-}ilmenite}$ with temperature determined from oxide-thermometry (as depicted in Fig.1) indicates that the Fe-isotopic composition of oxides in hydrothermally altered oceanic rocks is influenced by T. However, the shift of the trend towards higher $\Delta^{56}Fe_{magnetite\text{-}ilmenite}$ in Fig.1 indicates eiter that isotopic equilibrium was not attained or that additional factors control the distribution of Fe isotopes.

The strong variation of the $\delta^{56}Fe$ within single minerals (magnetite and ilmenite) shows that fluid-rock-interactions may have affected the isotopic composition of the Fe-oxides to different degrees. However, a clear distinction between primary magmatic signatures and different stages of hydrothermal alteration of the 1256D rocks is difficult to work out with the current data. Future investigations should include analysis of the other Fe-bearing phases such as olivine, cpx, opx, and also secondary phases to get a better image of the iron-isotopic cycle in the ocean crust. Including those minerals, it would be possible to shed light on the question if the negative $\delta^{56}Fe$ values of hydrothermal fluids is caused by leaching of ^{54}Fe in general or by preferential dissolution of isotopically light minerals.

References:

Beard, B.L., Johnson, C.M., Von Damm, K.L., Poulson, R.L., 2003. Iron isotope constraints on Fe cycling and mass balance in oxygenated Earth oceans. Geology 31, 629-632.

Beard, B.L., Johnson, C.M., 2004. Fe isotope variations in the modern and ancient earth and other planetary bodies. Rev. Mineralogy & Geochemistry 55, 319-357.

Chou I.-M. and Eugster H. P., 1977. Solubility of magnetite in supercritical chloride solutions. Am. J. Sci. 277, 1296–1314.

Dziony, W., Koepke, J., and Holtz, F., 2008. Data report: petrography and phase analyses in lavas and dikes from Hole 1256D (ODP Leg 206 and IODP Expedition 309, East Pacific Rise). In Teagle, D.A.H., Alt, J.C., Umino, S., Miyashita, S., Banerjee, N.R., Wilson, D.S., and the Expedition 309/312 Scientists, Proc. IODP, 309/312: College Station, TX (Integrated Ocean Drilling Program Management International, Inc.)(doi:10.2204/iodp.proc.309312.201.2008)

France, L., Ildefonse, B., Koepke, J., 2009. Interactions between magma and hydrothermal system in Oman ophiolite and in IODP Hole 1256D: Fossilization of a dynamic melt lens at fast spreading ridges. Geochem. Geophys. Geosyst., 10, Q10O10.(doi:10.1029/2009GC002652)

Koepke, J., D. M. Christie, W. Dziony, F. Holtz, D. Lattard, J. Maclennan, S. Park, B. Scheibner, T. Yamasaki, and S. Yamazaki (2008), Petrography of the dike-gabbro transition at IODP Site 1256 (equatorial Pacific): The evolution of the granoblastic dikes, Geochem. Geophys.Geosyst.,9,Q07O09.(doi:10.1029/2008GC001939)

Horn, I., von Blanckenburg, F., Schoenberg, R., Steinhoefel, G., Markl, G., 2006. In situ iron isotope ratio determination using UV-femtosecond laser ablation with application to hydrothermal ore formation processes. Geochim. Cosmochim. Acta 70, 3677–3688.

Johnson C. M. and Beard B. L., 2006. Tracing metasomatic and crystallization processes in the mantle through Fe isotopes. Geochim. Cosmochim. Acta 70(1), A295.

Poitrasson F. and Freydier R., 2005 Heavy iron isotope composition of granites determined by high resolution MC-ICP-MS. Chem. Geol. 222, 132–147.

Rouxel, O., Dobbek, N., Ludden, J., Fouquet, Y., 2003. Iron isotope fractionation during oceanic crust alteration. Chem. Geol. 202, 155-182.

Sauerzapf, U, Lattard, D, Burchard, M, Engelmann, R., 2008. The titanomagnetite-ilmenite equilibrium; new experimental data and thermo-oxybarometric application to the crystallization of basic to intermediate rocks. Journal of Petrology 49(6):1161-1185

Schoenberg R. and von Blanckenburg F., 2006. Modes of planetary-scale Fe isotope fractionation. Earth Planet. Sci. Lett. 252, 342–359.

Weyer S., Anbar A. D., Brey G. P., Münker C., Mezger K. and Woodland A. B., 2005. Iron isotope fractionation during planetary differentiation. Earth Planet. Sci. Lett. 240, 251–264.

IODP

Paleoenvironmental reconstruction of the Black Sea basin during the Eemian interglacial by means of geochemical and isotopic studies

S. ECKERT[1], B. SCHNETGER[1], C. MONTOYA-PINO[2], S. WEYER[3], J. KÖSTER[1], S. SEVERMANN[4], H. ARZ[5], H.-J. BRUMSACK[1]

[1] Institut für Chemie und Biologie des Meeres (ICBM), Universität Oldenburg, P.O. Box 2503, D-26111 Oldenburg, Germany (sebastian.eckert@uni-oldenburg.de)

[2] Institut für Geowissenschaften, Universität Frankfurt, Altenhofer Allee 1, D-60431 Frankfurt a. M., Germany

[3] Institut für Mineralogie, Leibniz Universität Hannover, Callinstraße 3, D-30167 Hannover, Germany

[4] Institute of Marine and Coastal Science, Rutgers University, 71 Dudley Road, NJ-08901 New Brunswick, USA

[5] Leibniz-Institut für Ostseeforschung Warnemünde (IOW), Seestraße 15, D-18119 Rostock, Germany

The Black Sea is the type locality of an anoxic basin with HS^- dissolved in the water column. Such reducing conditions favor preservation of organic matter, precipitation of sulfides, and scavenging of elements associated with organic matter and/or sulfide in sapropels. The Holocene sapropelic layer presently deposited in the Black Sea basin likely represents a recent analog for

ancient widespread black shale formation like during the Mid-Cretaceous. Here we report of a second sapropelic layer located beneath the glacial clays, which documents reducing euxinic conditions during the Eemian interglacial.

During DSDP Leg 42B (Site 379A) in the Black Sea a sapropel of presumably Eemian age was recovered 99 m below the recent (Holocene) one (USHER and SUPKO, 1978). In 2007 R/V *Meteor* again detected this second sapropelic layer during cruise M72/5. It was retrieved in two gravity cores (22-GC-3/7) off the Anatolian coast at only 8 m depth below seafloor. Both sapropel-cores were sub-sampled at high-resolution (2 to 6 mm). Because only one bulk sapropel sample was analyzed during the DSDP cruise (sample #19 in CALVERT and BATCHELOR, 1978) the sapropel interval was resampled at high-resolution in the Bremen Core Repository from the archive half. In all samples major elements (Al, Ca, Fe, K, Mg, Mn, Na, P, Si, and Ti) and trace metals (e.g. As, Ba, Co, Cr, Cu, Mo, Ni, Re, U, V, Y, Zn, and Zr), as well as the REE distributions were determined by WD-XRF, ICP-OES and HR-ICP-MS. Total organic and inorganic carbon (TOC, TIC) as well as total sulfur were measured by standard techniques. In selected samples $\delta^{56}Fe$, $\delta^{97}Mo$, and $\delta^{238}U$ were determined by MC-ICP-MS after chromatographic extraction. Furthermore some selected samples were extracted with dichloromethane/methanol by ASE and fractionated by column chromatography for GC-MS determination of derivatives of isorenieratane ($C_{40}H_{66}$), which are molecular indicators for photic zone anoxia.

The general inorganic-geochemical element profiles of the Eemian sapropel show vertical distributions comparable to the Holocene one. Especially the TOC and carbonate trends in the Eemian sapropel compare well with the Holocene. This fact allows creating a lithological classification analogous to the acknowledged unit classification of the Holocene sapropel (ARTHUR and DEAN, 1998). In addition the paleoenvironment of deposition was studied by means of the vertical distribution of selected redox-sensitive trace metals as well as Fe, Mo and U isotope ratios.

Comparable enrichments of redox-sensitive elements (e.g. Co, Cr, Cu, Fe, Mo, Ni, Re, U and V) indicate that both sapropels were deposited under euxinic conditions. The results also show that the transition from the glacial period to the Eemian interglacial slightly differed from the initial Holocene ingression of seawater from the Mediterranean over the Marmara Sea into the Black Sea. These trace metal enrichments suggest a similar formation mechanism, but a slightly different paleoenvironment during the two time periods. One possible explanation might be the different deposition mechanism in the Eastern Mediterranean Sea during the Eemian and the Holocene. While sapropel deposition in the Black Sea and Mediterranean Sea (S5) is expected to be synchronous during the Eemian, this was not the case during the Holocene since Units I and II in the Black Sea are not time-equivalent to the S1 sapropel. These differences between the two sapropels are documented by $\delta^{97}Mo$ and $\delta^{238}U$.

Both, $\delta^{97}Mo$ and $\delta^{238}U$ are redox-sensitive: Mo isotopes display large fractionation between seawater and oxic or suboxic sediments (towards low $\delta^{97}Mo$) but no fractionation between seawater and euxinic sediments (BARLING et al., 2001; NEUBERT et al., 2008). The latter is due to the quantitative removal of Mo (as MoS_4) from the water column and accumulation in the sedimentary archive when the sulfide-controlled geochemical action point switch (APS) at ~11 µM HS^- is exceeded (HELZ et al., 1996; NEUBERT et al., 2008). In contrast to Mo, U is never quantitatively removed from the water column and displays significant isotope fractionation between seawater and anoxic or euxinic sediments (towards high $\delta^{238}U$; WEYER et al., 2008; MONTOYA-PINO et al., 2010) Thus, the combination of $\delta^{97}Mo$ and $\delta^{238}U$ may help to reconstruct the redox history of the Black Sea. Both isotope proxies indicate that the paleoenvironment of the Eemian interglacial was anoxic but less euxinic than that of the Holocene during deposition of Unit I sediments. At least the $\delta^{97}Mo$ data of the lower Eemian samples imply incomplete removal of Mo from the water column into the sediment under non- or less euxinic conditions, more similar than those established during deposition of the Holocene Unit II sediments, assuming that the $\delta^{97}Mo$ value of the inflowing seawater was essentially constant. In the upper half of the Eemian profile, $\delta^{97}Mo$ are almost identical to those from Unit I sediments, indicating euxinic condition. A switch to euxinic conditions may be indicated by the peak in Mo/Al. U isotopes are similar to those of Holocene sediments for most of the Eemian, but become relatively light in the uppermost part of Unit V. This may indicate that water mass exchange with the Mediterranean Sea was very limited at the end of the Eemian and the Black Sea water column became depleted in Mo and U and heavy U isotopes, as the latter were preferentially incorporated into the sediments before.

On the basis of Fe/Al, Mo/Al and Re/Mo ratios a less dynamic transition of the water column from the limnic glacial to the brackish/marine Eemian interglacial is indicated. During the Holocene the redox-/pycnocline experienced some fluctuations, as recorded by distinctive maxima in the vertical Fe/Al distribution and variations of the Mo/Al ratio in depth profiles. In contrast, the Eemian depth profiles of these element ratios show more gradual changes.

The redox-sensitive and partly bio-associated trace metals (e.g. Cu, Ni, and V) are less enriched in the Eemian compared to the Holocene sapropel. This might be due to a reservoir effect induced by the assumed synchronous deposition of sapropel S5 in the Eastern Mediterranean. For this reason seawater which entered the Black Sea during the Eemian might have been depleted in redox-sensitive trace metals.

$\delta^{56}Fe$ values show the same systematics in the Eemian and the Holocene sapropels. In both sapropels low $\delta^{56}Fe$ values are accompanied by increased Fe/Al ratios and vice versa, due to dissolved microbially reduced iron originating from suboxic shelf sediments. During processes of microbial reduction, lateral transport from the shelf into the basin, and precipitation as iron sulfides always the lighter iron isotope is preferred. This finally leads to the enrichment of the lighter Fe isotope in Fe-enriched sediment layers (SEVERMANN et al., 2008). The comparison of the $\delta^{56}Fe$ values of the two sapropels with those from the glacial clay show that the Fe-isotopic composition of the background sediments drifted to higher $\delta^{56}Fe$ values with time. Thus, the effective Fe isotope fractionation ($\Delta^{56}Fe$) during the Holocene is slightly higher compared to the fractionation during the Eemian.

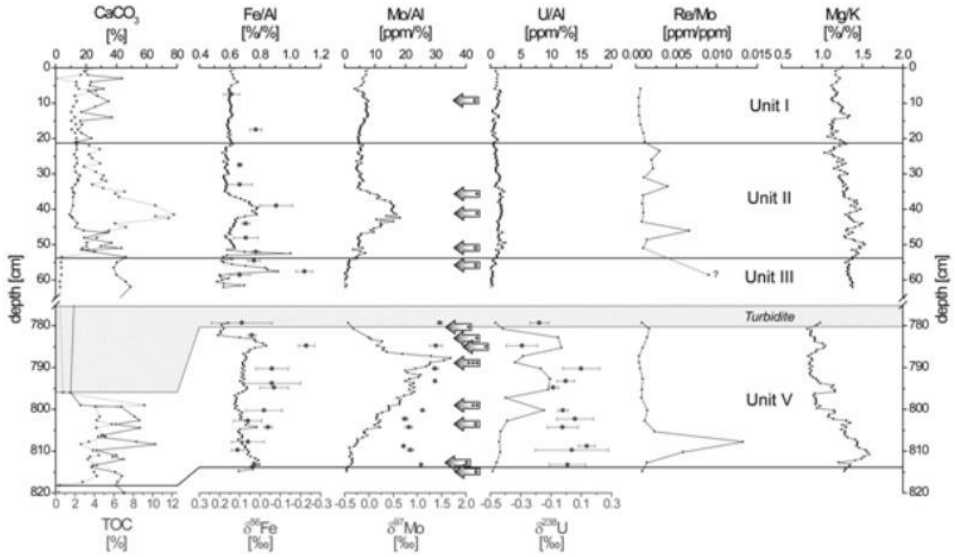

Fig. 1: Depth profiles of $CaCO_3$, TOC (dotted line), Fe/Al, δ^{56}Fe, Mo/Al, δ^{97}Mo, U/Al, δ^{238}U, Re/Mo, and Mg/K; Unit boundaries after Arthur & Dean (1998); Holocene Units I to III: 22-GC-7, Eemian Unit V: 22-GC-3 (except TOC and $CaCO_3$: 22-GC-7); hatched area: turbidite above Unit V; error bars correspond to 2σ; arrows with plus sign mark the samples and abundance of isorenieratane derivatives.

The detection of free (not sulfur-bound) isorenieratane derivatives fits perfectly into this context, because isorenieratane is a biomarker for green sulfur bacteria. These bacteria are capable of anoxygenic photosynthesis and indicate photic zone euxinia (KOOPMANS et al., 1996; BOSCH et al., 1998). In our data set these biomarkers occur after the redoxcline shifted from the sediment surface into the water column, as indicated by Mo deposition. It seems also evident that the redoxcline was located in the photic zone during the Eemian interglacial. This might be a further indicator for more gradual changes of the water column chemistry. By contrast, in the Holocene samples free isorenieratane derivatives were only found in the Unit II sapropel at the TOC and Mo/Al maxima, indicating the oscillation of the redoxcline around the photic zone.

Paleoproductivity proxies (e.g. Ba/Al, Cu/Al, Ni/Al, P/Al, and Sr_{xs}/Ca_{xs}) suggest an increase in paleoproductivity during the Eemian interglacial due to an increased riverine nutrient inflow and document increased deposition/preservation of organic matter during the warmer periods in the Black Sea. Detailed information on primary productivity rates or the distinction between increased preservation and enhanced deposition is rather complicated, because all paleoproductivity proxies mentioned owe certain disadvantages under euxinic conditions like in the Black Sea. Biogenic Ba, for example, is mainly deposited as $BaSO_4$, which may dissolve under reducing, sulfate-limited conditions. Cu and Ni are not only bound to organic matter but also to iron sulfides, which precipitate on a large scale in euxinic settings. The Sr_{xs}/Ca_{xs} ratio for itself is not a paleoproductivity proxy, but changes depending on the type of the deposited carbonate minerals. Furthermore this ratio changes with the transition from limnic (lower values) to marine conditions (higher values).

Mg/K ratios may be used to monitor the change of detrial input during the transition from glacial to interglacial. Mg/K shows lower ratios during a glacial period and higher ratios during an interglacial, where the ratio is decreasing with time. This might indicate increasing chlorite content (Mg rich) with enhanced fluvial input due to warmer temperatures.

To validate our new results a spatiotemporal comparison with the recent Black Sea sapropel (same location) and the Eastern Mediterranean S5 sapropel (same time period) was made. The enrichment of major and trace elements of the Eemian sapropel shows similarities with the Holocene sapropel from the same location, as well as with the S5 sapropel.

Our study implies that repeated sapropel formations in the Black Sea are linked to interglacial periods and reflect the global sea level rise and marine ingression through the Bosporus sill.

References:

Arthur, M. A. and Dean, W. E., 1998. Organic-matter production and preservation and evolution of anoxia in the Holocene Black Sea. Paleoceanography 13, 395-411.

Barling, J., Arnold, G. L., and Anbar, A. D., 2001. Natural mass-dependent variations in the isotopic composition of molybdenum. Earth Planet. Sci. Lett. 193, 447-457.

Bosch, H. J., Sinninghé Damsté, J. S., and de Leeuw, J. W., 1998. Molecular palaeontology of Eastern Mediterranean sapropels: Evidence for photo zone euxinia. In: Robertson, A. H. F., Emeis, K. C., Richter, C., and Camerlenghi, A. Eds.), Proceedings of the Ocean Drilling Program, Scientific Results, College Station, TX.

Calvert, S. E. and Batchelor, C. H., 1978. Major and minor element geochemistry of sediments from Hole 379A, Leg 42B, Deep Sea Drilling Project. In: Usher, J. L. and Supko, P. Eds.), Initial reports of the Deep-Sea Drilling Project. U.S. Government Printing office, Washington D.C.

Helz, G. R., Miller, C. V., Charnock, J. M., Mosselmans, J. F. W., Pattrick, R. A. D., Garner, C. D., and Vaughan, D. J., 1996. Mechanism of molybdenum removal from the sea and its concentration in black shales: EXAFS evidence. Geochim. Cosmochim. Acta 60, 3631-3642.

Koopmans, M. P., Köster, J., van Kaam-Peters, H. M. E., Kenig, F., Schouten, S., Hartgers, W. A., de Leeuw, J. W., and Sinninghé Damsté, J. S., 1996. Diagenetic and catagenetic products of isorenieratene: Molecular indicators for photic zone anoxia. Geochim. Cosmochim. Acta 60, 4467-4496.

Montoya-Pino, C., Weyer, S., Anbar, A. D., Pross, J., Oschmann, W., van de Schootbrugge, B., and Arz, H. W., 2010. Global enhancement of ocean anoxia during Oceanic Anoxic Event 2: A quantitative approach using U isotopes. Geology 38, 315-318.

Neubert, N., Nägler, T. F., and Böttcher, M. E., 2008. Sulfidity controls molybdenum isotope fractionation into euxinic sediments: Evidence from the modern Black Sea. Geology 36, 775-778.

Severmann, S., Lyons, T. W., Anbar, A., McManus, J., and Gordon, G., 2008. Modern iron isotope perspective on the benthic iron shuttle and the redox evolution of ancient oceans. Geology 36, 487-490.

Usher, J. L. and Supko, P., 1978. Initial Reports of the Deep Sea Drilling Project U.S. Government Printing office, Washington D.C.
Weyer, S., Anbar, A. D., Gerdes, A., Gordon, G. W., Algeo, T. J., and Boyle, E. A., 2008. Natural fractionation of U-238/U-235. Geochim. Cosmochim. Acta 72, 345-359.

IODP

Magnetic Measurements in Boreholes – Influence of Tool Strings

S. EHMANN[1], C. VIRGIL[1], A.HÖRDT[1], M. LEVEN[2]

[1]Institut für Geophysik und Extraterrestrische Physik, TU Braunschweig
[2]Institut für Geophysik, Universität Göttingen

Tools for magnetic measurements are often run in tool strings together with other instruments due to time constraints or operational requirements. A typical example is the General Purpose Inclinometry Tool (GPIT) that is run in Ultrasound Borehole Imager (UBI), Formation Micro Scanner (FMS) or Triple Combo tool strings. Even if some parts of the tool string are made out of nonmagnetic alloys, some parts can carry induced or remanent magnetization that can have a considerable influence on the magnetic field measurements. Depending on the use of the measurement, be it to reorient borehole images or to measure the magnetic field as main purpose, this can have a considerable effect on the measurement.

The influence of magnetized parts on the measurements is largest in the component of the magnetic field in line with the symmetry axis of the tool string. Unless the borehole is strongly inclined, this is mostly the vertical component of the magnetic field. Thus reorientation of borehole images is not strongly influenced but the values for the inclination of the magnetic field calculated from the measured data are erraneous.

The Göttingen Borehole Magnetometer (GBM) comprises three fluxgate magnetometers and three fibre optical gyros. The gyros record rotations of the tool with a high resolution ($9 \cdot 10^{-5}$ degree per increment) and thus enable reorientation of the magnetic field to the Earth's reference frame. The magnetometers have a range of ±50000nT (x- and y-sensor) and ±70000nT (z-sensor) paired with a high resolution of 6.1nT and 8.5nT, respectively. In addition to the gyros, two inclinometers are used to determine the deviation of the tool from the vertical.

One of the main goals of IODP Expedition 330 to the Louisville Seamount Chain is the determination of the paleo-latitude of the underlying hotspot and the history of the movement of the hotspot and the Pacific plate. This is done by measurements on core samples but also using *in-situ* measurements in the borehole using the GBM. The GBM measurements have the additional advantage that the reoriented data can be used to determine the declination of the magnetization in the rocks surrounding the borehole using inverse modelling of the data. This puts further constraints on the position of the Virtual Geomagnetic Pole (VGP).

The GBM is run in a tool string together with a sinker bar and a centralizer. The sinker bar is required to increase the weight on the wireline, the centralizer is required to both keep the magnetometer centered and to reduce rotations and vibrations of the tool to increase the accuracy of the measurement.

In August 2010, extensive equipment tests were made at the Schlumberger Office in Houston, Texas, to determine the magnitude of the magnetic influence of the accessories. Numerical modelling of the measurements suggested a high remanence of 5000-8000A/m in the sinker bar and 40000A/m in the centralizer, depending on the value used for the magnetic susceptibility in the models. Especially the result for the sinker bar was unexpectedly high, since it is made mostly out of a tungsten alloy and was thought to be basically non-magnetic. The tests showed that using these accessories could cause an error of about 350nT in the measurement. To avoid this error and to improve the quality of the measurement, a new sinker bar was made out of aluminum and included in the tool string finally used during Expedition 330 to increase the distance between the magnetometers and the magnetic accessories. This is expected to reduce their influence to below 100nT and significantly improve the determination of the VGP position.

IODP

Viruses in the deep biosphere

T. ENGELHARDT[1], H. CYPIONKA[1], B. ENGELEN[1]

[1]Institut für Chemie und Biologie des Meeres, Universität Oldenburg, Post Box 2503, D-26111 Oldenburg, www.pmbio.icbm.de

General introduction. Viruses might be the main "predators" in the deep biosphere and possibly have a major impact on indigenous microorganisms in providing labile organic compounds for this extremly nutrient depleted habitat. While direct counting of viruses along depth profiles of various ODP sites indicated a general decrease with depth, we could show that the ratio of viruses vs. cells increased. Prophages were induced from six out of thirteen representative deep-biosphere bacteria of our ODP Leg 201 culture collection, exhibiting different morphotypes of sypho- and myoviruses. Five of them were subjected to whole genome sequencing. This sequence information will be used to design specific primers for a molecular detection and quantification of these phages in the deep biosphere. Especially the number and distribution of phages that infect *Rhizobium radiobacter*, which is highly abundant in subsurface sediments, will be examined.

In a new project, our research will be extended to investigate samples from the extremely oligotrophic South Pacific Gyre (IODP Exp. 329). These mid-ocean gyres represent large parts of the world´s oceans, but were hardly explored, so far. The results will be compared to our previous studies on benthic viruses from continental margin sites, and finally provide a more realistic estimate of the viral impact on the deep biosphere. It should be clarified whether viruses might be the main controlling factor of the abundance and diversity of the deep biosphere communities. In general, we will focus on the following questions: How important is the viral shunt in providing essential nutrients for deep biosphere populations? How is the physiological state of indigenous microorganisms related to viral infections?

Identification of prophages in deep-biosphere isolates. The cell and viral abundance in deep-subseafloor were quantified in sediments recovered in the frame of Leg 201 of the Ocean Drilling Program. A phylogenetically

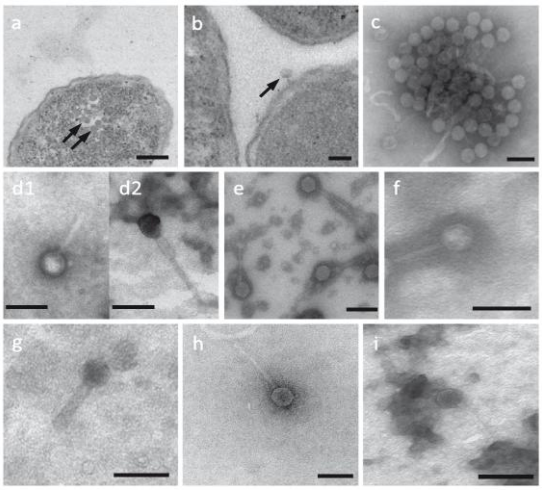

Fig. 1. Electron microscopic images of marine phages from deep-subseafloor bacteria. a,b: thin sections of a mitomycin C treated culture of *R. radiobacter* strain P007 showing (a) phage heads inside a cell (b) a phage attached to the cell surface; c: free phages induced from *Rho. capsulatus* strain E32; d-f: myoviruses from *R. radiobacter* strain P007 (d1/2), *V. diazotrophicus* strain P082 (e); *V. diazotrophicus* strain R6 (f); g-i: siphoviruses from *P. glucanolyticus* strain P073A (g); *Rho. capsulatus* strain E32 (h); *Rhb. sulfidophilum* strain P122A (i). scale bars: 100 nm.

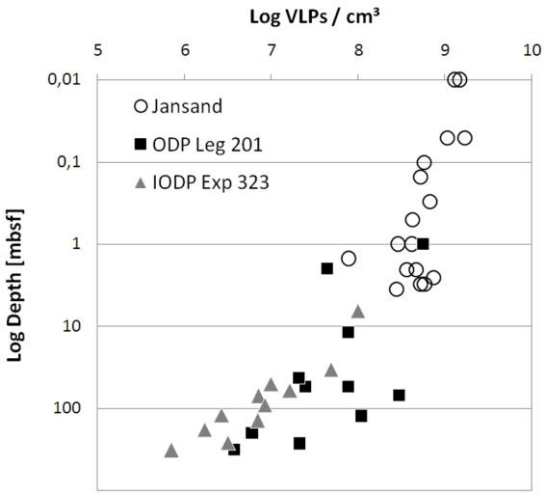

Fig. 2: Viral abundance in sub-surface sediments from selected sediment layers of three different sites: North Sea tidal-flat (site Jansand), Equatorial Pacific (ODP Leg 201; Sites 1225, 1227, 1228, 1229, 1230, 1231); Bering Sea (IODP Exp. 323; Site 1344). In general, a decrease of viral abundance with depth was observed.

diverse culture collection was tested for the presence of inducible prophages during stimulation experiments. After mitomycin C treatment as inducing agent, a drop of cell density in 6 out of 13 bacterial isolates indicated the presence of prophages. Different morphotypes of myoviruses and siphoviruses were detected by transmission electron microscopy (Fig. 1). Pulsed-field gel electrophoresis applied to viral DNA extracts showed their genetic diversity (Engelhardt et al. 2011). Fve of our induced phages for whole genome sequencing by an initiative of the Broad institute which is still in progress. The genetic information will be used to generate al molecular detection system for quantifying these phages in deep-biosphere samples.

Viral abundance in subsurface sediments. To quantify the amount of free viruses in subsurface sediments, we have performed direct counts on three different sets of sediment samples. First, we have analyzed sediment layers from ODP Leg 201 that were corresponding to the origin of our culture collection. As not enough material was available for all sites, we have ordered the respective material from the IODP core depository to complete our dataset. A high abundance of viruses ($2 \times 10^6 – 6 \times 10^8$ cm^{-3}) was determined by direct counting in selected sediment layers. Their numbers exceeded the total cell counts by a factor of 3 to 21 (Tab. 1). The increase of this ratio with depth might be due to a better preservation of viruses by adsorption on sediment particles. The second set of samples derived from IODP Exp. 323 (IODP Site 1344, Bering Sea) which was obtained by a sample request during the ongoing expedition. As a third set, we have chosen subsurface sediments from a German tidal flat (Site Jansand) that was shown to be a model site for the deep biosphere. In general, a decrease of viral abundance with depth was observed (Fig. 2). This plot will be expanded and compared to total cell counts to identify a global depth distribution of viruses in comparison to cell abundances.

ODP Site	Water Depth [m]	Sediment Depth [mbsf]	TCC [cells/cm³]	Viral counts [viruses/cm³]	Ratio [viruses:cells]	Investigated Strain	Phylogenetic Affiliation
1225	3760	198	$4.0 \cdot 10^5$	$1.6 \cdot 10^6$	15.3	P007 P073 A	*Rhizobium radiobacter* *Paenibacillus glucanolyticus*
1225	3760	320	$1.8 \cdot 10^5$	$3.8 \cdot 10^6$	20.9	R6	*Vibrio diazotrophicus*
1227	427	55	$2.5 \cdot 10^6$ *	$2.5 \cdot 10^7$	10.1	E24	*Oerskovia paurometabola*
1228	252	1	n. a.	$7.9 \cdot 10^7$	-	1288 II	*Brevundimonas sp.*
1229	151	12	$2.6 \cdot 10^7$	$7.8 \cdot 10^7$	3.0	P148	*Brachybacterium nesterenkovii*
1229	151	70	$5.5 \cdot 10^7$	$3.0 \cdot 10^8$	5.4	P045 A	*Bacillus firmus*
1230	5086	1	$1.4 \cdot 10^8$	$5.7 \cdot 10^8$	4.0	P082	*Vibrio diazotrophicus*
1230	5086	124	$1.1 \cdot 10^7$ *	$1.1 \cdot 10^8$	10.6	P118	*Psychrobacter okhotskensis*
1230	5086	268	$1.3 \cdot 10^6$ *	$2.2 \cdot 10^7$	17.0	E32 E33 A	*Rhodobacter capsulatus* *Marinobacter aquaeolei*
1231	4813	2	$7.0 \cdot 10^6$	$4.5 \cdot 10^7$	6.4	P114	*Oerskovia paurometabola*
1231	4813	43	$9.8 \cdot 10^5$	$2.1 \cdot 10^7$	21.1	P122 A	*Rhodovulum sulfidophilum*

Tab.1: Ratio of viral counts to total cell counts in different sites and sediment layers of ODP Leg 201. The investigated bacterial isolates from these layers are given. n.a., not available

The viral shunt as a potential source of nutrients for the deep biosphere. The question if viral lysis might support microbial life in deep sediments will be investigated in an experiment with preserved sediment samples from IODP Exp. 301 and IODP Exp. 329. Slurries will be prepared as replicates with artificial seawater and sediment samples from representative depth intervals. One set of slurries will be treated with mitomycin C, others will serve as controls. During the incubation period, subsamples will be analysed to determine total cell counts and to quantify free virus-particles. The number of microorganisms with lysogenic infections will be calculated as the ratio of produced virus-like particles, the burst size and the total cell counts. This will give the maximum number of cells that potentially contribute to the release of cytoplasmic material as labile organic compounds. The amount of organic matter that is released will be quantified in the supernatant by using a CN-

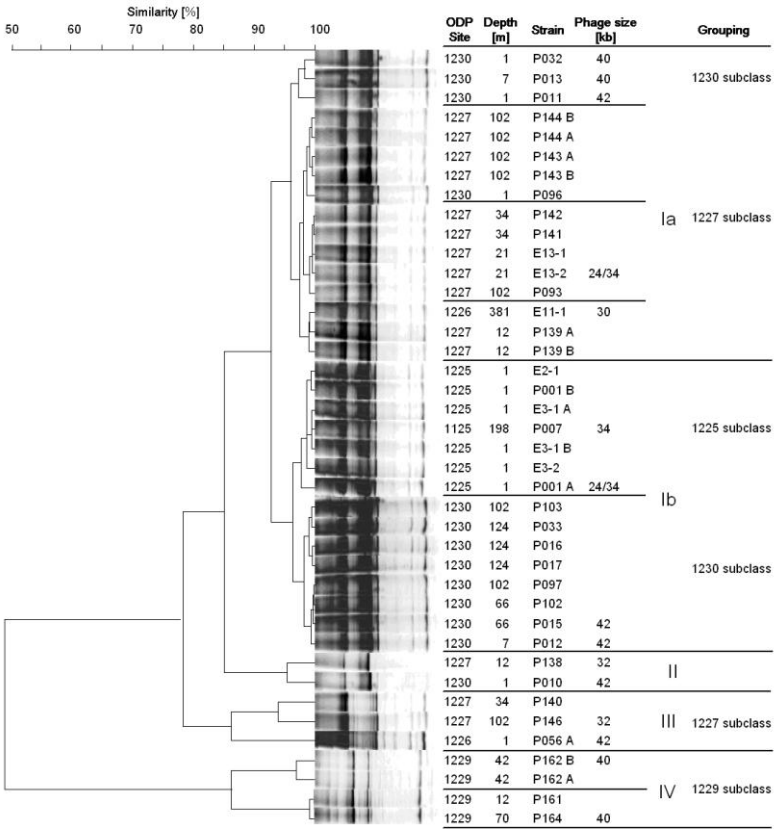

Fig. 3: Genetic heterogeneity of *R. radiobacter* isolates from ODP Leg 201 (ODP Sites 1225, 1227, 1229, 1230). The amplification of Enterobacterial Repetitive Intergenic Consensus (ERIC) sequences result in strain-specific fingerprints that allow a differenciation below the species-level. The site-specific grouping of *R. radiobacter* indicate that the populations have developed at these sites.

analyzer and a TOC monitor. The question which part of the natural microbial community can take advantage of the lysed cell material will be determined by PCR-DGGE of the 16S rRNA.

Host starvation and bacteriophage dynamics. To test whether bacteriophages from starving populations show evolutionary adaptations to the physiological state of their hosts will be performed by classical plaque assays. First experiments will be performed with bacterial cultures from a stationary growth phase in comparison to exponentially growing cultures. Furthermore, we will compare cultures that are incubated under oxic and anoxic conditions to identify difference between both life modes. In other experiments, it will be tested, if the plaques continue to expand even after the cells do not grow anymore as it was observed for phages from microorganisms thriving in oligotrophic environments. Additionally, we have kept some of our strains from the deep biosphere under starving conditions for several years now. These cultures will be compared with actively growing cells due to their response to phage induction. Furthermore, we will also compare our strains (e.g. *R. radiobacter*) with others from the same species that were isolated from habitats that are not characterized by starvation such as the plant rhizosphere.

Intraspecies diversity and biogeography of R. radiobacter-specific phages in deep-subsurface sediments. *Rhizobuim radiobacter* was chosen as the model organism because this species represents a substantial part of the deep biosphere making up up ~ 4% of the total bacterial communities. First molecular biological investigations by ERIC-PCR were carried out to analyse their intraspecies diversity and the biogeography of phages in deep-subsurface sediments (Fig. 3). Forty out of the 162 isolates from Leg 201 appear to have a close affiliation to *R. radiobacter*. Cluster analysis revealed four main genetically diverse groups. Interestingly, we found a site-specific grouping of *R. radiobacter*, indicating that the populations have developed at these sites. Analysis of the viral genomes by PFGE revealed a high diversity of viral genome sizes between 24 and 42 kb. Investigations on the biogeography of *R. radiobacter* and their phages, the so-called Rhizobiophages, will be completed by a comparison to other marine and terrestrial populations. The whole-genome information of the induced phages from our ODP Leg. 201 isolates will be used to generate primer systems for their specific quantification in subsurface sediments.

References:
Engelhardt T, Sahlberg M, Cypionka H, Engelen B (2011) Induction of prophages from deep-subseafloor bacteria. EMI Rep. doi:10.1111/j.1758-2229.2010.00232.x.

IODP

GGE as part of European Petrophysics Consortium: Activities for IODP Expedition 313 and 325

A. FEHR[1], F. P. BOSCH[1], J. INWOOD[2], J. LOFI[3], S. MORGAN[2], L. M. ANDERSON[2], S. J. DAVIES[2], R. PECHNIG[4], C. CLAUSER[1]

[1] Institute for Applied Geophysics and Geothermal Energy (GGE), E.ON Energy Research Center, RWTH Aachen University, Mathieutsr. 6,
D-52074 Aachen, Germany
[2] University of Leicester, Department of Geology, University Road, Leicester, LE1 7RH, UK
[3] Géosciences Montpellier, Université Montpellier, 2,Place E. Bataillon, F-34095 Montpellier cedex 5, France
[4] Geophysica Beratungsgesellschaft mbH, Lütticher Str. 32, D-52064 Aachen, Germany

As part of the European Petrophysics Consortium (EPC), the Institute for Applied Geophysics and Geothermal Energy (GGE) at RWTH Aachen University contributes to the Integrated Ocean Drilling Program (IODP) by providing staff and technical equipment for marine expeditions and performing logging and petrophysical lab analysis of rock samples drilled during IODP expeditions. The EPC comprises the Department of Geology at University of Leicester (UK) (coordinator), the Department of Geoscience at University of Montpellier (F) and the GGE at RWTH Aachen University (D). EPC carries out all geophysical logging and petrophysical activities for the European Science Operator (ESO).

The drilling of IODP expedition 313 New Jersey Shallow Shelf was proposed to obtain deep sub-seafloor samples and downhole logging measurements in the crucial inner shelf region. The inner to central shelf off-shore New Jersey is an ideal location to study the history of sea-level changes and its relationship to sequence stratigraphy, because it features rapid depositional rates, tectonic stability, and well-preserved, cosmopolitan fossils suitable for age control characterize the sediments of this margin throughout the time interval of interest. Today's sea levels are predicted to rise due to global warming. Therefore, sea-level change is one of the crucial issues affecting our planet, requiring careful study of past changes in sea level and a solid understanding of processes that govern the shoreline response to these changes. Past sea-level rise and fall is documented in sedimentary layers deposited during Earth's history. The main objectives of this expedition were (1) to date late Paleogene-Neogene depositional sequences and compare ages of unconforming surfaces that divide these sequences with times of sea level lowering predicted from the δ18O glacio-eustatic proxy; (2) to estimate the corresponding amplitudes, rates and mechanisms of eustatic sea-level changes; (3) to evaluate sequence stratigraphic facies models that predict depositional environments, sediment compositions and stratal geometries in response to sea-level change (Integrated Ocean Drilling Program Expedition 313 Preliminary Report). To reach these goals three boreholes were drilled in the so-called New Jersey/Mid-Atlantic transect. During IODP Expedition 313 New Jersey Shallow Shelf, two GGE scientists worked offshore as ESO petrophysicist to perform Multi Sensor Core Logger (MSCL) measurements. The MSCL measures density, resistivity, P-wave velocity and magnetic susceptibilty

L/B Kayd during IODP Expedition 313 (Picture A. Fehr).

from the whole round cores. Before the Onshore Party, one scientist and one technician from GGE performed thermal conductivity measurements on the NJSS cores using a needle probe device owned by GGE. TC measurements might be used for estimating thermal flow conditions, controlling cementation processes of sediments. Petrophysical and downhole logging data provided lithofacies characterization and greatly aided intersite correlations for intervals with no or only poor recovery.

IODP Expedition 325 Great Barrier Reef Environmental Changes was designed to investigate the fossil reefs on the shelf edge of the Great Barrier Reef and to establish the course and effects of the last glaciation in reef settings that developed in tectonically inactive areas located far from glaciated regions. The objectives of Expedition 325 are to establish the course of sea level change, to define sea-surface temperature variations, and to analyze the impact of these environmental changes on reef growth and geometry for the region over the period of 20–10 ka (Integrated Ocean Drilling Program Expedition 325 Preliminary Report). Expedition 325 drilled for cores and performed borehole logging operations at several offshore sites along transects on the Great Barrier Reef. For IODP Expedition 325 Great Barrier Reef, one GGE scientist participatetd in the Onshore Party working in total three weeks at the MARUM in Bremen on carrying out thermal conductivity measurements and line scan images. Line scan images provide high quality photographs of sediment cores and can be used to image, quantify, and archive sedimentological changes in marine sediment cores. The objective of this approach is to capture variations in sediment colour and texture before oxidization of the sediment surface takes place. For the onshore part of Expedition 325 in the core repository at Bremen (Germany), GGE provided a thermal conductivity meter to perform TC measurements in the lab.

References:

Expedition 313 Scientists, 2010. New Jersey Shallow Shelf: shallow-water drilling of the New Jersey continental shelf: global sea level and architecture of passive margin sediments. IODP Prel. Rept., 313. doi:10.2204/iodp.pr.313.2010.

Expedition 325 Scientists, 2010. Great Barrier Reef environmental changes: the last deglacial sea level rise in the South Pacific: offshore drilling northeast Australia. IODP Prel. Rept., 325. doi:10.2204/iodp.pr.325.2010.

ICDP

The petrology, geochemistry and age determination of impact melt from the USGS-ICDP drill core Eyreville-B into the late Eocene Chesapeake Bay impact structure

V. A. S. M. FERNANDES[1], M. TRIELOFF[2], N. A. ARTEMIEVA[3], J. P. FRITZ[4], W.U. REIMOLD[4]

[1]Institute of Physics University of Bern, Berne, Switzerland;
[2]Institut für Geowissenschaften, Univ. Heidelberg,Heidelberg, Germany;
[3]Institute for Dynamics of Geospheres RAS, Moscow, Russia;
[4]Museum für Naturkunde, Leibniz Institute, Humboldt Univ. Berlin, Berlin, Germany;

Introduction: In this abstract we introduce to the DFG-ICDP community our recently submitted project entitled "The petrology, geochemistry and age determination of impact melt from the USGS-ICDP drill core Eyreville-B into the late Eocene Chesapeake Bay impact structure", and the respective research group.

Project: Large impacts can distribute ejecta material globally, and these layers are important horizon markers that allow inter-correlation of sediments from different sites, e.g. for late Eocene sediments pre-dating the tipping point of Earth's climate at the Eocene/Oligocene boundary (e.g. [1]). The Global Stratotype Section and Point (GSSP) in Massignano (Italy) contains three Ir-rich ejecta layers [2] and shows an increase in the flux of ^{3}He-rich extraterrestrial material in the late Eocene [3] covering a 2 Ma time interval. Two of these Ir-rich layers have been attributed to the Chesapeake Bay (85 km Ø) and the Popigai (100 km Ø) impact structures. Current radiometric age determination for the Chesapeake Bay crater (located in Atlantic Coastal Plain centered near the present mouth of Chesapeake Bay in eastern Virginia, U.S.A.) of 35.3±0.1 Ma [4-7] is based on total fusion Ar ages of tektites (distal impact glasses). In preliminary ^{40}Ar-^{39}Ar work, we have shown that precise Ar ages on these tektites cannot be acquired by total fusion experiments but require step heating measurements. Consequently we have proposed to DFG-ICDP a systematic petrologic, geochemical and radiometric study of the first impact melt rocks found in the Chesapeake Bay structure [8&9] and to refine the ^{40}Ar-^{39}Ar ages for the related tektites. Another crater from which samples will be studied in detail is Popigai which is located north of the Siberian city of Norilsk, Russia. The current radiometric age for this crater is based on ^{40}Ar/^{39}Ar step heating experiments carried out by [10] on several impact melt rocks. The reported age is 35.7±0.2 Ma based on a single plateau. [10] argued that other Ar-Ar age spectra were likely affected by inherited ^{40}Ar or perturbed by some unclear mechanism. More recently, [11] recalculated the weighted mean of the best four plateaux and two "mini"-plateaux (displaying a disturbed age spectrum and a younger age for Popigai crater) given by [10]. The best age estimate of 36.42±0.81 Ma is based on the four plateaux showing ~70% of the total ^{39}Ar release [11]. Thus, [11] concluded that there is a need to further extend the work on age determination and petrologic characterization of several samples from Popigai to better evaluate the effects of inherited argon and other disturbances (e.g. weathering alteration) on Popigai impactites.

This study will be complemented by ^{40}Ar-^{39}Ar age determinations of impact melt rocks from two other late Eocene impact structures, Mistastin (28 km Ø; 36.4±4 Ma, [11]) and Wanapitei (7.5 km Ø; 37.8±1.6 Ma, [12]) with the aim of improving their current age determination and to verify the possibility of a late Eocene bolide shower.

Conclusion: There is a need to acquire a variety of well preserved impactites that will permit the thorough characterization of the material as well as hand-picking of the best suitable fragments for an extended ^{40}Ar/^{39}Ar study for precise age determinations of the Chesapeake, Popigai, Wanapitei and Mistastin craters. Radiometric and petrological results combined with new numerical models on impact ejecta distribution result in age, composition and distribution of global marker horizons in later Eocene sediments: a fundamental data set for investigations on the succession of events predating the tipping point of Earth's climate. Only the USGS-ICDP Eyreville B drill core provides the sample material for the main focus of this research: dating the Chesapeake Bay crater. Moreover, there are currently plans under development for a field excursion to the Popigai crater during the 2011 summer.

References:

[1] Hilgen F. J. and Kuiper K. F. (2009) The Geological Society of America Special Paper 452, 139-148.
[2] Montanari A., Asaro F., Michel H. V. and Kennett J. P. (1993) Palaios 8, 420–437.
[3] Farley K.A., Montanari A., Shoemaker E.M. and Shoemaker C.S. (1998) Science 280, 1250–1253.
[4] Glass B. P., Muenow D. W., and Aggrey K. E. (1986) Meteoritics 21, 369-370 (abstr.).
[5] Glass B. P., Koeberl C., Blum J. D., Senrle F., Ize G. A. , Evans B. J., Thorpe A. N., Povenmire H. and Strange R. L. (1995) Geochim. Cosmochim. Acta 59, 4071-4082.
[6] Albin E.F. and Wampler J.M. (1996) Lunar and Planet. Sci. Conf. XXVII, 5-6 (abst).
[7] Horton J. W., and Izett G. A. (2004) In Studies of the Chesapeake Bay Impact Structure, USGS Prof. Paper 1688, E1-E30.
[8] Wittmann A., Schmitt R.T., Hecht L., Kring D.A., Reimold W.U. and Povenmire H. (2009a) Geol. Soc Amer. Special Papers 458, 377-396.
[9] Wittmann A., Reimold. W.U., Schmitt R.T., Hecht L. and T. Kenkmann (2009b) Geol. Soc Amer. Special Papers 458, 349-376.
[10] Bottomley R., Grieve R., York D. and Masaitis (1997) Nature 388, 365-368.
[11] Jourdan F., Renne P.R., Reimold W.U. (2009) Earth Planet Sci. Lett. 286, 1-13.
[12] Mak E. K. C., York D., Grieve R.A.F. and Dence M.R. (1976) Earth Planet. Sci. Lett. 31, 345-357.
[13] Winzer, S. R., Lum, R.K.L. and Schuhmann S. (1976) Geochim. Cosmochim. Acta 40, 51-57.

ICDP

Neutron Computed Tomography: Adapted for the Earth Sciences

A.FLAWS[1], K.-U.HESS[2], M.J.MÜHLBAUER[2], B.SCHILLINGER[2], M.SCHULZ[2], E.CALZADA[2], D.B.DINGWELL[1], K.BENTE[3], A.FRANZ[3]

[1]Geo- und Umweltwissenschaften, Ludwig-Maximilians-Universität, Theresienstr. 41, 80333 Munich, Germany
[2]Forschungs-Neutronenquelle Heinz Maier Leibnitz, Technische Universität München, Lichtenbergstr. 1, 85747 Garching, Germany
[3]Institut für Mineralogie, Kristallographie und Materialwissenschaften, Universität Leipzig, Scharnhorststr. 20, 04275 Leipzig, Germany

The application of state-of-the-art detector systems at the Advanced Neutron Tomography And Radiography Experimental System (ANTARES) has led to significant improvements in spatial resolution and contrast for geomaterial imaging. Resolutions of approximately 16 µm → 100 µm are now possible with fields of view of 33 mm → 205 mm, a level which is now comparable with X-Ray Computed Tomography (XCT). Neutron Computed Tomography (NCT) is a non-destructive 3-dimensional imaging method. A collimated neutron beam generated by nuclear fission of ^{235}U passes through the specimen. The neutrons can be coherently/incoherently scattered, or absorbed by atomic nuclei within the sample. The remaining neutron flux is imaged using a scintillation screen placed behind the sample. Nuclear reactions between the neutrons and the scintillator material generate photons which are detected by a Charged Coupled Device (CCD) camera, (fig 1). The sample rests atop a manipulator, which is rotated by a fraction of a degree between each exposure. The resulting set of radiographs is then deconvolved using the inverse Radon transform [1] to

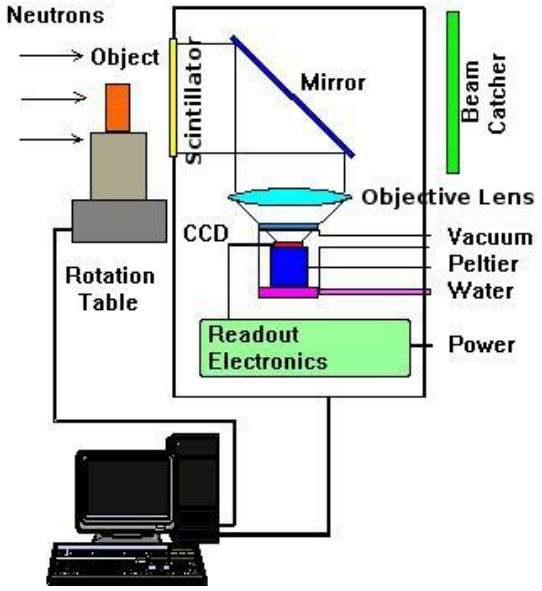

Fig.1: A collimated neutron beam, generated by an experimental nuclear reactor, passes through the specimen. The neutrons can be coherently/incoherently scattered, or absorbed by atomic nuclei within the sample. The remaining neutron flux is imaged using a scintillator screen placed behind the sample. Nuclear reactions between the neutrons and the scintillator material generate photons which are detected by a CCD camera (www.frm2.tum.de).

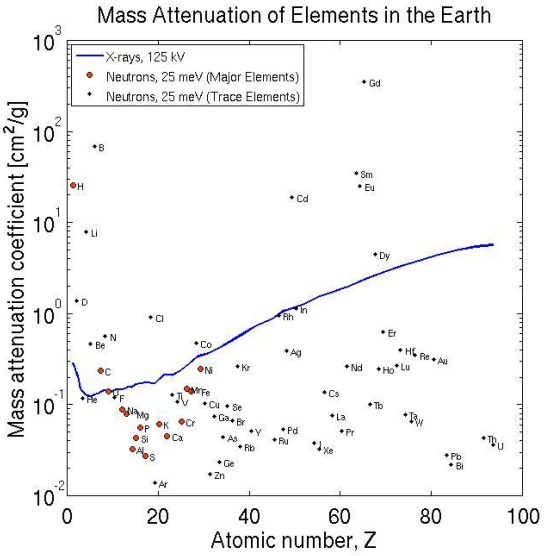

Fig.2: Comparison between X-ray and neutron mass attenuation coefficients as a function of atomic number (modified from Bücherl, 2004). The elements have been divided into major and trace elements.

generate a 3-dimensional image of the local attenuation within the object [2]. The mass attenuation coefficient may vary by several orders of magnitude without any obvious regularity with atomic number. Figure 2 shows a comparison between X-ray and neutron mass attenuation coefficients (modified from [3]) for elements in the Earth (silicate mantle and core). The elements in this figure have been divided into those contributing to 99.88 wt.% of the Earth: O, Mg, Si, Fe, Ca, Al, Na, Cr, Ni, Mn, S, C, H, P, K (sorted by decreasing occurrence in the silicate mantle) and trace elements [4]. What we see is that the attenuation measured by X-ray Computed Tomography (XCT) will be different from that observed by NCT. Hydrogen is a highly attenuating material for NCT, while it is almost invisible for X-rays; the opposite is true for Aluminum. So NCT is particularly well-suited for imaging hydrous minerals (and glasses) as well as hydrogen-bearing fluids [5]. In this way, the two methods provide complementary information about the sample.

Until recently [6], state of the art NCT imaging could only achieve a spatial resolution of 200 µm, which is too coarse to image many of the fine structures of interest to the geosciences, e.g. crystals, cracks, and pores. In this report we detail recent hardware developments at the ANTARES beam line which have turned NCT into a significantly improved tool for the Earth sciences. The application of state-of-the-art scintillator screens now allows us to achieve spatial resolutions as low as 16 µm. Our goal is to demonstrate that NCT can now achieve a comparable spatial resolution to XCT.

One of the current limitations in resolution is given by the scintillation screen itself due to an inherent blurring of the radiograph. Slow neutrons (defined as those with energies less than 0.4 eV) can only be detected by a nuclear reaction. The detection reaction, $^{6}Li + n \rightarrow {}^{3}H + {}^{4}He$, is exothermic with an energy of 4.7 MeV. This energy is distributed as kinetic energy among the reaction products, the ^{4}He and ^{3}H particles. The reaction products are then stopped within the Zinc sulfide (ZnS) scintillation material.

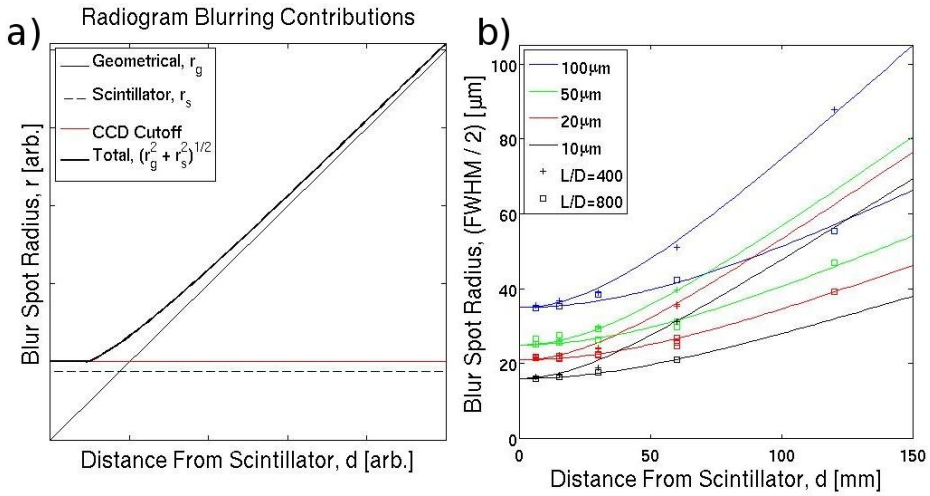

Fig.3: a) The size of the blur spot is the combination of 3 effects: (1) the geometrical spreading which increases with distance to the scintillator screen, d. (2) the stopping length of the reaction products within the screen itself. (3) a cutoff at the CCD camera pixel size. The total is calculated from these components and is represented by the thick black line. **b)** Measured resolution for each of the different scintillators (100 µm, 50 µm,20 µm, 10 µm thickness), indicating the higher resolution of thin scintillators. The 10 µm scintillator resolution may be better than indicated, as 16 µm was the CCD pixel size cutoff for these experiments.

The stopping path length of these particles blurs the location of each neutron event on the screen. For example, the average range in a standard 100 µm thick screen is on the order of 50-80 µm [7]. Since Gadolinium is very sensitive to neutrons, thinned X-ray scintillation screens made of Gadolinium oxisulfide (Gd_2O_2S) can be used for neutron detection. At present, Gd_2O_2S screens are the only neutron sensitive scintillators commercially available in the range of 10 to 20 µm thickness [8]. Spatial resolution is also limited by the geometrical spreading of the beam. This can be mitigated by increasing the beam collimation. We define beam collimation as the ratio of the flight length, L, to pinhole diameter, D. Naturally there is also a limit at the pixel / lens resolution of the CCD camera, as features smaller than this limit cannot be resolved on the radiograph. Figure 3a illustrates these 3 blurring components, and figure 3b shows the measured resolution for each of the different scintillators (100 µm, 50 µm, 20 µm, 10 µm thickness). As we see, thinner scintillators do indeed achieve better resolution. The 10 µm scintillator resolution may be better than indicated, as 16 µm was the CCD pixel size cutoff for these experiments. In this figure it can also be seen that geometrical spreading becomes significant for experimental scenarios with low beam collimation and high sample radius. The sample radius dictates the minimum possible distance of the rotation axis from the scintillator screen, *d*. The blur spot radius climbs more steeply as a function of *d* for lower values of L/D. For example, consider a sample of radius 70 mm imaged by a 20 µm scintillator. The blur spot size doubles from L/D = 800 to 400. At first glance this suggests that the best possible beamline setup is to use very thin scintillators and high beam collimation. However, we must also consider the image quality and exposure time for each radiograph.

Figure 4 shows that thinner scintillators require more exposure time to achieve the same image quality. The coloured squares show measured radiographs, while the lines represent different values of *c* from equation (2). The lower light output from Gd_2O_2S screens results in significantly longer exposure times to achieve the same image quality. We estimate the relative exposure time to be almost an order of magnitude higher for Gd_2O_2S, which is in agreement with previous work [8].

State-of-the-art NCT imaging can now achieve a spatial resolution of less than 20 µm. This can be done using a combination of high beam flux, high collimation and thin scintillator screens. However, this configuration results in either poor contrast or prohibitively long exposure times. For high contrast cases, such between air and rock, this configuration is ideal. For cases where a more subtle contrast between phases is expected, it may be better to use thicker scintillation screens. The optimum configuration must be determined on a case-by-case basis for each sample. High beam collimation is increasingly important for larger samples as the geometrical blurring quickly becomes the dominant effect at higher radii.

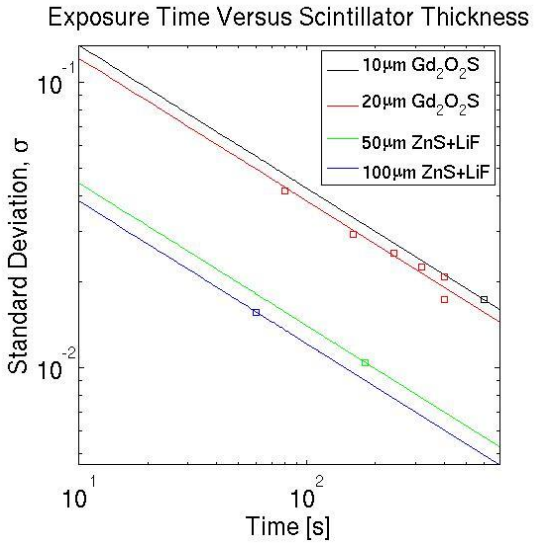

Fig.4: Standard deviation of the radiograph intensity with time for scintillators of different thickness. We clearly see that thinner scintillators require more exposure time to achieve the same image quality. The coloured squares show measured radiographs, while the lines represent different values of c from equation (1). The L/D ratio was 800 for these experiments

New software has been developed to aid in the advanced processing, segmentation and characterisation of tomographic data. This software package has been purpose built for the 3-d tomographic analysis of geomaterials. The unique datafile structure allows the user to explore datasets of many gigabytes in size without any loading times and using very little of the systems resources. This means that research groups can enjoy the benefits of 3-d tomographic analysis without investing in expensive high-end computer hardware. Sub-volumes can be selected from the dataset for advanced processing, rendering and characterisation. A broad range of data processing and morphology tools are available, allowing the user to remove noise and improve the overall image quality. It is possible to overlay and compare multiple datasets using interpolated slicing. For example, this feature can be used to study the relative attenuation of neutron and X-ray computed tomography, highlighting the presence of water. The software also features powerful and reliable segmentation algorithms to convert the dataset into a database of objects at the press of a button (isolating individual crystals, cracks and pores). These algorithms have been designed to cope with the subtle phase contrast and high image noise often present in geomaterial tomography. The database gives each object a unique label and stores information such as its location; volume, mean-attenuation and bounding-box. This database can then be augmented using ellipsoid fitting to characterise the sizes, shapes and orientations of the objects. This allows us to quantitatively study subtle features such as particle anisotropy and flow dynamics. Complex structures, such as crack networks, cannot be well described by an ellipsoid. For these features, a special anisotropy algorithm has been developed to quantify the 3-d anisotropy based on the edge-gradient.

We will now demonstrate the feasibility and complementary nature of the method by showing an example. This example has been selected from work that is in progress and will be presented in its entirety in future publications. Directional drilling at the Unzen Volcano, Japan in 2004 penetrated through the 1991-1995 magma conduit and successfully recovered samples from the lava dike. The dike was sampled about 1.3 km below the volcano's summit vent and intruded into a broader conduit zone that is 0.5 km wide. Unexpectedly, the lava dike sample was altered, suggesting that circulation of hydrothermal fluids rapidly cools the conduit region of even very active volcanoes [9].

Figure 5 shows a scientific drill core taken from Mt. Unzen. It has been taken from a hydrothermally altered ascent path for the volcanic conduit. In figures 5a) and 5b) we show 3 perpendicular cross sections of the drill core taken with XCT and NCT. The contrast between phases for the NCT image is noticeably better than XCT. The XCT reconstruction also suffers from strong image artefacts. This is a well known difference between the two methods. When using poly-chromatic neutron and X-ray spectra, the neutrons usually experience less beam-hardening than XCT. Beam hardening only becomes significant for NCT investigations involving either neutron absorber materials such as: boron, dysprosium, gadolinium, or a high content of water [10]. Hydothermal alteration is visible in the boxed region. In figure 5a) a faint ring-like shadow is visible in the image, possibly indicating a thin crack or grain boundary. The same feature in the NCT reconstruction (fig. 5b) attenuates very strongly, suggesting the presence of hydrogen as "water" (OH-, H_2O) incorporated in the newly developed mineral phases. The Mt. Unzen drill core is decorated with many such features. NCT provides the first opportunity to non-destructively map and study hydrothermal alteration and diffusion in 3-dimensions.

With its greatly improved spatial resolution, NCT now promises to be a useful tool for a much wider spectrum of geomaterial research. It can be used to study the formation of natural glasses and for the characterisation of precious samples from scientific drilling, where shear zones are often decorated with hydrous minerals. Such features can be found, for instance, in samples from the San Andreas Fault Observatory at Depth (SAFOD) and the Kontinentales Tiefbohrprogram der Bundesrepublik Deutschland (KTB), or the hydrothermally altered ascent path for volcanic conduits, e.g. the Mt. Unzen Scientific Drilling Project (USDP). In addition, the visualisation of stepwise rock deformation experiments allows us to observe the development of shear zones under controlled conditions. The availability of samples, both from the laboratory and the field, promises to shed light on the process of high temperature rock cracking and magma failure.

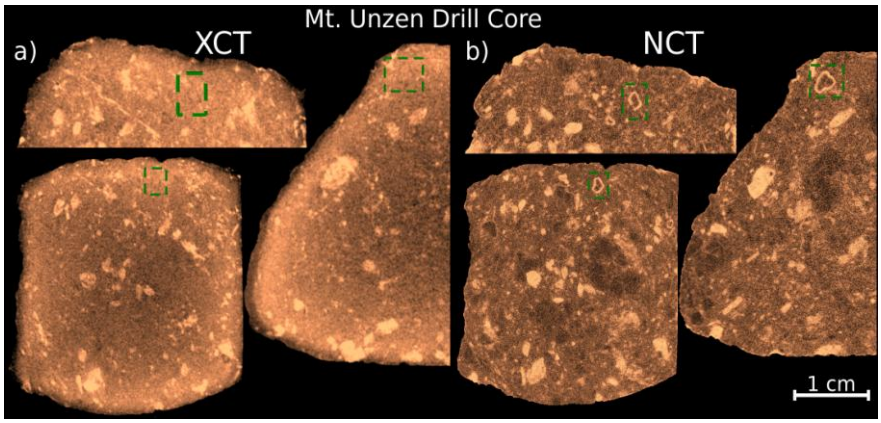

Fig.5: Section through the Mt. Unzen drill core, taken from the hydrothermally altered ascent path of the volcanic conduit. This sample has been imaged with both XCT and NCT. **a)** X-ray attenuation. In the boxed region a faint ring-like shadow is visible, possibly indicating a thin crack or grain boundary **b)** neutron attenuation. In the boxed region the same ring-like feature attenuates strongly, suggesting a high abundance of hydrogen.

References:
[1] Deans, S.R. (2007) Dover Pub. Co.
[2] Banhart, J. (2008) Oxford University Press, USA.
[3] Bücherl, T., et al. (2004) App. Rad. Isotopes, 61(4), 537-540.
[4] McDonough, W.F. (1995) Chem. Geology, 120, 223-253.
[5] Carlson, W.D. (2006) Earth Planet. Sci. Lett., 249(3-4), 133-147.
[6] Frei, G., et al. (2009) Nucl. Instr. Meth. Phys. Res. A, 605, 111-114.
[7] Spowart, A.R. (1969) Brit. J. Non-Destr. Testing, 11(1), 2-4.
[8] Baechler, S., et al. (2002) Nucl. Instr. Meth. Phys. Res. A, 491(3), 481-491.
[9] Kusakabe, K., et al. (1999) Japan J. Volcan. Geotherm. Res., 89(1-2), 231-242.
[10] Vontobel, P., et al. (2006) Physica B, 385–386(2006), 475–480.

IODP

Constraining ocean circulation modes and balancing the 14C-cycle of the last 40 ka based on dating of ultra-small carbonate samples from ODP Site 1063.

J. FOHLMEISTER [1], J. LIPPOLD[1], M. KUCERA[2]

[1] Heidelberger Akademie der Wissenschaften, Im Neuenheimer Feld 229, 69120 Heidelberg
[2] Eberhard-Karls-Universität Tübingen, Fachbereich Geowissenschaften, Sigwartstraße 10, 72076 Tübingen

The Atlantic Meridional Overturning Circulation (AMOC) is believed to have crucial influence on global climate. It affects global temperatures due to the redistribution of heat to the high latitudes and by removing and releasing carbon from or into the deep sea. Reconstructions of past ocean circulation changes suggest a strong link between the strength of AMOC and climate, especially circum North Atlantic temperatures. Additionally, the strength of this ocean circulation in the past seems to be a mayor player in controlling the past atmospheric carbon budget. The atmospheric carbon dioxide increase during the last termination is correlated with a synchronous decrease in atmospheric radiocarbon, suggesting that the ocean released large amounts of old carbon to the atmosphere. This increase in atmospheric CO_2 occurred mainly during Heinrich event 1 (H1) and the Younger Dryas (YD). At these times, the ocean circulation is believed to have been significantly reduced.

The overarching aim of this project is to carry out a comprehensive assessment of changes in past Ocean circulation as well as its impact in the global carbon cycle over the climatic key periods of the last 40,000 years. To this end, we will carry out ^{14}C measurements from planktonic and benthic foraminifera to reconstruct reservoir and ventilation ages. Combined with sortable silt and existing geochemical measurements this will provide a unique multi-proxy record of past ocean circulation carried out on the same sample material. This synergy is only possible due to the uniquely high sedimentation rate of the selected core location (enabling high time resolution), the availability of an ^{14}C independent age model ($CaCO_3$ preservation), and cutting edge AMS dating technique.

We will address the following questions:

To what extend was glacial and interstadial ocean circulation different to the Holocene? Were there Holocene-like conditions during this period, as suggest by new data?

It has been suggested that past ocean circulation has underwent vast variations, thus, significantly influencing global climate. We will reconstruct past ocean circulation by ^{14}C measurements on benthic and planktonic foraminifera from the North-West Atlantic to derive ventilation ages. These measurements will be set in context to additionally measured sortable silt data and existing $^{231}Pa/^{230}Th$ and ε_{Nd} records.

Which influence has ocean circulation on atmospheric radiocarbon?

Several studies reported an increase of ^{14}C reservoir ages during the last deglaciation cold events presumably due to weakening of ocean circulation. We will test this hypothesis by a new record of deep water ventilation covering the time period of the deglaciation extended to the last glacial (e.g. H2). Variations of the reservoir ages will be set in context to variations of atmospheric ^{14}C and the above mentioned proxies from the same location, directly testing the response of the carbon cycle to ocean circulation.

Specifically, the combination of four different proxies of ocean circulation will provide information about provenance (ε_{Nd}) and local current speed of bottom water (sortable silt), deep water export ($^{231}Pa/^{230}Th$) and ventilation age of deep water (^{14}C) in very high time resolution from the same sediments of a key position within the Atlantic. This will give us the opportunity to mutually test the sensitivity of each proxy in terms ocean circulation. As these proxies provide different parameter respectively, several suggested scenarios of past circulation modi can be excluded or supported.

ICDP

The Chew Bahir project – First steps towards a paleoenvironmental reconstruction for South Ethiopia

V. Foerster[1], O. Langkamp[1], F. Schaebitz[1], A. Asrat[2], H. Lamb[3], M. Trauth[4], M. Umer[5]

[1] University of Cologne, Seminar for Geography and Education
[2] University of Addis Ababa, Department of Earth Sciences
[3] University of Aberystwyth, Institute of Geography and Earth Sciences
[4] University of Potsdam, Institute of Earth and Environmental Science
[5] University of Addis Ababa, Department of Geology and Geophysics

Chew Bahir is a tectonically bounded basin in the southern part of the Main Ethiopian Rift and in close proximity to the Omo valley which contains some of the oldest known early modern human sites. Furthermore, Chew Bahir is located southwest of the area of deposition of the Konso Silver Tuff, dated to 154±7 ka BP. The basin has a nearly 5 km thick sediment infill, therewith presenting an opportunity to provide valuable insight into paleoenvironmental changes that could have influenced the evolution and the dispersal of our ancestors crucially.

This poster presents the first results of core studies based on six (9-22m) cores, taken along a NW-SE transect (Fig.1) right across the Chew Bahir basin. These are mainly dominated by lacustrine clays but already show in that early stage of our research that several climate shifts of the late Quaternary are recorded in that climate archive and therefore first results of the past climate conditions in Southern Ethiopia can be outlined. The collected data comprises the lithology and high resolution scans of the

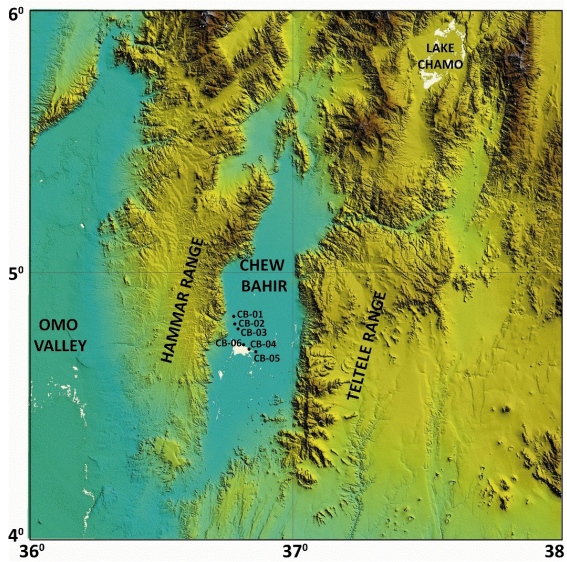

Figure 1: Location of six short (10-22m) cores from a NW-SE transect across the Chew Bahir basin in southern Ethiopa

magnetic susceptibility and X-ray fluorescence as well as first analyses organic matter and microfossils based on smear slides. Particularly a distinct layer of planktonic diatoms that ranges over several meters suggests that the African Humid Period (~ 15-5 ka BP) did have a considerable impact on the area of research. We aim to test hypotheses about the timing, magnitude and synchronicity of the African Humid Period including the possible abruptness, its internal variability and its influence on the biosphere.

Parallel to the applied multi proxy approach, we work on the identification of the sedimentation rate and its variation within the basin, in order to provide the necessary detailed information for the ICDP deep drilling initiative "Hominid Sites and Paleolakes Drilling Project". First AMS results suggest a sedimentation rate of ~0.5 mm per year; hence, a 200,000 year record requires coring to a depth of ~120 m.

IODP

Evolution of Cretaceous oceans - A 55 million year record of Earth's temperature and carbon cycle

O. FRIEDRICH[1], R.D. NORRIS[2], J. ERBACHER[3]

[1]Institut für Geowissenschaften, Goethe-Universität, Altenhöferallee 1, 60438 Frankfurt, Germany. E-Mail: o.friedrich@em.uni-frankfurt.de
[2]Scripps Institution of Oceanography, 9500 Gilman Drive, La Jolla, CA 92093, USA
[3]Bundesanstalt fuer Geowissenschaften und Rohstoffe, Stilleweg 2, 30655 Hannover, Germany

We produced new stable isotope data sets of Cenomanian to Santonian benthic foraminifera from the western equatorial Atlantic (ODP Leg 207) and from the tropical Pacific Ocean (DSDP Sites 305 and 463). Together with literature data our results are compiled into a global isotope compilation, resulting in a continuous benthic $\delta^{18}O$ record for the last 115 Ma. The new 115 million year global compilation of benthic foraminifera $\delta^{13}C$ and $\delta^{18}O$ shows that the Cretaceous super-greenhouse world saw the widespread formation of bottom waters with temperatures >20°C. These bottom waters filled the silled North Atlantic and probably originated as thermocline or intermediate waters in the tropical oceans.

The high temperatures are explained by a lack of cold bottom-water formation, the restricted nature of the North Atlantic, and the formation of warm saline bottom waters that sporadically were formed within epicontinental seas. The parallel positive trend in $\delta^{13}C$ is believed to reflect massive storage of C_{org} during Cretaceous black shale formation. Interestingly, however, $\delta^{13}C$ values of the tropical Atlantic show a similar trend but more negative values. We propose that this reflects a combination of extensive remineralization of ^{12}C and a long residence time due to the sporadic formation of warm and saline waters.

Overall, carbon burial during the Cretaceous OAEs produced a positive $\delta^{13}C$ shift in global carbon reservoirs, but this is not particularly large, especially by comparison with the remarkable late Paleocene carbon maximum. The inter-basin $\delta^{13}C$ gradient was unusually large during the Cretaceous super-greenhouse, probably because the North Atlantic was a silled basin filled with unusually old, poorly-exchanging deep water. The super-greenhouse and massive black shale deposition ended when the Equatorial Atlantic Gateway opened sufficiently to flood the deep North Atlantic with relatively cool polar waters formed in the Southern Ocean. This explanation is supported by the global decrease in $\delta^{13}C$, proposed to reflect the better connection of the former restricted North Atlantic that allows the oxidization of the organic-rich sediments formed in this basin.

ICDP

The Archaean to Palaeoproterozoic transition: U-Pb geochronology of detrital zircons and accompanying provenance analysis of siliciclastic sedimentary rocks from FAR-DEEP

C. GÄRTNER[1], A. P. MARTIN[2], H. BAHLBURG[1], A. LEPLAND[3], A.R. PRAVE[4], D.J. CONDON[2], V. MELEZHIK[3,5], J. BERNDT[6], E. KOOIJMAN[6] AND THE FAR-DEEP SCIENTISTS

[1]Westfälische Wilhelms-Universität Münster, Institut für Geologie und Paläontologie, Münster, Germany
[2]NERC Isotope Geosciences Laboratory, British Geological Survey, Keyworth, UK
[3]Geological Survey of Norway, Trondheim, Norway
[4]School of Geography and Geosciences, University of St. Andrews, UK
[5]University of Bergen, Centre of Geobiology, Bergen, Norway
[6]Westfälische Wilhelms-Universität Münster, Institut für Mineralogie, Münster, Germany

During the Fennoscandian Arctic Russia – Drilling Early Earth Project (FAR-DEEP), which is part of the International Continental Scientific Drilling Program (ICDP), volcano-sedimentary successions of early Palaeoproterozoic age were drilled in Russian Fennoscandia. They represent a 500 Ma interval containing the time period of the Archaean to Palaeoproterozoic transition recovered in rocks from the Pechenga and Imandra-Varzuga Greenstone belts (Kola Peninsula Province), as well as from the Onega basin (Karelian Province, Fig. 1). Our study focused on rocks from the Pechenga and Imandra-Varzuga Greenstone belts.

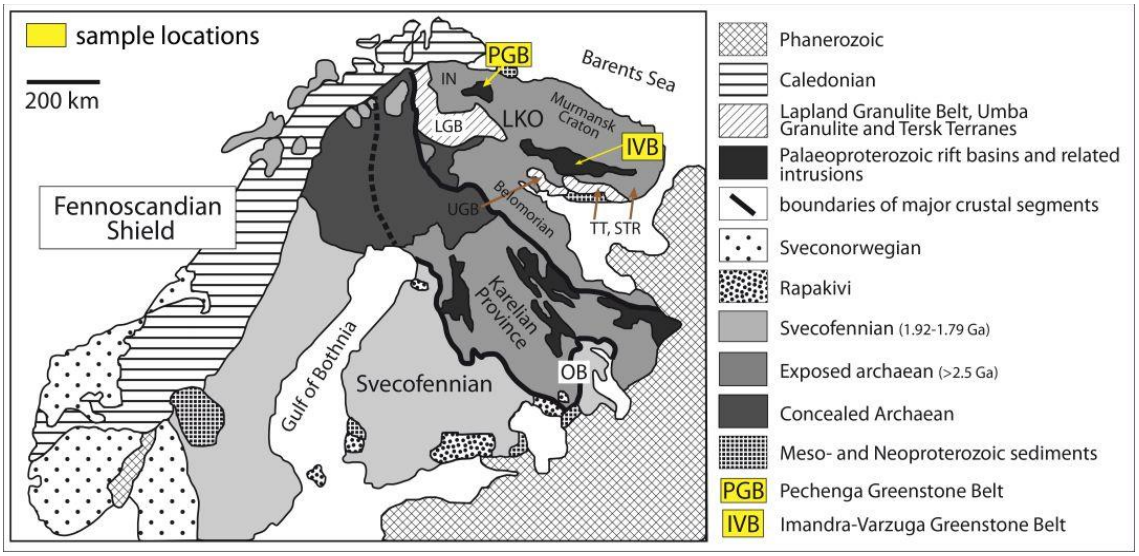

Fig. 1: Map of Fennoscandia, Northern Europe, with sample locations and different provinces and terranes in Fennoscandia, showing potential source areas of detrital zircons (after Daly et al., 2001). Ka - Karelian Province, LKO - Lapland- Kola-Orogen/ Kola Province, OB - Onega Basin, IVB - Imandra-Varzuga Greenstone Belt, PGB - Pechenga Greenstone Belt, STR - Strelna Domain, TT - Tersk Terrane, IN - Inari Terrane, LGB - Lapland Granulite Belt, UGB - Umba Granulite Belt.

Successions in these belts can be correlated, due to their similar stratigraphy. We applied U-Pb geochronology by LA-ICPMS on detrital zircons from siliciclastic sediments to improve age constraints on the duration of three environmental events characterizing the Archaean to Palaeoproterozoic transition. This transition from 2.5-2.0 Ga is marked by several major environmental events and plate tectonic reorganisations, e.g. the break-up of the supercontinent Kenorland (e.g. Melezhik et al., 2005b). Three of the environmental events are considered in this study: 1) the Huronian Glaciation, which is the first known worldwide glaciation from 2.45-2.22 Ga (Young et al., 2001), 2) the Lomagundi-Jatuli Event, occurring from 2.3-2.06 Ga (Karhu & Holland, 1996; Shields & Veizer, 2002, Melezhik et al., 2007), characterized by a large positive excursion of $\delta^{13}C$ in sedimentary carbonates and following the glaciation, and subsequently 3) the Shunga Event, which was the first deposition of C_{org}-rich sediments, so-called "shungites" (Melezhik et al., 2005a). Furthermore, the provenance of the sedimentary rocks will be investigated.

Fourteen core samples of sandstones, greywackes, siltstone and tuffs from five formations in the Pechenga and Imandra-Varzuga Greenstone belts were analysed, as well as three field samples from the Kolasjoki Sedimentary Formation (Fm.) in the Pechenga Greenstone Belt. The sampled formations were chosen due to their stratigraphic position below or above characteristic successions like glacial diamictites, isotopically heavy carbonates or C_{org}-rich sediments.

LA-ICPMS analysis focused on the outer zone of the zircons to obtain the youngest age of the grain, that should constrain the maximum depositional age of the host rock. CL images were used to avoid laser spots in different growth zones. Some zircons showed a high content of common lead (>1.5%), which effects the reliability of the U-Pb ages, and were discarded. Discordant zircons (on average 22% per sample) were excluded from the interpretation of age constraints, but were used to assess the timing of Pb-loss pointing to crystallization ages around 2.5 Ga or a metamorphic overprint around 550 Ma. Zircons with the youngest ages determined by LA-ICPMS analysis were subsequently analysed by ID-TIMS, employing the 'chemical abrasion' pre-treatment method to minimise Pb-loss, to further constrain age data in several formations.

The results of detrital zircon dating for all samples cover an age range from 3.5 to 1.9 Ga with one prominent age group between 2.9-2.6 Ga in all but two samples (Fig. 2). The youngest zircons from individual samples vary due to their stratigraphic position. Age constraints for the Huronian glaciation have been reported from the eponymous Huronian Supergroup in Canada (Young et al., 2001) and from the Pretoria Group in South Africa (Hannah et al., 2004). In the Imandra-Varzuga Greenstone Belt, the Seidorechka Sedimentary Fm. is underlying glacial deposits of conglomerates and varve-like sediments with dropstones of the Polisarka Sedimentary Fm. Age data from the Seidorechka Sedimentary Fm. yielded a maximum depositional age of 2.43 Ga, interpreted as close to the beginning of the Huronian glaciation. These ages were also reproduced by ID-TIMS analysis. Pb-Pb ages for metasediments from the Polisarka Sedimentary Fm. obtained a maximum depositional age of 2.34 Ga, which is interpreted to mirror the end of the glaciation. Younger ages around 2.2 Ga, being in accordance with the upper age limit for the glaciation reported from Young et al. (2002), could not be confirmed by ID-TIMS analysis, they yielded Archaean ages instead. We therefore interpret the next youngest zircon ages of 2.34 Ga as coninciding with previous data from South Africa for the onset of the third of three observed glacial events (Hannah et al., 2004) and with age data for the Polisarka and Neverskrukk Fm. (Sarioli Group) by Melezhik et al. (1997). Hence, maximum depositional ages of 2.37 Ga for the Neverskrukk Fm. from the Pechenga Greenstone Belt also seem to match with these previous ages.

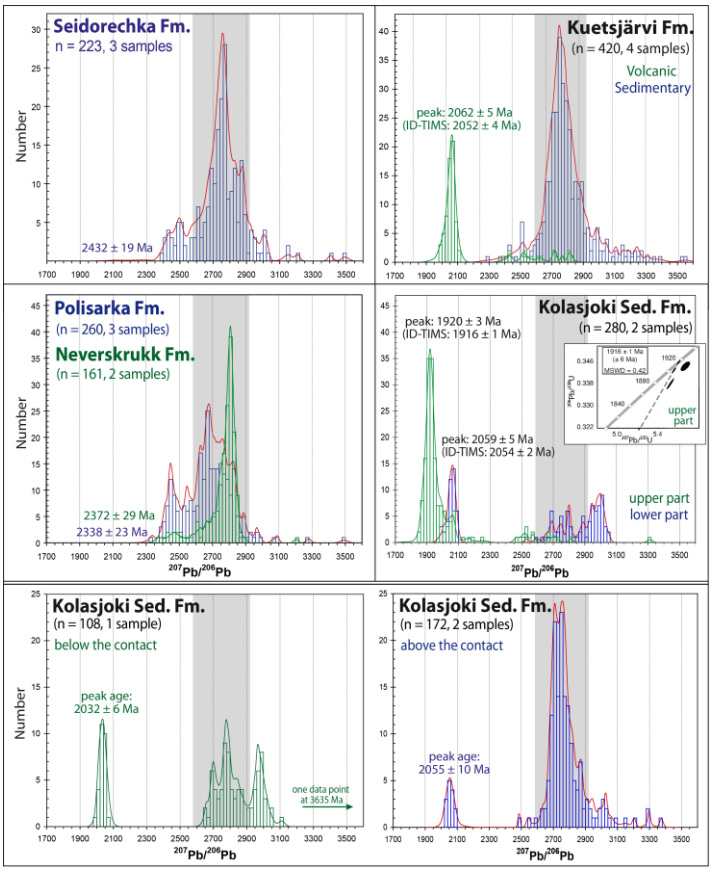

Fig. 2: Histograms showing U-Pb ages for all formations with peak ages, analysed by LA-ICPMS. The main age group of 2.9-2.6 Ga is marked by grey colours. The small rectangle shows young ages of 1.92 Ga from the Kolasjoki Sedimentary Fm. specified by ID-TIMS.

The Kuetsjärvi Sedimentary Fm. in the Pechenga Greenstone Belt contains isotopically heavy sedimentary carbonates which are associated with the Lomagundi-Jatuli positive $\delta^{13}C$ excursion. The Kuetsjärvi Sedimentary Fm. yielded a youngest age of 2.4 Ga pointing to a beginning of the event, in coincidence with previous age constraints of 2.36 Ga reported by Shields & Veizer (2002). Furthermore, the obtained ages are similar to the underlying Neverskrukk Fm. and the correlated Polisarka Sedimentary Fm. from the Imandra-Varzuga Greenstone Belt. In contrast, the sample from the middle Kuetsjärvi Volcanic Fm. that overlies Kuetsjärvi sediments yielded youngest ages of 1.94 Ga and a clear age peak at 2.1-2.0 Ga, with an average of 2.06 Ga, verified by ID-TIMS analysis.

To constrain the end of the Lomagundi-Jatuli Event and the beginning of the Shunga Event, two samples from the Kolasjoki Sedimentary Fm., stratigraphically above isotopically heavy carbonates and below C_{org}-rich sediments, have been analysed. The distance between these samples in the stratigraphic profile is about 200 m and they are separated by a thick carbonate succession. Interestingly, they yielded remarkable differences in the distribution of their detrital zircon ages. The sample below the carbonates (lower part, Fig. 2) provided a young age group of 2.1-1.99 Ga with the peak age of 2.06 Ga. This indicates the maximum depositional age and considering the error, it is in accordance with the middle Kuetsjärvi Volcanic Fm. and previous age determinations form these sediments (2.06 Ga; Melezhik et al., 2007) This points to a beginning of the Shunga Event < 1.99 Ga. In contrast, the sample above the carbonates (upper part, Fig. 2) has a clear age peak at 2.0-1.85 Ga (average = 1.92 Ga).

As U-Pb data from the Pilgujärvi Volcanic Fm., overlying the Kolasjoki Fm., gave an age of 1.97 ± 0.005 Ga (Hanski, 1992), which is inferred to constrain the sampled stratigraphic level, these young zircon ages of our samples do not fit into the hitherto established stratigraphy. Therefore, we repeated the age determination of some of the 'young' zircon grains by ID-TIMS analysis to refine the age of this youngest zircon population to around 1.916 ± 0.001 Ga (Fig. 2). Obtaining the same ages indicates, in addition to an eventually later onset of the Shunga Event, that the stratigraphical succession might not be as conformable as previously thought, and suggesting the presence of a potential unconformity between these two samples. An alternative hypothesis is that the zircons formed in association with later metamorphic overprinting. We therefore attempted to test these two ideas and refine the age relationships in this part of the succession by obtaining three more field samples located above and below the assumed unconformity, which is characterised by a conglomerate layer and lithological change. Detrital zircon ages of all three samples provided many discordant ages pointing to zero-age lead loss and a crystallization age of c. 2.05 Ga (i.e. a distribution comparable to a sample dated previously, which comes from strata beneath the purported unconformity), as well as to a metamorphic overprint around 550 Ma. Youngest concordant zircon ages of c. 2.05 Ga are interpreted as maximum depositional ages. To specify the origin of the younger ages and to define the contact between rocks of different ages,

additional samples will be processed for U-Pb geochronology.

Concerning the provenance, the detrital zircon ages of 2.9-2.6 Ga, which occur in most of the samples, point to orogenic processes during the generation of the Fennoscandian Shield as a source for the analysed zircons. Collisional and accretional processes during the Saamian (3.1-2.9 Ga) and Lopian orogeny (2.9-2.6 Ga) recycled detritus from the surrounding exposed Archaean basement, e.g. from the southern Karelian Province, the Kola Province and the northern Murmansk Craton (Fig. 1). From c. 2.5-2.35 Ga rifting of Archaean crust started, as indicated by layered mafic intrusions in northern Fennoscandia, leading to the break-up of Kenorland and the initiation of rift basins. Rifting continued until 2.1 Ga (Daly et al., 2006). Subsequently, new continental crust was formed and older crust was reworked by accretionary and collisional orogens at 2.0-1.8 Ga (Lahtinen et al., 2008). Zircons of such younger events of 2.1-1.85 Ga (Kuetsjärvi and Kolasjoki fms.) may be linked to this period of crustal growth in Fennoscandia, including also accretion of microcontinents and juvenile arcs, like the Umba Granulite Belt, Strelna Domain, Inari and Tersk Terrane (Lahtinen et al., 2009; Fig. 1). To constrain information about the source rocks and to permit a more detailed definition of the source areas, further provenance studies are necessary. At the moment we are awaiting results of whole rock geochemical analyses and Hf isotope analysis on dated zircons to further delimit provenance areas of the siliciclastic sedimentary rocks.

References:

Daly , J.S., Balagansky, V.V., Timmerman, M.J., Whitehouse, M.J., de Jong, K., Guise, P., Bogdanova, S., Gorbatschev, R., Bridgwater, D. (2001): Ion microprobe U-Pb zircon geochronology and isotopic evidence for a trans-crustal suture in the Lapland-Kola Orogen, northern Fennoscandian Shield. Precambrian Research, 105, p. 289-314.

Hannah, J.L., Bekker, A., Stein, H.J., Markey, R.J., Holland, H.D. (2004): Primitive Os and 2316 Ma age for marine shale: implications for Paleoproterozoic glacial events and the rise of atmospheric oxygen. Earth and Planetary Science Letters, v. 225, p. 43-52.

Hanski, E.J., (1992): Petrology of the Pechenga ferropicrites and cogenetic, Ni-bearing gabbro-wehrlite intrusions, Kola Peninsula. Geological Survey of Finland Bulletin, v. 367, 192 p.

Karhu, J.A. & Holland, H.D. (1996): Carbon isotopes and rise of atmospheric oxygen. Geology, v. 24, p. 867-870.

Lahtinen, R., Garde, A.A., Melezhik, V. (2008):Paleoproterozoic evolution of Fennoscandia and Greenland, Episodes, v. 31, no. 1, p. 20-28.

Lahtinen, R., Korja, A., Nironen, M., Heikkinen, P. (2009): Palaeoproterozoic accretionary processes in Fennoscandia, The Geolocigal Society, London, Special Publications, v. 318, p. 237-256.

Melezhik , V.A., Huhma, H., Condon, D.J., Fallick, A.E., Whitehouse, M.J. (2007): Temporal constraints on the Paleoproterozoic Lomagundi-Jatuli carbon isotopic event. Geology, v. 35, no. 7, p. 655-658.

Melezhik, V.A., Kump, L., Strauss, H., Fallick, A.E., Hanski, E., Hawksworth, C.J., Lepland, A., Prave, A., Philippov, N. (2005a): Fennoscandian Arctic Russia - Drilling Early Earth Project (FAR – DEEP). Full proposal to the International Continental Scientific Drilling Program.

Melezhik, V.A., Fallick, A.E., Hanski, E., Kump, L., Lepland, A., Prave, A., Strauss, H. (2005b): Emergence of the Modern Earth System during the Archean-Proterozoic Transition. GSA today, 15, p. 4-11.

Melezhik, V.A., Fallick, A.E., Makarikhin, V.V., Lyubtsov, V.V. (1997): Links between Palaeoproterozoic palaeogeography and rise and decline of stromatolites: Fennoscandian Shield, Precambrian Research, v. 82, p. 311-348.

Shields, G. & Veizer, J. (2002): Precambrian marine carbonate isotope database: Version 1.1. Geochemistry, Geophysics, Geosystems, v. 3, p. 1-12.

Young G.M., Long, D.G.F., Fedo, C.M., Nesbitt, H.W. (2001): Paleoproterozoic Huronian basin: product of a Wilson cycle punctuated by glaciations and a meteorite impact. Sedimentary Geology, 141-142, p. 233-254.

ICDP

Seismic reflection data from Lake Issyk-Kul, Kyrgyzstan

A. C. GEBHARDT[1], M. DE BATIST[2], L. NAUDTS[2], L. DE MOL[2]

[1]Alfred Wegener Institute of Polar and Marine Research, 27568 Bremerhaven, Germany
[2]Renard Centre of Marine Geology, University of Gent, 9000 Gent, Belgium

The planned project (Start: November 2011) is a key contribution to investigations at Lake Issyk-Kul, Central Asia, located in an intramontane basin of the Tien Shan mountains. The lake has formed in a tectonically active region (W-E striking major thrust zones N and S of the lake) and has experienced lake level changes of up to >400 m, which is well documented in two large delta systems at the W and E end of the lake. The lake contains the sediments of the past up to several million years, and has been proposed as a future target for deep drilling within ICDP.

The lake's modern surface level is at 1607 m above sea level, maximum depth in the central basin of the lake is roughly 670 m, and the total water volume is around 1736 km^3. The lake is elongated with 180 km in west-east and 60 km in south-north direction. With a surface area of 6232 km^2, Lake Issyk-Kul is the second largest lake in the higher altitudes (De Batist et al., 2002). The lake is characterized by two large delta areas at its western and eastern end, with the deltaic area being as wide as up to 60 km in the eastern and 40 km in the western part, and by steep slopes at the northern and southern shore with only a rather narrow shallower shelf area. At the delta areas, the shelf is divided into two parts, one shallower part with water depths down to 110 m with an average inclination of 0.5°, and the other with water depths between 110 and 300 m and an average inclination of 1° (De Mol, 2006). Incised channels of up to 2-3 km width and 50 m depth are visible on both the eastern and the western shelf, but are limited to the shallower part of the shelf. They lie in the prolongation of modern river mouths at the eastern part of the lake, and are quite likely connected to former in- and outlets of the Chu river at the western delta (De Mol, 2006). This river presently bypasses the lake. The deeper part of the shelf is characterized by a series of structural terraces that were interpreted as ancient shorelines.

First seismic data of lake Issyk-Kul were acquired in 1982 by the Moscow University with a total of 31 profiles across the lake. Unfortunately, only a few profiles were ever published (Stavinsky et al., 1984). In 1997, a second seismic survey of the lake was carried out by the group of Marc De Batist (Gent, Belgium) in cooperation with the Royal Museum of Central Africa (Tervuren, Belgium) and the SBRAS (Siberian Branch of the Russian Academy of Sciences, Novosibirsk, Russia). This survey resulted in 62 profiles (990 km) acquired with a 500 J multi-electrode sparker and a single-channel streamer. In 2001, a third survey was carried out by the same group, concentrating on some key locations identified from the 1997 campaign. These profiles are mainly located (a) in the vicinity of the city of Sadji Kai and (b) in the eastern delta of the lake (Fig. 2). In addition, a sidescan sonar survey was carried out in 2002 at several places along the slopes of Lake Issyk-Kul.

A third seismic survey is planned for summer/autumn 2011 to complete the seismic survey and to refine the planned drill site positions for future deep drilling within the framework of ICDP. Main tasks will be detailed investigations of four areas already chosen as potential drill sites at the eastern delta. In addition, refraction profiles are planned to image the deeper structures including the bedrock morphology of the lake.

Previous seismic surveys by our Belgian colleagues were so far only investigated by two master students (Naudts, 2002; De Mol, 2006), and data are not published yet. The seismic profiles shall be reinterpreted, and the study of the delta sequences and their internal structures will result in a refined lake level curve. This will allow to compare the lake's paleoclimate record with other global and regional records, e.g. from the Tarim Basin loesses located south of the Tien Shan mountains. Latest Pleistocene sediments cropping out at the northern and southern shore were interpreted as resulting from earthquakes and point at tectonic activity. Other tectonic features such as faults and folds are quite likely found in the lake sediments and will be mapped in the seismic profiles. This will help to reconstruct the tectonic history of the lake and its basin.

References:
De Batist, M., et al., 2002. Bathymetry and sedimentary environments of Lake Issyk-Kul, Kyrgyz Republic (Central Asia): a large, high-altitude, tectonic lake. In: J. Klerkx and B. Imanackunov (Editors), Lake Issyk-Kul: Its Natural Environment. NATO Science Series, Series IV: Earth and Environmental Sciences. Kluwer Academic Publishers, Dordrecht, pp. 101-123.
De Mol, L., 2006. Reconstructie van meerspiegelschommelingen in het Issyk-Kul Meer (Kirgizië) op basis van de geomorfologische en seismostratigrafische analyse van rivierdelta's. M.Sc. Thesis, University of Gent, Gent, 144 pp.
Naudts, L., 2002. Seismisch-stratigrafische interpretatioe van een complex deltasysteem in het Issyk-Kul Meer, Kyrghyzstan. M.Sc. Thesis, University of Gent, Gent, 133 pp.

IODP

Sedimentology of late Quaternary coral reefs, Great Barrier Reef, Australia (IODP 325)

E. GISCHLER[1], R. BOURILLOT[2], A.W. DROXLER[3], H. KAN[4], C. SEARD[5], J.M WEBSTER[6], Y. YOKOYAMA[7], AND EXPEDITION 325 SCIENTISTS[8]

[1]Goethe University, Frankfurt, Germany
[2]Université de Bourgogne, Dijon, France
[3]Rice University, Houston TX, USA
[4]Okayama University, Okayama, Japan
[5]Cerege, Aix-en-Provence, France
[6]University of Sydney, NSW, Australia
[7]University of Tokyo, Tokyo, Japan
[8]http://www.eso.ecord.org/expeditions/325/part325.php

IODP expedition 325 drilled 34 holes along four traverses across the Great Barrier Reef of Australia thereby penetrating some 750 m of reefal deposits of the late Quaternary in water depths ranging from 40-170 m. The expedition on the Greatship Maya took place during 12 February - 1 April and was followed by the onshore science party in Bremen, Germany, during 1-16 July 2010 involving 28 scientists from 9 countries. IODP expedition 325 has three major objectives. They include (1) a reconstruction of deglacial sea level for the period 20-10 kyrs BP with a focus on MWP 1A and 1B events, (2) to use the variability of sea surface temperature and sea-level change on reef growth patterns including drowning, and (3) to quantify paleoclimatic change in high-resolution by sampling skeletons of massive corals during the same time window. According to preliminary age dating, the majority of cores cover the time period of about 25-10 kyrs BP. These late Pleistocene sections appear diagenetically unaltered and comprise coralgal boundstone, coralgal-microbial boundstone, skeletal grainstone and rudstone, and unconsolidated sand. In five cores taken in depths of 40-85 m water depths at three traverses, older Pleistocene (>25 Kyrs BP) reefal deposits were recovered in lower core sections. Lithologies include skeletal grainstone to rudstone, some packstone, coralgal boundstone, and few occurrences of coral-microbial boundstone. Usually, they exhibit clear evidence of diagenetic modification in the meteoric realm, such as caliche phenomena, neomorphism, dissolution vugs, and low magnesium calcite cement growth.

References:
Expedition 325 Scientists, 2010. Great Barrier Reef environmental changes: the last deglacial sea level rise in the South Pacific: offshore drilling northeast Australia. *IODP Preliminary Report,* 325. doi:10.2204/iodp.pr.325.2010.
Webster, J.M., Yokoyama, Y., and Cotterill, C., 2009. Great Barrier Reef environmental changes: the last deglacial sea level rise in the South Pacific: offshore drilling northeast Australia. IODP Scientific Prospectus, 325. doi:10.2204/iodp.sp.325.2009.

ICDP

Microbial activity and abundance in sediments Lake Van (Turkey), first results from ICDP Project PALEOVAN

C. GLOMBITZA, J. KALLMEYER

University of Potsdam, Institute for Earth and Environmental Sciences, Geomicrobiology Group, Karl-Liebknecht Str. 25, Haus 27, 14476 Potsdam

Studies during the past two decades have demonstrated the importance of microbial life in the deep subsurface. So far, most studies focused on life in the subseafloor, only few dealt with terrestrial environments. With the exception of some very few and solitary projects, lacustrine sediments received almost no attention.

In summer 2010 the ICDP drilling operation at Lake Van (Eastern Anatolia, Turkey) recovered long sediment cores at two sites (Northern Basin and Ahlat Ridge). At both sites, sample material was obtained from undisturbed core catchers and selected whole round cores, ranging in depth from the sediment surface down to 140 mblf (meters below lake floor). Coring was mainly carried out by hydraulic piston coring, providing largely uncontaminated samples, as seen by the porewater composition in the sample. However, certain intervals with thick layers of volcanic ash required extended core barrel and rotary coring, the obtained cores were at least partially infiltrated by drilling fluid. Additionally, short gravity cores of 75 cm length were retrieved at both sites, providing the undisturbed sediment-water interface, which is too liquid to be recovered by hydraulic coring.

Radiotracer experiments for the quantification of sulfate reduction, anerobic oxidation of methane and methanogenesis were initiated on site, using the mobile Geomicrobiology Laboratory BugLab , owned by GFZ

Potsdam. Porewater was squeezed and split between the different working groups. Samples for cell enumeration and anion porewater analysis were preserved for analysis at the University of Potsdam.

Although the distance between the two sites is only approx. 7 km, they exhibit significant differences, both in porewater geochemistry and in microbial abundance and activity. The results of the cell enumeration are strikingly different to marine sediments. Whether these trends are the result of sedimentological changes or lateral fluid flow remains unclear at the moment, as a full sedimentological description of the cores is still lacking. Cell abundance appears to be slightly higher at the Northern Basin site, at which sulfate reduction rates measured by radiotracer are also generally higher than at Ahlat Ridge. Despite the higher sulfate reduction rates at the Norther Basin site, sulfate penetrates down to 40 mblf, about twice as deep than at Ahlat Ridge. This is most probably caused by the lateral influx of a saline brine between 20 and 40 mblf.

The significant biogeochemical differences between both sites indicate that lacustrine sediments are very sensitive to changes in sedimentary and organic matter input. Studies of the deep subsurface of lake sediments are still in their infancy but due to strong biogeographical gradients they may offer a unique chance to study the effects of even small physicochemical changes in on deep subsurface life.

IODP

The marine Ca isotope budget in response to Eocene carbonate accumulation events

N. GUSSONE[1], K. RABE[1] AND B.M.A. TEICHERT[2]

[1]Westfälische Wilhelms-Universität Münster, Institut für Mineralogie, Münster, Germany
[2]Westfälische Wilhelms-Universität Münster, Institut für Geologie und Paläontologie, Münster, Germany

Sediment samples recovered during IODP-Expeditions 320 and 321 (Pacific Equatorial Age Transect - PEAT) retrieved well preserved core material from the Equatorial Eastern Pacific providing an excellent archive for reconstructions of climate changes during the Cenozoic, which is known for its times of extreme climates and rapid climate changes. One of the main aims of this expedition was to enhance the understanding of carbon cycling, in particular the interplay of carbonate compensation depth (CCD), $CaCO_3$-dissolution and productivity. First results revealed several pronounced fluctuations in $CaCO_3$ concentrations (Lyle et al. 2010, Pälike et al. 2010), refining the carbonate accumulation events (CAE) previously described by Lyle et al. (2005). These events indicate not only dramatic changes in the carbonate but also in the Ca budget of the ocean. An ideal tool to study changes in the Ca budget is the Ca isotopic composition of the paleo-seawater which is recorded in marine biogenic carbonates.

In this study, we investigate the Eocene carbonate accumulation events CAE- 2 to 4 (~ 45-38 Ma), to better understand the role of Ca in terms of input, redistribution and output. Sediments samples were characterized in respect to their calcareous microfossil content, to select the best suited Ca isotope archive. We choose the benthic foraminifer *Nuttalides* spp. (mainly *N. trympi*) from the size-fraction >63µm. Foraminifer tests were hand-picked under the binocular and preservation was verified with scanning electron microscopy. The isolated foraminifers were cleaned from attached fine-grained material, organics and coatings following the method described in Gussone and Filipsson (2010). Calcium isotope ratios were analysed by Thermal Ionisation mass spectrometry. First results show that the $\delta^{44/40}Ca$ values of the benthic foraminifer-tests are significantly different during times of a deeep-lying carbonate compensation depth (corresponding to CAE) and times of a shallow CCD. Rather constant values are characteristic for the CAE, while heavier and more variable $\delta^{44/40}Ca$ values are typical for times of a shallow CCD. These results shed a new light on the previous understanding of the marine Ca budget.

References:

Gussone N. and Filipsson H. L. (2010) Calcium isotope ratios in calcitic tests of benthic Foraminifers, Earth and Planetary Science Letters 290, 108-117.

Lyle M. W., Olivarez Lyle A., Backman J., and Tripati A. (2005) Biogenic sedimentation in the Eocene equatorial Pacific: the stuttering greenhouse and Eocene carbonate compensation depth, in Proc. ODP, Sci Res 199, edited by Lyle, M., Wilson, P., Janecek, T.R., and Firth, J., College Station, TX, Ocean Drilling Program: 35 pp.

Lyle M., Pälike H., Nishi H., Raffi I., Gamage K., Klaus A., and the IODP Expeditions 320/321 Scientific Party (2010) The Pacific Equatorial Age Transect, IODP Expeditions 320 and 321: Building a 50-Million-Year-Long Environmental Record of the Equatorial Pacific Ocean. Scientific Drilling 9, 4-15

Pälike H., Nishi H., Lyle M., Raffi I., Gamage K., Klaus A., and the Expedition 320/321 Scientists, 2010. Proc. IODP, 320/321: Tokyo (Integrated Ocean Drilling Program Management International, Inc.). doi:10.2204/iodp.proc.320321.2010

ICDP

Seismic images of the tremor region at the San-Andreas-Fault system around Cholame (USA)

S. GUTJAHR[1], S. BUSKE[2]

[1]Freie Universität Berlin, Department of Geophysics, Malteserstrasse 74-100, 12249 Berlin, stine@geophysik.fu-berlin.de

[2]TU Bergakademie Freiberg, Institute of Geophysics and Geoinformatics, 09596 Freiberg, buske@geophysik.tu-freiberg.de

We present seismic images of the Coast Ranges and the San-Andreas-Fault system in Central California including the non-volcanic tremor region around Cholame. The seismic images have been obtained by applying advanced seismic imaging techniques (Fresnel volume migration, Buske et al., 2009) to the industry seismic reflection data set WSJ-6. The reflection profile was acquired in 1981 over a distance of about 180 km from Morro Bay to the Sierra Nevada foothills running across several prominent fault systems, e.g. the Rinconada fault in the western part as well as the San Andreas fault in its central part. The latter includes the region of increased non-volcanic tremor activity near Cholame, as reported by several authors.

We are able to to image the crust and the uppermost mantle down to approximately 40 km depth by recorrelating the original field data to 26 seconds two-way traveltime. A 3D tomographic velocity model derived from local earthquake data (Thurber et al., 2006, Lin et al., 2010) was used. The imaging technique was implemented in 3D taking into account the true shot and receiver locations. The imaged subsurface volume itself was divided into three separate parts to correctly account for the significant kink in the profile line near the San Andreas fault. The most prominent features in the resulting images are areas of high reflectivity down to 30 km depth in particular in the central western part of the profile corresponding to the Salinian Block between the Rinconada fault and the San Andreas fault. Southwest of the San Andreas surface trace a broad zone of high reflectivity is located at depths between 20 km to 35 km. Non-volcanic tremor events that were located by Nadeau et al. (2009) appear southwest of the San Andreas fault below the seismogenic zone down to depths of approximately 30 km. Most of the tremors are located at the top of the high reflectivity body and below a strong southwest dipping reflector that may be interpreted as the base of the Salinian Batholith.

In the area of the San Joaquin Valley along the eastern part of the profile line slightly west dipping sediments show up between depths of 2 km to 10 km. These sediments are folded and faulted below the region of the Kettleman Hills. Steeper west dipping reflectors can be identified below the uppermost sedimentary layers down to depths of approximately 20 km.

The resulting images are compared to existing interpretations (Trehu and Wheeler, 1987; Bloch et al., 1993) and discussed in the frame of the suggested non-volcanic tremor locations in that area.

References:

Bloch, R. B., von Huene, R., Hart, P. E.,Wentworth, C.M. (1993). Style and magnitude of tectonic shortening normal to the San Andreas fault across Pyramid Hills and Kettleman Hills South Dome, California. Bull. Seism. Soc. Am., 105, p.464–478.

Buske, S., Gutjahr, S., Sick, C. (2009). Fresnel Volume Migration of single-component seismic data. Geophysics, Vol.74, No.6, WCA47-WCA55.

Lin, G., Thurber, C. H., Zhang, H., Hauksson, E., Shearer, P. M., Waldhauser, F., Brocher, T. M., Hardebeck, J. (2010). California Statewide Three-Dimensional

Seismic Velocity Model from Both Absolute and Differential Times. Bull. Seism. Soc. Am., 100, pp.225-240.

Nadeau, R. M., Guilhem, A. (2009). Nonvolcanic Tremor Evolution and the San Simeon and Parkfield, California Earthquakes. Science, Vol325.

Thurber, C., Zhang, H., Waldhauser, F., Hardebeck, J., Michael, A., Eberhart-Phillips, D. (2006) Three-Dimensional Compressional Wavespeed Model, Earthquake Relocations, and Focal Mechanisms for the Parkfield, California Region. Bull. Seism. Soc. Am., 96,S38-S49

Trehu, A. M., Wheeler, W. H. (1987) Possible evidence in the seismic data of profile SJ-6 for subducted sediments beneath the Coast Ranges of California, USA. Open-File Report 87-73

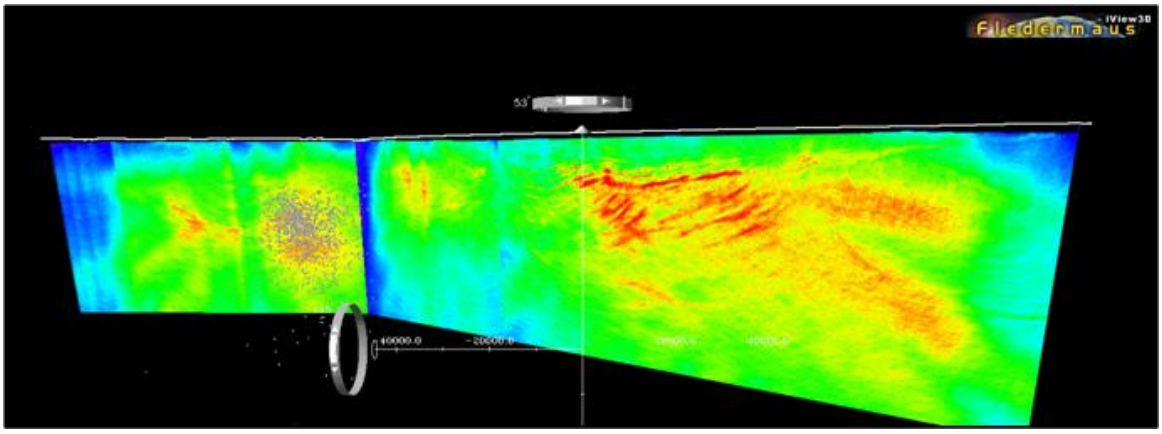

Fig. 1: 3D perspective view of obtained seismic reflection images and tremor locations

ICDP

Nam Co - a potential ICDP drilling site on the Tibetan Plateau?

T. HABERZETTL[1], G. DAUT[1], S. DOBERSCHÜTZ[1], T. KASPER[1], G. GLEIXNER[2], P. FRENZEL[3], R. HETZEL[4], K. REICHERTER[5], A. SCHWALB[6], T. SCHWENK[7], V. SPIEß[7], J. WANG[8], L. ZHU[8], R. MÄUSBACHER[1]

[1] Physical Geography, Institute of Geography, Friedrich-Schiller-University Jena, Löbdergraben 32, 07743 Jena, Germany
[2] Max Planck Institute for Biogeochemistry, Jena, Germany
[3] Institute of Geosciences, Friedrich-Schiller-University Jena, Burgweg 11, 07749 Jena, Germany
[4] Institut für Geologie und Paläontologie, Westfälische Wilhelms-Universität Münster, Corrensstr. 24, 48149 Münster, Germany
[5] Neotektonik und Georisiken, RWTH Aachen University, Aachen, Germany
[6] Institute of Environmental Geology, Technische Universität Braunschweig, Pockelsstr. 3, 38106 Braunschweig, Germany
[7] Department of Geosciences, University of Bremen, P.O. Box 330440, 28334 Bremen, Germany
[8] Chinese Academy of Sciences, Institute for Tibetan Plateau Research, 18, Shuangqing Rd., P.O. Box 2871, Beijing, 100085, China

Lake Nam Co (4718 m a.s.l., 30°45'N and 90°30'E) is a deep terminal lake located on the central Tibetan Plateau, China. The depth of this lakes assures that it did not desiccate during dry phases as paleoshorelines all arround the lake attest major lake level variations in the past. In this contribution we try to assess the potential of lake Nam Co for paleoenvironmental reconstruction in this case with an emphasis on magnetostratigraphical, sedimentological and geochemical methods.

Precise age control is a prerequisite for reliable paleoenvironmental research. However, almost all lakes on the Tibetan Plateau are affected by a reservoir effect due to carbonatious catchments. A radiocarbon date of bulk sediment from the top of a gravity core yielded an age of 1420 ±40 BP for the sediment/water interface. In order to test if this value can be constantly extrapolated back in time we established a reservoir corrected chronology with this value and ^{210}Pb and ^{137}Cs measurements. Subsequently, we compared inclination and declination data calculated from NRM to the CALS3k.3 (Donadini et al. 2009) and the CALS7k.2 (Korte et al. 2005) geomagnetic field models (Kasper et al. in prep.) which currently provide the best representation of the late Holocene geomagnetic field (Donadini et al. 2009). This showed excellent accordance for the period covered by the gravity core, i.e., ~4000 cal BP. This leads to the conclusion that the presented chronology is well suited for further paleoenvironmental investigations. This is important as this area lacks well-dated records. On the other hand, our data also support the validity of the CALS-models for the past ~4000 cal BP on the Tibetan Plateau, where paleomagnetic data are very scarce and also demonstrate that sediments from Nam Co are good recorders of paleomagnetic variations.

Further investigations on this gravity core covering the last 4 ka showed that minerogenic input proxies (e.g., Ti), grain sizes and the presence of Monohydrocalcite are well suited for the reconstruction of hydrological variations at Nam Co which seem to be coupled to the Indian Ocean Summer Monsoon (IOSM; Kasper et al. in prep.). According to our analyses on this short core, high monsoonal activity prevailed between 4000-1900 cal BP as well as between 1500-1200 cal BP. This pattern shows a very good correlation to the variability of the IOSM as recorded in a peat bog much further north-east of Nam Co (Kasper et al. in prep.).

Besides the mentioned short core four other gravity cores and one piston core (~10.5 m) were recovered at a water depth of 93 m in September 2008. A wide spectrum of sedimentological, geochemical and mineralogical investigations was carried out on all cores using a similar approach for the long piston core as for the gravity core. With 23 000 cal BP this is one of the longest records of lake sedimentation available on the Central Tibetan Plateau. Magnetostratigraphic analyses and 23 OSL measurements are currently underway to support the established chronology. Preliminary investigations reveal only minor variations from ~23 000 cal BP to ~13 800 cal BP, indicating stable conditions of the sedimentary regime. At ~13.8 ka cal BP the system obviously changes. Strong monsoonal pulses are reported from the Arabian Sea and dated to 13.5 ka cal BP, and 13.0 – 12.5 ka cal BP (Sirocko et al. 1993, Overpeck et al. 1996). These temporary confined upwelling events can probably be linked to an intensified moisture transport reaching the Tibetan Plateau. A ~13 800 cal BP event is clearly visible within our sequence, allowing the connection of monsoonal pulses and a sedimentary response of Lake Nam Co, interpreted as a hydrological signal of a freshwater pulse, coupled with enhanced fluvial transport of clastic material (e.g., Ti, Al). However, an even more pronounced increase in monsoonal activity can be obeserved after 9 300 cal BP. This provides the most prominent signal of paleoenvironmental change in the whole record. Records from the Arabian Sea indicate an abrupt increase in monsoon intensity from 10.0 to 9.5 ka cal BP (Overpeck et al. 1996), 9.9 ka cal BP and 8.8 ka cal BP (Sirocko et al. 1993), pointing to strong connection between marine processes in the Arabian Sea and the lake response on the Tibetan Plateau. Subsequent weak phases of monsoon, as documented in the Arabian Sea, are not visible within our geochemical record regarding the 2σ error range of our analysis. Only after 5 400 cal BP a similar trend can be observed.

In conclusion, the record from Nam Co is perfectly suited for paleoenvironmental as well as paleomagnetic studies. This natural archive seems to record the occurrence as well as the intensity of the IOSM in a comparably high resolution. As expected linkages exist between the source area of this monsoon type. However, there are also some dissimilarities which need to be investigated in future.

References

Donadini, F., M. Korte & C. G. Constable (2009) Geomagnetic field for 0-3 ka: 1. New data sets for global modeling. *Geochemistry Geophysics Geosystems*, 10.

Kasper, T., T. Haberzettl, S. Doberschütz, G. Daut, R. Mäusbacher, J. Wang, L. Zhu, V. Wennrich & N. Nowaczyk (in prep.) Monsoon variability for the past 4 ka derived from high-resolution analyses of sediments from Lake Nam Co, central Tibetan Plateau.

Korte, M., A. Genevey, C. G. Constable, U. Frank & E. Schnepp (2005) Continuous geomagnetic field models for the past 7 millennia: 1. A new global data compilation. *Geochemistry Geophysics Geosystems*, 6.

Overpeck, J., D. Anderson, S. Trumbore & W. Prell (1996) The southwest Indian Monsoon over the last 18000 years. *Climate Dynamics*, 12**,** 213-225.

Sirocko, F., M. Sarnthein, H. Erlenkeuser, H. Lange, M. Arnold & J. C. Duplessy (1993) Century-scale events in monsoonal climate over the past 24,000 years. *Nature*, 364**,** 322-324.

ICDP

The geochemical record of the ~51 ka Laguna Potrok Aike sediment sequence

A. HAHN[1], P. KLIEM[1], C. OHLENDORF[1], B. ZOLITSCHKA[1] AND THE PASADO SCIENCE TEAM[2]

[1] Geopolar, Institute of Geography, University of Bremen, Germany (anhahn@uni-bremen.de)
[2] PASADO Science Team as cited at: http://www.icdp-online.org/front_content.php?idcat=1494

During the lake deep drilling campaign PASADO in 2008 (ICDP expedition 5022) more than 500 m of lacustrine sediments were recovered from the maar lake Laguna Potrok Aike. From Site 2 a composite profile (5022-2CP) with the total length of 106 m was assembled. Discrete 2 cm thick samples from 5022-2CP were analyzed for total inorganic carbon (TIC), total organic carbon (TOC) and total nitrogen (TN) content at 8-16 cm spatial resolution using an elemental analyzer (EuroEA). Furthermore, the major element composition was assessed with a spatial resolution of 5 mm using an ITRAX XRF core scanner (COX analytical systems, Croudace et al., 2006). Prior to the interpretation of XRF-scanning data, some methodological aspects have to be taken into consideration.

The grain size of Laguna Potrok Aike sediments is often relatively coarse. This is known to affect count rates of XRF-scanning (Croudace et al. 2006). Moreover, fluctuations in sediment mineralogy, particle size and water content affect the mean atomic number of the sediment volume excited by the X-ray beam of the XRF core scanner. These effects are recorded as differences in the intensity of the scatter peaks (Rayleigh and Compton scattering) which therefore can be used to correct for mineralogy, particle size and water content (Potts et al. 1997). Despite the application of a Rayleigh scatter correction there are still indications for the necessity of a calibration using element concentrations determined on discrete samples and possibly water content corrections using the element Cl (Tjallingi et al. 2007).

Principal component analysis (PCA) is a useful tool for analyzing large datasets like element counts from XRF-scanning and this approach helps to reduce noise and/or element-specific biases (Shanahan et al. 2008). A PCA was applied to normalized counts of all elements if their profiles contain an interpretable geochemical signal defined by low noise, high variability and a sufficiently high number of counts.

The sharp boundary between the carbonate-bearing and the carbonate-free depositional systems at 15,6000 cal. BP (18.82 m composite depth) dominates the PCA of 5022-2CP marking the transition from the Glacial to the Late Glacial. Holocene and Late Glacial sediments can easily be distinguished by elements that are indicative of organic-rich sediments (Br, Cl) or of calcite (Ca). Ca in the Holocene sediments of Laguna Potrok Aike can be attributed to calcite precipitation (Haberzettl et al. 2005). Br and Cl have been related to organic sediment components (Br) containing Cl-bearing pore water (Thomson et al. 2006). For Laguna Potrok Aike a correlation is only detected between TOC and Br (R^2 = 0.64). Glacial sediments are characterized by elements that represent terrigenous sediment fluxes (Fe, Zn, Al, Si, K, Ti, Zr, Mn, Cu) (Cohen 2003).

Variations in the geochemistry of the clastic glacial sediments have been explored by excluding all data points from the PCA that are linked to the sediments above 18.82 mcd . As expected, elements indicative of clastic input (Fe, Zn, Al, Si, K, Ti, Cu) are responsible for positive scores in the first component and indicators of organic matter (Br) and calcite (Ca) have little importance. The accumulation of Mn along with the bulk of elements related to clastic input was probably inhibited by reducing conditions during glacial high lake levels conditions (Haberzettl et al. 2005). With regard to the PCA of the entire composite profile the loadings of Cl, Zr and to a lesser extent of Sr become inversed. During the Glacial Cl probably reflects the effect of highly porous sand layers and is therefore correlated with lithogenic elements. Sr is most common in biogenic carbonates; its strong negative loadings could therefore be attributed to occasional remains of calcareous organisms in the sediments. Negative loadings of the immobile element Zr may indicate that clastic input during the Glacial is characterized by fresh physical weathering products rather than by increased transport.

References:

Cohen A.S., (2003), Paleolimnology–the history and evolution of lake systems. Oxford University Press, Oxford.

Croudace, IW, Rindby, A. & Rothwell, R.G., (2006), ITRAX: description and evaluation of a new multifunction X-ray core scanner. In: Rothwell, R.G. (ed.) New Techniques in Sediment Core Analysis. Geological Society, London, Special Publications, 267, 51–63.

Haberzettl, T., Fey, M., Lücke, A., Maidana, N., Mayr, C., Ohlendorf, C., Schäbitz, F., Schleser, G. H., Wille, M., and Zolitschka, B. (2005). Climatically induced lake level changes during the last two millennia as reflected in sediments of Laguna Potrok Aike, southern Patagonia (Santa Cruz, Argentina). Journal of Paleolimnology 33, 283-302.

Shanahan, T. M., J. T. Overpeck, J. B. Hubeny, J. King, F. S. Hu, K. Hughen, G. Miller, and J. Black (2008), Scanning micro-X-ray fluorescence elemental mapping: A new tool for the study of laminated sediment records, *Geochem. Geophys. Geosyst.*, 9, Q02016, doi:10.1029/2007GC001800.

Thomson, J., Croudace, I.W. & Rothwell, R.G., (2006), A geochemical application of the ITRAX scanner to a sediment core containing eastern Mediterranean sapropel units. In: Rothwell, R.G. (ed.) New Techniques in Sediment Core Analysis. Geological Society, London, Special Publications, 267, 65–77.

Tjallingii, R., U. Ro¨hl, M. Ko¨ lling, and T. Bickert (2007), Influence of the water content on X-ray fluorescence corescanning measurements in soft marine sediments, Geochem. Geophys. Geosyst., 8, Q02004, doi:10.1029/2006GC001393.

Potts, P.J., Webb P.C., Williams-Thorpe O., (1997), Investigation of a correction procedure for surface irregularity effects based on scatter peak intensities in the field analysis of geologiclal and archaeological rock samples by portable x ray fluorescence spectrometry. J Anal Atom Spect 12, 769-776.

IODP

Tropical climate and vegetation response during the Last Glacial Maximum and Heinrich event 1 from two Earth System Model simulations

D.N. HANDIANI[1,2], A. PAUL[1,2], L.M. DUPONT[1], X. ZHANG[1,2], R. RACHMAYANI[1,2]

[1] MARUM - Center for Marine Environmental Sciences, University of Bremen, Leobener Strasse, 28359 Bremen
[2] FB-Geowissenschaften,Universität Bremen, Klagenfurter Straße, 28359 Bremen

The climate of last glacial is known to be different from the the present climate, and it is also marked by abrupt climate changes. Among these are the so-called Heinrich events, which correlate with massive iceberg discharges from the Northern Hemisphere ice sheets. These events likely caused changes in the circulation of the North Atlantic Ocean, which in turn - according to pollen assemblages from marine sediment cores - affected land areas as remote as the Tropics. Pollen records from Northeast Brazil are dominated by dry vegetation (e.g. shrubs and grassland) during the end of the last glacial period, but indicate a more humid period with robust dry forest and Atlantic rain forest around 16.5 and 15 kyrs BP. In contrast, in West Africa (Angola and southern Congo), pollen records show no response during Heinrich event 1 (~14.6–16. 3 kyrs BP).

To better understand these pollen records, we performed simulations of the Last Glacial Maximum (LGM, ~21 kyrs BP) and Heinrich event 1 (HE1, ~18–15 kyr BP) with an Earth System Model of Intermediate Complexity (the University of Victoria Earth System-Climate Model, UVic ESCM) and a comprehensive Earth System Model (the NCAR Community Climate System Model version 3, CCSM3). Both models contain a Dynamic Global Vegetation Model (DGVM), which can simulate changes in the vegetation distribution in response to changes in climate.

When comparing HE1 to the LGM, both models showed a cooling in the Northern Hemisphere due to the slowdown of the meridional overturning circulation caused by a freshening of the high-latitude Atlantic Ocean. At the same time the Southern Hemisphere experienced a slight warming. In both models, the tropical cooling was less than the cooling in the middle and high latitudes; however, the change was larger in the CCSM3: the surface temperature in the Tropics changed up to 2 ºC in the CCSM3 and up to 0.6 ºC in the UVic ESCM. The CCSM3 simulated a strong reduction in precipitation in Central America (e.g. Mexico, Costa Rica, Nicaragua) and northeast South America, whereas in the UVic ESCM, the reduction was more pronounced in West Africa and the Sahel region. In both models, the vegetation distribution changed accordingly: The CCSM3 simulated a reduction of tree cover and an increase of grasses in Central America and northeast South America, while the UVic ESCM arrived at an increase in grasses and shrubs in West Africa and the Sahel region. Large differences in the vegetation distribution as simulated by these two models occurred in South America, where a strong increase of trees and decrease of grasses in the CCSM3 had no counterpart in the UVic ESCM.

It turned out that no single model could reproduce the changes in the vegetation distribution as recorded in the pollen data. Rather, the CCSM3 results were similar to the Northeast Brazil pollen record, while the UVic ECSM results were similar to the Angola and southern Congo pollen records.

ICDP

Development of GESEPs new National Drillcore Data Repository

U. HARMS[1], R. CONZE[1], J. KLUMP[1],J. ERBACHER[2], H.J. WALLRABE-ADAMS[3], G. WEFER[3]

[1] GFZ Potsdam
[2] BGR Hannover
[3] MARUM Bremen

Samples and data retrieved from underground by drilling are of overarching long-term importance for geological research. This is due to the high acquisition costs and due to the scarcity of pristine samples from critical regions of the earth system and from *in situ* processes. Accordingly, detailed core handling and curation processes have been developed for various types of samples such as for soft sediment cores, ice cores or crystalline rocks. As far as possible, many scientific drilling projects follow the routines and protocols developed over the past decades. In addition, several institutions around the world, especially the Integrated Ocean Drilling Program, IODP, have set up sample curation facilities which ensure appropriate long-term storage and availability to the community at large.

However, a major gap in core sample facilities exists for continental drill cores. Main reasons for this are of legal nature, where national jurisdiction complicates core export, and of technical nature, as sample types, sizes and investigation routines vary considerably. Therefore, there is to date no core repository for the International Continental Scientific Drilling Program, ICDP even though cores from lacustrine sediments require unified sampling routines and constant low temperatures. Furthermore, continental and marine drilling-related research have develop many ties through joint projects, but a unified sample and data access does still not exist.

The German Scientific Earth Probing Consortium, GESEP e.V. has been founded to address this issue and to strengthen data and sample availability. In partnering with the MARUM in Bremen and the Federal Institute for Geosciences and Natural Resources, BGR, in Berlin-Spandau, GESEP has established a national core repository for continental cores. In order to allow for retrieving sample information, data, and associated metadata access via internet, GESEP is developing an overarching internet portal and a related database. Both will serve to make the wealth of data and samples available and assure their long-term availability for the community at large. It is intended to incorporate several existing software components developed for the large research programs, to assign International Geo Sample Numbers (IGSN) as unique sample identifiers, and to integrate the distributed sample repositories.

ICDP

Understanding the interplay of past environmental settings and biotic evolution – biodiversity of ancient Lake Ohrid

T. HAUFFE, K. SCHREIBER, C. ALBRECHT, T. WILKE

Department of Animal Ecology and Systematics, Justus Liebig University Giessen, Heinrich-Buff-Ring 26-32 (IFZ), 35392 Giessen, Germany.

The oldest European lake, ancient Lake Ohrid, is situated on the Balkan Peninsula, and was chosen to be the place for a future International Continental Scientific Drilling Program (ICDP). The SCOPSCO-Program (Scientific Collaboration on Past Speciation Conditions in Lake Ohrid) aims to unravel the onset of a lacustrine environment of Lake Ohrid and to reconstruct major environmental fluctuations over the past 2-3 million years. Thus, it will be the first drilling campaign worldwide that is primarily conducted to integrate information on geological and biological evolution of a specific ecosystem to unravel processes that have led to the extraordinary degree of endemic biodiversity. Preliminary studies have revealed lake-level fluctuations of up to 60 m during the last glacial-interglacial cycle (Lindhorst et al., 2010), climate dependent occurrence of micro algae (Reed et al., 2010), predictive power of fossil gastropod communities concerning the depth of drilling cores (Albrecht et al., 2010), and spatial variation of sediment features (Vogel et al., 2010). Yet little is known about the distribution of biodiversity and possible geological and environmental factors influencing its temporal and spatial scales.

Biodiversity, the variation among living organisms or ecosystems, is a multi-factorial concept. Ecosystem diversity can be assessed by a combination of α-diversity (i.e. species richness at one location), β-diversity (i.e. rate of change in species distribution along environmental gradients), and γ-diversity (i.e. the total number of species of the ecosystem). Lake Ohrid is a suitable model to study such spatial variability of biodiversity because of its well-defined physiogeographical boundaries. The Lake Ohrid Basin is classified into vertical zones (the lake, several spring systems, small rivers/pools and horizontal layers within Lake Ohrid), which are characterized by different hydrological features. The model character of Lake Ohrid for biodiversity studies is furthermore constituted by the high degree of endemic biodiversity, limiting the impact of widespread species, and the heterogeneous distributions of species and environmental factors in general.

We were using information from 224 collecting points for one of the most species-rich groups in Lake Ohrid, the Gastropoda to: (i) provide a comprehensive assessment of the gastropod diversity, (ii) identify potential faunal subdivisions of the Ohrid Basin utilizing a multivariate framework, (iii) provide a spatially-explicit description of biodiversity patterns within the lake proper including the identification of biodiversity hotspots, and (iv) assess the differential contribution of processes based on speciation, extinction or dispersal limitation of species or processes acting via environmental factors such as water depth.

We have found that the total number of 68 species of gastropods, with 73.5% of them being endemic does not substantially differ from the numbers provided decades ago (Hauffe et al., 2010). Additionally, we did not find significant differences in the frequency of species occurrences at sites. We do see a moderate trend indicating a decrease in endemic species and an increase of widespread species. Many endemic species are very common and relatively unconfined regarding their depth preferences. In contrast, non-endemic species are mostly rare species. Our study shows a strong correlation between the hydrological features of the Ohrid Basin and the spatial distribution of gastropod diversity. The variation of these community assemblages is likely to be explained by hierarchically structured effects acting on different scales. Large scale effects such as type of water body and lake depth do, indeed, cause broad differences in gastropod assemblages, resulting in little faunal similarity among vertical layers and horizontal zones. In the case of water bodies this is probably caused by the phenomenon of eco-insularity. Accordingly, well adapted ancient lake organisms may out-compete most invading species but are probably inferior outside the native lake. Small scale effects like environmental gradients typically cause minor differences in biodiversity distributions on a smaller spatial scale. However, a significant proportion of community variation seems to be driven by the dispersal capacity and evolutionary history of the species alone. Similar processes are assumed to have shaped the distribution of species richness with a highly heterogeneous distribution at the uppermost layer of Lake Ohrid. Biodiversity hotspots were found near lacustrine spring fields and at the feeder springs of Lake Ohrid. Those areas are known to be most affected by lake-level changes during the last glacial-interglacial cycle. Thus, the paradigm of long-term environmental stability causing high levels of biodiversity seems to be questionable in this case.

In order to reach a general conclusion on impacts of ecosystem instability that might have shaped the extraordinary rich biodiversity of Lake Ohrid, a deep-time perspective on environmental fluctuations is necessary. Such insights will be provided by the upcoming SCOPSCO drilling project at Lake Ohrid.

References:

Albrecht, C., Vogel, H., Hauffe, T., and Wilke, T.: Sediment core fossils in ancient Lake Ohrid: testing for faunal change since the Last Interglacial, Biogeosciences, 7, 3435-3446, 2010, doi:10.5194/bg-7-3435-2010.

Hauffe, T., Albrecht, C., Schreiber, K., Birkhofer, K., Trajanovski, S., and Wilke, T.: Spatially explicit analysis of gastropod biodiversity in ancient Lake Ohrid, Biogeosciences, 8, 175-188, 2011, doi:10.5194/bg-8-175-2011.

Lindhorst, K., Vogel, H., Krastel, S., Wagner, B., Hilgers, A., Zander, A., Schwenk, T., Wessels, M., and Daut, G.: Stratigraphic analysis of lake level fluctuations in Lake Ohrid: an integration of high resolution hydro-acoustic data and sediment cores, Biogeosciences, 7, 3531-3548, 2010, doi:10.5194/bg-7-3531-2010.

Reed, J. M., Cvetkoska, A., Levkov, Z., Vogel, H., and Wagner, B.: The last glacial-interglacial cycle in Lake Ohrid (Macedonia/Albania): testing diatom response to climate, Biogeosciences, 7, 3083-3094, 2010, doi:10.5194/bg-7-3083-2010.

Vogel, H., Wessels, M., Albrecht, C., Stich, H. B., and Wagner, B.: Spatial variability of recent sedimentation in Lake Ohrid (Albania/Macedonia), Biogeosciences, 7, 3333-3342, 2010, doi:10.5194/bg-7-3333-2010.

ICDP

Large-scale obsidian emplacement at Obsidian Cliff, Yellowstone (USA)

R.M. HEISTEK[1], Y. LAVALLÉE[1], C. DE CAMPOS[1], K.-U. HESS[1], K. HEIDE[2] AND D.B. DINGWELL[1]

[1] Department of Earth and Environmental Sciences, Ludwig-Maximilians Universität München (LMU), Theresienstrasse 41/III, 80333 München, Germany
[2] Department of Geosciences, Friedrich-Schiller-University Jena, Burgweg 11, 07749 Jena, Germany

During its eruptive history, the large volcanic system at Yellowstone has experienced large outpouring of silicic material, both explosively and effusively. The trigger mechanism for explosive activity in Yellowstone are enigmatic, as the magmas are considered to be relatively too hot (850 - 1100°C) to be explosive (Branney et al., 2008). The key to this enigma may reside in the concentration of volatiles present in the magmas. Here, we provide a study of magmatic volatiles present in a rhyolitic obsidian lava flow named Obsidian Cliff. Outcrop exposure at Obsidian Cliff (Yellowstone) exposes the interior of a thick rhyolitic lava flow erupted about 180,000 years ago. The rhyolitic lava flow has a thickness of 60m and extends for 6km down Obsidian Creek. The quenching of this obsidian trapped parts of the volatiles species present in the magma, thus providing the opportunity to study their rheological effects on eruption dynamics at Yellowstone. In detail, we investigate the volatile content, cooling rate and glass transition temperature of 15 samples across a 10m vertical section of the lava flow.

Bulk rock analysis using X-ray fluorescence technique, as well as glass analysis with an electron microprobe, show obsidian cliff to be a slight calc-alkaline rhyolite with 78% SiO2. In these analyses, only minor chemical variations were observed along the outcrop. Differential Scanning Calorimetric (DSC) analysis and the GRD model (2008) showed a glass transition (Tg) ranging between 730°C and 760°C (at a heating rate of 20K/min). The DSC data does not show systematic variations in Tg along the stratigraphy, but rather a 35°C range in Tg. The non-systematic variation in Tg of a glass with homogenous composition of major elements may be explained by the different volatiles in the melt phase. Directly Coupled Evolved Gas Analyzing System (DEGAS) data reveal that the obsidian contains H2O, OH, CO2, HF, F, SO2 and Cl. Detailed analysis are currently underway in order to distinguish the volatile content along the length of the cliff and shed light on the emplacement of this large obsidian lava flow.

IODP

Geotechnical and sediment physical characterization of glacial-interglacial cycles on a late Miocene to Holocene shelf-slope transect (Canterbury Basin, New Zealand)

D. A. HEPP[1], S.KREITER[1]

[1] MARUM – Center for Marine Environmental Sciences and Faculty of Geosciences, University of Bremen

Integrated Ocean Drilling Program (IODP) Expedition 317 aimed to understand the relative importance of global sea level changes and local tectonic and sedimentary processes in controlling continental margin sedimentary cycles (Fulthorpe et al., 2011). One focus was on the sequence stratigraphy of the late Miocene to recent, when the global sea level change was dominated by glacioeustasy.

Four shelf and upper slope sites were cored in the Canterbury Basin on the eastern margin of the South Island of New Zealand in shallow to moderate water depths (85-344 m). Upper Miocene to recent sedimentary sequences were cored in a landward to basinward transect of three sites on the continental shelf (Sites U1353, U1354, and U1351) and one on the continental slope (Site U1352).

The transect holds a stratigraphic record of depositional cycles across the shallow-water environment most directly affected by relative sea-level change. Seismic sequence boundaries have been correlated to lithological boundaries in cores from each site. Additionally, Sites U1353 and U1354 provide a high resolution record of recent glacial cycles in a continental shelf setting. The Canterbury Basin middle Miocene to recent sedimentary sequence correlates generally well with the New Jersey Margin sequence drilled during Ocean Drilling Program (ODP) Leg 174A (Christie-Blick et al., 2003). The Canterbury Basin IODP Expedition 317 complements ODP Leg 181 drilling (Carter et al., 2004), which focused on drift development at the more oceanic part of the Eastern New Zealand oceanic sedimentary system.

Lithologic-seismostratigraphic correlations provide insights into the origin of the seismically identified sequences. Nineteen middle Miocene to Pleistocene seismostratigraphic sequence boundaries were recognised along this continental margin transect. The interpretation of these erosional unconformities is limited due to the poorly defined time gaps comprising the missing intervals. A nearly continuously sedimentary record is crucial for, e.g., age-depth estimation, correlation with lithological sequences among each site, and two dimensional backstripping. In intervals with poor core recovery where “missing strata” were indicated, an underestimation of sedimentation rates and thicknesses of lithological sequences is unavoidable. This again constrains the potential of the interpretation of sedimentary processes in controlling continental margin sedimentary cycles on the basis of a reconstructed initial sedimentary record.

An approach to bridge these gaps in the sedimentary record is the reconstruction of these “missing strata” using the reaction of clayey sediments to changing overburden stresses. The compaction characteristics of clayey sediments are determined by the maximum effective overburden stress, they experienced since their depostion.

This allows to constrain the former overburden and ultimatly the thicknesses of "missing strata" from geotechnical tests, e. g. from one-axial consolidation tests performed in oedometers. At present 56 representative whole-round samples from above and below the unconformities are tested one axially. Shipboard measurements of sediment strength (fall cone penetrometer, automated vane shear) and whole-round logging data (magnetic susceptibility, natural gamma radiation) are used to constrain the interpretation of the geotechnical tests and lithological and sequence analyses. Preliminary results show that the compaction history can be traced horizontally across a shelf-slope transect and vertically down to a sediment depth of more than 980 m. This confirms the applicability of the oedometer tests in deeper sediments and exclude the possibility of diagenetic alteration of the geotechical properties.

The results and additional analyses of physical property, down-hole logging and sedimentological shipboard data will support the quantitative analysis of subsidence and sea level change in Canterbury Basin.

References:
Carter, R.M., McCave, I.N., and Carter, L., 2004. Leg 181 synthesis: fronts, flows, drifts, volcanoes, and the evolution of the southwestern gateway to the Pacific Ocean, eastern New Zealand. In Richter, C. (Ed.), Proc. ODP, Sci. Results, 181: College Station, TX (Ocean Drilling Program), 1–111. doi:10.2973/odp.proc.sr.181.210.2004.
Christie-Blick, N., Austin, J.A., Jr., and Malone, M.J. (Eds.), 2003. Proc. ODP, Sci. Results, 174A. doi:10.2973/odp.proc.sr.174a.2003.
Fulthorpe, C.S., Hoyanagi, K., Blum, P., and the Expedition 317 Scientists, 2011. Proc. IODP, 317: Tokyo (Integrated Ocean Drilling Program Management International, Inc.). doi:10.2204/iodp.proc.317.2011.

IODP

Masked millennial-scale climate fluctuations in SW Africa during the last glacial

I. HESSLER[1], L. DUPONT[1], D. HANDIANI[1], S. STEINKE[1], J. GROENEVELD[2], U. MERKEL[1], A. PAUL[1]

[1] MARUM-Center for Marine Environmental Sciences, University of Bremen, Bremen, Germany
[2] Alfred Wegener Institut for Polar and Marine Research, Bremerhaven, Germany

Large and abrupt shifts between extreme climatic conditions characterise the last glacial period. They are not restricted to the North Atlantic, but transmitted by the atmospheric and oceanic circulation. It has been suggested that the abrupt shifts associated with North Atlantic Heinrich Stadials (HS) are the effect of a reduction of the strength of the Atlantic meridional overturning circulation. According to the hypothesis of interhemispheric climate coupling a reduced overturning circulation leads to the accumulation of heat in the South Atlantic. Additionally, HS are thought to influence the vegetation composition on land due to the linkage between ocean and atmosphere.

To investigate the connection between tropical African vegetation and oceanic conditions during HS, we reconstructed the vegetation development in Angola and the sea surface temperatures (SST) of the eastern South Atlantic using marine sediments of ODP Site 1078 (11°55'S, 13°24'E). Combining both high-resolution records from the same site we can directly study variations in the marine and terrestrial realm and their interactions.

Mg/Ca SSTs of *Globigerinoides ruber* (pink) were 1°-2°C warmer SSTs during HS. SST obtained from *Globigerina bulloides*, however, do not show much response during HS. We suggest that changes in the *G. bulloides* SST indicate changes in the position of the Angola-Benguela Front and the Benguela upwelling system. In contrast, *G. ruber* represents water masses of the Angola Current which are restricted north of the front. Surprisingly, the prevalent vegetation development on the African subcontinent reflects no changes during HS. Indeed, it seems that the vegetation response during HS is disguised by mechanisms that cancel out each other. Modelling experiments conducted with an Earth system climate model including a dynamical vegetation component corroborate our conclusion.

IODP

The early stage of Shatsky Rise plateau formation: Isotope-geochemical characterization (Sr, Nd, Pb and Hf) of volcanic rocks from IODP site U1347 (Shatsky Rise, Northwest Pacific)

K.HEYDOLPH[1], J.GELDMACHER[2], K.HOERNLE[1]

[1] Leibniz Institute of Marine Sciences, IFM-GEOMAR-East Shore Campus, Wischhofstr. 1-3. D-24148 Kiel, Germany
[2] Integrated Ocean Drilling Program, Texas A&M University, 1000 Discovery Drive, College Station, Texas 77845-9547

The submarine Shatsky Rise plateau, a unique large igneous province (LIP) in the northwest Pacific Ocean ca. 1500 km east of Japan, is the only large intraoceanic plateau worldwide, which formed during the Late Jurassic to Early Cretaceous. Numerous reversals of the Earth's magnetic field during this time period caused alternating magnetic lineation in the ocean floor, which allowed a detailed reconstruction of the original tectonic setting. Accordingly the three main volcanic edifices Tamu, Ori and Shirshov massif formed along a southwest - northeast trending, rapidly spreading triple junction. However, Shatsky Rise shows characteristics for both a ridge-controlled and a plume head origin. Therefore the main objective of IODP Expedition 324 was to test both hypotheses (plume head versus ridge-controlled) for the plateau genesis.

During Expedition 324 five sites on all three main volcanic edifices have been cored, with one site (U1346) on the summit of Shirshov Massif and two sites on Ori (U1349 and U1350) and on Tamu (U1347 and U1348) respectively. With the exception of site U1348 all sites revealed basaltic lava flows, which occur as packages of pillow basalt and massive inflation units, frequently interbedded with volcaniclastic sediments. The largest massive inflation flows have a maximum thickness ~ 23m and the thickest occur on Tamu Massif, comparable to massive flows cored on Ontong Java Plateau during ODL Leg 192. Massive flows are also found at Sites U1349 and U1350, on Ori Massif summit and flank, respectively, though an entire ~50 m succession of igneous rocks from Site U1346 (Shirshov Massif summit) consists of pillow lavas. Ori Massif flow units are generally thinner than on Tamu Massif, presumably indicating that the average eruptions become smaller and less effusive from Tamu to

Ori to Shirshov massifs. Cores from site U1348 contained a thick sequence (~120 m) of highly altered volcaniclastic sediments with shallow-water carbonaceous sandstones on top. The cored basaltic lava flows ranging from relatively fresh (Sites U1347 and U1350) to moderately to highly altered (Sites U1346 and U1349). Additional recovered basement rocks from two summit sites (U1346 and U1349) showed the most severe alteration, whereas rocks from Sites U1347 and U1359 are apparently less affected by fluid flow and temperatures. Preliminary shipboard geochemical data (Expedition 324 Scientists, 2010) show that the recovered lava flows consist of variably evolved tholeiitic basalts, with Sites U1347 and U1350 samples having similar compositions to basalts from previous ODP Site 1213 on Tamu Massif. In general, their compositions overlap with Ontong Java Plateau samples as well as with mid-ocean-ridge basalts (MORB). Some samples from Site U1350 have Zr/Ti ratios similar to MORB values. This led to the first broad assumption that the source of Shatsky Rise basalts is slightly enriched in incompatible elements compared to MORB, consistent with slightly lower degrees of partial melting and possibly the presence of residual garnet. Alteration-resistant element ratios (e.g. Zr/ Ti) seem to indicate, that the more altered basalts from Sites U1346, U1348 and U1349 are also of tholeiitic composition. Basaltic lava flow samples from Site U1349 appear to represent significantly less differentiated magmas than those from other sites and have similarities to picritic Ontong Java Plateau basalts.

We present here first isotope-geochemistry results from the southernmost site U1347A, situated on the upper flank east of the summit of Tamu massif. The analyzed volcanic rocks were sampled from a depth range of ~160 m to ~300 mbsf, and comprise relatively fresh basaltic lava flows, which occur as packages of pillow basalt and massive inflation units.

We present new Sr-Nd and Pb and for the first time Hf isotope data from Shatsky Rise. The $^{176}Hf/^{177}Hf$ and $^{143}Nd/^{144}Nd$ isotopic compositions are fairly uniform throughout the entire hole and ranging between 0.283130 and 0.283160 and 0.513080 and 0.513150 respectively, showing no distinct MORB or intraplate (plume) affinity. Combined Nd and Hf isotope form a tight field below the mantle array with values also in between MORB or intraplate (plume)-like compositions.

At this stage neither the plume-head nor the ridge-controlled hypotheses for the plateau genesis can be rulled out.

References:
Expedition 324 Scientists, 2010. Testing plume and plate models of ocean plateau formation at Shatsky Rise, northwest Pacific Ocean. IODP Prel. Rept., 324. doi:10.2204/iodp.pr.324.2010.

ICDP

Lake Ohrid: Insights into the tectonic evolution

N.HOFFMAN[1], K. REICHERTER[1]

[1] Lehr und Forschungsgebiet Neotektonik und Georisiken, RWTH Aachen, Lochnerstr. 4-20, 52056 Aachen; mail: n.hoffmann@nug.rwth-aachen.de

The future ICDP deep drilling site of Lake Ohrid is located along the southwestern border of Macedonia (FYROM) with Albania and is considered being an active tectonic region in the Balkanides. The area is controlled by the progressive roll-back and detachment of the subducted slab of the Northern Hellenic Trench. This results in a compressive regime along the coast of Albania, whereas the east of Albania and the west of Macedonia are presently subject to extension. The lake itself stretches over a length of c. 30 km and a width of c. 15 km. A multidisciplinary approach was chosen to reveal the stress history of the region. Tectonic morphology, paleostress analysis, remote sensing and geophysical investigations have been taken out to trace the landscape evolution. Furthermore, apatite fission-track (A-FT) analysis and t-T-path modelling was performed to constrain the thermal history and the exhumation rates.

The apatite fission-track analysis shows a range of apparent ages from 56.5±3.1 to 10.5±0.9 Ma. The spatial distribution of ages suggests different blocks with a variable exhumation and rock uplift history. From the data and modelling results we assume a westward migration of the extensional basin so that the initiation of the Prespa Basin occurred well before the formation of the Ohrid Basin. The structural data, like paleostress data (fault-slip data) and mapping of folds, joints and fractures gives us a stress history of the area. After separation and classification of the data the results show three major deformation phases: NW-SE shortening, NE-SW shortening and a present-day extension. In addition resent earthquake focal mechanisms show active N-S normal faulting with horst and graben structures. This is also reflected in a seismogenic landscape with several features expressed. A geomorphological analysis was carried out to characterize these features. The fault scarps along the steep flanks of Mokra and Galicica Mountain chains are long-lived reflections of repeated surface faulting in tectonically active regions. Others like wind gaps, wineglass-shaped valleys and triangular facets, are accompanying morphological features. Additionally, mass movement bodies within the lake and also onshore (rockfalls, landslides, sub-aquatic slides, homogenites, turbidites) are likely to have been seismically triggered. Earthquakes larger than magnitude M 6.0 at Lake Ohrid may also be accompanied by secondary effects like liquefaction, seeps, dewatering structures, rock falls landslides and others. These morphotectonic observations correspond to focal mechanisms of earthquakes in the greater Lake Ohrid area. A sedimentological study mainly based on GPR, electric resistivity and drilling data was carried out along the present-day coastline of Lake Ohrid, including locations in the northern and southern plains as well as accumulation areas along the eastern shore where a steep relief is exposed. The data revealed, that the northern and southern

plains are dominated by fluvial sequences including channel structures which are underlain by deltaic sediments and foresets. No evidence for a higher lake-level during the Holocene was found in the plains, except of rare temporal floodings, which are also documented historically and by lacustrine faunal elements (ostracods, Chara) encountered within the sediments. The Velestovo site to the east of the basin provides evidence for a shallow lagoon or marsh environment. An abrupt change in the sediment composition of the core can be related to a sudden lake-level drop, enhanced discharge of the karstic springs or to tectonic activities. Considering the tectonic activity of the region and the landscape architecture a tectonic event is likely the cause of this effect.

IODP

Trace element geochemistry of upper oceanic crust formed at a superfast spreading rate – Insights from fresh volcanic glasses of IODP/ODP – Site 1256 (Guatemala Basin, Cocos Plate)

T. HÖFIG[1], K. HOERNLE[1], S. DUGGEN[1], D. GARBE-SCHÖNBERG[2]

[1] Leibniz Institute of Marine Sciences IFM-GEOMAR, Dynamics of the Ocean Floor,Wischhofstraße 1-3, D-24148 Kiel, Germany

[2] Institute of Earth Sciences, Kiel University, Ludewig-Meyn-Straße 10, D-24118 Kiel, Germany

The investigation of the accretion of ocean crust formed at mid-ocean ridges (MORs) during fast to superfast spreading (more than 80 mm/a full rate) is of critical importance due to the fact that ca. 50 % of the recent ocean crust is derived from such a rapid spreading process. So far, IODP/ODP – Site 1256, located on the Cocos Plate (eastern equatorial Pacific), represents the most complete drilled in-situ section of oceanic crust formed ca. 15 Ma ago at a superfast spreading centre.

The extrusive layer of Site 1256 igneous basement extends from ca. 250 m below seafloor (mbsf) to a depth of about 1,004 mbsf (Expedition 309/312 Scientists, 2006). The upper 502 m of this section were penetrated during ODP Leg 206. This lava package consists mainly of sheet and subordinate massive flows as well as minor pillow lavas, and hyaloclastites (TEAGLE & WILSON, 2007). Throughout this lava section, glassy chilled margins are detectable.

Fresh glass shards of remarkable quality were separated from glassy margins of thirteen lava samples (flows and hyaloclastites) obtained during ODP Leg 206. These samples are distributed all over the upper extrusive crustal section representing different depths between 250 and 700 mbsf. Up to now, major and trace element analyses have been carried out using the electron microprobe (EMP) technique and laser ablation – inductively coupled plasma – mass spectrometry (LA-ICP-MS), respectively, in order to generate a precise geochemical dataset. Associated with the stratigraphical sampling the interpretation of this data is aimed at yielding fundamental information on melting processes and mantle heterogeneity at a superfast spreading MOR system in a temporal resolution not known so far.

The SiO_2 contents of the volcanic glasses cover a range from 51.2 to 54.8 wt%, thus, encompassing basalt and basaltic andesite in composition with the vast majority being basaltic andesite. Though a more or less considerable scattering is obvious, broad trends of decreasing MgO and increasing FeO towards the top of the lava sequence are unambiguous. The Mg# [= 100^{x}MgO/(MgO + FeO*) (atomic)] ranges from 30 to 55 showing an overall slight decreasing upwards with the most primitive (less evolved) samples (sheet flows) between 450 and 550 mbsf. The most differentiated sample (highest SiO_2, lowest Mg#) is a basaltic andesite represented by a sheet flow at a depth of 398 mbsf (Unit 1256D-4C). It has the lowest MgO, CaO, Al_2O_3, and highest FeO and K_2O contents. On the primitive mantle – normalized multi-element plot it shows the most enriched pattern being enriched by three to four orders of magnitude compared to samples of the same crustal level. Furthermore, this plot reveals distinctive negative Sr and Eu anomalies indicating removing of these elements from the melt by fractionation of plagioclase during magma evolution. This sample forms a distinct outlier in almost every geochemical plot. However, it indicates that this sheet flow constitutes the most differentiated sample of a fractionation trend formed by the sheet flows at depths between 370 and 420 mbsf (Units 1256D – 3-4D).

Another discrete group is presented by the deepest volcanics sampled for this study. They comprise sheet flows and a hyaloclastite spanning depths between 450 and 700 mbsf. Most of them constitute the most primitive lavas sampled, although being partly silica-enriched (52.5-53.1 wt% SiO_2) to some extent compared to the flows above. The deep flows display fractionation trends in variation diagrams with decreasing CaO and Al_2O_3 as well as increasing FeO, TiO_2, K_2O, and Na_2O contents with decreasing MgO concentration. The hyaloclastite sample (Unit 1256D-21) shows the lowest abundances of compatible trace elements (e.g., Cr, Co, V) and the highest contents of highly incompatible trace elements (e.g., Th, Nb, Hf, Zr) in this group, hence, every displayed fractionation trend of these deep volcanics seems to point to this sample. However, it contemporaneously shows the lowest silica concentration whereas having also the lowest Mg# within this group. Therefore, these indicators of magmatic evolution maybe suggest a different origin compared to the deep flows. In fact, with respect to a supposed fractionation trend characterizing the group of these lavas, the hyaloclastite sample represents a kind of mediator to the sample collected from the thick (> 74 m) ponded lava flow which caps the whole lava section on the top. In addition, it resembles the lava pond sample in almost every major element concentration and highly incompatible element abundances. However, the uppermost sample is more enriched in rare earth elements (REEs) compared to the hyaloclastite. Nonetheless, apart from the enrichment degree, both samples reveal a very similar REE pattern in chondrite – normalized REE plot (Fig. 1). Thus, in general these two samples are akin to each other.

The sheet flow (Unit 1256D-2) sampled at a depth of ca. 360 mbsf is a unique one among the volcanics investigated in this study. It is quite different from any other single sample. It represents the most mafic composition revealing basaltic chemism with 51.2 wt% SiO_2 and showing the highest Mg# (51) within the upper lava flows. Although it has the lowest silica content, this high-alumina basalt shows the second highest concentration of alkalis (Na_2O, K_2O) only excelled by the

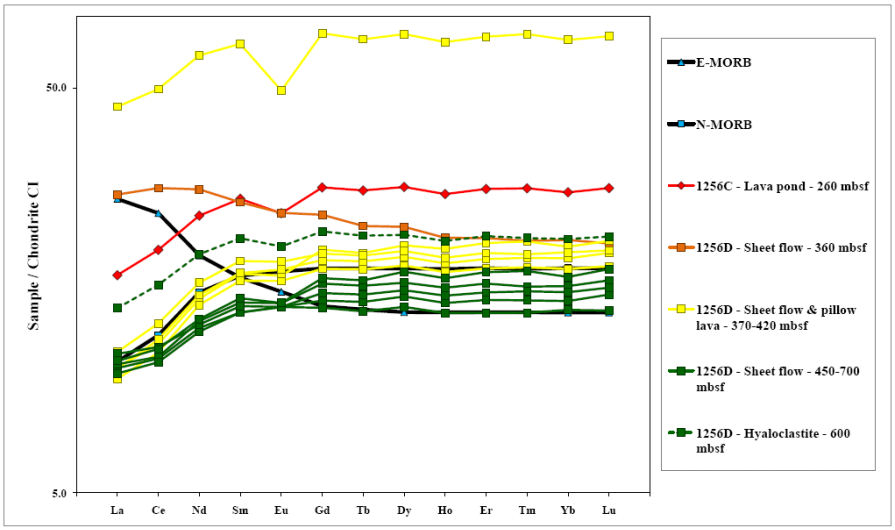

Fig. 1: Chondrite (CI) – normalized REE plot displaying the principle differences in REE geochemistry between the glass samples from discrete flows penetrated in different depths ranging from 250 to almost 700 mbsf during ODP Leg 206 at Site 1256. Values for CI chondrite, E-MORB, and N-MORB are from SUN & MCDONOUGH (1989).

most differentiated volcanic glass sampled from Unit 1256D-4C. Both immobile element ratios (Zr/Ti, Zr/Y) and the La/Yb ratio as a function of the degree of REE fractionation significantly differ from the other glass samples. This most likely points to a variation in the composition of the primitive magma at Site 1256.

For fresh MOR lavas the ratio K/Ti (= $K_2O/TiO_2{}^x100$) can serve as a reliable tool for discriminating between N-type MORB (MOR basalt) and E-type MORB, i.e., establishing the degree of MORB enrichment (SMITH et al., 2001, and references therein). Applied to our samples, this gives rise to E-MORB enrichment of the unique upper sheet flow revealing K/Ti of more than 14. This ratio is quite similar to that of the most differentiated sheet flow from below. However, this is likely to be related to the pretty high evolutional stage of this lava sample. The E-MORB nature of the uppermost sheet flow is confirmed by the chondrite – normalized REE plot which shows the similarity to the E-MORB pattern (Fig. 1). In addition, it substantiates that the pattern of the most differentiated sheet flow from the middle of the section with the most enriched REE contents is most likely the result of fractionation processes.

In the next analytical step Sr-Nd-Pb-Hf isotope studies will be implemented in order to constrain the source of the lavas generated during superfast spreading at Site 1256.

References:

Expedition 309/312 Scientists (2006): Expedition 309/312 summary. In: Teagle, D.A.H., Alt, J.C., Umino, S., Miyashita, S., Banerjee, N.R., Wilson, D.S., and the Expedition 309/312 Scientists [eds.]: Proceedings of the Integrated Ocean Drilling Program, 309/312, Washington, D.C. (Integrated Ocean Drilling Program Management International, Inc.): 1–127.

SMITH, M. C., PERFIT, M. R., FORNARI, D. J., RIDLEY,W. I., EDWARDS, M. H., JURRAS, G. J. & Von DAMM, K. L. (2001): Magmatic processes and segmentation at a fast spreading mid-ocean ridge; detailed investigation of an axial discontinuity on the East Pacific Rise crest at 9°37'N. In: Geochemistry, Geophysics, Geosystems, 2, paper number 2000GC000134.

SUN, S. S., MCDONOUGH, W. F. (1989): Chemical and isotopic systematics of oceanic basalts: implications for mantle composition and processes. In: SAUNDERS, A. D., NORRY, M. J. [eds.]: Magmatism in ocean basins. Geological Society of London Special Publication, 42: 313-345.

TEAGLE, D.A.H., WILSON, D.S. (2007): Leg 206 synthesis: initiation of drilling an intact section of upper oceanic crust formed at a superfast spreading rate at Site 1256 in the eastern equatorial Pacific. In: TEAGLE, D.A.H., WILSON, D.S., ACTON, G.D., VANKO, D.A. [eds.]: Proceedings of the Ocean Drilling Program, Scientific Results, 206, College Station, TX (Ocean Drilling Program): 1-15.

IODP

The trace element and Sr-Nd-Pb isotopic record of IODP/ODP – Site 1256 sedimentary overburden and its implications for the Neogene paleoceanographic evolution of the eastern equatorial Pacific

T. HÖFIG[1], K. HOERNLE[1], S. DUGGEN[1], F. HAUFF[1]

[1] Leibniz Institute of Marine Sciences IFM-GEOMAR, Dynamics of the Ocean Floor,Wischhofstraße 1-3, D-24148 Kiel, Germany

The investigation of the sediment package of IODP/ODP – Site 1256 (Guatemala Basin, Cocos Plate) is of particular interest, since it provides valuable insights into the evolution of the eastern equatorial Pacific Ocean from mid-Miocene to Pleistocene times. By means of correlation with deep-sea drilling holes further to the east offshore Central America there is the opportunity to shed light on the entire Neogene paleoceanography of the central eastern Pacific.

Site 1256 is characterized by a 250 m thick sediment section deposited on ca. 15 Ma old basement (TEAGLE & WILSON, 2007). The sediment column comprises 40 m of terrigenous silty-clay (Unit I) capping 210 m of calcareous nannofossil ooze (Unit II) which sporadically shows intercalated layers of diatomaceous ooze (TEAGLE & WILSON, 2007). Unit I consists of two subunits: The upper subunit (Unit IA) comprises silty clays incorporating 40 wt% biogenic sediment and 60 wt% of terrigenous material mainly involving smectite and volcanic glass (TEAGLE & WILSON, 2007; ZIEGLER et al., 2007). The deeper subunit (Unit IB) reveals a coarser clastic component than Unit IA, thus, considered to be a coarser silty-clayey nannofossil ooze which contains less than 20 wt% carbonate (WILSON et al., 2003; ZIEGLER et al., 2007).

There are several factors acting as controlling mechanisms contributing to and impacting on the geochemical pattern. The trace element sedimentary record shows significant variabilities through time. In the following, this will be exemplified for some trace element and isotopic data.

At the beginning of sediment accumulation, a constantly high level of Sr concentration is obvious. Since the Sr content underlies the control of carbonate sedimentation, it is not surprising that values between 1,000 and >1,500 ppm are revealed in the carbonate-rich Unit II. This high amount of carbonate reflects the formation area of Site 1256 oceanic crust near the paleoequator (approximately 1° N) at the East Pacific Rise and, thus, is subsequently characterized by high carbonate mass accumulation rates within the zone of high productivity (WILSON et al., 2003; JIANG et al., 2007). However, at ca. 11 Ma radical changes took place leading to a sharp drop of carbonate concentration and sedimentation rates termed the "carbonate crash" (FARRELL et al., 1995; LYLE et al., 1995; JIANG et al., 2007). Instead, thick diatom mats deposited. Naturally, this opaline sediment is associated with a low Sr content (here: around 400 ppm). The lowest Sr content in a calcareous nannofossil ooze is revealed by a sample collected at a depth of ca. 88 mbsf which corresponds to an estimated age of 9.6 Ma. This age marks the time of the "carbonate crash nadir" according to JIANG et al. (2007). With the increasing amount of terrigenous matieral as a consequence of the approach to Central America through continuous mid-ocean ridge spreading and the simultaneous leaving of the high-productivity zone, the Sr content persistently decreases pointing to the onset of the predominance of clastic sedimentation at 5 Ma. Afterwards, the Sr value is chiefly controlled by the nature of the terrigenous component. In Unit IB, there is an increasing abundance of smectite clay and volcanic glass (as well as volcanic ash) with decreasing age (WILSON et al., 2003). This trend shows the lowest Sr content (220 ppm) of all samples in a volcanic ash layer at ca. 1.6 Ma. Subsequently, an increase of the strontium concentration (up to almost 500 ppm) is recorded, as a calcareous nannofossil bearing smectite clay characterizes the younger Pleistocene sedimentation at Site 1256.

The barium concentration is mainly governed by the mineralogical composition of the sediment. As barite becomes a minor component with growing amount in the sediment pile from about 104 mbsf upwards (WILSON et al., 2003), the Ba content rises constantly reaching its highest value in Unit IB. The alkalis (K, Rb, Cs) are put in by detrital phases in marine sediments (ZIEGLER et al., 2007). Thus, their concentration is largely controlled by the ratio detritus/biogenic phases. This ratio increases with decreasing age, hence, the alkali contents rise continuously up to the base of Unit IB. Potassium reaches its highest value with the deposition of the probably arc-derived volcanic ash layer and dropping afterwards in Unit IA back to Unit IB levels.

The lowermost sample, i.e., closest to the basement, collected at a depth of ca. 245 mbsf, is distinctively different from the other samples above in the carbonate-rich Unit II. The alkali values are four- to eightfold elevated compared to the samples upwards. Therefore, it is assumed that these concentrations reflect a kind of basement signal as it might represent a halo of the metalliferous sediment detectable between the lowermost carbonates and the top of the igenous basement.

The lead isotopes move to more radiogenic compositions with declining age (decreasing depth) reaching the highest ratios in Unit IB for $^{207}Pb/^{204}Pb$ and $^{208}Pb/^{204}Pb$. Regarding the Pleistocene tephra layer and smectite clays, there is a drop of Pb isotope ratios before a new increasing trend is indicated towards the Holocene. The highest $^{206}Pb/^{204}Pb$ ratio is presented by the diatomite which marks the onset of the "carbonate crash". In the $^{206}Pb/^{204}Pb$ plots it is the only sample which is aside the general isotope trend. The $^{207}Pb/^{204}Pb$ and $^{208}Pb/^{204}Pb$ graphs show continuously increasing ratios from the bottom of the sediment column through the carbonates towards the siliciclastic units. Hence, they are more or less unaffected by the late Miocene "carbonate crash" while the $^{206}Pb/^{204}Pb$ trend shows significant shifts and variations during the crash period. The constantly high "pre-crash" $^{87}Sr/^{86}Sr$ values mainly reflect the seawater ratio whereas the "post-crash" sediments show the increasing impact of terrigenous material derived from the Central American Volcanic Zone (CAVZ). The $^{143}Nd/^{144}Nd$ ratios represent also seawater compositions during the "pre-crash" sedimentation. However, afterwards there is a shift to significantly higher ratios reflecting the continental detritus input.

Correlations of Site 1256 with the DSDP Site 495 (Leg 67) located near the Central American trench yield that the trace element and isotope compositions of the carbonate-rich sediments form a continuation downwards the sediment layer which has a thickness of ca. 400 m at Site 495. Accordingly, the sedimentation at this location started almost 23 Ma ago (Leg 67 Shipboard Scientific Party, 1982). Towards the upper hemipelagic units the geochemical pattern is quite similar to Site 1256 apart from some exceptions such as the U and Th concentrations which are shifted to higher values at a given age in the hemipelagic unit at Site 495.

The studies on the sediment package of Site 1256 done so far reveal a relatively complex interplay of different factors affecting the geochemical record. Above all, there is the progressive evolution from high-productivity to low- and non-productivity and their balance over the period of sedimentation in the eastern equatorial Pacific. The available data give rise to the assumption that the record of Site 1256 represents a mixing line between the basement signal (profoundly developed at the sediment base) and the arc signal of the CAVZ. Indeed, the deepest samples of the carbonate unit and the siliciclastic samples of hemipelagic Unit I have opposed endmember character particularly displayed by the isotope plots.

References:

FARRELL, J.W., RAFFI, I., JANECEK, T.R., MURRAY, D.W., LEVITAN, M., DADEY, K.A., EMEIS, K.-C., LYLE, M., FLORES, J.-A., HOVAN, S. (1995): Late Neogene sedimentation patterns in the eastern equatorial Pacific Ocean. In: PISIAS, N.G., MAYER, L.A., JANECEK, T.R., PALMER-JULSON, A., VAN ANDEL, T.H. (eds.): Proceedings of the Ocean Drilling Program, Scientific Results, 138, College Station, TX (Ocean Drilling Program): 717–756.

JIANG, S., WISE, S.W., JR., WANG, Y. (2007): Cause of the middle/late Miocene carbonate crash: dissolution or low productivity? In: TEAGLE, D.A.H., WILSON, D.S., ACTON, G.D., VANKO, D.A. (eds.): Proceedings of the Ocean Drilling Program, Scientific Results, 206, College Station, TX (Ocean Drilling Program): 1–24.

Leg 67 Shipboard Scientific Party (1982): Site 495: Cocos Plate – Middle America Trench Outer Slope. In: AUBOUIN, J., VON HUENE, R., et al.

(eds.): Initial Reports of the Deep Sea Drilling Project, 67, Washington (U.S. Government Printing Office): 79-141.

LYLE, M., DADEY, K.A., FARRELL, J.W. (1995): The late Miocene (11–8 Ma) eastern Pacific carbonate crash: evidence for reorganization of deep-water circulation by the closure of the Panama Gateway. In: PISIAS, N.G., MAYER, L.A., JANECEK, T.R., PALMER-JULSON, A., VAN ANDEL, T.H. (eds.): Proceedings of the Ocean Drilling Program, Scientific Results, 138, College Station, TX (Ocean Drilling Program): 821–838.

TEAGLE, D.A.H., WILSON, D.S. (2007): Leg 206 synthesis: initiation of drilling an intact section of upper oceanic crust formed at a superfast spreading rate at Site 1256 in the eastern equatorial Pacific. In: TEAGLE, D.A.H., WILSON, D.S., ACTON, G.D., VANKO, D.A. [eds.]: Proceedings of the Ocean Drilling Program, Scientific Results, 206, College Station, TX (Ocean Drilling Program): 1-15.

WILSON, D.S., TEAGLE, D.A.H., ACTON, G.D., and the Shipboard Scientific Party (2003): Site 1256. In: WILSON, D.S., TEAGLE, D.A.H., ACTON, G.D., et al.: Proceedings of the Ocean Drilling Program, Initial Reports, 206, College Station, TX (Ocean Drilling Program): 1-396.

ZIEGLER, C.L., MURRAY, R.W., HOVAN, S.A., REA, D.K. (2007): Resolving eolian, volcanogenic, and authigenic components in the pelagic sediment from the Pacific Ocean. Earth and Planetary Science Letters, 254: 416-432.

IODP

Developing an early to middle Miocene benthic foraminiferal isotope chronostratigraphy across the Pacific „paleoequator transect“ (IODP Expedition 320/321)

A. HOLBOURN[1], W. KUHNT[1], M. LYLE[2], N. ANDERSEN[3]

[1] Institute of Geosciences, Christian-Albrechts-University, D-24118 Kiel, Germany
[2] Department of Oceanography, Texas A&M University, College Station, Texas 77843, USA
[3] Leibniz Laboratory for Radiometric Dating and Stable Isotope Research, Christian-Albrechts-University, D-24118 Kiel, Germany

Our primary goals are to develop an early to middle Miocene (20-13 Ma) astronomically-calibrated benthic isotope chronostratigraphy in a “mega-splice” constructed from continuous and expanded sedimentary successions from multiple drill holes across the Pacific „paleoequator transect“. The PEAT Expedition 320/321 (March to June 2009) targeted key time slices in the evolution of the Cenozoic climate at locations across the paleo-equator that were not deeply buried, thus allowing optimum accumulation and preservation of calcareous sediments (Pälike et al., 2008; 2010). Specific targets included the prominent oscillations in ice volume and/or ocean temperatures during the early Miocene leading on to the “Monterey Excursion” (Vincent and Berger, 1985) and Miocene Climatic Optimum followed by the punctuated expansion of ice sheets towards the end of the middle Miocene. Although these intervals were drilled during previous cruises, considerable information is still missing, as previous records are incomplete due to patchy core recovery and/or poor preservation of sedimentary successions, especially within the 20-16 Ma time interval, which is not yet firmly anchored within the geological timescale and still requires major clarification.

Based on improved understanding of Pacific sedimentation patterns and the past movement of plates, the position of each PEAT drill site was selected to ensure optimum recovery of well-preserved carbonate-rich sediments (Pälike et al., 2010). Cores were retrieved mainly with the APC coring system from multiple holes at each site, thus ensuring optimum sediment recovery and preservation. When spliced together, three primary sites (U1335, U1337 and U1338) provide a continuous paleoceanographic record over the 20-13 Ma interval. Remarkably high sedimentation rates (20-30 m/Myr) over this time slice allow unparalleled resolution of major climatic events (Climatic Optimum “warm events” and Mi-1-3 glaciations) as well as fresh insights into early-middle Miocene ice volume changes, Pacific paleoceanography and deep-water circulation changes. Our study is primarily based on stable isotope analysis of epibenthic foraminifers *(Planulina wuellerstorfi* and/or *Cibicidoides mundulus)* in high-resolution samples (5-10 cm interval equivalent to ~ 1.5-5 kyr time resolution) from Sites U1335, U1337 and U1338. Time series analysis of core logging, coarse fraction residue >63 μm and XRF scanning data (collaboration with Prof. M. Lyle), which exhibit prominent orbital periodicities, are performed in paralllel to complement the stable isotope investigation and to develop an astronomically-tuned chronostratigraphy.

Our initial stable isotope measurements in Site U1338 (10 cm spacing, ~ 3 kyr time resolution over 13-16 Ma) resolve middle Miocene climate evolution in unprecedented resolution. The U1338 record already shows prominent periodicities (equivalent to ~ 40, 100 and 400 kyr), when plotted in the depth domain, thus demonstrating its suitability for astronomical calibration without risk of artificial distortion during the tuning process. Over critical intervals (prelude events to Mi-3 glacial shift, Climatic Optimum transient warm events) we will increase the temporal resolution to 1.5 kyr in order to elucidate phase relationships between the carbon cycle, equatorial Pacific circulation, and ice volume change. XRF scanning data (Si, Ba, Fe and Ca) further indicate a strong orbital control on the Miocene paleoceanographic evolution of the equatorial Pacific, and geochemical signals (Log(Ba/Ca, Log(Fe/Ca) closely follow variations in eccentricity and tilt, even in our minimally tuned record. Between 14.05 and 13.84 Ma, two prominent productivity spikes reveal major increases in equatorial upwelling associated with Antarctic ice expansion (Mi-3 glaciation). The PEAT stable isotope and XRF scanning data thus provide the first records with sufficient time resolution to clearly resolve the pacing of rapid climate events and to closely track interactions between Antarctic ice sheet development, Pacific circulation and climate evolution. While ancient climates are not exact analogues for the modern world, understanding past changes in a warmer world has major implications for evaluating scenarios of future warmer climate with elevated atmospheric CO_2 and unipolar ice concentration.

References:

Pälike, H., Lyle, M.W., Ahagon, N., Raffi, I., Gamage, K., and Zarikian, C.A., 2008. Pacific equatorial age transect. IODP Sci. Prosp., 320/321. doi:10.2204/iodp.sp.320321.2008.

Pälike, H., Lyle, M.W., Nishi, H., Raffi, I., Gamage, K., and Klaus, A., and the Expedition 320/321 Scientists, 2010. Proc. IODP, 320/321: Tokyo (Integrated Ocean Drilling Program Management International, Inc.). doi:10.2204/iodp.proc.320321.109.2010.

Vincent, E. and Berger, W.H., 1985. Carbon dioxide and polar cooling in the Miocene: The Monterey hypothesis, in: Broecker, W. S. and Sundquist, E. T., eds., The Carbon Cycle and Atmospheric CO_2: Natural Variations Archean to Present. Geophysical Monograph Series, 32, American Geophysical Union, Washington, DC, pp. 455-468.

IODP

Experimental investigation of smectite dehydration and pore water geochemistry at stress and temperature conditions similar to the shallow subduction zone

A. HÜPERS[1], A.J. KOPF[1]

[1] MARUM - Center for Marine Environmental Sciences, University Bremen, P.O. Box 330440, 28334 Bremen, Germany
Email of corresponding author: ahuepers@uni-bremen.de

At subduction zones the incoming sediments expel fluids in the course of consolidation and by mineral dehydration at greater depth. For most subduction zone complexes smectite dehydration is the dominant mineral dehydration reaction, and is hence believed to be a key player for the hydrology and mechanical behavior. It has been hypothesized that illitization generates overpressures at depth, which reduce the shear strength of faults and wall rocks by decreasing effective normal stress. Smectite dehydration is commonly referred to the mainly temperature driven transition of smectite to illite which starts at temperatures above 60°C. Because the expelled water is fresh, low chlorinity fluids are generally interpretated as a signal for lateral fluid flow. However, laboratory tests have shown that smectite dehydrates at room temperature and at low stresses of 1.3-1.6MPa. This finding suggests that smectite dehydration is much more complicated than previously assumed. The aim of the present study is, therefore, the investigation of smectite deyhdration and associated fingerprints in pore water geochemistry in dependence of stress and temperature.

For the study we used a new approach in form of a heatable and drainable consolidometer. Compared to undrained rocking autoclaves, which are widely used for hydrothermal testing, the system has the advantage that the effective stress increases and the porosity decreases during an experiment. Together with increasing temperature, the experiments simulate enhanced burial conditions. We ran 3 experiments with stresses up to 70 MPa, which is equal to 6-7 km depth. We held temperatures constant at 20°C, 60°C and 100°C to distinguish between stress and temperature effects. Sample material was smectite from Wards Scientific with ~70wt-% smectite. This is comparable to smectite-rich sediments found at the Nankai or Costa Rican margin. For each individual experiment the sediment was remoulded with seawater several times before it was placed into the consolidometer. The fluids expelled throughout the experiments were analyzed for major and trace elements representing different stress and temperature intervals.

Measured chlorinities corroborate that fluid freshening begins at a stress level of approximately 1.6 to 2.5MPa for all tests. We calculated the dehydrated smectite fraction in the sample from the chlorinity data after Fitts and Brown (1999). The calculations show that smectite loses one of the three water layers in its interlayer spacing within a stress interval of 2MPa to ~25MPa. The comparison of the experiments at three temperatures show an increasing dehydration rate with increasing temperature. We propose that the observed smectite dehydration is driven by the availability of free water in the water-rock system, which is best presented by a reversible solid-solution equilibrium reaction where the hydrated smectite (hSM) is on one side and the dry mectite (aSM) on the other plus n moles of released water: $hSM \leftrightarrow aSM + nH_2O$. When abundant water is present, the equation is driven to the left side of the equation. When free water is removed, for example by consolidation, the equation is driven to the right side. Proof for this process is given by the data of Zhang and Low (1989) who measured the relationship between interlayer spacing and the water-rock mass ratio. Their data show an incremental decrease of interlayer spacing which begins at a water-rock mass ratio of 0.44 and reaches 0.27 when one water layer is totally removed. This interval fits very well with calculated mass ratio from our tests, where a ratio of 0.44 denotes the onset of freshening and at 0.27 the total loss of one layer of water.

For heated tests pore water analyzes reveal the removal of Mg and enrichment of K, Ca and volatiles (B, Li). This can be related to the temperature dependence of cation exchange reactions. Instead, the onset of fluid freshening is characterized by the strong removal of K while divalent cations (Mg and Ca) remain conservative. Na and the volatiles B and Li are slightly enriched with progressing smectite dehydration. The collapse in interlayer spacing upon smectite dehydration initiation is associated with a change of cations selectivity for weakly hydrated ions like K. In expanded smectite interlayers strongly hydrated cations like Na or Ca are preferred. The slight enrichment of Na and B in the expelled fluids also document this selectivity. The strong depletion of K in the pore fluid suggests that the process seems to be dominant over the temperature dependence of cation exchange.

Based on the pore water geochemistry we propose three different depth-temperature stages of smectite dehydration in the subduction zone. At shallow depths with water-rock mass ratios greater than 0.44 and low temperature occurs no smectite dehydration. With increasing burial depth the temperature increases while the the water-rock mass ratio decreases. This stage is characterized by less K and Mg and increased concentrations of Na as well as volatile elements (B, Li, Si). The last stage is facilitated by higher temperatures and smaller water-rock mass ratios but the pore fluid is overprinted by the smectite–illite transition due to temperatures >60°C.

References:

Fitts, T.G., Brown, K.M., 1999. Stress-induced smectite dehydration: ramifications for patterns of freshening and fluid expulsion in the N. Barbados accretionary wedge. Earth and Planetary Science Letters 172 (1-2), 179-197.

Laird, D.A., Shang, C., 1997. Relationship between cation exchange selectivity and crystalline swelling in expanding 2:1 phyllosilicates. Clays Clay Miner. 45 (5), 681-689.

Zhang, Z.Z., Low, P.F., 1989. Relation between the heat of immersion and the initial water content of Li-, Na, and K- montmorillonite. J. Colloid Interface Sci. 133 461-472.

IODP

Preliminary results of modeling drainage efficiency of sand layers in underthrust sediments of the Nankai subduction zone, Japan.

A. HÜPERS[1], A.J. KOPF[1]

[1] MARUM - Center for Marine Environmental Sciences, University Bremen, P.O. Box 330440, 28334 Bremen, Germany
Email of corresponding author: ahuepers@uni-bremen.de

At subduction zones the sediment on the incoming plate is accreted as a wedge shaped sedimentary body to the overriding plate or is subducted with the downgoing plate. In this geologically dynamic setting the low permeable marine sediments are subjected to rapid burial and tectonic stresses that commonly generate pore fluid pressures in excess of hydrostatic. Excess pore pressures modify the effective normal stress and thus fault and rock shear strength. Pore pressures within underthrust sediments are of particular importance because they affect the shear strength of the plate boundary fault, the taper angle of the accretionary wedge and the up-dip limit of the seismogenic zone.

Evidence for excess pore pressure at shallow depths comes from direct measurements (<2km) while pore pressures at greater depths are inferred from seismic reflection surveys and numerical modeling. Especially numerical models have been extensively used to study the role of fluids in subduction zone. Despite the lithostratigraphic variability of incoming sediments at active margins (e.g. Nankai, Barbados), these models commonly deal with homegenous sediments. To consider the full range of hydrostratigraphic variability, we measured permeability of core samples of different lithologies in the laboratory. Samples were taken during IODP Expedition 322 at IODP Sites C0011 and C0012 located ~15km seaward of the deformation front offshore Kii peninsula. The results are combined with a coupled loading and pore pressure diffusion model to study the pore pressure evolution within the underthrust sequence. The preliminary results focus on the western Nankai subduction zone, the so called Ashizuri transect, where at least 5% of the incoming underthrust sequence comprise permeable sand layers.

Measured permeabilities show characteristic trends for mudstones and sandstones. Mudstone permeability follows a trend, which is best described by the following linear relationship between permeability (k) and porosity (n): log(k)=-20.45+6.93*n. This trend is similar to previously documented mudstone permeabilities from numerous studies at the Nankai margin. The more important result comes from the sandstone measurements, which are here reported for the first time for the Nankai subduction zone. The sands are proximately 100 times more permeable than mudstones and their permeability-porosity relationship is represented best by log(k)=-17.93+6.83*n. Model scenarios with varying sandlayer geometries show that thickness and location of sandlayer in underthrust sediments influence excess pore pressure generation. The average excess pore pressure in the underthrust sequence decreases when the sand layer thickens or the location is moved to the impermeable base. The lower pore pressure is associated with more efficient lateral drainage along the permeable sand layer. For a more realistic model scenario we incorporated a sand layer distribution profile based on the sedimentological description of the incoming sediment at ODP Site 1177 from the Ashizuri transect. In addition, boundary conditions are adjusted until modeled pore pressures at the deformation front met corresponding pore pressures inferred from the non-cohesive critical taper theory. With these settings the highest excess pore pressures are observed along the decollement thoughout the first 30km of underthrusting. The lower basal excess pore pressure suggests a better lateral drainage along the permeable sand layer than through the decollement.

The preliminary results presented from a coupled loading and pore pressure diffusion model show the significance of lateral fluid flow along permeable sand layers in underthrust sediments of the Nankai subduction zone. Future tasks of this study will be the application of the model to different transects along strike the Nankai subduction zone to investigate the lateral differences in hydrostratigraphy. Another task will be the quantification of fluid budgets, which is important for mass balancing of subduction zones.

ICDP

A new organic carbon isotopic record for the Fennoscandian early Paleoproterozoic

C. J. ILLING*[1], H. STRAUSS[1], R.E. SUMMONS[2], A.E. FALLICK[3], L. KUMP[4], V.A. MELEZHIK[5,6] AND THE FAR-DEEP SCIENTISTS

[1] Institut für Geologie und Paläontologie, Westfälische Wilhelms-Universität, Münster, Germany
[2] Department of Earth, Atmospheric and Planetary Sciences, Massachusetts Institute of Technology, Cambridge, USA
[3] Scottish Universities Environmental Research Centre, Glasgow, United Kingdom
[4] Department of Geosciences, Pennsylvania State University, University Park, USA
[5] Geological Survey of Norway, Trondheim, Norway
[6] Centre for Geobiology, University of Bergen, Bergen, Norway

The scientific goal of this project is to reconstruct ancient microbial ecosystems and the evolution of key metabolic pathways during the Archean-Proterozoic Transition of Fennoscandia using molecular and organic isotopic evidence. This work is part of the Fennoscandian Arctic Russia - Drilling Early Earth Project (FAR-DEEP) that recovered fifteen drill cores with a total length of 3650 m. Cores were retrieved in three areas in northern Russia, namely the Imandra/Varzuga and Pechenga Greenstone belts and the Onega Basin and cover a time interval of some 700 million years. Several global perturbations are archived in the FAR-DEEP drillcores, among them the Great Oxygenation Event (GOE) at ca. 2350 million years ago that resulted in large-scale environmental changes (e.g. Melezhik et al., 2005). Of similar importance, and specifically relevant for global carbon cycling, are the Lomagundi-Jatuli Event (LJE; e.g. Melezhik et al., 1999a, 2007) and the Shunga Event (SE; e.g. Melezhik et al.,1999b, 2009).

This work presents new carbon isotope data for sedimentary organic matter ($\delta^{13}C_{org}$) from all major sedimentary formations cored by FAR-DEEP. Approximately 120 archive samples were analyzed for

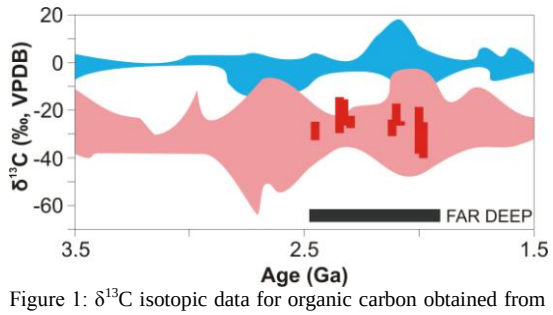

Figure 1: $\delta^{13}C$ isotopic data for organic carbon obtained from FAR-DEEP cores compared to published data for carbonate (blue) and organic carbon (reddish) isotopic records (carbonate data taken from Prokoph et al., 2009; organic carbon isotopic data taken from Eigenbrode & Freeman, 2006)

their bulk organic carbon isotopic composition at the University Münster via sealed-tube combustion.

The total variation in $\delta^{13}C_{org}$ was between -40 and -12‰ and agrees generally well with previously published data (Fig. 1). However, more informative than the organic carbon isotopic composition is the isotopic difference ($\Delta^{13}C$) between the organic ($\delta^{13}C_{org}$) and the carbonate carbon ($\delta^{13}C_{carb}$) isotopic composition:

$$\Delta^{13}C = \delta^{13}C_{carb} - \delta^{13}C_{org}$$

This parameter comprises information about the isotopic fractionation associated with biosynthesis and carbon cycling (e.g., Des Marais, 2001). Accordingly, $\delta^{13}C_{org}$ is shown here together with $\delta^{13}C_{carb}$ versus the stratigraphy of the three investigated areas (Fig. 2). The carbonate carbon isotope dataset was obtained by Fallick and Brasier at SUERC also from the archive samples.

Throughout most of the sedimentary succession $\delta^{13}C_{org}$ displays limited variability (-27 to -22 ‰), and an isotopic difference between both carbon fractions ($\Delta^{13}C$) of 20 to 30‰ suggests autotrophic carbon fixation as the prime biosynthetic process. In contrast, sediments from the lower Kuetsjärvi Formation (core 5A) and the Tulomozero Formation (cores 10A, 10B, 11A), covering the LJE, display comparable $\delta^{13}C_{org}$ values around -27 ‰, yet $\Delta^{13}C$ values range from 32 to 40‰. The consistency of $\delta^{13}C_{org}$ for that interval, suggests that the variations of $\Delta^{13}C$ might not only reflect a primary change in the biological fractionation processes. Melezhik et al. (1999b) showed also the strong temporal influence of the environmental setting on $\delta^{13}C_{carb}$. Sediments of the shungite/maksovite bearing Zaonega Formation show a more structured temporal evolution in $\delta^{13}C_{org}$, but $\Delta^{13}C$ returns to the pre-LJE level.

In general, the broad parallel evolution of $\delta^{13}C_{org}$ and $\delta^{13}C_{carb}$ indicates that respective perturbations affected the global carbon cycle.

The carbon isotopic record is relative robust against alteration, at least compared to other geochemical biosignatures. But it is important to keep in mind that high thermal maturity of organic matter is associated with a kinetic effect on the isotopic composition that could overprint the original isotope signature. This would affect samples with low total organic carbon content (TOC) more than samples characterized by a higher TOC. However, new samples reveal no discernible correlation between a lower TOC and a higher $\delta^{13}C_{org}$ value. The present data set still needs more refinement in respect to temporal resolution but also with regard to the significance of apparent 'outliers'.

Based on the information gained from bulk rock carbon isotopic composition more detailed insights prevailing metabolic pathways can be addressed by biomarker analysis. This is currently being pursued. Unfortunately however, like most lithologies of this age the rocks of Fennoscandia have significantly suffered from post-depositional thermal processes. Initial organic petrologic analyses for a small sample set from the Onega Basin revealed a high bituminite reflectance (above 5%). Rock Eval (e.g. Espitalie et al., 1977) pyrolysis also documented their high maturity. However, successful biomarker studies from time-equivalent sedimentary succession such as in South Africa (e.g. Waldbauer et al., 2009) leave the search for molecular fossils promising.

References:

Des Marais, D.J. (2001): Isotopic evolution of the biogeochemical carbon cycle during the Precambrian. Rev. Mineral. Geochem. 43, 555 – 578.

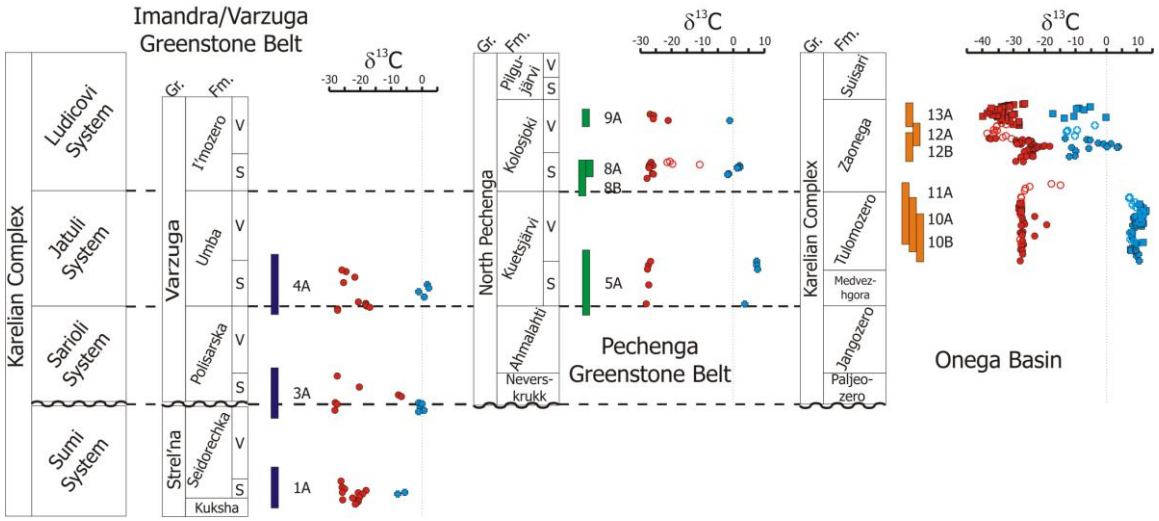

Figure 2: Carbon isotopic composition of bulk organic matter ($\delta^{13}C_{org}$; red) and whole-rock carbonate ($\delta^{13}C_{carb}$; blue) for cores retrieved by FAR-DEEP (chronostratigraphic correlation after Melezhik & Hanski, in preparation). Cored intervals are marked by coloured boxes (purple: Imandra/Varzuga Greenstone Belt, green: Pechenga Greenstone Belt, orange: Onega Basin) and core numbers are listed next to it.

Eigenbrode, J.L. & Freeman, K.H. (2006): Late Archean rise of aerobic microbial ecosystems. Proc. Nat. Acad. Sci. 103, 15759 – 15764.
Espitalie, J., Laporte, J.L., Madec, M., Marquis, F., Leplat, P. & Paulet, J. (1977): Methode rapide de characterisation des roches meres et de leur potentiel petrolier et de leur degre d'evolution. – Rev. Inst. Francais du Petrole 32, 23 – 42.
Melezhik, V.A., Fallick, A.E., Filipov, M.M. & Larson, O.(1999a): Karelian Shungite-an indication of 2000 Ma-year-old metamorphosed oil-shale and generation of petroleum: geology, lithology and geochemistry. Earth Sci. Reviews 47, 1 – 40.
Melezhik, V.A., Fallick, A.E., Medvedev, P.V. & Makarikhin, V.V. (1999b): Extreme δ13Ccarb enrichment in ca 2.0 Ga magnesite-stromatolite-dolomite-'red beds' association in a global context: a case for the worldwide signal enhanced by a local environment. Earth Sci. Reviews 48, 71 – 120.
Melezhik, V.A., Fallick, A.E., Hanski, E., Kump, L., Lepland, A. Prave, A. & Strauss, H. (2005): Emergence of the aerobic biosphere during the Archean-Proterozoic transition: Challenges of future research. GSA Today 15, 4 – 11.
Melezhik, V.A., Huhma,H., Condon, D.J., Fallick, A.E. & Whitehouse, M.J. (2007): Temporal constraints on the Paleoproterozoic Lomagundi-Jatuli carbon isotopic event. Geology 35, 655 – 658.
Melezhik, V.A., Fallick, A.E., Filipov, M.M., Lepland, A., Rychanik, D.V., Deines, J.E., Medvedev, P.V., Romashkin, A.E., Strauss, H. (2009): Petroleum surface oil seeps from Palaeoproterozoic petrified giant oilfield. Terra Nova 21, 119 – 126.
Prokoph, A., Shields, G.A. & Veizer, J. (2008): Compilation and time-series analysis of a marine carbonate $\delta^{18}O$, $\delta^{13}C$, $^{87}Sr/^{86}Sr$ and $\delta^{34}S$ database through Earth history. Earth Sci. Reviews 87, 113 – 133.
Waldbauer, J.R., Sherman, L.S., Sumner, D.Y. & Summons, R.E. (2009): Late Archean molecular fossils from the Transvaal Supergroup record the antiquity of microbial diversity and aerobiosis. Precambr. Res. 169, 28 – 47.

ICDP

Fault zone damage and chemical reactions at depth in the San Andreas Fault Zone: A study of SAFOD drill core samples

C. JANSSEN[1], R. WIRTH[1], E. RYBACKI[1], H.-R. WENK[2], G. DRESEN[1]

1GFZ German Research Centre for Geosciences, Telegrafenberg, 14473 Potsdam, Germany
2Department of Earth and Planetary Science, University of California, Berkeley, CA 94720, USA

Microstructures and chemical composition of four core samples from the San Andreas Fault drill hole (SAFOD; Fig 1a-c) have been examined using scanning and transmission electron microscopy (SEM, TEM), X-ray diffraction analyses (XRD), mercury porosimetry, Brunauer, Emmett and Teller (BET) gas adsorption methods and stable isotope analyses. Optical inspection of thin sections, SEM, TEM, and XRD analysis revealed that the cataclasites and fault breccias are mainly composed of quartz, clay minerals (illite/smectite, chlorite), feldspar (plagioclase), amorphous material, and calcite with grain sizes between 200 nm and 500 µm. The fine-grained (< 1µm) gouge matrix contains clasts (feldspar, quartz) and is frequently cut by fault-related calcite veins. Observed microstructures in the fine-grained matrix indicate intense shearing and dissolution-precipitation as main deformation processes.

Amorphous material

Based on our TEM observations we consider the previously undetected presence of abundant amorphous phases in two SAFOD samples (Fig. 2a-e) as a potential key factor reducing shear strength and promoting the absolute weakness of the SAF. We observed (1) amorphous material on a slickenside surface, (2) glassy bands contained in an ultracataclastic matrix and (3) amorphous rims surrounding quartz and feldspar grains. Chemical analyses of the amorphous material reveal that the silica content is slightly enriched or similar in comparison to the adjacent matrix.

We suggest that all amorphous material was formed by comminution of grains (crush-origin pseudotachylytes) rather than by melting (melt-origin pseudotachylytes). The observed amorphous material may behave like a viscous fluid film lubricant that is sheared between fault surfaces and gouge fragments reducing friction in the fault zone. We propose that the occurrence of amorphous material within the fault rocks is an essential factor in understanding the mechanically weak behavior of the San Andreas Fault [Janssen et al., 2010].

Nano-scale porosity

Concerning the question if the fault zone is weak because of elevated fluid pressure our findings show that nano-scale porosity may play an important role in the formation of elevated pore pressure [Janssen et al, 2011].

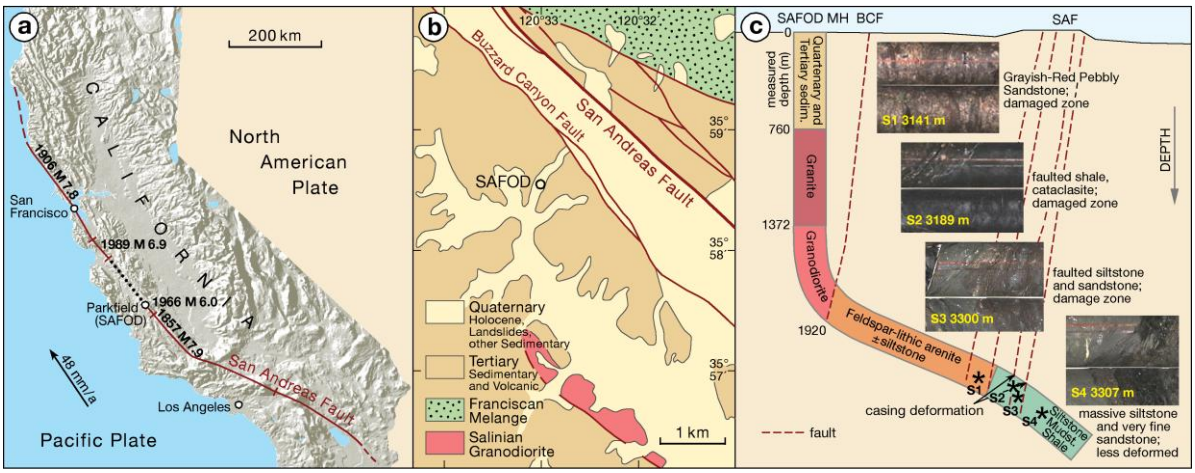

Figure 1. Location map of the study area. (a) The San Andreas Fault with the SAFOD drill site. The arrow shows the sense of plate movement [*Hickman et al.*, 2004]. Some major historical earthquakes are indicated. The dotted line characterizes the creeping segment. (b) Geological map of the drilling site [modified after *Dibblee et al*., 1999 and *Bradbury et al*., 2007]. (c) Simplified depth profile of the SAFOD MH (Main Hole) with different rock lithologies and sample positions (synchronized to the Phase 2 Baker-Atlas Open-hole logs). The red stars mark the positions of the two samples with amorphous material. BCF-Buzzard Canyon fault, SAF-San Andreas Fault.

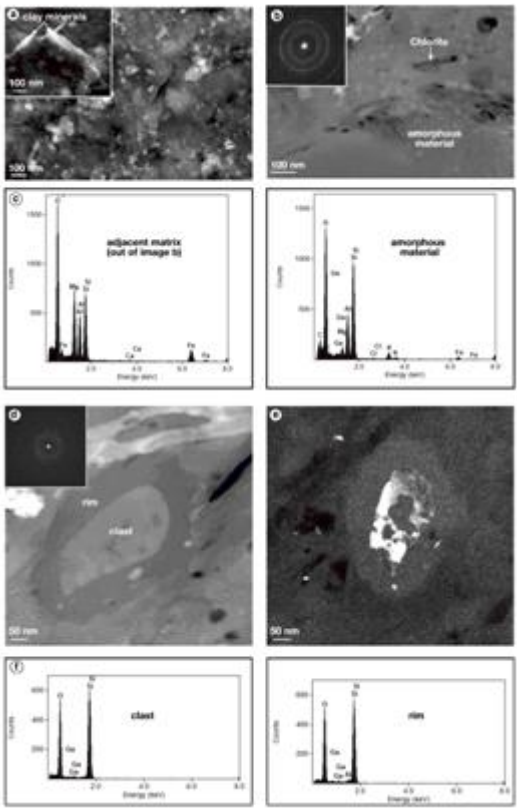

Fig. 2: (a) SEM micrograph illustrates a fault surface of sample 3 covered by silica thin-film coatings. The upper-left corner shows newly formed clay minerals with a characteristic flaky shape. (b) TEM bright field image illustrates the presence of authigenic chlorites in an amorphous matrix. The upper-left corner shows the broad diffuse scattering intensity of amorphous material additional to individual reflections from crystalline material in the diffraction pattern. (c) EDX spectra of adjacent matrix and amorphous material. (d) TEM HAADF image of a Quartz grain surrounded by a small amorphous rim containing rutile/anatase crystals (bright crystals). The upper-left corner shows the diffraction pattern of the rim. (e) TEM dark field image shows an eroded and etched quartz clast. (f) EDX spectra of clast and amorphous rim.

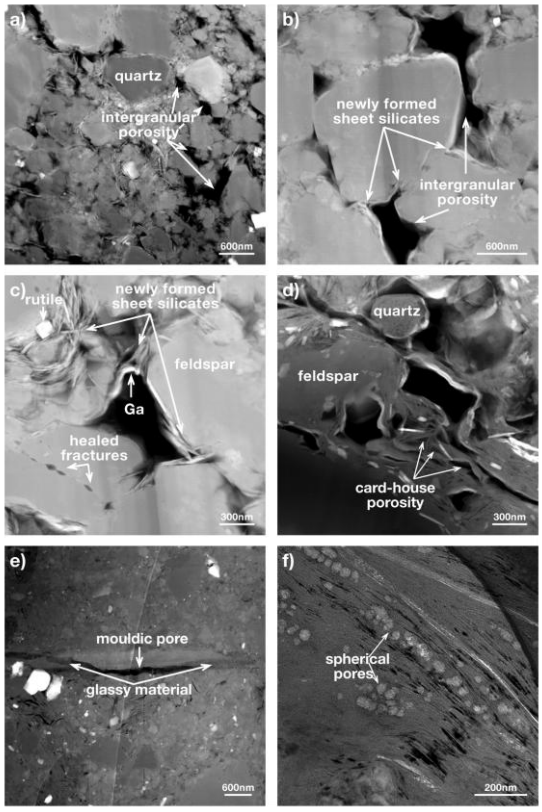

Fig. 3: Microphotographs of in-situ pore types. (a) TEM high-angle annular dark field (HAADF) image illustrates the distribution of intergranular porosity of sample S4. (b) TEM HAADF image of open pore spaces located around quartz and feldspar grains. (c) A single open pore lined with newly formed sheet silicates indicating porosity formation during or after deformation. Gallium is redeposited on the pore surface during sample preparation (d) Clay flakes in edge-to-face contact form card house structures with small open pore spaces between the clay flakes. (e) Large mouldic pore with an elongated shape. The open pore space is partly filled with amorphous material. (f) TEM bright field image shows round-shaped nano-pores agglomerated or lined up like pearls on a string.

We observed nanometer-sized pores in all four gouge/ultracataclastic and fractured core samples using TEM. Cutting of foils with the focused ion beam technique (FIB) allowed identifying porosity down to the nm scale. Between 40-50% of all pores could be indentified as in-situ pores showing no signs of damage related to sample preparation. The total porosity estimated from TEM micrographs (1-5%) is comparable to the connected fault rock porosity (2.8-6.7%) estimated by mercury injection. Permeability estimates for gouge/ultracataclastic fault rocks are 10^{-21} – 10^{-19} m^2 and 10-17 m^2 for fractured fault rocks. Porosity and permeability are independent of sample size. TEM images reveal that the porosity is intimately linked to fault rock composition and to the degree of deformation. The TEM-estimated porosity of the samples increases with increasing clay content. Based on pore morphology we distinguish different pore types varying with fault rock fabric and alteration (Fig. 3). The pore geometry derived from TEM observations and BET gas adsorption/desorption hysteresis curves indicates pore-blocking effects in the fine-grained matrix. Observations of isolated pores in TEM micrographs and high pore-body to pore-throat ratios inferred from mercury injection suggest elevated pore fluid pressure in the low permeability gouge, reducing shear strength of the fault [Janssen et al, 2011].

Fluid-rock interactions

The influence of fluid-rock interactions on mineralogical and geochemical changes in fault rocks is visible in pronounced dissolution-precipitation processes (stylolites, solution seams) as well as in the formation of new phases. Detrital quartz and feldspar grains are partially dissolved and replaced by authigenic illite-smectite (I-S) mixed–layer clay minerals (Fig.4). TEM imaging of these grains reveals that the alteration processes initiated within pores and small fissures inside these grains. In one sample syntectonic fluid-assisted overgrowth of chlorite-rich films on slickensides partly replaced sedimentary quartz grains. In addition quartz and feldspar grains are partially dissolved with sutured boundaries [Janssen et al., 2009].

Low-temperature deformation in calcite veins

Besides the investigation of the fault rock matrix we analyzed microstructures in calcite veins within all four

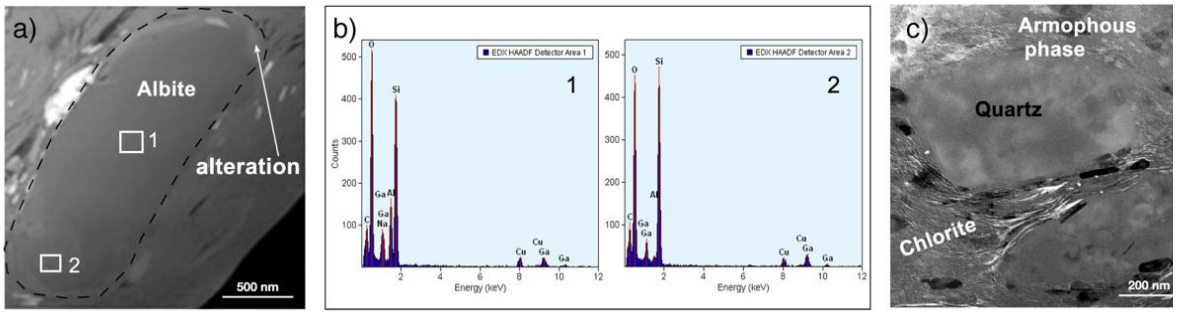

Fig. 4: TEM images of altered grains. (a) Albite grain in the initial stages of alteration at its margin; the squares mark points of analyses. (b) Analysis 1 represents pure albite; analysis 2 shows that Na is leached. (c) Quartz grain partly dissolved and replaced by chlorite (TEM-HAADF).

samples. First, we described microstructures examined under optical and transmission electron microscopes with the aim of providing information on the fault evolution. Second, we interpret dislocation and twin densities measured in the calcite veins in terms of stress estimation based on paleo-piezometric relationships. Preliminary results reveal that all calcite veins are fault-related as their abundance increases towards the active fault trace. Under the cathodoluminescence (CL)-microscope, all calcite veins show uniform yellow to orange CL-colors, suggesting that the original fluids from which the calcite precipitated had similar composition. In addition, the missing zoning of crystals may indicate a fast precipitation of vein calcites [Gratier and Gamond, 1990].

Calcite cements with different deformation features occur in most of the inspected samples. Vein cements with strong deformation show evidence for intense intracrystalline plasticity. Many curved dislocations are present, indicating active dislocation climb (Fig. 5a). The dislocations are spatially variable, sometimes forming cell-like networks. Evidence for subgrain formation like dislocation walls was not detected. The average dislocation density in the most strongly deformed calcite veins is about $(2.7 \pm 1.3) \cdot 10^{13}$ m^{-2} indicating a local maximum stress of about 135 MPa [Rybacki et al., 2011]. In comparison, the weakly deformed vein calcites contain much less dislocations (Fig. 5b). They appear to be more straight than in veins with high dislocation density, which probably points to limited climb activity. Dislocation densitiy in the most weakly deformed calcites is about $(2.9 \pm 1.1) \cdot 10^{12}$ m^{-2}. The corresponding differential stress is about 33 MPa.

Analyses of stable isotopes

Stable isotope data of different deformed vein generations in samples S2-S4 were used to identify fluid sources. The isotopic composition for all veins varies for $\delta^{18}O$ between 16.9‰ and 19.6‰ SMOW and for $\delta^{13}C$ between 0.79‰ and -9.61‰ PDB. Carbon isotope ratios scatter more than the oxygen isotope ratios, indicating only small differences between vein generations. Assuming an isotopic equilibration temperature from 110° C [see Schleicher et al., 2009 and Mittempergher et al., 2009] the oxygen-isotope water fractionation [O'Neil et al., 1969] yield $\delta^{18}O$ values of 0.855-3.55‰ for the fluid from which the calcite precipitated. This range of estimated $\delta^{18}O$ H_2O values indicate that vein calcite was probably precipitated from seawater and precludes a meteoric origin. The depleted $\delta^{13}C$ values suggest that calcite precipitated in an environment influenced by organic matter.

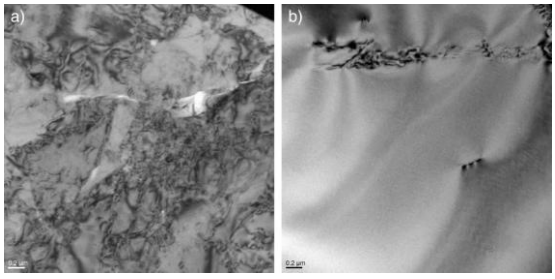

Fig. 5: Vein calcite with dislocations. (a) Vein calcite with a high dislocation density. Note that the dislocations are forming cell networks (b) Weakly deformed vein calcite with only few dislocations.

References

Bradbury, K.K., Barton, D.C., Solum, J.G., Draper, S.D., Evans, J.P., 2007. Mineralogical and textural analyses of drill cuttings from the San Andreas Fault Observatory at Depth (SAFOD) boreholes: Initial interpretations of fault zone composition and constraints on geological models. Geosphere 3, 299-318.

Dibblee, T.W., Graham, S.E., Mahony, T.M., Blissenbach, J.L., Mariant, J.J., Wentworth, C.M., 1999. Regional geologic map of San Andreas and related faults in Carrizo Plain, Temblor, Caliente and La Panza Ranges and vicinity, California: A digital database. U.S. Geological. Survey, Open File Report 99–114.

Gratier, J.P., Gamond, J.F., 1990. Transition between seismic and aseismic deformation in the upper crust. Geol. Soc. Spec. Publ. 54, 461-473.

Hickmann, S., Zoback, M., Ellsworth, W., 2004. Introduction to special section: Preparing for San Andreas Fault Observatory at Depth. Geophys. Res. Lett., 31, doi:10.1029/2004GL020688

Janssen, C.; Wirth, R.; Rybacki, E.; Naumann, R.; Kemnitz, H., 2009. Micro- and Nanostructures of SAFOD Core Samples - First Results. EOS Trans. AGU 90(52), Fall Meet. Suppl., Abstract T53C-1598.

Janssen, C., Wirth, R., Rybacki, E., Naumann, R., Kemmnitz, H., Wenk, H.-R., Dresen, G., 2010. Amorphous material in SAFOD core samples (San Andreas Fault): Evidence for crush-origin pseudotachylytes? Geophys. Res. Lett., 37, doi: 10.2029GL040993.

Janssen, C., Wirth, R., Reinicke, A., Rybacki, E., Naumann, R., Kemmnitz, H., Wenk, H.-R., Dresen, G., 2011. Nanoscale porosity in SAFOD core samples (San Andreas Fault). Earth and Planetary Science Leters, 301, 179-189.

Mittempergher, S., Toro, G.D., Gratier, J., Hadizadeh, J., Smith, S.A., Desbois, G., Spiess, R., 2009. Evidence of transient increase of fluid pressure in isolated patches of the San Andreas Fault in SAFOD phase III cores. EOS Trans. AGU 90(52), Fall Meet. Suppl., Abstract T52B-04.

O'Neil, J.R., Clayton, R.N. and Mayeda, T.K., 1969. Oxygen isotope fractionation in divalent metal carbonates. J. Chem. Phys., 51: 5547-5558.

Rybacki, E., Janssen C., Wirth, R., Chen, K., Wenk, H.-R., Dresen, G., 2010. Low-temperature deformation in calcite veins of SAFOD core samples (San Andreas Fault) – microstructural analysis and implications for fault rheology. Tectonophysics, submitted

Schleicher, A.M., Warr, L.N., van der Pluijm, B.A., 2009. On the origin of mixed-layered clay minerals from the San Andreas Fault at 2.5-3 km vertical depth (SAFOD drillhole at Parkfield, California). Contributions to Mineralogy and Petrology 157, 173-187.

IODP

Calcareous nannofossil ecology and paleoredox conditions across the Paleocene-Eocene Thermal Maximum at Demerara Rise, western Atlantic (ODP Leg 207)

C. JOACHIM[1], J. MUTTERLOSE[1], P. SCHULTE[2], H.- J. BRUMSACK[3]

[1] GMG, Ruhr-University Bochum, Universitätsstr. 150, D-44801 Bochum, Germany

[2] GeoZentrum Nordbayern, University Erlangen, D-91056 Erlangen, Germany

[3] ICBM, Oldenburg Univerity, D-26111 Oldenburg, Germany

Calcareous nannofossil assemblage changes as well as variations of redox conditions during the Paleocene-Eocene thermal maximum (PETM) are currently investigated to constrain the spatial and water depth-dependent pattern of warming, carbon input, and O2 deficiency in the global ocean (e.g., Chun et al., 2010; Gibbs et al., 2010; Leon-Rodriguez & Dickens, 2010; Nicolo et al., 2010; Raffi, et al., 2009). Here, we investigate the PETM in the tropical, western Atlantic (ODP Leg 207, Site 1258C Demerara Rise) by a set of calcareous nannofossils as well as stable isotope and element geochemical data. Generally, the PETM record on the Demerara Rise (lower-bathyal to upper-abyssal paleodepth, ~2000 m) shows a pronounced and sharp lithologic change from calcareous chalks to laminated, clay-rich beds present in several drill sites across a depth transect.

Calcareous nannofossils were studied on a high-resolution scale of 2 to 5 cm, resulting in 168 settling slides. In the pre–PETM interval the species richness ranges from 20 to 32. The lowermost 22 cm of the PETM interval shows a sharp drop to an assemblage of low abundance and low diversity (6 species). Subsequently, in the upper 1,25 m of the PETM sequence, species richness increases almost to pre-PETM values of about 19 species and remains on this level also in the post-PETM succession. Absolute abundances amount to a maximum of 2.3x109 specimens/g sediment in the pre-PETM interval. At the base of the PETM abundances drop to values slightly above zero, stay below 2.5x106 specimens/g sediment during the event, and increase slowly above the PETM. Abundances are below 1.0x109 specimens/g sediment for the remaining part of the PETM succession. Calcareous nannofossils show pronounced changes in the assemblage composition. Increased abundances of Campylosphaera sp. and Chiasmolithus sp. precede the onset of the PETM and may indicate eutrophic conditions. The nannofossil record during the PETM onset is obscured by carbonate dissolution, causing low total abundances in the lowermost 35 cm of the PETM. Small taxa including Coronocyclus bramlettei and Coccolithus minimus seem to have favoured the conditions prevailing during the early phase of the PETM, even if the assemblage is heavily distorted by deep water acidification. During the recovery stage of the PETM, the large - sized species Coccolithus bownii appears with high percentages and remains highly abundant throughout the remaining interval. Discoasterids indicating warm surface-waters become more frequent and diversify concomitant to the PETM onset. Discoaster araneus is characterized by a reduction of its rays from a maximum of 9 in the lowermost part of the PETM to a minimum of 5 to 6 rays in the later stage. Deformed discoasterids are common throughout the entire PETM interval, paralleled by C. bownii and Rhomboaster cuspis as well as by small sized Campylosphaera spp. Mutterlose et al. (2007) suggested productivity, pH and salinity changes at Demerara Rise during the PETM, based on a low resolution study. The assemblage shifts observed in this study suggest, however, a concert of three different ecological factors: productivity increases significantly in the pre-PETM interval, deep water acidification appears for a short periode synchronous to the PETM onset, and higher temperatures dominate the entire “core” and early “recovery” interval.

The typical stable isotope pattern anomaly across the PETM is somewhat disturbed at this site since carbon isotopes show a negative anomaly with values as low as –10 ‰, whereas oxygen isotopes reveal a positive excursion. These isotopic signatures indicate the early diagenetic formation of 13C-depleted carbonates in the claystone after burial. However, as outlined above, calcareous nannofossil faunal assemblages and the CaCO3 distribution both show typical PETM patterns similar to other deep-sea sites. A strong drop in Si/Al ratios concomitant to the onset of the PETM points to reduced Si input derived from silicic organisms (e.g., radiolarians). Subtle changes are evident for certain other element/Al ratios indicative for provenance change (K, Na, Ti, Fe, Rb, Zr). However, Mn/Al ratios and bulk Mn enrichment factors (EF) compared to crustal values show a substantial drop during the PETM onset, followed by a gradual recovery to pre-event values. In contrast to the depletion of Mn, other typical redox-sensitive elements (e.g., V, Cr, Co) or element/Al ratios show no major changes across the PETM, and U as well as Mo stay close to the detection limit. These results indicate that W Atlantic deep waters were oxygenated before and after the PETM, but lower in dissolved oxygen content during the onset of this hyperthermal event, suggesting a considerable vertical expansion of the oxygen minimum zone correlative to carbonate dissolution (Chun et al., 2010, Gibbs et al., 2010).

References:

Chun, C.O.J., Delaney, M.L., and Zachos, J.C., 2010, Paleo-redox changes across the Paleocene-Eocene Thermal Maximum, Walvis Ridge (ODP Sites 1262, 1263, and 1266): Evidence from Mn and U enrichment factors. Paleoceanography, 25, PA4202.

Gibbs, S.J., Stoll, H.M., Bown, P.R., and Bralower, T.J., 2010, Ocean acidification and surface water carbonate production across the Paleocene-Eocene thermal maximum. Earth Planet. Sci. Lett., 295, 583-592.

Leon-Rodriguez, L., and Dickens, G.R., 2010, Constraints on ocean acidification associated with rapid and massive carbon injections: The early Paleogene record at Ocean Drilling Program Site 1215, Equatorial Pacific Ocean. Palaeogeogr. Palaeoclimatol. Palaeoecol., 298, 409-420.

Mutterlose, J., Linnert, C., and Norris, R., 2007, Calcareous nannofossils from the Paleocene-Eocene Thermal Maximum of the equatorial Atlantic (ODP Site 1260B): Evidence for tropical warming. Mar. Micropal., 65, 13-31.

Nicolo, M.J., Dickens, G.R., and Hollis, C.J., 2010, South Pacific intermediate water oxygen depletion at the onset of the Paleocene-Eocene Thermal Maximum as depicted in New Zealand margin sections. Paleoceanography, 25, PA4210.

Raffi, I., Backman, J., Zachos, J.C., and Sluijs, A., 2009, The response of calcareous nannofossil assemblages to the Paleocene Eocene Thermal Maximum at the Walvis Ridge in the South Atlantic. Mar. Micropal., 70, 201-212.

IODP

Late-stage veining in samples from Leg 304/305 provides insights into the uplift history of the Atlantis Massif oceanic core complex

N. JÖNS[1], W. BACH[1], M. ROSNER[1,2,3], B. PLESSEN[2]

[1] FB 05 Geowissenschaften, Universität Bremen
[2] Helmholtz-Zentrum Potsdam, Deutsches GeoForschungsZentrum GFZ
[3] Fachbereich Geowissenschaften, Freie Universität Berlin

Although slow- and ultraslow spreading ridges are common types of oceanic spreading centers, their general anatomy and evolution is poorly understood. It is known that most of the extension at slow-spreading ridges is tectonic, with episodes of magmatic accretion, and overall low magma budgets. This tectonically driven extension has recently been recognized as a mode of seafloor spreading that is fundamentally different from the established models valid for fast-spreading ridges (e.g., Escartín & Canales, 2011). The differences in spreading rate manifest in a distinct crustal anatomy with large-offset oceanic detachment faults leading to oceanic core complex formation. Furthermore, the lithosphere is heterogeneous in composition, strongly tectonized and large outcrops of gabbroic rocks and peridotites occur at the seafloor. The diversity in lithospheric composition and structure opens possibilities for the occurrence of variable types of hydrothermal systems and thus for a great diversity in the seafloor and sub-seafloor biosphere.

The Atlantis Massif is a prominent example of an oceanic core complex. It formed during the past 1.5-2.0 Ma (Blackman et al., 1998, 2002) at the Mid-Atlantic Ridge at ca. 30°N, near the intersection of the Atlantis Transform fault with the mid-oceanic ridge. IODP expeditions 304/305 (Blackman et al., 2006) drilled into the footwall (Site U1309) and hanging wall (Sites U1310 & U1311) of the detachment fault that is interpreted to be related to the exhumation of the Atlantis Massif. Late-stage mineral veins (e.g. consisting of anhydrite, calcite, prehnite or zeolite) that formed from sub-seafloor fluid-rock interactions provide a key to gaining a deeper understanding of the history of cooling and fluid flow during exhumation. We focused our study on footwall samples from Site U1309D, where the corrugated detachment fault surface was penetrated.

Despite the nearby Lost City hydrothermal vent field being hosted in ultramafic rocks, drill cores from U1309D are dominated by gabbros and troctolites. Just minor amounts of ultramafic (ca. 5 vol.%) and basaltic (ca. 3 vol.%) rocks are present. The drilled section is fractured and metamorphosed and shows evidence for extensive retrograde overprint, recorded by granulite- to zeolite-facies alteration assemblages. The most intense retrogression stage is characterized by greenschist-facies P-T conditions and the presence of hydrous fluids. Ultramafic rocks are strongly serpentinized and foliated; gabbros and troctolites show secondary mineral assemblages indicative of rodingitization and chloritization.

Syn- to postkinematic calcite forms as vein networks in both mafic and ultramafic rocks. Calcite is the only carbonate phase present. It is characterized by high Fe and Mn contents, whereas Mg contents are low. Concentrations of incompatible trace elements (e.g., U, Sr, Li) are low compared to calcite formed in the oceans. Measurements of rare earth elements (REE) reveal flat chondrite-normalized REE+Y patterns with a pronounced positive Eu anomaly. The overall variability in REE concentrations is high, ranging from ca. 10^{-2}x to 10x chondritic values. This points to differences in intensity of fluid-rock interactions. Moreover, REE+Y patterns show that the calcite precipitating fluids are similar to basalt-hosted high-T vents and indicate no affinity to the nearby serpentinization-derived Lost City vent field. The deep origin of the fluids and the low degrees of admixture of a seawater component is highlighted by low $^{87}Sr/^{86}Sr$ (0.704 to 0.708) as well as mantle-like $\delta^{7}Li_{LSVEC}$ (+0.8 to +9.4‰; n=3) and $\delta^{13}C_{PDB}$ (-6 to -2‰). Low $\delta^{13}C$ values indicate the absence of thermal methanogenesis and suggest peak fluid temperatures below 350°C. Accordingly, $\delta^{18}O_{VSMOW}$ values point to minimum temperatures of calcite precipitation in the range from 150 to 220°C. However, no systematic trend of $\delta^{18}O$ with depth is observed, indicating upwelling of already conductively cooled basement fluids. Thus, calcite precipitation temperatures do not record a past local geothermal gradient of the oceanic crust.

From a depth of about 740 mbsf, two massive cm-wide veins were recovered, consisting of anhydrite and anhydrite

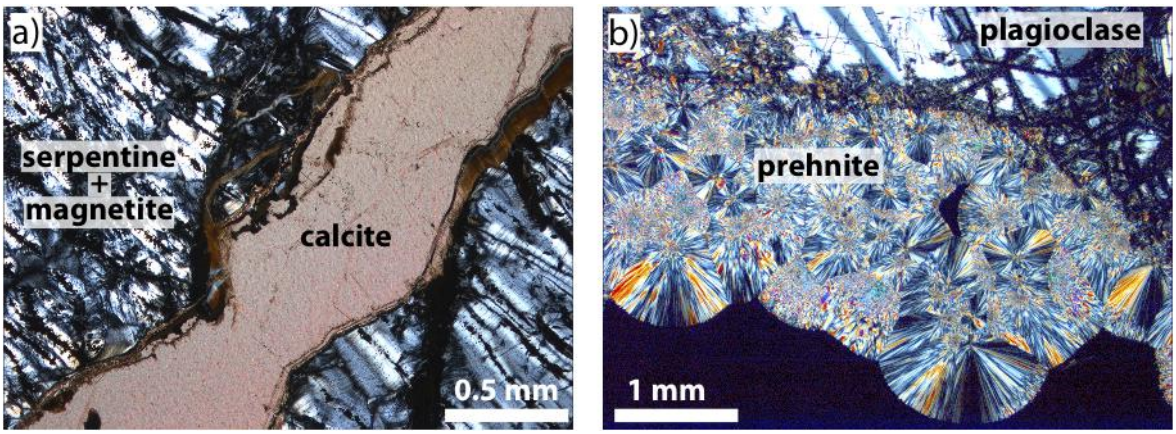

Figure 1: a) Massive calcite vein crosscutting a strongly foliated and serpentinized peridotite (cross-polarized light; sample 304-65R1_31-36cm). b) Radially fibrous prehnite as vein filling in gabbro (cross-polarized light; 305-231R2_123-127cm).

+ zeolite, respectively. In situ LA-MC-ICP-MS $^{87}Sr/^{86}Sr$ data display different Sr isotope compositions for the two samples, with uniform Sr isotope ratios across each vein. Five discrete analyses of the pure anhydrite vein indicate a very constant $^{87}Sr/^{86}Sr$ ration of 0.70774 (±0.00005 2SD, n=5). The slightly deeper composite anhydrite-zeolite vein is much more unradiogenic and shows more variable $^{87}Sr/^{86}Sr$ (0.70631 ± 0.00017 2SD, n=5). The latter is close to high end $^{87}Sr/^{86}Sr$ values of calcite veins. Comparing the anhydrite $^{87}Sr/^{86}Sr$ values from U1309D with TAG and PACMANUS hydrothermal sites, we infer anhydrite formation from down-flowing seawater heated to ≈150°C. The occurrence of anhydrite veins at ca. 740 mbsf reveals local penetration of seawater to relatively great depths. The $^{87}Sr/^{86}Sr$ ratios of anhydrite transitional between seawater and hydrothermal fluid reveals that the infiltrating seawater leached unradiogenic Sr from the basement on its way down. REE patterns indicate that admixed hydrothermal fluids at depth played a minor role, as the anhydrite vein has no pronounced positive Eu anomaly.

Silicate veins – both monomineralic and composite – occur throughout the entire 1415.5m of the U1309D core. Monomineralic veins consist of prehnite, quartz and plagioclase. The $\delta^{18}O_{VSMOW}$ values of pure quartz veins range from +11.4 to +12.1‰. This corresponds to precipitation temperatures of ca. 200-210°C (assuming a fluid $\delta^{18}O$= 0‰). An almost end-member albite vein records higher formation temperatures of ca. 270°C ($\delta^{18}O$= +6.47‰). That fluid circulation persisted upon cooling is documented by a prehnite vein with $\delta^{18}O$= +9.22‰, pointing to a precipitation temperature of ca. 145°C. Composite veins consisting of plagioclase + quartz or prehnite + thomsonite range in $\delta^{18}O$ from +7.0‰ to +12.3‰. Here, the thomsonite-bearing veins have the lowest $\delta^{18}O$ values, whereas plagioclase-quartz mixtures have $\delta^{18}O$ similar to pure quartz veins. Strontium isotope analyses of silicate veins reveal comparatively unradiogenic compositions ($^{87}Sr/^{86}Sr$= 0.703300-0.704580). The $^{87}Sr/^{86}Sr$ ratios from silicate veins are even lower than in calcite veins and may again be explained by leaching of unradiogenic Sr from the basement rocks or by mixing with unradiogenic hydrothermal fluids. The comparison of $^{87}Sr/^{86}Sr$ ratios from anhydrite- (depth ca. 740 mbsf) and prehnite-bearing veins (depth > 1100m), which have formed at similar temperatures, points to a decreasing influence of seawater infiltration with increasing depth.

In summary, late-stage veins in Leg 304/305 Site U1309D samples provide critical insights into the fluid regime and temperature conditions within the detachment fault footwall during formation of the Atlantis Massif oceanic core complex. The lack of systematic isotopic downhole trends indicates that already conductively cooled basement fluids are responsible for precipitation of vein minerals. Furthermore, the fluid chemistry of the nearby Lost City vent field is dominated by ultramafic rocks, while the U1309D calcite veins point to fluids with affinities to basalt-hosted hydrothermal systems. This finding emphasizes that the heterogeneous composition of slow-spreading crust offers possibilities for pronounced differences in hydrothermal systems on small spatial and/or temporal scales. Additionally, although rocks below the detachment fault surface are strongly tectonized, the seawater influence on the fluids is insignificant and thus dominantly mantle carbon is sequestered within the examined calcite veins.

References:
Blackman DK, Cann JR, Janssen B, Smith DK (1998) Origin of extensional core complexes: Evidence from the Mid-Atlantic Ridge at Atlantis Fracture Zone. Journal of Geophysical Research 103(B9):21315-21333.
Blackman DK, Karson JA, Kelley DS, Cann JR, Früh-Green GL, Gee JS, Hurst SD, John BE, Morgan JP, Nooner SL, Ross DK, Schroeder TJ, Williams EA (2002) Geology of the Atlantis Massif (Mid-Atlantic Ridge, 30° N): Implications for the evolution of an ultramafic oceanic core complex. Marine Geophysical Researches 23:443-469.
Blackman DK, Ildefonse B, John BE, Ohara Y, Miller DJ, MacLeod CJ, Expedition 304/305 Scientists (2006) Oceanic Core Complex formation, Atlantis Massif (Expedition 304/305 summary). Proceedings of the Integrated Ocean Drilling Program 304/305.
Escartín J, Canales JP (2011) Detachments in oceanic lithosphere: Deformation, magmatism, fluid flow, and ecosystems. EOS Transactions 92:31.

IODP

The Campanian – Maastrichtian (Late Cretaceous) climate transition: the history of palaeoceanographic changes

C. JUNG[1], S. VOIGT[1], O.FRIEDRICH[1], M. FRANK[2]

[1] University of Frankfurt am Main, Institue of Geology, Altenhöferallee 1, 60438 Frankfurt am Main, Germany
[2] Leibniz-Institute for Marine Science, IFM-GEOMAR, Wischhofstr. 1-3, 24148 Kiel, Germany

The Late Cretaceous was a period of long-term climate cooling succeeding the extreme warmth of the mid-Cretaceous greenhouse world. The cooling is mainly considered as a result of changes in ocean circulation due to plate-tectonic movements resulting in progressive deep-water exchange between the deep oceanic basins and a parallel drop in pCO2 concentrations. The aim of this project is the reconstruction of changes in ocean circulation and deep-water formation in the tropical Pacific (Shatsky Rise) relative to carbon isotope events in the latest Campanian to late Maastrichtian carbon isotope events (CMBE and MME). The main objectives of this project are 1) to develop a high-resolution carbon isotope stratigraphy at Shatsky Rise (DSDP-Site 305, ODP-Site 1210B), 2) to reconstruct the history of changes in tropical surface- and deep-water temperatures, and 3) to decipher changes in ocean circulation and the source regions of different deep- and intermediate water masses.

During Year 1, a new high-resolution $\delta^{13}C$ record was measured for Site 1210B in order to improve the stratigraphic resolution (Figure 1). The new $\delta^{13}C$ record from Site 1210B allows for a detailed correlation with the previously generated $\delta^{13}C$ record of Site 305 that represents a deeper site at Shatsky Rise (Voigt et al. 2010). The correlation is validated by FO ages of planktic foraminifera and provides evidence for two major gaps below and above the CMBE of Site 305, each representing a 1 to 2 Ma long period of erosion and non-deposition. The Campanian-Maastrichtian Boundary Event (CMBE) is characterized by a distinct long-lasting negative carbon isotope excursion and a short-term increase in oxygen isotopes recorded from the tropical Pacific, the Indian Ocean and the Southern Ocean. In fact, the first results of this project clearly show that the detection of sedimentary gaps is a serious issue in the paleoceanographic interpretation of deep-sea cores.

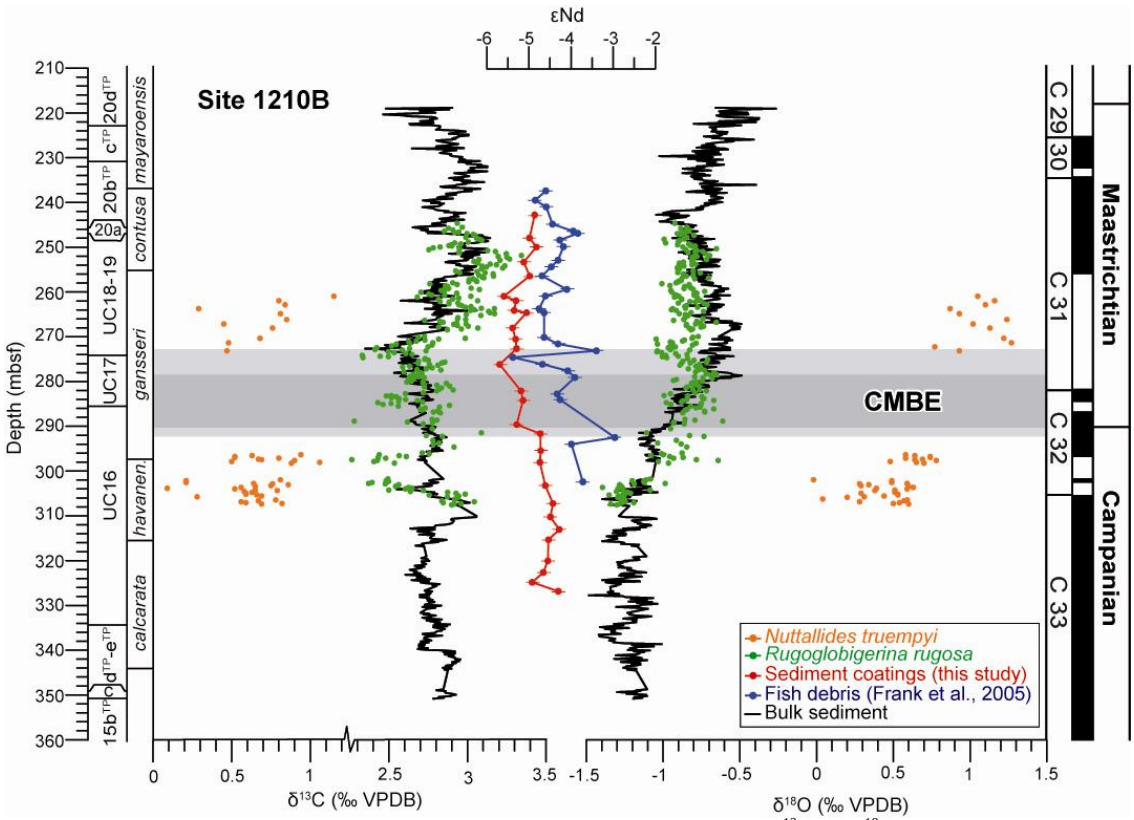

Figure 1. Preliminary compilation of bulk-carbonate and planktic and benthic foraminiferal $\delta^{13}C$ and $\delta^{18}O$ data together with Nd isotopes from sediment coatings (this project) and fish debris (Frank et al. 2005) at Site 1210B, Shatsky Rise. The decrease towards less radiogenic εNd values during the CMBE suggests the Southern Ocean as an intermittent deep-water source.

Another question addressed in our proposal was the occurrence of a late Campanian negative carbon isotope event (LCE) in the tropical Pacific. The new 1210B $\delta^{13}C$ record does not show such a distinct carbon isotope excursion as it is recorded from European shelf records (sections in Gubbio, Italy, Norfolk, UK, Lägerdorf, N-Germany, Tercis, France; Voigt et al. 2010 and unpublished data). Possible reasons could be 1) regional effects restricted to locations in Europe or to shallower shelves, 2) a hiatus at Shatsky Rise, or 3) a much smaller magnitude of the event which makes it indistinguishable from the background noise.

Nevertheless, the new high-resolution $\delta^{13}C$ stratigraphy provides a reliable stratigraphic framework that enables us to attend the history of changes in surface- and deep water temperatures. At Site 1210B, a total of 400 samples were processed to analyse the $\delta^{13}C$ and $\delta^{18}O$ of the planktic foraminifera Rugoglobigerina rugosa and the benthic foraminifera Nuttallides truempyi, representing the interval from the late Campanian up to the mid-Maastrichtian. Here, we present the first 250 planktic and 50 benthic isotope data (Figure 1). Two preliminary conclusions can be drawn at present. First, the planktic $\delta^{18}O$ record of R. rugosa closely resembles the $\delta^{18}O$ record of bulk-carbonates and displays a period of surface-water cooling that accompanies the negative carbon isotope excursion of the CMBE. Second, the benthic $\delta^{18}O$ data of N. truempyi show a distinct cooling trend in bottom waters that is of higher magnitude (~2°C without ice).

Changes in ocean circulation and the source regions of different deep and intermediate water masses will be deciphered by using radiogenic isotopes (Nd). In this project we used ferromanganese oxide coatings of bulk sediments as archive to analyse Nd isotopes (Gutjahr et al. 2007, Martin et al. 2010). A total of 55 samples was processed from the CMBE interval in the tropical Pacific (Site 1210B) and the Southern Ocean (Site 690) using the lab facilities at the IFM-GEOMAR. This approach is rather new for Cretaceous sediments. However, Nd extracted from bulk deep-sea sediment offers the potential to expand Nd isotopic studies on longer timescales beyond the spatial and temporal limitations of the presence of fossil fish debris. It was demonstrated that both archives deliver indistinguishable results for Cretaceous sediments (Martin et al. 2010).

Relatively high concentrations of Nd were extracted from the nannofossil chalks of Site 1210B. The analysis of sediment coatings is thus a promising tool to generate more continuous Nd isotope records of paleo-seawater from Cretaceous sediments. Especially, given that the amount of detrital material is very low and thus there is essentially no danger of contamination of the signature by partial leaching of detrital particles. Another preliminary observation is a small offset of Nd isotopes between sediment coatings and fish debris with lower values for the coatings (Figure 1). It is not clear at present how this offset can be explained. Possible reasons include different times of Nd uptake in the two archives during early diagenesis or different proportions of pore-water contributions of Nd. Importantly, however, the trend of the data is essentially identical to one extracted from the fish debris but shows less scatter.

The first 28 data show relative radiogenic Nd isotopic signatures for the tropical Pacific (Site 1210B; ε_{Nd}= -4.3 to

-5.7; Figure 1). At Shatsky Rise (Site 1210B), the bottom-water Nd isotope composition shows a distinct trend towards less radiogenic values that was enhanced during the CMBE interval (Figure 1). Concomitant to the termination of the CMBE the εNd values became more radiogenic again parallel to the long-term δ13C trend. The interval with the lowest Nd isotope signatures coincided with the major cooling of surface and bottom waters and suggests a change in ocean circulation with an intermittent influx of intermediate and/or deep waters from the Southern Ocean. At present, our data suggest that most of the planktic and benthic isotopic variability was related to shifts in the sources and mixing of deep waters and consequently the reconfiguration of ocean currents. The long duration of the CMBE (> 2 Ma) exclude a glaciation as the single mechanism and supports tectonically driven processes (Voigt and Schönfeld 2010).

The aim of for the third year will focus on the reconstruction of changes in ocean circulation and deep-water formation relative to the early and mid-Maastrichtian carbon isotope excursions (CMBE, MME). The high-resolution carbon isotope stratigraphy of bulk-carbonates successfully developed at Shatsky Rise (DSDP/ODP Sites 305, 1210B) during Year 1 forms the stratigraphic framework for the studies supposed in the renewal proposal. The reconstruction of the history of changes in surface- and deep-water temperature, water-column stratification and intermediate-to-deep-water mass sources (focus of Years 1 and 2) will be extended into the higher Maastrichtian with special focus on the 68-69 Ma interval of the MME. In addition to the already processed Nd isotope data of Site 1210B, we plan to extend the Nd isotope record of Fe-Mn oxide coatings from the tropical Pacific (Site 1210B) and to add new data from the South Atlantic (Site 525) and the Southern Ocean (Sites 690 and 761).

References:

Frank, T.D., Thomas, D.J., Leckie, R.M., et al., 2005. The Maastrichtian record from Shatsky Rise (northwest Pacific): A tropical perspective on global ecological and oceanographic changes. Paleoceanography, 20, PA1008, doi:10.1029/2004PA001052.

Gutjahr, M., Frank, M., Stirling, C.H., Klemm, V., van de Flierdt, T. and Halliday, A.N., 2007. Reliable extraction of a deepwater trace metal isotope signal from Fe-Mn oxyhydroxide coatings of marine sediments. Chemical Geology, 242, 351-370.

Martin, E.E., Blair, S.W., Kamenov, G.D., et al., 2010, Extraction of Nd isotopes from bulk deep sea sediments for paleoceanographic studies on Cenozoic time scales: Chemical Geology, v. 269, p. 414-431.

Voigt, S., Schönfeld, J. 2010. Cyclostratigraphy of the reference section for the Cretaceous white chalk of northern Germany, Lägerdorf — Kronsmoor: a late Campanian-early Maastrichtian orbital time scale. Palaeogeography, Palaeoclimatology, Palaeoecology, 287, 67-80.

Voigt, S., Friedrich, O., Norris, R .D. et al. 2010. Campanian – Maastrichtian carbon isotope stratigraphy: shelf–ocean correlation between the European shelf sea and the tropical Pacific Ocean. Newsletters on Stratigraphy, 44/1, 57-72.

IODP

The impact of tropical gateways on ocean circulation and climate during the Pliocene

C. KARAS[1,2], D. NÜRNBERG[2], R. TIEDEMANN[3], D. GARBE-SCHÖNBERG[4]

[1] Biodiversity and Climate Research Centre (BIK-F), Institute of Geosciences, Goethe-University Frankfurt, D-60438, Germany
[2] Leibniz Institute of Marine Sciences (IFM-GEOMAR), University of Kiel, Wischhofstrasse 1-3, D-24148 Kiel, Germany
[3] Alfred Wegener Institute for Polar and Marine Research, Am Alten Hafen 26, D-27568 Bremerhaven, Germany
[4] Institute of Geosciences, University of Kiel, D-24118 Kiel, Germany

The impacts of the constrictions of the Indonesian Gateway and the Central American Seaway on ocean circulation are among the keys to understand Pliocene climate evolution, including the intensification of the Northern Hemisphere Glaciation between 3.5 and 2.5 Ma. Plate tectonic reconstructions show that the main reorganization of one such seaway, the Indonesian Gateway, occurred between 4 and 3 Myr ago. Model simulations have suggested that this would have triggered a switch in the source of waters feeding the Indonesian throughflow into the Indian Ocean, from the warm salty waters of the South Pacific Ocean to the cool and relatively fresh waters of the North Pacific Ocean. Here, we show $\delta^{18}O$ and Mg/Ca ratios of planktonic foraminifera from different depth habitats to reconstruct the thermal structure at sensitive core sites in the Indian and Pacific Oceans from ~6 to 2 Myr ago: DSDP Site 214 in the tropical eastern Indian Ocean, ODP 763A in the subtropical east Indian Ocean under the influence of the Leeuwin Current, and DSDP Site 590B in the southwest Pacific Ocean at the Tasman Front.

In the outflow region of the Indonesian throughflow (DSDP Site 214), we find that sea surface conditions remained relatively stable throughout the mentioned Pliocene interval, while subsurface waters (300-450 m water depth) freshened and cooled by about 4°C between 3.5 and 2.95 Myr ago. We suggest that the constriction of the Indonesian Gateway led to the cooling and shoaling of the thermocline in the tropical Indian Ocean and might have contributed to cooling in various (sub)tropical upwelling regions. At Site 763, we found evidence for a ~2°C decrease in sea surface temperatures during the Mid-Pliocene pointing to a Leeuwin Current, which weakened since ~3.3 Myr ago in line with the hydrographic changes in the Indonesian Throughflow region. Most likely, a reduced surface Indonesian Throughflow led to a diminished poleward heat transport resulting in a weakened Leeuwin Current and a cooling of the Benguela upwelling system. The Tasman Front Site 590B data suggest influences by both gateways, the Central American and the Indonesian Gateway. We relate our observed gradual cooling of ~2°C, and freshening of the sea surface during ~4.6- 4 Ma to the constriction of the Central American Seaway, which reached a critical threshold during this time and presumably cooled the southwest Pacific through heat piracy by the Northern Hemisphere. After ~3.5 Ma, the ongoing restriction of the Indonesian Gateway might have amplified the southward heading East Australian Current,

allowing still warm sea surface temperatures at Site 590B when the global climate gradually cooled. In contrast, the cooling and freshening of the subsurface level in line with a marked increase in the sandfraction points to a fostered northward circulation of Subantartic Mode- and Antartic Intermediate waters, possibly a first step towards the present Antarctic Frontal System.

IODP

North Atlantic water mass distribution and Meridional Overturning Circulation, 3.3 – 3.0 Ma

N. KHÉLIFI[1], M. FRANK[1], D. NÜRNBERG[1], C. TESCHNER[1]

[1] Leibniz Institute of Marine Sciences (IFM–GEOMAR) at the University of Kiel

This project focuses on changes in the North Atlantic Meridional Overturning Circulation (MOC) and aims to provide a detailed reconstruction of intermediate and deep water mass distribution and circulation in the North Atlantic over the most recent global warm period in the Pliocene from ~3.3 to 3.0 Ma. During this 300 kyr interval, global temperature was ~3°C warmer than today, which is predicted to be reached before the end of this century due to anthropogenic climate change.

The Pliocene warm period is considered to be one of the closest and the most recent analogs for future global climate. It is thus uniquely suited for a case study with the goal to better understand the oceanographic and climatic processes controlling and responding to the global warming. On the basis of 5 core transects in the North Atlantic, we propose to constrain the water-mass composition and flow patterns, and to assess the changes of North Atlantic deep and intermediate water circulation over the Pliocene warm period. This systematic approach will help to more accurately evaluate the past variability of the North Atlantic MOC and its effects on climate under environmental conditions similar to our near future.

A glimpse into changes in intermediate and deep circulation in the northeast Atlantic during the Pliocene warm period is obtained at a first depth transect of four IODP/ODP drill sites by using combined ε_{Nd}, stable isotope, and Mg/Ca-based bottom water temperature records. First results show that during that time the Southern Ocean Water may have influenced substantial volumes of the deep North Atlantic reaching depths as shallower as ~2400 m. On longer timescale, a first significant re-organization of the intermediate-to-deep circulation in the North Atlantic towards the modern conditions appears to start after 1.5 Ma. This study will extend based on further core transects in order to better understand how water masses were distributed, how ocean circulation changed, and in which state the North Atlantic MOC was during this key period of past climate.

IODP

Towards a numerical model to constrain the time scales for vertically moving axial magma chambers at fast-spreading ocean ridges on the basis of natural samples drilled at IODP Site 1256D

C. KIRCHNER[1], J. KOEPKE[1], H. BEHRENS[1]

1 Institut fuer Mineralogie, Leibniz Universitaet Hannover, Callinstr. 3, 30167 Hannover, Germany, (c.kirchner@mineralogie.uni-hannover.de)

It is well accepted that AMCs ("axial magma chamber") under fast spreading ocean ridges located at the boundary between lower and upper crust are dynamic systems with the potential to move up and down. Nevertheless, the time scales of these vertical movements are poorly constrained up to now with very rough estimations, varying between 10 and 10000 years. This project focuses on a close investigation on the gabbro/sheeted dike transition, which is part of a reference profile of the upper oceanic crust recently drilled by IODP multi-cruise mission „Superfast Spreading Crust"(Site 1256, equatorial East Pacific Rise). Of substantial interest is a specific horizon defined as CBL ("conductive boundary layer"), separating the AMC and the hydrothermally altered dikes. The ascent of the AMC leads to the formation of "granoblastic dikes" due to an intense metamorphic overprint under granulite facies conditions [Koepke et al. 2008].

In order to quantify the vertical oscillations of the AMC described above, we are applying tools of diffusion profile modeling to relictic, zoned plagioclase and clinopyroxene phenocrysts within the granoblastic dikes, which were metamorphosed by the thermal imprint of the AMC (~1200°C) in a high position. Provided that the zoning patterns in the crystals studied are due to temperature-induced diffusion processes, the conditions of metamorphic overprint (temperature, volatile fugacities), and diffusion coefficients are known, the detailed analysis and modeling of the concentration profiles allows us a quantification of the residence time of the heat source (AMC) in a high position and hence, temporal information about the vertical fluctuations of the AMC can be constrained.

Here we report the current status of the project, including first results as well as some difficulties encountered during the diffusion modeling approach. Additionally, we also report about the experimental subproject, which is embedded in this study.

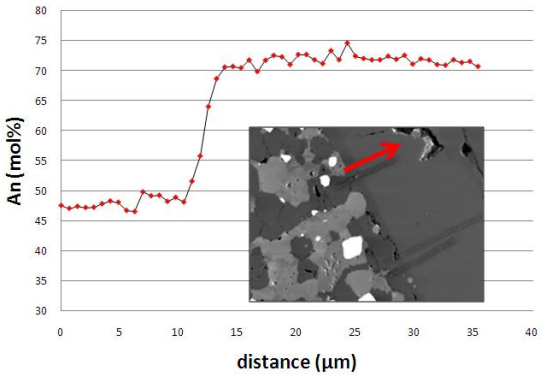

Figure 1. Backscattered electron image showing a relictic plagioclase with idiomorphic shape (medium grey) surrounded by plagioclase of the granoblastic matrix (dark grey) within a typical granoblastic dike drilled at Site 1256D (sample number **312-1256D-203-1-10-14**) The red arrow marks the location where the concentration profile was measured with the electron microprobe. The light grey and withish phases are hornblende, pyroxene, and oxides of the granoblastic matrix (including products of secondary alteration).

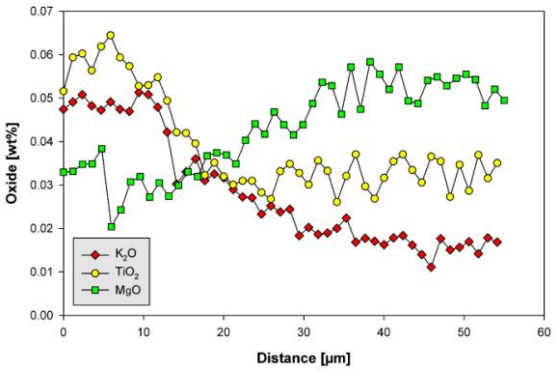

Figure 2: K_2O, TiO_2 and MgO profiles through the marginal part of a relictic plagioclase phenocryst and adjacent plagioclase grains of the granoblastic matrix

At this stage of the project, we are collecting a high number of concentration profiles with respect to CaAl-NaSi diffusion (An-Ab content and selected trace elements) in several relictic plagioclases with electron microprobe. Analysis of concentration profiles have been performed using a Cameca SX100 electron microprobe with standard operating conditions (beam current: 15nA, acceleration potential: 15KV). The first measurements were focused on the An-Ab content of preselected, zoned plagioclase phenocrysts which survived the metamorphic overprint, but show now distinct concentration profiles imposed by the thermal overprint.

We realized soon, that with standard operating conditions, we were not able to measure the An-concentration profiles with sufficient spatial resolution and precision. The diameter of the electron beam can be focused on ~ 1µm and due to the fact, that the profiles are very short (ranging from approximately 4-10µm), we could not achieve enough data points for a reliable fit of the profiles. Because of that, we applied the possibility to reduce the acceleration potential to 8kV in subsequent analysis sessions. This leads to a smaller excitation area in the sample and we could improve the precision of the measurements considerably. Thus, we could almost double the data points along a given traverse. The measured An-profiles show the typical shape of diffusion profiles resulting from the exchange between plagioclase and matrix as presented in Figure 1. Trace element measurements were conducted with a high precision trace element setting, with high beam current of 40nA and counting times of 20 to 120s, in order to make the analysis of very low amounts of MgO, K_2O, TiO_2 feasible. Figure 2 shows three exemplary trace element concentration profiles. Note that compared to the An-profiles shown above, the shape and the length of the profiles are different, reflecting the varying diffusion behavior of the components.

The first calculations were conducted on the basis of the An-profiles in relictic plagioclases. The profiles were fitted with TableCurve2D using the appropriate solution of Fick´s second law (Crank, 1975) assuming constant diffusivity and an initially homogenous plagioclase (r^2=0.999). First estimations yield average time scales of 19000 years for the development of these concentration profiles.

The calculations based on the Mg profiles obtained so far revealed quite different results: this approach estimates the duration of the modification of the profiles as being much shorter with ~150-400 years. These times scales are similar to the ones obtained by Gillis (2008). However, they do not fit to the much longer ones derived from the An-profiles in this study. This discrepancy remains unclear up to now and has to be evaluated in the near future. It is even unclear, if Mg profiles were probably caused by other processes than intermineral diffusion (grain boundary diffusion; dissolution/precipitation effects).

A requirement for the diffusion modeling method is the knowledge on initial concentration distribution of the elements. Concerning that issue, the conditions are excellent, since we investigated many fresh dike rocks not affected by the granoblastic overprint in the framework of routine basic research on the 1256D core (diploma thesis of Dziony 2007; Dziony et al. 2008b). For plagioclase phenocrysts, this work shows that many are virtually unzoned (at least for those elements analyzed with electron microprobe), and some show smooth normal zoning. So, for plagioclase, we assume initially homogeneous condition as first approach for the calculation of the time scales. However, we measured a new series of concentration profiles in relictic plagioclases in samples unaffected by the granoblastic overprint with enhanced analysis settings which revealed that several profiles depart from the previously expected distribution patterns and show also short profiles.

Provided that the examined dike diverges with a maximum rate of 11 cm/a away from the spreading center, the highest calculated residence times derived from An-profiles (19000 years) of the AMC in a high position are obviously too high because after these times the corresponding dike would have leaved the on-axis environment where AMC's reside exclusively. However, these high values can presumably be explained by the unexpected initial distribution patterns in the plagioclases unaffected by the thermal imprint which are not yet incorporated into the evaluation of the time scales. Nevertheless, this overestimation will be addressed in the final numerical model, which will lower the calculated values to more reasonable time scales as a consequence.

Table 1: Composition of starting glass											
Oxide [wt%]	**Na_2O**	**SiO_2**	**Al_2O_3**	**CaO**	**K_2O**	**TiO_2**	**FeO**	**MgO**	**MnO**	**P_2O_5**	**Total**
	2.74	51.62	13.79	10.81	0.08	1.78	12.55	6.69	0.25	0.19	100.54
	(0.32)	(0.45)	(0.23)	(0.36)	(0.02)	(0.03)	(0.4)	(0.21)	(0.08)	(0.1)	
1 σ standard deviation are given in parenthesis											

It has to be mentioned that many of the measured profiles up to now exhibit irregularities most likely caused by alteration reactions or inclusions and cannot be used for our modeling approach. Thus, a statistical approach of collecting a high number of (An and trace elements) diffusion profiles is necessary in order to develop a final numerical model. Practically, a discretized form of the suitable continuity equation (for details see Costa et al. 2008) in combination with the initial and boundary conditions, allows the calculation of concentration profiles for different durations, if diffusion coefficients are known. The calculations will be performed by using the explicit finite difference method which will be implemented into a Mathematica© notebook.

In addition to the diffusion modeling, an experimental subproject has just started, which aims on the simulation of melt/rock interactions occurring during the up-ward burning of the AMC into the previously altered sheeted dike complex. By aligning small, one side polished cylinders of natural sheeted dike material and MORB glass, we will perform a series of diffusion couple experiments at different temperatures and run durations. It is to expect, that comlex fluid-triggered partial melting reactions in the sheeted dikes will occur, making the detailed evaluation of newly formed phase compositions and relations feasible. By measuring the width of the reaction zone, we attempt to gain knowledge about the dissolution rates and hence, information about the amount of assimilation.

In this context, we highly benefit from the direct access to natural samples both from the lower sheeted dikes and representive MORB drilled at IODP site 1256D. On the basis of chemical bulk-analyses we selected at least 4 different fresh MORB unaffected by the granoblastic overprint and 4 different samples from the lowermost sheeted dikes. The MORB starting material was subsequently ground and fused twice at 1 atm and 1600°C to get a dry, homogeneous glass. Before using, the starting material was checked carefully for homogeneity and for major and trace element bulk composition. The composition of the MORB glass determined by electron microprobe analysis is listed in Table 1.

Figure 3: Picture obtained from optical microscope (transmitted light) of the interface between MORB glass and material from the sheeted dikes after the experiment

Subsequently, small, one-side polished cylinders were drilled from both the starting materials and aligned in a sample capsule with the polished sides at the contact. The first sample was run for 4 hours in a special designed IHPV at 1140°C, 1 kbar, fO_2: QFM+1. Figure 3 shows the interface between the two aligned sample cylinders of the very first experiment of this study. Obviously, a run duration of 4 hours is too long to preserve a disequilibrium, capable to investigate reaction rates or magmatic reactions. Further run durations will be decreased to 1 hour down to 30 minutes.

To summarize, the combination of the modeling approach and the experimental study bears great potential to extent our knowledge on the dynamics of fast spreading ocean ridges and the underlying magmatic reactions, regarding processes like stoping, assimilation and contamination.

References:

Costa F, Dohmen R, Chakraborty S (2008) Time scales of magmatic processes from modeling the zoning patterns of crystals. Rev Mineralogy & Geochemistry 69: 545-594

Crank, J. (1975), The Mathematics of Diffusion, 414 pp., Oxford Univ. Press, Oxford, U. K.

Dziony W, 2007. Petrographie von MOR-Basalten vom East Pacific Rise (IODP-Site 1256D – Leg 206 und Exp.309). Diploma thesis Thesis, Leibniz Universitaet Hannover, Hannover, 110 pp.

Dziony W, Koepke J, Holtz F (2008b) Data report: Petrography and phase analyses in lavas and dikes from the hole 1256D (ODP Leg 206 and IODP Expedition 309, East Pacific Rise). In: Teagle DAH et al. (eds) Proc. IODP, Sci. Results, 309/312, doi:10.2204/iodp.proc.309312.201.2008. College Station, TX, Ocean Drilling Program

Gillis KM (2008) The roof of an axial magma chamber: A hornfelsic heat exchanger. Geology 36: 299-302

Koepke, J. et al. (2008) Petrography of the dike-gabbro transition at IODP Site 1256 (equatorial Pacific): The evolution of the granoblastic dikes. Geochem.Geophys Geosyst, vol. 9, doi:10.1029/2008GC001939

ICDP

Dating, age-depth modeling and hydrological interpretation of the 51 cal. ka BP composite profile from Laguna Potrok Aike in southern Patagonia, Argentina (ICDP expedition 5022 – PASADO)

P. KLIEM[1], J.P. BUYLAERT[2,3], D. ENTERS[1], A. HAHN[1], C. OHLENDORF[1], B. ZOLITSCHKA[1] AND THE PASADO SCIENCE TEAM[4]

[1] Geopolar, Institute of Geography, University of Bremen, Germany (kliem@uni-bremen.de)
[2] The Nordic Laboratory for Luminescence Dating, Aarhus University, Risø DTU, Denmark
[3] Radiation Research Division, Risø DTU, Denmark
[4] PASADO Science Team as cited at: http://www.icdp-online.org/front_content.php?idcat=1494

Different dating methods (AMS radiocarbon, OSL, Ar/Ar-dating of tephra layers) are applied in order to obtain absolute dates and a reliable chronology for the sedimentary sequence recovered during the lake deep-drilling project PASADO (ICDP expedition 5022) at Laguna Potrok Aike, southernmost Argentina. In this contribution we first report on the results of radiocarbon dating on organic plant remains along the entire 106 m long composite record from Site 2 (5022-2CP). These ages were used to establish a chronology for this unique late Pleistocene record from the Southern Hemisphere. With regard to age-depth modeling we present methodological aspects and discuss the criteria that were applied for the selection of ages that had to be excluded from the final age-depth model. Secondly, a first interpretation of 31 currently available OSL dates in support of the radiocarbon chronology is discussed as well as the potential for additional Ar/Ar-dating of the frequent volcanic ash layers. Finally, we interpret the resulting sedimentation rates in terms of climatic fluctuations which are mainly driven by changes in precipitation and evaporation in this part of the world, e.g. by hydrological variations as reflected by lake level changes of the lacustrine system.

The selection of 37 radiocarbon dates is restricted to samples from below 18 mcd (meter composite depth) of 5022-2CP. For the topmost 18 m an additional set of 16 radiocarbon ages was correlated to 5022-2CP from the published chronology elaborated for the composite sediment record of PTA-03/12+13 (Haberzettl et al., 2007) by means of lithology and supported by magnetic susceptibility. For the Holocene and the Late Glacial part of the lacustrine record from Laguna Potrok Aike radiocarbon dating was carried out on calcites that were precipitated from the water column (no hard-water effect was recognized), bulk sediment and on different organic macro remains (Haberzettl et al., 2007). But almost no calcite occurs in the sediments of 5022-2CP older than the Late Glacial. Hence, AMS ^{14}C dating could not be applied to calcites below 18 mcd. Macro remains of aquatic mosses were the only component available in a sufficient quantity on which to perform radiocarbon dating. These aquatic mosses are concentrated in layers intercalated within pelagic sediment sections as well as dispersed in mass movement deposits. The former were preferred because for mass movement deposits the likelihood of obtaining too old ages that do not represent the time of deposition for the surrounding pelagic sediment is high.

However, the occurrence of aquatic mosses in the pelagic facies is limited. Moreover, it has to be kept in mind that the origin of this organic material is the littoral zone of the lake. Hence, it is not surprising that some dates from pelagic sediments distinctly tend towards higher ages indicating some degree of reworking. For this reason, an inspection of dated samples including an interpretation of the outliers was indispensable prior to, as well as during age-depth modeling. This was carried out on the event-corrected record from 5022-2CP by running two iterations with a mixed-effect regression procedure as described by Heegaard et al. (2005), a method which is relatively robust with regard to outliers. The first iteration reveals that (1) some radiocarbon dates considerably exceed the confidence interval of the age-depth model and (2) the age-depth modeling below 81 mcd produces an age reversal caused by a lack of reliable material for dating and because the radiocarbon method as such is very close to its lower limit (>45 cal ka BP). Therefore, the second iteration using the mixed-effect regression was restricted to dates of the upper 81 m of the record and excluding dates considerably exceeding the confidence interval of the first iteration. The resulting age-depth model V.2 was extrapolated below 81 mcd back to the final depth of 106 mcd.

To obtain a chronology independent from radiocarbon dating OSL dating was performed on sand-sized K-feldspar grains. The analyses were carried out at the Nordic Laboratory for Luminescence Dating (Aarhus University, Risø DTU, Denmark). A post-IR IRSL dating protocol (modified from Buylaert et al., 2009) was employed which isolates a more stable K-feldspar signal and thus avoids undesirable fading corrections. Dating was successful for 31 OSL samples, while 7 samples did not contain the necessary amount of sand-sized K-feldspar grains and thus were not datable with this method. In general, post-IR IRSL dates confirm the radiocarbon-based age-depth model. Between 65 and 80 mcd the match between both independent dating methods is almost perfect. Below 80 mcd and for the topmost 15 m the post-IR IRSL dates seem to overestimate the radiocarbon based age-depth model. Insufficient bleaching can explain overestimations in both parts. In the bottom part differences might also result from dating at the limit of the radiocarbon method. Surprisingly, between 20 and 65 mcd post-IR IRSL ages seem to underestimate the radiocarbon-based chronology. An additional source of error is related to the fact that OSL samples – for the sake of obtaining enough material for dating – integrate along several centimeters or even decimeters of the record and thus could integrate small-scaled redeposited sediment layers.

The third method applied is Ar/Ar-dating. Altogether, for this approach five samples were taken from tephra layers. Because of the age ranges and errors involved with this method only volcanic ashes below 55 mcd were sampled. Even though these tephra layers reach several decimeters in thickness they contain very few minerals suitable for Ar/Ar-dating; volcanic glass, pumice and amorphous clasts dominate. However, four of the five samples contain amphibole and plagioclase but no K-rich mineral phase (e.g. sanidine). Consequently, amphiboles are the target for the ongoing Ar-Ar measurements.

Results of the radiocarbon-based age-depth modelling were used to calculate sedimentation rates for the entire record. Previously, a time window with high sedimentation rates during the early Holocene was interpreted as a period with a low lake level; as a result we hypothesize that low lake levels can also be assumed for older sections with increased sedimentation rates. We recognized two such additional periods that could match these conditions: 24-31 cal. ka BP and 45-51 cal. ka BP. There is evidence that at least the older phase with high sedimentation rates was caused by low lake levels: according to seismic reflection data this sediment depth corresponds to a phase dominated by aeolian dune morphologies in the eastern part of the lake basin (Gebhardt et al., in prep.). This fact supports a very low lake level or even desiccation.

References:
Buylaert, J.P., Murray A.S., Thomsen, K.J., Jain, M., 2009. Testing the potential of an elevated temperature IRSL signal from K-feldspar. *Radiation Measurements* **44**, 560–565.
Gebhardt, A.C., C. Ohlendorf, F. Niessen, M. De Batist, F.S. Anselmetti, D. Ariztegui, B. Zolitschka. Seismic evidence of a highly dynamic lake development in Southeastern Patagonia during the Late Pleistocene. *in prep.*
Haberzettl, T., Corbella, H., Fey, M., Janssen, S., Lücke, A., Mayr, C., Ohlendorf, C., Schäbitz, F., Schleser, G. H., Wille, M., Wulf, S., and Zolitschka, B. (2007). Lateglacial and Holocene wet-dry cycles in southern Patagonia: chronology, sedimentology and geochemistry of a lacustrine record from Laguna Potrok Aike, Argentina. *The Holocene* **17,** 297-310.
Heegaard, E., Birks, H. J. B., and Telford, R. J. (2005). Relationships between calibrated ages and depth in stratigraphical sequences: an estimation procedure by mixed-effect regression. *The Holocene* **15,** 612-618.

IODP

Campanian-Maastrichtian deep-water changes in the high latitudes: benthic foraminiferal evidence

M.C. KOCH[1], O. FRIEDRICH[2]

[1] Institut für Geowissenschaften, Goethe-Universität, Altenhöferallee 1, 60438 Frankfurt, Germany
E-Mail: Mi.Koch@em.uni-frankfurt.de
[2] Institut für Geowissenschaften, Goethe-Universität, Altenhöferallee 1, 60438 Frankfurt, Germany
E-Mail: o.friedrich@em.uni-frankfurt.de

During the latest Cretaceous cooling phase, a superimposed positive shift in benthic $\delta^{18}O$ values lasting about 1 Ma (71-70 Ma) can be observed in the South Atlantic Ocean (Campanian-Maastrichtian Boundary Event, CMBE). This oxygen isotope excursion is either interpreted in terms of a change in deep-water circulation or as a temporal built-up of ice sheets in Antarctica. In this study we test if benthic foraminiferal assemblages from a southern high-latitudinal site near Antarctica (Ocean Drilling Program Site 690, Maud Rise, Weddell Sea, southern South Atlantic) are influenced by the CMBE. If the positive oxygen isotope excursion reflects a change in deep-water circulation from low-latitude to high-latitude water masses, this change would result in cooler temperatures, higher oxygen concentration, and possibly lower organic matter flux at the seafloor. As a consequence, a major shift in benthic foraminiferal assemblages would be expected. If, however, the $\delta^{18}O$ excursion was exclusively triggered by ice formation, no considerable compositional difference in benthic foraminiferal assemblages would be expected. Samples of Site 690 were taken in a mean resolution of 35 kyr spanning the latest Campanian to late Maastrichtian time interval (73.0 – 68.0 Ma). Our data show a clear separation of the studied succession into two parts with distinctly different benthic foraminiferal assemblages. Species dominating the lower part (73.0 to 70.5 Ma) tolerate less oxygenation and higher organic matter flux (e.g., *Globorotalites* spp., *Paralabamina hillebrandti*) or are typical components of low-latitude assemblages (*Reusella szajnochae*). In contrast, the upper part (70.0 to 68.0 Ma) is characterized by species that indicate well-oxygenated bottom waters under more oligotrophic conditions (e.g., *Nuttallides truempyi*) or species common in high-latitude assemblages (*Pullenia* spp.). The benthic foraminiferal assemblages therefore clearly respond to the CMBE. We interpret the observed changes in benthic foraminiferal assemblages towards a well-oxygenated environment associated with the CMBE to reflect the onset of a shift from low-latitude dominated deep-water masses towards the dominance of a high-latitude deep-water source. As the benthic fauna would not be influenced by ice formation in Antarctica, the formation of an ice sheet as sole cause for the oxygen isotope excursion can be excluded.

ICDP

The Oman Ophiolite Drilling Project – a new ICDP drilling proposal

J. KOEPKE[1], P. KELEMEN[2], A.. AL RAJHI[3], S. ARAI, W. BACH, D. BLACKMAN, G. CEULENEER, L. COOGAN, M. GODARD, S. GOLDSTEIN, P. GOUZE, G. HIRTH, A. HOFMANN, B. JAMTVEIT, C. LANGMUIR, C. MACLEOD, C. MANNING, J. MATTER, K. MICHIBAYASHI, J. MILLER, S. NASIR, B. SHERWOOD LOLLAR, E. SHOCK, E. SONNENTHAL, D. TEAGLE, S. UMINO, J. WARREN, W. ZHU, F. BOUDIER, K. M. GILLIS, F. KLEIN, B. ILDEFONSE, S. MIYASHITA, A. NICOLAS, P. PÉZARD, S. SINGH, E. TAKAZAWA

[1] Institut fuer Mineralogie, Leibniz University Hannover, Callinstraße 3, 30167 Hannover; Germany, koepke@mineralogie.uni-hannover.de
[2] Lamont Doherty Earth Observatory, Columbia University, Palisades NY 10964, USA; peterk@ldeo.columbia.edu
[3] Geological Survey of Oman; Ministry of Commerce and Industry, Sultanate of Oman; alialrajhi66@yahoo.com

Here we propose an ICDP sponsored workshop to develop a full proposal for drilling in the Samail ophiolite in the Sultanate of Oman. The Samail ophiolite is composed of igneous crust and upper mantle formed at a submarine spreading center, via processes very similar to those at today fast-spreading mid-ocean ridges. Drilling will provide key data on the processes of melt extraction from the mantle, igneous accretion of oceanic crust, and hydrothermal modification of that crust. Drilling will also investigate present day alteration processes, their relationship to the deep biosphere, and their potential for acceleration to achieve carbon capture and storage via in situ mineral carbonation.

The scientif rationale behind can be devided in different major themes:

(1) **Geodynamics of mid-ocean ridges** with topics like the nature of heat and mass transfer from the mantle to the hydrosphere, mechanisms of melt extraction from the mantle beneath ridges, the geometry and nature of mantle upwelling beneath ridges, the architecture of the oceanic

crust, the nature of igneous accretion of the oceanic crust, the characterization of the dynamics of the axial magma chanber and melt lens, the hydrothermal circulation / alteration of newly formed igneous oceanic crust.

(2) **Alteration and weathering of oceanic lithosphere** away from the ridges with topics related to hydration, carbonation and oxidation of minerals in peridotite and mafic rocks, the role of fluid flow during mineral hydration and carbonation reactions, the mechanism of maintaining and controlling of fluid porosity and permeability, the role of abiotic hydrocarbon synthesis.

(3) **Enhanced peridotite carbonation** and the potential role in CO_2 storage with topics related to technical and engeneering aspects of practical and inexpensive route to geological CO_2 capture and storage, quantification of reactions and processes behind, and the importance to learn from natural systems what are the spontaneous mechanisms for natural mineral carbonation, which can then be emulated and enhanced in order to achieve rapid reaction with minimal additional energy input.

We propose a diamond drilling program in two phases; all drill holes will be 500 to 600 m deep because this is the maximum capability of available equipment in Oman, which we plan to use to maximize the impact of limited funding. In Phase I, we will use diamond coring techniques that are standard in the mineral exploration industry, we will drill preliminary holes in three settings: (a) a hole sited to sample the deeper parts of the reaction zone in the ongoing alteration of mantle peridotite, (b) a hole sampling the dike/gabbro transition in the upper part of the crustal section, and (c) a hole sampling the crust/mantle transition at the base of the crustal section. Pending successful results from these three holes, in Phase II we will drill a series holes that together comprise a full crustal section through the ophiolite. Additional sites will be drilled to evaluate spatial variability along strike in crucial horizons. Downhole logging of geophysical properties will provide a key element in linking micron to centimeter scale observations of samples from drill core to 100 m to 10 km scale geophysical observations of active ocean ridges. Similarly, downhole measurements of fracture spacing, permeability, fluid flow, and fluid composition (via CTD and gas-tight samplers), will be combined with core observations of primary lithology, extent and nature of alteration, and small scale permeability to yield a multi-scale understanding of reactive fluid flow. Pressure-tight biological sampling will be an important part of our investigation.

IODP

SmartPlug and GeniusPlug - Two simple borehole observatories and their application in NanTroSEIZE

A. KOPF [1], S. HAMMERSCHMIDT [2], H. VILLINGER [2]

[1] MARUM, Universität Bremen, Leobener Str., 28359 Bremen
[2] Fachbereich Geowissenschaften, Universität Bremen, Postfach 330440, 28334 Bremen

At the Nankai Trough south off Japan, the Philippine Sea Plate is subducted at a rate of 4 – 6 cm /yr beneath the Eurasian Plate, causing several smaller earthquakes (EQs) throughout the year and also more destructive events such as the 1944 Tonankai M8.1 rupture on occasion. Based on seismic and tsunami waveform inversion models it is assumed that a major splay fault cutting through the accretionary prism, termed the "Megasplay Fault" (MSF), showed coseismic slip in the past and can therefore be assumed to have an important role in seismogenesis and tsunamigenesis in this area (Park et al., 2002). In order to understand the overall EQ-triggering mechanisms the NanTroSEIZE project has been implemented as the IODP Seismogenic Zone Experiment. In the course of this project, IODP Expedition 319 (Saffer et al., 2009), penetrated the MSF at Hole C0010A, and a first simple borehole observatory, a "mini-CORK" was installed (Davis et al., 2009). This instrument termed SmartPlug measures temperature and pore fluid pressure and was mounted to a retrievable bridge plug that sealed the cased hole at a depth of ~ 374 mbsf, directly above a screened casing interval at one shallow branch of the MSF. Pore fluid pressure data is of particular interest since the fault probably serves as drainage boundary and thus influences the seismogenic behavior at the plate boundary and subsequently the earthquake and tsunami generation (Scholz, 1998; Moore and Saffer, 2001; Tobin and Saffer, 2009). Moreover, by monitoring pore fluid pressure it is possible to make assumptions for the prevailing strain and its change over time.

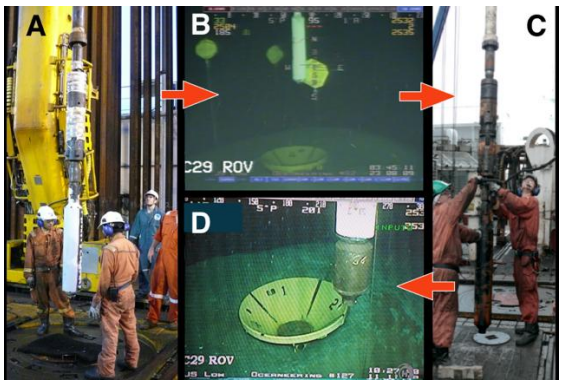

Flow chart showing deployment and recovery of the different borehole observatories during IODP Expeditions 319 and 332. (A) Deployment of the SmartPlug during IODP Expedition 319. The SmartPlug sits inside the white painted lower part, which is connected to the bridge plug. Bright tape is surrounding the packer at the bridge plug to prevent its inflation before deployment. (B) ROV picture from the SmartPlug's housing prior to the deployment into Hole C0010A. (C) Recvovery of the SmartPlug during IODP Expedition 332. After its 15 month lasting installation, the housing rusted and lost its color - however, the instruments and sensors remained unharmed. (D) ROV picture of the GeniusPlug prior to its installation in Hole C0010A. Clearly visible is the bulkhead extension below the white painted structural shell of the SmartPlug, housing the OsmoSamplers and the FLOCS microbial chambers.

The SmartPlug incorporates two Paroscientific Digiquartz sensors located in two pressure transducers, one data logger and four temperature sensors, all connected to the data logger and PPC frequency counter via an underwater connector. Disturbances caused by drilling and installation of the SmartPlug will cease over the planned observation period, so that previous *in situ* conditions are reestablished. This development in pressure and temperature can be monitored by one pressure transducer being connected to a pressure gauge which is passed through the bottom seal via 1/16-inch hydraulic tubing. Hydrostatic reference pressure and temperature are obtained by the other pressure transducer being connected to a pressure gauge above the bottom seal in the drowned section.

Fifteen months after its initial deployment, the SmartPlug was recovered during IODP Expedition 332 (Kopf et al., 2011), and the data were downloaded via the AWQ connector. A first look at the data reveals that the deployment was successful with all sensors fully functional. Although mainly influenced by periodic tidal signals, the obtained pore fluid pressure data showed distinct transient signals which can be attributed to tectonic events, e.g. farfield p-wave, s-wave and tsunami wave signals from the M8.8 Maule EQ in Chile in February 2010 could be correlated to distinct peaks in the pressure data. In further analysis the pressure data will be de-tided and compared with local earthquake catalogues like the HI-NET (Okada et al., 2004) to reveal the role of the MSF in seismogenesis and tsunamigenesis. The collected temperature data showed an exponential adjustment to in situ temperatures, proving the sufficient sealing of the fault zone and a subsequent reestablishment of *in situ* conditions.

Before a more sophisticated CORK can be installed in the following years, a temporary replacement is represented by an enhanced version of the SmartPlug, termed GeniusPlug. It has basically the same configuration except for a 30 cm extension at the lower end of the SmartPlug main hull. This section, where an OsmoSampler (Jannasch et al., 2003) and a FLOCS microbial chamber (Orcutt et al., 2010) are situated, allows only formation fluid from the fault zone to enter. The OsmoSampler consists of one or several pumps being driven by an osmotic pressure gradient caused by fluids of different salinity separated by a semipermeable membrane. The configuration used here allows a draw rate of 73 ml/yr at a temperature of 20°C. The FLOCS system takes advantage of two osmotically driven pumps being attached via a tee, which doubles the pump rate thus increasing the inflow of formation water to a rate of 146 ml/yr (at 20°C). This would fill the 150 m long teflon tubing within 14 months, however, due to the high saline gradient, the pumps will not stop working. As a result, only the last 14 months will be sampled.

The FLOCS microbial unit consists of four chambers. One chamber is divided in two different parts, separated by autoclaved glass wool and 5 mm borosilicate glass beads. Both parts are filled with autoclaved rock chips of different lithology (in our case mudstones from the Nankai accretionary wedge IODP Exp 316, basalt glass, crushed barite, and crushed olivine). This configuration will allow microbial growth experiments under controlled, *in situ* chemical conditions on different substrates (Wheat et al., 2010). The GeniusPlug is set to measure and sample for geochemistry and microbiology for at least 24 months and will be recovered during an upcoming NanTroSEIZE expedition with *D/V Chikyu*.

References:

Davis, E. E., Saffer, D. M., Kopf, A., MacDonald, R., Labonte, A., Bennest, J., Meldrum, R., and S. Toczko (2009), A "Mini-CORK" smart bridge plug for initial NanTroSEIZE borehole monitoring, paper presented at American Geophysical Union, Fall Meeting 2009, AGU.

Jannasch, H., Davis, E., Kastner, M., Morris, J., Pettigrew,, and P. T., J.N., Solomon, E., Villinger, H., and Wheat, C.G. (2003), CORK-II: long-term monitoring of fluid chemistry, fluxes, and hydrology in instrumented boreholes at the Costa Rica subduction zone., paper presented at Proceedings of the Ocean Drilling Program, Initial Reports, 205.

Kinoshita, M., Tobin, H., Ashi, J., Kimura, G., Lallement, S., Screaton, E.J., Curewitz, D., Masago, H., Moe, K.T., and the Expedition 314/315/316 Scientists (2009), Proceedings of the Integrated Ocean Drilling Program, 314/315/316.

Kopf, A., Araki, E., Toczko, S., and the Expedition 332 Scientists (2011), NanTroSEIZE Stage 2: Riserless Observatory, IODP Preliminary Report, 322.

Moore, J. C., and D. Saffer (2001), Updip limit of the seismogenic zone beneath the accretionary prism of southwest Japan: An effect of diagenetic to low-grade metamorphic processes and increasing effective stress, Geology, 29(2), 183-186.

Orcutt, B., C. G. Wheat, and K. J. Edwards (2010), Subseafloor Ocean Crust Microbial Observatories: Development of FLOCS (FLow-through Osmo Colonization System) and Evaluation of Borehole Construction Materials, Geomicrobiology Journal, 27(2), 143 - 157.

Okada, Y., Kasahara, K., Hori, S., Obara, K., Sekiguchi, S., Fujiwara, H., and A. Yamamoto (2004), Recent progress of seismic observation networks in Japan: Hi-net, F-net, K-NET and KiK-net, Earth Planets Space, 56, 15 - 28.

Park, J.-O., T. Tsuru, S. Kodaira, P. R. Cummins, and Y. Kaneda (2002), Splay Fault Branching Along the Nankai Subduction Zone, Science, 297(5584), 1157-1160

Saffer, D., McNeill, L., Araki, E., Byrne, T., Eguchi, N., Toczko, S., Takahashi, K. and the Expedition 319 Scientists (2009), NanTroSEIZE Stage 2: NanTroSEIZE Riser/Riserless Observatory, IODP Preliminary Report, 319, 83 pp.

Scholz, C. H. (1998), Earthquakes and friction laws, Nature, 391(6662), 37-42.

Tobin, H. J., and D. M. Saffer (2009), Elevated fluid pressure and extreme mechanical weakness of a plate boundary thrust, Nankai Trough subduction zone, Geology, 37(8), 679-682.

Wheat, C. G., Jannasch, H.W., Kastner, M., Hulme, S., Cowen, J., Edwards, K., Orcutt, B.N., and B. Glazer (2010), Fluid Sampling from Oceanic Borehole Observatories: Design and Methods for CORK Activities (1990-2010), Proceedings of the Ocean Drilling Program, 327.

ICDP

PIER-ICDP: Spatial and temporal seismic imaging of fluid migration through the crust in the W-Bohemia/Vogtland earthquake swarm region

M. KORN [1], M. FALLAHI [1], U. WEGLER [2], M. KEYSER [2], D. RÖSSLER[3], K. BAUER [4]

[1] Institut für Geophysik und Geologie, Universität Leipzig, Talstrasse 35, 04103 Leipzig
[2] Bundesanstalt für Geowissenschaften und Rohstoffe, Stilleweg 2, 30655 Hannover
[3] Kopenhagen, Denmark
[4] Helmholtzzentrum Potsdam Deutsches Geoforschungszentrum, Telegrafenberg, 14473 Potsdam

The western Eger rift area is dominated by presently ongoing magmatic processes in the intra-continental lithospheric mantle. These processes take place in absence of any presently active volcanism at the surface. However, they are expressed by a series of phenomena distributed over a relatively large area, like occurrence of repeated earthquake swarms, surface exhalation of mantle-derived and CO2-enriched fluids, mofettes, mineral springs and enhanced heat flow, among others. This area is the "locus typicus" for the term "earthquake swarm" (in German "Erdbebenschwarm", established by Credner more than 100 years ago) and, at present this is the only known intra-continental region where such deep-seated, active lithospheric processes currently occur.

Geodynamic nature and implications of these processes are far from being understood. Is it a magmatic activity in the upper mantle or in the lower crust? Is it possibly a developing large-scale faulting zone (like a future analogue of the San Andreas Fault system) or a zone of developing volcanism? What is the geodynamic role of fluids in general and of CO_2 in particular? What is the geodynamic relationship between geophysical and geochemical signatures of these magmatic processes?

Continuous seismic monitoring, active seismic surveys, fluid and groundwater level monitoring as well as GPS measurements have been carried out in this region for many years. It is therefore an excellent location for an ICDP drilling project targeted to a better understanding of the mantle - crust (including also the deep biosphere) interaction in an area of active magmatic underplating.

The newly established program Probing of Intracontinental magmatic activity: drilling the Eger Rift (PIER-ICDP) will create a common geophysical and geochemical frame between the former KTB site and Eger Rift, bounded at its Western and Eastern endings by scientific drilling data. In this way, it will significantly contribute to understanding the intra-continental mantle-crust interaction in a broader scale. It will contribute to the research areas of

Volcanic Systems and Thermal Regimes
Mantle Plumes and Rifting
Active Faulting and earthquake Processes
Geobiosphere and Early Life
Natural Ressources
Climate Change and Global Environment.

Within PIER-ICDP several projects using active and passive seismic methods with the integrating focus "fluids triggering lithospheric activity" have recently started.

In the project "Spatial and temporal seismic imaging of fluid migration through the crust in the W-Bohemia/Vogtland eartquake swarm region" the three-dimensional structure of the Earth's crust in the W-Bohemia/Vogtland region, where the existence of crustal fluid reservoirs is postulated and numerous spatially distributed anomalies exist, is analyzed with advanced seismological methods using existing data. Moreover, temporal variations in the crustal structure are studied. The prinicpal goals are

- to obtain a structural image of P- and S-velocities by travel-time tomography and by ambient noise surface wave tomography
- to obtain a structural image of seismic attenuation and to separate scattering and intrinsic attenuation by attenuation tomography and by the inversion of small-scale structure based on radatiive transfer of seismic energy
- to explore the potential of monitoring time variations of seismic parameters by using coda wave interferometry and passive image interferometry.

We will test the hypothetical existence of a fluid reservoir and estimate its spatial extent. We will measure the temporal evolution of stress and fluid dynamics giving information about changes in the upper crust during a swarm earthquake cycle. The 3D and 4D seismological models delivered by this project will constrain the decision for an optimal ICDP drilling location in the Eger Rift system..

This project is closely related to the presentation Buske et al.: Seismic and seismological features of the Vogtland-Bohemia earthquake swarms – in preparation for a high resolution seismic survey and scientific drilling.

IODP

What pines and elms can tell: vegetation and climate development on the Atlantic Coastal Plain and implications for sea-level reconstruction

U. KOTTHOFF[1], F. M. G. MCCARTHY[2], M. E. KATZ[3], R. WILLIAMS[3], R. ZANATTA[2]

[1] Department of Geosciences, Hamburg University, Bundesstrasse 55, D-20146 Hamburg, Germany, e-mail: ulrich.kotthoff@uni-hamburg.de
[2] Department of Earth Sciences, Brock University, 500 Glenridge Avenue, St. Catharines, Ontario, L2S 3A1, Canada
[3] Earth and Environmental Sciences, Rensselaer Polytechnic Institute, 110 8th St., Troy NY 12180, United States of America

The major aims of IODP Expedition 313 are estimating amplitudes, rates and mechanisms of sea-level change and the evaluation of sequence stratigraphic facies models that predict depositional environments, sediment compositions, and stratal geometries in response to sea-level change. Several hundred cores from three sites (313-M0027A, M0028A, and M0029A; 45 to 67 km off the coast of New

Jersey) from the New Jersey shallow shelf (water depth approximately 35 m) were retrieved during May to July 2009, using an ECORD "mission-specific" jack-up platform. The recovery rate for the three sites exceeded 80%, resulting in more than 1300 m total core length. The oldest sediments were recovered from Hole M0027A, and dated as late Eocene according to biostratigraphy, magnetostratigraphy and Sr-isotopy-based age estimates.

In the project presented here, the ratio between organic-walled dinoflagellate cysts and pollen grains found in late Eocene (Priabonian) to Miocene (Serravallian) sediments from Hole M0027A is used to estimate the site-shoreline distance. These estimations are compared with quantitative paleodepths reconstructions based on assemblages of benthic foraminiferal species, primarily on faunas characterized by various species of *Elphidium*, *Hanzawaia*, *Pseudononion*, *Buliminella*, *Uvigerina*, *Cibicidoides*, and/or *Oridorsalis*. Paleodepth estimates based on benthic foraminiferal data show close agreement with the distance-from-shoreline estimates derived from the palynomorphs, and together these parameters allow us to infer paleo-sea-level.

Furthermore, the micropaleontology-based reconstructions of paleodepth and site-shoreline distance contribute to a pollen-transport model, allowing more reliable pollen-based reconstructions of the vegetation development in the hinterland of the New Jersey margin. While oak forests dominated the vegetation on the Atlantic Coastal Plain during the Eocene and Oligocene, the Miocene witnessed the spreading of hickory-oak forests. At the Aquitanian-Burdigalian boundary different hemlock pine (*Tsuga*) species were present on the Atlantic Coastal Plain, indicating humid, but probably relatively cool conditions, consistent with the documented Mi-1 glaciation. The interval of extraordinary-high *Tsuga*-pollen percentages was also detected at sites M0028A and M0029A, and can be used as a biostratigraphic tie-point.

Subsequently, the spreading of deciduous oaks and further broad-leaved tree taxa during the late Burdigalian points to warmer temperatures representing the Mid-Miocene Climatic Optimum. Similarly to the "*Tsuga*-horizon" found at the Aquitanian-Burdigalian boundary, an interval of particularly frequent elm (*Ulmus*) pollen grains can be used to identify the late Burdigalian in all three sites of IODP Expedition 313. During the Langhian to Tortonian, grass- and herb-dominated landscapes expanded, probably due to a decrease in humidity resulting from ice sheet growth in Antarctica.

ICDP

Classification and characteristics of mass movement deposits in the 3.6 Ma sediment record of Lake El'gygytgyn, Chukotka, NE Siberia

M. KUKKONEN[1], O. JUSCHUS[2], V. WENNRICH[1], T. COOK[3], C. GEBHARDT[4], M. MELLES[1], LAKE EL'GYGYTGYN SCIENTIFIC PARTY

[1] University of Cologne, Institute of Geology and Mineralogy, Cologne, Germany maaret.kukkonen@uni-koeln.de
[2] TU Berlin, Institute for Applied Geosciences, Berlin, Germany
[3] University of Massachusetts, Department of Geosciences, Amherst, MA, USA
[4] AWI Bremerhaven, Geosystems, Bremerhaven, Germany

Lake El'gygytgyn (67°30' N, 172°05' E), formed after a meteorite impact 3.6 million years ago, is situated in the high Arctic of Chukotka, NE Siberia, 100 km north of the Arctic Circle in an area thought to have escaped continental wide glaciation. The lake was drilled by the ICDP El'gygytgyn Drilling Project in spring 2009 near the center of the lake at a depth of 170 m. Three overlapping cores were recovered forming a unique 315-m long paleoclimate archive from the terrestrial Arctic reaching back to the Pliocene. The coring site was selected based on a pre-site survey that indicated undisturbed and layered units in the lake center. On the lake slope, seismic survey and pilot cores have revealed thick debris flows thinning toward the lake floor.

Detailed studies of earlier pilot cores, with a maximum length of 16 m blf, revealed altogether 28 mass movement events incised into pelagic sediment in the lake center (Melles et al. 2007, Juschus et al. 2009). These event layers are for the most part normally graded beds, interpreted as non-erosive turbidites (Juschus et al. 2009) that originated as debris flows on the steep lake slope and transformed into turbidity flows on their way toward the lake floor. Since mass movement deposits potentially erode the underlying sediment and therefore cause hiatuses in the paleoclimatic record, investigations of the mass movement events in all of the new cores are underway.

The recovered lacustrine sediment record is repeatedly interrupted by short-lived mass movement deposits. These deposits are macroscopically distinguishable from the pelagic sedimentation according to their characteristics, e.g. normal grading, grain size and color. Their macroscopical identification was further confirmed by evaluation of radiographs, high-resolution magnetic susceptibility measurements and elemental analyses. These methods, as well as thin-section analyses, revealed more details and internal structures of the mass movement deposits.

Cores 5011-1A and 1B, reaching 147 m and 112 m blf, respectively, have approximately 30 % mass movement deposits. Most commonly these are normally graded beds (turbidites), which have a sharp contact to the underlying sediment. Thicknesses of the turbidite beds vary between millimeters and tens of centimeters. The grain sizes are from sand to clay and show often clear internal boundaries indicating changes in grain size. Densites, massive silty sections with a thin graded top occur only rarely. In several sections of the Lake El'gygytgyn sediment record fragments of different pelagic facies are repeated, tilted

and/or deformed. These redeposited sections are found also in the parallel core but might have partly different characteristics. Poorly sorted gravelly/sandy to silty sediments are found deeper in the cores. They are frequently overlain by disturbed or occasionally undisturbed lenses of pelagic sediment and caped by a turbidite. In addition, sequences of folded or bended sediment were discovered in the core, a result of more extensive deformation of sediment. These units have thicknesses between half a meter and a few meters and show distinct repetition of specific layers, e.g. tephra or turbidite. The new cores were correlated to the pilot core to create a record of mass movement deposits covering the whole history of the lake.

References:
Juschus O., Melles M., Gebhardt A.C. & Niessen F. (2009): Late Quaternary mass movement events in Lake El´gygytgyn, north-eastern Siberia. Sedimentology, 56, 2155-2174. DOI: 10.1111/j.1365-3091.2009.01074.x
Melles M., Brigham-Grette J., Glushkova O. Yu., Minyuk P., Nowaczyk N. R. & Hubberten H.-W. (2007): Sedimentary geochemistry of a pilot core from El´gygytgyn Lake - a sensitive record of climate variability in the East Siberian Arctic during the past three climate cycles. Journal of Paleolimnology, 37, 89-104.

IODP

Paleogene sedimentation changes along a depth transect at the northern flank of the Walvis Ridge (ODP Leg 208), South Atlantic Ocean

D.C. LEUSCHNER[1], W. EHRMANN[1]

[1] Institut für Geophysik und Geologie, Universität Leipzig, Talstr. 35, 04103 Leipzig, mail: dcleu@rz.uni-leipzig.de

The aim of the EPASA project (**E**arly **Pa**leogene deep-water overturning in the **S**outh **A**tlantic) is to reconstruct variations in the circulation of deep- and bottom-water masses in the eastern South Atlantic. In this study we analysed a large number of sediment samples recovered from a depth transect along the northern flank of the Walvis Ridge (ODP Leg 208, Fig. 1) for their grain size distribution and clay mineral composition. The late Paleocene to early Eocene sections at all five sites, spanning a water depth range of more than 2000 m, were studied on high resolution. Additional samples, covering the entire Cenozoic record, were taken from the two intermediate sites (1265 and 1267) in order to obtain an overview of the general, long-term variations that occur on site.

The long-term record

The clay mineral assemblages indicate that environmental conditions in the eastern South Atlantic underwent significant changes during the late Paleogene. Illite and smectite are the main components of the terrigenous clay fraction at Sites 1265 (Fig. 1) and 1267, forming more or less a two-component clay mineral system during the entire Cenozoic record. Therefore, the records of the two minerals show opposing trends. Kaolinite and chlorite are almost absent in the late Paleocene to early Eocene period. However, these minerals become more abundant at the end of the early Eocene and show a persistent and increasing trend throughout the younger Paleogene and Neogene. The onset of the kaolinite and chlorite occurrences is almost contemporary with the Early Eocene Climatic Optimum (EECO) about 50 Ma ago. At the same time smectite shows its highest concentrations within a broad maximum ranging from the early Eocene until the end of the Eocene, while the illite content drops down to minimum values. In the late Eocene illite concentrations increase up to >60%, whereas smectite concentrations decrease. The younger part of the sequences recovered at Sites 1265 and 1267 is characterized by an overall decrease in illite and an increase in smectite concentrations.

The variations in the sediment composition at the end of the early Eocene and the Eocene / Oligocene boundary are likely to reflect severe changes in sediment source areas, oceanic circulation and/or sediment preservation at the northern Walvis Ridge. In the late Eocene / early Oligocene we observe an increase in the illite content, associated with a shift towards a better illite crystallinity (Illite-IB), indicating a switch from a mixed–layer dominated association to the predominance of well crystallised illites across this boundary. This change occurs almost contemporaneous with the onset of the Antarctic glaciation and the onset of North Atlantic deep-water production and its export into the South Atlantic (Via and Thomas, 2006). Global changes, that were associated with a reorganization of oceanic currents and the global carbon cycle. Moreover, at the Walvis Ridge these climatically induced changes are accompanied by the incision of a channel structure crossing the Ridge adjacent to the study area, starting to develop between 50 and 40 Ma (Bartels et al., 2007). In combination with the ongoing subsidence of the aging oceanic plate, this channel may have provided a new transport path allowing a sediment supply from a different source than before.

Prior to the Early Eocene Climatic Optimum, in the early Eocene section the mineral clinoptilolite, an authigenic zeolite, is common in the clay fraction of the sediments, indicating a strong diagenetic overprint of the sediments of this period. At the same time the kaolinite and chlorite values break down. Their concentrations within these section are generally below the detection limit of the XRD method. Therefore, the kaolinite/chlorite ratio, which is highly indicative for deep-water masses and source areas of South Atlantic sediments in the Quaternary record (Petschick et al., 1996; Diekmann et al., 1999), is not applicable for the late Paleocene / early Eocene section. However, this ratio does not show a consistent pattern for the younger late Eocene, Oligocene and Neogene records at Sites 1265 and 1267.

The amount of non-calcareous material, the silt and clay content, is mainly a function of winnowing and carbonate dissolution. The most striking feature in the late Eocene and Neogene record is the occurrence of three strong carbonate dissolution phases, as indicated by the increase of the terrigenous silt and clay fraction with a broad maxima in the late Eocene, the late Oligocene and at the end of the early Miocene. All three maxima are even more pronounced at the deeper Site 1267. The paleodepth of this Site was ranging from about 3600 m in the late Eocene to 4200 m in the middle Miocene (Lindsey and Schellenberg, 2006). Therefore, it is most likely that the implied strong carbonate dissolution is caused by the oscillation of the carbonate compensation depth (CCD) in association with the subsidence of the oceanic plate. The observed periods of intense carbonate dissolution at the

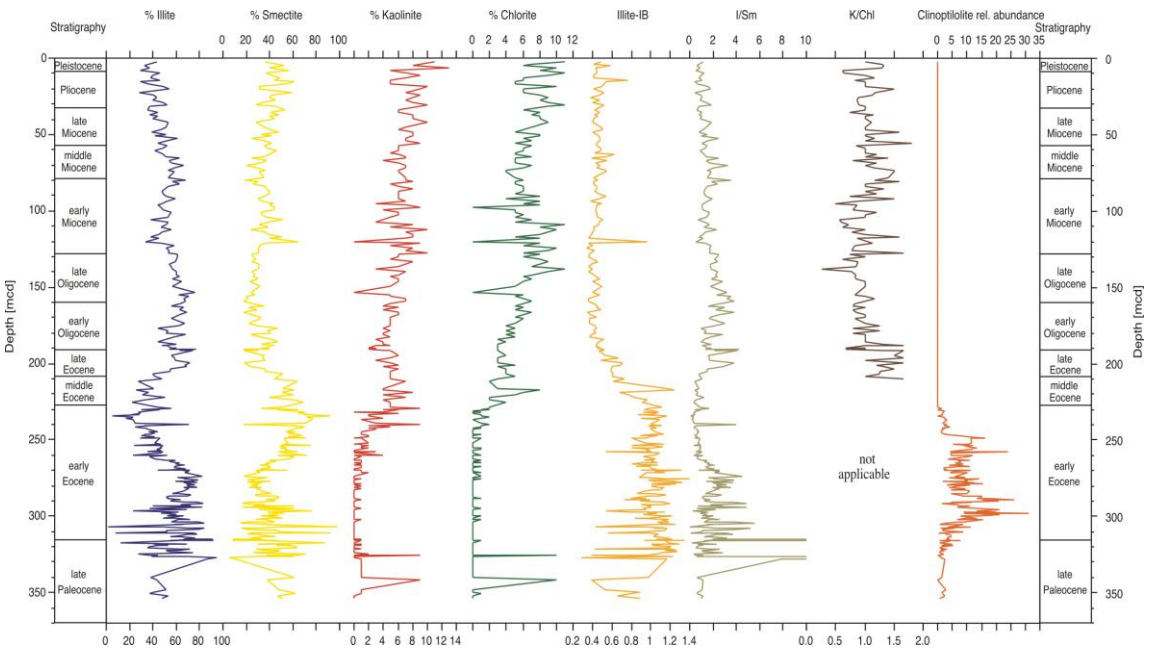

Fig. 1: Percentage distribution of the main clay mineral groups illite, smectite, kaolinite and chlorite and records of the illite integral breadth ("crystallinity", Δ°2Θ), the illite/smectite ratio, the kaolinite/chlorite ratio and the relative abundance of clinoptilolite in sediments recovered at ODP Site1265.

Walvis Ridge are contemporaneous with non-permanent or ephemeral ice sheets in Antarctica. On the other hand the carbonate dissolution is low during the Oligocene glaciation and the entire Plio- and Pleistocene, i.e. during periods of permanent Antarctic glaciations. Moreover, there is a short but distinct decrease in the clay content, indicating better carbonate preservation, right at the Oligocene / Miocene boundary, that is contemporaneous with the Miocene Mi-1 glaciation. This implies that during periods of instable ice sheets the oceanographic conditions were favourable for the advection of corrosive deep-water into the basin north of the Walvis Ridge, and/or generally high carbonate consumption in the oceans forced the CCD to rise significantly.

The abrupt deepening of the CCD at the Eocene / Oligocene boundary is also documented by changes in the lithologic composition, carbonate content, colour reflectance and coarse fraction of the sediments at Sites 1262 and 1265 (Liu et al., 2004) and stable isotope records at Site 1263 (Riesselman et al., 2007). This shift is commonly attributed to a major reorganization of the global carbon cycle, probably demonstrating the sudden increase in organic carbon burial associated with the first appearance of large, permanent ice sheets on Antarctica and possibly coupled to deep sea cooling and/or Northern Hemisphere ice growth.

The late Paleocene / early Eocene record and short climatic events

The silt and clay contents in the late Paleocene / early Eocene record at Site 1265 are highly variable, due to the short lasting hyperthermal events. However, the short lasting carbonate dissolution events during the generally warm climates of the late Paleocene and early Eocene were driven by complete different mechanisms than mentioned before. Strong carbon isotope excursions indicate that these events are commonly associated with a strong acidification of the ocean, most likely caused by the massive dissociation of oceanic methane hydrate (Dickens et al., 1995).

The comparison of the illite content at the three Sites 1265, 1266 and 1267 (Fig. 2) shows that the conditions for clay mineral deposition changed more or less simultaneous along transect, representing a 1300 m water-depth range from 4355 m (Site 1267) over 3798 m (Site 1266) to 3060 m (Site 1265). At Site 1266 the illite and smectite records exhibit the known inverted trends with highest abundances of smectite at the EECO, indicating that the smectite deposition is generally increasing during warm climates. However, the maximum in the smectite record is certainly not as pronounced and long lasting as the Eocene warm phase as indicated by oxygen isotopes, for instance.

The abrupt climatic events of the late Paleogene, so called hyperthermals (Cramer et al., 2003,), like the P/E boundary (PETM or ETM1) and the Eocene Thermal Maximum 2 (ETM2 or "ELMO"-event) (Sluijs et al., 2009) had a strong impact on the temperature, oceanic environment and water chemistry (Zachos et al., 2005; Hodell et al., 2007). Acidification of the ocean affected the preservation of carbonate and forced a shoaling of the CCD of more than 2000 m in the South Atlantic associated with the PETM (Zachos et al., 2004). Such short but extreme events are also documented in the clay mineral assemblages at Walvis Ridge. However, in contrast to the general pattern with smectite concentrations increasing during warmer climates, the illite concentrations appear to increase within the carbonate depleted clay layers of the PETM at Sites 1265 and 1267, as well as in the ETM2-layer at Site 1267. On the other hand the illite content within the ETM2-layer at 1265 is slightly decreasing. However, the observed variations do not exceed significantly the general background variations. Therefore, we have no indication for exceptional changes in the oceanic circulation and/or the provenance of the clay minerals deposited at the Walvis Ridge in association with these events.

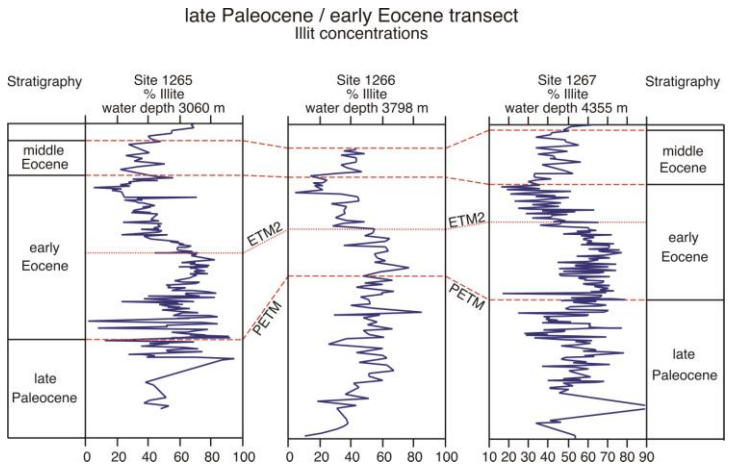

Fig. 2: Illite content variations in the late Paleocene to early Eocene sections at sites 1265, 1266 and 1267. Red lines indicate the positions of the PETM (dashed) and ETM2 (dotted).

References:

Bartels, T., Krastel, S., and Spiess, V., 2007. Correlation of high-resolution seismic data with ODP Leg 208 borehole measurements. In Kroon, D., Zachos, J.C., and Richter, C. (Eds.), Proc. ODP, Sci. Results, 208: College Station, TX (Ocean Drilling Program), 1–27. doi:10.2973/odp.proc.sr.208.204.2007

Cramer, B.S., Wright, J.D., Kent, D.V. and Aubry, M.-P., 2003. Orbital climate forcing of $\delta^{13}C$ excursions in the late Paleocene–early Eocene (chrons C24n–C25n). Paleoceanography, 18(4): 21.1-21.25. doi:10.1029/2003PA000909.

Dickens, G.R., O'Neil, J.R., Rea, D.K., and Owen, R.M., 1995. Dissociation of oceanic methane hydrate as a cause of the carbon isotope excursion at the end of the Paleocene. Paleoceanography, 10: 965–971.

Diekmann, B., Kuhn, Mackensen, A., Petschick, R., Fütterer, D.K., Gersonde, R., Rühlemann, C., and Niebler, H.-S., 1999. Kaolinite and Chlorite as tracers of modern and late Quaternary deep-water circulation in the South Atlantic and the adjoining Southern Ocean. In Fischer, G. and Wefer, G., Use of Proxies in Paleoceanography: Examples from the South Atlantic. Springer-Verlag, Berlin Heidelberg New York, 285-313.

Hodell, D.A., Kamenov, G.D., Hathorne, E.C., Zachos, J.C., Röhl, U., and Westerhold, T., 2007. Variations in the strontium isotope composition of seawater during the Paleocene and early Eocene from ODP Leg 208 (Walvis Ridge). Geochem. Geophys. Geosyst., 8: Q09001. doi:10.1029/2007GC001607

Lindsey, M.M., and Schellenberg, S.A., 2006. Early Eocene to late Miocene variations in the South Atlantic CCD: constraints from the Walvis Ridge depth-transect (ODP Leg 206). Eos, Trans. Am. Geophys. Union, 87(52)(Suppl.): PP23A-1737. (Abstract)

Liu, Z., Tuo, S., Zhao, Q., Cheng, X., and Huang, W., 2004. Deep-water earliest Oligocene Glacial Maximum (EOGM) in South Atlantic. Chin. Sci. Bull., 49(20): 2190–2197.

Petschick, R. Kuhn, G., and Gingele, F.X., 1996. Clay mineral distribution in surface sediments of the South Atlantic: sources, transport, and relation to oceanography. Mar. Geol., 130: 203-229.

Riesselman, C.R., Dunbar, R.B., Mucciarone, D.A., and Kitasei, S.S., 2007. High resolution stable isotope and carbonate variability during the early Oligocene climate transition: Walvis Ridge (ODP Site 1263). Open-File Rep.—U.S. Geol. Surv., 2007-1047:095.

Sluijs, A., Schouten, S., Donders, T.H., Schoon, P., Röhl, U., Reichart, G.-J., Sangiorgi, F., Kim, J.-H., Sinninghe Damsté, J.S., Brinkhuis, H., 2009. Warm and Wet conditions in the Arctic region during Eocene Thermal Maximum 2. Nature Geoscience, 2: 777 - 780. doi:10.1038/ngeo668

Via, R.K., and Thomas, D.J., 2006. Evolution of Atlantic thermohaline: Early Oligocene circulation onset of deep-water production in the North Atlantic. Geology, 34: 441-444. doi: 10.1130/G22545.1

Zachos, J.C., Kroon, D., Blum, P., et al., 2004. Proc. ODP, Init. Repts., 208: College Station, TX (Ocean Drilling Program), doi:10.2973/odp.proc.ir.208.2004

Zachos, J.C., Röhl, U., Schellenberg, S.A., Sluijs, A., Hodell, D.A., Kelly, D.C., Thomas, E., Nicolo, M., Raffi, I., Lourens, L.J., McCarren, H., and Kroon, D., 2005. Rapid acidification of the ocean during the Paleocene-Eocene Thermal Maximum. Science, 308: 1611-1615. doi:10.1126/science.1109004

ICDP

A hydroacoustic data set from pre-site surveys for the SCOPSCO ICDP-campaign in Lake Ohrid (Macedonia and Albania)

K. LINDHORST[1], S. KRASTEL[1], T. SCHWENK[2], M. GRÜN[1], B. WAGNER[3]

[1] Leibniz-Institut für Meereswissenschaften (IFM-GEOMAR), Kiel, Germany, klindhorst@ifm-geomar.de
[2] Fachbereich Geowissenschaften, Universität Bremen, Germany
[3] Institute für Geologie und Mineralogie, Universität Köln, Germany

The transboundary Lake Ohrid is situated on the Balkan Peninsula with approximately two thirds of its surface area belonging to the Former Yugoslav Republic of Macedonia and about one third belonging to the Republic of Albania. Lake Ohrid is not only considered to be the oldest, continuously existing lake in Europe but also host more than 210 endemic species which makes it a hotspot of biodiversity (Albrecht and Wilke, 2008). Its unique aquatic ecosystem was highlighted when Lake Ohrid was declared a UNESCO World Heritage Site in 1979. However, still several factors such as the exact age and origin of the lake as well as the causes for the abundance of endemic spices are poorly understood.

The drilling proposal entitled SCOPSCO (Scientific Collaboration On Past Speciation Conditions in Lake Ohrid) is approved by ICDP and will start in 2011 by drilling a few shallow sites. Deep drilling in 2012 will address the impact of major geological and environmental events (e.g. tephra input, sudden environmental changes) on the general evolutionary patterns, which might influence the extraordinary degree of endemic biodiversity as a matter of global significance. In addition, drilling will provide important information on age and origin of Lake Ohrid. It will help to unravel the seismotectonic history of the lake area including effects of major earthquakes and associated mass wasting events. Since information on hydrological changes in the northern Mediterranean borderland are relatively spare over long time scales a continuous record of paleoenvironmental history obtained from Lake Ohrid would provide an important database for historic climate changes as well as for volcanic activity.

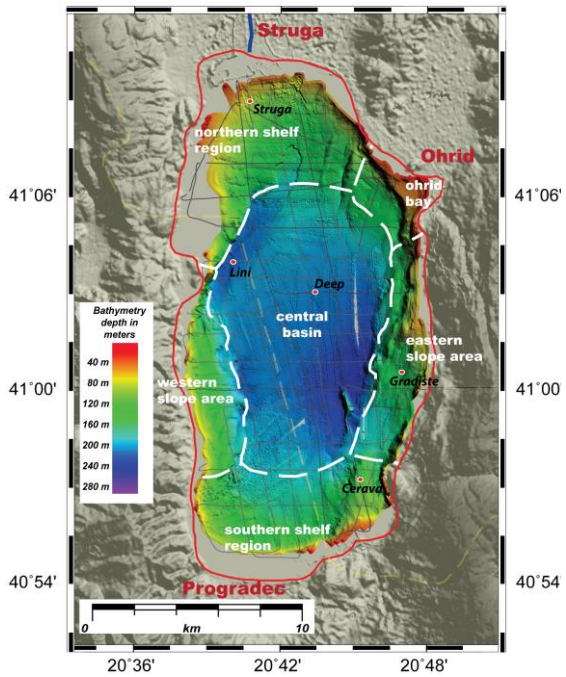

Figure 1: Bathymetry map of Lake Ohrid showing four primary morphological areas. Black lines indicate seismic profiles; proposed drill sites are marked by the red dots.

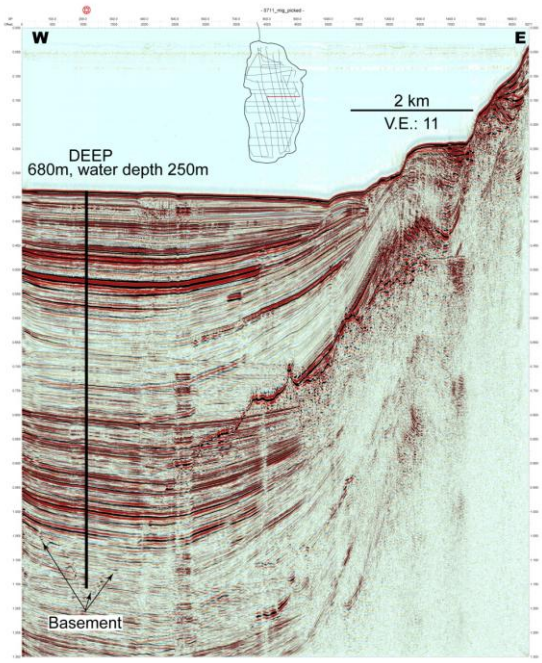

Figure 2: Multichannel seismic line crossing the DEEP-Site in the central basin of Lake Ohrid.

Pre-site surveys have been carried out between 2004 and 2009 and allowed to collect an integrated hydroacoustic data consisting of multichannel seismic, sediment echo sounder, and bathymetric data (Fig. 1). Lake Ohrid can be divided into four morphological provinces based on the bathymetric data: Ohrid Bay (with well distinguished terrace structures), the steep slope areas with gradients of 6° - 20° (marking the eastern and western part of the lake), the relatively flat northern and southern shelf regions, as well as a large central basin (Figure 1). Multibeam data illustrates that the basin covers more than one third of the total lake floor with an average depth of ca. 250 m including two deeper areas: one along a prominent half graben fault system marking the north-western boundary of the basin and the deepest zone of the lake (with max. 293 m) at the south-eastern part of the basin.
For the ICDP campaign five sites have been selected as potential drilling locations (Fig. 1): the central basin site (labeled DEEP on Fig. 1) will provide a continuous archive of maximal age. Cores from four drill sites in proximity to the shore will shed light on (i) major changes of the hydrological regime, (ii) ages of ancient clinoforms that are linked to lake level fluctuations, as well as (iii) its neotectonic activity and associated mass wasting events.

The central goal of the SCOPSCO campaign is to collect an almost 700 m-long core from the deep central basin of Lake Ohrid (DEEP site on Figure 1). Seismic profiles from this area show thick undisturbed sediments overlying a rough basement (Fig. 2). No indications for a hiatus or major mass transport deposits are found at this location. Major objectives to be addressed with this site include the age and origin of the lake, its environmental history, tephra deposition, and the link between evolutionary changes and geological events.

The Lini drill site is located on the Albanian side at the active half graben fault north-west of the central basin (Figure 1). Bathymetric and seismic data shows that the western slope area is characterized by several mass movement events that are probably related to active fault systems. Two mass wasting deposits are found close to the proposed drill site, they probably occurred during the younger Pleistocene. Another drill site (Gradiste, at the eastern part of Lake Ohrid, Figure 1) is placed along the eastern active lake-bounding normal fault.

Two drill sites were chosen to investigate clinoform structures that are visible in the seismic data within the northern and southern part of the lake (Struga and Cerava, Fig. 1). The proposed Struga site close to the out flowing river Crni Drim at the northern part of Lake Ohrid, will provide information about changes in sediment input over time and allow determining the ages of such events. Five distinct clinoforms are found close to the Cerava Site within the southern part of the lake (Figs 1, 3). They indicate considerably lower lake levels in the past with subsequent sudden lake level rises, which is of major importance for the hydrological history of Lake Ohrid. Tracing reflections directly above or below the clinoforms is a first attempt of dating and allocating these events but deep drill cores are needed for exact age estimation and to reconstruct the subsidence history of the entire basin. The drill cores will also improve dating of mass movement events (indicated by chaotic slide deposition bodies, Figure 3) and therefore provide a promising possibility to assess paleaoseismicity of this active tectonic region.

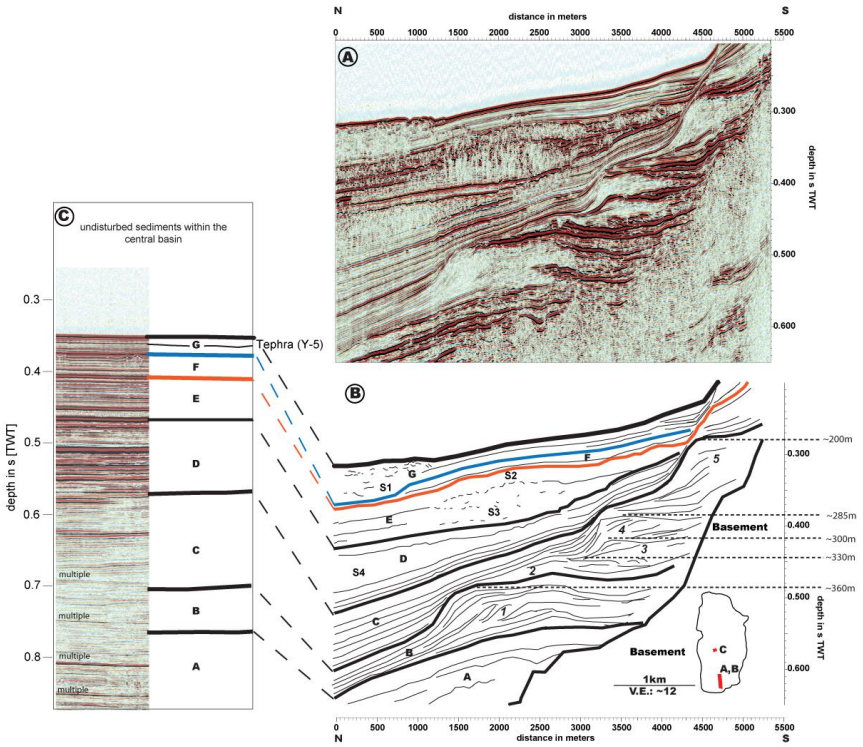

Figure 3: Multichannel seismic data within the southern area close to the Cerava Drill site. (A) uninterpreted and (B) interpreted sections showing complex sedimentary evolution with step-wise lake-level rise as suggested by five major clinoform structures as well as subaquatic slide deposits. (C) illustrates well stratified sediments in the central basin of Lake Ohrid, which can be traced to the clinoforms.

IODP

Implications for the Late Cretaceous oceanic circulation of the proto-North Atlantic from calcareous nannofossils of DSDP Sites 549 and 551

C. LINNERT[1], J. MUTTERLOSE[1]

[1] Institut für Geologie, Mineralogie und Geophysik, Ruhr-Universität Bochum, Universitätsstraße 150, 44801 Bochum

The recent oceanic circulation of the Atlantic is driven by the large difference of sea surface temperatures between the equator (~30°C) and the polar region (<0°C). The thermohaline circulation is characterised by deep water formation in the high latitudes and equatorial upwelling. Large surface water currents such as the Gulf Stream transport heat from the equator into the high latitudes. The low pole-to-equator-gradient of the early Late Cretaceous (<10°C, e.g. Huber et al., 2002), however, did not allow a thermohaline circulation like those of recent oceans. Hay (2008) proposed that the Cretaceous ocean was bare of any modern circulation patterns such as gyres or the Gulf Stream. According to Hay (2008) the surface water circulation was limited to various eddy systems ("Eddy Ocean").

In order to better understand the circulation of the Cretaceous ocean, 77 samples from the Late Cretaceous (Cenomanian – Maastrichtian) of DSDP Sites 549, 551 have been examined for calcareous nannofossils (Linnert et al., 2011). The abundance patterns of calcareous nannofossils from DSDP Sites 549, 551 have been compared to previous studies of the Late Cretaceous from the European shelf. The early Late Cretaceous (Cenomanian) was characterised by calcareous nannofossil assemblages evenly distributed in the proto-North Atlantic and in the European shelf. Taxa with an affinity to open ocean waters such as *Watznaueria* spp. and *Retecapsa* spp. were abundant in the open ocean (DSDP Sites 549, 551) and on the European shelf. On the other hand taxa with an affinity to near shore waters such as *Biscutum* spp. and *Tranolithus orionatus* were quite common in both open ocean and shelf based sections. Calcareous nannofossil assemblages of similar composition imply stable palaeoecologic conditions (nutrient content, surface water temperature, salinity) in the Cenomanian proto-North Atlantic and in European shelf seas. Starting with the Turonian calcareous nannofossil assemblages became different in the open ocean and shelf based sections. Open ocean taxa dominate the assemblages of DSDP Sites 549, 551, whereas near shore taxa are the common assemblages of the European shelf sections. Our findings suggest that the open ocean became more oligotrophic whereas mesotrophic conditions prevailed in the European shelf seas.

This shift from evenly spread calcareous nannofossil assemblages in the Cenomanian to a differentiation of pelagic and neritic assemblages in the Turonian hints towards a shift of the proto-North Atlantic circulation patterns. An "Eddy Ocean" (Hay, 2008) may have existed during the Cenomanian. The absence of large surface water current systems (gyres, Gulf Stream) may have resulted in stable palaeoecologic conditions (nutrient content, surface water temperature) in the proto-North Atlantic as well in

the European shelf seas. During the Turonian the ocean circulation then shifted towards a modern circulation pattern. This way the open ocean became more oligotroph and perhaps warmer compared to the European shelf seas. The differences of the proto-North Atlantic palaeoenvironments and those of the European shelf seas prevailed until the Maastrichtian suggesting a long term stability of the new mode of oceanic circulation. The change of ocean circulation was perhaps supported by the Late Cretaceous high latitude cooling. The pole-to-equator-gradient increased from 9°C in the Cenomanian towards 20°C in the Maastrichtian (Huber et al., 2002). This increased pole-to-equator-gradient may have allowed the establishment of a thermohaline circulation similar to the modern one.

References:
Hay, W.W., 2008. Evolving ideas about the Cretaceous climate and ocean circulation. Cretaceous Research, 29, 725-753.
Huber, B.T., Norris, R.D., MacLeod, K.G., 2002. Deep-sea paleotemperature record of extreme warmth during the Cretaceous. Geology 30, 123-126.
Linnert, C., Mutterlose, J., Herrle, J.O., 2011. Late Cretaceous (Cenomanian-Maastrichtian) calcareous nannofossils from Goban Spur (DSDP Sites 549, 551): Implications for the palaeoceanography of the proto North Atlantic. Palaeogeography, Palaeoclimatology, Palaeoecology 299, 507-528.

Cell wall components, membrane lipids, and microbial communities in the deep subsurface at Canterbury Basin and Peru Margin (ODP Leg 201 and IODP Expedition 317)
(DFG Project Hi 616/11-1)

J.S LIPP[1], R. ZHU[1], G. VERSTEEGH[1], K.-U. HINRICHS[1]

[1] MARUM Center for Marine Environmental Sciences & Department of Geosciences, University of Bremen, 28359 Bremen, Germany

Introduction

The discovery of a subseafloor biosphere in both deep sediments and crustal rocks has fundamentally changed our perception of life on Earth. Evidence for the existence of live microorganisms in the subseafloor is based on the staining of intact cells with specific dyes (Parkes *et al.*, 1994) and on the detection of a group of highly labile molecules such as membrane lipids and DNA (Schippers *et al.*, 2005; Lipp *et al.*, 2008). Both cells and lipids have been found down to great depths and form the basis for current estimates of total microbial biomass in marine sediments. These estimates suggest that subsurface microbial communities constitute a sizeable fraction of total biomass on Earth that exceeds the standing stock of total biomass in the ocean by about two orders of magnitude (Parkes *et al.*, 1994; Whitman *et al.*, 1998; Lipp *et al.*, 2008).

Despite continuous efforts, the most comprehensive recent studies based on culture-independent molecular tools have not yet provided a coherent picture, even when applied to identical environments, as to whether Archaea or Bacteria dominate the subsurface biosphere. Partially responsible is the difficulty of distinguishing signals from dead and live biomass – no matter whether cells are studied directly or molecular methods based on lipids or DNA are being applied. Since cultivation is particularly difficult, detection strategies independent of direct cell counts can principally focus on chemical compounds that represent microbial biomass for the purpose of quantifying specific members of microbial populations. The two biomass pools that have been used so far are DNA (e.g., Schippers *et al.*, 2005; Inagaki *et al.*, 2006) and intact membrane lipids (Lipp *et al.*, 2008).

Study area

IODP Expedition 317 cored four shelf-upper slope sites in the Canterbury Basin on the eastern margin of the South Island of New Zealand in water depths of 85-344 m. Eocene to recent sedimentary sequences, influenced by a high rate of sediment supply from the uplifting Southern Alps, were cored in a transect of three sites on the continental shelf (landward to basinward, Sites U1351, U1353, U1354) and one site on the continental slope (U1352). While IODP Expedition 317 aimed to derive an understanding of the relative importance of global sea level changes versus local tectonic and sedimentary processes in controlling continental margin sedimentary cycles (Fulthorpe *et al.*, 2011), it provided excellent opportunities to study the relation between size, composition, and carbon metabolism of the subsurface biosphere and both the availability of organic matter which is controlled by paleo-sedimentation conditions with highly variable sedimentation rates (1 to 40 cm/ky, Böttcher *et al.*, 2004), and the quality of organic matter which largely results from terrestrial sources. Moreover, it provided the unique opportunity to study the link of microbial communities and geochemistry at burial depths of up to 1.9 km.

Project goals and results

The overarching goal is to develop and apply new methods to exploit molecular pools other than lipids and DNA in order to gain a better understanding of the quantity, taxonomic composition, and metabolic pathways of microbial communities in marine sediments and to integrate the results with geochemical data. An attractive target are cell wall components consisting of polymers such as peptidoglycan, which is characteristic for most Bacteria, and pseudomurein, which is indicative for certain methanogenic archaea. During the project we have added an additional approach based on pyrolysis gas chromatography coupled to mass spectrometry (pyr-GC/MS) which generates low-molecular-weight fingerprints of organic macromolecules including proteins and nucleic acids. This method is independent of specific molecular structures only found in certain organisms and targets bulk biomass.

More specific research questions of this project include:

- Is microbial biomass detectable down to great burial depths of 1.9 km?
- What is the link between geochemistry and microbial communities and how does it change from surface to burial depths of 1.9 km?
- Does the strong terrestrial predominance in organic matter type result in distinct patterns of biomass concentration and taxonomic composition compared to marine organic matter found at Peru Margin?

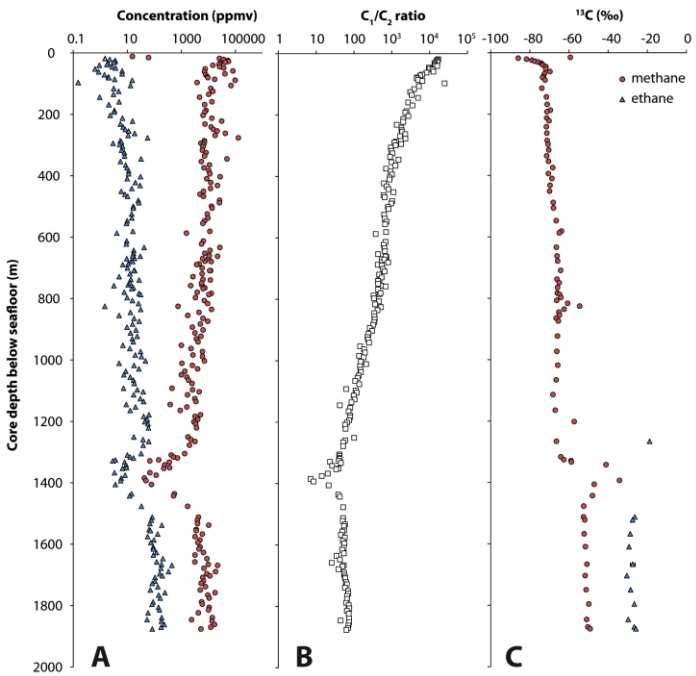

Figure 1: Plots of headspace methane and ethane concentrations (**A**), C_1/C_2 ratios (**B**) and $\delta^{13}C$ values (**C**) vs. depth of sediment samples from IODP Site U1352.

1) Sediment geochemistry

Cores at all four sites at IODP Expedition 317 were routinely sampled for traces of residual dissolved gas, both as a hydrocarbon safety procedure and as a sensitive technique to determine the status of the microbial and thermal degradation of organic matter. In combination with pore water samples, this approach led to detailed profiles covering the biogeochemical zones of sulfate reduction, anaerobic oxidation of methane (AOM), and methanogenesis at all sites (Fulthorpe *et al.*, 2011). Site U1352 is the deepest IODP site which was systematically sampled for molecular biological and chemical analyses and covers a complete section from modern slope terrigenous sediment to Eocene limestone reaching into the early oil-generating window. Preliminary analysis of hydrocarbon gases shows signs of microbial activity and the influence of depth and temperature (Fig. 1). The methane to ethane ratio (C_1/C_2) decreases three orders of magnitude to the bottom of the hole at 1920 m as $\delta^{13}C$ values gradually increase, which is in accordance with an increase of thermogenic methane with depth. At an apparent unconformity near 1400 m, C_1/C_2 ratios drop to minimum values of 7, while $\delta^{13}C$ values of methane increase from ~-70‰ to ~-50‰, suggesting an abrupt, substantial increase in the proportion of thermogenic gas below this depth. Confirmation of the relative importance of thermogenic and biogenic gas in this depth interval will come from analysis of stable hydrogen isotopes which is scheduled for summer 2011.

2) cell wall components

Peptidoglycan, also known as murein, is a polymer responsible for the rigid structure of cell wall sacculi in Bacteria. It is particularly abundant in gram-positive bacteria in which it can account for up to 90% of the cell wall. The monomers of high taxonomic specificity for Bacteria are a number of D-amino acids and muramic acid. Most cultured archaea lack this type of cell wall polymer except for select methanogens, which synthesize a different type of peptidoglycan, the so-called pseudomurein (Kandler and König, 1998). In pseudomurein, the peptide moiety is composed of L-amino acids, and *N*-acetyltalosaminuronic acid is the substitute of muramic acid found in bacterial cell walls. The pool of cell wall polymers is potentially attractive as it provides an alternative means to quantify the biomass of Bacteria and select methanogenic archaea.

We have implemented two methods: one based on liquid chromatography (LC; Boschker *et al.*, 2008) and the other based on gas chromatography (GC; Guerrant and Moss, 1984). The first method has the advantage that no special sample treatment is necessary before analysis, while the GC protocol needs conversion of the polar compounds to volatile derivatives before analysis. Both techniques are in principle suitable for compound-specific stable carbon isotope analysis, however, only the GC-based method can be easily adapted to additionally monitor nitrogen isotope ratios. First tests with standard compounds and different derivatization techniques were successful and all target molecules were identified with both methods. Due to the lacking availability of a suitable detector on the LC side we put more emphasis on the improvent of the GC-based protocol. In a next step, we extracted cell wall components from four ODP samples of ODP Legs 201 and 204. After clean-up by ion exchange resin and subsequent derivatization to aldononitrile derivatives (Guerrant and Moss, 1984), several aminosugars could be detected in the extract. However, muramic acid as the most important target compound was not detected, possibly due to incomplete derivatization or insufficient purification leading to low sensitivity.

3) bulk biomass analysis (pyr GC-MS)

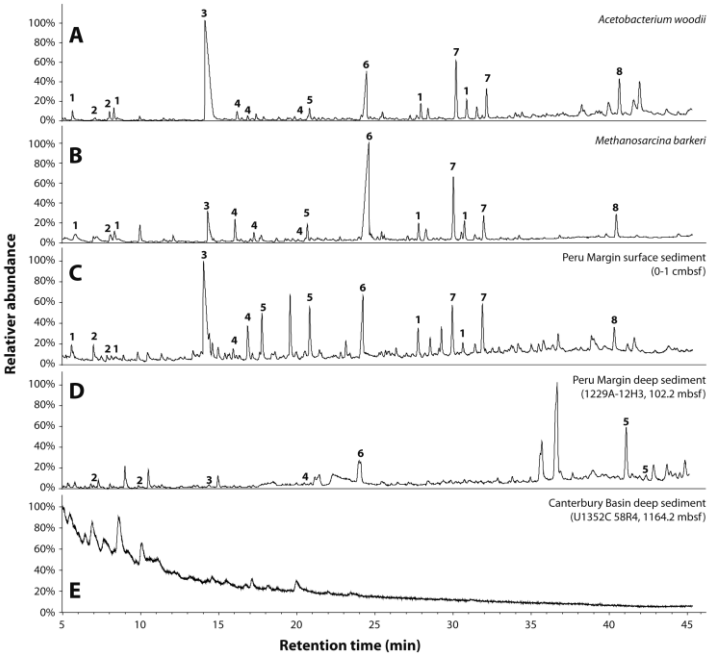

Figure 2. Characteristic partial pyrolysis-GC/MS chromatograms of (**A**) *Acetobacterium woodii*, (**B**) *Methanosarcina barkeri*, (**C**) surface sediment from the Peru Margin, (**D**) a deeply buried sediment of Peru Margin (ODP 1229A), and (**E**) a deeply buried sediment of Canterbury Basin (U1352). (1: nitrile derivatives; 2: pyridine and derivatives; 3: acetic acid; 4: pyrrole and derivatives; 5: furan derivatives; 6: acetamide; 7: phenol and derivatives; 8: indole).

Pyrolysis-GC/MS has been successfully used to characterize microorganisms and differentiate between them (Irwin, 1979; Snyder *et al.*, 2004). These previous studies of microbial cultures relied on ratios of diagnostic fragments and multivariate analyses such as principal component analysis to differentiate between the taxa. Therefore, pyrolysis-GC/MS can be used as a method to rapidly screen for the presence of labile macromolecules associated with living microbes in the deep biosphere. In order to adapt the pyrolysis-GC/MS method to the analysis of sedimentary matrices, we first pyrolyzed cells of different archaeal and bacterial lineages (Fig. 2A,B) as well as reference substances and model compounds to obtain a fingerprint for living microbial biomass. Pyrolysis products derived from proteins, carbohydrates and nucleic acids generally dominated the pyrolysates. Although the relative distributions of these compounds varied between the strains, no specific archaeal or bacterial fingerprint could be identified so far. By pyrolyzing surface sediments from the Peru Margin (Fig. 2C), we tested to what extent the fingerprint of microbial biomass could be recovered from the benthic ecosystem. As expected some nitrogen-bearing fragments derived from proteins, amino sugars and nucleic acids occur both in microbial cultures and surface sediments. Although in the surface sediments, proteins, amino sugars and nucleic acids may also be derived from fresh organic matter from the overlying water column, such contribution is not expected to play a role in more deeply buried sediment. Preliminary analyses show that at around 100 m below the sea floor signals can be still detected at Peru Margin ODP Site 1229 where cell concentrations were on the order of 10^7 cells/mL sediment (Fig. 2D). On the other hand, initial results of pyrolysis-GC/MS in sediments spanning the unconformity depth interval at Site U1352 from 1110 to 1630 m showed only empty pyrograms and no typical microbial signals (Fig. 2E). This is in concordance with the lack of signals during intact polar lipid (IPL) analysis of the same samples and reflects generally low biomass concentrations at the great burial depths. Cell concentrations of Site U1352 are not yet available, but on-board counts of Site U1351 point to cell concentrations generally 1-2 orders of magnitude lower than the established global dataset (Fulthorpe *et al.*, 2011; Parkes *et al.*, 2000). We are currently improving the pyrolysis-GC/MS method and are generating a calibration curve as basis for estimating sedimentary microbe concentrations from pyrolysates and to establish a detection limit. Further analytical improvements will include the use of a trap to pre-concentrate the pyrolysates before chromatographic separation. The expected increase in detection limit will enable the analysis of biomass in previously inaccessible sediments with very low organic carbon concentrations.

Outlook

Subseafloor samples from Exp. 317 with burial depths greater than 1 km are particularly challenging due to their presumed low concentrations of microbial cells. This results in increased requirements for method adaptation to the system-specific requirements. Subsequently, we will generate molecular down-core records for Sites U1351, U1352, U1353, and U1354 by combined analysis of cell wall components, total biomass by pyrolysis-GC/MS, and intact polar lipids. The latter analytical approach will benefit from other ongoing projects funded by DFG and ERC in which we currently develop new separation and mass spectrometric protocols aimed at reducing the detection limit. If concentrations permit, we intend to generate data by stable isotope analysis of carbon and nitrogen in cell wall components and total biomass. This approach targets substrates and nutrient cycling of subsurface microbial communities and will be especially informative with respect to the mechanisms and dynamics of N-uptake in bacteria and selected archaea, respectively.

References:

Boschker HTS, Moerdijk, TCW, van Breugel P, Houtekamer M, Middelburg JJ (2008). A versatile method for stable carbon isotope

analysis of carbohydrates by high-performance liquid chromatography/isotope ratio mass spectrometry. *Rap. Comm. Mass Spec.* **22**, 3902-3908.

Böttcher ME, Khim BK, Suzuki A, Gehre M, Wortmann UG, and Brumsack HJ (2004). Microbial sulfate reduction in deep sediments of the Southwest Pacific (ODP Leg 181, Sites 1119-1125): evidence from stable sulfur isotope fractionation and pore water modeling. *Mar. Geol.* **205**, 249-260.

D'Hondt SL, Jørgensen BB, Miller DJ, Batzke A, Blake R, Cragg BA, Cypionka H, Dickens GR, Ferdelman T, Hinrichs KU, Holm NG, Mitterer R, Spivack AJ, Wang G, Bekins B, Engelen B, Ford K, Gettemy G, Rutherford S, Sass H, Skilbeck CG, Aiello IW, Guerin G, House CH, Inagaki F, Meister P, Naehr T, Niitsuma S, Parkes RJ, Schippers A, Smith DC, Teske A, Wiegel J, Padilla CN, Acosta JLS (2004). Distributions of Microbial Activities in Deep Subseafloor Sediments. *Science* **306**, 2216–2221.

Fulthorpe CS, Hoyanagi K, Blum P, and the Expedition 317 Scientists, 2011. *Proc. IODP, **317***: Tokyo (Integrated Ocean Drilling Program Management International, Inc.). doi:10.2204/iodp.proc.317.2011.

Guerrant GO, Mass GW (1984). Determination of Monosaccharides as Aldononitrile, O-Methyloxime, Alditol, ans Cyclitol Acetate Derivatives by Gas Chromatography. *Anal. Chem.* **56**, 633-638.

Inagaki F, Nunoura T, Nakagawa S, Teske A, Lever M, Lauer A, Suzuki M, Takai K, Delwiche M, Colwell FS, Nealson KH, Horikoshi K, D'Hondt S, Jørgensen BB (2006). Biogeographical distribution and diversity of microbes in methane hydrate-bearing deep marine sediments on the Pacific Ocean Margin. *Proc. Natl. Acad. Sgci. USA* **103**, 2815-2820.

Irwin WJ (1979) *J. Anal. Appl. Pyrolysis.* **1**, 89-122.

Kandler O, König H (1998). Cell wall polymers in Archaea (Archaebacteria). *Cell. Mol. Life Sci.* **54**, 305-308.

Lipp JS, Morono Y, Inagaki F, Hinrichs KU (2008). Significant contribution of Archaea to extant biomass in marine subsurface sediments. *Nature* **454**, 991-994.

Parkes RJ, Cragg BA, Bale SJ, Getliff JM, Goodman K, Rochelle PA, Fry JC, Weightman AJ, Harvey SM (1994). Deep bacterial biosphere in Pacific Ocean Sediments. *Nature* **371**, 410-413.

Parkes RJ, Cragg BA, Wellsbury P (2000). Recent studies on bacterial populations and processes in subseafloor sediments: A review. *Hydrogeol. J.* **8,** 11–28.

Schippers A, Neretin LN, Kallmeyer J, Ferdelman TG, Cragg BA, Parkes RJ, Jørgensen BB (2005). Prokaryotic cells of the deep sub-seafloor biosphere identified as living bacteria. *Nature* **433**, 861-864.

Snyder AP, Dworzanski JP, Tripathi A, Maswadeh WM, Wick CH (2004). Correlation of Mass Spectrometry Identified Bacterial Biomarkers from a Fielded Pyrolysis-Gas Chromatography-Ion Mobility Spectrometry Biodetector with the Microbiological Gram Stain Classification Scheme. *Anal. Chem.* **76**, 6492-6499

Whitman WB, Coleman DC, Wiebe WJ (1998). Prokaryotes: The Unseen Majority. *Proc. Natl. Acad. Sci. USA* **95,** 6578–6583.

ICDP

Lake Van Drilling Project 'PaleoVan', a long continental record of Eastern Anatolia: Report of the ICDP drilling operation in 2010

T. LITT[1], F.S. ANSELMETTI[2], N. CAGATAY[3], R. KIPFER[1], S. KRASTEL[4], S. ÖCEN[5], M. STURM[1] AND 'PALEOVAN' SCIENTIFIC DRILLING PARTY

[1] Steinmann Institute of Geology, Mineralogy and Palaeontology, University of Bonn; Germany (t.litt@uni-bonn.de)
[2] Eawag, Swiss Federal Institute of Aquatic Science and Technology, Switzerland
[3] Eastern Mediterranean Centre for Oceanography and Limnology, Istanbul Technical University, Istanbul, Turkey
[4] Leibniz Institute of Marine Sciences (IFM-GEOMAR), Kiel, Germany
[5] Department of Geology, University of Yüzüncü Yil, Van, Turkey

Lake Van is the fourth largest terminal lake in the world (volume 607 km^3, area 3,570 km^2, maximum depth 460 m), extending for 130 km WSW-ENE on the Eastern Anatolian High Plateau, Turkey. Lake Van is a key site for the investigation of the Quaternary climate evolution in the Near East. The geochronological precision on a decadal or even annual scale will allow comparisons not only with astronomical cyclicity but also signals below the frequency of Milankovitch cycles, such as North Atlantic Oscillation, which may have also affected the past climate system of the eastern Mediterranean region. As a closed and saline lake, Lake Van reacts very sensitively with lake level changes to any alterations in the hydrological regime in response to climate change. These changes do affect water chemistry and water physics, which in turn alter the sediments so that they record these past fluctuations with distinct changes in lithology. Lake Van's annually laminated sediment record covers several glacial-interglacial cycles and holds thus potentially 400'000 years of depositional history. It is considered a jewel for high-resolution paleoenvironmental, paleoclimatic and paleotectonic research. The sedimentary succession of the lacustrine subsurface was recovered in summer 2010 by the ICDP (International Continental Scientific Drilling Program) project ‚PaleoVan'. The ICDP drilling operation was carried out from July 2 to August 23, 2010. DOSECC, as operator of the deep drilling, has built the new Deep Lake Drilling System (DLDS), which was specifically designed for sampling sediments from deep lakes and which made its maiden voyage on Lake Van. The DSDL was operated at water depths of up to 360 m. Two sites were drilled and cores of 140 m (Northern Basin) and 220 m (Ahlat Ridge) depth were retrieved. The sediments of the very bottom document the initial phase of the lake formation, which was characterized by fresh water conditions. We collected a total recovered sediment core length of over 800 m, which allow an unprecedented look back in time at the scale of at least three glacial-interglacial cycles. Several meter thick tephra layers originating from volcanoes surrounding the lake were also recovered, allowing reconstructions of larger volcanic events and related environmental impacts. The cores are stored in the Bremen IODP-core repository (MARUM). All facilities of the IODP-core repository have been be used for splitting, scanning of the split half, core descriptions and sampling during an international sampling party 2011 (17 January – 11 February). Samples have been taken for palaeomagnetic investigations, sedimentology, anorganic geochemistry, pollen and isotope analyses, and black carbon especially from the cores obtained from Ahlat Ridge (priority site for paleoclimate research).

ICDP

Scientific Collaboration On Past Speciation Conditions in Ohrid (SCOPSCO): Recent and fossil Ostracodes from Lake Ohrid as indicators of past environments: A coupled ecological and molecular genetic approach with deep-time perspective

J. LORENSCHAT[1], B. SCHARF[1], T. PETKOVSKI[2], H. KANAFA[1], M. LIST[1], F. VIEHBERG[3], A. SCHWALB[1]

[1] Institut für Umweltgeologie, Technische Universität Braunschweig, Langer Kamp 19 c, 38106 Braunschweig, Germany (j.lorenschat@tu-bs.de)
[2] Macedonian Museum of Natural History, Boulevard Ilinden 86, MK-1000 Skopje, Macedonia
[3] Institut für Geologie und Mineralogie, Universität zu Köln, Zülpicherstraße 49 a/b, 50674 Köln, Germany

Introduction:

Ancient Lake Ohrid is characterized by a high degree in endemism and an unresolved geological history. Ostracodes, small crustaceans, are preserved in adequate abundances in at least two interglacial sediment sequences and thus provide a unique record to test the aquatic ecosystem response to environmental changes. Because knowledge of ecological dependences is insufficient to interpret fossil assemblages from long sediment cores, and taxonomy is difficult, we (1) perform autecological and taxonomic analyses of recent ostracodes and environmental parameters to characterize habitats, (2) unravel the response of the lake system and the ostracode assemblages during the Eemian and the Holocene, and (3) determine the degree of extinction due to anthropogenic pressure. Recent ostracodes are also being used to (4) establish phylogeny and date speciation events using genetic techniques. This will allow to verify ostracode taxonomy and degree of diversity as well as ages of speciation events provided by other organisms analyzed by our cooperation partners Wilke and Albrecht (Universität Giessen). The coupling of taxonomic and autecological analyses with genetic techniques and results from fossil assemblages will be used to narrow down age and causes of speciation events, and the origin of Lake Ohrid.

Autecology and taxonomy of recent ostracodes:

Because it is essential to understand the ecology of individual ostracode species and species assemblages when working with fossil assemblages, we carried out four seasonal field campaigns to unravel the ecology of ostracodes in Lake Ohrid as well as in its catchment by characterizing sediment and water characteristics. Initial results from our survey of living ostracodes based on 117 samples taken in Lake Ohrid provided 29 species belonging to 13 genera including *Candona*, *Fabaeformiscandona, Candonopsis*, *Cypria*, *Cyclocypris, Ilyocypris, Eucypris, Prionocypris, Dolerocypris, Leptocythere, Paralimnocythere, Cytherissa, and Darwinula.* Identification was based on valve and soft part characteristics. Another five species were identified using empty carapaces and valves. The most prominent species is *Cypria lacustris* that occurred in all water depths ranging from the littoral down to 280 m. The most common group are the Candonidae representing about 52% of all species. Restricted to the littoral zone were *Candona litoralis*, C*andonopsis kingsleii*, *Eucypris virens*, *Eucypris* sp., *Prionocypris zenkeri*, *Bradleystrandesia reticulata*, *Dolerocypris sinensis*, and *Darwinula stevensoni*. Even in 280 m water depth living ostracodes were found (*Candona candida*, *Candona hadzistei*, *Candona media*, *Candona ovalis*, *Fabaeformiscandona krstici*, *Cypria lacustris*, and *Cypria obliqua*). In the catchment of Lake Ohrid 21 species were discovered of which 14 also occurred in the lake itself.

Eemian and holocene ostracode assemblages:

Ostracode species assemblages from core CO1202, taken in 2007, spanning the past approximately 136 ka (Wagner et al., 2010), and $\delta^{18}O$ and $\delta^{13}C$-signatures of their valves will serve to determine the regional expression of global climate change on the Balkans, the influence of geologic perturbations such as volcanic eruptions on the diversity of ostracodes, and how ostracode assemblages recovered from these perturbations. Furthermore, we are testing if these perturbations play a role for speciation by comparing fossil assemblage data and speciation events dated by DNA analysis. A preliminary set of 34 samples shows that ostracode valves are present in all analyzed interglacial samples of Eemian and Holocene age. We found only sporadically valves in the glacial sediments that are carbonate-free or have low carbonate contents (< 10 %). So far we identified 21 ostracode species (exclusively juveniles) out of which five species were not yet found in our recent sediment samples. In contrast, Belmecheri et al. (2009) reported only a total of 12 species from a sediment core spanning the past approx. 140 ka. The presence of *Leptocythere*, a genus that typically occurs in sea- and brackwater, in this core and in our surface sediment samples may provide evidence for a marine origin of Lake Ohrid. Maximum number of species in a single sample was 11 (ca. 6.7 ka), and diversity during the Eemian is lower than during the Holocene. This also contradicts results by Belmecheri et al. (2009) who suggest that there is no significant change in species diversity between these two interglacial periods. These discrepancies also underline the need for accurate taxonomy.

Antropogenic impact on species assemblages:

Based on ostracode assemblages we assess human impact, determin the degree of extinction due to anthropogenic pressure, and use ostracodes as indicators for ecosystem health. This may help to clarify whether the ecological threshold has already been reached and if remedial measures should be considered. To reach this goal we have taken sediment short cores in Lake Ohrid from polluted sites (nearby the cities of Struga and Ohrid on the northern and north-eastern shore) and from a pristine site (near Sveti Naum at the south-eastern shore). The cores were documented and described, water content, organic matter and carbonate content were determined by loss on ignition, and ^{210}Pb and ^{137}Cs dating were carried out. Preliminary results suggest sedimentation rates of 0.083 cm yr^{-1} near the city of Ohrid, 0.4 cm yr^{-1} near the city of Struga, and 0.46 cm yr^{-1} near Sveti Naum. To date, we identified 14 ostracode species in the core “Sveti Naum” and 25 species in the core “Ohrid”. The dominant species in the core “Sveti Naum” was *Candona trapeziformis* and in “Ohrid” *Candona hadzistei*. Higher ostracode diversity and abundances occur near the cities of Ohrid and Struga than near Sveti Naum. This suggests that the modern anthropogenic pressure has rather a positive effect on ostracode species assemblages and that nutrient-poor water

off Sveti Naum cause lower ostracode abundances and diversity. Thus, a critical state that would call for remedial measures has not yet been reached. However, it cannot be ruled out that increasing water pollution will lead to extinction of highly specialized endemic species.

DNA analysis:

Ostracodes have the advantage of being preserved in the sediments of Lake Ohrid in high abundances. Thus, fossil species assemblages allow calibration of the molecular clock by dating when specific species started to colonize the lake. This question can be addressed once long cores going further back in time will become available after ICDP drilling. By means of DNA analysis we will test if the lake served as a refuge for certain species during the cold periods of the Pleistocene, if species survived in the lake while other lakes in the region had, for example, dried up, and if there were repeated immigration events or if intralacustrine speciation occurred. Studies based on detailed anatomical analyses and fast evolving nuclear markers will help to unravel the uncertainties in the total number of species, e.g. in the genus *Candona*. In a pilot study we isolated the mitochondrial cytochrome oxidase I (COI) gene from five ethanol-preserved ostracode species (*Candona hadzistei*, *Candona ovalis*, *Cypria obliqua*, *Leptocythere karamani*, and *Paralimnocythere karamani*; one to four specimens per species) utilizing the protocol of Winnepenninckx et al. (1993). The calcified valves were separated from the soft tissues of the individuals because they can inhibit enzymes in subsequent molecular biological methods such as the Taq polymerase in the polymerase chain reaction (PCR; Schön and Martens, 2003). For both PCR and sequencing universal primers for COI were used (Folmer et al., 1994). In the next series of analysis we will screen the 16S, 18S and 28S region, different subunit RNA molecules of the ribosome. These are slow evolving genes that may be more suited for our purposes, the reconstruction of long evolutionary histories (Schön and Martens, 2003). Another reason for the choice was that Schön and Martens (2003) have successfully used 16S on ostracodes. Furthermore, we will increase the number of DNA amplification cycles and add bovines serum albumin (BSA) during the PCR to stabilize enzymes in the DNA digestion and to prevent adhesion of enzymes to reaction tubes. During screening we will add universal primers for crustaceans.

References:

Belmecheri, S., Namiotko, T., Robert, C., von Grafenstein, U. & D.L. Danielopol, 2009. Climate controlled ostracod preservation in Lake Ohrid (Albania, Macedonia). Palaeogeography, Palaeoclimatology, Palaeoecology 277: 236-245.

Folmer, O., Black, M., Hoeh, W., Lutz, R.A. & R.C.Vrijenhoek, 1994. DNA primers for amplification of mitochondrial cytochrome c oxidase subunit I from diverse metazoan invertebrates. Molecular Marine Biology and Biotechnology 3: 294-299.

Martens, K. & I. Schön, 1999. Crustacean biodiversity in ancient lakes: A review. Crustaceana 72: 899-910.

Schön, I. & K. Martens, 2003. Phylogenetic reconstructions of ostracodes - a molecular approach. In: L.E. Park, A.J. Smith (eds), Bridging the Gap, Trends in the Ostracode Biological and Geological Sciences. Paleontological Society Papers 9: 71-88.

Wagner, B., Vogel, H., Zanchetta, G. & R. Sulpizio, 2010. Environmental changes on the Balkans recorded in the sediments from lakes Prespa and Ohrid. Biogeosciences 7: 3365-3392.

Winnepenninckx, B., Backeljau, T. & R. De Wachter, 1993. Extraction of high molecular weight DNA from molluscs. Trends in Genetics 9: 407.

ICDP

Shock deformation and nucleation of magnetic minerals in suevites of the Chesapeake Bay Impact Crater, USA

C. MANG[1], A.KONTNY[1], D. HARRIES[2], L. HECHT[3], F. LANGENHORST[2]

[1] Institut für Angewandte Geowissenschaften, Karlsruher Institut für Technologie, Hertzstraße 16, D-76187 Karlsruhe
[2] Bayrisches Geoinstitut, University of Bayreuth, D-95440 Bayreuth
[3] Museum für Naturkunde, Humboldt Universität zu Berlin, Invalidenstraße 43, D-10115 Berlin

We investigated the dominant magnetic minerals in scientific drill cores from the Chesapeake Bay impact crater (CBIS), USA. This crater is characterized by an irregular magnetic anomaly (Shah et al., 2009). The goal of our work was to determine and characterize the dominant magnetic minerals and to separate the particular impact units by means of their magnetic mineralogy and magnetic properties. As these features differ from each other in all impact units, this characterization allows to estimate the discrete contribution of each unit to the bulk magnetic field. This approach is reasonable for a characterization of impact craters rocks in general, but particularly for Chesapeake Bay since the magnetic anomaly is neither circular nor confined to the crater rim as observed in many other craters (e.g. Melosh and Ivanov, 1999). On a microscopic scale our investigations lead to a possible link between chemical composition, deformation structures and the rock magnetic behaviour of the main magnetic minerals. The latter studies were particularly done with respect to a possible change in the crystal structure and the magnetic behaviour due to shock.

The regional negative, NW - SW tending magnetic anomaly around CBIS is disturbed within the crater by irregular field deviations (Shah et al., 2009) Positive magnetic anomalies at the western and eastern side of the inner ring of the crater structure are considered to be impact-related. We studied samples of the ICDP-USGS Eyreville and NASACape Charles drill core and characterized each unit with respect to its rock magnetic behaviour (Tab. 1). Except the suevites, all units contributing significantly to the bulk magnetization are unshocked basement megablocks, which occur within the crater fill. In the Eyreville core a magnetite bearing granite- and a pyrrhotite bearing schist megablock form these unshocked lithologies. The grains of the magnetic carriers are partly altered and their origin can clearly be linked with the regional geological history of the parent rock material. The Cape Charles core comprises severals blocks of gneiss and a layer of suggested “impact melt”. The suevites in both core profiles differ in their magnetic mineralogy. Magnetite is present in both suevites, but pyrrhotite is exclusively present in the Eyreville suevite. Magnetization of the suevite is significantly higher in the Eyreville Core, especially in the upper part. This part is also enriched in melt components (Wittmann et al., 2009). However, the Cape Charles suevite and gneiss, and the Eyreville granite block do not carry a stable magnetization. NRM mean values published by Shah et al. (2009) suggest 2 – 6 A/m for the layer of “impact melt”. This assumption cannot be confirmed by our measurements, as the measured values range from 0.1 to 1 A/m. Thus we believe magnetic contribution of the impact melt to be overestimated. NRM and suceptibility values of the studied units indicate that only few units contribute to the bulk magnetic field. Thus, the latter is strongly dependent on where these units occur and what size they have. The irregular magnetic field can consequently be explained by a random arrangement of units with higher magnetization.

The impact event, did not only change the bulk

Eyreville	**n**	**NRM**	**SD**	**χ**	**SD**	**Q**
		A/m		SI		
Sediment	41	0.016	0.0196	2.06E-04	0.0001	1.91
Granite	88	0.084	0.3954	1.61E-02	0.0075	0.13
Sandstone 2	4	0.000	0.0001	1.78E-04	0.0002	0.04
Suevite	46	0.125	0.1350	1.60E-03	0.0016	1.91
Schist	18	0.754	0.7271	4.85E-03	0.0100	3.79
Pegmatite	15	0.017	0.0041	6.31E-05	0.0001	6.56
Amphibolite	39	0.002	0.0004	6.64E-04	0.0007	0.09
Bayside						
Granite	37	0.045	0.0486	1.06E-02	0.0076	0.10
Cape Charles						
Amphibolite	15	0.003	0.0003	5.63E-04	0.0003	0.12
Gneiss	32	0.007	0.0074	1.55E-03	0.0018	0.12
Suevite	27	0.010	0.0116	5.22E-04	6.7120	0.48
(Melt) basalt dyke	8	0.434	0.2143	1.57E-02	0.0015	0.67
Langley						
Granite	41	0.031	0.1053	1.51E-03	0.0031	0.50

Table 1: Mean values of rock magnetic properties for all rocks in the Chesapeake Bay impact structure. n: number of analyses, NRM Natural Remanent Magnetization, χ: susceptibility, Q: Königsberg ratio, SD: standard deviation

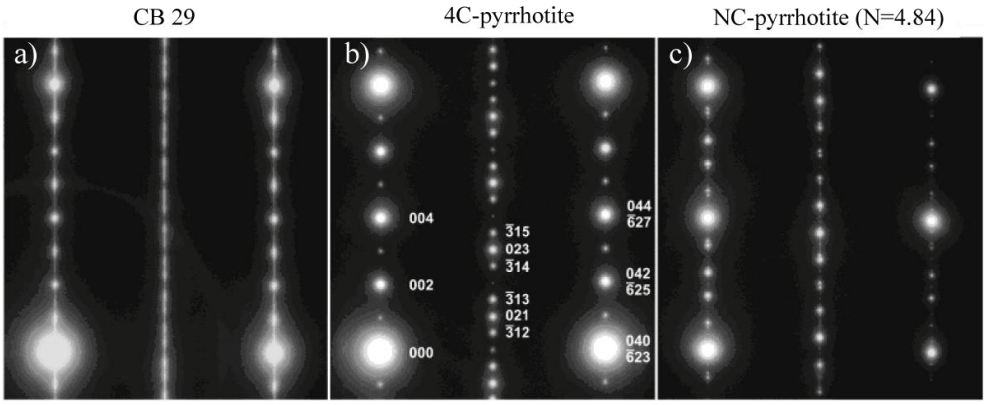

Fig.1 SAED pattern of different pyrrhotite modifications. a) shocked pyrrhotite from the suevite of the Chesapeake Bay impact structure. The outer rows match with b) but the inner row indicate a deviating superstructure. The streaking within the inner row is in accordance with a high amount of crystal defects. b) 4C pyrrhotite. c) NC pyrrhotite is also not in accordance with the pattern in a).

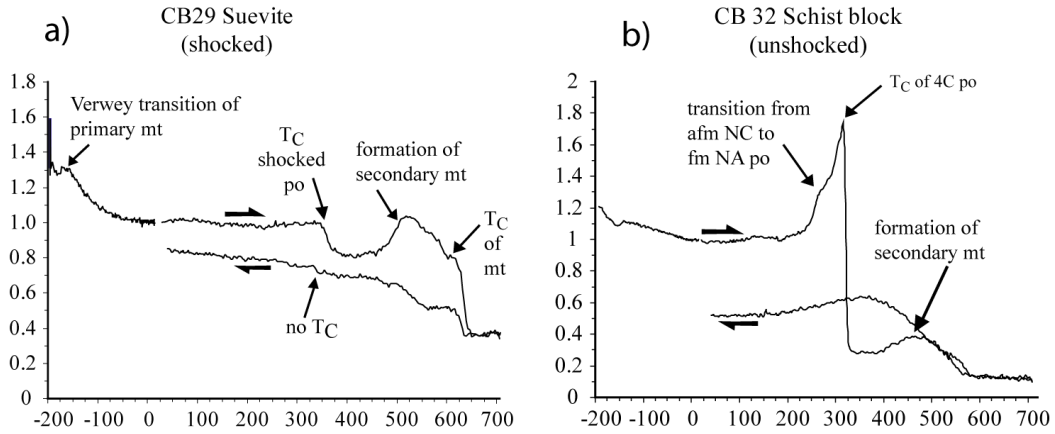

Fig 2: Temperature-dependent suceptibility measurements of a suevite and a schist sample. a) T_C of shocked pyrrhotite is at ~350°C. A small peak at -170°C and T_C above 580°C is related to post-impact formed magnetite of varying grain sizes. The Curie temperature of pyrrhotite lies at ~350°C. b) the schist sample contains monocline and hexagonal pyrrhotite. mt: magnetite, po: pyrrhotite, T_C: Curie temperature, fm: ferrimagnetic, afm: antiferromagnetic

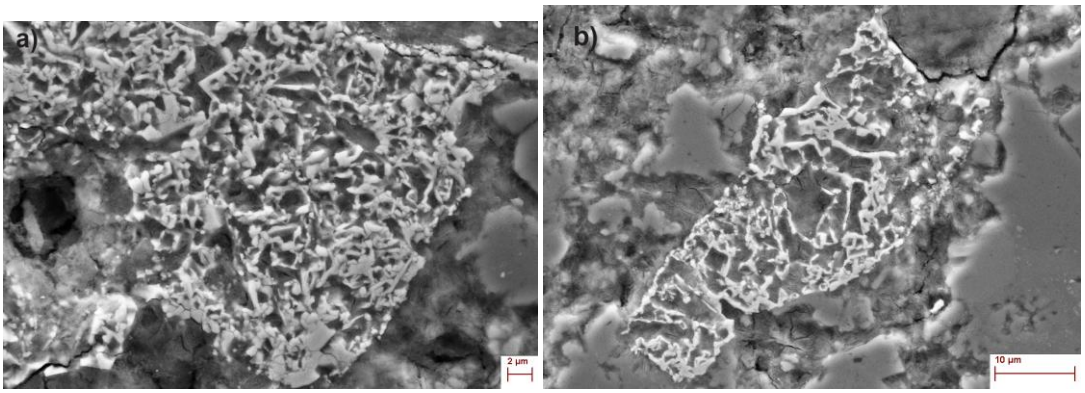

Fig. 3: Clusters of secondary formed magnetite. a) network of single needles and denser domains. The latter consist of nm-sized magnetite crystallites. b) Magnetite network consisting mainly of µm sized intergrown magnetite rods.

magnetization by disordering the pre-impact units. Within the suevites PDF's in quarz and various other shock indicators (Schmitt et al., 2009) display shock induced structural changes within the affected minerals. To characterize the consequences of shock on the rock magnetic behaviour it is thus indispensable to accurately analyse the magnetic mineralogy and restrict their occurrence to a pre- or postimpact origin. In case of the suevites from the CBIS our studies clearly define pyrrhotite as a shocked pre-impact, and magnetite as a secondary post-impact phase as SEM and TEM investigations at the KIT in Karlsruhe and the Geoinstitut in Bayreuth have shown. Additional microprobe analysis at the Museum für Naturkunde in Berlin were important to determine the exact chemistry of the occuring phases.

Magnetic minerals, can be relieably identified using reflecting light microscopy and by coating the thin section with a ferrfluid. The ferrofluid sticks on pyrrhotite and magnetite in the suevites as well as on magnetite in granite, gneiss and basalt (impact melt). Pyrrhotite in the schist rock is present as a ferrimagnetic, monoclinic 4C modification and an antiferromagnetic hexagonal NC modification. As this schist block is until now the only pyrrhotite-bearing pre-impact lithlogical unit in the crater, we interpret this unit as the source of the shocked pyrrhotites in the suevite. In contrast to unshocked pyrrhotite the shocked one, present in the suevites, hold unusual high amounts of crystal defects and thus reveal its shocked pre-impact nature This is visible on HRTEM micrographs. Most likely due to partial vacancy reordering after shock, reflexes in the SAED pattern do not entirely fit with the ones of 4C pyrrhotite and also not with any known pyrrhotite modification (Fig. 1). Probably a new superstructure developed during that process. Pyrrhotite has a chemical formula of $Fe_{1-x}S$ with $0<x<0.125$. The shocked sulfide minerals of CBIS, in contrast, have a bulk composition of $Fe_{0.808}S$ and $Fe_{0.811}S$. This composition falls significantly below the minimum percentage of iron described for pyrrhotites (0.875). The composition varies between individual grains but remains fairly constant within each grain. No chemical zonation could be found among the studied grains. We thus exclude alteration processes to have caused the present Fe/S ratio. A calculated mineral formula lies between $(Fe,Ni)_4S_5$ (0.80) and $(Fe,Ni)_9S_{11}$ (0.818). The latter formula represents the stoiciometry of smythite, an iron depleted sulfide mineral. It forms during rapid quenching from above 500°C (Furukawa and Barnes, 1996) or low temperature oxidation of 4C pyrrhotite (Taylor and Williams, 1972). Although its composition is close to the one of the shocked pyrrhotites of CBIS, the presence of intense lattice defects in the latter hampers the structural identification as smythite. In both formation scenarios one would assume an, at least partial, annealing of the defect structure. We thus assume that the iron depleted Fe/S ratio has to be linked to a shock transformation in the mineral rather than to subsequent alteration processes. Furthermore, the iron defiency has a direct consequence on the Curie temperature (T_C) of pyrrhotite. This becomes obvious in temperature-dependent susceptibility measurements, where T_C was determined at temperatures between 350 and 365°C (Fig. 2). Shock experiments on pyrrhotite have been conducted by several authors and indicate a shock induced transition of 4C pyrrhotite at ~3.5 GPa (e.g. Louzada et al., 2010). Ahrens (1979) found a high pressure phase (hpp) of pyrrhotite forming at shock pressures between 2.5 – 3.5 GPa. A transformation of 4C pyrrhotite to such a hpp in CBIS is therefore a reasonable assumption for the recent mineral properties of the shocked pyrrhotite. After compression of the crystal lattice, rapid pressure release is assumed to have caused the main fraction of crystal defects. The low Fe/S ratio indicates a higher amount of vacancies and thus a lower density. Explosive extensional movements can lower the density by producing distrubances in the crystal lattice without changing the present crystal structure. For this model, a transformation into a hpp is necessary, as both, hexagonal and monoclinic pyrrhotite were transformed to one single shocked sulfide phase. The formation of the hpp would then have "homogenized" the previous compositions of the different pyrrhotite modifications.

Temperature-dependent susceptibility measurements reveal that these clusters do not have a clear defined Curie temperature. In fact the suceptibility drops slowly and beyond 580°C (Fig 3), the typical T_C of magnetite. The early onset of the Curie point can be explained by the nm-sized crystallites. Tang et al (2004) found that the Curie temperature of magnetite grains in the nm range is progressively depressed with decreasing grain size. In return, this effect decreases with increasing grain size. We interpret the early drop in susceptibility around 510°C as a sucessive onset of T_Cs derived from individual nm-sized grains with slightly deviating grain sizes.

Both, magnetite and pyrrhotite show a stable remanence direction of the same orientation. The schist rocks, in contrast, do not show a stable NRM direction. As magnetite clearly carries a Chemical Remanent Magnetization (CRM), which has been acqiured after shock, we interpret the acquisition of both magnetizations to have taken place in a similar time intervall. This implies that pyrrhotite has lost its previous magnetization due to shock and was subsequently able to acquire a new and stable magnetization.

In the next stage of our project, we plan to conduct shock experiments on pyrrhotite to compare the features of naturally shocked pyrrhotite with the ones of pyrrhotite shocked under known conditions.

References:

Ahrens, T. J. 1979. Equations of State of Iron Sulfide and Constraints on the Sulfur Content of the Earth. Journal of Geophysical Research. 84, B3, 985-998

Furukawa, Y., Barnes, H.L., 1996, Reactions forming smythite, Fe_9S_{11}. Geoch. Cosmoch. Acta 60, 3581 – 3591

Louzada, K.L., Steward, S.T., Weiss, B.P., Gattacceca, j., Bezaeva, N., 2010, Shock and static pressure demagnetization of pyrrhotite and implications for the martian crust. Earth and Planetary Science Letters (290) 90 - 101

Melosh, H.J., Ivanov, B.A., 1999, Impact crater collapse, Earth and Planetary Sciences (27) 385-415

Schmitt, R.T., Bartosova, K., Reimold, W.U., Mader, D., Wittmann, A., Koeberl, C., Gibson, R.L., 2009, Geochemistry of impactites and crystalline basement-derived lithologies from the ICDP-USGS Eyreville A and B cores, Chesapeake Bay impact structure, Virginia, USA. The geological Society of America Special Paper (458) 481 - 543

Shah, A.K., Daniels, D.L., Kontny A., Brozena, J., 2009, Megablocks and melt pockets in the Chesapeake Bay impact structure constrained by magnetic field measurements and properties of the Eyreville and Cape Charles cores. Geol. Soc. Am. Spec. Pap. 458, 195 – 209.

Tang, N.J., Zhong, w., jiang, H.Y., Wu, X.L., Liu, W., Du, Y.W., 2004, Nanostructured magnetite (Fe_3O_4) thin films prepared by sol-gel method. Journal of. Magnetism and magnetic Minerals 282, 92 – 95

Taylor, L. A., Williams, K. L., 1972, Smythite, $(Fe, Ni)_9S_{11}$ A Redefinition. American Mineralogist. 57, 1571-1577

Wittmann, A., Schmitt, R.T., Hecht, L., Kring D.A., Reimold, W.U., Povenmire, H., 2009, Petrology of impact melt rocks from the Chesapeake Bay crater, USA. The geological Society of America Special Paper 458, 377 – 396

IODP

Reconstruction of the Atlantic Circulation back to the Last Interglacial by a combined proxy approach from ODP Leg 172 Site 1063 sediments

A. MANGINI[1], J. LIPPOLD[1], E. BÖHM[1], S. WEYER[2], M. GUTJAHR[3], M. CHRISTL[4]

[1] Academy of Science, Heidelberg, Germany
[2] University of Köln, Germany
[3] University of Bristol, UK
[4] ETH Zürich, Switzerland

The Atlantic Meridional Overturning Circulation (AMOC) is believed to have crucial influence on global climate. It affects global temperatures due to the redistribution of heat energy to the high latitudes and by removing and releasing carbon from or into the deep sea. Reconstructions of past ocean circulation changes suggest a strong link between the strength of AMOC and climate especially in circum North Atlantic temperatures.

Theoretical studies and measured data suggest that the AMOC has different circulation modes and that transitions between these modes can be triggered by variations of freshwater runoff into the North Atlantic [Rahmstorf 2002; Rickaby and Elderfield 2005]. Further, glacial climate in the North Atlantic region was characterized by short term climatic cycles referred to as Dansgaard-Oeschger- and Heinrich- Events (HE), which are also believed to be tightly correlated to the strength of North Atlantic Deep Water formation and hence AMOC.

Within the last years two different proxies turned out to be promising in order to reconstruct past deep water provenance and strength of the AMOC, as both proxies are not subject to diagenetic processes. First, the ratio of the in seawater in situ produced ^{231}Pa and ^{230}Th in the sediment, and second the isotopic ratio of ^{143}Nd to ^{144}Nd (ε_{Nd} hereafter) in the post depositional Fe-Mn coatings of the sediment (e.g. [Henderson and Anderson 2003; Frank 2002]). Due to the observation that in the Atlantic Ocean ^{231}Pa is subject to advective transport (while ^{230}Th is a constant flux tracer) the ^{231}Pa/^{230}Th ratio can be applied a tracer for the strength of AMOC in the past. By additionally using the water mass proxy ε_{Nd}, complementary information about the source of the prevailing water mass is available. For this reason, a synthesis of both proxies from the same sediment samples holds the opportunity to provide new insights on the modes of deep ocean circulation in the past.

In this project samples of ODP Leg 172 Site 1063 will be investigated. The oceanic region of ODP Site 1063 on the northeast Bermuda Rise holds a key position in the interaction of Northern Component Water and Southern Component Water and is therefore ideal for detecting past changes in southward water mass export. These variations are recorded in marine sediments and can be reconstructed by analysing ^{231}Pa/^{230}Th and ε_{Nd}. ODP Site 1063 displays constantly very high sedimentation rates (>10cm/ka) enabling a high time resolution.

This study is the first to directly compare water mass source changes, reconstructed by using ε_{Nd} isotopes, with ^{231}Pa/^{230}Th ratios, which records the overturning rate, from identical samples on a timescale back to the last Interglacial (Eemian). The time interval of the planned measurements (35 ka back to 130 ka) spans several severe climate incidents like Heinrich Events (HE-4 to HE-6), numerous Dansgaard-Oeschger Cycles, the Last Glacial Inception and the last Interglacial [McManus et al. 2004; Lippold et al. 2009; Gutjahr et al. 2008; Roberts et al. 2010].

First measurements of the water mass source proxy ε_{Nd} have been accomplished within the time range from 60 to 154 ka with a temporal resolution of in average 3 ka. The data display the presence of Southern Sourced Water (SSW) during MIS 6 to MIS 6.4 and indicates an active deep water formation in the north at the beginning of the Eemian Interglacial (MIS 5.5). The transition between these two different modes in AMOC is marked by a distinct drop in the ε_{Nd} values (-11.5 to -14). This is consistent with ε_{Nd} results obtained from the same core [Gutjahr and Lippold 2011] and from a sister core [Roberts et al. 2010] at the transition from MIS 2 to MIS 1.1. The similar temporal behaviour of ε_{Nd} during Termination I and II implies recurring millennial-scaled identical processes converting the AMOC from a Glacial mode into an Interglacial mode.

References:

Frank, M. (2002), Radiogenic Isootpes: Tracers of Past Ocean Circulation and Erosional Input, Reviews of Geophysics 40(1).

Gutjahr, M., M. Frank, C. Stirling, L. Keigwin and A. Halliday (2008), Tracing the Nd isotope evolution of North Atlantic Deep and Intermediate Waters in the western North Atlantic since the LGM from Blake Ridge sediments, Earth and Planetary Science Letters 266: 61–77.

Gutjahr, M. and J. Lippold, 2011. Invasion of Southern Source Water into the deep North Atlantic. Paleoceanography. submitted.

Henderson, G. and R. Anderson (2003), The U-series toolbox for paleoceanography, "Uranium Series Geochemistry", Reviews in Mineralogy and Geochemistry 128.

Lippold, J., J. Grützner, D. Winter, Y. Lahaye, A. Mangini and M. Christl (2009), Does sedimentary 231Pa/230Th from the Bermuda Rise monitor past Atlantic Meridional Overturning Circulation?, Geophyscial Research Letters 36: L12601.

McManus, J. F., R. Francois, J. M. Gherardi, L. D. Keigwin and S. Brown-Leger (2004), Collapse and rapid resumption of Atlantic meridional circulation linked to deglacial climate change, Nature 428: 834-837.

Rahmstorf, S. (2002), Ocean circulation and climate during the past 120,000 years, Nature(419): 207-214.

Rickaby, R. and H. Elderfield (2005), Evidence from the high-latitude North Atlantic for variations in Antarctic Intermediate water flow during the last deglaciation, Geochemistry Geophysics Geosystems 6: Q05001.

Roberts, N., A. Piotrowski, J. McManus and L. Keigwin (2010), Synchronous deglacial overturning and water mass source changes, Science, accepted.

IODP

Complex sedimentation processes and bottom water redox conditions across the Eocene-Miocene “hiatus” in the Central Arctic Ocean (IODP Expedition 302)

C. MÄRZ[1,2], C. VOGT[3], B. SCHNETGER[1], H.-J. BRUMSACK[1]

[1] Mikrobiogeochemie, ICBM, Carl-von-Ossietzky-Universität Oldenburg, 26111 Oldenburg, Germany
[2] Present address: Biogeochemistry, School of Civil Engineering and Geoscience, Drummond Building, Newcastle University, NE1 7RU Newcastle upon Tyne, UK
[3] Kristallographie/ZEKAM, Fachbereich Geowissenschaften, Universität Bremen, 28334 Bremen, Germany

In 2004, Expedition 302 of the Integrated Ocean Drilling Program (Arctic Coring Expedition, ACEX) to the Central Lomonosov Ridge recovered the first composite sediment record from the Central Arctic Ocean, stretching

from the Upper Cretaceous to the Holocene (Backman, Moran, McInroy, Mayer et al., 2006). One of the major findings of this expedition was that the Paleogene Arctic Ocean was a semi-enclosed anoxic basin in a subtropical climate, and only developed into the modern well-mixed oxic basin due to the Neogene opening of the Fram Strait. The inorganic geochemistry of the sediments reflects this major paleo-environmental transition, despite partly significant diagenetic overprint of the primary sediment composition. While biosiliceous deposits rich in organic matter, pyrite and redox-sensitive/sulfide-forming trace metals dominate the Paleogene section, the Neogene part is mostly siliciclastic, organic-poor, and enriched in Mn and adsorbed trace metals (e.g. Backman, Moran, McInroy, Mayer et al., 2006; Moran et al., 2006; Stein et al., 2006; Stickley et al., 2008; März et al., 2010).

The exact transition from anoxic to oxic conditions in the Central Arctic is still a matter of debate, because its lithological expression on Lomonosov Ridge is affected by a sedimentological hiatus of ~26 Ma duration, separating Eocene from Miocene strata (e.g. Moore et al., 2006; Sangiorgi et al., 2008). Recently, however, an alternative hypothesis for the transition from an anoxic to oxic Arctic Ocean questioned the existence of a hiatus, but favoured the continuous deposition of sediments on Lomonosov Ridge through the Eocene, Oligocene and Miocene (Poirier and Hillaire-Marcel, 2009). Here we present high-resolution major and minor element and mineralogical records across the anoxic-oxic transition in the ACEX record to reconstruct the development of the depositional regime and the variations in bottom water redox conditions. Our results strongly indicate that sedimentation across the Eocene-Miocene boundary was not steady, but was interrupted by several hiati of unknown duration that are clearly expressed in the detrital element records. Below the palynologically defined hiatus, we found evidence for a drastic change in sediment provenance and/or weathering intensity in the terrigenous source area. Above the hiatus, the composition of the Zebra interval suggests repeated erosion and re-deposition of material, supporting its tilted bedding. Regarding redox conditions, our data support the view of an anoxic to euxinic setting on the Eocene Lomonosov Ridge, with high enrichments in pyrite and redox-sensitive/sulfide-forming trace metals (e.g. Cd, Cu, Mo, Ni, Re, U). Before the palynological hiatus, euxinic conditions were even more extreme, leading to strong authigenic pyrite and trace metal enrichments, probably assisted by much lower sedimentation rates. However, despite extreme euxinia in a semi-restricted Arctic basin, we find no indication for trace metal drawdown from the water column throughout the Eocene, revealing that the Arctic water masses were continuously renewed through connections to the world ocean. Assuming that sediments of the Zebra interval are at least partly autochthonous and not entirely re-deposited, reconstructed redox conditions during its deposition were highly variable (Jakobsson et al., 2007), but there are clear signs of an at least periodically well-oxygenated water column. The strongest indication for oxic conditions during the Zebra interval are the extreme positive Ce anomalies in several samples. Interestingly, although positive Ce anomalies in marine sediments are usually related to an intense Mn cycle in the water column, comparable sedimentary Mn enrichments are missing in the Zebra interval, which might be related to selective post-depositional remobilisation of Mn due to microbial Mn (oxyhydr)oxide reduction. Significant Mn enrichments only occur in the sediments above the Zebra interval, documenting the Miocene establishment of fully and persistently oxic conditions in the Arctic Ocean. In summary, our data strongly argue against continuous sediment deposition on the Late Eocene to Mid-Miocene Lomonsov Ridge, but support extremely low sedimentation rates, various intervals of non-deposition and/or erosion.

References:

Backman, J., Moran, K., McInroy, D.B., Mayer, L.A., Expedition 302 Scientists, 2006. Arctic Coring Expedition (ACEX), Proc. IODP 302, doi:10.2204/iodp.proc.302.2006.

Jakobsson, M., Backman, J., Rudels, B., Nycander, J., Frank, M., Mayer, L., Jokat, W., Sangiorgi, F., O´Regan, M., Brinkhuis, H., King, J., Moran, K., 2007. The early Miocene onset of a ventilated circulation regime in the Arctic Ocean. Nature 447, 986–990.

März, C., Schnetger, B., Brumsack, H.-J., 2010. Paleoenvironmental implications of Cenozoic sediments from the Central Arctic Ocean (IODP Expedition 302) using inorganic geochemistry. Paleoceanography 25, PA3206, doi:10.1029/2009PA001860.

Moore, T.C., Expedition 302 Scientists, 2006. Sedimentation and subsidence history of the Lomonosov Ridge. In: Backman, J., Moran, K., McInroy, D.B., Mayer, L.A., Expedition 302 Scientists. Proc. IODP 302, doi:10.2204/iodp.proc.302.105.2006.

Moran, K., Backman, J., Brinkhuis, H., Clemens, S.C., Cronin, T., Dickens, G.R., Eynaud, F., Gattacceca, J., Jakobsson, M., Jordan, R.W., Kaminski, M., King, J., Koc, N., Krylov, A., Martinez, N., Matthiessen, J., McInroy, D., Moore, T.C., Onodera, J., O´Regan, M., Pälike, H., Rea, B., Rio, D., Sakamoto, T., Smith, D.C., Stein, R., St. John, K., Suto, I., Suzuki, N., Takahashi, K., Watanabe, M., Yamamoto, M., Farrell, J., Frank, M., Kubik, P., Jokat, W., Kistoffersen, Y., 2006. The Cenozoic palaeoenvironment of the Artic Ocean. Nature 441, 601-605.

Sangiorgi, F., Brumsack, H.-J., Willard, D.A., Schouten, S., Stickley, C.E., O'Regan, M., Reichart, G.-J., Sinninghe Damsté, J.S., Brinkhuis, H., 2008. A 26 million year gap in the central Arctic record at the greenhouse-icehouse transition: Looking for clues. Paleoceanography 23, PA1S04, doi:10.1029/2007PA001477.

Stein, R., Boucsein, B., Meyer, H., 2006. Anoxia and high primary production in the Paleogene central Arctic Ocean: First detailed records from the CLR. Geophys. Res. Lett. 33, L18606, doi:10.1029/2006GL026776.

Stickley, C.E., Koc, N., Brumsack, H.-J., Jordan, R.W., Suto, I., 2008. A siliceous microfossil view of middle Eocene Arctic paleoenvironments: A window of biosilica production and preservation. Paleoceanography 23, PA1S14, doi:10.1029/2007PA001485.

ICDP

Methodology and paleoenvironmental significance of carbonate isotope records from the ICDP-site Laguna Potrok Aike

C. MAYR[1,2,3], M. OEHLERICH[1], A. LÜCKE [4], C. OHLENDORF[5], B. ZOLITSCHKA[5], F. SCHÄBITZ [6], M. WILLE[6], T. HABERZETT[7] AND THE PASADO SCIENCE TEAM

[1] Dept. of Earth and Environmental Sciences, Ludwig-Maximilians Universität München, Richard-Wagner-Str. 10, D-80333 Munich, Germany
[2] Geo-Bio-Center, Ludwig-Maximilians Universität München, Richard-Wagner-Str. 10, D-80333 Munich, Germany
[3] present address: Institute of Geography, Friedrich-Alexander-Universität Erlangen-Nürnberg, Kochstr. 4/4, D-91054 Erlangen, Germany
[4] Institute of Bio- and Geosciences, IBG-3: Agrosphere, Forschungszentrum Jülich, D-52425 Jülich, Germany
[5] GEOPOLAR, Institute of Geography, University of Bremen, Celsiusstr. FVG-M, D-28359 Bremen, Germany
[6] University of Cologne, Gronewaldstr. 2, D-50931 Cologne, Germany
[7] Institute of Geography, University of Jena, Löbdergraben 32, D-07743 Jena, Germany

The ICDP site Laguna Potrok Aike (51°57´S, 70°23´W) is a polymictic lake in the Patagonian steppe of Argentina. A 106 m long sediment composite profile from the profundal zone was recovered in 2008 that corresponds to an environmental archive covering the last ~51,000 years. The carbonate isotopes from this lake bear the potential to reconstruct past water temperatures and hydrological variability. However, the low carbonate content of these sediments is often combined with relatively high organic matter content. Moreover, the carbonate content of Laguna Potrok Aike sediments is high in the Holocene (up to 20 wt. %) but low or even absent during the last glacial period. The study of the isotopic composition ($\delta^{13}C_{carb}$ and $\delta^{18}O_{carb}$) of bulk carbonates is hampered by the release of CO_2 derived from organic matter. The frequently used NaOCl-treatment-method to remove organic matter prior to carbonate stable isotope analyses is not applicable for these sediment samples, because with decreasing carbonate content (represented by Total Inorganic Carbon, TIC) and increasing organic matter content (given as Total Organic Carbon, TOC) the very small amount of CO_2 liberated from organic matter by acid preparation of samples increasingly biases carbonate isotope values (Fig. 1). Preliminary results with artificial mixtures of carbonate standard and different organic substances show that isotope analyses to a minimum

TIC/TOC ratio of about 0.1 are reliable and no pre-treatment is needed (Fig. 2). However, for samples of Laguna Potrok Aike only isotope values from samples with TIC/TOC > 0.4 seem to provide reliable carbonate isotope values (Fig. 1). The $\delta^{18}O_{carb}$ values of the resulting sediment record from the composite profile 5022-2CP decrease from the early Mid-Holocene to the present (Fig. 3). The steadily decreasing $\delta^{18}O_{carb}$ values of the Mid-Holocene correlate with an increasing lake level inferred from previous sedimentological and seismic investigations (Anselmetti et al., 2009) suggesting changes in the water balance as the main control mechanism for Holocene $\delta^{18}O_{carb}$ values.

The new carbonate isotope record from the ICDP expedition 5022 “PASADO” match the carbonate isotope values from a previous piston core composite profile (PTA 03/12&13) from the centre of Laguna Potrok Aike (Fig. 3) and agree well with other proxies from the same record (Fig. 4). The early Mid-Holocene $\delta^{18}O$ maximum agrees

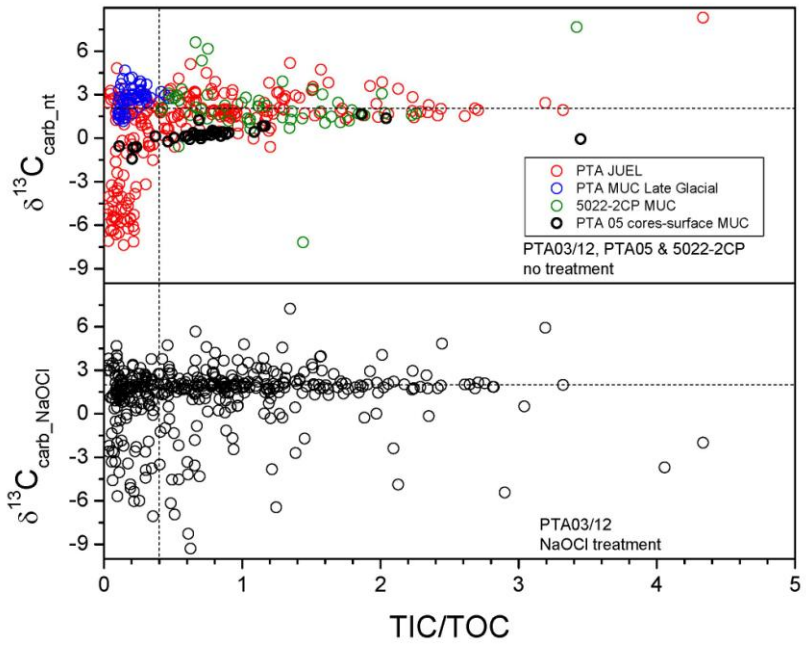

Fig. 1 Effects of NaOCl treatment on Laguna Potrok Aike sediments. $\delta^{13}C$carb values show frequent outliers towards more negative values (lower panel) than untreated samples from the same composite profile (upper panel, red dots). Moreover the effect of low TIC/TOC ratios on isotopic analysis is shown. TIC/TOC ratios below 0.4 (dotted vertical line) evoke more negative $\delta^{13}C$ values due to increasing dominance of CO_2 liberated from organic matter with falling TIC/TOC.

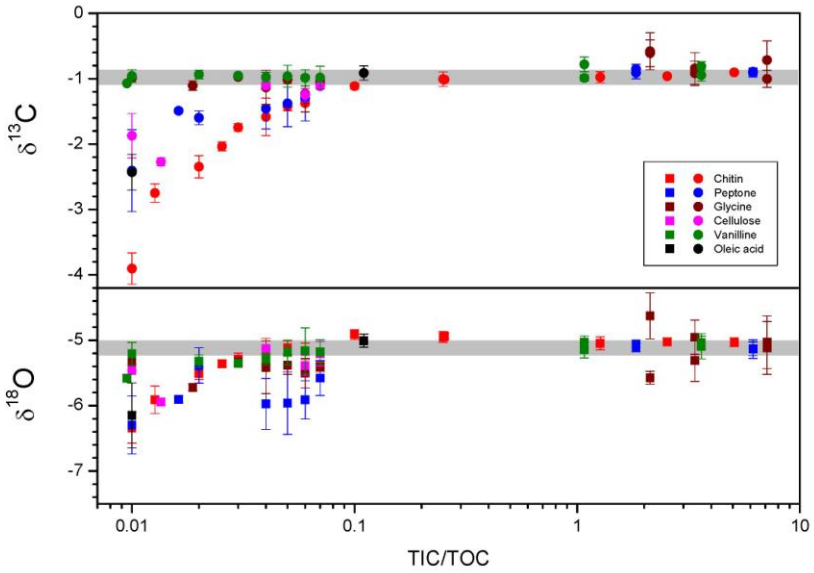

Fig. 2 Effect of varying TIC/TOC ratios on carbon and oxygen isotope values. Artificial mixtures of lab-standard carbonate with various organic compounds were isotopically analysed. Grey bars represent isotope composition of pure lab-standard.

with an increase of Andean forest pollen taxa in the pollen spectrum previously interpreted as the onset of enhanced westerly winds in that region (Mayr et al., 2007). An increased sedimentation of eroded soil organic matter was inferred from sedimentation rates and organic matter isotopic composition (Mayr et al., 2009) exactly in the period of highest carbonate isotope values. Thus, the period around 8000 cal yrs BP can be interpreted as an interval of maximum wind intensity leading to most negative water balance since the Early Holocene in the south-eastern Patagonian steppe.

References:

Anselmetti, F., Ariztegui, D., De Batist, M., Gebhardt, C., Haberzettl, T., Niessen, F., Ohlendorf, CV., Zolitschka, B. (2009). Environmental history of southern Patagonia unravelled by the seismic stratigraphy of Laguna potrok Aike. Sedimentology 56: 873-892.

Mayr, C., Wille, M., Haberzettl, T., Fey, M., Janssen, S., Lücke, A., Ohlendorf, C., Oliva, G., Schäbitz, F., Schleser, G.H. & Zolitschka, B. (2007). Holocene variability of the Southern Hemisphere westerlies in Argentinean Patagonia (52°S). Quaternary Science Reviews 26: 579-584.

Mayr, C., Lücke, A., Maidana, N.I., Wille, M., Haberzettl, T., Corbella, H., Ohlendorf, C., Schäbitz, F., Fey, M., Jansen, S., Zolitschka, B., 2009. Isotopic and geochemical fingerprints of lacustrine organic matter sources reflect environmental changes during the last 16,000 years in semi-arid Patagonia. Journal of Paleolimnology 42: 81-102.

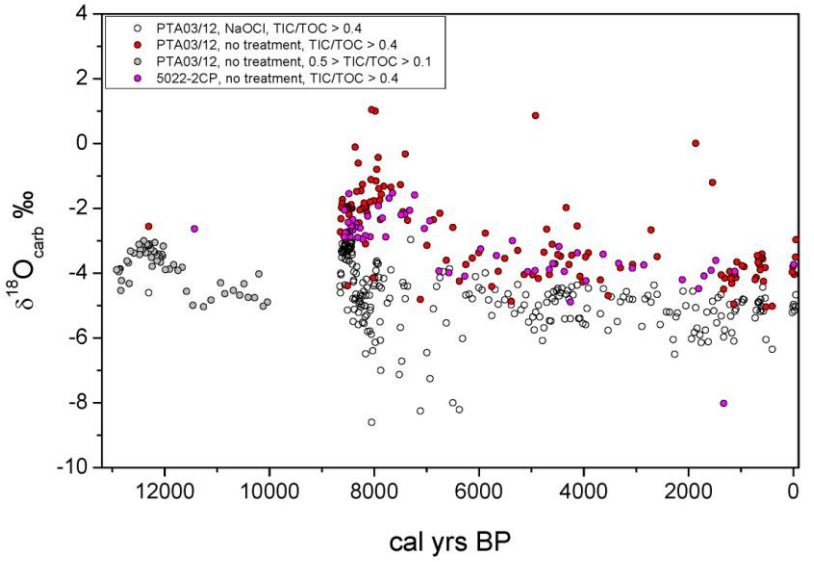

Fig. 3 Preliminary $\delta^{18}O$ records of ICDP-profile 5022-2CP and piston core PTA 03/12&13. The effects of NaOCl treatment are shown (black open dots) compared to untreated samples (magenta and red dots). All analyses are from samples with TIC/TOC >0.4, except of Late Glacial samples.

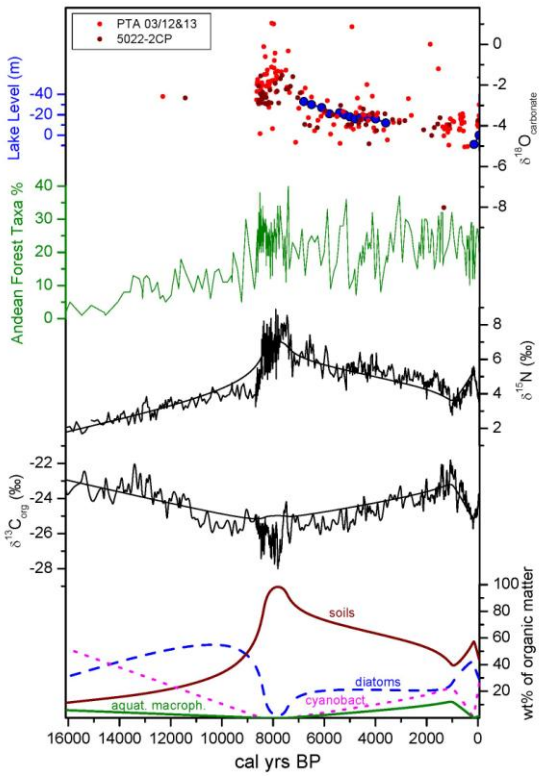

Fig. 4 Holocene $\delta^{18}O$ values of bulk carbonates compared to other proxies from Laguna Potrok Aike. In the course of the Middle Holocene the lake level increases (from Anselmetti et al., 2009, inverse scale relative to present-day). The Andean forest taxa index indicates increased westerly winds since 8700 cal yrs BP (Mayr et al., 2007), carbon and nitrogen isotope records of organic matter are caused by varying proportions of different organic matter types as modelled in the lowermost panel (modified from Mayr et al., 2009).

ICDP

Comparison of Petrophysical Properties of Impactites for four Meteroritic Impact Structures

MAYR S.[1], BURKHARDT H.[2], POPOV YU.[3], ROMUSHKEVICH R.[3], WILHELM H.[4]

[1] Geophysics, Freie Universität, Malteserstrasse 74-100, D-12249 Berlin, Germany
[2] Geophysics, Applied Geosciences, Technische Universität Berlin, Germany
[3] Moscow State Geological Prospecting University, Russia
[4] Geophysical Institute, University of Karlsruhe, Germany

Combined petrophysical and geothermal investigations have been carried out on four impact structures: the Puchezh-Katunki impact structure (Vorotilovo borehole, Russia), the Ries impact structure (Noerdlingen-73 borehole, Germany), the Chicxulub structure (ICDP Yaxcopoil-1 borehole, Mexico), and the Chesapeake impact structure (ICDP-USGS-Eyreville borehole, USA). Thermal properties were measured on densely sampled cores of the boreholes drilled into these impact structures using the optical scanning technique. For the cores of the Noerdlingen-73 and the two ICDP boreholes additionally porosity and partly p-wave velocity were measured on the same cores. The resulting data (Popov et al., 1998; Popov et al., 2003; Popov et al., 2004; Mayr et al., 2008; Mayr et al., 2010) is a unique data base and allows to establish joint peculiarities and differences in physical properties of various impactites.

For the Puchezh-Katunki and Ries impact structures the target lithology is more or less homogeneous and consists of crystalline rocks. The Vorotilovo borehole is drilled in the center of the Puchezh-Katunki impact structure and the rocks crossed by the well display shock-thermal metamorphism. Noerdlingen-73 was drilled about 3.5 km west of the center of the Ries impact structure. The target rocks of these two structures display moderate, low shock metamorphism; and weak shock effects (so called "Shocked Target Rocks"). Here a decrease of porosity and an increase of thermal conductivity with depth is observed and can be correlated to shock metamorphism. The Chicxulub and Chesapeake impact structures have a complex target lithology. The boreholes Yaxopoil-1 (located at the edge of the Chicxulub impact structure) and Eyreville (located in the center of the Chesapeake impact structure) cross displaced megablocks. Samples of these boreholes show practically no indication for high temperature shock metamorphism, therefore no correlation can be found, but the physical properties are influenced by lithology and geological history.

The Lithic Impact Breccia and Suevites are inhomogeneous on core scale. For these breccia the following distinction can be made: The various Suevites of the Puchezh-Katunki, Ries and Chicxulub impact structure have high porosity and close values of thermal conductivity. Possibly this is due to different deformation transformations (clastation, planar fractures, planar elements, deformation bands) caused by the impact load, which dominate over the differences in mineralogical and chemical compositions. The Polymict Melt Breccia (Lower Suevite) of the Chicxulub impact structure and Suevites and Lithic Breccia of the Chesapeake impact structure are characterized by lower porosity values, higher values of thermal conductivity and p-wave velocity compared to the above mentioned Suevites. These differences are possibly due to a higher content of rock clasts and diaplectic glasses next to differences in the texture. Additionally the Suevites and Lithic Breccia of the Chesapeake impact structure have a distinct different mineralogical composition (e.g. higher content of SiO_2).

Dense sampling for physical property measurements as well as mineralogical and chemical information is mandatory for this type of investigation. The investigations confirm, that the physical properties allow conclusions with respect to shock metamorphism (target rocks). They allow to distinguish between different types of breccia (Lithic Impact Breccia and Suevites incl. Polymict Impact Melt Breccia) due to differences in the texture and chemistry and the different amount of melt and rock clasts.

References:

Popov, Yu., Pimenov, V., Pevzner, L., Romushkevich, R., and Popov, E. (1998), Geothermal characteristics of the Voritilivo deep borehole drilled into the Puchezh-Katunki impact structure. Tectonophysics, 291, 205-223.

Popov, Yu., Pohl, J., Romushkevich, R., Tertychnyi, V., and Soffel, H. (2003), Geothermal characteristics of the Ries impact structure. Geophysical Journal International, 154, 355-378.

Popov, Y., Romushkevich, R., Bayuk, L., Korobkov, D., Mayr, S., Burkhardt, H. and Wilhelm, H. (2004), Physical properties of rocks from the upper part of the Yaxcopoil-1 drill hole, Chicxulub crater. Meteoritics & Planetary Science, 39 (6), 700-812.

Mayr, S.I., A. Wittmann, H. Burkhardt, Yu. Popov, R. Romushkevich, I. Bayuk, P. Heidinger, and H. Wilhelm (2008), Integrated Interpretation of Physical Properties of Rocks of the Borehole YAXCOPOIL-1

(Chicxulub impact structure), J. Geophys. Res., v. 113,21 p. B07201, doi:10.1029/2007JB005420.

Mayr S.I., Burkhardt H., Popov Yu., Romushkevich R., Miklashevskiy D., Gorobtsov D., Heidinger P., Wilhelm H. (2010), Physical Rock Properties (Borehole Eyreville) - Results and First Interpretations of Laboratory Measurements. GSA Special Paper "Chesapeake Bay Impact Structure Deep Drilling Project".

IODP

Late Aptian cooling and superimposed punctuated climate events recorded in sediments from the eastern subtropical Atlantic (Mazagan Plateau, DSDP Site 545).

A. MCANENA[1], P. HOFMANN[1], J. HERRLE[2], J. PROSS[2], J. RETHEYER[1], H. TALBOT[3], T. WAGNER[3]

[1] Institut für Geologie und Mineralogie, Universität zu Köln (amcanena@uni-koeln.de)
[2] Institut für Geowissenschaften, Goethe Universität, Frankfurt am Main
[3] School of Civil Engineering, Newcastle University, UK

The Late Aptian-Early Albian reflects a period of global transition towards the mid-Cretaceous greenhouse, with heightened tectonic, volcanic and hydrothermal activity and an increase in organic carbon burial in combination leading to a global adjustment of climate conditions. In order to document the response of the tropical North Atlantic to this global climatic readjustment we investigated the sea surface temperature development over 5 million years in the late Aptian expressed in marine sediments from DSDP Site 545, Mazagan Plateau (NW Africa).

Detailed new records of TEX_{86}-derived sea surface temperature (SST), organic carbon (TOC) and carbonate content, grain size composition, $\delta^{13}C_{carbonate}$ and $\delta^{13}C_{organic}$ confirm a >1.5 million year long cooling trend off NW Africa that culminated in the Late Aptian 'cold snap' before the onset of OAE 1b. Superimposed on this long term cooling trend three short term intervals are identified where surface waters either markedly cooled or warmed. Notably, these short-term SST perturbations are linked to small (<1.5‰) negative isotope excursions. The regular spacing and duration of these punctuated climate events, approximately every 400ka with a duration between 50-150ka based on current biostratigraphy, suggest a causal link to orbital forcing.

The long term surface water cooling towards the Late Aptian 'cold snap' is recorded by a ~4°C drop of sea surface temperature from ~32°C to 28°C. Corresponding element records of Zr/Al and Si/Al very moderately decline parallel to SST indicating an overall decrease in grain size of the siliciclastic sediment fraction suggesting a gradual but minor weakening of the atmospheric circulation over West Africa over the study period. At the onset of maximum SST cooling, within the 'cold snap', a distinct and abrupt decline in the abundance of *Nannoconus* spp. is observed that may indicate an intensification of water circulation prior to OAE1b.

Superimposed upon the long term trend in climate and biotic response we observe three to our knowledge previously undescribed punctuated climate perturbations. A rapid increase in SST by +4°C coinciding with a sharp negative $\delta^{13}C$ excursion (~ 1.25‰) and a rapid drop in continental climate proxies (Zr/Al, Si/Al, Na/Al and K/Al ratios) argue for a period of significant African humidity consistent with geochemical signatures which are well known for other hyperthermal events in the Paleogene-Mesozoic. This hyperthermal event in the Late Aptian has not yet been described but may well be a precursor event to OAE1b (Wagner et al., 2007, 2008).

Interestingly the new SST profile also shows two surface water cooling events below the new hyperthermal event, with drops in SST of 2-2.5°C; The rather constant element composition of the siliciclastic (terrigenous) fraction in these sediments support the conclusion that they are not a result of the intensification of to local upwelling conditions. Instead they may rather reflect short periods of enhanced mixing of colder waters along the NW African margin.

The source of cooler intermediate and/or deep waters is currently unknown however its periodic shoaling off West Africa may manifest the response to a large-scale reorganization of deep ocean circulation in the mid Cretaceous North Atlantic. Recent studies (Poulsen et al. 2003: Trabucho Alexandre et al., 2011) propose that variable inflow of cooler and nutrient enriched intermediate and deep waters from the Cretaceous Pacific Gateway into the proto North Atlantic would have caused the establishment of an estuarine circulation in the Atlantic basin, that would have focused colder subsurface waters along the NW African margin.

The causal relationships of the observed hyperthermal event, as a possible precursor to OAE1b, and the drastic biotic response of calcareous nannoplankton to these short and long term fluctuations in climate and large-scale oceanography are not yet fully understood however the new records from Mazagan Plateau show interesting new aspects that warrant further molecular and geochemical research.

References:

Poulsen, C.J., Gendaszek, A.S., Jacob, R.L., 2003. Did the rifting of the Atlantic Ocean cause the Cretaceous thermal maximum? Geology, 31, 115-118.

Trabucho Alexandre,j., Tuenter, E., Henstra,g.A., van der Zwan, K.J., van de Wal, R.S.W., Dijkstra, H.A., de Boer, P.A. 2010. The mid-Cretaceous North Atlantic nutrient trap: Black shales and OAEs. Paleoceanography 25, PA4201, doi:10.1029/2010PA001925, 2010

Wagner, T. Wallmann, K, Herrle J.O., Hofmann P. Stüsser I., 2007. Consequences of moderate ~ 25,000 yr lasting emission of light CO2 into the mid-Cretaceous ocean. EPSL 259, 200-211.

Wagner, T., Herrle, J.O., Stüsser, I., Hofmann, P., Schouten, S., Sinninghe Damsté, J.S., 2008. Instant heating of Cretaceous surface waters off subtropical Africa in response to light carbon emission to the atmosphere. Geology 36, 203-206.

ICDP

Resolving sedimentary sulphur cycling during the Shunga Event (early Palaeoproterozoic) with sulphur isotopes

D. MEISTER[1], H. STRAUSS[1], V.A. MELEZHIK[2,3], A. LEPLAND[2], and the FAR DEEP scientists

[1] Westfälische Wilhelms-Universität Münster, Institut für Geologie und Paläontologie, Münster, Germany
[2] Geological Survey of Norway (NGU), Trondheim, Norway
[3] University of Bergen, Centre of Geobiology, Bergen, Norway

Several major environmental changes occurred during the early Palaeoproterozoic with profound consequences for the global carbon and sulphur cycles (Melezhik et al. 2005). These include the accumulation of an unprecedented amount of organic matter during the Shunga-Event at c. 2.05 Ga ago (Hannah 2008), postdating the Lomagundi-Jatuli Event (e.g. Melezhik et al. 1999a) during which isotopically heavy carbonates accumulated. Moreover, the irreversible oxygenation of Earth's atmosphere c. 2.4 Ga ago (termed the Great Oxidation Event, cf. Holland, 1999) enhanced the terrestrial oxidative weathering, among other consequences resulting in the delivery of sulphate to the ocean. This input of sulphate into the ocean likely triggered a more dominant role of sulphate reducing bacteria in the microbial turnover of sedimentary organic matter. This sequence of intimately related events is reflected in secular variations of the carbon and sulphur isotopes. The isotopic composition of different forms of sulphur embedded in the organic-rich sediments deposited during the Shunga Event will be utilized in order to resolve the sedimentary sulphur cycling during this important period in Earth history.

The Fennoscandia Arctic Russia - Drilling Early Earth Project (FAR DEEP) recovered some ~744 m of drillcore from three drillholes within the c. 2.05 Ga old Zaonega Formation (ZF). This unit comprises sedimentary as well as volcanic rocks. It was suggested that rhythmically bedded sedimentary rocks of the ZF were deposited in a low-energy, non-euxinic brackish-water environment and are typically of grey to black colour. They contain substantial amounts of organic matter which is most likely of algal or bacterial origin (Melezhik et al. 1999b). Iron sulphides are very abundant in these rocks with pyrite being the most common iron sulphide occuring in variable morphologies. These include larger euhedral cubic as well as irregular shaped, zoned or finely disseminated forms of pyrite. Postdepositional processes resulted in the generation and migration of bitumen within the ZF and through the overlying stratigraphy (Melezhik et al. 2009) with a complex pattern of iron sulphide formation trailing organic matter degradation. These processes are archived in the sulphur isotopic composition of sedimentary pyrite that shows highly variable $\delta^{34}S$ values between -22 and +31‰ (reviewed in Melezhik et al. 1999b).

Based on the newly acquired drillcore material and building upon previous work, the present study under the auspices of ICDP's FAR DEEP initiative aims at reconstructing sedimentary sulphur cycling in an environment characterized by a high supply of organic matter and the presence of dissolved sulphate. Different forms of sulphur will be analytically separated including acid volatile sulphur (AVS), chromium reducible sulphur (CRS), and kerogen-bound sulphur. For these different sulphur fractions traditional sulphur isotopes ($\delta^{34}S$) will be measured in order to reconstruct prevailing metabolic pathways as well as to assess primary versus secondary processes. For selected samples, this will be supplemented by multiple sulphur isotope analyses. Geochemical work will be paralleled by detailed petrographic studies (reflected and transmitted light microscopy) in order to reconstruct the sedimentological and diagenetic evolution of the shungite rocks. Resolution will range from bulk rock to single mineral grains. First $\delta^{34}S$ results for AVS and CRS ranging from -8.1 to +25.6‰ agree with previous data (Melezhik et al. 1999b), but more detailed interpretations have to await further work.

Acknowledgements: This project forms part of the Fennoscandian Arctic Russia – Drilling Early Earth Project (FAR-DEEP). Financial support through the Deutsche Forschungsgemeinschaft (SPP 1006) is gratefully acknowledged.

References:

Hannah, J.L. (2008). Re-Os geochronology of a 2.05 Ga fossil oil field near Shunga, Karelia, NW Russia. Abstract, 33rd International Geological Congress, Oslo, 2008, 6-14 August

Holland, H.D. (1999). When did the Earth's atmosphere become oxic? The Geochemical News 100: 20-22.

Melezhik, V.A., Fallick, A.E, Filippov, M. M. Larsen, O. (1999b). Karelian shungite - an indication of 2.0-Ga-old metamorphosed oil-shale and generation of petroleum: geology, lithology and geochemistry. Earth-Science Reviews 47: 1-40.

Melezhik, V.A., Fallick, A.E., Medvedev, P.V., Makarikhin, V.V. (1999a). Extreme $^{13}C_{carb}$ enrichment in ca. 2.0 Ga magnesite-stromatolite-dolomite-`red beds´ association in a global context: A case for the world-wide signal enhanced by a local environment: Earth-Science Reviews 48: 71–120.

Melezhik, V.A., Fallick, A.E., Hanski, E., Kump, L., Lepland, A., Prave, A.R. and Strauss, H. (2005). Emergence of the aerobic biosphere during the Archean-Proterozoic transition: challenges of future research. GSA Today 15, No. 11: 4-11.

Melezhik, V.A., Fallick, A.E., Filippov, M.M., Lepland, A., Rychanchik, D.V., Deines, Y.E., Medvedev, P.V., Romashkin, A.E., Strauss, H. (2009). Petroleum surface oil seeps from a Palaeoproterozoic petrified giant oilfield. Terra Nova 21: 119–126.

IODP

A dynamic sulphate/methane transition zone at Peru Margin Site 1229 (ODP Leg 201) reproduced by reactive transport modelling

P.H. MEISTER[1], B. LIU[1], S. CONTRERAS QUINTANA[1,2], A. KHALILI[1], T.G. FERDELMAN[1], M. KUYPERS[1], B. BARKER JØRGENSEN[1,3]

[1] Max Planck Institute for Marine Microbiology, Celsiusstrasse 1, 28359 Bremen, Germany; email: pmeister@mpi-bremen.de
[2] Large Lakes Observatory (LLO), University of Minnesota, Research Laboratory Building 205, 2205 E. 5th St., Duluth, MN 55812, USA
[3] Center for Geomicrobiology, Århus University, Ny Munkegade 116, 8000 Århus, Denmark

Microbial degradation of organic matter deposited on the seafloor and buried over geological time within marine sediments leads to the onset of a redox zonation. The thickness of these redox zones is essentially controlled by geochemical gradients, which are a result of metabolic turnover and burial rates. Redox zonations may leave characteristic imprints in the geological record, and therefore document the diagenetic history of a particular biogeochemical setting. Diagenetic imprints, such as barite enrichments, dolomite layers and abundance of specific microbial biomarkers (Contreras et al., in prep.) can

	Time interval dt (ka)	Sedimentation rate v (m/ka)	Init. TOC TOC_0 (wt%)	Initial age *a* (ka)
Interglacial	95	0,0421	1	10000
Glacial	5	0,2000	8,2	0,1

A. Input variables for one glacial/interglacial cycle.

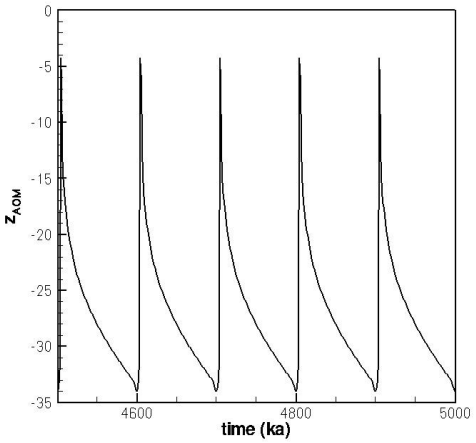

B. Simulated depth of the sulphate methane transition zone (z_{AOM} or z_{SMT}) as a function of time. Input values from table 1 were periodically repeated until a dynamic steady state was reached, which was the case after about 4 ka.

document how subsurface redox zonation evolved in response to past oceanographic conditions thereby serving as potential proxy for fluxes of diverse geochemical compounds and their contribution to biogeochemical cycling.

While steady state geochemical conditions are generally assumed to drive subsurface fluxes, episodic upward migration of the sulphate/methane interface were suggested (Riedinger et al., 2005; Kasten and Jørgensen, 2006). Meister et al. (2007, 2008) interpreted the episodic formation of dolomite layers at the sulphate methane interface and variable carbon isotope values in these layers as a result of upward and also downward migration of the sulphate methane interface in a non-steady diffusive porewater system at ODP Site 1229 drilled on the Peruvian Shelf.

We present the results of a reactive transport model based on the model described in Arndt et al. (2009), in which an upward and downward migrating sulphate/methane transition zone was simulated for a diffusive porewater system at Site 1229 over a depth range of 30 m (below seafloor) and within a time period of glacial interglacial cycles. Input variables were sedimentation rate (v), initial total organic carbon content (TOC_0) and reactivity of organic matter (*a*; Fig. A), whereby the organic decay follows a Middelburg (1989) type function: $TOC = TOC_0.\exp[3.2(a^{0.05} - (a + t)^{0.05})]$.

Different input values were tested, but to achieve an upward and downward migration within the time period of glacial interglacial cycles (Fig. B), it must be assumed that sedimentation rate varies between glacial and interglacial times and organic matter is composed of two or more differently reactive pools. It is important to note that under strongly variable conditions, steady state in porewater chemistry is never reached. By applying a continuous periodic input, however, a constant minimal and maximal depth of the SMTZ is reached.

The modelling results demonstrate that sub-surface redox zonation is more dynamic than we would expect from just looking at porewater profiles, and non-steady state conditions must be taken into account for a global assessment of diffusive fluxes to and from marine sediments to the water column. The model provides a theoretical basis in order to understand how variable oceanographic conditions controlling organic matter input and sedimentation rates (e.g. at glacial interglacial timescales) indirectly affect subsurface redox zonation and therefore global biogeochemical cycling.

References:

Arndt, S., Hetzel, A. and Brumsack H.-J. (2009) Geochim. Cosmochim. Acta 73, 2000-2022.
Contreras, S., Meister, P.H., Liu, P., Hinrichs, K.-U., Khalili, A., Ferdelman, T.G., Kuypers, M. and Jørgensen, B.B. (in prep.).
Kasten and Jørgensen (2006) In: H.D. Schulz and M. Zabel: Marine geochemistry. Springer press. Berlin, Heidelberg.
Meister, P., Bernasconi, S., McKenzie, J.A., Vasconcelos, C., Frank, M., Gutjahr, M. and Schrag, D. (2007) Sedimentology 54, 1007-1032.
Meister, P., Bernasconi, S., McKenzie, J.A. and Vasconcelos, C. (2008) Marine Geology 252, 166-173.
Middelburg, J.J. (1989) Geochim. Cosmochim. Acta 53, 1577-1581.
Riedinger, N., Pfeifer, K., Kasten, S., Garming, J.F.L., Vogt, C. and Hensen, C. (2005) Geochim. Cosmochim. Acta 69, 4117-4126.

ICDP

The El´gygytgyn Drilling Project in NE Siberia – present results and ongoing work supported by DFG funding

M. MELLES[1], G. SCHWAMBORN[2], H. MEYER[2], H.-W. HUBBERTEN[2], D. WAGNER[2], K. MANGELSDORF[3], J. WILLENBRING[3], U. REIMOLD[4], R. SCHMITT[4], O. JUSCHUS[5], AND EL´GYGYTGYN SCIENTIFIC PARTY

[1] University of Cologne, Institute of Geology and Mineralogy, Zülpicher Str. 49a, D-50674 Cologne
[2] Alfred Wegener Institute for Polar and Marine Research, Research Unit Potsdam, Telegraphenberg A43, D-14473 Potsdam
[3] GeoForschungsZentrum Potsdam, Telegraphenberg, D-14473 Potsdam
[4] Museum für Naturkunde, Humboldt University of Berlin, Invalidenstr. 43, D-10115 Berlin
[5] Technical University Berlin, Institute of Applied Geosciences, Ackerstr. 76, D-13355 Berlin

Lake El'gygytgyn is located 100 km to the north of the Arctic Circle (67°30' N, 172°05' E) in a crater of 18 km diameter that was formed 3.6 Ma ago by a meteorite impact event (Gurov et al. 1978, Layer 2000). Following a comprehensive pre-site survey (Melles 2005, Brigham-Grette et al. 2007, and references therein), an international drilling campaign was conducted at Lake Elgygytgyn from Oct. 2008 until May 2009, achieving its three major objectives (Melles et al. in press).

First, drilling from the ice cover in the lake center penetrated the entire, 315 m thick lake sediment succession in 170 m water depth. The sediments show no indications for hiatuses due to glaciation or desiccation. Hence, their temporal length and geologic significance is absolutely unprecedented, for the first time providing deep and widely continuous insights into the climatic and environmental

evolution of the terrestrial Arctic since Pliocene times. This is particularly true for the lowermost 40 m and uppermost 150 m of the sequence, which were drilled with almost 100 % recovery and, using the chronological information we have available, likely reflect the initial lake stage during the Pliocene and the last ca. 2.9 Ma, respectively. In between, the quality of the record is restricted due to lower recovery as a consequence of technical problems and/or sequences of coarse sand and gravel interbedded with lacustrine mud.

Second, a ca. 200 m thick, almost complete section of impact breccias was recovered underneath the lake sediments, consisting of a ca. 100 m thick suevite layer above broken and fractured volcanic basement rocks. Investigation of this core sequence promises new information concerning the El´gygytgyn impact event, including the composition and nature of the meteorite, the energy released, and the shock behavior of the volcanic basement rocks.

Third, a 142 m long sequence was recovered from the permafrost deposits in the western lake catchment, only a few hundred meters from the lake shore. The core consists of gravelly and sandy alluvial fan deposits, which are continuously frozen and rich with ground ice. The sediment and ice composition promises to provide complementary information on the regional climatic history and lake-level fluctuations. Besides, a thermistor chain installed in the drill hole as part of the "Thermal State of Permafrost Network" of the International Permafrost Association will contribute to the understanding of the permafrost behavior in light of contemporary rapid climate change.

The drilling operation was mainly funded by the International Continental Scientific Drilling Program (ICDP), the US National Science Foundation (NSF), and the German Federal Ministry of Education and Research (BMBF). The BMBF is also supporting the time-consuming processing and subsampling of the lake sediment and permafrost cores at the University of Cologne and the Alfred Wegener Institute in Bremerhaven, respectively, along with some basic analyses on discrete core samples. This work commenced in autumn 2009 and will be completed by summer 2011, shortly before the BMBF funding will terminate in autumn 2011.

The DFG priority program "ICDP" since 2007 is providing complementary funding for both the pre-site survey and the drill-core investigation. The site survey at Lake El´gygytgyn was supported by initial analyses on permafrost deposits in the lake catchment and oxygen isotope measurements on diatoms in a 16 m long lake sediment core. Besides, dating of the permafrost drill core with cosmogenic nuclides as well as microbiological, mass movement, and pollen analyses on the drilled lake sediments are funded by the DFG. Funding also is provided for specific analyses on the impact rocks, whose subsampling and distribution was defined and agreed on a sampling party held at the Humboldt University of Berlin in May 2010.

The presentation will summarize the objectives and operational success of the drilling campaign, and highlight the scientific results obtained so far based on the limited onsite and ongoing offsite core processing. Special attention will be put on the results obtained within the scopes of the DFG projects funded.

References:

Brigham-Grette J., Melles M., Minyuk P. & Scientific Party (2007): Overview and significance of a 250 ka paleoclimate record from El´gygytgyn Crater Lake, NE Russia. - *Journal of Paleolimnology*, 37: 1-16.

Gurov, E.P., Valter, A.A., Gurova, E.P., and Serebrennikov, A.I., 1978. Meteorite impact crater El'gygytgyn in Chukotka. *Doklady Akademii Nauk USSR*, 240: 1407-1410 [in Russian].

Layer, P., 2000. Argon-40/argon-39 age of the El´gygytgyn impact event, Chukotka, Russia. *Meteoritics and Planetary Science*, 35: 591-599.

Melles, M., Minyuk, P., Brigham-Grette, J., and Juschus, O., (Eds.) 2005. The Expedition El´gygytgyn Lake 2003 (Siberian Arctic). *Repts. Polar and Marine Res*., 509: 139 pp .

Melles M., Brigham-Grette J., Minyuk P., Koeberl C., Andreev A., Cook, T., Fedorov G., Gebhardt C., Haltia-Hovi E., Kukkonen M., Nowaczyk N., Schwamborn G., Wennrich V. & El´gygytgyn Scientific Party (in press): The El´gygytgyn Scientific Drilling Project - conquering Arctic challenges through continental drilling. - *Scientific Drilling*, 11, March 2011.

ICDP

Peering into the Cradle of Life: multiple sulfur isotopes reveal insights into environmental conditions and early sulfur metabolism some 3.5 Ga ago

A. MONTINARO, H. STRAUSS

Institut für Geologie und Paläntologie, Westfälische Wilhelms-Universität Münster, Münster, Germany

During the early stages of Earth's evolution, environmental conditions were much different from today. One of the most intriguing questions in Earth and Life Sciences is where, when and under which conditions life emerged on our planet. The record of early life on Earth comprises three principal lines of evidence: microfossils, stromatolites, and chemofossils, i.e. chemical and isotopic signatures that relate to metabolic processes including biomass production via autotrophic processes and/or the aerobic/anaerobic mineralisation of sedimentary organic matter. These processes leave behind reaction products that can be archived as organic or mineral matter in the rock record. Their chemical and isotopic characteristics are, by inference from the modern world, biosignatures for a set of biological driven reactions. Among the chemofossils, the stable isotopes of carbon, sulfur, and nitrogen – all elements that represent the building blocks of life – have an established record as tracers for life on Earth (e.g., Thomazo et al., 2009).

The record of well preserved rock successions from the earliest part of Earth history is rather limited. The Barberton Greenstone Belt in South Africa represents one of the oldest well preserved rock successions (3.5 – 3.2 Ga). The succession is known for komatiites and for sedimentary rocks, of which the latter have yielded some of the earliest records of early life. The sedimentary rocks were deposited in shallow and deep marine environments, probably on normal Archean oceanic crust and possibly associated with hydrothermal activity (Tice and Lowe, 2004, 2006; Westall et al 2001). Samples for this study will be obtained under the auspices of the International Continental Drilling Programme (ICDP) "Peering into the Cradle of Life" (http://www.icdp-online.org), and drilling will commence in April 2011.

The ability to utilize the stable isotopic composition of sulfur as a biosignature results from the fact that microbial sulfur metabolism is associated with a distinct and

frequently substantial isotopic fractionation. Recent multiple sulfur isotopes studies of time-equivalent sedimentary rocks from Western Australia provided rather controversial results in respect ot early sulfur metabolism (Philippot et al., 2007; Ueno et al., 2008; Shen et al., 2009). Both the microbial reduction of sulfate as well as the disproportionation of sulfur have been suggested. In addition, a multiple isotope approach on barite from the Barberton Greenstone belt revealed inconclusive data with regard to the ultimate source of that sulfate (Bao et al., 2007).

From previous work, two key questions result as scientific objectives that will be central to this research:

- Can an unequivocal signal of microbial sulfur cycling be deduced from the sulfur isotope data of sedimentary sulfide?
- Does the barite reflect the sulfur isotopic compositions of Archean seawater?

Considering existing and in part controversial results from traditional and multiple sulfur isotopes, a systematic and comprehensive sulfur isotope study of the key sedimentary units in the Barberton Greenstone Belt appear highly warranted and promising at the same time. A detailed characterization of the environmental and in particular the redox conditions will provide the necessary information about the geochemical framework in which life could emerge and develop.

References:

Bao, H., Rumble III, D., Lowe, D.R., 2007. The five stable isotope compositions of Fig Tree barites: implications on sulphur cycle in ca. 3.2 Ga oceans. Geochim. Cosmochim. Acta 71: 4868-4879.

Lowe, D.R., Byerly G.R., 1999. Geologic evolution of the Barberton Greenstone Belt, South Africa. Geological Society of America Special Paper 329, 312p.

Pavlov, A.A., and Kasting, J.F., 2002. Mass-independent fractionation of sulphur isotopes in Archaean sediments: strong evidence for an anoxic Archaean atmosphere. Astrobiology 2: 27-41.

Philippot, P., Van Zuilen, M., Lepot, K., Thomazo, C., Farquhar, J., van Kranendonk, M., 2007. Early Archean microorganisms preferred elemental sulfur, not sulfate. Science 317: 1534-1537.

Shen, Y., Farquhar, J., Masterson, A.M., Kaufman, A.J., Buick, R. (2009) Evaluating the role of microbial sulfate reduction in the early Archean using quadruple isotope systematics. Earth Planet Sci Lett 279:383–39.

Thomazo, C., Pinti, D.L., Busigny, V., Ader, M., Hashizume, K., Philippot, P., 2009. Biological activity and the Earth's surface evolution: insights from carbon, sulphur, nitrogen and iron stable isotopes in the rock record. Comptes Rendus Palevol 8: 655-678.

Tice, M.M., Lowe, D.R., 2004. Photosynthetic microbial mats in the 3.416-Myr-old ocean. Nature 431: 549-552.

Tice, M.M., Lowe, D.R., 2006. The origin of carbonaceous matter in pre-3.0 Ga greenstone terrains: A review and new evidence from the 3.42 Ga Buck Reef Chert. Earth-Science Reviews 76: 259-300.

Ueno, Y., Ono, S., Rumble III, D., Maruyama, S., 2008. Quadruple sulphur isotope analysis of ca. 3.5 Ga Dresser Formation: new evidence for microbial sulfate reduction in the early Archean. Geochim. Cosmochim. Acta 72: 5675-5691.

Westall, F., de Wit, M.J., Dann, J.C., van der Gaast, S., de Ronde, C.E.J., Gerneke, D., 2001. Early Archean fossil bacteria and biofilms in hydrothermally influenced sediments from the Barberton greenstone belt, South Africa. Precambrian Research 106: 93-116.

ICDP

The role of magma mixing between rhyolitic and basaltic magmas in the Bruneau-Jarbidge eruptive center, Snake River Plain (USA): an experimental study

D. MORGAVI[1], D. PERUGINI[2], C. DE CAMPOS[1], Y. LAVALLÉE[1], LISA MORGAN[3], D. B. DINGWELL[3]

[1] Dept. Earth and Environmental Sciences, Ludwig-Maximilians München (LMU), Theresienstrasse 41/III, 80333 München, Germany. (morgavidaniele@hotmail.com)

[2] Dept. Earth Sciences, University of Perugia, Piazza Universitá, 06100 Perugia, Italy.

[3] U.S. Geological Survey, 973 Federal Center, Box 25046, Denver, CO 80225-0046, USA

Volcanic and magmatic activities in the Snake River Plain (SRP) have been characterised by a rhyolitic-basaltic bimodal geochemical character. The Bruneau-Jarbidge eruptive center (BJEC; southwestern SRP) is a 95 km by 55 km structural basin formed, ca.12 to 8 Ma, by multiple eruptions of rhyolitic pyroclastic and lava flows. The rhyolitic units are intercalated with a series of basaltic lava flows (e.g. Bonnichsen et al., 2008). The BJEC is an example in which basalt underplating induced partial melting of the crust and where mantle and crustal derived melts experienced mutual interaction (Leeman et al., 2008).

The aim of this work is to study experimentally the physical and chemical interaction of basaltic and rhyolitic magmas and to evaluate whether this process can explain the variation in major and trace elements in the BJEC rhyolitc units.

Following on geochemical studies by Cathey and Nash (2009), Leeman (2008) and Bonnichsen (1982), the Mary's Creek basalt and the Cougar Point Tuff rhyolite unit V were chosen as end-members for mixing experiments. Petrographic analyses indicate that the basalt contains phenocrysts of plagioclase, clinopyroxene, and olivine in a glassy groundmass with micro-crystals of plagioclase. The rhyolite contains phenocrysts of plagioclase, quartz, sanidine, elongated vesicles, in a glassy groundmass.

Chaotic mixing experiments were performed using completely molten end-members in a newly developed experimental apparatus (De Campos et al., 2010) working at constant temperature (1450°C) and under controlled flow fields. The determination of the temperature dependence of the viscosity of each sample has been performed using concentric cylinder and micropenetration methods in order to gain insights into the rheological properties of the end-member magmas. Samples resulting from the mixing experiments have been analyzed for their major and trace elements contents, and compared to natural data.

Experimental results indicate that efficient physical and chemical mixing between the end-members can occur (despite the high viscosity ratio, of the order of 10^3). In our experiments, this produced a strong modulation of compositional variability leading to the complete extinction of the basaltic composition and to significant compositional variations in the rhyolitic magma. The geochemical variability in inter-elemental plots display a clear similarity to the compositional variability of natural samples indicating that magma mixing may have played a role to the compositional variability in the SRP magmatism.

References:
Bonnichsen B. Idaho Bureau of mines and Geology Bull. 26. P.237-254
Bonnichsen B. et al. Bull. Volcanology 70, 315-342
De Campos C. et al., 2010, Contrib. Mineral. Petrol., in press.
Cathey H.E. Nash, B.P. 2009. J.Volcanol. Geotherm. Res. 188, 173-185
Leeman W.P. et al, 2008. In: Dynamics of crustal magma transfer, storage and differentiation.

IODP

Eirik Drift: Archive of palaeoenvironmental information of climate development and oceanic circulation in the Greenland and Labrador Seas

A. MÜLLER-MICHAELIS[1], G. UENZELMANN-NEBEN[1]

[1] Alfred-Wegener-Institut für Polar- und Meeresforschung, Am Alten Hafen 26, 27568 Bremerhaven

The Eirik Drift off the southern tip of Greenland contains sedimentary records since the Miocene. This archive of depositional processes has been shaped by the Western Boundary Undercurrent (WBUC), the Greenland ice sheet, and the material input from the Labrador Sea through the Davis Strait. The incorporation of high resolution seismic reflection data acquired during RV *Maria S. Merian* cruise MSM 12/2 in June/July 2009 with geologic information from ODP and IODP sites will lead to information on the development of the WBUC as well as the dimensions and expansion/retreat of the Greenland ice sheet and a much clearer understanding of the evolution of the climate southwest of Greenland.

A first step in this reconstruction comprised the computation of synthetic seismograms based on density and P-wave velocity data from ODP Leg 105 Site 646 and IODP Expedition 303 Sites 1305, 1306, and 1307. Those are correlated with the processed seismic reflection profiles to allow a spatial extrapolation of the geological information. This way we can identify four seismic units and the reflectors R1 (onset of ice rafting), R2 (higher carbonate content, increased deep circulation), and R3/R4 (brief hiatus and/or increased sedimentation rate) as defined by *Arthur et al. (1989).* The next steps will include tracking and mapping of both reflectors and units.

IODP

Strengthening of North American dust sources during the late Pliocene (2.7 Ma)

B.D. A. NAAFS[1,2], J. HEFTER[1], R. PANCOST[2], R. STEIN[1], G.H. HAUG[3,4]

[1] Alfred Wegener Institute for Polar and Marine Research, Department of Marine Geology and Paleontology, D-27568 Bremerhaven, Germany
[2] Leibniz Center for Earth Surface and Climate Studies, Institute for Geosciences, Potsdam University, D-14476 Potsdam, Germany
[3] Organic Geochemistry Unit, Bristol Biogeochemistry Research Centre, School of Chemistry, University of Bristol, Cantock's Close, BS8 1TS Bristol, United Kingdom
[4] Geological Institute, ETH Zürich, 8092 Zürich, Switzerland

Dust plays an important role in global climate as it influences the radiative forcing of the atmosphere[1], can be a source of nutrients to the open ocean[2,3], and affects the albedo of ice sheets[4]. More over, the increased dust emission during the most recent glacials has been argued to cause part of the 100 to 80 ppm change in CO_2 between glacials and interglacials[5]. However, most record of dust fluxes focus on the Southern Hemisphere. Here we present orbitally resolved records of the accumulation of lipids derived from terrestrial higher plants waxes at IODP Site U1313 in the North Atlantic over the last 3.4 million years. These lipids are a major component of dust, even in remote ocean areas[6], and thus have a predominantly aeolian origin in marine sediments[7-9]. We therefore use variations in their accumulation to for the first-time infer changes in aeolian input to the mid-latitude North Atlantic Ocean. The results show that the intensification of the Northern Hemisphere glaciation around 2.7 million years ago (Ma) was accompanied by a drastic increase in aeolian input to the North Atlantic. During every glacial of the Quaternary the input of aeolian material into the North Atlantic was up to 30 times higher compared to interglacials. We suggest that the increased aeolian input during glacials is predominantly related to a strengthening of the North American sources in the late Pliocene. The close correspondence between aeolian input to the North Atlantic and dust fluxes in Antarctica over the last 800 thousand years (ka)[10] indicates a globally uniform response of dust sources to Quaternary climate variability.

References:
[1] Mahowald, N. M. et al., Climate response and radiative forcing from mineral aerosols during the last glacial maximum, pre-industrial, current and doubled-carbon dioxide climates. *Geophysical Research Letters* **33** (20), L20705 (2006).
[2] Fung, I. Y. et al., Iron supply and demand in the upper ocean. *Global Biogeochemical Cycles* **14** (1), 281 (2000).
[3] Ridgwell, A. J., Dust in the Earth system: the biogeochemical linking of land, air and sea. *Philosophical Transactions of the Royal Society of London. Series A: Mathematical, Physical and Engineering Sciences* **360** (1801), 2905 (2002).
[4] Ganopolski, A., Calov, R., and Claussen, M., Simulation of the last glacial cycle with a coupled climate ice-sheet model of intermediate complexity. *Clim. Past* **6** (2), 229 (2010).
[5] Watson, A. J. et al., Effect of iron supply on Southern Ocean CO2 uptake and implications for glacial atmospheric CO2. *Nature* **407** (6805), 730 (2000).
[6] Conte, M. H. and Weber, J. C., Long-range atmospheric transport of terrestrial biomarkers to the western North Atlantic. *Global Biogeochem. Cycles* **16** (2002).
[7] López-Martínez, C. et al., Abrupt wind regime changes in the North Atlantic Ocean during the past 30,000 - 60,000 years. *Paleoceanography* **21**, PA4215 (2006).
[8] Madureira, L. A. S. et al., Late Quaternary High-Resolution Biomarker and Other Sedimentary Climate Proxies in a Northeast Atlantic Core. *Paleoceanography* **12**, 255 (1997).
[9] Martìnez-Garcia, A. et al., Links between iron supply, marine productivity, sea surface temperature, and CO2 over the last 1.1 Ma. *Paleoceanography* **24** (1), PA1207 (2009).
[10] Lambert, F. et al., Dust-climate couplings over the past 800,000 years from the EPICA Dome C ice core. *Nature* **452** (7187), 616 (2008).

IODP

Warm North Atlantic waters allow for Heinrich events but prevent major deglaciations

B.D. A. NAAFS[1,2], J. HEFTER[1], P. FERRETTI[3,4], R. STEIN[1], G.H. HAUG[2,5]

[1] Alfred Wegener Institute for Polar and Marine Research, Department of Marine Geology and Paleontology, D-27568 Bremerhaven, Germany
[2] Leibniz Center for Earth Surface and Climate Studies, Institute for Geosciences, Potsdam University, D-14476 Potsdam, Germany
[3] The Godwin Laboratory for Palaeoclimate Research, Department of Earth Sciences, University of Cambridge, Cambridge CB2 3EQ, United Kingdom
[4] GRC Marine Geosciences, Department of Stratigraphy, Palaeontology and Marine Geosciences, Faculty of Geology, University of Barcelona, E-08028 Barcelona
[5] Geological Institute, ETH Zürich, 8092 Zürich, Switzerland

Hudson Strait (HS) Heinrich events, massive ice-rafting events in the North Atlantic originating from the Laurentide ice sheet (LIS), are among the most dramatic examples of millennial-scale climate variability[1]. Recently, HS Heinrich events have been proposed to drive intense deglaciations through a feedback in which the event shuts off North Atlantic overturning, leading to an increase in Antarctic overturning[2-4]. However, it is debated as to whether the occurrence of HS Heinrich events in the (eastern) North Atlantic depends on greater ice discharge, or simply from the longer survival of icebergs in cold waters[1,5]. Using sediments from the North Atlantic spanning the period between 960 and 320 ka, here we show that sea surface temperatures (SSTs) did not control the first occurrence of HS Heinrich(-like) events in the sedimentary record. We detect the first HS Heinrich(-like) event in our record around 643 ka (Marine Isotope Stage (MIS) 16), but this first HS Heinrich(-like) event did not coincide with low SSTs. Thus, the HS Heinrich events do indeed indicate enhanced ice discharge from the LIS at this time, not simply the survivability of icebergs due to cold conditions in the North Atlantic. In addition, the general lack of HS Heinrich Events prior to the Mid-Brunhes Event (MBE) at ~450 ka is consistent with the absence of intense deglaciations and the "luke-warm" Antarctic conditions and intermediate atmospheric CO_2 levels of pre-MBE interglacials[6,7]. An exception is the large HS Heinrich Event in stage 16, which was also followed by a luke-warm interglacial. We propose that the high North Atlantic SSTs during stage 16 are indicative of relatively strong North Atlantic overturning, which the HS Heinrich Event was unable to quench.

References:
[1] Hemming, S. R., Heinrich events: Massive late Pleistocene detritus layers of the North Atlantic and their global climate imprint. *Rev. Geophys.* **42** (1), RG1005 (2004).
[2] Denton, G. H. et al., The Last Glacial Termination. *Science* **328** (5986), 1652 (2010).
[3] Sigman, D. M., Hain, M. P., and Haug, G. H., The polar ocean and glacial cycles in atmospheric CO2 concentration. *Nature* **466** (7302), 47 (2010).
[4] Barker, S. et al., Interhemispheric Atlantic seesaw response during the last deglaciation. *Nature* **457** (7233), 1097 (2009).
[5] Hodell, D. A. et al., Onset of "Hudson Strait" Heinrich events in the eastern North Atlantic at the end of the middle Pleistocene transition (~640 ka)? *Paleoceanography* **23**, PA4218 (2008).
[6] Lüthi, D. et al., High-resolution carbon dioxide concentration record 650,000-800,000 years before present. *Nature* **453** (7193), 379 (2008).
[7] Jouzel, J. et al., Orbital and Millennial Antarctic Climate Variability over the Past 800,000 Years. *Science* **317** (5839), 793 (2007).

ICDP

Holocene Dust Storms and Flood Events in the Dead Sea Region – Establishing a New Methodological Approach of High-Resolution Dead Sea Sediments Analyses for the ICDP Dead Sea Deep Drilling Project (DSDDP)

I. NEUGEBAUER, U. FRANK, M. J. SCHWAB, P. DULSKI, A BRAUER

Helmholtz Centre Potsdam, GFZ German Research Centre for Geosciences, Telegrafenberg, D-14473 Potsdam, Germany

Since the early 1990s several cooperations between Israeli and German scientists were performed in order to increase our knowledge about the climatic variability and its influence on human history in the Dead Sea and Jordan region. Using sedimentological, microstratigraphical, palynological and magnetic methods, it turned out that lacustrine sediments of the Dead Sea are an ideal mirror of the interactions between climate and environmental response in this climate sensitive region. Changes in precipitation, evaporation and runoff are therefore directly reflected in the succession, composition and thickness of sediment layers. Alternating fine layers of authigenic aragonite and detrital clay layers, with intercalated sand, halite and gypsum layers build the main components of these lacustrine depositions.

High-resolution analyses of a varved sediment sequence of Lake Lisan (Prasad et al., 2009), the Late Pleistocene precursor of the Dead Sea, already revealed, that solar influenced climate variabilities are reflected in laminae thickness during MIS2, resulting in a remarkable accordance of drier events in the Lisan formation with colder events in the GISP2 record (Prasad et al., 2004). First studies of the Holocene Dead Sea sediments in respect to their use to reconstruct long and short term climatic variations in this climate sensitive environment have been performed by Heim (1998). Furthermore, investigations of Holocene sea level variations reflecting regional climate variability in the Dead Sea basin have been carried out on several well dated sediment cores and profiles recovered from three sites on the western Dead Sea shore (Ken-Tor et al., 2001; Migowski et al., 2004; Migowski et al., 2006). The results of these palaeoclimate studies emphasize the great potential of the Dead Sea sediments for climatic and environmental reconstructions in the Near East but also the need of further high-resolution investigations.

The aim of this new study is to apply novel methodological standards to identify flood and dust storm layers in Dead Sea sediments and to establish Holocene time series of these extreme event deposits. Currently a combination of petrographic thin section microscopy, µXRF element scanning and high-resolution magnetic susceptibility analysis is being carried out to identify clastic to evaporitic phases of sedimentation, which are related to periods of abrupt seasonal changes in rainfall/evaporation in the northern Dead Sea region. The geochemical measurements allow to characterise the limnic, fluvial and aeolian sediments in respect of their origin. Furthermore, the high resolution of the multi-proxy

data set on a microscopic scale enables the identification of individual dust storm and flood events. The investigations are performed on existing material from the sediment cores Ein Feshka, Ein Gedi and Ze'elim that were obtained during a drilling campaign in 1997 on the western shore of the Dead Sea basin. The current ICDP Dead Sea Deep Drilling sediment cores DSEg1 and DSEg2 will be integrated in the analyses in order to synchronise and compare sedimentation processes of the onshore profiles with those from the northern deep basin of the Dead Sea. Varve chronologies will be created for all profiles and anchored in improved AMS- 14C- chronologies. Establishing long time series of individual extreme events as well as recognising decadal-scale variability in the eastern Mediterranean climate system during the Holocene will be feasible using this data set. Thereby it will be particularly focussed on determining the influence of the North Atlantic Oscillation (NAO) and solar irradiation changes. A further objective of this investigation is to enable the use of rock magnetic records, especially the magnetic susceptibility, as a proxy for arid periods in further studies of Dead Sea sediments by calibrating this parameter against the sedimentological and geochemical results.

The scientific standards developed during this research plan provide a guideline for dealing with the specific problems of the unique Dead Sea sediments, especially regarding the new long record of the ICDP Dead Sea Deep Drilling Project (DSDDP).

References:
Heim, C. (1998). Holozäne Sedimente aus dem Toten Meer als Paläoklima-Indikatoren. GeoForschungsZentrum Potsdam, Scientific Technical Report STR98/12, 98pp.
Ken-Tor, R., A. Agnon, Y. Enzel, M. Stein, S. Marco & J. F. W. Negendank (2001). High-resolution geological record of historic earthquakes in the Dead Sea basin. J. Geophys. Res. 106: 2221-2234.
Migowski, C., A. Agnon, R. Bookman, J. F. W. Negendank & M. Stein (2004). Recurrence pattern of Holocene earthquakes along the Dead Sea transform revealed by varve-counting and radiocarbon dating of lacustrine sediments. Earth Planet. Sci. Lett. 222: 301-314.
Migowski, C., M. Stein, S. Prasad & J.F.W. Negendank (2006). Holocene climate variability and cultural evolution in the Near East. Quaternary Research 66(3): 421-431.
Prasad, S., H. Vos, J.F.W. Negendank, N. Waldmann, S.L. Goldstein & M. Stein (2004). Evidence from Lake Lisan of solar influence on decadal- to centennial scale climate variability during marine oxygen isotope stage 2. Geology 32: 581-584.
Prasad, S., J.F.W. Negendank & M. Stein (2009). Varve counting and its potential for determining reservoir age fluctuations in palaeolake Lisan. Journal of Quaternary Science 24(7): 690-696.

IODP

Calcium adsorption and ion exchange in marine sediments

C. OCKERT[1], L. M. WEHRMANN[2], T. G. FERDELMANN[2], S. KAUFHOLD[3], B.M.A. TEICHERT[4], N. GUSSONE[1]

[1] Institut für Mineralogie, Corrensstraße 24, 48149 Münster
[2] Max Planck Institut für Marine Mikrobiologie, Celsiusstraße 1, 28359 Bremen
[3] Bundesanstalt für Geowissenschaften und Rohstoffe, Stilleweg 2, 30655 Hannover
[4] Institut für Geologie und Paläontologie, Corrensstraße 24, 48149 Münster

Introduction

Calcium (Ca) isotope ratios of marine organic and inorganic mineral precipitates have been used to monitor changes in the oceanic Ca-budget and in paleo-temperature, and as a proxy for the trophic level of organisms in the food chain (Zhu & Macdougall, 1998; Skulan et al., 1997). Nonetheless, little is known about processes influencing the Ca isotopic composition of marine pore waters through interaction between sediments and pore water. Besides partial dissolution of calcareous tests, diagenetic processes such as release of organically bound Ca, Ca-release from altered volcanic material and ion exchange processes with clay minerals may introduce Ca into the pore fluid and thus have the potential to affect the proxy signal of the respective archives. Calcium-ion exchange with clay minerals has not been taken into account as an important process when interpreting the Ca-isotope ratios of pore water profiles. However, this process could explain findings which could not be explained up to now (Teichert et al., 2009).

Pore water analyses of drill core samples from the Cascadia accretionary margin (ODP Leg 204) show a correlation of ammonium-concentration (NH_4^+) and $\delta^{44/40}Ca$ ratios (Teichert et al., 2009). A comparable correlation was found by von Breymann et al. (1990) for magnesium and ammonium in marine pore waters which was attributed to interaction of cations with sediment particles. While von Breymann et al. (1990) observed a correlation between Mg- and NH_4^+-concentration, Teichert et al. (2009) detected a correlation between ammonium

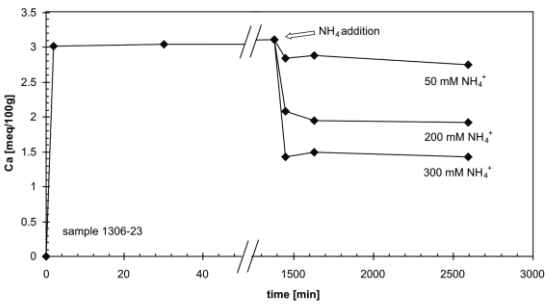

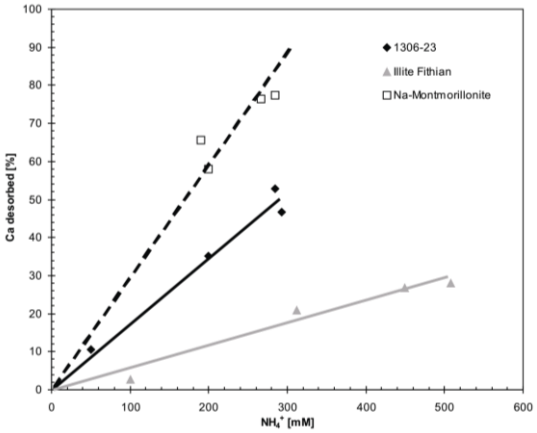

Fig. 1a: Adsorption of Ca (shown in meq/100g) occurs within the first 2 to 5 minutes. Also the desorption of Ca through ammonium addition occurs immediately.
Fig. 1b: Desorbed Ca (in % of Ca originally adsorbed in a seawater medium) as a function of the ammonium-concentration: Illit, Na-Montmorillonite and one sediment sample show a different response to ammonium addition.

concentration and Ca-isotope ratios, rather than Ca-concentration. This indicates that Ca-isotope fractionation is occuring as Ca is displaced from clay minerals by ammonium, while the Ca-concentration in marin pore water is dominated by other processes, like Ca-carbonate precipitation.

In order to approach Ca-isotope-fractionation mechanisms during adsorption and desorption to clay minerals laboratory experiments on well characterized clay minerals as well as analyses of natural pore waters from the North Atlantic were carried out.

Calcium-ammonium ion exchange experiments with clay minerals

To study if Ca-ammonium-exchange at clay mineral surfaces is a significant process in the marine environment, experiments were conducted with an artifical sea water (asw) medium. The Ca-uptake capacity for different clay mineral separates and natural marine sediments as well as the rate of this process were investigated with a radioactive Ca-tracer method. This method has an important advantage over element concentration measurements, since even small changes in the Ca-concentration are detectable. In addition, desorption behaviour of Ca as a function of ammonium introduction was investigated.

Equilibrated suspensions of clay minerals (cations on interlayer of clay minerals are in equilibrium with cations in the surrounding seawater matrix) and artificial seawater were doped with radioactive ^{45}Ca. A time series of samples was taken to determine how fast Ca is adsorbed by the different clay minerals (montmorillonite, illite, kaolinite) and marine sediment (from IODP Expedition 303, Site U1306A). The adsorption of Ca onto the clay minerals was determined by monitoring the decrease of radioactivity in the fluid phase. After equilibration of the radioactive tracer with the suspension, different amounts of ammoniumchloride (resulting in NH_4^+-concentrations of 50, 100, 200, 300 and 500 mM) were added to induce Ca-desorption. This desorption was visible in terms of an increase of radioactivity in the asw solution.

These experiments revealed that after introducing the radioactive tracer, Ca was adsorbed to the clay minerals within minutes for all samples (Fig. 1a). The subsequent admixture of ammonium also showed an immediate effect as Ca was desorbed (Fig. 1a). Depending on the mineral-type and its respective CEC (cation exchange capacity) different amounts of Ca and ammonium were adsorbed (Fig. 1b). However, in a seawater medium about 19 % (9 to 26 %) of the possible interlayer spaces are occupied by Ca.

Since the experiments showed that the cation load equilibrates within minutes, it can be assumed that in natural marine systems a steady state between pore water cation concentration and cations adsorbed to clay minerals exists. Consequently, an increase of ammonium in pore water due to increased organic matter decomposition would lead to desorption of calcium into the pore water.

Natural marine pore waters

With these new insights into the ion exchange behavior of Ca, it is now possible to better understand the natural occuring processes controlling Ca-isotope fractionation. Three sites (U1304A, U1306A, U1308A from the North Atlantic sampled in 2004 during IODP Expedition 303 of JOIDES Resolution) with different lithologies and Ca-pore water profiles indicate that different diagenetic processes play a role.

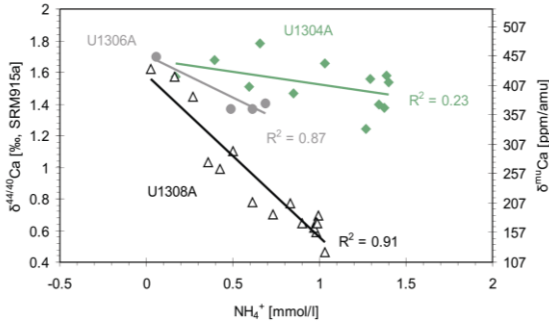

Fig. 2: Calcium isotope ratios as a function of ammonium concentration in the pore waters of Sites U1304A, U1306A and U1308A. When clay minerals are a major component in the lithologic succession (as for Site U1306A and U1308A) the coefficient of determination shows a value closer to 1 than at sites with less clay content.

As indicated from earlier findings (Teichert et al., 2009) and above described experiments a clay mineral rich Site should show an interaction of Ca and ammonium. At the clay mineral rich sites U 1306A and U1308A the relation between $\delta^{44/40}Ca$ and ammonium concentration is stronger pronounced than at the the diatom- and nannofossil ooze dominated Site U1304A (Fig. 2).

Sediments of Site U1304A are dominated by interbedded nannofossil ooze and diatom ooze (Fig. 3). In the upper 100 mbsf (meters below sea floor) of the core a decrease of Ca from seawater concentration to lower concentration is evident. This low concentration remains approximately constant downcore. The $\delta^{44/40}Ca$ values for Site U1304A show only small excursions and range around an average of 1.6 ‰, which is slightly lower than seawater. The absence of a strong correlation between ammonium and Ca isotope values indicates that cation exchange does not play a great role for this site.

The lithologic sequence of Site U1306A is quite homogeneous and consists mainly of silty clay (Fig. 3). The Ca-concentration strongly decreases in the upper 50 mbsf from seawater values of ~10 mM to values around 4 mM and increases again from 100 m depth to 7.5 mM. This feature points to Ca-carbonate precipitation, which is also mirrored in the $\delta^{44/40}Ca$-signal. When assuming Rayleigh-carbonate precipitation for this depth interval the theoretical and measured development show a good match. Whereas for the profile section from 0 to 50 mbsf the signal is most likely the result of the release of light Ca from clay mineral interlayer spaces by ammonium exchange.

Site U1308 reveals a lithology composed of mainly nannofossil ooze and minor silty clay. Here the Ca-concentration decreases to a minimum in the upper 100 mbsf of the core and then increases to above sea water concentration (Fig. 3). Data of Site U1308A demonstrate a trend from seawater-like to low (0.46 ‰) $\delta^{44/40}Ca$ values. This suggests a deep source of Ca that could be either from $CaCO_3$ dissolution or from interaction with the basement. A pronounced negative correlation of NH_4^+-concentration and $\delta^{44/40}Ca$ is evident, which supports the suggested interaction of Ca and ammonium with clay minerals (Fig. 2).

Analysis of $^{87}Sr/^{86}Sr$-isotope ratios of the lowermost samples of the three sites identified the deep source to

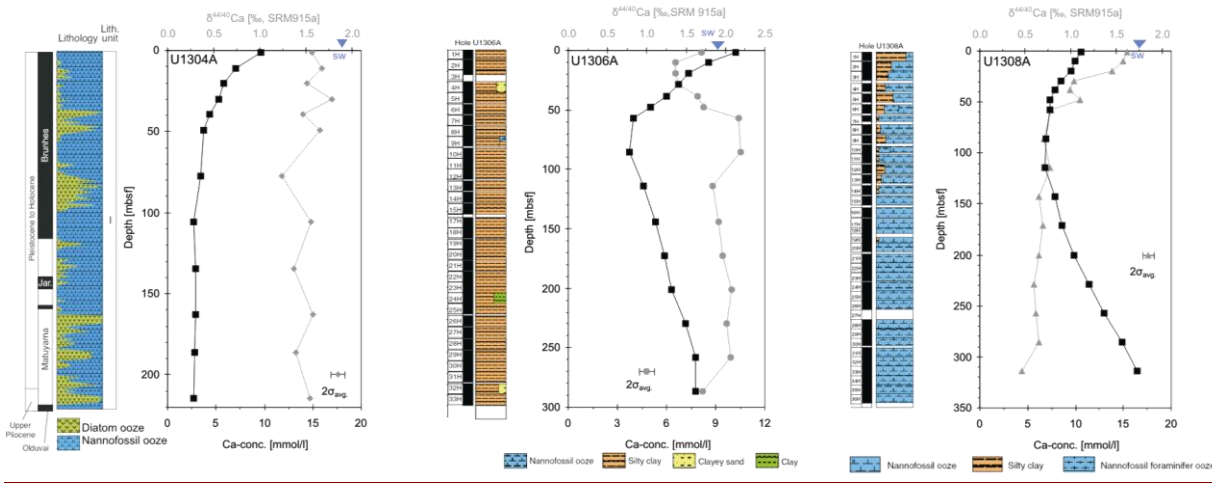

Fig. 3: Lithologic sequences and Ca-concentration and Ca-isotope ratios in the pore water of the three cores from the North Atlantic.

originate from dissolution of marine biogenic $CaCO_3$. This finding is consistent with the Ca-isotopic composition of biogenic marine carbonates of that age (Heuser et al., 2005).

According to these findings it can be proposed that the different behavior for Ca-isotope signals in the pore water profiles are strongly influenced by lithologic differences. The data obtained in this study point to a general diagenetic process in siliciclastic, organic-bearing sediments where light Ca is released into the pore waters.

Summary

In a seawater matrix generally about 20 % of the possible cation uptake capacity of any clay mineral is occupied by Ca and a constant exchange of the cations on the interlayers and the pore water cations is occurs. The amount of organic material and therewith the ammonium concentration of the pore water consequently have an effect on the amount of Ca being desorbed from the marine sediments. To obtain light $\delta^{44/40}$Ca-values like in the upper 50 mbsf of Site U1306A, it is likely that Ca is isotopically fractionated during adsorption and desorption from the clay mineral sites.

In ongoing experiments the fractionation factors for these adsorption and desorption processes are determined. Since we determined how much Ca adsorbs to different clay types and how ammonium affects desorption of Calcium only the isotopic fractionation factors of the adsorption and desorption process are missing for quantifying the system.

References:

Heuser A., Eisenhauer, A., Böhm, F., Wallmann, K., Gussone, N., Pearson, P.N., Nägler, T.F., Dullo, W.-C. (2005): Calcium isotope ($\delta^{44/40}$Ca) variations of Neogene planktonic foraminifera. Paleoceanography 20(2). PA2013, doi:10.1029/2004PA001048,2005.

Skulan, J., DePaolo D.J., and Owens T.L. (1997): Biological control of calcium isotopic abundances in the global calcium cycle. Geochimica et Cosmochimica Acta 61(12), 2505-2510.

Teichert, B.M.A., Gussone, N., Torres M.E. (2009): Controls on calcium isotope fractionation in sedimentary porewaters. Earth and Planetary Science Letters 279(3-4), 373-382.

von Breymann, M.T., Collier, R., Suess, E. (1990): Magnesium adsorption and ion exchange in marine sediments: a multi-component model. Geochimica et Cosmochimica Acta 54(12), 3295-3313.

Zhu, P. & Macdougall D. (1998): Calcium isotopes in the marine environment and the oceanic calcium cycle. Geochimica et Cosmochimica Acta 62(10), 1691-1698.

ICDP

Evidence for a rapid lake level rise after 51,000 cal BP as revealed by a combination of seismic evidence and sediment core data from Laguna Potrok Aike, Argentina

C. OHLENDORF[1], C. GEBHARDT[2], A. HAHN[1], P. KLIEM[1], B. ZOLITSCHKA[1] AND THE PASADO SCIENCE TEAM[3]

[1] Geopolar, Institute of Geography, University of Bremen, Germany (ohlen@uni-bremen.de)
[2] Alfred Wegener Institute for Polar and Marine Research, Bremerhaven, Germany
[3] PASADO Science Team as cited at: http://www.icdp-online.org/front_content.php?idcat=1494

In the framework of the ICDP expedition 5022 (PASADO: Potrok Aike Maar Lake Sediment Archive Drilling Project, Zolitschka et al., 2009) in total 510 m of lacustrine sediments were recovered from the profundal sediments of the maar lake Laguna Potrok Aike (52°S, 70°W; 116 m asl.; diameter: 3.5 km, water depth: 100 m) in southern Patagonia, Argentina. Quadruplicate and triplicate cores down to a maximum depth of 101.5 m below lake floor (blf) were taken with a total core recovery of 94.4 % from two drill sites located 750 m apart in the central profundal plain of the lake (Fig. 1). All cores were handled following a core processing strategy that was developed to consider all the needs of multidisciplinary lake drilling projects (Ohlendorf et al., submitted). For site 2 a 106.08 m long composite profile (5022-2CP) was created by splicing of the three cores drilled. After the non-destructive core scanning was accomplished, 5022-2CP was sampled in consecutive 2 cm steps. 5089 samples with 35,623 sub-samples were taken which are currently analysed by the different international research teams involved in the project.

In this contribution we present a first comparison of results from non-destructive sediment core scanning and lithological description of 5022-2CP on the one side, with results obtained during several seismic surveys of the lake on the other side. First paleoenvironmental interpretations are given using a chronology based on 51 AMS ^{14}C dates.

Seismic refraction data reveal a funnel-shaped structure originating from phreatomagmatic maar explosions

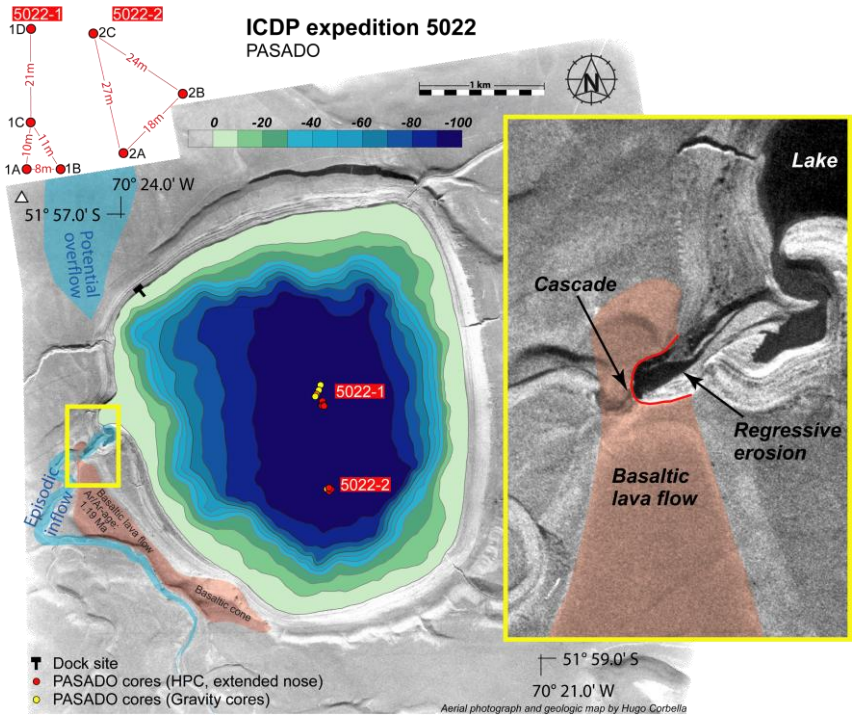

Figure 1: Bathymetric map of Laguna Potrok Aike superimposed on an aerial photograph. PASADO drill sites are indicated by red and yellow dots. The inset close-up (yellow frame) shows the northern end of a basaltic lava flow that was eroded by the main lake tributary (see text for explanation).

embedded in the sandstone rocks of the surrounding Santa Cruz Formation. The funnel is filled by lacustrine sediments of up to 370 m in thickness with seismic velocities of 1500-2350 m s^{-1} which are underlain by a unit of probably volcanoclastic origin (>2400 m s^{-1}). Seismic reflection data of the uppermost 100 m of the sediments reveal stratified lacustrine sediments reflecting a rather dynamic development of the lake: at approx. 90 m blf a desiccation horizon was recognised on top of pelagic sediments. This horizon is characterised by sand dunes in the eastern part of the lake basin, and followed by a series of paleo shorelines documenting the history of a lake level rise during the early stage of re-flooding of the lake basin. While this new lake formed in the central and eastern part of the maar depression, the western part was filled by stacked coarse-grained, delta-type sediments probably derived from the inlet that is only episodically active at present time. After this early filling of the new lake, a rapid lake level rise is observed in the seismic reflection data.

In the sedimentary record of site 2 several features occur that can be used to verify these seismic findings. The lithostratigraphy of 5022-2CP exhibits contrasting lithologies down core especially in the Pleistocene part of the record. The uppermost unit A down to 8.82 m composite depth (mcd) is characterised by carbonaceous, light to dark grey, greenish to bluish grey and brownish grey laminated silts (Fig. 2). In unit B, between 8.82 and 18.72 mcd carbonate poor and sand-layered, brownish (lower part) and dark grey (upper part) laminated silts occur. Intercalated are dark grey to black and several millimeters thick fine sand and coarse silt layers that show sharp contacts to the underlying laminated silts. Plant macro remains and gastropods are abundant in unit B, whereas ball and pillow structures and normal graded beds occur occasionally. The lowermost unit C (18.72 to 106.09 mcd) is characterised by a down core increase in the percentage of mass movement deposits that are intercalated in thinly sand-layered, greenish and bluish grey laminated silts. Lamination is poor compared to lithostratigraphic units A and B. Mass movement deposits like normal graded beds, ball and pillow structures as well as structureless sand and fine gravel layers prevail. The percentage of mass movement deposits averaged over 5 m intervals increases from 14% at the top to 100% at the base of unit C (Fig. 2). Averaged over the entire 5022-2CP sequence 52% of the record consist of re-deposited sediments.

A first chronology was established for 5022-2CP using 51 AMS radiocarbon dates determined on macro remains of aquatic mosses. For age-depth modelling a corrected composite depth (ccd) was calculated that discards all sections with re-deposited sediments (54.88 m) and gaps (5.06 m) but only considers pelagic sediments (46.15 m). After exclusion of ages originating from re-deposited sediments age-depth modeling was done with 39 AMS ^{14}C-dates using the CalPal_2007_HULU calibration curve (Weninger and Jöris, 2008) and the mixed-effect regression procedure (Heegaard et al., 2005). Thus a basal age of ca. 51,000 cal BP was obtained.

Unit A and B represent the Holocene and the Late Glacial lake system that is characterised by authigenic carbonate precipitation with calcite contents of up to 35%, low percentages of re-deposited sediments, and lake level variations between +21 m and -35 m with respect to present day lake level (Anselmetti et al., 2009; Haberzettl et al., 2007). In contrast, unit C with its carbonate-free sediments represents the Weichselian part of the record that is dominated by clastic input of fluvial and eolian origin and a high proportion of re-deposition. The shift between these two modes occurs rather abruptly at 18.82 mcd. At

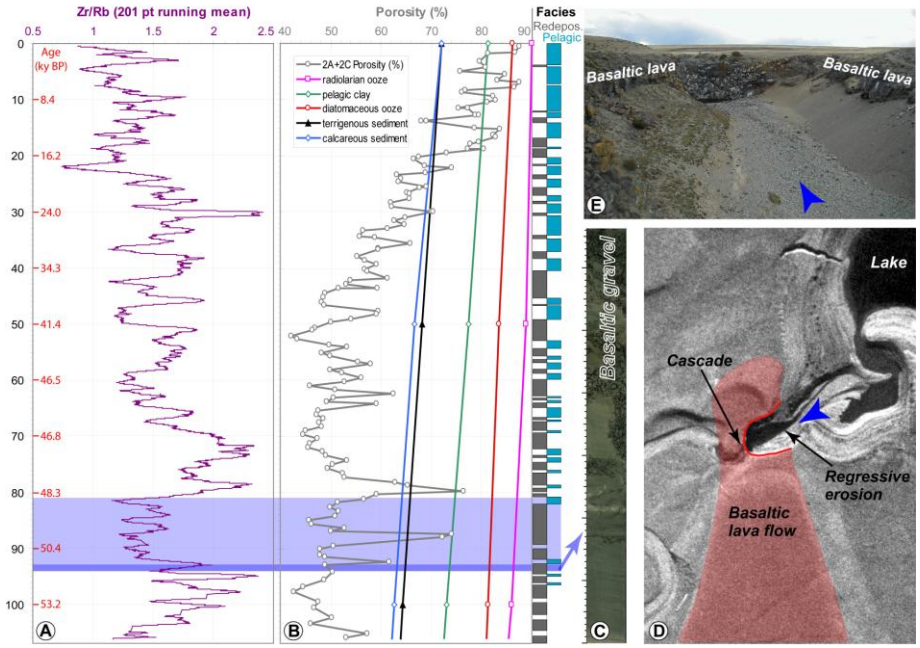

Figure 2: Erosion of a basaltic lavaflow occurred at the western shore of the lake around ca. 51,000 cal. BP. A) Zr/Rb-ratio indicating a short transport distance for the interval highlighted in purple. B) Porosity values indicate overcompacted sediments below ca. 19 mcd. C) Gravel layer deposited at 93 mcd (dark purple line). D) Aerial photograph showing the northern end of the basaltic lavaflow where the cascade was eroded. Blue arrow indicates the position where the photograph shown in E) was taken. E) Photograph of the cascade, view to the WSW.

this level, corresponding to ca. 15,600 cal BP, a more than 1 m thick layer with a fundamentally different geochemical composition follows immediately above a ca. 1 cm thick tephra layer that originated from an eruption of the Reclus volcano. Down core from this level a distinct shift of field-determined porosity values occurs (Fig. 2). Whereas porosity values follow compaction trends expected for pelagic clays (Hamilton, 1976) for the uppermost 18.72 m, porosity shifts away from values that would be expected for normal sediment compaction of any type of deep sea sediments below this depth (Hamilton, 1976). Thus, if compared to normally compacted deep-sea sediments, the sediments of Laguna Potrok Aike seem to be overcompacted below 18.72 mcd, i.e. the overburden pressure was higher than it would be expected from the respective burial depth. According to Faas (1982) such a feature may result from e.g. 1) removal of sedimentary overburden through erosion or faulting, 2) dessication, 3) cementation and recrystallization in the sediment, or 4) lateral compression. All of these possible reasons would have important implications for the interpretation of the sedimentary record because these would indicate that the sediments below 18.72 mcd are either heavily disturbed due to the effects of slumping or diagenetic processes or that drastic erosion occurred that gave rise to hiatuses of yet unknown duration. To verify these field-based porosity estimations a high resolution and more precise calculation of sediment densities, porosities and compaction rates is currently under way applying the analysis of sediment core logging data acquired with a Multi Sensor Core Logger with 1 to 2 cm spatial resolution for the entire record of 5022-2CP.

However, apart from porosity data there are other lithological and geochemical evidences for the possible occurrence of a hiatus especially in the lower part of unit C. Between 82 and 98 mcd several basaltic gravel layers (Fig. 2) indicate highly dynamic hydrological conditions. These layers resemble in appearance poorly rounded fluvial gravel. Above these layers often component supported chaotic fine-grained deposits with ball and pillow structures as well as folded sediments are observed. In between these layers short sequences of fine-grained, laminated sediments occur that can be interpreted as shallow lacustrine deposits. We hypothesise that this sequence reflects a delta type situation and may thus represent an initial flooding of a previously desiccated lake as it has been interpreted from seismic data. Although XRF-scanning data is of poor quality for the coarse intervals of this section, there are indications for a different elemental composition of these sediments. For instance, the observation of slightly reduced Zr/Rb- and Zr/Ti-ratios between 81 and 92 mcd may point towards a rather short transport distance of sediments in this section (Fig. 2). These gravel components were macroscopically described as poorly rounded basaltic clasts. Together, all this information suggests that the source of the described coarse-grained layers probably can be related to the basaltic lava flow that outcrops at the south-western shore of the lake (Fig. 2). This lava flow was eroded at its lakeward facing side. At its northernmost end regressing erosion by the main tributary led to the formation of a waterfall (plunge) with a plunge pool and a short gorge downstream of the basaltic ridge where today the tributary enters the lake. The waterfall itself recedes upstream and carves deeper into the basalt (Figs. 1, 2). The volume of basalt missing in this gorge was estimated to 72000 m^3 which today would be enough to cover the entire deep basin with an approx. 4 cm thick basaltic gravel layer.

In conclusion, combining seismic evidence with sediment core results we hypothesise the following lake

development: Sand dunes in the eastern part of the lake basin detected on seismic profiles indicate a desiccation of the lake prior to ca. 51,000 cal BP. After this date a delta-type sediment sequence in 5022-2CP suggests considerable erosion of the basaltic lava flow and a relatively rapid refilling of the lake. Delta-type sediments are also documented on seismic profiles for the western part of the basin, whereas a sequence of paleo shorelines documents a rising lake level at the eastern shore. The lake level rise must have occurred relatively fast because sediment deposition on the lake shoulder located at 35 m water depth today probably started around 48,000 to 50,000 cal BP. This would imply a lake level rise of about 150 m within a time period of approximately 2000 years, i.e. a mean value of 7.5 cm/yr. This would also compare in magnitude to the mean value obtained for the lake level fall (10 m) since the last lake level high stand of the "Little Ice Age" (6.3 cm/yr). At present, the lake level of Laguna Potrok Aike fluctuates at a comparable magnitude.

References:

Anselmetti, F. et al., 2009. Environmental history of southern Patagonia unravelled by the seismic stratigraphy of Laguna Potrok Aike. Sedimentology, 56: 873-892.

Faas, R.W., 1982. 30. Gravitational Compaction Patterns Determined from Sediment Cores Recovered during the Deep Sea Drilling Project Leg 67 Guatemalan Transect: Continental Slope, Middle America Trench, and Cocos Plate. Initial Reports DSDP, 67: 617-638.

Haberzettl, T. et al., 2007. Wet-dry cycles in southern Patagonia - Chronology, sedimentology and geochemistry of a lacustrine sediment record from Laguna Potrok Aike (Argentina). The Holocene, 17: 297-311.

Hamilton, E.L., 1976. Variations of density and porosity with depth in deep-sea sediments. Journal of Sedimentary Petrology, 46(2): 280-300.

Heegaard, E., Birks, H.J.B., Telford, R.J., 2005. Relationships between calibrated ages and depth in stratigraphical sequences: an estimation procedure by mixed-effect regression. The Holocene, 15(4): 612-618.

Ohlendorf, C. et al., submitted. The PASADO core processing strategy – a new standard for sediment core treatment in multidisciplinary lake drilling projects. Sedimentary Geology.

Weninger, B., Jöris, O., 2008. A 14C age calibration curve for the last 60 ka: the Greenland-Hulu U/Th timescale and its impact on understanding the Middle to Upper Paleolithic transition in Western Eurasia. Journal of Human Evolution, 55(5): 772-781.

Zolitschka, B. et al., 2009. The Laguna Potrok Aike Scientific Drilling Project PASADO (ICDP Expedition 5022). Scientific Drilling, 8: 29-34.

IODP

The evolution of surface, intermediate and deep water connections during the closure of the Central American Seaway

A. OSBORNE[1], M. FRANK[1], R. TIEDEMANN[2]

[1] IFM-GEOMAR, Leibniz-Institut für Meereswissenschaften an der Universität Kiel, Wischhofstrasse 1-3, 24148 Kiel.
[2] AWI, Alfred-Wegener-Institut für Polar- und Meeresforschung, Am Alten Hafen 26, 27568 Bremerhaven.

The goal of this project is to use radiogenic isotopes to reconstruct the history of shallow, intermediate and deep water connections between the Caribbean Sea and the eastern Equatorial Pacific Ocean during the shoaling of the Central American Seaway (CAS), 5.0 to 2.0 million years ago (Ma). The progressive closure of the CAS and the associated reorganisation of ocean circulation have been controversially reported as contributing to a warming and a cooling of global climate, as well as increasing moisture supply to the northern hemisphere and hence preconditioning the inception of Northern Hemisphere Glaciation. This study will use samples from ODP sites 999 and 1000 in the Caribbean and 1241 in the eastern tropical Pacific. For each site we will measure the Nd isotope composition of planktonic foraminiferal calcite in order to characterise surface water exchange and mixing, and the Nd and Pb isotope composition of early diagenetic ferromanganese coatings of the same sediment samples to characterise intermediate and deep water exchange and to assess differences and potential phase lags between surface and deeper water signatures. Sampling resolution will initially be at 100 thousand years (kyr), increasing to less than 21 kyr (i.e. sub-Milankovitch) for key periods identified in the 100 kyr resolution study. The aim of this project is to reconstruct the exact timing of CAS closure to deep, intermediate and shallow waters. These results will be compared with the evolution of the strength of North Atlantic Deep Water (NADW) formation and with the timing of changes in the distribution of heat and moisture to high northern latitudes. It will thus allow to better constrain causes and consequences during this key period of global climate evolution.

Here we present results from an ongoing preliminary core-top survey, comparing the radiogenic isotopes of Nd and Pb in the foraminfera and the sediment coatings with expected water mass. Leaches of the < 63 μm fraction are compared with bulk sediment leaches from core top sediments taken from the region of ODP 1000 in the central Caribbean Sea. The isotopic composition of Nd shows little or no offset between the two leached fractions and gives values between -7.5 and -10.2 ε_{Nd}. These results are broadly consistent with published data from ferromanganese crusts in the Lesser Antilles (Frank *et al.* 2006), although seawater compositions from the central Caribbean Sea are required to confirm the expectation that intermediate and surface waters will have a more radiogenic Nd signature. The isotopic composition of Pb is more radiogenic in the bulk leachate samples than the < 63 μm samples, which might indicate that a fraction of the Pb was adsorbed to clay-size particles in another location and then transported. However, the seawater origin of the leached fraction is confirmed by $^{87}Sr/^{86}Sr$ values.

Frank, M., Marbler, H., Koschinsky, A., van de Flierdt, T., Klemm, V., Gutjahr, M., Halliday, A. N., Kubik, P. W. and Halbach, P. (2006), Submarine hydrothermal venting related to volcanism in the Lesser Antilles: Evidence from ferromanganese precipitates, *Geochemistry, Geophysics, Geosystems, 7*, Q04010, doi: 10.1029/2005GC001140.

IODP

Main bottom channel dynamic during last 300 yrs in the Swatch of No Ground Shelf Canyon offshore the Ganges-Brahmaputra Delta – Implications for a new IODP proposal

L. PALAMENGHI[1,2], T. SCHWENK[3], V. SPIESS[4], H-R. KUDRASS[5]

[1,3,4] Department of Geosciences, University of Bremen, Klagenfurter Str. 28359 Bremen, Germany
[2] Bremen International Graduate School for Marine Sciences (GLOMAR), University of Bremen, Leobener Straße, 28359 Bremen, Germany
[5] MARUM — Center for Marine Environmental Sciences, University of Bremen, Leobener Straße, 28359 Bremen, Germany

1) Introduction

Submarine canyons represent a key link between continent erosion and oceanic sedimentation but indeed they are expected to be mostly sediment bypassing zones. The Swatch of No Ground Canyon, SoNG, incises the Bengal Shelf up to the topset beds of the Ganges-Brahmaputra subaqueous delta and connects the Bengal Basin to the Bengal Fan (Figure 1). Sedimentation is active in present day with accumulation rates in the vicinity of the main bottom channel that range from 50 cm/a in the canyon head to 15 cm/a down to -500 m water depth (Michels et al., 2003), demonstrating that the canyon is not only acting as a bypass, but also as a (temporary) sediment sink. A very close relationship between cyclone activity and sedimentation rate has already been established from the late 60's to the early 90's (Kudrass et al., 1998). A main goal of this research is to decipher the sedimentation processes within the canyon by means of seismo-acoustic datasets. The results will be used to develop a drilling strategy for a new IODP Proposal to study the climate dynamics controlled by the monsoon wind and precipitation with respect to tectonic activity at different timescales from ultra-high yearly resolution to high centennial to millennial resolution.

2) Methods:

The data sets (Figure 1) used for this study are:

(a)Parasound data collected during SO93 Expedition in 1993, during SO126 in 1996 and SO188 in 2006 (ultra-high resolution).

(b) Multichannel seismic, MCS, data collected during SO188 in 2006 from 300 to 0 m water depth using a 0,4 l GI Gun and a 50 m long streamer especially designed for shallow water (48 channels with spherical single hydrophones) that allows imaging of sedimentary deposits in shallow water depth with extremely high lateral resolution (high-resolution).

(c) MCS data collected during SO188 in 2006 from 2000 to 300 m water depth using a 4,1 l GI Gun and a SYNTRON seismic streamer with 96 channels and 600 m length (medium-high-resolution).

The data set has been processed and loaded in and interpretation software and each specific acquisition strategy contributes to unreveal the complex interaction between different transport agents and sedimentary processes.

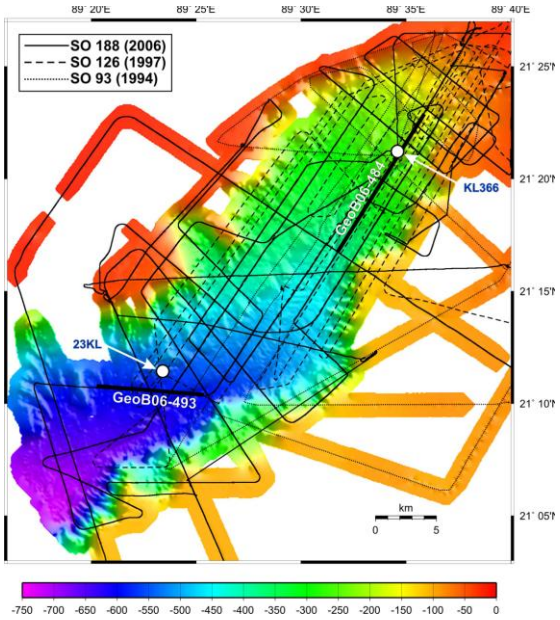

FIGURE 1. Bathymetric map of the Swatch of No Ground canyon cruise tracks of SO93, SO126 and SO188 Expeditions.

3) Results:

The canyon head is fed by daily-yearly sediment supply from the shelf region transported downward by tide+current-supported gravity flows (Palamenghi et al., in press) and cyclone wave-supported gravity flows (Kudrass et., 1998). These sedimentation processes lead to regular deposits suitable for high resolution climatic studies.

However, as another main process, episodic liquefaction flows have been reported from the canyon margin caused by hydrostatic cyclic loading during the Sidr cyclone in November 2007. They have been identified and measured as several kilometers wide units but with minimal run-out distances in the order of 300 m (Rogers and Goodbred, 2010). A Wadati–Benioff Zone of earthquakes illuminating the subducted oceanic lithosphere characterizes the very close India–Sunda boundary and some of the plate-boundary earthquakes are huge (Steckler et al, 2008). Liquefaction flows caused by cyclic load produced by plate boundary earthquakes have been identified and measured in the foreset beds of the subaqueous delta for the last 300 years as wide-spread Transparent Units (TUs) (Palamenghi et al., in press). In particular three TUs have been mapped along the foreset beds and attributed to the specific plate boundary earthquakes of 1762 (Arakan Earthquake, magn. 8.8), 1897 Great India Earthquake, magn. 8.7) and 1950 (Assam Earthquake, magn. 8.2). According to these findings and to the general sensitivity to liquefaction of the G-B delta sediments, it is expected also in the canyon some kind of deposits associated to these tectonic events.

This wide range of sediment transport results in a very complex architectural pattern with channel-levees systems as main elements. The channels are characterized by migrations within relative short time scale and significant amplitude changes associated to specific types of deposition. In the canyon head, the right and left levees of the active main bottom channel present a very high degree of asymmetry where the right section aggraded when the left has a wavy growth pattern (Figure 2). The

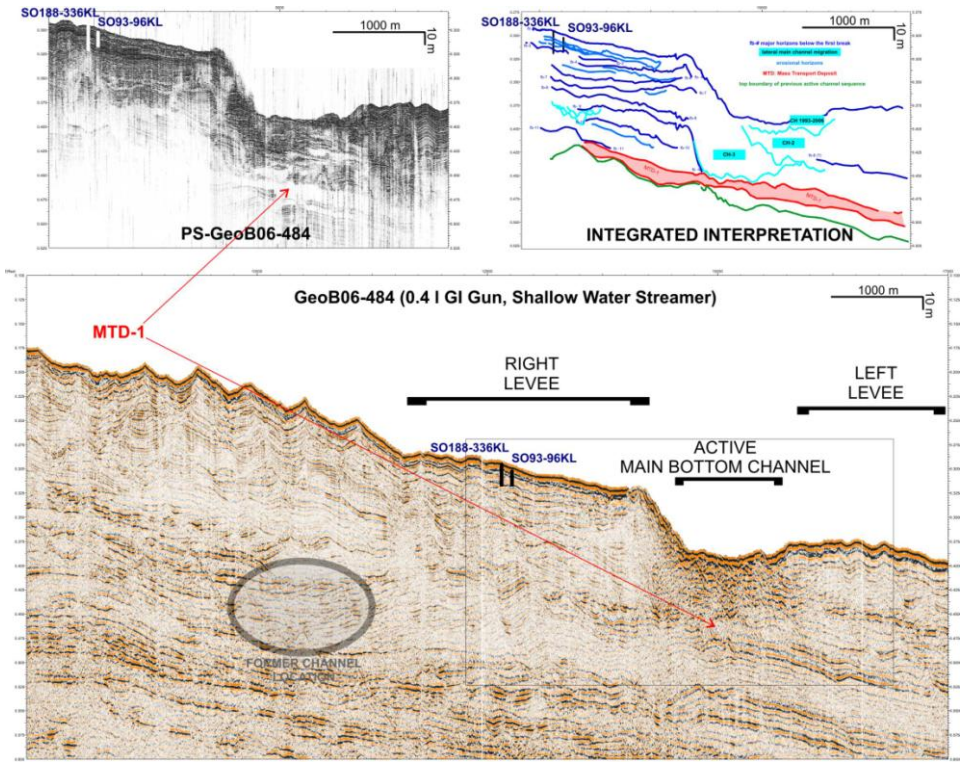

FIGURE 2. MCS and Parasound echosounder equivalent of Line GeoB06-484 from the canyon head. See Figure 1 for profile and core location.

origin of the asymmetry is maybe due to the slope angle of the canyon floor and the interaction of the gravity flows with the very close canyon flank. The 96KL (SO93) core was collected at 280 mbsl in 1993 in the right levee and a repetition has been retrieved during the SO188 Expedition in 2006. The new core, 336KL, has penetrated the ^{137}Cs base and therefore a more accurate dating could be performed that further confirms the given accumulation rate. In the Parasound record an acoustic transparent unit up to 15 m thick extending beneath the entire channel-levees system in a depth of ca. 40 mbsf with erosive base associates in the MCS data to a unit with a chaotic seismic facies (Figure 2). This body is interpreted as a Mass Transport Deposit (MTD) and represents the base of the main bottom channel-levees system as we observe in the present day canyon drainage. The projection of the accumulation rate of ~50 cm/a down to this MTD-1 event that probably influenced the initiation of the activation of the main bottom channel ranges in the order of 150-200 years.

A very similar situation is found for the SO126-23KL core collected at 580 mbsl again in the right levee of the main bottom channel-levees system. Here, two MTDs are recorded: a shallower one approx. 9 m thick and a deeper one more than 20 m thick (Figure 3). The projection of the accumulation rate of ~15 cm/a down to these MTDs gives an estimate of their age for MTD-1 ca. 170 years and of MTD-2 ca. 320 years. As a preliminary interpretation we

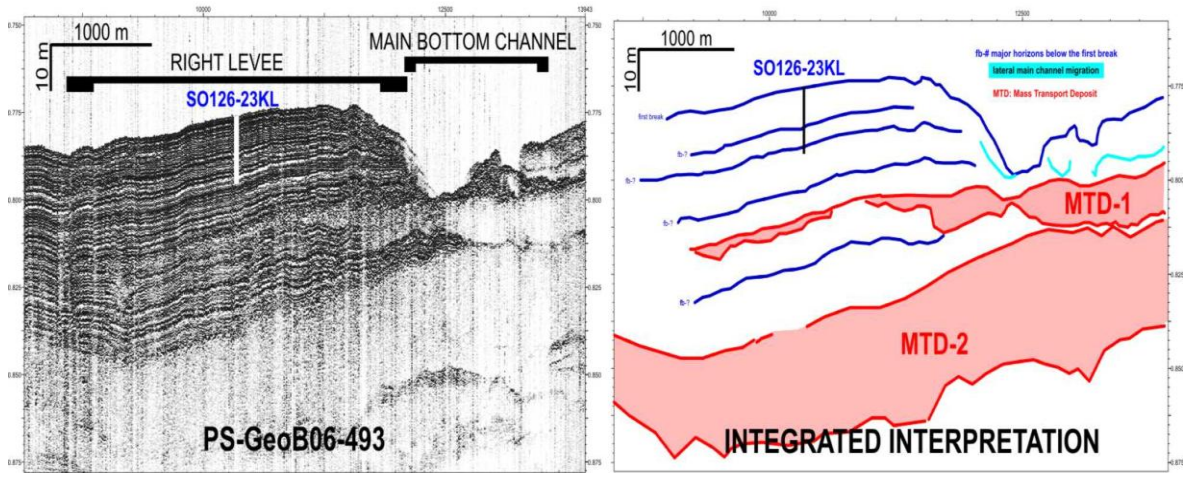

FIGURE 3. MCS and Parasound echosounder equivalent of Line GeoB06-493 from the central canyon section. See Figure 1 for profile and core location.

attribute the origin of these MTDs units to an earthquake trigger mechanism that generated them but further investigation will follow to validate this hypothesis.

4) Conclusion:

The surface sedimentary sequence record of the right levee of the main active bottom channel-levee system archived a continuous ultra-high to high resolution history of the monsoon variability. This might be especially true in the deeper region of the canyon where less lateral shift of the main bottom channel occurred. Therefore the Swatch of No Ground seems to be a very promising target for an IODP drilling. Additionally, the canyon offers the opportunity to evaluate the tectonic activity within this region by drilling the identified MTDs.

5) Outlook:

The surface sedimentary sequence record could be probably used as analogue to reconstruct the canyon history over longer time scales. In fact, while the canyon flanks mostly aggraded, 700 meters thick sediment sequences fill the canyon region down to a very pronounced, horizontal to sub-horizontal unconformity. These peculiar conditions make the Swatch of No Ground Canyon not only a potential climatic archive but also an interesting target to general considerations on the relationship between shelves growth and canyons fill, sediment resident time in a canyon and the mechanisms that might trigger the sediment transfer from offshore basins to the deep-sea fans independently from high- or low-stand sea level conditions.

References:

Kudrass, H.R., Michels, K.H., Wiedicke, M., Suckow, A., 1998. Cyclones and tides as feeders of a submarine canyon off Bangladesh. Geology 26, 715–718.

Michels, K.H., Suckow, A., Breitzke, M., Kudrass, H.R., Kottke, B., 2003. Sediment transport in the shelf canyon ‘‘Swatch of No Ground’’ (Bay of Bengal). Deep-Sea Research II 50, 1003–1022.

Palamenghi, L., Schwenk, T., Spiess, V., Kudrass, H.-R., 2011. Seismostratigraphic Analysis with Centennial to Decadal Time Resolution of the Sediment Sink in the Ganges-Brahmaputra Subaqueous Delta,. Continental Shelf Research, in press.

Rogers, K.G., and Goodbred, S.L. Jr, 2010. Mass failures associated with the passage of a large tropical cyclone over the Swatch of No Ground submarine canyon (Bay of Bengal). Geology 38, 1051-1054.

Steckler, M.S., Akhter, S.H., Seeber, L., 2008. Collision of the Ganges–Brahmaputra Delta with the Burma Arc: Implications for earthquake hazard. Earth and Planetary Science Letters 273, 367–378.

ICDP

Fluid inclusions in the Outokumpu Deep Drill Core: implications for paleofluid evolution and composition of modern deep saline fluids

C. PIRIBAUER[1], F. M. MEYER[1], S. SINDERN[1], T. W. VENNEMANN[2], W. PROCHASKA[3]

[1] Institute of Mineralogy and Economic Geology, RWTH Aachen University, Wüllnerstraße 2, D-52056 Aachen, piribauer@iml.rwth-aachen.de
[2] Institut de Minéralogie et Géochimie, Université de Lausanne, BFSH-2, CH-1015 Lausanne
[3] Department Angewandte Geowissenschaften und Geophysik, Montanuniversität Leoben, 8700 Leoben

Fluid inclusions in quartz veins in the Outokumpu Deep Drill core are characterised by high salinities and high homogenisation temperatures in excess of 330°C. In addition to an aqueous phase, fluid inclusions also contain gaseous phases such as CO_2 und CH_4. Cation ratios of the dissolved salts are higher than seawater with Li/Na ratios indicating the influence of magmatic water in deeper parts of the drill hole. Stable isotope (δD, $\delta^{18}O$) signatures point to a metamorphic origin of the paleofluids. Deep groundwaters in the Outokumpu crystalline basement deviate significantly from fluid inclusions in their stable isotope ratios, which plot to the right of the global meteoric water line in a δD - $\delta^{18}O$ diagram. This suggests that they may have formed as a mixture of meteoric and saline waters. In addition, Cl/Br and Na/Br ratios point to chemical exchange with the host rocks. Many models have been proposed to account for the enhanced salinity of deep groundwaters and the shift in the stable isotopes, but our data indicate that the saline fluids are derived primarily through water–rock interaction. The role of fluid inclusions as important contributors to the saline fluids is not supported.

The drill site is located within the Outokumpu allochthon in eastern Finland, which represents a 1 - 5 km thick remnant of folded and imbricated overthrust terrane, dominated by 1.92 - 1.90 Ga old metaturbidites, emplaced over a basement complex consisting of late Archean gneisses and a thin Palaeoproterozoic cover. The lithologies comprise (1) metasediments, now metamorphosed to amphibolite facies mica schists and black schists, and (2) serpentinites, skarns and sulphide-rich black schists, commonly referred to as the Outokumpu assemblage (Gaál et al. 1975, Koistinen 1981, Park 1988, Peltonen et al. 2008, Säntti et al. 2006).

The uppermost 33 m of the drill core are made up of sand and silt. This is followed by a sequence of metasediments, which mainly consist of biotite-muscovite schist, biotite schist, black schist and biotite-rich gneiss. The metasediments are underlain by serpentinite, skarn and black schist of the Outokumpu assemblage, which extends to a depth of 1515 m. The base of the sequence (1515m – 2516m) is composed of amphibolite facies metasediments, which are locally intruded and crosscut by pegmatite dykes. Pegmatitic granite dominates at depth beyond 2000m. In all lithologies, except the black schist, fluid inclusion bearing quartz and carbonate veins can be observed. A sketch of the drillcore can be seen in figure 1.

Mica schist, biotite mica schist and biotite gneiss contain quartz, biotite, chlorite, and feldspars as main components and accessory minerals like hematite, pyrrhotite, garnet and tourmaline. Fine grained quartz is orientated along bedding planes and/or foliation. Some grains show undulous extinction and incipient recrystallisation. Biotite defines bedding planes and/or foliation and is partly replaced by chlorite. Plagioclase is rarely replaced by white mica and alkali feldspar shows signs of incipient alteration. The mineralogy and texture of the ultramafic rocks of the Outokumpu assemblage show an amphibolite facies overprint (Peltonen et al. 2008). The samples studied are addressed as serpentinites. Microscopically serpentine, calcite, Mg-chlorite and sericite can be distinguished. Because of the strong serpentinisation and the metamorphic conditions, no relicts of the primary magmatic minerals could be identified. In addition, magnetite and pyrite occur as opaque phases. The skarn rock mainly consists of diopside and tremolite, which are arranged in a herringbone pattern. Talc, carbonates and opaque phases are also present. The opaque phases, like pyrrhotite and chalcopyrite, replace the primary minerals. The skarn rocks are often penetrated by calcite veins. In

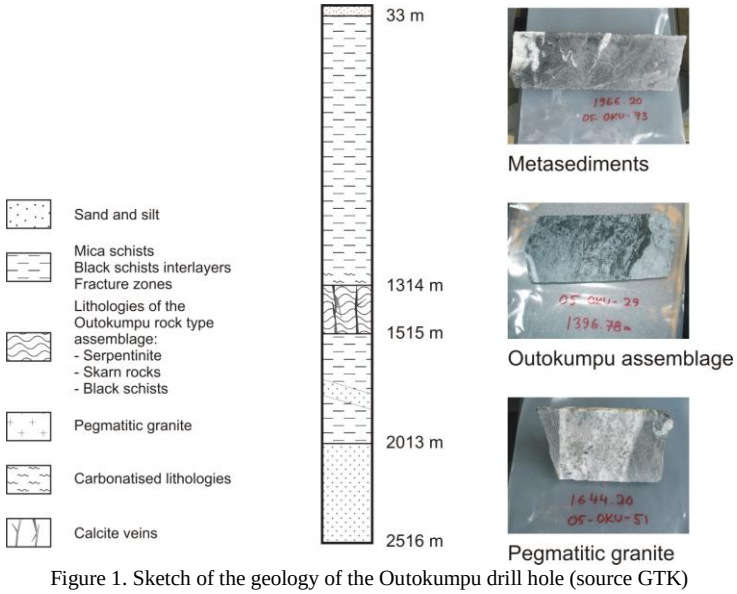

Figure 1. Sketch of the geology of the Outokumpu drill hole (source GTK)

addition to these main lithologies other strongly carbonatized rock types were found. The pegmatites and pegmatitic granites consist of alkali feldspar, plagioclase, muscovite, quartz and partly garnet. Apatite, epidote, and opaque phases occur as accessories. Quartz shows partly undulous extinction and no recrystallisation has been observed. The strip-shaped plagioclase shows beginning alteration and a myrmekitic intergrowth with quartz. Alkali feldspar is not as strongly altered as plagioclase and muscovite forms large crystals within the interstices.

The chemical composition of the biotites within the metasediments plot in the centre of the annite, phlogopite, siderophyllite and eastonite diagram, with a Mg/(Mg+Fe) ratio between 0.4 and 0.5 and Al IV between 2.2 and 2.6. No chemical variance could be noticed in correlation with depth and contact to other rock types. Rare garnets within the metasediments have almandine-rich compositions. Amphiboles and pyroxene, occurring within the skarn rocks, are of tremolite and diopside composition. Some rare Cr-diopside was detected within skarn rocks close to metaultramafic rocks. Feldspar in pegmatites and pegmatitic granites shows perthitic exsolution. The hosting alkali feldspar has a composition of about 90% orthoclase. The plagioclase lamellae are of albite and oligoclase compositions.

Various mineral and isotopic thermometers were applied to obtain an understanding on the formation temperatures of the lithologies occurring in the drill core. This data, together with the micro-thermometrical measurements of fluid inclusions enabled the construction of a P-T path. The isotopic thermometer used is based on the exchange of oxygen isotopes within bitotite and quartz. The formula from Bottinga and Javoy (1975) was applied to calculate the temperatures. Ti has been measured in quartz with LA-ICP-MS technique. The Ti concentrations have been used to calculate a formation T of quartz with the formula of Wark & Watson (2006). Ti in biotite was applied for geothermometry using the calibration of Henry et al. (2005). The temperatures measured and calculatet vary with depth and method. The Ti in quartz thermometer gives temperatures between 558 and 697°C with a $a\mathrm{TiO_2}$ of 0.2 and 460 – 567°C with $a\mathrm{TiO_2}$ of 0.8. The temperatures of the method from Henry et al. (2005) plot between 612 and 746°C. The isotopic thermometers give temperatures between 504 and 545°C.

The primary, pseudosecondary and secondary fluid inclusions observed in quartz veins contain up to three different phases: vapour phase (V), liquid phase (L) and sometimes a solid phase (S) as accidentally trapped crystals. Within the veins, fluid inclusions occur on intragranular trails, on transgranular trails, in clusters or as single inclusions in the veins. Fluid inclusions within the carbonate veins are smaller than 5 µm and cannot be analysed with microthermometry. Three different types of primary isolated fluid inclusions can be distinguished within the quartz veins, based on their composition:

Type 1: LV → $\mathrm{H_2O}$-NaCl
Type 2: LV → $\mathrm{H_2O}$-$\mathrm{CaCl_2}$-NaCl
Type 3: L → $\mathrm{CO_2}$

Type 1 fluid inclusions show a melting temperature (T_m) between -2 and -22°C, which corresponds to a salinity of 2 – 22 mass% NaCl eq. The size of the inclusions range from <2 µm to 40 µm. The homogenisation temperatures

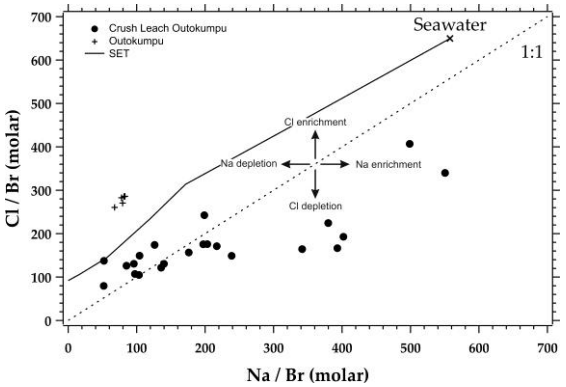

Figure 2, Na/Br vs. Cl/Br plot of fluid inclusion leachates from Outokumpu and groundwater values from Outokumpu (Nurmi et al. 1988).

(T_h (LV→L)) of the type 1 fluid inclusions plot between 100 and 400 °C. Type 2 fluid inclusions have a lower eutectic melting (T_E) than type 1 fluid inclusions. T_E is between -30 and -60 °C, which suggests the presence of $\mathrm{CaCl_2}$ in addition to NaCl. Final melting occurs between -45 and -5 °C, which points to a variable salinity of the fluid inclusions next to a variable composition of the $\mathrm{CaCl_2}$-rich type. The $\mathrm{CO_2}$ bearing, type 3, inclusions are characterised by a T_m(ice) between -57° and -60°C, which indicates the presence of another gas phase, most likely $\mathrm{CH_4}$. They show different homogenisation temperatures $T_h(\mathrm{CO_2}$ LV→L) between -11°C and +6°C. The homogenisation of the $\mathrm{CO_2}$ occurs into the liquid phase.

The results of crush-leach analyses show cation ratios of Ca/Na (0.255 – 0.948 molar), K/Na (0.097 – 0.204 molar), Li/Na (0.001 – 0.085 molar) and Mg/Na (0.024 – 0.344 molar), which are partially higher than seawater (Ca/Na 0.022; K/Na 0.021; Li/Na >0.001; Mg/Na 0.113; seawater values from Turekian, 1968). The Li/Na ratio rises in the vicinity of the deeper pegmatites, which suggests an influence of magmatic water. Within the Cl/Br-Na/Br diagram (Fig. 2) most of the crush-leach samples differ significantly from the seawater evaporation trajectory (SET). They also plot mainly below the 1:1 line, indicating a change of the Cl/Br-Na/Br ratios during halite precipitation and halite dissolution. The molar Cl/Br ratios range from 100 to 400 and are significantly lower than seawater, suggesting a higher Br concentration than seawater. The molar Na/Br ratios are between 80 and 580 and are similar to seawater ratios.

The $\delta^{18}O$ values of the fluid inclusions were calculated under the assumption of isotopic equilibrium between the fluid phase and the host mineral (quartz, Hu & Clayton 2003) at a temperature of 500 - 540°C as indicated by geothermometry. The δD values of the fluid inclusions show a broad scatter; however, all values plot in the field of metamorphic fluids with the biotite values being distinctly lighter in $\delta^{18}O$ straddling the field of magmatic fluids. In contrast, the isotopic composition of the Outokumpu groundwater (Nurmi et al. 1988) plots to the left of the meteoric water line (Fig. 3).

On the basis of the cation and anion composition as well as stable isotope characteristics of fluid inclusions we conclude that fluid inclusions do not significantly contribute to the deep saline groundwaters of the Outokumpu crystalline basement. Rather, Cl/Br and Na/Br

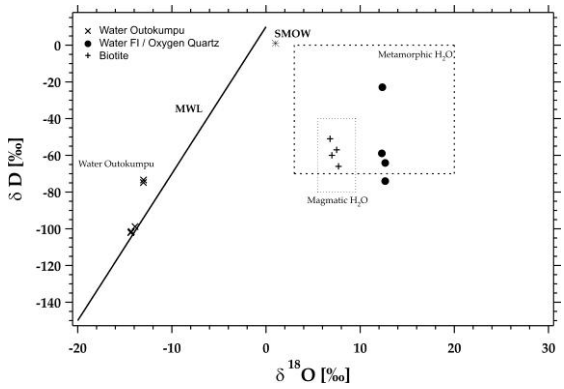

Figure. 3 Plot of $\delta^{18}O$ vs. δD for fluid inclusions and biotites from Outokumpu compared with Groundwater values from Outokumpu (Nurmi et al. 1988).

ratios point to chemical exchange of the groundwaters with the host rocks.

References:
Bottinga, Y & Javoy, M. 1975. Oxygen Isotope Partitioning Among the Minerals in Igneous and Metamorphic Rocks. Reviews of Geophysics and Space Physics 13 (2), 401-418.
Gaál, G., Koistinen, T. & Mattila, E. 1975. Tectonics and stratigraphy of the vicinity of Outokumpu, North Karelia, Finland: Including a structural analysis of the Outokumpu deposit. Geological Survey of Finland, Bulletin 271, 67p.
Koistinen, T.J. 1981. Structural evolution of an early Proterozoic stratabound Cu-Co-Zn deposit, Outokumpu, Finland. Transactions of the Royal Society of Edinburgh: Earth Sciences 72, 115-158.
Henry, D. J., Guidotti, C. V. & Thomson, J. A. 2005. The Ti-saturation surface for low-to-medium pressure metapelitic biotite: Implications for Geothermometry and Ti-substitution Mechanisms. American Mineralogist 90 (2-3), 316-328.
Hu, G. & Clayton, R. N. 2003. Oxygen isotope salt effects at high pressure and high temperature, and the calibration of oxygen isotope geothermometers. Geochimica et Cosmochimica Acta 67 (17), 3227–3246.
Nurmi, P. A., Kukkonen, I. T. & Lahermo, P. W. 1988. Geochemistry and origin of saline groundwaters in the Fennoscandian Shield. Applied Geochemistry 3 (2), 185-203.
Park, A. F. 1988. Nature of the early Proterozoic Outokumpu assemblage, Eastern Finland. Precambrian Research 38 (2), 131-146.
Peltonen, P., Kontinen, A., Huhma H. & Kuronen, U. 2008. Outokumpu revisited: New mineral deposit model for the mantle peridotite – associated Cu-Co-Zn-Ni-Ag-Au sulphide deposits. Ore Geology Reviews 33 (3-4), 559-617.
Säntti, J., Kontinen, A., Sorjonen-Ward, P., Johanson, B. & Pakkanen, L. 2006. Metamorphism and chromite in serpentinized and carbonate-silica-altered peridotites of the Paleoproterozoic Outokumpu-Jormua ophiolite belt, Eastern Finland. International Geology Review 48 (6), 494-546.
Turekian, K.K. 1968. Oceans. Prentice-Hall, 149 pp.
Wark, D.A. & Watson, E.B. 2006. TitaniQ: a titanium-in-quartz geothermometer. Contributions to Mineralogy and Petrology 152 (6), 743-754.

IODP

Paleotemperature reconstructions on cold-water coral mound Challenger (IODP Site 1317)

J. RADDATZ[1], V. LIEBETRAU[1], A. RÜGGEBERG[2], E. HATHORNE[1], A. EISENHAUER[1], J. FIETZKE[1], D. NÜRNBERG[1], C. DULLO[1]

[1] IFM-GEOMAR Leibniz-Institute of Marine Sciences at Kiel University, Wischhofstrasse 1–3, D-24148 Kiel, Germany
[2] Department of Earth and Envionmental Sciences, K.U. Leuven, Celestijnenlaan 200 E, B-3001 Heverlee, Belgium

The Integrated Ocean Drilling Program (IODP) Expedition 307 drilled the 155 m high cold-water coral mound Challenger in the Porcupine Seabight (SW off Ireland) in order to understand the paleoenvironment during initiation and early development of this spectacular cold-water coral site.

Up to now stratigraphic work carried out by Kano et al. (2007) and Foubert & Henriet (2009) showed that growth of Challenger Mound was initiated around 2.6 Ma. A major hiatus separates the mound record into a period of fast growth (2.6-1.7 Ma) and slower growth (1.0-0.5 Ma). In this study we combined three different age determinations, radiogenic strontium ($^{87}Sr/^{86}Sr$), U/Th, and U/U ratios and suggest a mound growth different from what has been published earlier. Age determinations of *Lophelia pertusa* samples originating from IODP Site 1317 Core C reveal that coral growth was active during MIS 1 (U/Th age 1292 ys ± 15) and MIS 5 (U/TH age 104 ka ± 1.4, U/U age 117 ka ± 7.5). Moreover U/Th and U/U and Sr ages indicate a significant hiatus in Core C at around 5 m. Below this hiatus coral growth was active in MIS 13.U/Th isotope data close to the ($^{230}Th/^{234}U$) activity equilibrium indicate time intervals of coral growth around 430 ± 40 ka, 435 ± 50 ka, and 500 ±85 ka, supported by ($^{234}U/^{238}U$)exc. activity ratios resulting in U/U age determinations of 490 ± 15 ka, 495 ±15 ka and 488 ±11 ka, respectively (taking modern seawater ratios as starting value into account) as well as overlapping $^{87}Sr/^{86}Sr$ SIS (strontium isotope stratigraphy) age estimates. Moreover, ($^{234}U/^{238}U$)exc. activity ratios imply coral growth during MIS 21 (855 ± 50 ka) and probably also during MIS 19 (811 ± 35 ka). Addititonal 87Sr/86Sr SIS age determinations identify clearly the major hiatus and show that mound growth ceased around 1.53 Ma.

On the basis of these well-dated corals we carried out paleotemperature recontsructions of intermediate water masses. Potential paleotemperature proxies (Sr/Ca, Mg/Li and $\delta^{88/86}Sr$ ratios) were all calibrated against living *in situ* sampled *L. pertusa* along the European continental margin. For $\delta^{88/86}Sr$ determinations we used the new developed Double-Spike-TIMS technique and found results different to those published earlier (Fietzke and Eisenhauer 2006; Rüggeberg et al., 2008). Our results show that downcore coral $Sr/Ca_{Lophelia}$ ratios give unrealistic low values. Whereas downcore coral $Mg/Li_{Lophelia}$ and $\delta^{88/86}Sr_{Lophelia}$ ratios result in reasonable temperature values in the order of ~6°C and ~12°C for the mound record investigated. Additional foraminiferal $Mg/Ca_{Planulina}$ temperatures support coral temperatures with values of about 9.5°C to 12.5°C for the upper mound interval.

Our reconstructed paleotemperatures from cold water coral *L. pertusa* are interpreted as a warming of intermediate water masses since the onset of Challenger mound formation. We suggest that this trend reflects possible vertical movements (shallowing) of the Mediterranean Outflow Water (MOW) influencing and triggering mound growth.

References:
Fietzke J. and Eisenhauer A. (2006) Determination of temperature-dependent stable strontium isotope ($^{88}Sr/^{86}Sr$) fractionation via bracketing standard MC-ICP-MS. *Geochemistry Geophysics Geosystems* **7**.
Foubert, A., Henriet, J.-P., 2009. Nature and Significance of the Recent Carbonate Mound Record. Lecture Notes in Earth Sciences 126. Springer-Verlag, Berlin. pp. 298.
Kano, A., Ferdelman, T.G., Williams, T., Henriet, J.-P., Ishikawa, T., Kawagoe, N., Takashima, C., Kakizaki, Y., Abe, K., Sakai, S., Browning, E.L., Li, X., IODP Expedition 307 Scientists, 2007. Age constrains on the origin and growth history of a deepwater

coral mound in the northeast Atlantic drilled during Integrated Ocean Drilling Program Expedition 307. Geology 35, 1051–1054

Rüggeberg A., Fietzke J., Liebetrau V., Eisenhauer A., Dullo W. C., and Freiwald A. (2008) Stable Strontium Isotopes ($\delta^{88/86}$Sr) in Cold-Water Corals - A new Proxy for Reconstruction of Intermediate Ocean Water Temperatures. *Earth and Planetary Science Letters* 269(3-4), 569-574.

Sakai, S., Kano, A., Abe, K., 2009. Origin, glacial–interglacial responses, and controlling factors of a cold-water coral mound in NE Atlantic. Paleoceanography 24, PA2213. doi:10.1029/2008PA001695.

ICDP

Preliminary stratigraphy and first petrographic and geochemical results for the ICDP drill core from the El´gygytgyn impact structure (Russia).

U. RASCHKE[1], W.U. REIMOLD[1], R.T. SCHMITT[1],AND THE EL´GYGYTGYN SCIENTIFIC PARTY

[1] Museum für Naturkunde – Leibniz Institute at Humboldt University Berlin, Invalidenstr. 43, D-10115 Berlin, Germany (ulli.raschke@mfn-berlin.de , uwe.reimold@mfn-berlin.de , ralf-thomas.schmitt@mfn-berlin.de)

Introduction: El´gygytgyn (67°30'N and 17°05'E), a 3.6 Ma [1], 18-km-diameter impact structure, is located in the Late Mesozoic Ochotsk-Chukotsky Volcanic Belt of Chukotka (Northeast Siberia). It is one of the best-preserved impact structures on Earth [2]. The complex crater structure was formed in a silicious volcanic target [3,4]. The volcanic rocks of the crater area were described as the Late Cretaceous Pykarvaam and Milguveem series [5-7] (schematic geology: Fig.1). ^{40}Ar-^{39}Ar dating of some volcanic rocks from the crater area gave ages of 86-89 Ma [8]. The average stratigraphy for the target area includes (from top of section): ignimbrites (250 m), tuffs and rhyolitic lava (200 m), tuffs and andesitic lava (70 m), and ash tuffs and welded tuffs of rhyolitic and dacitic compositions (100 m). Thus, rhyolitic rocks amount to 89% and andesitic rocks to 11% of the target composition [9]. After the impact a 12 km wide crater lake was formed. The lake is somewhat offset from the center of the crater. Undisturbed and continuous lacrustrine sedimentation took place to establish a long-term reservoir of paleoenvironmental information. The crater was never covered by glaciers or ice shields, which allowed the development of a unique arctic climate archive. Thus, in spring 2009 a drilling campaign by the "International Continental Drilling Project (ICDP)" recovered a nearly complete, 315 m sequence of lake sediments and 202 m of impactites.

Methods: Our first goal was the core curation in collaboration with ICDP staff. We recorded the core material and carried out a first lithological description. This was followed by a sampling party in May 2010. By now we have obtained 102 polished thin sections of core samples and a further 20 from country rocks (collections of the MfN and from GFZ Potsdam, representing samples from ca 60% of the crater rim). Optical microscopy was used for lithological classification and first shock deformation analysis; the core is strongly altered which is providing a nice challenge. RAMAN spectrometry is used together with optical microscopy for the identification of secondary minerals and sulfides. We have also begun with

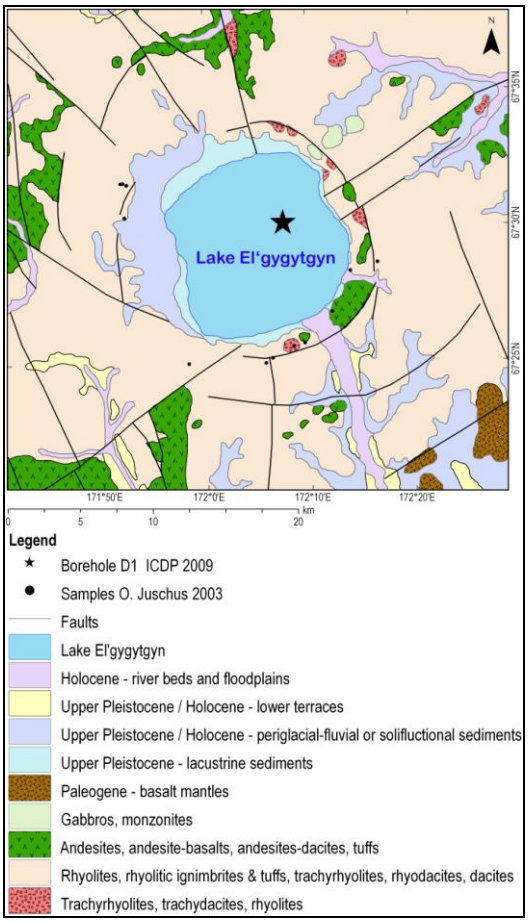

Fig. 1: Geological Map from El´gygytgyn, mod. after [10].

detailed analysis of volcanic melt phases (in tuff and ignimbrite) and impact-generated melts. XRF analysis has been conducted on both impact breccia and bedrock samples.

Preliminary lithostratigraphy: Within the impactite sequence between 316 and 517 m depth we can distinguish three different lithologies (see Fig. 2). At the top there is a 19 m wide transition zone between lake sediments and underlying suevite. This transition is composed of a weakly consolidated mixture of shocked and unshocked lithic and mineral clasts and fine- to coarse-grained sediment particles. Below this follow 88 m of polymict impact breccia that contains impact melt clasts and variably shocked lithic/mineral clasts (Fig. 3), and consequently is classified as suevite. It includes four volcanic clasts/blocks of different thickness and mineral compositions; in all four cases the more mafic portions are strongly altered and transected by numerous thin calcite veins. Near the transition from suevite to underlying bedrock, a strongly altered, dark greenish zone occurs. Below 423 m depth the lowermost lithology comprises brecciated bedrock. It consists of a porphyric rhyodacite with a fine-grained matrix. Small phenocrysts of mostly altered feldspar and melt particles are prominent. The melt clasts are elongated (up to 1 cm thick and 2 to 6 cm long). Their long axes have varied orientations of 15 to 75 ° to the core axis. Open and filled fractures occur abundantly throughout this core section and have a similar variation of orientations with respect to the core axis. The fractures in this lowermost lithology are filled by calcite and zeolites (e.g., analcite).

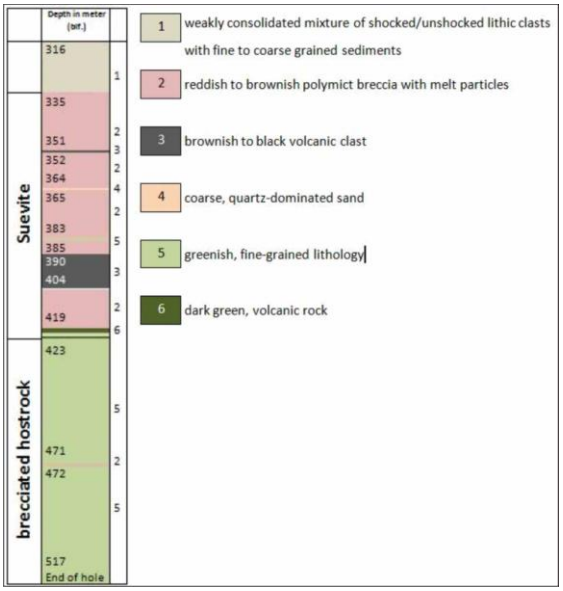

Fig. 2: Preliminary stratigraphic table (blf.= below lake floor).

At 471 m a 0.5 m thick vein of polymict impact breccia (suevite) occurs, with sharp contacts to the surrounding volcanic rock.

First petrographic results: The suevite sequence consists of clasts and matrix grains ranging in size from mud to stone (0.002 mm to 20 cm). Target lithologies identified include a range of volcanic rocks, some of which resemble the lithologies of the bedrock sequence from the crater rim region. We also identified some particles of clayey and fine-grained sediment which have been pressed into fractures in the uppermost suevite. This material could contain fine deposit from the vapor plume, because it contains ~100 µm sized glass spherules and small quartz grains with planar deformation features (PDF, Fig. 4). Some of these spherules are filled with zeolites (e.g., heulandite). We have found three shatter cones in volcanic clasts (rhyolite and tuff) within suevite, at the depths of 351, 368 and 376 m (compare Fig. 5).

The lower unit represents brecciated bedrock material generally of rhyodacitic composition. Besides feldspathic (plagioclase as well as albite and alkali feldspar) phenocrysts, there are also quartz and mafic (biotite, amphibole) phenocrysts. The groundmass is composed of the same minerals. The igneous melt particles contained in this lithology also contain some very fine-grained feldspar and quartz phenocrysts embedded in a brownish glassy matrix.

Geochemistry: XRF major element compositions of target rocks had been previously determined by Gurov and Koeberl (2004). We have obtained further country rock analyses for a suite of samples collected by O. Juschus in 2003 and including rhyolite, dacite, andesite and basalt (Fig. 6 – TAS plot after [11]). Our first XRF results of suevite samples from the D1 drill core cover the same compositional range as the country rock lithologies. Samples of brecciated bedrock plot into the rhyo-dacite field. The altered horizon between the two main sequences is more mafic (SiO_2 < 50 wt%). This layer is also characterized by very high (in comparison to all other samples analysed so far) concentrations of Ti, Al, Fe, Mn, Mg, Ca, Ni, Co, Cr).

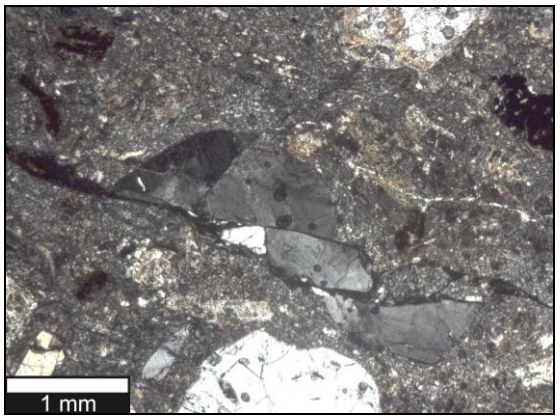

Fig. 3: Shearfracture displaying quartz aggregate and possibly friction melt, 352.25 m,cross polarized light.

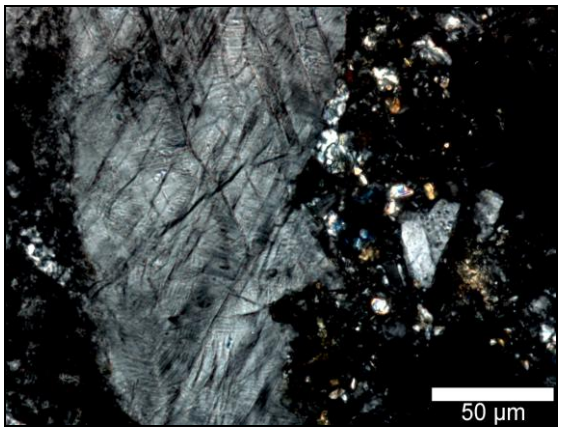

Fig. 4: Planar deformation feature and planar fractures in quartz clast in weakly consolidated material at 317.64 m, cross polarized light.

Fig. 5: Shatter cone in volcanic clast from 351 m below lake floor.

Conclusion: The El´gygytgyn ICDP drill core consists of two main impactite types: an upper suevite package with clasts that show abundant evidence of shock metamorphism in the shock pressure range from < 10 to 50 GPa (PF, PDF, mosaicism in quartz, shatter cones, impact melt); and a lower part of monomict breccia after volcanic

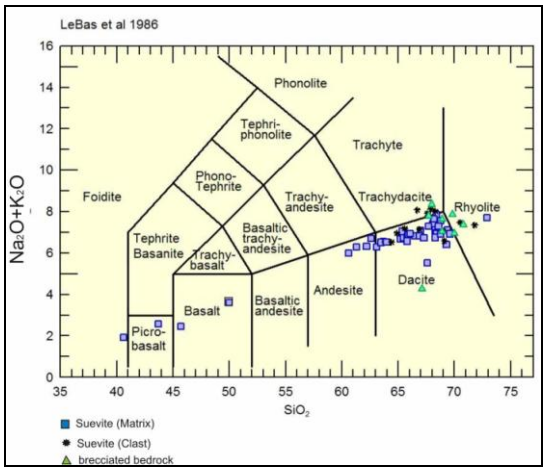

Fig. 6: Chemical classification (TAS diagram after [11]).

(rhyodacitic) rock that is only weakly shocked (quartz grains rarely show 1 or 2 sets of PDF; most quartz shows normal extinction). The intensity of shock metamorphism seems to rapidly decrease in the bedrock lithology with depth, as indicated by almost unshocked material at the end of the drill core (517 m).

Acknowledgements: This project is funded by DFG (German Research Foundation) grant RE 528/10-1). N. Nowaczyk and O. Juschus are thanked for providing some country rock samples. Drilling and logistics were supported by ICDP, the US National Science Foundation, the German Ministry of Research and Education, the Russian Academy of Sciences, and the Austrian Ministry for Science and Research.

References:
[1] Layer, P. (2000) Meteoritics & Planet. Sci, v. 35, p. 591–599;
[2] Gurov, E.P. et al. (2007), Meteoritics & Planet. Sci. v. 42, Nr 3, p. 307–319;
[3] Gurov, E.P. et al., (1979), LPS X, p. 479–481;
[4]Gurov, E.P. & Gurova, E.P. (1991), Nauk. Dumka Press, 160 p;
[5] Beliy, V.F. (1969) Nauk. Dumka Press 138 p;
[6] Beliy, V.F. (1982) Tichook. Geol., no. 5, p. 85–92;
[7] Feldman,V.I. et al., (1981), Marak., A.A., ed., Impactites: Moscow St. Univ. Press, p. 70–92;
[8] Ispolatov,V.O. et al., (2004), The J. of Geol., 2004, vol. 112, p. 369–377;
[9] Gurov, E.P. et al.(2005), GSA, Spec.Pap. 384, p. 391-412;
[10] Melles, M.et al. (2003), Ber. Polar & Meeresforsch.509,ISSN 1618-3193;
[11] Le Bas, M.J. et al. (1986), J. Geol. Soc. London 148, 825-833.

IODP

Calcium carbonate veins in ocean crust record a threefold increase of seawater Mg/Ca and Sr/Ca in the past 30 Million years

S. RAUSCH[1], F. BÖHM[2], A. EISENHAUER[2], A. KLÜGEL[1], W. BACH[1]

[1] Geoscience Department, University of Bremen, Germany; srausch@uni-bremen.de / akluegel@uni-bremen.de / wbach@uni-bremen.de
[2] IfM-GEOMAR, 24148 Kiel, Germany; fboehm@ifm-geomar.de

Seawater infiltration into the ocean floor has profound effects on both the physical and chemical properties of the oceanic crust. In particular, water circulation through the flanks of mid-ocean ridges — where the crust is young and therefore comparatively permeable — is the most important mechanism for cooling the lithosphere. Associated with circulation of seawater-derived fluids, precipitation of vein minerals is lowering porosity and permeability upon ageing. Mineral precipitation is also of major importance from a chemical perception: carbonates are forming most abundantly during low-temperature alteration, changing the overall composition of the oceanic lithosphere and making seawater-related alteration of oceanic crust a significant component of the global carbon cycle.

Element transfer between seawater and rocks of the oceanic crust has been quantified by different authors using either the rock record (e.g., Alt & Teagle, 1999; Bach et al., 2003) or ridge flank fluid compositions (e.g., Elderfield et al., 1999; Wheat & Mottl, 2000). A more integrative approach for estimating chemical exchange budgets is analysing vein minerals from basaltic crust and using their composition to reconstruct element ratios of the seawater-derived fluid from which they precipitated. Coggon et al. (2004) successfully derived fluid parameters (Sr isotopes, temperatures, Mg/Ca and Sr/Ca ratios) from calcium carbonate veins, and more recently expanded the approach to use the composition of calcium carbonate veins as archives for past seawater composition (Coggon et al., 2010). The general applicability of this method is corroborated by comparison with combined data from calcareous fossils (Dickson, 2002; Lear et al., 2002) and halite-hosted fluid inclusions (Horita et al., 2002; Lowenstein et al., 2003; Timofeeff et al., 2006).

Based on the record from calcite carbonate veins, Coggon et al. (2010) propose that Mg/Ca and Sr/Ca ratios of seawater were essentially uniform throughout the period between 170 and 24 Ma, but at 24 Ma a sudden increase by a factor of 4 to present-day seawater composition occurred. This increase is interpreted as an effect of decreasing ridge flank hydrothermal activity, which seems to concur with a proposed decrease in ocean crust production rate in the late Cretaceous (e.g., Spencer & Hardie, 1990). However, data are sparse for the time period critical for determining the onset of increase in Sr/Ca and Mg/Ca ratios. In the present study, we fill this gap by complementing the published data with Sr/Ca and Mg/Ca reconstructions for eleven drill sites in young (mostly ≤57 Ma) cold ridge flanks (Rausch et al., submitted).

Samples from eleven drill sites were examined. Calcium carbonate (calcite and aragonite) veins were sampled by micro-drilling or handpicking from crushed core material. Sr/Ca and Mg/Ca ratios were analyzed by means of ICP-OES, and $^{87}Sr/^{86}Sr$ ratios by TIMS. Oxygen and carbon isotopic compositions were determined by gas-source mass spectrometry. Retrieving past seawater compositions involves a number of steps: Firstly, formation temperatures from $\delta^{18}O$ were calculated using empirical calibrations (aragonite: Böhm et al., 2000; calcite: Friedman & O'Neil, 1977). Second, temperature-dependent Sr/Ca and Mg/Ca distribution coefficients were calculated using calibrations by Gaetani & Cohen (2006) for aragonite and Rimstidt et al. (1998) for calcite. Third, data for sites with elevated formation temperatures were extrapolated to 10°C. Finally, using the $^{87}Sr/^{86}Sr$ seawater data through time (McArthur & Howarth, 2004), carbonate vein formation ages were determined for samples that show higher $^{87}Sr/^{86}Sr$ ratios than seawater at the time of basement formation. This procedure is also used by

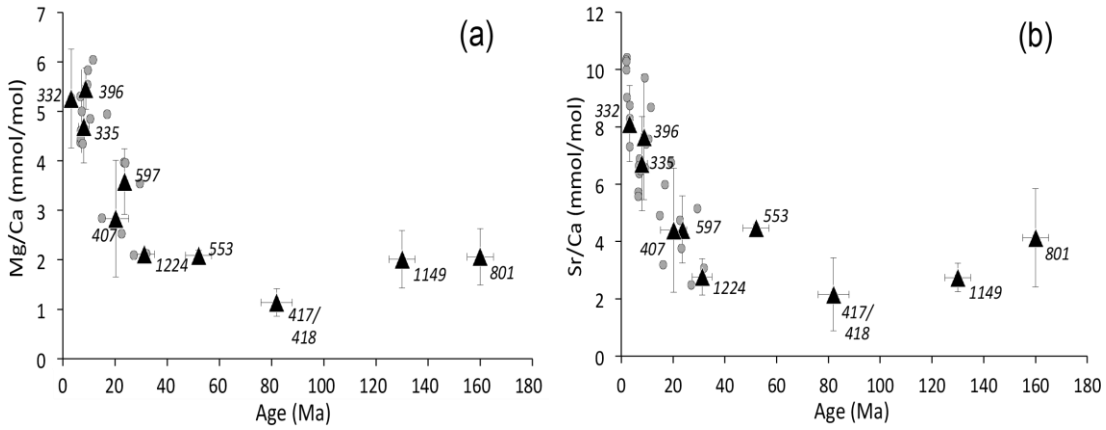

Figure 1: Reconstruction of past seawater Mg/Ca (a) and Sr/Ca (b) ratios based on calcium carbonate veins from the ocean crust. The large triangles with error bars (2SD) are averages for different drill sites. Gray dots are data for individual veins for which Sr isotope seawater dating was possible.

Coggon et al. (2010) and thus comparison of both datasets is not biased by different methodologies.

Seawater compositions derived from the new data (Fig. 1) show fairly uniform Mg/Ca of 1-2 mol/mol for the time older than ca. 30 Ma. From about 30 Ma on, a steady increase in Mg/Ca is observed and the present-day value of 5.4 mol/mol is reached a few million years ago. Similarly, the almost constant Sr/Ca ratios of ca. 2-4 mmol/mol derived from samples older than 30 Ma increased within the same time frame to the present-day value of ca. 9 mmol/mol (see Fig. 1). Comparison of our dataset with the results of Coggon et al. (2010) shows an overall agreement. However, while Coggon et al. (2004) propose the onset of increasing Mg/Ca and Sr/Ca to occur at 24 Ma, some of our older data show an increase of both ratios too. Hence we propose that an increase in seawater Mg/Ca and Sr/Ca ratios started as early as 30 Ma.

The observed trend in evolution of seawater composition shows considerable deviations from data derived from benthic foraminifera (e.g., Delaney & Boyle, 1986; Lear et al., 2002); however, physiological effects have likely occurred upon carbonate formation, making it difficult to obtain consistency between seawater evolution trends obtained from biogenic and from abiogenic carbonate. Furthermore, our data are indirectly confirmed by a general agreement with model predictions (e.g., Wallmann, 2001; Spencer & Hardie, 1990), which account for variations in hydrothermal and weathering fluxes, ocean floor alteration, sedimentation, subduction, volcanism, metamorphism and carbonate accumulation.

Models for seawater compositional changes published in the literature assume a decrease in ocean crust production rate by a factor of 2 to 2.5 in the late Cretaceous (e.g., Spencer & Hardie, 1990; Wallmann, 2001), which would consequently lead to decreasing global hydrothermal flux. However, new assessments of spreading rate changes point to a significantly lower decrease in ocean crust production rates at the Cretaceous-Cenozoic boundary (only by a factor of 1.5; Seton et al., 2009) and lowering of the hydrothermal flux may also be less pronounced than previously estimated. But Coggon et al. (2010) argue that decreasing hydrothermal activity is the main driver for increasing Sr/Ca and Mg/Ca ratios, whereas continental runoff is thought to be insufficient to explain the changes in seawater chemistry (this would increase only Mg/Ca but not Sr/Ca ratios). But hydrothermal fluids have Sr/Ca ratios around 3 mmol/mol and Mg/Ca near zero (Wheat & Mottl, 2000) and therefore the observed seawater trend cannot solely be explained by decrease in hydrothermal activity (Fig. 2).

Our data indicate that Sr/Ca and Mg/Ca ratios derived for seawater from carbonate veins are strongly correlated (Fig. 2). Moreover, the regression line goes through the origin, suggesting that Sr/Mg ratios of seawater have remained constant throughout the past 165 Myrs, which is difficult to reconcile with hydrothermal fluctuations. In addition, the proposed models fail to explain why changes in Sr/Ca and Mg/Ca of seawater took place millions of years after the spreading rates decreased. This indicates that an additional factor must have influenced the seawater chemistry.

The increase in seawater Sr/Ca and Mg/Ca ratios at constant Sr/Mg can be explained by a sink flux of carbon

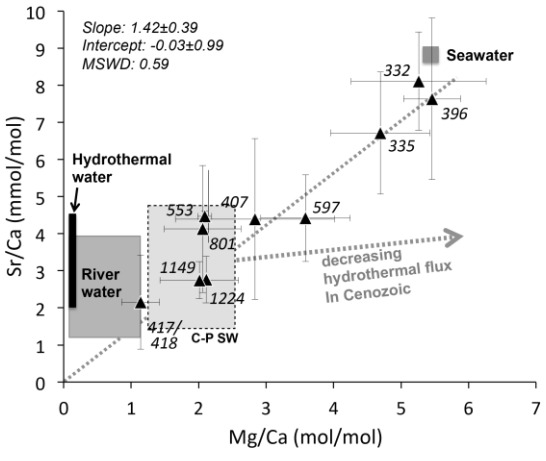

Figure 2: Plot of reconstructed seawater Sr/Ca versus Mg/Ca, with compositions of modern seawater, river waters and hydrothermal fluids as reference values. The gray box labelled "C-P SW" marks the area in which the Paleogene-Cretaceous seawater reconstructions from Coggon et al. (2004) plot. Regression through our data yield a linear trend, which – within error – goes through the origin of the diagram. This indicates that the Sr/Mg ratio of seawater has remained constant throughout the past 165 Myrs. Furthermore, hydrothermal fluxes alone could not have shifted Cretaceous seawater to modern seawater compositions.

that was greater than the source flux for Ca during the past 30 Myrs. We suggest that the following szenario, first proposed by Wallmann (2001), can explain the observed trend: The late Cenozoic decrease in ocean crust production rate led to an increase in the average age of the crust und thus to a sea level drop. Lower sea level caused a shift of the major carbonate deposition areas from the shelves to the pelagic ocean. This — delayed by a few million years — increased the amount of carbonate subducted at convergent margins and the subsequent increase in subaerial CO_2 flux related to arc volcanism. An increased flux of CO_2 to the atmosphere promoted continental silicate weathering and caused a major increase in carbonate alkalinity flux to the oceans. As the concomitant flux of dissolved Ca to the oceans shows a lesser increase, Ca is depleted from the seawater by enhanced calcium carbonate formation.

Although hydrothermal waning (as proposed by Coggon et al., 2010) certainly played a significant role in changing the seawater composition, we conclude that this mechanism alone is incapable of producing the observed dramatic chemical changes during the past 30 Myrs. Our proposed model involves increased erosion and a subduction-recycle delayed transfer of CO_2 from deep-sea carbonates to volcanic arcs, which finally boosted tha Ca sink flux by carbonate formation due to increased carbonate alkalinity input to the seawater.

References:

Alt, J.C., Teagle, D.A.H., 1999. The uptake of carbon during alteration of ocean crust. Geochimica et Cosmochimica Acta 63, 1527-1535.

Bach, W., Peucker-Ehrenbrink, B., Hart, S.R., Blusztajn, J.S., 2003. Geochemistry of hydrothermally altered oceanic crust: DSDP/ODP Hole 504B - Implications for seawater-crust exchange budgets and Sr- and Pb-isotopic evolution of the mantle. Geochemistry, Geophysics, Geosystems 4.

Böhm, F., Joachimski, M.M., Dullo, W.-C., Eisenhauer, A., Lehnert, H., Reitner, J., Wörheide, G., 2000. Oxygen isotope fractionation in marine aragonite of coralline sponges. Geochimica et Cosmochimica Acta 64, 1695-1703.

Coggon, R.M., Teagle, D.A.H., Cooper, M.J., Vanko, D.A., 2004. Linking basement carbonate vein compositions to porewater geochemistry across the eastern flank of the Juan de Fuca Ridge, ODP Leg 168. Earth and Planetary Science Letters 219, 111-128.

Coggon, R.M., Teagle, D.A.H., Smith-Duque, C.E., Alt, J.C., Cooper, M.J., 2010. Reconstructing past seawater Mg/Ca and Sr/Ca from mid-ocean ridge flank calcium carbonate veins. Science 327, 1114-1117.

Delaney, M.L., Boyle, E.A., 1986. Lithium in foraminiferal shells: implications for high-temperature hydrothermal circulation fluxes and oceanic crustal generation rates. Earth and Planetary Science Letters 80, 91-105.

Dickson, J.A.D., 2002. Fossil echinoderms as monitor of the Mg/Ca ratio of Phanerozoic oceans. Science 298, 1222-1224.

Elderfield, H., Wheat, C.G., Mottl, M.J., Monnin, C., Spiro, B., 1999. Fluid and geochemical transport through oceanic crust: a transect across the eastern flank of the Juan de Fuca Ridge. Earth and Planetary Science Letters 172, 151-165.

Friedman, I., O'Neil, J.R., 1977. Compilation of stable isotope fractionation factors of geochemical interest, In: Data of Geochemistry, U.S. Geological Survey Professional Paper, 440-KK, 6th ed.

Gaetani, G.A., Cohen, A.L., 2006. Element partitioning during precipitation of aragonite from seawater: A framework for understanding paleoproxies. Geochimica et Cosmochimica Acta 70, 4617-4634.

Horita, J., Zimmermann, H., Holland, H.D., 2002. Chemical evolution of seawater during the Phanerozoic: Implications from the record of marine evaporites. Geochimica et Cosmochimica Acta 66, 3733-3756.

Lear, C.H., Rosenthal, Y., Slowey, N., 2002. Benthic foraminiferal Mg/Ca-paleothermometry: a revised core-top calibration. Geochimica et Cosmochimica Acta 66, 3375-3387.

Lowenstein, T.K., Hardie, L.A., Timofeeff, M.N., Demicco, R.V., 2003. Secular variation in seawater chemistry and the origin of calcium chloride basinal brines. Geology 31, 857-860.

McArthur, J.M., Howarth, R.J., 2004. Strontium isotope stratigraphy, in: Gradstein, F., Ogg, J.G., Smith, A. (Eds.), A Geological Time Scale, 1st ed, Cambridge, pp. 96-105.

Rausch, S., Böhm, F., Eisenhauer A., Klügel, A., Bach, W. Calcium carbonate veins in ocean crust record a threefold increase of seawater Mg/Ca and Sr/Ca in the past 30 Million years, submitted

Rimstidt, J.D., Balog, A., Webb, J., 1998. Distribution of trace elements between carbonate minerals and aqueous solutions. Geochimica et Cosmochimica Acta 62, 1851-1863.

Seton, M., Gaina, C., Müller, R.D., Heine, C., 2009. Mid-Cretaceous seafloor spreading pulse: Fact or fiction? Geology 37, 687-690.

Spencer, R.J., Hardie, L.A., 1990. Control of seawater composition by mixing of river waters and mid-ocean ridge hydrothermal brines, in: Spencer, R.J., Chou, I.-M. (Eds.), Fluid-mineral interactions: A tribute to H. P. Eugster, Geochemical Society Special Publication 19, pp. 409-419.

Timofeeff, M.N., Lowenstein, T.K., da Silva, M.A.M., Harris, N.B., 2006. Secular variation in the major-ion chemistry of seawater: Evidence from fluid inclusions in Cretaceous halites. Geochimica et Cosmochimica Acta 70, 1977-1994.

Wallmann, K., 2001. Controls on the Cretaceous and Cenozoic evolution of seawater composition, atmospheric CO_2 and climate. Geochimica et Cosmochimica Acta 65, 3005-3025.

Wheat, C.G., Mottl, M.J., 2000. Composition of pore and spring waters from Baby Bare: global implications of geochemical fluxes from a ridge flank hydrothermal system. Geochimica et Cosmochimica Acta 64, 629-642.

IODP

Veining and alteration in rocks from the Louisville Seamount Chain (IODP Leg 330) – consequences for crust-seawater exchange budgets

S. RAUSCH[1], F. DESCHAMPS[2], M. DORAIS[3] , W. BACH[1], A. KLÜGEL[1], IODP EXPEDITION 330 SCIENCE PARTY

[1] Geoscience Department, University of Bremen, Petrology of the Ocean Crust, Klagenfurter Str. (GEO), 28359 Bremen, Germany, srausch@uni-bremen.de

[2] Géosciences Montpellier, Université Montpellier 2, Place Eugène Bataillon, cc 060, 34095 - Montpellier cedex 05, France fabien.deschamps@gm.univ-montp2.fr

[3] Department of Geological Sciences Brigham Young University, Prowo Utah, USA

IODP Expedition 330 drilled five seamounts in the Louisville seamount chain, ranging in age between 80 and 50 Ma. One main goal of this expedition was to drill a large number of in situ lava flows at each seamount for high-quality estimates of their paleolatitudes using paleomagnetic measurements, for improving constraints on the overall age progression using high-precision $^{40}Ar/^{39}Ar$ geochronology, and for detailed geochemical studies of the volcanic evolution of these seamounts.

The ages of the five volcanic structures are similar to those of four guyots drilled in the Hawaiian – Emperor seamount chain (ODP Leg 197). There, workers have documented a rapid southward motion of the Hawaiian hotspot. From determining the relations between age and paleolatitude for the Louisville seamount chain and comparing them with the Leg 197 results, the proponents of Exp. 330 plan to test hotspot motion hypotheses. Either the Hawaii and Louisville hotspots move coherently and show minimal inter-hotspot motion as predicted by some (Wessel & Kroenke, 1997; Courtillot et al., 2003), or the hotspots show different motions, which is what other workers have proposed based on mantle flow model calculations (e.g., Koppers et al., 2004; Steinberger et al., 2004).

Apart from this primary goal of unraveling mantle flow patterns, the drill cores from these sites provide an unparalleled opportunity for investigating exchange fluxes between seamounts and the ocean. Seamounts are believed to rival mid-ocean ridge flanks in terms of mass flux of seawater that circulates through the basement, and therefore they likely play a critical role in regulating crust-

ocean exchange fluxes. With this regards, ocean ridge flank systems have been studied by several authors (e.g. Alt & Teagle, 1999; Alt & Teagle 2003; Bach et al., 2003); however, the alteration and veining history of seamounts has not yet been studied in any detail.

We plan a systematic and comprehensive study of seamount-ocean interaction manifest in rock alteration and veining. Whole-rock geochemical studies as well as Sr-, O-, H-, C-isotopic analyses of veins and other alteration mineral assemblages will provide the basis for reconstructions of the quantity and physico-chemical conditions of seawater-rock interaction throughout the lifetime of hydrologic activity.

The first goal is to determine the extent of veining related to sub-seafloor water-rock interaction. At all Sites of Leg 330 either carbonate veins or carbonate cemented breccias are abundant (Figure). The carbonate vein record from the Louisville drill cores will help to improve the assessment and quantification of seamounts as a global CO_2 sink, and will further our understanding of the processes and timescales involved. We also plan to estimate the timing, sequence, and formation conditions of other secondary vein minerals (e.g., zeolites, clay minerals) from compositional and isotopic characteristics, e.g., the Sr isotope systematics will provide a rough indicator of the duration of seawater circulation in volcanic basement.

We hypothesize – based on our experience with ridge flank settings – that open circulation of seawater will leave the circulating fluids essentially unmodified so that carbonate veins can be used as a recorder of past seawater composition (Coggon et al., 2010; Rausch et al., submitted). To estimate the amount of chemical exchange of vein carbonates with their host rocks, the REE and Y inventory will be used.

The carbonates that are uninfluenced by the volcanic host rocks are expected to be significantly younger than the volcanic basement and will provide $^{87}Sr/^{86}Sr$ seawater ages <38 Ma (the point in time when seawater 87Sr/86Sr began to increase). Carbonates with rock-dominated REE and Y characteristics cannot be used for reconstruction of palaeo-seawater compositions, but they will instead yield information about exchange reactions of seawater with the basement rocks (Coggon et al., 2004; Eickmann et al., 2009). Zeolites and clays can provide additional useful information on formation temperature and geochemical changes during aging of the oceanic crust (Révillon et al., 2007).

In 521 m deep Hole U1374A, the drill cores show abundant carbonate veins, as well as vesicles and voids filled with carbonates in the 300 first mbsf. These rocks are altered under subzeolite to zeolitefacies conditions, indicating that the carbonates fromed from seawater-derived hydrothermal fluids at a relatively low temperature (< 100°C). But with increasing depth below the seafloor, the abundance of zeolites goes up. A succession of zeolites, from phillipsite to analcite and possibly to stilbite, suggests an alteration temperature gradient. By comparison with drill core from other locations (Eastern Iceland: Walker, 1951; Kerguelen Island: Giret et al., 2003; East Greenland: Neuhoff et al., 2011) the zeolite mineral succession may represent temperatures startign between 40-80 °C and increase to 140°C.

Carbonate infillings in vesicles and veins are the dominant secondary mineral at all other sites of Exp.330. In Hole U1376A, a total of 1190 veins and 280 vein networks were counted. The core features an average of 8.1 veins per meter, and the majority are filled with carbonate (Mg-calcite and aragonite). For Holes U1377A and B we also discovered a high density of veins, between 4 and 9 per meter. Both vesicles and veins were mostly filled with zoned carbonates (Mg-calcite, siderite, ankerite). The appearance of siderite and ankerite could point to an influence of hydrothermal fluids, providing Fe and Mn.

References:

Alt, J. C. and Teagle, D. A. H., 1999. The uptake of carbon during alteration of ocean crust. *Geochim. Cosmochim. Acta* 63, 1527-1535.

Alt, J.C. and Teagle, D.A.H. 2003. Hydrothermal alteration of upper oceanic crust formed at a fastspreading ridge: mineral, chemical, and isotopic evidence from ODP Site 801. *Chem. Geol.*

Bach, W., Peucker-Ehrenbrink, B., Hart, S. R., and Blusztajn, J. S. 2003a. Geochemistry of hydrothermally altered oceanic crust: DSDP/ODP Hole 504B – Implications for seawater-crust exchange budgets and Sr- and Pb-isotopic evolution of the mantle. *Geochem. Geophys. Geosys.* 4(3), 10.1029/2002GC000419.

Coggon, R.M., Teagle, D.A.H., Cooper, M.J. and Vanko, D.A., 2004. Linking basement carbonate vein compositions to porewater geochemistry across the eastern flank of the Juan de fuca Ridge, ODP Leg 168. Earth and Planetary Science Letters, 219: 111-128.

Coggon, R.M., Teagle, D.A.H., Smith-Duque, C.E., Alt, J.C., Cooper, M.J., 2010. Reconstructing past seawater Mg/Ca and Sr/Ca from mid-ocean ridge flank calcium carbonate veins. Science 327, 1114-1117.

Courtillot, V., Davaille, A., Besse, J., and Stock, J., 2003. Three distinct types of hotspots in the Earth's mantle. *Earth and Planetary Science Letters, 205: 295-308.*

Eickmann, B., Bach, W. and Peckmann, J. (2009) Authigenesis of carbonate minerals in ocean-floor hard rocks: modern and Devonian examples. Journal of Geology 117: 307-323.

Giret, A., Weis, D., Grégoire, M., Mattiellli, N., Moine, B., Michon, G., Scoates, J., Tourpin, S., Delpech, G., Gerbe, M.C., Doucet, S., Ethien, R., and Cottin, J-Y., 2003. L'Archipel de Kerguelen: les plus vieilles îles dans le plus jeune océan. Géologues, 137: 15-23.

Honnorez, J., 2003. Hydrothermal alteration vs. ocean floor metamorphism. A comparison between two case histories: the TAG hydrothermal mound (Mid-Atlantic Ridge) vs. DSDP/ODP Hole 504B (equatorial East Pacific). Comp. Rendus Geosci., 335(10–11):781–824. doi:10.1016/j.crte.2003.08.009

Neuhoff, P.S., Watt, W.S., Bird, D.K., and Pedersen, A.K., 2011. Timing and structural relations of regional zeolite zones in basalts of the East Greenland continental margin. Geology, 25:803-806.

Révillon, S., Teagle, D.A.H., Boulvais, P., Shafer, J. and Neal, C.R., 2007. Geochemical fluxes related to alteration of a subaerially exposed seamount: Nintoku seamount, ODP Leg 197, Site 1205. Geochemistry, Geophysics, Geosystems, doi: 10.1029/2006GC001400

Rausch, S., Böhm, F., Eisenhauer A., Klügel, A., Bach, W. Calcium carbonate veins in ocean crust record a threefold increase of seawater Mg/Ca and Sr/Ca in the past 30 Million years, submitted

Rouxel O., Ono S. H., Alt J., Rumble D., Ludden J. (2008) Sulfur isotope evidence for microbial sulfate reduction in altered oceanic basalts at ODP Site 801. *Earth and Planetary Science Letters*, **268**, 110-123.

Steinberger, B., Sutherland, R., and O'Connell, R. J. 2004. Mantle flow models constrained by revised global plate motions successfully predict the Emperor-Hawaii and other hotspot-related seamount chains. *Nature, 430, 167-173, doi:10.1038/nature02660.*

Walker, G.P.L., 1951. The amygdale minerals in the Tertiary lavas of Ireland. I. The distribution of chabazite habits and zeolites in the Garron plateau area, County Antrim'. Am. Min., 29:773.

Wessel, P., and Kroenke, L.W., 1997. A geometric technique for relocating hotspots and refining absolute plate motions. *Nature, 387: 365-369.*

IODP

Paleodiversity reconstruction in Antarctic Neogene Radiolarians

J. RENAUDIE[1], D. LAZARUS[1]

[1]Museum für Naturkunde, Leibniz-Institut für Evolutions- und Biodiversitätsforschung an der Humboldt Universität zu Berlin, Invaliden-straße 43, 10115 Berlin.
johan.renaudie@mfn-berlin.de

Introduction

Antarctic Neogene sediments record major changes in oceanography linked to climate cooling and increased glaciation of the polar regions and are a key archive for paleoceanographic and paleoclimate studies. Because these sediments mostly lack carbonate microfossils and also because of widespread hiatuses and rapid changes in sedimentation rate, even with paleomagnetic stratigraphy it has been difficult to develop a robust, unambiguous geochronologic framework, the lack of which significantly hinders paleoceanographic/climatic research. In addition to the more widely employed diatoms, Antarctic Neogene sediments contain abundant well preserved radiolarians. These faunas are diverse, evolve rapidly and offer in principle a major resource for improved biostratigraphy and thus improved geochronology. However, studies to date have employed only a fraction of the fauna and the available biostratigraphic resolution is only moderate. Equally of interest is the increasing use in recent years of fossil data in macroevolutionary studies, primarily analyzing patterns from databases of taxa occurrences compiled from the published literature. Our hope is that the extraordinarily complete species-level fossil record of marine microfossils may circumvent problems with less-complete shallow marine or terrestrial macrofossil data. However, the same incompleteness of data collection that limits biostratigraphy also limits use of this record for evolutionary research.

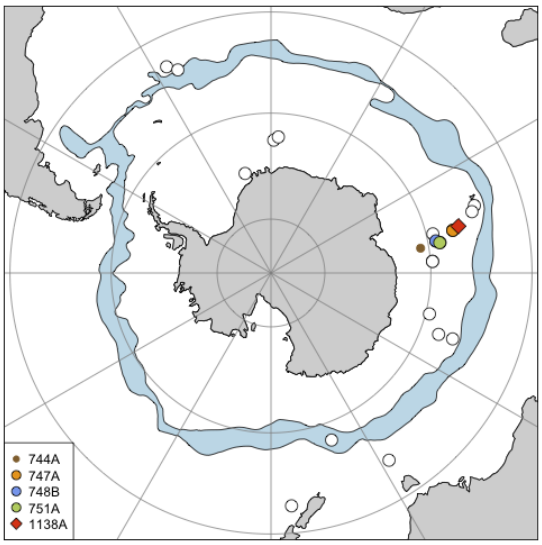

Figure 1: Location of studied ODP and DSDP samples. Samples included in our whole-fauna dataset are from leg 119 site 744, leg 120 site 747, 748 and 751 and leg 183 site 1138. White circles are the other sites included in the Neptune dataset. Polar front (blue zone) from Orsi et al, 1995.

The goals of our project are 1) to document as completely as possible the species level diversity of Antarctic Neogene radiolaria; to determine the stratigraphic range of these species in several Neogene sections; 2) to analyze the patterns of species first and last occurrences to better understand patterns and processes of macroevolution in these faunas; and lastly to analyze the same data set using modern methods to increase biostratigraphic resolution in Antarctic Neogene sediments.

The taxonomic work has been largely completed; while quantitative occurrence data collection is well advanced and macroevolutionary analysis has begun. In the context of this analysis, we compared the observed diversity trends in our material to reconstructions produced using modern, computationally-intensive, statistical tools based on occurrence data extracted from database, in order to test the adequacy of such methods.

Whole-fauna data

The main focal point of the study was to document Antarctic Neogene radiolarian fauna as exhaustively as possible. In a preliminary taxonomical survey of ca 250 samples, we isolated nearly 500 species, including approximately 100 new to science and another 100 never previously reported from the Southern Ocean.

To collect our abundance data, we counted between 7000 and 9000 specimens per samples (i.e until the species accumulation curve actually flattens). Extrapolation using Chao1 or ACE methods (Chao, 1984; Chao and Lee, 1992) suggests that between 80 and 90% of the taxa present in the assemblage are actually being recorded in our count data. We are thus quite confident that we are successfully capturing a reasonably complete quantitative dataset on this fauna.

Testing the accuracy of classic paleodiversity reconstruction methods

We compared our results to two datasets extracted from the Neptune database of previously published DSDP-ODP microfossil data (Lazarus 1994; Spencer-Cervato 1999); one 'Full Antarctic' using all data below 40°S, the other using only data from the Kerguelen Plateau). We used standard statistical tools for paleodiversity reconstructions (e.g. Alroy et al, 2001; Rabosky and Sorrhannus, 2009): subsampling either by specimens (classical rarefaction, CR) or by collections (unweighted, UW, occurence-weighted, OW, or occurrence-squared-weighted, O2W) and range-through diversity based on boundary-crossers (Foote, 2000). These subsampling methods are frequently used in paleobiology literature: they are supposed to correct the data to account for the unequal sampling of the fossil record.

Subsampling the Neptune data seem relatively successful in retrieving our diversity pattern (Figure 2 - compare B and C to A), despite the presence of some small secondary, artefactual trends. Yet, when we compute extinction and origination rates (Figure 3), the equivalence between our whole-fauna analysis and the subsampling-based methods declines (compare A and D to B, C and E, F; respectively).

The most probable explanation for such a divergence is the common use (in the data contained in databases such as Neptune) of checklists of biostratigraphic markers instead of true fauna inventories: instead of subsampling data collected to be representative of the actual assemblages,

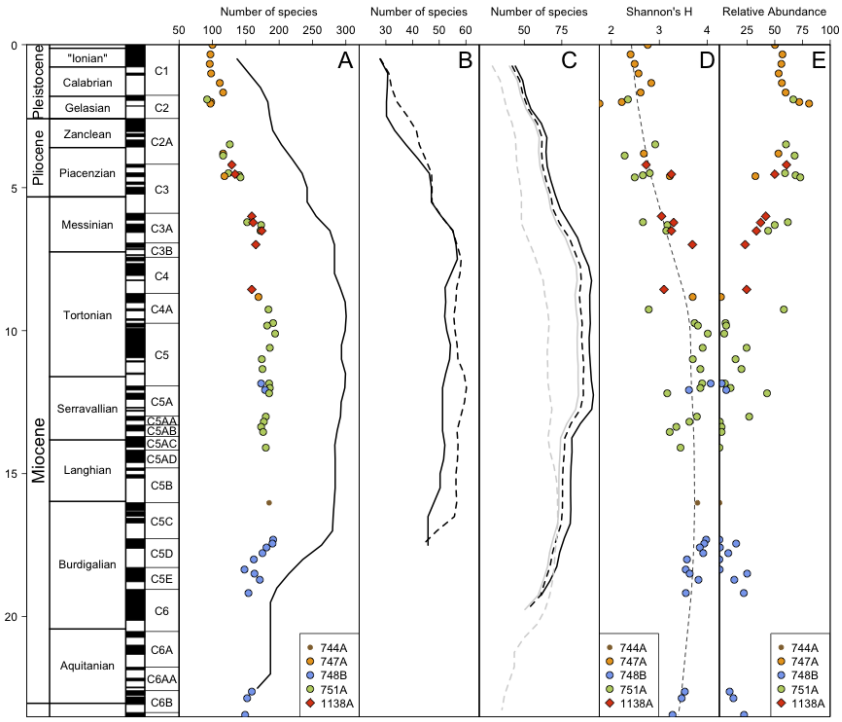

Figure 2: Antarctic Neogene radiolarian diversity. A. Whole-Fauna Dataset: Species richness in samples along with range-through diversity (using boundary-crossers) (black line). B. Kerguelen-Only Neptune dataset: range-through diversity (using boundary-crossers) based on UW (black line) and OW (dotted line) subsampled data. C. Complete Antarctic Neptune dataset: range-through diversity (using boundary-crossers) based on UW (black line), OW (black dotted line), CR (grey line) and O2W (grey dotted line) subsampled data. D. Shannon's H Index for the Whole-Fauna dataset with Loess regression curve. E. Relative abundance of the Antarctissids (genera Antarctissa and Helotholus) in percentage.

we subsample data pre-screened to emphasize only a subset of species.

Checklists used for Antarctic Neogene radiolarians are classically composed of ca 20 to 40 biostratigraphic markers and ca 50 to 100 'wildcard' taxa, depending mostly on the paleontologist's own interest: the pre-screening is thus here moderate, hence a rather accurate main diversity trend. Extinction and origination rates, however, being more sensitive derived data, are not accurate.

Implications of the diversity pattern

The diversity trend found with our whole-fauna dataset shows a strong decrease starting in the Messinian, at ca 6/5.5 Ma Figure 2A). As seen with Shannon's evenness index (Figure 2D), it is preceded (starting at the end of the Tortonian, at ca.8/7Ma) by a change in the community structure, most specificly an increase in dominance.

The evenness drop itself is directly linked to the rise of the Antarctissids (i.e. genera Antarctissa and Helotholus), which dominate the assemblages since ca 8Ma (Figure 2). Diversity loss appears to be thus preceded by ecologic reduction in relative abundance.

The triggering event of this episode is yet to be found. However, the Late Miocene Carbon Shift (recognized in subantarctic material at ca 7.7Ma in Tedford and Kelly, 2004) might be a putative lead.

Outlook

Counting will continue throughout most of the first semester of 2011 in order to obtain a sufficient number of stratigraphic sequences so we can proceed, by the summer, with the planned biostratigraphical analysis using the CONOP method: as seen with the diversity trend of our fauna, the end Miocene/early Pliocene was marked by a strong change in the community composition, hence a large number of bioevents in perspective. Substantial work is still also needed to document our new, more exhaustive taxonomy for Antarctic Neogene radiolarians (mostly new species description).

References:

J. Alroy et al, 2001. Effects of sampling standardization on estimates of Phanerozoic marine diversification, *PNAS*, 98(11): 6261-6266.

A. Chao, 1984. Non-parametric estimation of the number of classes in a population. *Scandinavian Journal of Statistics*, 11: 265-270.

A. Chao, S. M. Lee, 1992. Estimating the number of classes via sample coverage. *Journal of American Statistical Association*, 87: 210-217.

M. Foote, 2000. Origination and extinction components of taxonomic diversity: general problems, *Paleobiology*, 26(sp4): 74-102.

D. B. Lazarus, 1994. Neptune: a Marine Micropaleontology Database. *Mathematical Geology*, 26(7): 817-832.

A. H. Orsi, T. Whitworth III, W. D. Nowlin Jr, 1995. On the meridional extent and fronts of the Antarctic Circumpolar Current, *Deep-Sea Res.*, 42(5): 641-673.

D. L. Rabosky, U. Sorhannus, 2009. Diversity dynamics of marine planktonic diatoms across the Cenozoic, *Nature*, 457: 183-187.

C. Spencer-Cervato, 1999. The Cenozoic Deep Sea Microfossil Record: explorations of the DSDP/ODP sample set using the Neptune datasbase. *Palaeontologica Electronica*, 2(2): 268pp.

R. A. Tedford, D. C. Kelly, 2004. A deep-sea record of the late Miocene carbon shift from the Southern Tasman Sea. *Geophysical Monograph*, 151: 273-290.

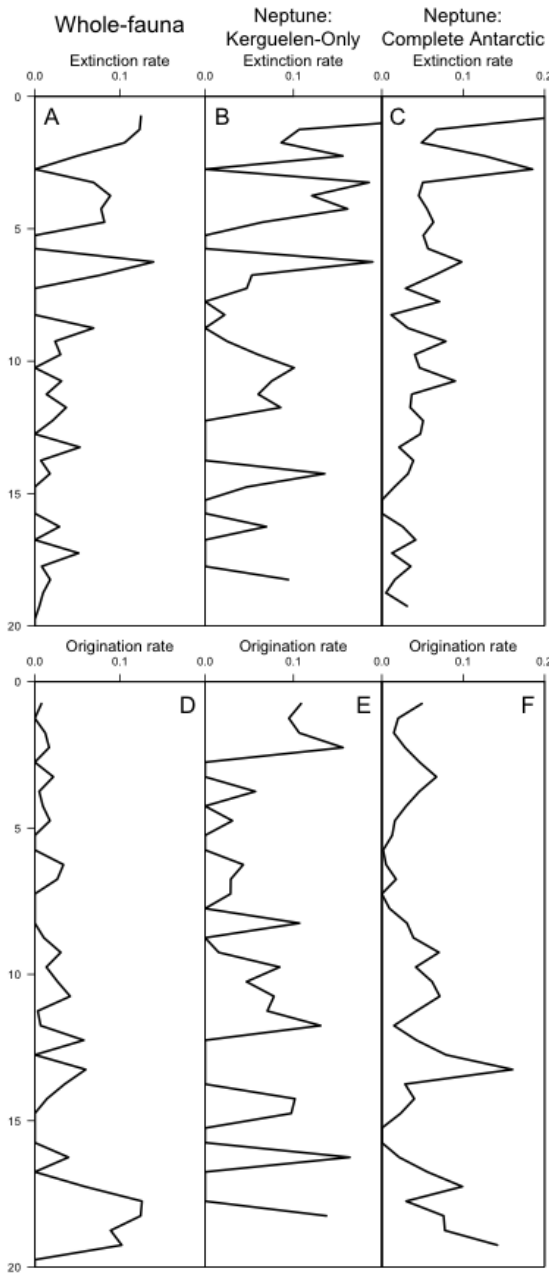

Figure 3: Extinction and Origination Rates for our whole-fauna dataset (A and D, respectively), the Kerguelen-Only Neptune dataset (B and E) and the complete Antarctic Neptune dataset (C and F).

ICDP

Geochemical fingerprints of an evolving oxic atmosphere in the Paleoproterozoic– A sulfur isotope approach

M. REUSCHEL[1], H. STRAUSS[1], V.M. MELEZHIK[2, 3], A. LEPLAND[2], L.R. KUMP[4]

[1] Westfälische Wilhelms-Universität Münster (Germany)
[2] Geological Survey of Norway (Norway)
[3] Centre for Geobiology, University of Bergen (Norway)
[4] Pennslvanina State University, Department of Geosciences (United States of America)

The availability of free oxygen in the modern Earth's atmosphere distinguishes our planted from all others in the solar system. It makes the Earth to a comfortable living space for multicellular organisms, like plants, fungi and animals. However, shortly after its formation, some 4.5 billion years ago, the planet Earth must also have been devoid of oxygen like its neighbors. The unraveling of those processes that lead to the development of this complex world around us, from its lifeless beginnings to its modern diversity is a great challenge for Earth system science.

It is by now accepted, but not collectively, that the initial and irreversible rise in atmospheric oxygen occurred in the early Palaeoproterozoic, between 2.45 and 2.32 Ga (Guo et al., 2009, Papineau et al., 2007, Bekker et al., 2004). This is right in the time interval between 2.5 and 2.0 Ga, the Archean-Paleoproterozoic transition (APT), which represents one of the most critical periods in Earth history. Fundamental changes in the biogeochemical cycles of redox sensitive elements like carbon, sulfur, iron or phosphorus characterize this time period together with geotectonic and climatic upheavals.

From the geochemists point of view, there are plenty of approaches to constrain the redox conditions in ocean and atmosphere, but up to now only sulfur isotope data can provide a trustworthy number on the oxygen concentration in the Earth's atmosphere. The occurrence of mass independent fractionation of sulfur isotopes (MIF-S) among the minor stable isotopes of sulfur (^{33}S and ^{36}S) in sulfur bearing minerals constrains the concentration of atmospheric oxygen to < 10^{-5} PAL (present atmospheric level) (Farquhar et al., 2000, Pavlov and Kasting, 2002). The loss of the MIF-S signal is thought to mirror the rise in atmospheric oxygen, as far as MIF-S can only be produced, transferred and archived in Earth surface environments in an anoxic atmosphere and hydrosphere. A further consequence of the Earth's atmospheric oxygenation and the concomitant onset of oxidative weathering of sulfides, the oceanic sulfate concentration began to rise. This process significantly affected the sulfur cycling in the marine realm. With the increasing availability of sulfate in the water column, the microbial turnover of sulfate, associated with a significant mass dependent sulfur isotope fractionation, became more and more important and altered the sulfur isotope composition of water column sulfate and the reduced sulfur pool, preserved in sedimentary sulfate minerals and sulfides.

The Russian part of the Fennoscandian Shield provides exceptional rock successions of the Paleoproterozoic, spanning nearly 700 Ma of Earth history. The rocks provide a unique record of the APT and thus help to further investigate the geotectonic, climatic and biochemical

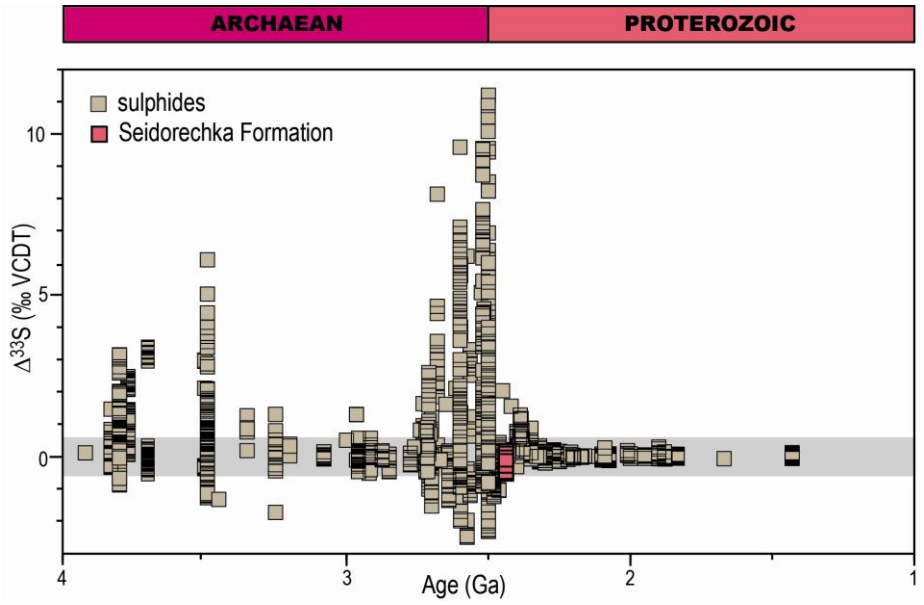

Fig.1. Variations in $\Delta^{33}S$ throughout the first 4 Ga of Earth history. The grey bar indicates the range of mass dependent sulfur isotope fractionation. Data from the Seidorechka Formaion is shown with pink squares. (Literature data: cf. Farquhar et al., 2010)

changes during that time (Melezhik et al., 2005). In summer 2007, the ICDP FAR-DEEP (Fennoscandian Arctic Russia - Drilling Early Earth Project) drilled 15 holes in three areas of the Fennoscandian Shield. Two of these are situated in the Kola Peninsula, including the Pechenga Greenstone Belt located in the north-west, close to the Norwegian boarder, and the Imandra/Varzuga Greenstone Belt, in the south-east. The third drilling area, the Onega basin, is located in Karelia. A total of 3650 m of drill core has been stored and archived at the Norwegian Geological Survey in Trondheim. To date, more than 300 samples (archive samples and selected samples) have been

studied for their sulfur geochemistry, including total sulfur abundances and sulfur isotope measurements for monosulfide sulfur, pyrite sulfur and carbonate-associated sulfate (CAS).

The Seidorechka Sedimentary Formation from the Imadra/Varzuga Greenstone Belt represents the oldest formation of the FAR-DEEP succession with an age constraint of ca. 2.44 Ga (U-Pb, Amelin et al., 1995). This formation could still capture the interval of Earth's initial oxygenation of the Earth's surface environments. Hence, 50 samples (archive and research samples and outcrop material) have been analyzed for their sulfur isotopic composition. Sulfide $\delta^{34}S$ varies between -15.1 and +3.3 ‰ with distinct temporal variations. The overall range in $\delta^{34}S$ throughout the succession indicates bacterial sulfate reduction in the depositional environment with low seawater sulfate concentrations. For a subset of 16 samples multiple sulfur isotopes (^{32}S, ^{33}S, ^{34}S amd ^{36}S) have been measured. MIF-S (i.e $\Delta^{33}S$) values range between 0.06 and -0.42 ‰ (with an average of -0.20±0.15 ‰) (Fig.1). These small, but still significant deviations from mass dependent fractionated signatures in $\Delta^{33}S$, combined with a $\Delta^{33}S/\Delta^{36}S$ plot clearly reveal the influence of MIF-S producing reactions in the atmosphere for the Seidorechka sulfides. It is therefore suggested that the atmospheric oxygen concentration was still below 10^{-5} PAL, low enough for UV induced photochemistry of SO_2 to cause MIF-S in atmospheric sulfur species. The largely negative character of the $\Delta^{33}S$ suggests a dominance of oxidized sulfur species in the atmosphere, since the reduced species and elemental sulfur carry a positive anomaly in $\Delta^{33}S$. The negative $\Delta^{33}S$ signature could thus be a sign of low concentrations of elemental sulfur in the atmosphere and this in turn could point to a low concentration of reduced gases like CH_4 and H_2 in the atmosphere. The dominance of oxidized sulfur species in the atmosphere and subsequently in the hydrosphere has likely stimulated bacterial sulfate reduction together with increasing availability of sulfate in the depositional environment. This in turn triggered the anaerobic oxidation of methane, which would have drawn down the methane concentration of the hydrosphere and finally in the atmosphere. Because methane is a greenhouse gas, its drawdown would lead to a cooling of Earth's surface and may have triggered the onset of the Huronian Glaciation, represented by the glacial deposits of the overlying Polisarka Sedimentary Formation on the Fennoscandian Shield and elsewhere in the world.

The Polisarska Sedimentary Formation overlies the 2.44 Ga Seidorechka Volcanic Formation and its sedimentary rocks are thought to be of glacial origin, reflecting the Fennoscandian equivalent of the Huronian glaciation. The isotopic composition of the sulfides ranges between -30.7 and -2.4 ‰. Although the major part of the succession is suggested to display high influence of a igneous sulfur source ($\delta^{34}S$=-1.6±1.5 ‰), the lower part shows fractionated sulfur isotope data with an average $\delta^{34}S$ of -16.7±7.5 ‰. This pronounced negative sulfur isotope compositions are indicative of enhanced microbial turnover of sulfate.

Rocks recovered in the Onega basin during FAR-DEEP drilling include the Tulomozero Formation dolostones and siliciclastic sediments with abundant Ca-sulfates. 32 carbonate samples of the 2.0 Ga Tulomozero Formation from the drillcores 10A, 10B and 11A have been selected for CAS extraction. The carbonates are suggested to represent a shallow marine sabkha environment and as the

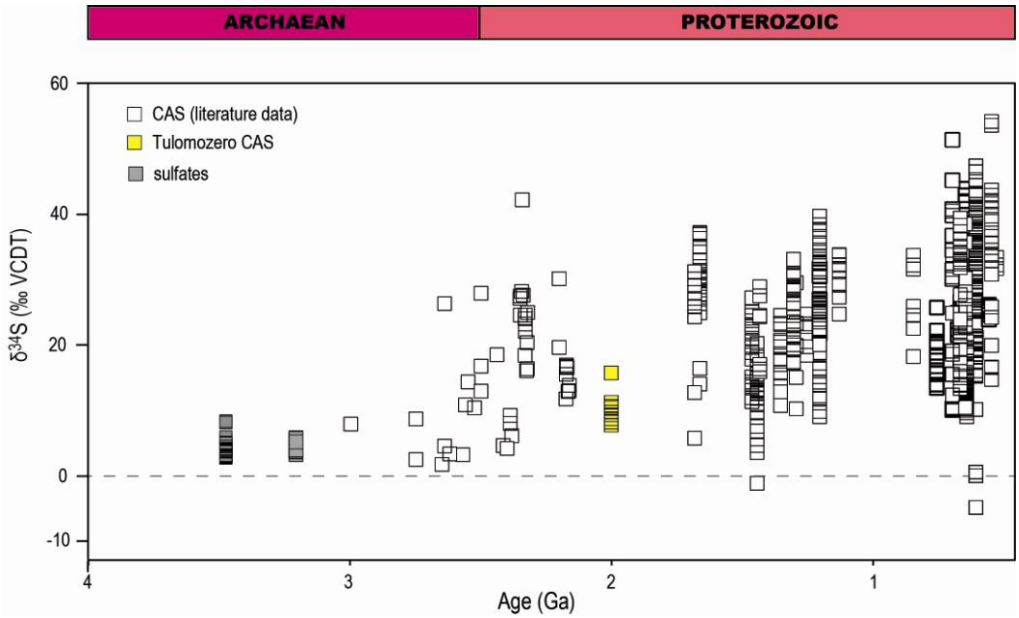

Fig. 2.: The carbonate associated sulfate sulfur isotope record throughout the Precambrian. CAS sulfur isotope data obtained from the Tulomozero Formation is marked with yellow squares. The grey squares show sedimentary sulfate sulfur isotope data by Shen et al., (2001) and Bao et al., (2007). Literature data: Chu et al., (2007), Domagal-Goldman et al. (2009), Gellatly and Lyons (2005), Guo et al., (2009), Goldberg et al., (2005), Fike et al., (2006), Hurtgen et al., (2000, 2005), Kah et al. (2004), Kaufman et al., (2007), McFadden et al., (2008), Shen et al., (2008).

incorporation of sulfate in the carbonate lattice is not associated with a substantial sulfur isotope fractionation effect, the gained sulfur isotope data should reflect the sulfate isotopic composition of the coeval seawater sulfate (e.g. Burdett et. al., 1989, Kampschulte et al., 2001, Gellatly and Lyons, 2005, Guo et al., 2009). The CAS data of the Tulomozero carbonates provide an unique opportunity to constrain the seawater sulfate sulfur isotope composition some 400 Ma after the initial rise in atmospheric O_2. However only 8 samples yielded measurable amounts of CAS and CAS abundance varied between 65 and 310 ppm. Modern carbonates yield CAS concentrtions up to 1000 ppm, but up to now the incorporation mechanism for seawater sulfate in carbonates is still ambigeous. The highly variable CAS content is suggested to be owed to extensive meteoric diagenesis (Gill et al., 2008), which affected the shallow water carbonates during exposure to air. The diagenesis however does not change the sulfur isotopic composition of the CAS (Gill et al., 2008), and thus the observed $\delta^{34}S$ (av. 10.9±2.7 ‰) should mirror the water column sulfate.

The observed $\delta^{34}S_{SO4}$ values of the Tulomozero Formation are considerably different from the values observed in Archean strata (Fig. 2). It is suggested that bacterial sulfate reduction in the anoxic part of the water column shifted the sulfur isotopic composition of the seawater sulfate towards more positive values (Fig. 2), presumably since 3.5 Ga (Shen et al., 2001). But the dominance of this sulfur metabolism is suggested to have started in response to an increasing availability of sulfate in the water column after the initial rise in atmospheric oxygen around 2.4 Ga. The homogeneity of the $\delta^{34}S$ data throughout the Tulomozero Formation indicates that a substantial seawater sulfate reservoir most likely existed only 400 Ma after this initial rise in atmospheric oxygen. Pseudomorphs after sulfate evaporites throughout the Tulomozero Formation (Melezhik et al., 2005b) further underline the existence of a seizeable seawater sulfate reservoir at that time.

The redox-evolution of the atmosphere can be traced sucessfully with the geochemical fingerprints of sulfur bearing minerals preserved in FAR DEEP core material, showing that the rise in atmospheric oxygen in the Early Paleoproterozoic changed the system Earth fundamentaly.

References:

Amelia, Y.V., Heaman, L.M., Semenov, V.S. (1995) U–Pb geochronology of layered mafic intrusions in the eastern Baltic Shield: implications for the timing and duration of Paleoproterozoic continental rifting. Precambrian Res. 75, 31–46.

Bao, H., Rumble, D., Lowe, D.R. (2007) The five stable isotope compositions of Fig Tree barites: implications on sulfur cycle in ca. 3.2. Ga oceans. Geochim.Cosmochim. Acta 71, 4868-4879.

Chu, X., Zhang, T., Zhang, Q., Lyons, T.W. (2007) Sulfur and carbon isotope records from 1700 to 1800 Ma carbonates of the Jixian section, northern China: implications for secular isotope variations in Proterozoic seawater and relationships to global supercontinents. Geochim. Cosmochim. Acta 71, 4668-4692.

Bekker, A., Holland, H.D., Wang, P.L., Rumble, D., Stein, H.J., Hannah, J.L., Coetzee, L.L., Beukes, N.J. (2004) Dating the rise of atmospheric oxygen. Nature 427. 117-120.

Burdett J. W., Arthur M. A. and Richardson M. (1989) A Neogene seawater sulfur isotope age curve from calcareous pelagic microfossils. Earth Planet. Sci. Lett. 94, 189–198.

Domagal-Goldman, S.D., Kasting, J.F., Johnston, D.T., and Farquhar, J. (2008) Organic haze, glaciations and multiple sulfur isotopes in the Mid-Archean Era. Earth and Planetary Science Letters 269, 29–40.

Farquhar, J., Bao, H.M., Thiemens, M. (2000) Atmospheric influence of Earth's earliest sulfur cycle. Science 289, 756–758.

Farquhat, J., Wu, N, 2010

Gellatly A. M., Lyons T. W. (2005) Trace sulfate in mid-Proterozoic carbonates and sulfur isotope record of biospheric evolution. Geochim. Cosmochim. Acta 69, 3813–3829.

Gill, B., Lyons, T.W., Frank, T.D. (2008) Behavior of carbonates associated sulfate during meteoric diagenesis and implications for the sulfur isotope paleoproxy. Geochim. Cosmochim. Acta 72, 4699-4711.

Guo, Q., Strauss, H., Kaufman, A.J., Schröder, S., Gutzmer, J., Wing, B., Baker, M.A., Bekker, A., Jin, Q., Kim, S., Farquhar, J. (2009) Reconstructing Earth's surface oxidation across the Archean Paleoproterozoic transition. Geology 37, 399-402.

Goldberg, T., Poulton, S.W., Strauss, H. (2005) Sulphur and oxygen isotope signatures of late Neoproterozoic to early Cambrian sulphate, Yangtze

Platform, China: diagenetic constraints and seawater evolution. Precamb. Res. 137, 223-241.
Fike, D.A., Grotzinger, J.P., Pratt, L.M., Summons, R.E. (2006) Oxidation of the Ediacaran ocean, Nature 444, 744-747.
Hurtgen, M.T., Arthur, M.A., Suits, N.S., Kaufman, A.J. (2002) The sulfur isotopic composition of Neoproterozoic seawater sulfate: implications for a snowball Earth? EPSL 203, 413-429.
Hurtgen, M.T., Halverson, G.P., Arthur, M.A., Hoffman, P.F. (2005) Sulfur cycling in the aftermath of a 635-Ma snowball glaciation: evidence for a syn-glacial sulfidic deep ocean. EPSL 245, 551-570.
Kampschulte A., Bruckschen P. and Strauss H. (2001) The sulphur isotopic composition of trace sulphates in Carboniferous brachiopods: implications for coeval seawater, correlation with other geochemical cycles and isotope stratigraphy. Chem. Geol. 175, 149–173.
Kaufman, A.J., Corsetti, F.A., Varni, M.A., (2007) The effect of rising atmospheric oxygen on carbon and sulfur isotope anomalies in the Neoproterozoic Johnnie Formation, Death Valley, USA. Chem. Geol. 237, 47-63.
Kah, L.C., Lyons, T.W., Frank, T.D. (2004) Low marine sulphate and protracted oxygenation of the Proterozoic biosphere. Nature 431, 834-838.
McFadden, K.A., Huang, J., Chu, X., Jiang, G., Kaufman, A.J., Zhou, C., Yuan, X., Xiao, S. (2008) Pulsed oxidation and biological evolution in the Ediacaran Doushantuo Formation. PNAS 105, 3197-3202.
Melezhik, V.A., Fallick, A.E., Hanski, E.J., Lepland, A., Prave, A.R., Strauss, H. 2005a: Emergence of the aerobic biosphere during the Archean-Proterozoic transition: Challenges of future research. GSA Today,15,4.
Melezhik, V.A., Fallick, A.E., Rychanchick, D.V., Kuznetsov, A.B. (2005) Palaeoproterozoic evaporites in Fennoscandia: implications for seawater sulphate, the rise of atmospheric oxygen and local amplification of the $\delta^{13}C$ excursion. Terra Nova 17, 141-148.
Ohmoto, H., Watanabe, Y., Ikemi, H. Poulson, S.R., Taylor, B.E. (2006) Sulphur isotope evidence for an oxic atmosphere. Nature 442, 908-911.
Papineau, D., Mojzsis, S.J. Schmitt, A.K. (2007) Multiple sulfur isotopes from Paleoproterozoic interglacial sediments and the rise of the atmospheric oxygen. Earth a. Planetary Science Letters 255, 188-212.
Pavlov, A.A., Kasting, J.F., 2002. Mass-independent fractionation of sulfur isotopes in Archean sediments: strong evidence for an anoxic Archean atmosphere. Astrobiology 2, 27–41.
Shen, Y., Buick, R., Canfield, D.E. (2001) Isotopic evidence for microbial sulphate reduction in the early Archaean era. Nature 410, 77-81.
Shen, B., Xiao, S., Kaufman, A.J., Bao, H, Zhou, C., Wang, H. (2008) Stratification and mixing of a post glacial Neoproterozoic ocean: evidence from carbon and sulfur isotopes in a cap dolostone from Northwest China. EPSL 265, 209-228.

IODP

Onset of Quaternary glaciations near 3 Ma induced by final closure of Panama and reduction of atmospheric CO2

M. SARNTHEIN[1]

[1] Institut für Geowissenschaften, Universität Kiel, D 24098 Kiel, Germany

Various models and paleoceanographic records suggest that the climatic deterioration between 3.1 Ma and 2.82 (MIS G10) – 2.72 Ma (MIS G6) was possibly linked to both a major decrease in atmospheric CO2 and the final closure of the Central American Seaways (CAS). The latter forcing is inferred from rising salinity contrasts between the Caribbean and the equatorial East Pacific (Groeneveld, 2005). Each closing event strengthened the poleward transport of salt and heat in the North Atlantic (warmings of 2° – 3°C), thus enhanced meridional overturning circulation and in turn, reduced the atmospheric CO_2 level. Also, the closing led to a slight rise in the poleward atmospheric moisture transport to northwest Eurasia. Most important, model and data show that the final closure of the CAS implied a major drop in sea surface salinity and rise in the stratification and steric height of the subarctic North Pacific. Consequently, CO_2 outgassing from the North Pacific was barred and the low-saline Arctic Throughflow from the Bering Strait to the East Greenland Current (EGC) at least doubled. This throughflow resulted in reduced sea surface salinity and increased sea-ice cover in the Arctic Ocean, thus promoting polar albedo, a crucial feedback, and the build-up of continental ice sheets, in harmony with the effect of reduced atmospheric CO_2. This trend toward Quaternary-style conditions was corroborated by an abrupt and irreversible cooling of the East Greenland Current by 6°C and freshening by 2 psu from 3.2–~3.05 Ma, right after a first but still short-lived full closing of CAS (Sarnthein et al., 2009; Sarnthein, subm. 2011).

References:

Groeneveld, J., 2005: Effect of the Pliocene closure of the Panamaian gateway on Caribbean and east Pacific sea surface temperatures and salinities by applying combined Mg/Ca and $\delta^{18}O$ measurements (5.6–2.2 Ma). – PhD Thesis University of Kiel.
Sarnthein, M., Bartoli, G., Prange, M., et al., 2009: Mid-Pliocene shifts in ocean overturning circulation and the onset of Quaternary-style climate. – Climate of the Past, 5 (2), 269-283.
Sarnthein, M., 2011: Ch. 8.16. History of Quaternary glaciations. Transition from Late Neogene to Early Quaternary environments. – Encyclopedia of Quaternary Sciences, 2nd Edition. J. Ehlers, edit., 30 ms-pp. (subm.)

IODP

African climate changes during C_4 plant evolution and expansion

E. SCHEFUß, L. DUPONT, F. ROMMERSKIRCHEN

MARUM – Center for Marine Environmental Sciences, University of Bremen. Leobener Str. DE-28359 Bremen

Climatic changes in the Earth's history are responsible for the evolution and distribution of vegetation types on the continents. In general, the atmospheric pCO_2 level, temperature, amount and seasonality of precipitation are major factors to control the balance between two types of plants using different carbon fixation pathways for photosynthesis. Most trees, shrubs and temperate grasses are C_3 plants evolved during times of high pCO_2 levels and preferring a relatively cool and humid climate, while most tropical grasses and sedges are C_4 plants thriving in warm and dry regions and have adapted to low pCO_2 levels due to an additional CO_2-concentrating mechanism (e.g. Ehleringer et al. 1997, Sage 2004). The evolution of plants using C_4 photosynthesis occurred independently in several groups potentially triggered by a sharp drop in global pCO_2 level during the Oligocene between 34 and 23 Ma BP (Edwards et al. 2010). However, global C_4 plant expansion delayed until the late Miocene/Pliocene boundary (6-8 Ma) and took place under climatic conditions of general global cooling and relatively stable levels of pCO_2 similar to the present (Tipple & Pagani 2007). The temporal mismatch between the large-scale expansion of C_4 grasslands and globally low pCO_2 levels leaves the causes of the C_4 plant evolution unexplained. It has been suggested that enhanced low-latitude aridity and changes in seasonal precipitation patterns might play a yet underestimated role in driving large-scale vegetation changes (Pagani et al. 1999).

The aim of the project is to characterize the climatic and environmental evolution in the Miocene and how these changes have been linked to the C_4 plant expansion. The focus of our studies lies on marine sediment cores of the South-East Atlantic receiving predominantly aeolian-transported terrestrial material from areas in southern Africa. The study area is sensitive to changes in the ocean circulation and Antarctic ice expansion. Previous published pollen records suggested a late Miocene change in vegetation composition to enhanced occurrence of arid plant types along the Namibian coast and the Cape region (Coetzee 1986).

To reconstruct time-series of environmental changes, a variety of organic geochemical techniques combined with marine palynology have been applied to sediment samples of several ODP cores, in particular ODP Site 1085 situated in front of the Orange River mouth. Sedimentary pollen and spore assemblages provide evidence about changes in the extension of tropical forest, fynbos, dry forest, savannahs, grasslands, and deserts. Stable carbon and hydrogen isotope analyses of terrestrial plant waxes record the relative terrestrial proportion of C_4 and C_3 plants in the vegetation cover and hydrological changes on the continent, respectively. In addition, we studied the development of the southern Benguela upwelling system from the middle Miocene to the early Pliocene using two different sea temperature proxies, $Temp_{TEX}$ (after Schouten et al. 2002 and Kim et al. 2010) and SST_{UK} (after Prahl & Wakeman 1987 and Müller et al. 1998) in combination with total organic carbon measurements and a proxy for fluvial discharge, the BIT index (after Hopmans et al. 2004) reflecting relative soil organic matter contributions.

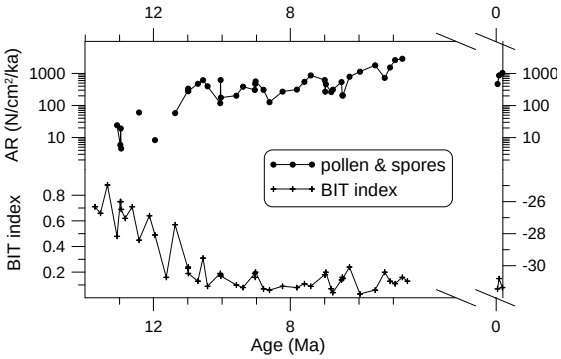

Figure 1. BIT index (crosses) and accumulation rates (AR) of total pollen and spores on a ^{10}log scale (black dots) of ODP Site 1085 against age (Ma). Youngest samples are of late Pleistocene age.

Terrestrial organic matter was brought to ODP Site 1085 via fluvial transport by the adjacent Orange River and via aeolian transport by easterly winds. As a proxy for relative fluvial soil run-off the BIT index indicates a decrease in the contribution of organic matter by the river until 10 Ma (Fig. 1). After 10 Ma the low BIT index values suggest that the fluvial organic matter contribution almost completely ceased or deflected due to changing current patterns. The increase in pollen and spore accumulation rates, however, indicates an increasing terrestrial contribution, probably by more vigorous easterly or south-easterly winds after 11 Ma. The increased trade wind strength might have led to increased marine productivity and cooling of sea surface temperatures in association with intensified Benguela upwelling.

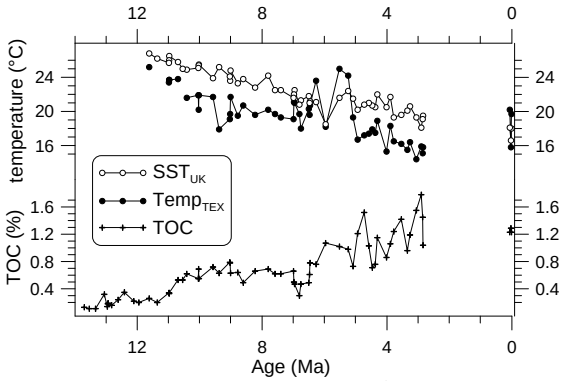

Figure 2. Water temperature estimates after the alkenone based $U^{K'}_{37}$ index (SST_{UK}, open circles), the TEX_{86} index ($Temp_{TEX}$, black dots), and total organic carbon (TOC, crosses) in weight percentages at ODP Site 1085.

The initiation of Benguela upwelling has been dated in the late Miocene (e.g. Siesser 1980), but estimates of its sea surface temperature evolution are not available. In concordance with global cooling during the Miocene, SST_{UK} and $Temp_{TEX}$ exhibit a decline of about 8 and 16°C, respectively (Fig. 2). The temperature trends suggest an inflow of cold Antarctic waters triggered by Antarctic ice sheet expansion and intensification of Southern Hemisphere southeasterly winds. A temperature offset between both proxies developed with the onset of upwelling, which can be explained by differences in the habitat of the organisms that produce the temperature records, SST_{UK} and $Temp_{TEX}$: alkenone-producing phytoplankton live in the euphotic zone and record sea-surface temperatures (SST_{UK}), while Thaumarchaeota are displaced to colder sub-surface waters in upwelling-influenced areas and record sub-surface water temperatures ($Temp_{TEX}$). We suggest that variations in sub-surface water temperatures were driven by advection of cold Antarctic waters and thermocline adjustments. Decline in surface temperatures, increased offset between the temperature proxies and increase in primary productivity (Diester-Haass et al. 2004) suggest establishment of Benguela upwelling at 10 Ma. During the Messinian Salinity Crisis, between 7 and 5 Ma, however, surface and sub-surface temperature estimates became similar, likely due to a strong reduction in the Atlantic overturning circulation. During the Pliocene the offset between the temperature estimates and the cooling trend was re-established.

The stable carbon isotope ratios of sedimentary odd carbon-numbered long-chain *n*-alkanes with carbon number of 27 to 33 ($\delta^{13}C_{wax}$) are in the typical range for plant leaf waxes. The $\delta^{13}C_{wax}$ values exhibit a continuous increase from -30 ‰ at around 13 Ma to -27 ‰ at the end of the late Miocene (Fig. 3). Typical of modern African plants are $\delta^{13}C_{wax}$ values of around -21 ‰ for C_4 grasses (Rommerskirchen et al. 2006) and, -37.1 ‰ and -33.8 ‰ for rain forest and savannah C_3 plants, respectively (Vogts et al. 2009). These values suggest a Miocene contribution of C_4 plants of 30-50 % compared to the Pleistocene contribution of around 70 %. However, the shift in $\delta^{13}C_{wax}$ is also in the range of C_3 plants growing under conditions varying from closed canopy to open vegetation (Medina & Minchin 1980). Pollen records show a high relative abundance of grass pollen already between 11 and 10 Ma and between 7 and 5 Ma. The high grass pollen percentages

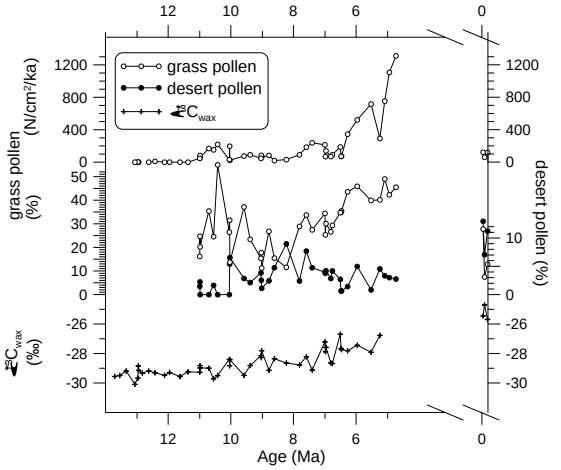

Figure 3. Vegetation records of ODP Site 1085 against age (Ma). Bottom, stable carbon isotope ratios of long-chain odd carbon-numbered *n*-alkanes in the carbon number range from 27 to 33 ($\delta^{13}C_{wax}$) in pro mille against the V-PDB standard (crosses). Middle, percentages of total pollen and spores of desert plants (black dots, right axis) and grasses (open circles, left axis). Top, grass pollen accumulation rates (AR) in grains (N) per square cm and per 1000 year (ka).

and the pollen assemblages indicate an open vegetation cover in southwestern Africa from the beginning of the record in the middle Miocene. Increasingly higher grass pollen accumulation rates occurred between 7 and 5 Ma. The combination of pollen and stable isotope results suggest a maximum in the development of C_4 grasslands around 6 Ma (Fig. 3). After 9-8 Ma terrestrial floral assemblages started to resemble those of the Pleistocene and the flora gradually got more affinity with that of the drier parts of the greater Cape Flora. Pollen percentages of desert plants are higher between 10 and 7 Ma and in the Pleistocene samples indicating that desert vegetation had increased in the late Pleistocene compared to the end of the Miocene. The increase in C_4 plants as recorded by the stable isotope composition might be the result of a shift from savannah grassland toward desert and semi-desert.

Preliminary stable hydrogen isotope analyses of plant waxes (δD_{wax}) indicate a pronounced aridification from about 10 Ma to 5 Ma, which is in concordance with the C_4 grass expansion at that time. The continental environmental changes are connected to the intensification of the Benguela upwelling current bringing cold, nutrient-rich waters from the sub-polar South Atlantic and the Antarctic circumpolar current, probably driven by the formation of the West Antarctic ice sheet. Overall, a stepwise aridification in southwestern Africa is in accordance with intensification and northward shifting of the subtropical high pressure cell of the Southern Hemisphere.

Combining the data from ODP Site 1085 (29°S) with limited data from ODP Site 1087 (32°S) and preliminary results from ODP Site 1081 (20°S), it becomes obvious that the C_4 plant expansion was delayed in the southernmost site, whereas it started around 8 Ma in the more northern sites. Results of all sites indicate that the C_4 plant expansion was not concluded in the Miocene and lasted into the Pliocene. The most well-defined shift is found in ODP Site 1081 and it appears that this more tropical (warmer) site shows a more pronounced increase of C_4 plants.

References:

Coetzee JA, 1986. Palynological Evidence for Major Vegetation and Climatic-Change in the Miocene and Pliocene of the Southwestern Cape. *South African Journal of Science* 82, 71-72.

Diester-Haass L, Meyers PA, Bickert T, 2004. Carbonate crash and biogenic bloom in the late Miocene: Evidence from ODP Sites 1085, 1086, and 1087 in the Cape Basin, southeast Atlantic Ocean. *Paleoceanography* 19, PA1007, 19p.

Edwards EJ, Osborne CP, Stromberg CAE, Smith SA, Consortium CG, 2010. The Origins of C-4 Grasslands: Integrating Evolutionary and Ecosystem Science. *Science* 328, 587-591.

Ehleringer JR, Cerling TE, Helliker BR, 1997. C_4 photosynthesis, atmospheric CO_2, and climate. *Oecologia* 112, 285-299.

Hopmans EC, Weijers JWH, Schefuss E, Herfort L, Sinninghe Damste JS, Schouten S, 2004. A novel proxy for terrestrial organic matter in sediments based on branched and isoprenoid tetraether lipids. *Earth and Planetary Science Letters* 224, 107-116.

Kim JH, Schouten S, Hopmans EC, Donner B, Damsté JSS, 2008. Global sediment core-top calibration of the TEX_{86} paleothermometer in the ocean. *Geochimica Cosmochimica Acta* 72, 1154-1173.

Medina E, Minchin P, 1980. Stratification of $\delta^{13}C$ values of leaves in Amazonian rain forest. *Oecologia* 45, 377-378.

Müller PJ, Kirst G, Ruhland G, von Storch I, Rosell-Melé A, 1998. Calibration of the alkenone paleotemperature index $U^{k'}_{37}$ based on core-tops from the eastern South Atlantic and the global ocean (60°N-60°S), *Geochimica Cosmochimica Acta* 62, 1757-1772.

Pagani M, Freeman KH; Arthur MA, 1999. Late Miocene atmospheric CO_2 concentrations and the expansion of C_4 grasses. *Science*, 285, 876-879.

Prahl FG, Wakeham SG, 1987. Calibration of unsaturation patterns in long-chain ketone compositions for paleotemperature assessment. *Nature* 330, 367-369.

Rommerskirchen F, Plader A, Eglinton G, Chikaraishi Y, Rullkotter J, 2006. Chemotaxonomic significance of distribution and stable carbon isotopic composition of long-chain alkanes and alkan-1-ols in C_4 grass waxes. *Organic Geochemistry* 37, 1303-1332.

Sage RF, 2004. The evolution of C_4 photosynthesis. *New Phytologist* 161, 341-370.

Schouten S, Hopmans EC, Schefuß E, Sinninghe Damsté JS, 2002. Distributional variations in marine crenarchaeotal membrane lipids: a new tool for reconstructing ancient sea water temperatures. *Earth and Planetary Science Letters* 204, 265-274.

Siesser WG, 1980. Late Miocene origin of the Benguela Upwelling System off northern Namibia. *Science* 208, 283-285.

Tipple BJ, Pagani M, 2007. The early origins of terrestrial C_4 photosynthesis. *Annual Review of Earth and Planetary Sciences* 35, 435-461.

Vogts A, Moossen H, Rommerskirchen F, Rullkötter J, 2009. Distribution patterns and stable carbon isotopic composition of alkanes and alkan-1-ols from plant waxes of African rain forest and savanna C_3 species. *Organic Geochemistry* 40, 1037-1054.

IODP

Heterogeneous mantle underneath the North Atlantic: Evidence from water in spinel peridotite from different locations at the Mid-Atlantic Ridge

E. SCHMÄDICKE[1], J. GOSE[1], T.M. WILL[2]

[1] University of Erlangen-Nürnberg, GeoZentrum Nordbayern, Schlossgarten 5a, D-91054 Erlangen

[2] University of Würzburg, Geodynamics and Geomaterials Research Division, Am Hubland, D-97074 Würzburg

Contrasting water contents are present in nominally anhydrous minerals in oceanic spinel peridotite from the Mid-Atlantic Ridge near 15˚N (ODP-Leg 209) and 23˚N (ODP-Leg 153). Orthopyroxene in oceanic spinel peridotite from Leg 2

09 (site 1274A) contains only up to 16 wt.-ppm water that is bound as hydroxyl defect in the mineral structure (Table 1). In contrast, the orthopyroxene water content of peridotite from Leg 153 (site 920D) is one order of magnitude higher (up to 270 wt.-ppm). This value is identical with both, the water contents in sub-continental spinel peridotite xenoliths and the maximum amount of water that can be incorporated in enstatitic orthopyroxene

ODP sample number	Depth [mbsf]	Water content [wt.-ppm]
Leg 209		
1274A-6R3-72	33.54	12 16
1274A-7R1-95	36.75	10
Leg 153		
920D-15R1-80	124.70	189
920D-21R4-79	192.59	174 159
920D-22R4-27	193.70	233 200 270

Table 1. Water contents of orthopyroxene determined by quantitative infrared spectroscopy. Data of Leg 153 samples are from Gose et al. (2009)

Leg	209	153
residual opx, measured	16	270
melting degree	18 %	12 %
original opx, estimated	300	3500
original peridotite, estimated	120-130	1400-1500

Table 2. H_2O contents (wt.-ppm) of original orthopyroxene and peridotite prior to partial melting, estimated from the H_2O content of residual orthopyroxene measured in this study. The used modal composition is 25 % orthopyroxene (opx), 5 % clinopyroxene (cpx), and 70 % olivine (ol). The applied H partition coefficients are: 0.01 (mineral/melt), 0.1 (ol/opx), 1.5-2 (cpx/opx).

at pressures of the spinel-peridotite facies (c. 200-300 wt.-ppm; Rauch and Keppler, 2002).

The water contents in orthopyroxene from the sub-oceanic mantle at the Mid-Atlantic Ridge, which range from about 10-15 (= highly depleted) to nearly 300 wt.-ppm (= water saturation in orthopyroxene) compare well with the highly variable water contents of Atlantic MORB glass that also extend over one order of magnitude. Mineral trace element data indicate different degrees of partial melting: 18 % for peridotite samples from Leg 209 and 12 % for those from Leg 153. The mantle equilibrium temperatures differ by 200 ˚C (Leg 209: 1150-1200 ˚C, Leg 153: 950-1000 ˚C). The orthopyroxene water contents of Leg 209 are compatible with residual values after c. 18 % partial melting of a peridotitic source with a bulk rock water content of c. 120-130 wt.-ppm and of c. 300 wt.-ppm in the original orthopyroxene, respectively (Table 2). In contrast, the water content of 270 wt.-ppm in orthopyroxene of Leg 153 peridotite cannot be reconciled with residual amounts of water to be expected after 12 % partial melting. This is because an unrealistically high initial water content of c. 3500 wt.-ppm would be required for the original orthopyroxene – exceeding the water storage capacity of orthopyroxene at an ambient pressure of c. 20 kbar by one order of magnitude.

Thus, following earlier melt depletion, the water contents of Leg 153 peridotite must have re-equilibrated. Re-equilibration must have occurred in the spinel-peridotite facies. Modificaion of water contents by ocean-floor processes can be excluded. First, the diffusion of H in orthopyroxene is too sluggish (Stalder et al., 2007) at the temperatures ≤ 300 ˚C that were estimated for ocean-floor alteration (e. g. Alt and Shanks, 2003; Bach et al., 2004). Second, water incorporation in mantle minerals positively correlates with pressure (e. g. Rauch and Keppler, 2002), and the measured contents in Leg 153 samples as well as the calculated original values of Leg 209 samples reflect spinel-peridotite facies pressure conditions (but not ocean-floor conditions).

Re-equilibration of water in the spinel-peridotite facies may have been facilitated by a longer mantle residence time of Leg 153 peridotite (compared to Leg 209) after partial melting and prior to tectonic exhumation from c. 60 km depth. An extended mantle residence time is compatible with isobaric cooling from >1200 ˚C to 950-1000 ˚C (at c. 20 kbar pressure) as documented for Leg 153 peridotite and, furthermore, facilitates re-introduction of water from less or non-depleted mantle regions due to the high diffusivity of H.

References:

Alt, J.C., Shanks, W.C., 2003. Serpentinization of abyssal peridotites from the MARK area, Mid-Atlantic Ridge: Sulfur geochemistry and reaction modeling. Geochimica et Cosmochimica Acta 67, 641-653.

Bach, W., Garrido, C.J., Paulick, H., Harvey, J., Rosner, M., 2004. Seawater-peridotite interactions: First insights from ODP Leg 209, MAR 15°N: Geochemistry, Geophysics, Geosystems 5, Q09F26, doi: 10.1029/2004GC000744.

Gose, J., Schmädicke, E., Beran, A., 2009. Water in enstatite from Mid-Altantic Ridge peridotite: Evidence for the water content of suboceanic mantle? Geology 37, 543-546.

Rauch, M., Keppler, H., 2002. Water solubility in orthopyroxene. Contributions to Mineralogy and Petrology 143, 525-536.

Stalder, R., Purwin, H., Skogby, H., 2007. Influence of Fe on hydrogen diffusivity in orthopyroxene. European Journal of Mineralogy 19, 899-903

ICDP

Heavy mineral analysis of Archaean-Palaeoproterozoic rocks of the Fennoscandian Shield

K. SCHOLONEK[1], H. BAHLBURG[1], C. GÄRTNER[1], A. LEPLAND[2], V. MELEZHIK[2,3] AND THE FAR-DEEP SCIENTISTS[3]

[1] Westfälische Wilhelms-Universität Münster, Institut für Geologie und Paläontologie, Münster, Germany
[2] Geological Survey of Norway, Trondheim, Norway
[5] University of Bergen, Centre of Geobiology, Bergen, Norway

In order to contribute to the improvement of biostratigraphic age control for the Neogene sequences in the High Northern Latitudes we examined palynomorphs from ODP Hole 907A at a 100 kyr resolution. Diverse and well-preserved dinoflagellate cyst and acritarch assemblages, comprising 42 genera and 154 species are recorded for the period from 14.5 - 2.5 Ma. The section investigated has a good magnetostratigraphic age control (Channell et al., 1999), thus allowing us to firmly calibrate our identified dinocyst events to the Astronomical Tuned Neogene Timescale (ATNTS; Lourens et al., 2004). These dinocyst events have been compared with those recorded in other DSDP, ODP and IODP sites, and outcrops and boreholes from the U.S. East Coast, the adjacent North Sea and Mediterranean basins (Schreck et al., in prep.; Fig. 1).

Twenty two bioevents have been selected from Hole 907A, most of which are defined by the highest occurrence of species. Only taxonomically well-defined species have been chosen but a number of acritarchs and informally

described dinocyst taxa show a temporal distribution in Hole 907A and adjacent sites which may be promising as additional biostratigraphic markers. Comparison of these events across the Norwegian-Greenland Sea, North Atlantic and adjacent basins revealed that most are useful to correlate sequences on a regional scale but a number of events are suitable for supra- regional correlation of sequences.

References:
Zack, T., Moraes, R., Kronz, A., 2004. Temperature dependence of Zr in rutile: empirical calibration of a rutile thermometer. Contributions to Mineral and Petrology 148: 471-488.
Smythe, D. J., Schulze, D. J., Brenan, J. M., 2008. Rutile as kimerlite indicator mineral: minor and trace element geochemistry. 9. International Kimberlite Conference Extended Abstract, no. 9 IKC-A00193.

Twenty two bioevents have been selected from Hole 907A, most of which are defined by the highest occurrence of species. Only taxonomically well-defined species have been chosen but a number of acritarchs and informally described dinocyst taxa show a temporal distribution in Hole 907A and adjacent sites which may be promising as additional biostratigraphic markers. Comparison of these events across the Norwegian-Greenland Sea, North Atlantic and adjacent basins revealed that most are useful to correlate sequences on a regional scale but a number of events are suitable for supra- regional correlation of sequences.

References:
Channell, J.E.T., Amigo, A.E., Fronval, T., Rack, F. and Lehman, B., 1999. Magnetic stratigraphy at Sites 907 and 985 in the Norwegian-Greenland Sea and a revision of the Site 907 composite section. In: M.E. Raymo, E. Jansen, P. Blum and T.D. Herbert (Editors), Proceedings of the Ocean Drilling Program, Scientific Results 162, pp. 131-148.
Lourens, L., Hilgen, F., Shackleton, N.J., Laskar, J. and Wilson, J., 2004. The Neogene. In: F.M. Gradstein, J.G. Ogg and A.G. Smith (Editors), A geological timescale 2004. Cambridge University Press, Cambridge, U.K., pp. 409-430.

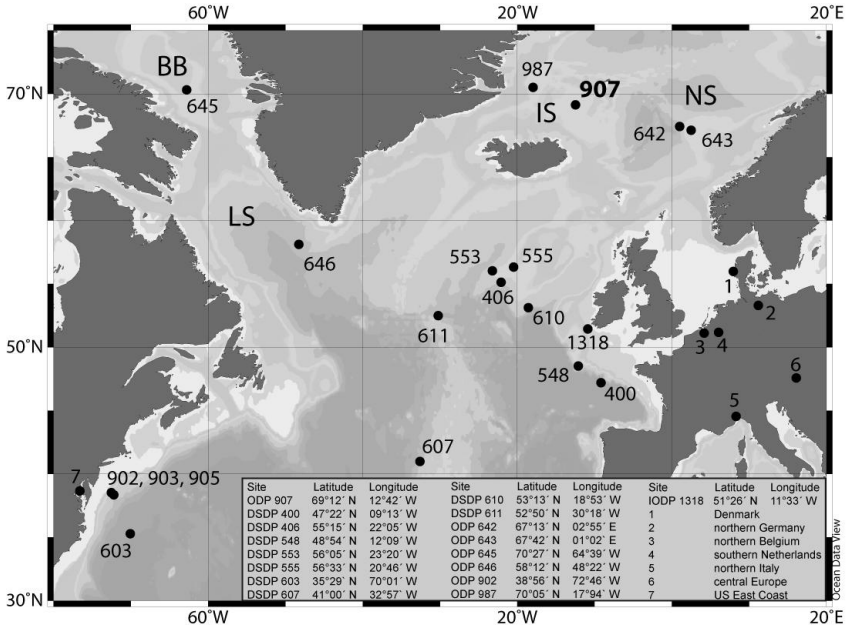

Fig.1: Location of ODP Hole 907A in the Iceland Sea, together with DSDP, ODP, IODP and other Sites discussed in the text. BB = Baffin Bay, LS = Labrador Sea, IS = Iceland Sea, NS = Norwegian Sea.

Mid-Miocene to Pliocene Dinoflagellate Cyst Datums in ODP Hole 907A (Iceland Sea)

M. SCHRECK, J. MATTHIESSEN

Alfred Wegener Institute for Polar and Marine Research, Bremerhaven

In order to contribute to the improvement of biostratigraphic age control for the Neogene sequences in the High Northern Latitudes we examined palynomorphs from ODP Hole 907A at a 100 kyr resolution. Diverse and well-preserved dinoflagellate cyst and acritarch assemblages, comprising 42 genera and 154 species are recorded for the period from 14.5 - 2.5 Ma. The section investigated has a good magnetostratigraphic age control (Channell et al., 1999), thus allowing us to firmly calibrate our identified dinocyst events to the Astronomical Tuned Neogene Timescale (ATNTS; Lourens et al., 2004). These dinocyst events have been compared with those recorded in other DSDP, ODP and IODP sites, and outcrops and boreholes from the U.S. East Coast, the adjacent North Sea and Mediterranean basins (Schreck et al., in prep.; Fig. 1).

ICDP

Do major evolutionary events in ancient Lake Ohrid indicate its origin?

K. SCHREIBER[1], T. HAUFFE[1], C. ALBRECHT[1], T. WILKE[1]

[1] Department of Animal Ecology and Systematics, Justus Liebig University Giessen, Heinrich-Buff-Ring 26-32 (IFZ), 35392 Giessen, Germany.

The Balkan Lake Ohrid is the most outstanding European ancient lake with a high degree of endemic biodiversity, particularly in invertebrates (reviewed in Albrecht & Wilke, 2008). By applying the normalized endemic species area index (Albrecht & Wilke, 2008) and taking the surface area into account, Lake Ohrid, for example, outnumbers other worldwide ancient lakes in

terms of endemic gastropod diversity (Albrecht et al., 2009). Whereas the geology of the basin and the hydrology of the lake are fairly well studied, the limnological history and age of Lake Ohrid are largely unknown. In fact, basically all hypotheses for the origin of extant Lake Ohrid (including all 4 hypotheses tested in this study) were established almost 100 years ago and none of these hypotheses has been tested within a modern scientific framework. Moreover, there is controversy about whether the outstanding degree of endemism in Lake Ohrid is the result of presumed long-term environmental stability or rapid breaks of the lake's environment due to major geological, hydrological or climatic changes.

This leads to the main goals of this work, which uses independent phylogeographical data from several invertebrate groups:

a) to unravel the origin of extant Lake Ohrid faunas, thus yielding information on the lakes limnological history,
b) to provide a timing of major evolutionary events in the Ohrid Basin triggering bursts of speciation and leading to the extraordinary diversity and endemism in many taxa,
c) to test for a correlation of these data with major geological/limnological/environmental changes, and
d) to understand the effect of geological, physico-chemical, and/or environmental stasis vs. changes onto the evolutionary history of the lake.

In order to answer these questions, we proposed to genetically study several invertebrate taxa in Lake Ohrid:

1) the subfamilies Pyrgulinae and "Orientalinae" (Gastropoda: Caenogastropoda),
2) the genus Carinogyraulus (Gastropoda: Basommatophora),
3) the genus Dina (Annelida: Hirudinea),
4) the Dreissena "stankovici" complex (Bivalvia: Heterodonta), and
5) the genus Candona (Crustacea, Ostracoda) (primary taxon of grant of Antje Schwalb Schw 671/11-1).

To obtain material of the respective taxa, four field campaigns to the Balkan Peninsula were performed within the framework of the current project (May 2009, September 2009, February 2010, September 2010). The fifth campaign is currently in preparation and will start in early April 2011. To date, we have successfully sampled a total of 430 sites in lakes Ohrid and Prespa, and another 111 sites in the Balkans to be used for comparisons.

The origin of extant Lake Ohrid faunas (Goal 1) was investigated with (preliminary) Bayesian phylogenies based on COI mitochondrial DNA data and partly in addition with LSU ribosomal DNA data. The subfamily Pyrgulinae and the leech genus Dina seem to form an ancient lake species flock (i.e., monophyletic groups of endemic taxa that presumably evolved within the lake). This indicated a single colonization event of Lake Ohrid for both taxa. This pattern is also seen in another taxon studied, the subfamily "Orientalinae". However, these three taxa showed different biogeographical affiliations. The Pyrgulinae form an species flock comprising species from lakes Ohrid and Prespa (including adjacent springs) and one widespread taxon from the northern Balkans, whose ancestor most likely lived in Lake Ohrid and spread along the north-eastern Adriatic coast via Lake Ohrids' effluent Drim River. The Dina and "Orientalinae" species flocks consist exclusively of endemic species.

In contrast to the Pyrgulinae, "Orientalinae" and Dina species flocks, the Lake Ohrid endemics of Carinogyraulus seem to had colonized Lake Ohrid in at least two independent events. This pattern is called a "species scatter" as was detected before in Lake Ohrid *Valvata* spp. (Hauswald et al., 2008).

For *Dreissena* spp. on the Balkans could be shown that they probably originated from an ancestral *Dreissena* population in Lake Ohrid (Wilke et al., 2010). Specimens of this population possibly invaded lakes in the southern Ionian region and became reproductively isolated. A second independent and probably later emigration of specimens out of Lake Ohrid invaded Lake Prespa. This population became the source for the spreading of the respective species in the Vardar and Thrace regions after a demogarphic expansion.

Although our data for the evolutionary history of the species flocks/species groups discussed above are still incomplete, some interesting patterns have already emerged. First of all, most endemic taxa in Lake Ohrid are members of ancient lake species flocks, that is, they evolved intralacustrine. Secondly, the respective sister groups of endemic Lake Ohrid taxa reside in the Balkans and typically not in the Aegean or Pannonian region. Thirdly, most sister groups occur in either spring or riverine habitats and not in marine or brackish-water settings. And fourthly, within endemic taxa from the Ohrid Basin, spring species are often distinct and typically comprise old haplotypes.

Thus, there currently is strong evidence against the "Mesohellenic Trough derivate hypothesis", the "Tethys derivate hypothesis", and the "Lake Pannon hypothesis" of limnological origin of extant Lake Ohrid. Instead, our preliminary data support the "de novo hypothesis", that is, that Lake Ohrid has formed de novo in dry poljes (flat depressions of karst limestone) from springs or rivers.

Due to the unknown exact age of Lake Ohrid (for a review of available data see Albrecht & Wilke, 2008), we estimated timing of major evolutionary events in the Ohrid Basin triggering bursts of speciation and leading to the extraordinary diversity and endemism in many taxa (Goal 2). We have performed molecular clock, lineages through time plot and analyses of spatial and demographic expansion of populations from the species groups mentioned above.

Given the conflicting geological information on the age of Lake Ohrid, molecular clock estimates of major evolutionary events in Lake Ohrid species flocks may help to refine these dates by establishing lower and upper constraints. Molecular clock analyses in the Pyrgulinae and "Orientalinae", for example, indicate that the diversification of the groups started some 1.7±0.8 and 2.4±1.1 Million years ago, respectively. Similar analyses were performed for other Lake Ohrid species flocks and are summarized in Fig. 1. This figure also shows suggested geological ages derived from the literature. Though the available geological data are not consistent, most workers agree that the geological age of Lake Ohrid is in the range of 2-3(5) Million years (reviewed in Albrecht & Wilke, 2008).

If we assume that speciation occurred intralacustrine, the first divergence event in the respective flock would constitute the minimum age of Lake Ohrid because at this time, the lake must have already existed. In contrast, if we calculate the divergence time of the most recent common

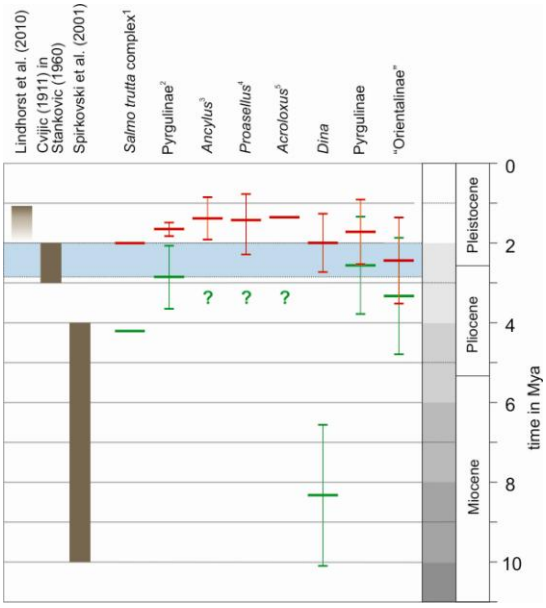

Figure 1: Comparisons of geological and evolutionary estimates for the age of Lake Ohrid. Brown bars indicate geological estimates (note that the estimate of Lindhorst et al., 2010 represents a minimum age). The narrow red bars indicate the onset of intralacustrine diversification in groups of endemic Lake Ohrid taxa together with their standard deviations. The narrow green bars indicate the average timing and standard deviations of the split with their respective sister groups outside the lake. These estimates set the minimum and a potential maximum time frame for the origin of Lake Ohrid faunas (blue band) based on evolutionary data (extended from Trajanovski et al., 2010).
1 Sušnik et al., 2006; 2 Wilke et al., 2007, 2009 (Note that the workers did not include all species of the Pyrgulinae species flock in their analysis. Therefore, the onset of intralacustrine diversification in this group is very likely underestimated and is recalculated in this study.); 3 Albrecht et al., 2006; 4 Wysocka et al., 2008; 5 Albrecht & Wilke, 2006.

ancestor of lake taxa with the presumed sister taxon from outside the lake, then we would receive a potential maximum age for the lake. Of course, to do so, we would have to assume that the divergence event happened outside the lake and that the lake did not already exist at that time. While data on, for example, the population structure and ecology of the taxa involved may help to provide some evidence for that, these assumptions appear to be difficult to test. Therefore, the lower constraint suggested here should be treated with caution (for details see Trajanovski et al., 2010). Moreover, missing taxa (either not sampled or already extinct) may also affect the clock estimations. Overall, the data summarized in Fig. 1 provide good support that the minimum age of Lake Ohrid is some 2 Million years. As mentioned above, support for the maximum age estimation is weaker and approximately 3 Million years is a rough estimate. Interestingly, this preliminary time frame of approximately 2-3 Million years for the origin of Lake Ohrid, generated solely based on evolutionary data, almost exactly fits the time frame most often used in the literature by geologists.

In order to test for variation in speciation rates over time within the Lake Ohrid *Dina* species flock, we used two independent approaches. First, we tested for lineage specific bursting, i.e., whether subsets of taxa were likely to speciate faster than others. Then we investigated whether, over the whole tree, there are changes in speciation rates over time by testing for deviation from a constant speciation model. Preliminary analyses (results not shown here) do not indicate a significant deviation from the constant speciation model. At no time, the estimated number of lineages exceeds the confidence interval of the expected number of lineages under a constant speciation model. Nonetheless, the actual plot indicated an initial lag phase followed by two phases of faster speciation.

To test for a correlation between evolutionary data with major geological/limnological/environmental changes, and to understand the effect of geological, physico-chemical, and/or environmental stasis vs. changes onto the evolutionary history of the lake (Goals 3 and 4) it is necessary to possess paleolimnoligical and geological information about Lake Ohrid. Relatively little was known about the paleolimnology and geology of the lake. Recently a special issue of the journal Biogeosciences "Evolutionary and geological history of Balkan lakes Ohrid and Prespa" was published with new insights from several Lake Ohrid projects conducted within the priority program ICDP (SPP 1006) and the ICDP project "SCOPSCO". These new insights can now be used to study the correlation between changes in geology, limnology and environment, and major evolutionary events in our model invertebrate groups. Such changes could be, for example, major volcano eruptions, which were examined with tephrostratigraphical methods (e.g., Vogel et al., 2010a, b), major lake level changes, examined by stratigraphy of lake sediments (e.g., Lindhorst et al., 2010), and major temperature changes, inferred from pollen records of sediment cores (e.g., Lézine et al., 2010). Furthermore fossils of molluscs were reported for the first time (Albrecht et al., 2010) for Lake Ohrid.

Despite the fact that the work on goals 3 and 4 has started only very recently and that only a small portion of the newly available geological data has been assessed, we would like to point again at three major findings already mentioned above. 1) Our preliminary data on the origin of extant Lake Ohrids fauna support the hypothesis that Lake Ohrid has formed de novo in dry poljes from springs or rivers. 2) We estimated a preliminary time frame of approximately 2-3 Million years for the origin of Lake Ohrid. 3) We did not find significant deviations from a constant speciation model in the Lake Ohrid *Dina* species flock.

References:

Albrecht, C., Hauffe, T., Schreiber, K., and Wilke, T.: Mollusc biodiversity and endemism in the putative ancient Lake Trichonis (Greece), Malacologia, 51, 357–375, 2009.

Albrecht, C., Trajanovski, S., Kuhn, K., Streit, B., and Wilke, T.: Rapid evolution of an ancient lake species flock: freshwater limpets (Gastropoda: Ancylidae) in the Balkan lake Ohrid, Org. Div. Evol., 6, 294–307, 2006.

Albrecht, C., Vogel, H., Hauffe, T., and Wilke, T.: Sediment core fossils in ancient Lake Ohrid: testing for faunal change since the Last Interglacial, Biogeosciences, 7, 3435-3446, 2010.

Albrecht, C. and Wilke, T.: Testing the "old lakes – old taxa assumption": freshwater limpets (Gastropoda: Acroloxidae) in the European ancient lakes, Berliner Palöaobiol. Abh., 9, 7, 2006.

Albrecht, C. and Wilke, T.: Lake Ohrid: biodiversity and evolution, Hydrobiologia, 615, 103–140, 2008.

Cvijić, J.: Fundamentals of geography and geology of Macedonia and Old Serbia, Book III, Serbian Academy of Sciences, Special Edition, Beograd (in Serbian), 1911.

Hauswald, A.-K., Albrecht, C. and Wilke, T: Testing two contrasting evolutionary patterns in ancient lakes: species flock versus species scatter in valvatid gastropods of Lake Ohrid, Hydrobiologia, 615, 169-179, 2008.

Lézine, A.-M., von Grafenstein, U., Andersen, N., Belmecheri, S., Bordon, A., Caron, B., Cazet, J.-P., Erlenkeuser, H., Fouache, E., Grenier, C., Huntsman-Mapila, P., Hureau-Mazaudier, D.,Manelli, D., Mazaud, A., Robert, C., Sulpizio, R., Tiercelin, J.-J., Zanchetta, G., and Zeqollari, Z.: Lake Ohrid, Albania, provides an exceptional multi-proxy record of environmental changes during the last glacial–interglacial cycle, Palaeogeogr. Palaeoclimatol. Palaeoecol., 287, 116–127, 2010.

Lindhorst, K., Vogel, H., Krastel, S., Wagner, B., Hilgers, A., Zander, A., Schwenk, T., Wessels, M., and Daut, G.: Stratigraphic analysis of lake level fluctuations in Lake Ohrid: an integration of high resolution hydro-acoustic data and sediment cores, Biogeosciences, 7, 3531-3548, 2010, doi:10.5194/bg-7-3531-2010.

Spirkovski, Z., Avramovski, O., and Kodzoman, A.: Watershed management in the lake Ohrid region of Albania and Macedonia, Lakes Reserv. Res. Manage, 6, 237–242, 2001.

Stanković, S., The Balkan Lake Ohrid and is Living World, Monographiae Biologicae Vol. IX., Uitgeverij Dr. W. Junk, Den Haag, 1960.

Sušnik, S., Knizhin, I., Snoj, A., and Weiss, S.: Genetic and morphological characterization of a Lake Ohrid endemic, *Salmo* (*Acantholingua*) *ohridanus* with a comparison to sympatric *Salmo trutta*, J. Fish Biol., 68, Supplement A, 2–23, 2006.

Trajanovski, S., Albrecht, C., Schreiber, K., Schultheiß, R., Stadler, T., Benke, M., and Wilke, T.: Testing the spatial and temporal framework of speciation in an ancient lake species flock: the leech genus *Dina* (Hirudinea: Erpobdellidae) in Lake Ohrid, Biogeosciences, 7, 5011–5045, 2010, doi:10.5194/bgd-7-5011-2010.

Vogel, H., Wagner, B., Zanchetta, G., Sulpizio, R., and Rosén, P.: A paleoclimate record with tephrochronological age control for the last glacial-interglacial cycle from Lake Ohrid, Albania and Macedonia, J. Paleolimnol., 44, 295–310, 2010a.

Vogel, H., Zanchetta, G., Sulpizio, R., Wagner, B., and Nowaczyk, N.: A tephrostratigraphic record for the last glacial-interglacial cycle from Lake Ohrid, Albania and Macedonia, J. Quat. Sci., 25, 320–338, 2010b.

Wilke, T., Albrecht, C., Anistratenko, V. V., Sahin, S. K., and Yildirim, M. Z.: Testing biogeographical hypotheses in space and time: Faunal relationships of the putative ancient lake Egirdir in Asia Minor, J. Biogeogr., 34, 1807–1821, 2007.

Wilke, T., Schultheiß, R., and Albrecht, C.: As time goes by: A simple fool's guide to molecular clock approaches in invertebrates, From the symposium "Molluscs as models in evolutionary biology: from local speciation to global radiation" presented at the World Congress of Malacology, held from 15 to 20 July 2007 in Antwerp, Belgium, American Malacological Bulletin, 27, 25–45, 2009.

Wilke, T., Schultheiß, R., Albrecht, C., Bornmann, N., Trajanovski, S., and Kevrekidis, T.: Native Dreissena freshwater mussels in the Balkans: in and out of ancient lakes, Biogeosciences, 7, 3051–3065, doi:10.5194/bg-7-3051-2010, 2010.

Wysocka, A., Kostoski, G., Kilikowska, A., Wr ´ obel, B., and Sell, J.: Proasellus (Crustacea, Isopoda) species group endemic to the Balkan Lake Ohrid: a case of ecological diversification?, Fund. Appl. Limnol., 172, 301–313, 2008.

IODP

Earliest Paleogene climate events – A multiproxy study from the Demerara Rise, western equatorial Atlantic

P. SCHULTE[1], A. BORNEMANN[2], T. WESTERHOLD[3], J. MUTTERLOSE[4]

[1] GeoZentrum Nordbayern, Universität Erlangen, Schlossgarten 5, D-91056 Erlangen, Germany
[2] Institut für Geophysik und Geologie, Universität Leipzig, Talstraße 35, D-04103 Leipzig, Germany
[3] MARUM – Center for Marine Environmental Sciences, University of Bremen, Leobener Strasse, 28359 Bremen, Germany
[4] GMG, Ruhr-University Bochum, Universitätsstr. 150, D-44801 Bochum, Germany

The climatic and oceanographic evolution during the recovery from the K-Pg boundary mass extinction (~ 65 Ma) is still poorly constrained although this ~0.5 to 1 My long interval is characterized by strong fluctuations in carbonate content, stable isotope records, and benthic faunal diversity [e.g., 1,2]. This period correlates to the "strange interval" [3], which shows a marked change in amplitude of the eccentricity-related cycles compared to the latest Maastrichtian and a possible switch of the deep water production from the Southern Ocean to the North Pacific [4]. Moreover, evidence for a transient warming event that occurred about 200 ky after the K-Pg boundary [5] has been provided, an interval which may represent the first hyperthermal of the Cenozoic. Here, we investigate this critical interval by a multi-proxy study including stable isotopes, mineralogy, XRF core scans, and calcareous nannofossils in several cores from the ODP Leg 207 in the western Atlantic.

Lithology: Immediately above the Chicxulub ejecta layer at the K-Pg boundary, all cores show a greenish, laminated interval that grade into an approximately two meter thick sequence with multiple intensively red-stained intervals encompassing Biozone P1a and P1b. The onset of the most intense red coloration is always observed about 30-50 cm above the K-Pg boundary in 8 of the 13 holes drilled. The red-stained intervals correspond to peaks in Fe content and magnetic susceptibility, reflecting the presence of Fe-oxides and hydroxides, as well as rapid changes in gamma ray attenuation with density values as low as 1.5 g/cm^3, which may indicate enhanced porosity due to carbonate dissolution. Further upcore, red staining ceases and pervasively bioturbated cycles of alternating light/dark greenish gray calcareous chalk are present (Biozone P1c). A prominent pyrite-rich surface marks a prominent hiatus at the Biozone P1c/P3a transition.

Mineralogy: Calcite, quartz, feldspars as well as phyllosilicates (smectite, some illite and kaolinite), and zeolites are the major mineral phases. Zeolites are mainly clinoptilolite and some heulandite; whereas no phillipsite or analcime was detected. Accessory mineral phases are dolomite, hematite (up to 0.8% in the red-stained intervals), goethite, and pyrite. Except for a short interval immediately above the K-Pg boundary that includes high abundances of illite, there is no marked change in the clay assemblage during the Maastrichtian-Danian as also revealed by relatively constant major element/Al ratios. Within the lowermost Paleocene red interval during Biozone P1a, three, about 4 to 10 cm-thick carbonate-poor layers with rapid lowering to <25 wt% calcite occur. These clay layers are separated by dm-thick carbonate-rich intervals (>55 wt% calcite). There is also a prominent increase of the zeolite contents across the lowermost two red intervals, reaching values up to 12 wt% in the second red stained interval. Rietveld refinement of the calcite crystallinity data in concert with the lowered residue in the >63 µm fraction suggest severe calcite dissolution associated with the red-stained intervals.

Stable isotopes: The carbon isotopes of the <63 µm fine fraction show a large, abrupt negative shift from stable late Maastrichtian values of about 1.8 ‰ to values as low as –0.5 ‰ in Biozone P0 directly above the K-Pg boundary, followed by immediate recovery to values of 0.1 ‰ during the lower part of Biozone Pα. Within the clay layers in the red-stained interval, the $\delta^{13}C$ record shows three abrupt negative shifts of about 0.5 ‰. Subsequently, there is a gradual increase of $\delta^{13}C$ values finally stabilizing at about 1.2 ‰ (Biozone P1c). Generally, the oxygen isotopes of the fine fraction show considerably wider scatter than the $\delta^{13}C$ values. The K-Pg boundary is associated with a positive excursion from typical late Maastrichtian values of about –2 ‰ to values as high as –1 ‰ during Biozone P0 and the lower part of Biozone Pα.

Within the lowermost red-stained interval, $\delta^{18}O$ values show two negative excursions (ca. –2.5 ‰).

In conclusion, our first results support relatively stable late Maastrichtian environments and indicate that a 0.5 my-long period of substantial environmental changes started at the K-Pg boundary including: (i) a brief period (several thousand years) with oxygen-deficiency immediately following the K-Pg. Although this is not a common feature observed in K-Pg boundary sites, intermediate water oxygen minima were widely developed during the earliest Danian in sections from the Tethys. It is noteworthy, that this period correlates with heavier oxygen isotope values that may indicate several degrees cooler surface waters of the Western Atlantic, although this interpretation needs to be confirmed by $\delta^{18}O$ analysis of foraminifera shells. Our results, however, support similar observations from the Walvis Ridge in the southern Atlantic [6]. (ii) The three clay layers within the red-stained interval (Biozone P1a) may be correlated to the 2 to 3 clay layers found at other ODP sites that were interpreted as a series of transient warming events ("Dan C2 event" [e.g., 5]). (iii) The red-stained intervals likely formed during deposition and early diagenesis as the result of low accumulation rates of organic matter and/or an increase in the content of dissolved oxygen in bottom waters due to changes in ocean circulation.

References:
[1] D'Hondt, S., Donaghay, P., Luttenberg, D., Lindinger, M., 1998, Organic carbon fluxes and ecological recovery from the Cretaceous-Tertiary mass extinction. Science, 282, 276-278.
[2] Alegret, L., Thomas, E., 2007, Deep-sea environments across the Cretaceous/Paleogene boundary in the eastern South Atlantic Ocean (ODP Leg 208, Walvis Ridge). Marine Micropaleontology, 64, 1-17.
[3] Westerhold, T., Röhl, U., Raffi, I., Fornaciari, E., Monechi, S., Reale, V., Bowles, J., Evans, H.F., 2008, Astronomical calibration of the Paleocene time. Palaeogeography, Palaeoclimatology, Palaeoecology, 257, 377-403.
[4] Thomas, D.J., 2004, Evidence for deep-water production in the North Pacific Ocean during the early Cenozoic warm interval. Nature, 430, 65-68.
[5] Quillévéré, F., Norris, R.D., Kroon, D., Wilson, P.A., Wilson, P., 2008, Transient ocean warming and shifts in carbon reservoirs during the early Danian. Earth Planetry Science Letters, 265, 600-615.
[6] Kroon, D., et al., 2007. Leg 208 Synthesis: Cenozoic climate cycles and excursions. Proceedings of the ODP. Scientific Results, 208, 1-55.

IODP

Ultrasonic wave velocity changes during experimental deformation of water-rich sediments from the Nankai accretionary prism (offshore SW Japan)

K.SCHUMANN, M. STIPP, D. KLAESCHEN, J.H. BEHRMANN

Marine Geodynamik, IFM-GEOMAR, Wischhofstraße 1-3, 24148 Kiel, Germany, kaschumann@ifm-geomar.de

IODP expeditions 315 and 316 investigated the shallow frontal thrusts, and the hanging wall to a major active splay fault of the active frontal thrust system of the Nankai accretionary prism. We analyse the composition, the microstructure and the deformation behaviour of a core sample set from a depth range of 48-128 m from the drilling sites of these expeditions in order to quantify their influence on the elastic properties of these sediments. The rather uniform silty clay samples consist of 16-25 % quartz, 13-34 % feldspar, up to 14 % calcite, and 34-41 % clay minerals (total clay content: 16-33 % smectite, 33-45% illite, up to 10 % kaolinite, and 15-30 % chlorite; GUO and UNDERWOOD, subm.). Particle size distribution measurements show 60-85% clay, 10-34% fine silt, 4-8% medium silt and less than 0.3% of coarser fractions. Smear slide analyses indicate a sample composition of 11-63 % lithics and minerals, 33-78% submicroscopic, < 9% volcaniclastic and up to 46% biogenic material. Microfossils found in the samples are mainly foraminifera, diatoms, silicoflagellates, sponge needles and radiolaria.The samples were deformed in a triaxial cell, using sample cylinders of 50 mm in diameter and up to 100 mm length, under consolidated-undrained conditions, confining pressures of 400-1000 kPa, axial displacement rates of 0.01-9.0 mm/min and up to ~50 % axial compressive strain. Three different types of tests were conducted: (1) single step compression experiments at constant confining pressure and displacement rate, (2) pressure stepping compression experiments at constant displacement rate and three different confining pressures, and (3) displacement rate stepping experiments at constant confining pressure and increasing displacement rate.

Bender element velocity measurements were carried out during the triaxial shear tests. While increasing the confining pressure, p- and s-wave velocity measurements were conducted in 100 kPa steps. After reaching the final confining pressure, pore pressure relaxation was ensured by keeping the sample under static conditions overnight. During the deformation phase of the experiment, p- and s-wave velocities were measured in arbitrary time intervals. Problems in the incorrect first arrival detection time of an automatic single trace algorithm were identified by sorting the time series data into common shear test gathers. By seismic time series analysis primary, multiple, and converted phase could be identified. Manually picked travel times in the common shear test gathers were used to calculate propagation velocity variations for each experiment. Ultrasonic p- and s-wave velocity measurements yield velocities of 300 – 2400 m/s for the p-waves and 100 – 1000 m/s for the s-waves. Based on these velocity data refinements, systematic changes in the elastic properties can be determined and correlated to changes in bulk density and pore space as well as to compositional and

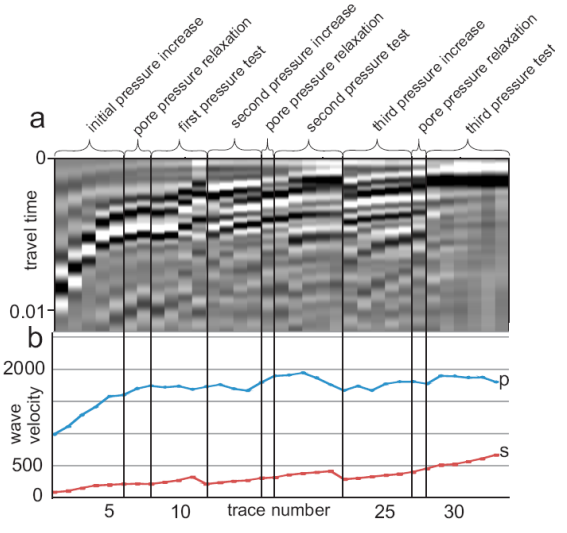

Fig.1: a) Typical p-wave travel time plot of a pressure stepping compression experiment (316-C0007C-7X-1, 63 m depth).
b) P- and s-wave velocity plot of the experiment 316-C0007C-7X-1.

microstructural differences between the samples.

A typical plot of a p-wave velocity measurement is given in Fig. 1. Changes in the p-wave velocity of a characteristic pressure stepping experiment can be described as follows: During the initial pressure increase there is a strong p-wave velocity increase (from 1000 m/s to 1600 m/s) in the data set. This velocity increase continues into the following phase of pore pressure relaxation. At the beginning of the first deformation test at 400 kPa confining pressure, p-wave velocity slightly increases. Then, after a few percent strain there is a decrease in the velocity. When reducing the deviatoric stress by retracting the σ1-piston at the end of the test the p-wave velocity returns to the high level recorded previously. The next confining pressure increase to 640 kPa is characterised by a p-wave velocity decrease, while it increases during the phase of relaxation. In the second deformation test, p-wave velocity increases only slightly, reaches its maximum (1940 m/s) and decreases strongly towards the end of deformation. During the next confining pressure increase, the velocity increases slightly and remains constant during the following pore pressure relaxation. In the third deformation test at 1000 kPa confining pressure, p-wave velocity increases at the beginning and decreases slightly until finite strain is reached.

Microstructural analyses were carried out on BSE (backscattered electron) images of the undeformed starting material and the experimentally deformed samples. The long axis-orientation of pores and mineral grains were determined using image analysis software. In the undeformed state, the sample pores do not show any preferred orientation, while illite grains show a weak preferred orientation oblique to the core axis, which we interpret as the original sedimentary bedding plane. After deformation, the pores display a long axis orientation maximum approximately perpendicular to the core axis. Long axis-orientation of the illites are rotated depending on the amount of axial strain. Some of the samples show two distinct illite orientation maxima indicative of the original bedding plane and a newly formed foliation. These microstructural results will be correlated with the velocity measurements in order to determine the influence of microstructural and deformation parameters on the elastic properties of the investigated sediments.

References:

Guo, J. and UNDERWOOD, M. (subm.): Data Report: Clay Mineral Assemblages from Nankai Trough and Kumano Basin, IODP Expedition 315 and 316, NanTroSEIZE Stage1.

ICDP

Tracing NE-Siberian palaeo-permafrost with multi-proxy core data

G. SCHWAMBORN [1], J. WILLENBRING[2], H. MEYER[1], A. ANDREEV[3], G.B. FEDOROV[4], N. OSTANIN[4], L. SCHIRRMEISTER[1], AND EL`GYGYTGYN SCIENTIFIC PARTY

[1] Alfred Wegener Institute for Polar and Marine Research, 14473 Potsdam (Germany)
[2] University of Pennsylvania, Department of Earth & Environmental Science, Philadelphia, PA 19104-6316 (USA)
[3] University of Cologne, Zülpicher Str. 49, 50674 Cologne (Germany)
[4] Arctic and Antarctic Research Institute, Bering Street, 199397 St. Petersburg (Russia)

The El'gygytgyn Meteorite Crater in Chukotka holds the unique opportunity to trace frozen ground conditions back to the Pliocene. The basin was not glaciated in Quaternary time and terrestrial deposits accumulate episodically at piedmont settings and continuously in a central lake basin. Drilling into sedimentary permafrost at the shore of the El'gygytgyn Crater Lake recovered a 141 m long core of frozen deposits that belong to an alluvial fan setting entering the lake basin from the west. The permafrost core contains ground ice throughout and largely consists of sandy gravels with volcanic clasts embedded in a sandy matrix. Pollen assemblages, ground ice hydrochemistry (i.e. stable water isotopes, main cations and anions) and mineralogical proxies of cryogenic weathering are used as palaeoenvironmental indicators for reconstructing late Cenozoic climate, landscape and permafrost dynamics. Reconstruction of the local erosional and depositional history is supported by tracing palaeo-permafrost with meteoric ^{10}Be and in-situ ^{26}Al/^{10}Be in an ongoing DFG project. This research aids our understanding of permafrost history over long time scales in far NE Siberia, an area yet underexposed in palaeo-permafrost research.

Permafrost conditions through time are inferred from proxy data of cryogenic weathering based on studying the mineral debris. The indicative weathering features (i.e. quartz grain enrichment in the fine fractions, single quartz grain micromorphology) originate from frost weathering on the exposed crater slopes in the (palaeo) active layer. Mineral grains are transported subsequently downslope and accumulate in the subaerial and subaquatic parts of the alluvial fan. These grains are then traced within our core. These two indicators reflect the continuity of thaw and freeze dynamics; i.e. of permafrost, in the catchment, which drive the production of the mineral debris in the area.

The discontinuous pollen dataset suggests that the upper 9 m represent a record back to the Allerød period. According to the pollen assemblages the Holocene is indicated by high amounts of alder and birch and is restricted to the upper 1.8 m where organic matter can occur in amounts of >1 weight-%. Below, where organic matter decreases to negligible values, the Younger Dryas is represented by the interval 1.8 - 2.5 m and a lack of birch and alder whereas the underlying Allerød down to 9.50 m core depth again contains those tree pollen. Sediments at ~20 m depth were probably formed during interglacial MIS 5.5 or 7 as inferred from the occurrence of alder and birch

pollen, which can be correlated with other regional records. Whilst the pollen assemblages at ~36 m and ~ 51 m depth still indicate cold Pleistocene environmental conditions, those at about 62 - 65 m depth may belong already to the warmer Pliocene epoch based on high pollen counts of pine, larch, fir, spruce, and hemlock.

The inferred climate oscillations for the transition from the Allerød to the Younger Dryas and into the Holocene are also suggested in the water isotope record of the ground ice occurring mainly as pore ice. $\delta^{18}O$ and δD minima and maxima support the inferred vegetation history as indicated by the pollen record. Below the Allerød core portion, the $\delta^{18}O$ values show less variation and tend toward more negative values. From exposed ancient lake terraces surrounding the lake at 10 m and 40 m above the modern shore line, we conclude that the coring site was flooded prior to the Allerød before lake level fall gave way to the modern outline of the alluvial fan setting. The $\delta^{18}O$ and δD values observed below 10 m core depth thus must be discussed in the framework of a basinward migration of the freezing front that marked the unfrozen zone (i.e. talik) below the water body of El'gygytgyn Crater Lake in the past. A marginal lake environment prior to the Allerød is also indicated by the occasional occurrence of distinctly rounded pebbles, suggesting shore-line processes, and well sorted sandy layers, possibly deposited on the upper lake slope.

IODP

Potential drill sites offshore NW-Africa to study the Neogene climate and related sediment dynamics – results of the pre-site survey MSM 11/2

T. SCHWENK[1], S. KRASTEL[2], T. BICKERT[1], S. FRICKE[1], MATHIAS MEYER[2]

[1] MARUM – Center for Marine Environmental Sciences and Faculty of Geosciences, University of Bremen, Klagenfurter Str., 28359 Bremen, Germany.
[2] IFM-GEOMAR, Wischhofstr. 1-3, 24148 Kiel, Germany.

The climate of NW Africa is driven by the interaction between the trade wind system and the African Monsoon, which control the distribution of the humidity over the continent and thereby the location of different vegetation-zones from the tropical rain forest over the Sahel zone to the dry Sahara. It is suggested that on longer timescales this distribution of the humidity has been significantly shifted between Sahel and Sahara, leading finally to an aridification of NW Africa. To reveal these climate changes within the last 15 Ma years, a new IODP drilling is proposed. On this poster, we show the relevant seismic data gathered during a pre-site survey in spring 2009.

Five different areas between Cap Bojador, southeast of the Canary Islands, and the deltas of Senegal and Gambia Rivers were investigated during cruise MSM 11/2 to collect high-resolution, multichannel seismic data. In total 10 potential sites have been selected. 4 out of 10 sites should cover at least the last 10 to 15 Ma to reconstruct the Neogene development of the African Monsoon and to document the early Pliocene aridification of the North African continent. Further 6 sites should explore sediments in high accumulation areas for a high resolution study of rapid climate changes in the subtropics and related sediment transport. It has been postulated, that the timing and frequency of gravity driven sediment transport is linked to climate change and related sea level change, though the direct link is not well understood.

One focus of the survey is the area offshore Cape Blanc (around 21° N), where ODP Site 658 was drilled in 1986. This site is located beneath a prominent, stable upwelling zone and is characterized by the expected high-accumulation rates. However, the drill core revealed a hiatus from 1.573 to 0.731 Ma and does not cover the change from the 41 ka glacial-interglacial cycles to the 100 ka cycles. The hiatus could be identified in the seismic data as result of a slope failure. New potential drill sites without the hiatus and an average accumulation rate of around 15 cm/ka can be proposed.

ICDP

Magma storage conditions and degassing processes of low-K and high-Al island-arc tholeiites: Experimental constraints for Mutnovsky volcano, Kamchatka

T. SHISHKINA[1], R. ALMEEV[1], R. BOTCHARNIKOV[1], F. HOLTZ[1]

[1] Institut für Mineralogie, Leibniz Universität Hannover, Callinstrasse 3, 30167 Hannover, Germany

Introduction

Mutnovsky volcano is located in the southern part of the Eastern volcanic front of Kamchatka peninsula (Russia). The mafic lavas of the volcano are typical island arc high-Al, low-K tholeiitic basalts. Mutnovsky is the object of the proposed ICDP drilling project which is focused on the investigation of the interaction between active magmatic and adjacent hydrothermal systems. It has two central scientific issues: (1) the identification of magmatic component in fluids proximal to conduits and (2) the determination of the overall volatile and thermal budget of the Mutnovsky volcano.

The experimental data and natural observations obtained in the course of our running DFG-project should provide new constraints on the magma storage conditions, especially on the pressures (depths), temperatures and volatile contents in the magma chamber of Mutnovsky volcano. The project consists of three main parts: (1) experimental study of the H_2O-CO_2 solubilities in basaltic melts relevant to Mutnovsky primitive magmas, since H_2O and CO_2 contents in magmas can be used as indexes of magma storage conditions; (2) determination of pre-eruptive conditions and depths of basaltic magma chamber beneath Mutnovsky volcano based on crystallization experiments; and (3) the study of natural samples: petrography and mineralogy of the rocks and compositions and volatile abundances in glass inclusions in minerals.

The data obtained for Mutnovsky volcano have a broad application and can be used to constrain a general genetic model for the formation of island arc tholeiitic series and will provide estimates on the budget and contribution of magmatic volatiles to the magmatic-hydrothermal volcanic systems.

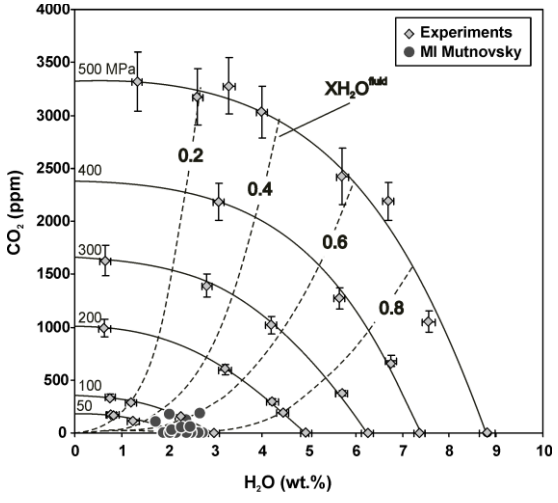

Fig. 1. Solubility plot for H_2O- and CO_2-bearing fluids in basaltic melts at 1250°C and pressures from 50 to 500 MPa. The solid lines represent isobars, the dashed lines are isopleths of constant fluid composition for the melts saturated with H_2O-CO_2-bearing fluids. Dark grey circles are compositions of melt inclusions in olivine from Mutnovsky volcano (see part 3).

1. Experimental investigation of solubility of H_2O and CO_2 in basaltic melts

This part of the project is devoted to the quantitative determination on H_2O-CO_2 solubility in tholeiitic basaltic melts in the range of pressures (50-500 MPa) corresponding to the crustal depths of magma chambers and conduits beneath typical island arc volcanoes. The experimental results of this part of the project were recently published (Shishkina et al., 2010).

As a starting composition for the experiments we used basaltic glass produced by air-melting of natural low-K high Al tholeiitic basalt from Mutnovsky volcano (sample N72, provided by M. Portnyagin; Duggen et al., 2007). Experiments were conducted in an internally heated pressure vessel (IHPV) at pressures of 50 to 500 MPa and temperature of 1250ºC with Ar as pressure- medium. Run products were analysed by different methods (IR, KFT, electron microprobe, colorimetry).

The results show that concentrations of H_2O and CO_2 in the glasses significantly increase with increasing pressure as well as with H_2O/CO_2 and CO_2/H_2O proportions in the coexisting fluid, respectively. The solubility of H_2O in equilibrium with pure H_2O fluid increases from about 2.2 wt.% at 50 MPa to about 8.8 wt.% at 500 MPa. The concentration of CO_2 increases from about 200 to 3400 ppm in glasses which were in equilibrium with the most CO_2-rich fluids. In general, the solubilities of both H_2O and CO_2 in basaltic melt show a non-linear dependence on the mole fraction of H_2O and CO_2 in the equilibrium fluid.

The diagram shown in Fig. 1, containing fluid-saturation isobars and isopleths of constant fluid composition (Fig. 1), was constructed from the solubility experiments and can be used as a tool for the evaluation of magma storage conditions and for the reconstruction of the dynamics of magma degassing. In particular, it can be applied for the determination of pressures and volatile compositions for natural basaltic glasses, for example, for melt inclusions in minerals. H_2O-CO_2 contents in the melt inclusions in olivines from Mutnovsky were analysed (see part 3) and plotted on the solubility diagramm (Fig. 1).

2. Crystallization experiments

Phase relationships of the Mutnovsky parental magma were investigated as a function of pressure, fO_2 and aH_2O. The experimental results are used to construct a set of phase diagrams at different pressures and temperatures for basaltic magma coexisting with H_2O-CO_2 fluid phase. The obtained experimental data provide quantitative information on the influence of pressure, aH_2O and fO_2 on stability fields of oxide and silicate phases, as well as on evolutionary trends of island-arc tholeiitic magma of Mutnovsky volcano.

We have conducted two sets of crystallization experiments on the tholeiitic basalt (sample N72) previously investigated for H_2O-CO_2 solubilities (part 1): (1) at 300 MPa and between 950-1200°C and (2) at 100 MPa and in range of 1000-1125°C. All experiments have

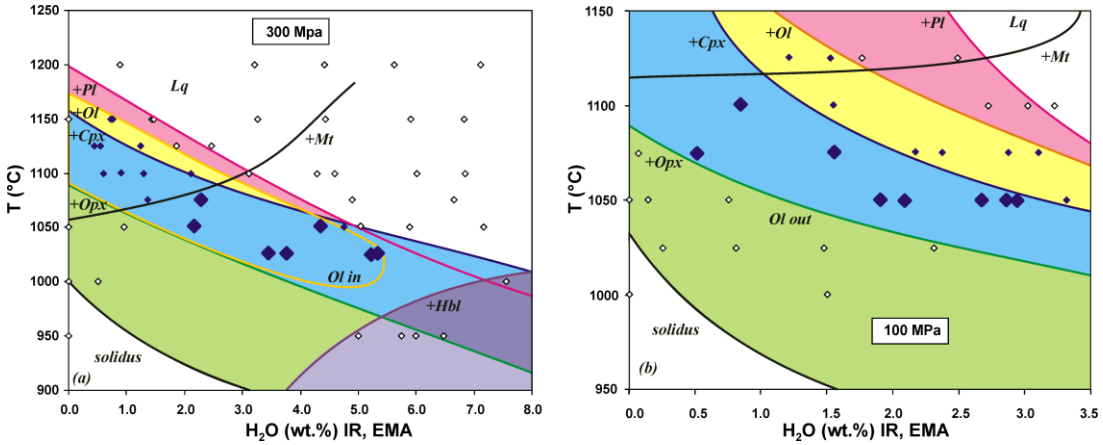

Fig. 2. Phase diagrams. (Temperature (°C) vs. water content in the residual melt, H_2O (wt.%)) for Mutnovsky tholeiitic basalt at 300 (a) and 100 (b) MPa. Mineral associations in equilibrium with melt (*Lq*) are shown by fields of different colors. Big dark diamonds represent runs where Ol+Pl+CPx+Mt association crystallized. Small dark diamonds are runs where mineral associations similar to natural ones were observed (Ol+Pl, Ol+Pl+CPx, Pl+CPx+Mt). White diamonds are all other runs.

been carried out in an IHPV at intrinsic oxygen fugacity, corresponding to the value of QFM+3.3 at water-saturated conditions, and to ~QFM at nominally dry conditions. The phase diagrams (T vs. H_2O in the residual melt) for both pressures are shown in Fig. 2.

(1) 300 MPa experiments (950-1200°C) (Fig. 2a)

At 1200°C Mutnovsky basalt is above the liquidus for the whole range of investigated aH_2O. At around 1175°C crystallisation of the first minerals (plagioclase (Pl) and olivine (Ol) was observed in runs with low H_2O content. In general, with decreasing temperature, the crystallization sequence in melts containing ~ 3 wt% H_2O is as follows: Mt → Mt + Pl → Mt + Pl + Ol → Mt + Pl + Ol + CPx→ Mt + Pl + Cpx + Opx, where Cpx and Opx are high and low-Ca pyroxene respectively. At higher water activities this crystallization sequence is complicated by the presence of amphibole (Hbl) at temperatures below 1000°C. In the presence of Hbl, Cpx and Opx do not crystallize simultaneously. Magnetite does not crystallize in runs above 1050°C from melts with low H_2O content.

(2) 100 MPa experiments (1000-1125°C) (Fig. 2b)

Experiments at temperatures higher than 1025°C were not performed and the exact position of the liquidus curve can not be defined. In contrast to experiments at 300 MPa, no amphibole was detected in any runs at 100 MPa. In conditions at which melts contain ~ 3 wt% H_2O, the crystallization sequence is identical to that at 300 MPa. The crystallization temperatures of the minerals are slightly different, in particular for CPx (larger stability field at high pressure). As for the 300 MPa dataset, the crystallization of OPx is accompnied by the absence of Ol (Ol and Opx have not been found as co-existing phases). . Magnetite is present at all conditions except for runs at 1125°C.

The compositions of minerals and glasses observed in the crystallisation experiments were measured by electron microprobe and were compared with those of natural rock samples from Mutnovsky volcano (see part 3).

3. Study of natural samples from Mutnovsky volcano

Rock samples from Mutnovsky volcano representative for the current project were collected during a fieldworks in 2009. We have sampled several young fresh cinder cones on the south-west slope of Mutnovsky volcano. The lavas of these cones are composed of clinopyroxene-olivine-plagioclase-bearing basalts (8 wt.% MgO, 50 wt.% SiO_2). For studying melt inclusions in olivines we collected basaltic tephra (pieces of scoria and ash) from holocene

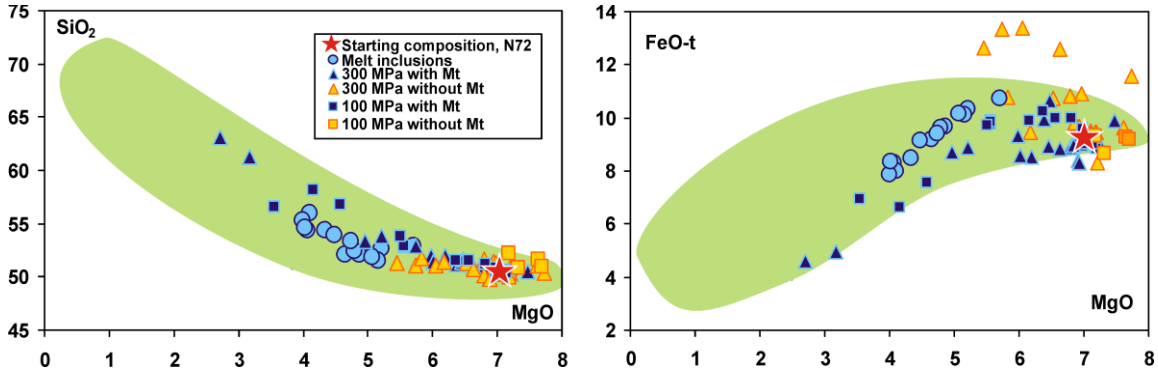

Fig. 3. Compositions of natural volcanics (filled field) and melt inclusions in olivines (circles) from Mutnovsky volcano in comparison with residual melt compositions produced in experiments at 300 and 100 MPa (symbol description is in the legend) on Mutnovsky parental basalt N72 (red star).

eruptions of Mutnovsky. Due to the explosive eruption and rapid cooling, olivines from tephra usually contain naturally quenched glassy inclusions with well preserved pre-eruptive volatile abundances.

Mineral associations and their compositions have been studied in basaltic lavas from Mutnovsky volcano. Three major types of basalts can be distinguished: CPx-Ol-Pl-, Ol-Plag- and rare OPx-CPx-Pl-bearing rocks. Phenocrysts vary in composition from sample to sample and in general are in a range from Fo_{75} to Fo_{83} in olivine, from An_{82} to An_{92} in plagioclase, from $Mg\#_{70}$ to $Mg\#_{80}$ in high-Ca pyroxene and from $Mg\#_{71}$ to $Mg\#_{74}$ in low-Ca pyroxene. No hydrous phases such as amphibole have been observed in basalts and more evolved andesites.

The character of natural mineral assemblages in Mutnovsky basalts suggest that parental melts probably evolved along Ol+Pl and Ol+Pl+Cpx low-pressure cotectics, similar to MORB-type magmas. However, in contrast to MORBs, Mutnovsky volcanics exhibit a pronounced FeO and TiO_2 depletion and weak SiO_2 enrichment (Fig. 3), suggesting earlier Fe-Ti-oxide onset crystallization, which, in turn, can be achieved only in the presence of significant amounts of water at more oxidized conditions. These assumptions are confirmed by our observations made for the natural samples and crystallzation experiments.

In the crystallization experiments performed at 300 and 100 MPa (part 2) we observed mineral associations similar to natural rocks of Mutnovsky. The main association Ol+Pl+CPx observed in natural samples was found to be stable over a wide range of temperatures and water concentrations in the melt (Fig. 2). A crucial point is the crystallization of magnetite together with the Ol+Pl+CPx association. Mineral compositions in the runs with complete Ol+Pl+CPx+Mt association are close to the compositions of the phenocrysts from the natural basalts, especially in runs at 300 MPa and 1125-1175°C (300 MPa: Ol (Fo_{79-84}), Pl (An_{83-89}), Cpx (Mg# 77-80, $Fs_{12-13}En_{43-46}Wol_{41-45}$; 100 MPa: Ol ($Fo_{79-85}$), Pl ($An_{77-81}$), Cpx (Mg# 77-80, $Fs_{11-14}En_{46-47}Wol_{39-42}$). In contrast, in the runs without Mt the compositions of Ol, Pl and CPx are quite different from the natural phenocrysts, usually with lower Mg# olivines and clinopyroxenes and with more Na-rich plagioclases.

Noteworthy, most of the experimental residual glasses produced at 100 and 300 MPa reproduce the Mutnovsky liquid lines of descent indicating a genetic link between parental basaltic compositions and their differentiates (Fig. 3).In addition, most Mt-free runs do not follow the general differentiation trend. Compositions of the Mt-free glasses from the runs at 300 MPa show strong deviation from the trend: enrichement in FeO-total and TiO_2 and depletion in Al_2O_3. Mt-free glasses from 100 MPa runs show no differentiation due to low degree of crystallization.

Glass inclusions from tephra of Mutnovsky volcano (with diameter more than 20 µm in olivines (Fo 75-80)) were studied using different methods. Major-element compositions as well as S and Cl content were determined by electron microprobe. H_2O and CO_2 concentrations were determined by SIMS in Yaroslavl`, Russia and in Nancy, France and S^{+6}/S^{-2} proportions in the glasses by XANES (Karlsruhe, Germany).

The studied melt inclusions have basaltic compositions and overlap with the general petrochemical trend of Mutnovsky volcanic series (Fig. 3), indicating that they are evolved derivates of the parental Mutnovsky melts, formed by crystallisation processes.

The inclusions contain 1.7-2.7 wt.% H_2O and 0-180 ppm CO_2. Plotting these values on the experimentally calibrated H_2O-CO_2 solubility plot (see part 1, Fig.1) shows that most of studied inclusions were trapped into olivines at relatively low pressures (less then 110 MPa) that correspond to the shallow depths (less then 3 km) when magma was already significantly degassed (especially in CO_2). Moreover, values of H_2O analysed in melt inclusions are similar to the H_2O-contents in experimental residual glasses where Ol+Pl+CPx+Mt association was crystallized.

Data on S^{+6}/S^{-2} ratios in the natural glasses were used for the calculations of the oxygen fugacity according to the method described by Jugo et al. (2010). In the glassy inclusions of Mutnovsky $S^{6+}/\Sigma S$ vary from 0.4 to 1, which corresponds to fO_2 within the range of QFM+0.9 to QFM+1.7. These fO_2 values are in a good agreement with previous estimations of redox conditions for island arc magma systems.

The combination of the natural and experimental observations gives us the possibility for evaluation of magma storage and pre-eruptive conditions for Mutnovsky. We can expect a magma chamber below Mutnovsky volcano at depth not deeper than 9 km (300 MPa), in which H_2O-rich magma was stored at approximately 1025-1075°C and relatively oxidized redox conditions (QFM+0.9 to QFM+1.7) and in which the mineral association Ol+Pl+CPx+Mt wasstable. The low water concentrations (and extremely low CO_2 concentrations) analyzed in glass inclusions in olivine can indicate that there is a shallow magma chamber (~ 100 MPa) in which olivine crystallized from an already partially degassed magma.

References:

Duggen, S., Portnyagin, M.V., Baker, J., Ulfbeck, D., Hoernle, K., Garbe-Schonberg, D., Grassineau, N. (2007) Drastic shift in lava geochemistry in the volcanic-front to rear-arc region of the Southern Kamchatkan subduction zone: Evidence for the transition from slab surface dehydration to sediment melting. Geochim. Cosmochim. Acta 71, 452-480.

Jugo, P.J., Wilke, M., and Botcharnikov, R.E. (2010): Sulfur K-edge XANES analysis of natural and synthetic basaltic glasses: Implications for S speciation and S content as function of oxygen fugacity, Geochim. Cosmochim. Acta 74, 5926-5938

Shishkina, T., Botcharnikov, R.E., Holtz, F., Almeev, R.R., and Portnyagin, M. (2010): Solubility of H_2O and CO_2-bearing fluids in tholeiitic basalts at pressures up to 500 MPa Chemical Geology 277, 115-125

IODP

Compositions of phyllosilicates from the TAG hydrothermal system at 26°N on the Mid-Atlantic Ridge as guide to subseafloor entrainment of seawater: Results from ODP Leg 158

L. SHU[1], W. BACH[1], A. KLÜGEL[1], N. JÖNS[1]

[1] Fachbereich Geowissenschaften, Universität Bremen, Klagenfurter Straße, 28359 Bremen

The TransAtlantic Geotraverse (TAG) hydrothermal system east of Mid-Adlantic Ridge at 26°N in a water depth of 3670 m is one of the largest known massive sulfide accumulations on the seafloor (2.7 million tonnes of sulfide; Hannington et al., 2005). TAG is a sulfide mound, 200 m in diameter and 45 m high, hosting several sites of hydrothermal venting of fluids with temperatures up to 360°C. TAG has been drilled during ODP Leg 158 (17 holes with depths up to 125 m below seafloor (mbsf). The drill cores indicate that much of the sulfide precipitation took place in the subseafloor (Humphris et al., 1998) and that the metals are redistributed within the mound by zone-refining processes (Humphris and Tivey, 2000). Both sub-seafloor precipitation and metal remobilization are due to entrainment of seawater into the hydrothermal upflow zone underneath the TAG hydrothermal mound. TAG hence offers a unique natural laboratory for studying the effect of seawater entrainment and wall rock interaction in massive sulfide deposit formation and evolution.

Previous studies of mineralogical, chemical and isotopic compositions of whole rocks and minerals have shown that the basement underneath TAG is zoned in terms of alteration type. The peripheral parts of the upflow zone are chloritized, with magnesian or ferroan chlorite

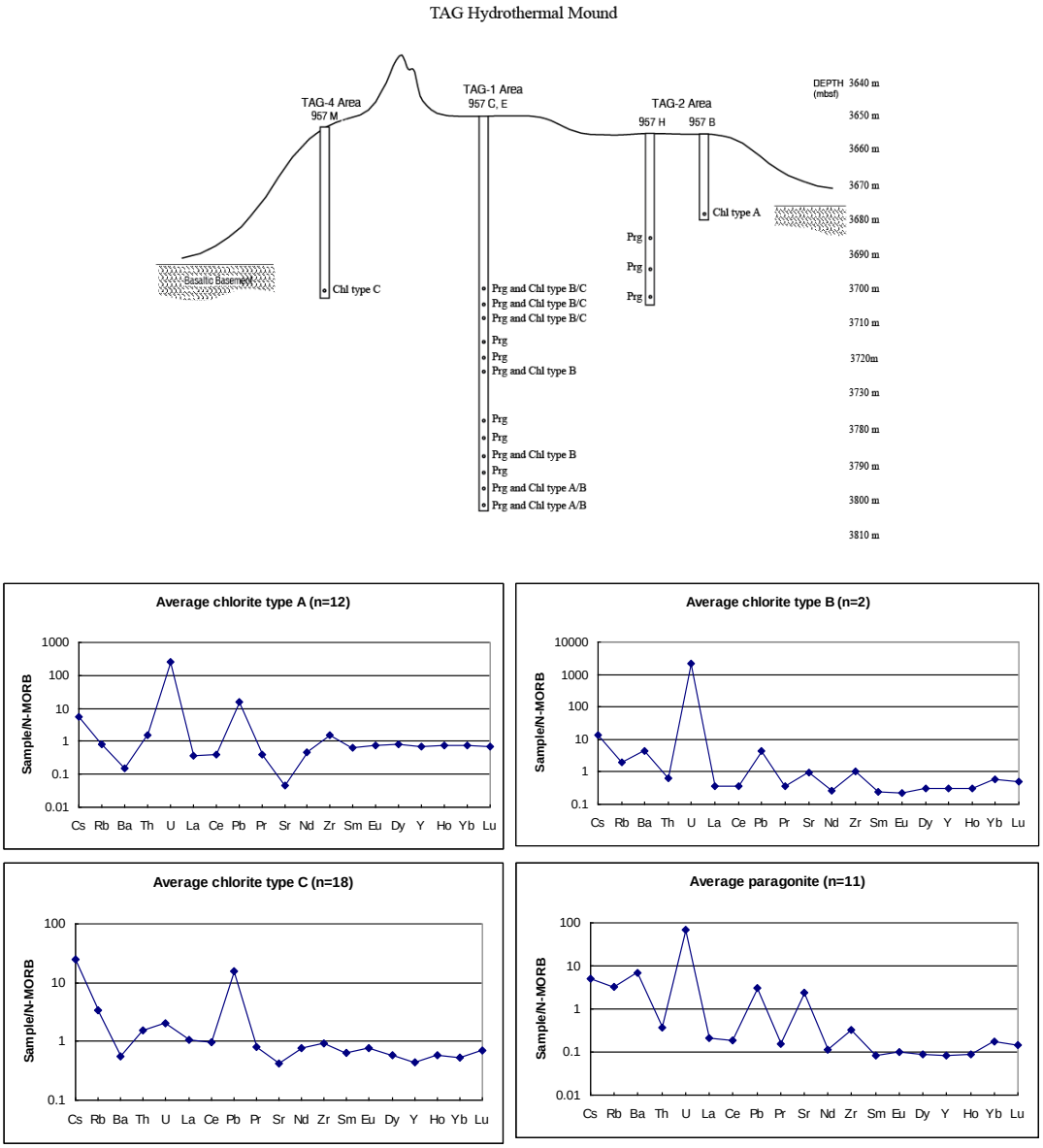

The top panel shows a schematic cross-section through the TAG hydrothermal mound, including the sample positions and mineral compositions. Chl=chlorite, Prg=paragonite. The bottom four panels present average trace element compositions (normalized to N-MORB (Sun and McDounough, 1989)) of different chlorite types and paragonite (see text) , 'n' is the number of the measured minerals.

dominating in different areas. Ferroan chlorite is also developed in the deepest drill cores (100-125 mbsf), but that zone grades into one enriched in paragonite at shallower depths. The uppermost basement underneath the mound is composed of silicified and sulfidized basalt, while the mound itself is composed of sulfide (mainly pyrite and lesser chalcopyrite) and anhydrite (Humphris et al., 1995). Anhydrite veining is developed throughout the drill core but is scarce below 60 mbsf. Anhydrite compositions provide valuable information about precipitation temperatures and seawater: hydrothermal fluid mixing ratios (Teagle et al., 1998; Mills and Tivey, 1999; Humphris and Bach, 2005). In this study, we focused on trace element systematics of chlorite and paragonite. The rationale behind this approach is that seawater (high U, low Pb, no Eu anomaly) has trace element characteristics different from hydrothermal fluids (low U, high Pb, positive Eu anomaly). Either chlorite or paragonite (and sometimes both) are abundant in almost every rock sample, even in areas in which anhydrite is missing. The phyllosilicate record may therefore provide additional constraints on subseafloor fluid mixing processes underneath the TAG mound.

The major element compositions of the phyllosilicates were measured by electron micoprobe at the University of Kiel. Chlorite from the upflow zone has Mg#s around 50 and shows variable extents of Tschermak-substitution (amesite). Chlorite in peripheral parts is either low in amesite component and magnesian (Mg#s of 70-90), e.g., in breccia cement from Hole 957B, or complex talc–smectite–Fe-chlorite intergrowths in alteration halos from Hole 957M. The presence of Mg-chlorite testifies to the seawater-dominated nature of the fluid percolating through the breccia, while the complex mineralogy and ferroan chlorite in the alteration halo from Hole 957M indicates low fluid flux and rock-dominated conditions. Paragonite is uniform in composition, but the chemical analyses reveal a notable amount of beidellite (or pyrophyllite).

Trace element concentrations were determined by laser-ablation ICP-MS at the University of Bremen. The paragonite patterns (see figures below) are fairly uniform and – compared to N-MORB – show positive Ba, U, Pb, Sr anomalies. In contrast, chlorite patterns are variable and can be divided into 3 different types: chlorite type A(see figures below) occurs in the breccia and in the deepest part of Hole 957E underneath the mound. Type A shows negative Sr and Ba anomalies and positive U and Pb anomalies. Chlorite type B occurs throughout Holes 957E and 957C in the central part of the mound, but is lacking in samples from the periphery of the upflow zone. Type B shows no or rare Sr anomaly but positive U, Ba, and Pb anomalies. Chlorite type C occurs in the halo from the peripheral part and in the uppermost basement from underneath the mound. It shows no significant U anomalies, but negative Ba anomalies and large positive Pb anomalies.

We propose that the different chlorite pattern types relate to sub-seafloor fluid flow dynamics, which are variably dominated by (i) seawater entrainment and heating, (ii) mixing of seawater and hydrothermal fluid, and (iii) pooling and conductive cooling of hydrothermal fluids. Our preliminary interpretation of the data collected thus far is that four stages can be distinguished:

Stage 1 (open to seawater): Entrainment and flash-heating of seawater caused formation of chlorite type A. The presence of type A chlorite deep in Hole 957E is consistent with anhydrite showing seawater-like Sr isotope compositions in the same core (Teagle et al, 1998; Tivey et al., 1998). Anhydrite precipitation seals conduits of seawater recharge.

Stage 2 (less open to seawater): Under reduced influx rates, seawater mixing with upflowing hydrothermal fluid is more prominent. Chlorite type B with positive U anomalies (from seawater) and positive Pb anomalies (from hydrothermal fluids) forms. Anhydrite with lower $^{87}Sr/^{86}Sr$ represents this stage (Teagle et al, 1998; Tivey et al., 1998). Precipitation of abundant anhydrite leads to competitive exclusion of Sr in chlorite, hence the negative Sr anomalies. Paragonite appears.

Stage 3 (little seawater entrainment): Fluid flow is reduced and reactions between mixed fluids and rocks in the upflow strongly affect fluid composition. Chlorite transitional type B/C forms; also, bulk of paragonite forms.

Stage 4 (seawater entrainment has ceased altogether): System is now entirely rock-dominated. Subordinate chlorite type C forms, which has no U anomaly; sparse paragonite; quartz dominates.

Our results show that phyllosilicate compositions of wall rock can be used to provide useful constraints on sub-seafloor seawater entrainment, which supplement and extend the record in gangue (e.g., anhydrite). Anhydrite is an ideal tracer in active hydrothermal systems, but (unlike phyllosilicates) it dissolves after hydothermal activity has ceased. Calibrating the phyllosilicate record of fluid evolution against that of anhydrite in the TAG subseafloor may hence provide us with a useful tool in studying fluid mixing in hydrothermal stockwork zones underlying ancient volcanigenic massive sulfide deposits.

References:

Hannington, M.D., de Ronde, C.E.J., Petersen, S., 2005. Sea-floor tectonics and submarine hydrothermal systems, in Hedenquist, J., et al., eds., 100th Anniversary Volume of Economic Geology: Littleton, Colorado, Society of Economic Geologists, p: 111–141.

Humphris, S. E., & Tivey M.K., 2000.A synthesis of geological and geochemical investigations of the TAG hydrothermal field: Insights into fluid flow and mixing processes in a hydrothermal system, in Ophiolites and Oceanic Crust: New Insights From Field Studies in the Ocean Drilling Program, edited by Y. Dilek et al., Spec. Pap. Geol. Soc. Am., 349: 213–235.

Humphris, S.E., et al., 1995. The Internal Structure Of An Active Sea-floor Massive Sulfide Deposit. Nature 377(6551): 713-716.

Humphris, S.E. & Bach, W., 2005. On the Sr isotope and REE compositions of anhydrites from the TAG seafloor hydrothermal system. Geochimica et Cosmochimica Acta, 69(6):1511– 1525.

Smith, S.E. & Humphris, S.E., 1998. Geochemistry of basaltic rocks from the TAG hydrothermal mound (26°08¢N), Mid-Atlantic Ridge. In Herzig, P.M., Humphris, S.E., Miller, D.J., and Zierenberg, R.A. (Eds.), Proc. ODP, Sci. Results, 158: College Station, TX (Ocean Drilling Program): 255–276.

Mills, R.A. & Tivey, M.K., 1999. Sea water entrainment and fluid evolution within the TAG hydrothermal mound: evidence from analyses of anhydrite. In: Cann, J.R., Elderfield, H., Laughton, A. (Eds.), Mid-Ocean Ridges. The Royal Society, Cambridge, pp: 225-263.

Teagle, D.A.H., Alt, J.C., Chiba, H., Humphris, S.E., Halliday, A.N., 1998. Strontium and oxygen isotopic constraints on fluid mixing, alteration and mineralization in the TAG hydrothermal deposit. Chem. Geol. 149: 1-24.

Sun, S.-S. & McDonough, W. F., 1989. Chemical and isotopic systematics of oceanic basalts: implications for mantle composition and processes. In Magmatism in the ocean basins (ed. A. D. Saunders & M. J. Norry). Geol. Soc. Lond. Spec. Publ. 42: 313-345.

Tivey, M.A., et al., 1998. Direct measurement of magnetic reversal Polarity boundaries in a cross-section of oceanic crust. Geophys. Res. Lett, 25: 3631-3634.

IODP

Estimation of endospore numbers in marine sediment samples by quantification of dipicolinic acid

M. SIEVERDING[1], B. ENGELEN[1], H. SASS[2], B. SCHOLZ-BÖTTCHER[1], H. CYPIONKA[1], J. RULLKÖTTER[1]

[1] Institute for Chemistry and Biology of the Marine Environment (ICBM), Carl von Ossietzky University of Oldenburg P.O. Box 2503, D-26111 Oldenburg, Germany
[2] School of Earth, Ocean and Planetary Sciences, Cardiff University, Park Place, Main Building, Cardiff CF10 3YE, Wales, U.K.

For more than 20 years, the scientific drilling community has studied microbial life in deeply buried sediments [1,2]. During these studies, prokaryotes were detected even at 1600 mbsf [3]. Extrapolation of direct counts of microbial cells leads to the estimate that one tenth to one third of the world's living biomass may be stored in the marine sub-seafloor biosphere [4]. Until today, it is unclear as to what extent these prokaryotes are active, since fluorescence dyes, like acridine orange or DAPI, do not discriminate between metabolically active, dormant or dead cells. These dyes even stain endospores.

In our study we show that in marine sediments endospores contribute up to 19 % to the total cell numbers at some tens of meters depth. Our results suggest that the relative contribution of endospores to the microbial community may generally increase with depth and age of the sediment. Furthermore, endospores are able to germinate within minutes if environmental conditions change (e.g. inflow of nutrients). Hence, knowledge about the number of endospores also gives an impression of the microbiological potential in the respective area. For this reason, we quantified the number of endospores and point out their significance as an important fraction of total cell numbers within sediments from the deep biosphere.

Dipicolinic acid (DPA), which is a major chemical cell component of endospores, was used to quantify endospores in up to 20 m long sediment cores collected from a tidal flat area near Spiekeroog Island, NW Germany, as well as in several sediment samples from ODP Leg 201. DPA contents were determined fluorimetrically using a highly sensitive post-column complexation HPLC approach [6]. DPA contents ranged from 0.004 to 1.7 nmol DPA g^{-1} sediment dry weight, corresponding to 1.6×10^4 to 7.7×10^6 spores g^{-1} sediment dry weight.

For conversion of dipicolinic acid contents into endospore numbers an average DPA content of 2.24×10^{-16} mol per endospore was assumed; the calibration is based on volume-DPA content relationships in cultures spores from the study area. The endospore depth profiles of the tidal flat sediments were non-linear, but reflected the vertical changes in lithology. The highest endospore numbers were found in muddy samples, while significantly lower numbers were detected in sandy sediments. The contribution of endospore numbers to total cell counts increased with sediment depth reaching up to 10 % of total cell counts in the deepest layer. In sediment samples from IODP Leg 201 the contribution of endospores to total cell numbers is even higher, ranging from 3 to 19 %. The relative increase of endospore contribution to total cell numbers with sediment age is explained by the longevity of endospores, whereas numbers of vegetative cells are expected to decrease more rapidly due to starvation.

References:

[1] Whelan, J.K., Oremland, R., Tarafa, M., Smith, R., Howarth, R., Lee,C., 1986. Evidence for sulfate-reducing and methane-producing microorganisms in sediments from sites 618, 619, and 622. Initial Reports of the Deep Sea Drilling Project 96, 6578-6583.
[2] Parkes, R.J., Cragg, B.A., Bale, S.J., Getliff, J.M., Goodman, K., Rochelle, P.A., Fry, J.C., Weightman, A.J., Harvey, S.M. 1994. Deep bacterial biosphere in Pacific-Ocean sediments. Nature 371, 410-413.
[3] Roussel, E.G., Cambon-Bonavita, M.A., Querellou, J., Cragg, B.A., Webster, G., Prieur, D., Parkes, R.J., 2008. Extending the sub-sea-floor biosphere. Science 320, 1046.
[4] Whitman, W.B., Coleman, D.C., Wiebe, W.J., 1998. Prokaryotes: The unseen majority. Proceedings of the National Academy of Sciences of the USA 95, 6578-6583.
[5] Parkes, R.J., Cragg, B.A., Wellsbury, P., 2000. Recent studies on bacterial populations and processes in subseafloor sediments: A review. Hydrogeology Journal 8, 11-28.
[6] Fichtel, J., Köster, J., Scholz-Böttcher, B., Sass, H., Rullkötter, J., 2007. A highly sensitive HPLC method for determination of nanomolar concentrations of dipicolinic acid, a characteristic constituent of bacterial endospores. Journal of Microbiological Methods 70, 319-327.

ICDP

Carbonation of porous rocks by interaction with magmatic and hydrothermal fluids - a case study on Unzen volcano, Japan

A. SIMONYAN[1], S.DULTZ[2], H. BEHRENS[1], J.FIEBIG[3], K.VOGES[1]

[1] Institute for Mineralogy, Leibniz University of Hannover, Callinstr. 3, D-30167 Hannover
[2] Institute of Soil Science, Leibniz University of Hannover, Herrenhäuser Str. 2, D-30419 Hannover
[3] Institute for Geosciences, J.W. Goethe University of Frankfurt, Altenhöferallee 1, D-60438 Frankfurt am Main

Unzen is a large composite volcano of dacite to andesite composition, characterized by non-explosive activity throughout its history (Hoshizumi et al., 1999). The Unzen drilling project was the first attempt to get insights into the mechanisms of volcanic eruptions by drilling into an active volcano shortly after eruption. The strong alteration of drilled rocks with large amounts of secondary minerals such as carbonates, chlorite and pyrite, supposed to be products of reactions of discharged volcanic fluids with the host rocks, inspired us to use the drilling cores in combination with experimental work to have closer look on the mechanisms of fluid-rock interaction, in particular the carbonation and decarbonation of rocks. This research is not only important for understanding the deep degassing of volcanoes, but it has also major impacts for storage of CO_2 in cavities or in porous/brecciated volcanic rocks. For instance, the formation of carbonate immobilizes CO_2 and may strongly change the permeability of rocks by closing open paths.

From microprobe investigations and back scattered electron images it is visible that amphiboles are strongly altered in all samples. The largest contents of Ca,Mg-carbonates were determined by image analyses in the samples C13-C16. The content of carbonate is up to 20 wt.%. These rocks were sampled at depth of 1975-2000 m in the magmatic conduit of Unzen. The most abundant phenocrysts in the rocks are plagioclases and amphiboles, whereby plagioclases are much more stable against alteration. Alteration of amphiboles is related to the formation of two types of carbonates, i.e., Ca-rich and Mg-rich, quartz, fine-grained muscovite and chlorite (Fig. 1). Carbonates are also observed in cracks and pores of the groundmass. The altered hornblende has a complicated microstructure and contains amphibole relicts and various minerals such as plagioclase, calcite and/or dolomite, quartz, chlorite, mica, pyrite and rutile. Typically, chlorites are formed at the outer rim of the altered hornblende crystal.

Pore volume of connected pores and the distribution of pore sizes were determined by mercury intrusion porosimetry (MIP). The pore size distribution was calculated from the minimum pressure required to fill pores of a certain radius with Hg by using the Washburn equation. The specific surface area (SSA) was calculated from the pore volume and the distribution of pore sizes. Further information about SSA and pore volume of fine pores in the range from 0.5 nm to 200 nm was obtained from N_2-adsorption. Adsorption and desorption isotherms, obtained for unaltered and altered dacites have the normal form of isotherm obtained for a nonporous or macroporous adsorbent (Dullien, 1992). A maximum in the micropore size distribution from N_2-adsorption method was observed at 3 - 5 nm in all core samples (Fig. 2a) and is attributed to the presence of chlorite. For the unaltered dacite the proportion of micropores is insignificant. The MIP data indicate broad maxima in the sub-micrometer range. The inflection points in Fig.2b mark the maxima in pore size distribution. The most frequent pore sizes for coherent altered dacites are observed in the range between 30 and 400 nm, whereas only few pore radii are larger than 10 µm. For the brecciated dacite C5-4-2-20 three inflection points

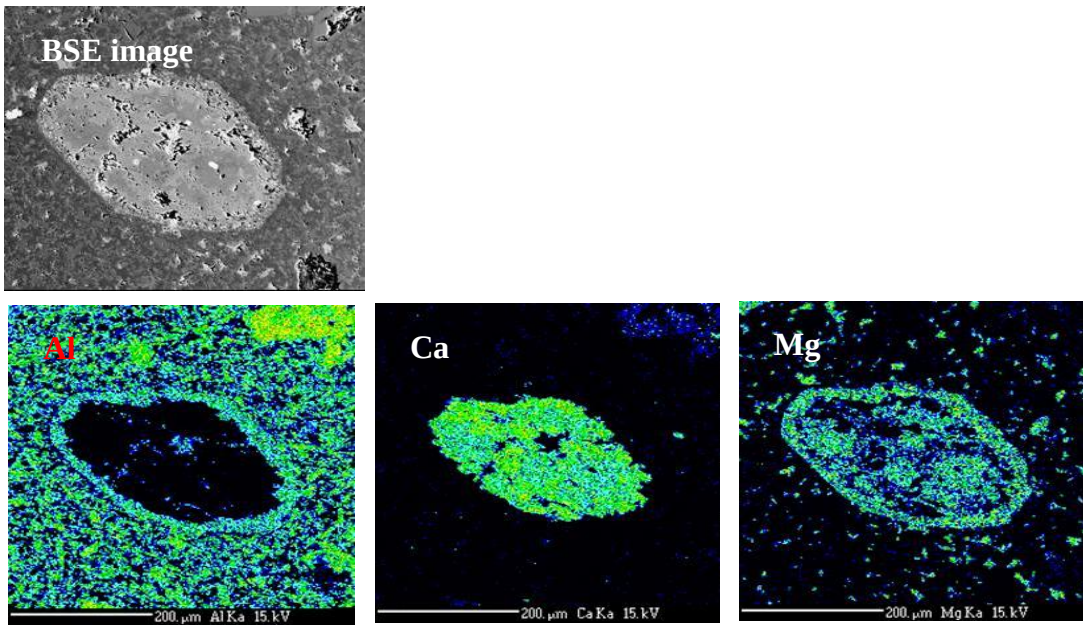

Fig. 1. Back scattered electron image of amphibole alteration in a polished section of sample C13-2-10 and element maps for Al, Ca and Mg obtained by electron microprobe. The presence of different mineral phases in the samples together with aggregates of layer silicates is a challenge for image analysis, where it is tried to separate the regions of pores and carbonates.

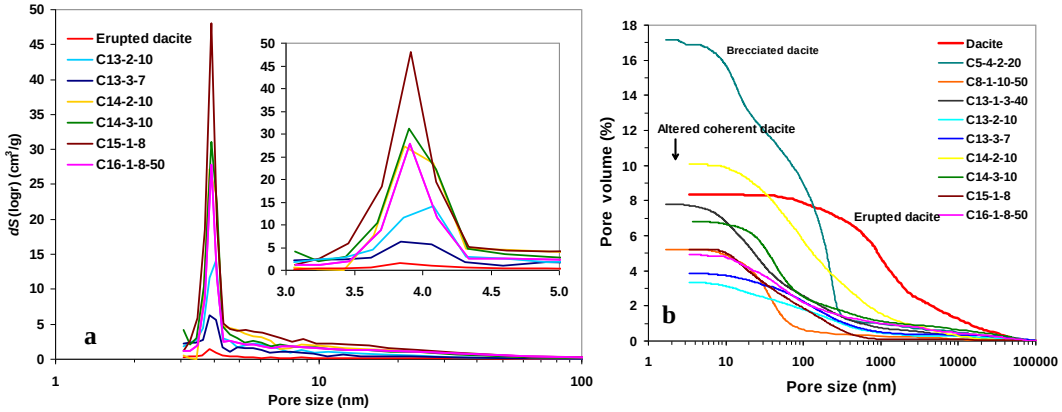

Fig. 2 (a) Pore size distribution of the altered and unaltered dacites determined by N_2-adsorption. (b) Cumulative normalized (volume-based) pore size distribution of the altered and unaltered samples determined by MIP. The inflection point on the branch shows the maximum in pore size.

are observed indicating difference in density and structure compared to the other samples and implying that this sample can potentially have different transport properties. Based on MIP unaltered dacite has pores in the range from 100 nm to 10 µm. For the altered samples (e.g., C15-2-8) and unaltered dacite the difference in pore size distribution both for micropores and mesopores is obvious and different control of diffusion transport can be expected.

Impregnation with Wood's metal shows that interconnected porosity is characteristic for all samples as illustrated for samples C13-2-10 (Fig. 3a,b) and C15-1-80-20 (Fig. 3c) from the conduit depth of 1975-2000 m. A marked tortuosity of the pores is visible at higher magnification (Fig. 3b,c). This image shows the outer rim of the altered hornblende, where chlorite is formed. The altered rims of amphibole, which contain chlorite, have very high porosity while the cores, formed mainly by carbonates, are very dense. Here the intrusion of the alloy results in an excellent contrast for the layer silicates. From Fig. 3c it can be seen, that chlorite is arranged during mineral replacement in different microstructures, dense arrangements are observed on the left side, and pore fillings with chlorite on the right side. These microstructures suggest a chronological sequence of formation of chlorite.

The spatial distribution of pores and carbonates of the altered hornblende phenocryst is shown in Fig. 4 a,b. The images were obtained using microtomography at the TOMCAT beamline of the synchrotron light source of the Paul Scherrer Institute, Villigen, Switzerland) and created with the 3D graphic program OpenGL. From the distribution of carbonates as well as pores the shape of the replaced crystal can be reconstructed and also zones where chlorite is formed can be seen in the outer rim.

The assignment of different areas obtained by cluster analysis to pores and mineral phases was based on microscopic observations and on the amount of carbonates and pores quantified in the samples. For the area of carbonates shown in Fig. 4a, b the content (8.3 wt.%) obtained by cluster analysis is in good agreement with the one determined by image analysis (8.1 vol.%). Carbonates are not only observed in altered hornblende phenocrysts but also finely distributed in the matrix of the rock. The pore volume was found to be underestimated by image analysis. For the sample shown in Fig. 4, pore volume determined by Hg-porosimetry is 3.3 vol.%, whereas with the image analysis it is only one third of this value. This underestimation can be assigned to the fact that small pores less than the pixel width of 350 nm and pores which were not fully imaged within one pixel are not detectable by image analysis.

The investigated amphiboles exhibit a quite homogeneous oxygen isotopic composition, with their $\delta^{18}O$ vs VSMOW varying between 6.6 and 7.0‰. Chen et al. (1999) reported $\delta^{18}O$VSMOW values of 8.0 to 8.4‰ for

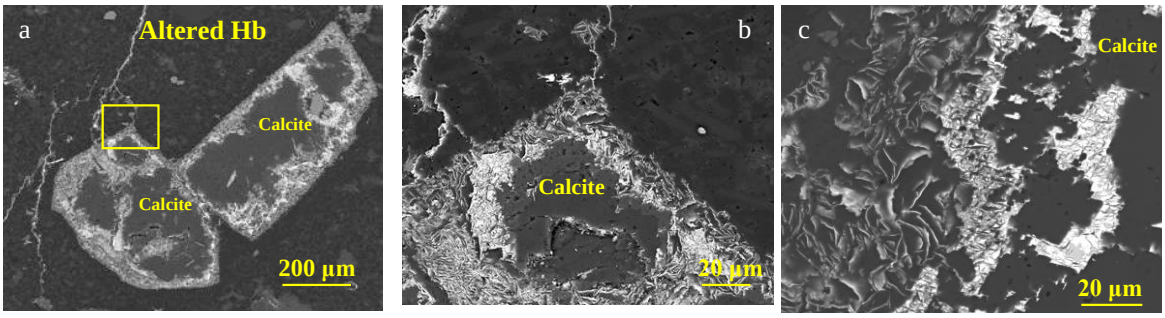

Fig. 3 (a) Back scattered electron images showing the heterogeneity of connective pore networks after intrusion of the molten alloy "Wood`s metal": (a, b) sample C13-2-10 and (c) sample C15-1-80-20. Tortuosity of pores is shown for the outer rim of the altered hornblende phenocryst where chlorite was formed in the pores. Bright: Wood`s metal.

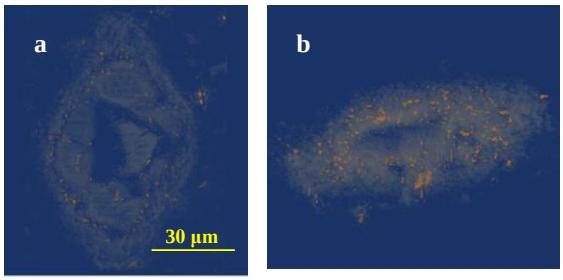

Fig.4 (a, b): Images of pores (orange) and carbonates (grey) of an altered hornblende phenocryst. Displayed are the areas of the separated regions. Perspective view are along the length-axis (a) and from the side (b). In the latter one the connected (orange) pores are visible.

fresh, unaltered dacitic lava deriving from two eruptions in 1991. These values are well within the range of 8.1 to 8.9‰ obtained for historic dacitic lava products. The oxygen isotope fractionation factor between bulk dacite and hornblende at magmatic temperatures is unknown. However, from the data provided by Zheng (1993) and Zhao & Zheng (2003) it can be calculated that the oxygen isotope fractionation between andesite and hornblende ranges from 1.3 to 1.6‰ and that between rhyolite and hornblende between 1.9 and 2.3‰, respectively, at crystallization temperatures of 800-1000°C. The oxygen isotope fractionation between dacite and hornblende during crystallization can be expected to lie within the range defined by these two end-member fractionations, i.e. being not smaller than 1.3‰ and not larger than 2.3‰. Considering that the δ^{18}OVSMOW of recent and historic dacite lava at Unzen varies between 8.0 and 8.9‰, the measured δ^{18}OVSMOW values of 6.6 to 7.0‰, therefore, point to a primary magmatic origin of the hornblende. From oxygen isotope analysis alone, however, we cannot exclude secondary alteration of the hornblende at low water/rock ratios, because at low water/rock ratios the oxygen isotopic composition of the exchanging hornblende would remain unaffected.

The carbonate carbon isotopic composition varies between –4.7 and –6.4‰ vs VPDB, whereas its oxygen isotopic composition ranges from 6.0 to 9.1‰ vs VSMOW. Carbonate δ^{13}C VPDB values are identical to those measured for the magmatic CO_2 discharging at Unzen volcano (δ^{13}CVPDB = –3.9 to –6.4‰; Ohba et al., 2008; Shinohara et al., 2008), whereas carbonate δ^{18}OVSMOW values are indistinguishable from those reported for fumarolic water vapor (7.4‰ < δ^{18}OVSMOW < 10.0‰; Ohba et al., 2008) and primary volcanic rocks (6.9‰ < δ^{18}OVSMOW < 8.9‰, Ohba et al., 2008). Carbonate δ^{18}OVSMOW values are, however, different from those characteristic for the local meteoric water (δ^{18}OVSMOW ~ –6‰; Mizota & Kusakabe, 1994). It, therefore, appears that magmatic CO_2 and primary silicates provide the sources for the carbonate carbon and carbonate oxygen, respectively.

Hydrogen isotope composition of unaltered amphiboles shows typical magmatic signatures (δD=-48‰) without any evidence for late- or post-magmatic contamination by meteoric waters. The analysis of several altered samples showed that presumably chlorite or matrix glass are the main water-bearing phases in samples (the bulk δD varies from -84 to -92‰). These values are lower than those reported for local meteoric water, having δD values around -40‰ (Mizota & Kusakabe, 1994) and even lower than those reported for the high temperature gases discharging from Unzen (δD = -25 to -40‰; Ohba et al., 2008; Shinohara et al., 2008). Hydrogen isotope fractionation factors between chlorite and water are poorly constrained. However, empirical and experimental studies imply that chlorite is depleted in D relative to water by 50 to 30‰ in a temperature range of 100-500°C (Chacko et al., 2001). In this respect, chlorite might have been generated from an interaction of silicates especially hornblende, indicated by layers of chlorite at the rim of phenocrysts, with fumarolic water vapor and/or meteoric water.

A series of hydrothermal fluid /rock interaction experiments in different systems, i.e., dacite or pure amphibole + H_2O, $H_2C_2O_4{\cdot}2H_2O$, $Ag_2C_2O_4$, Pl, $CaCO_3$ in different proportions were conducted at temperatures from 300 to 700°C and at pressures from 100 to 150 MPa, respectively. The run duration was varied from one to five weeks, whereas the fluid/rock ratio was varied between 0.3 and 9.5. The first analyses of the experimental products show that amphiboles participate in exchange reactions with the formation of new mineral phases, however the size of produced phases was too small for proper identification. It turned out to be crucial to separate the fluid from the solid material, i.e. to distinguish quench phases produced by oversaturation of the fluids during cooling, from phases grown under experimental conditions. For doing so, we have developed a new sample assemblage in which a clamp narrows the capsule above the solids (the applicability of this tecnique was confirmed by a reproduction of experiments with olivines after Dufaud et al., 2009).

Raman spectroscopy on our experimental products shows that new phases have spectral characteristics different from calcite. On the other hand, Raman spectra confirm that carbonates are indeed present as secondary phases in altered amphiboles. Further experiments are required to reproduce natural mineral assemblages and to determine typical conditions for carbonate formation in Unzen conduit.

The next steps of our work are the in-situ investigation of solution and element transport within the pore system and the experimental study of formation/dissolution of carbonate in rock samples. The results of our research will be combined with findings from other research groups working on Unzen volcano to improve our understanding of fluid-rock interaction and volcanic degassing.

References:

Chacko et al., 2001; Chen et al., 1999; Dufaud et al., 2009; Dullien et al., 1992; Hoshizumi et al., 1999; Mizota & Kusakabe, 1994; Ohba et al., 2008; Shinohara et al., 2008; Zhao and Zheng, 2003; Zheng, 1993.

IODP

Cold Aspects of past neogene warm Climates – interim Results

P.P. SMOLKA

University Muenster

Neogene climates appear(ed) to be suitable to study the upper limit of climate change. The time interval 4–5 Ma is the warmest time interval with persisting "El–Nino"–type temperature distributions. Coupling this ocean with an atmospheric GCM yields non–reconstructable parameters such as wind–fields and snow–fall. The resulting snow–rich and cold winters on the Northern Hemisphere (NH) continents are consistent with observed ice rafted debris (IRD) during the Pliocene in the Norwegian Sea (ODP site 642B) and respective sites in the North Pacific. The IRD is data, independent of SST reconstructions and modelings. Thus the Pliocene had colder aspects than generally thought. Other reconstructed Neogene time intervals, such as 5–6 Ma appear in northern higher latitudes, using the same reconstruction method, considerably colder, even though in the tropical oceans high SSTs occur. In addition threfore for *one* aspect of present climates (selected years with high tropical SSTs in coexistence with present Arctic sea ice and observed high snowfall in subsequent winter on NH continents) results from Neogene environments might be used as early indicator of one of several possible trajectories of climate change.

Neogene and Pleistocene environments might appear useful as proven scenarios for future climate change:

All Pleistocene warm time intervals are characterized by the co–ocurrence of temperatures of 3°C above preindustrial levels *and* IRD (e.g. ice floes) in the Norwegian Sea and the North Pacific. High Pleistocene "greenhouse"–temperatures did not prevent IRD in the Norwegian Sea and Arctic Sea ice further north. Thus in the Neogene an ice covered Arctic ocean coexisted with high tropical SSTs. Today these Pleistocene high temperatures are still not reached. The temperature levels of warm Pleistocene times – with IRD in the Norwegian Sea – appeared in the past as one upper limit of climate change.

Today, at least in the Norwegian Sea at ODP site 642B, no IRD occurs, neither in summer nor in winter. Thus, data based, one boundary condition of the climate system is today different from the Pleistocene and Pliocene. Thus the Holocene appears not be one of several interglacials any more. Only in this case IPCC scenarios of future climates, that regard +6°C, e.g. well above the +3°C of Pleistocene warm times, as possible, might apply. In this case (Holocene no interglacial) Neogene climates might only *partially* be a key to the future.

Alternatively, which needs to be tested, high SSTs in coexistence with Arctic Sea ice generate conditions (wind fields during NH winter, ice floes) that lead to IRD in the Norwegian Sea.

To test this, long (ideally 3 Ma) transient runs of coupled atmosphere/ocean models are needed. If the climate fluctuations of the past are met (overall) correct, the used boundary conditions, such as depth of the Greenland–Scotland Ridge through time, details of the Straits of Florida, apply. If the boundary conditions need to be modified until the model reproduces the known climate fluctuations testing by subsequent drilling provides the data.

IODP

A SEAWAT-2000 approach for modeling the fresh and salt water genesis in the New Jersey Shallow Shelf, Exp. 313

S. STADLER [1], H. HOLLÄNDER[2], T. HAYASHI[3], M. MOTTL[4] AND THE EXP313 SCIENCE PARTY[5]

[1] Federal Institute for Geosciences and Natural Resources (BGR), Hanover, Germany
[2] State Authority of Mining, Energy and Geology (LBEG), Hanover, Germany
[3] Akita University, Akita City, Japan
[4] University of Hawaii, Honululu, USA
[5] ECORD Science Operator, Edinburgh, United Kingdom

During the Integrated Ocean Drilling Program (IODP) Expedition 313 to the New Jersey Shallow Shelf off the east coast of the United States three boreholes were drilled (Holes M0027A, M0028A, M0029A) 45-67 km offshore to depths up to 757 meters below seafloor. Tertiary aquifers were penetrated during drilling which contained saltwater. The respective underlying lowly permeable layers showed salt concentrations down to 5 g Cl/L. Onshore and coastal-near offshore investigations of the USGS showed the existence of fresh water in all tapped aquifers. They suggested that fresh water could be available more than 100 km offshore (Cohen et al., 2010).

Using the density-driven flow model SEAWAT-2000 we test our hypothesis that freshwater aquifers were built when the sea level was lower (Vail et al., 1977). Rising sea levels resulted in higher hydraulic heads which caused salt water to intrude into the aquifers from the margins of the shelf. The salt water diffused from the aquifers into the lowly permeable layers causing the Cl concentration to still be low. The present situation appears to be a function of the interplay of recharge from onshore outcrops of the aquifers and the salt water intrusion from the margins of the shelf. In addition, the deeper layers of the system are influenced by evaporites (Mountain et al., 1994), where diffusive profiles can be found.

References:

Cohen, D., Person, M., Wang, P., Gable, C.W., Hutchinson, D., Marksamer, A., Dugan, B., Kooi, H., Groen, K., Lizarralde, D., Evans, R.L., Day-Lewis, F.D., and Lane Jr., J.W. (2010): Origin and Extent of Fresh Paleowaters on the Altantic Continental Shelf, USA. Groundwater, 48(1):143-158.

Mountain, G.S., Miller, K.G., Blum, P., et al., (1994): Leg 150: New Jersey Continental Slope and Rise. Proc. ODP, Init. Repts., 150: College Station, TX (Ocean Drilling Program). doi:10.2973/odp.proc.ir.150.1994.

Vail, P.R., Mitchum Jr., R.M., and Thompson III, S. (1977): Seismic stratigraphy and global changes of sea level-pt 4, Global cycles of relative changes of sea level. Seismic stratigraphy-application to hydrocarbon exploration: American Association of Petroleum Geologists Memoir, 26:83-97.

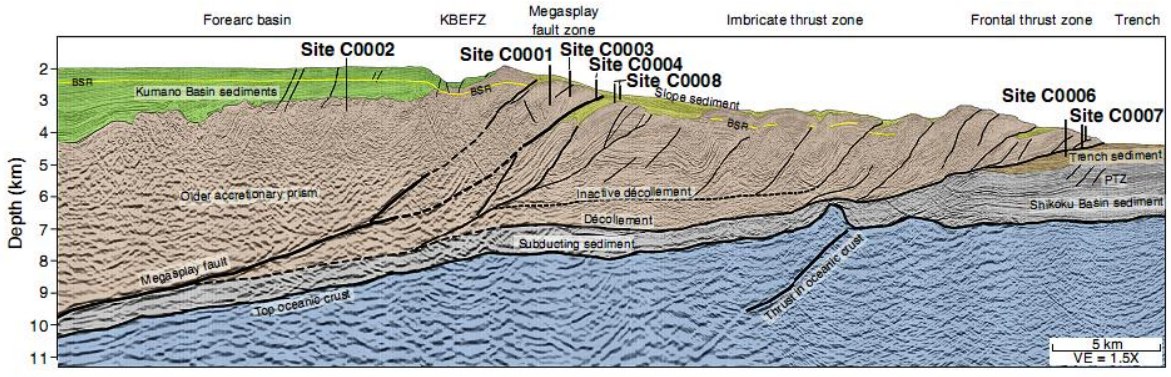

Fig. 1: Seismic cross section of the plate boundary from Park et al., [2002] with tectonic interpretation of Moore et al. [2009]. NanTroSEIZE drilling sites cored during IODP expeditions 315 and 316 are shown.

IODP

Structurally weak sediments indicate a high tsunami risk for the Megasplay fault of the Nankai accretionary prism (Japan)

M. STIPP[1*], M. ROLFS[2], Y. KITAMURA[3], J.H. BEHRMANN[1]

[1] Marine Geodynamics, IFM-GEOMAR, Kiel, Germany; [*]mstipp@ifm-geomar.de
[2] TU Hamburg-Harburg, Germany, malte.rolfs@tuhh.de
[3] JAMSTEC, Yokusuka, Japan, ykitamura@ifm-geomar.de

1. Introduction

The NanTroSEIZE (Nankai Trough Seismogenic Zone Experiment) drilling project of IODP in the SW Japan forearc is the first-ever attempt to core and instrument the updip end of the seismogenic part of a subduction zone (see review in Dixon & Moore, 2007). Hence, the project is dedicated to plate boundary deformation, accretionary prism formation and the upper seismogenic zone of the Nankai trench at which the Philippine sea plate is subducted below the Japanese islands Honshu and Shikoku (Eurasian plate; Fig. 1). IODP expeditions 315 and 316, from which our experimental sample material is recovered, investigated the shallow frontal thrusts, and the hanging wall to a major active splay fault of the active frontal thrust system in the Nankai accretionary prism (e.g., Kinoshita et al., 2009). For the tsunamigenic potential of this thrust system it is important to know if the sediments are dominated by localized brittle deformation and related near-surface fault slip, or alternatively, by distributed deformation and strain weakening causing a strain-dissipative creep-like behavior.

To answer this question, 17 core samples of IODP expeditions 315 and 316 from a depth range of 48-128 m below sea floor were experimentally deformed in a triaxial cell using sample cylinders (5 cm in diameter, up to 10 cm in length) under consolidated and undrained conditions at confining pressures of 400-1000 kPa, room temperature, axial displacement rates of 0.005-0.1 mm/min and up to axial compressive strains of ~48%. After saturation and consolidation three different geotechnical deformation tests were performed: (1) single step compression at constant confining pressure and displacement rate (Fig. 2), (2) pressure stepping compression at constant displacement rate and three different confining pressures (Fig. 3), and (3) displacement rate stepping compression at constant confining pressure and increasing displacement rate.

2. Results

Despite the consistent low depth range and the lithological similarity of the sample cores, the samples can be separated into two distinct 'rheological groups'. The first sample group shows deviatoric peak stress after only a few percent of compressional strain (< 10%) and a continuous stress decrease after peak conditions (Fig. 2A; Fig. 3). Simultaneous to this decrease there is a pore pressure increase indicating contractant behavior characteristic of structurally weak material (Fig. 2B; e.g.

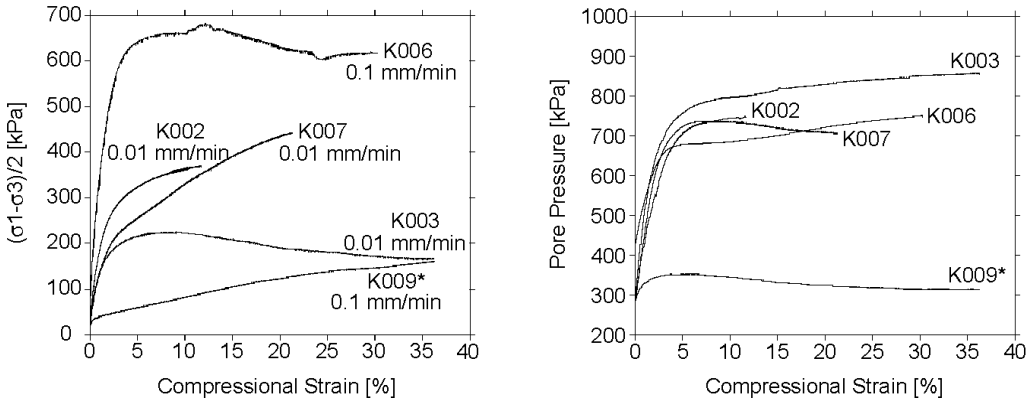

Fig. 2: Creep test results (single step axial compression experiments) at constant displacement rates and constant confining pressure of 1000 kPa except for sample K009 carried out at 400 kPa (marked by a star). A) Stress/strain-records, sample numbers and displacement rates are indicated. B) Related pore pressure/strain-records, sample numbers are indicated in correlation to A.

Sultan et al., 2004). The second sample group does not weaken at all, but displays strengthening characteristics until finite strain (Fig. 2A; Fig. 3). These samples are structurally strong (e.g. Sultan et al., 2004), and they are characterized by a decreasing pore pressure with increasing compressional strain indicating dilatant behavior after a maximum pore pressure at < 10% strain (Fig. 2B). A few exceptional samples with somewhat intermediate behavior reach high deviatoric peak stresses after significantly higher strain (> 10%) than the structurally weak samples. They weaken only moderately to a relatively high residual strength level or they show a steady-state like behavior at constant deviatioric stress (e.g., K006; Fig. 2A. Their pore pressure/strain-relationships more or less correspond to what is commonly expected for structurally weak material with some slight variations.

overburden previously removed by tectonic or erosive processes. Considering a specific weight under buoyancy with respect to the high porosity and pore water content nearly hydrostatic pressure conditions would have acted on the samples. For most of them an effective preload of 600-750 kPa can therefore be assumed. Only the cores C0001E-11H (91 m) and C0006E-20X (128 m) came from significantly greater depth. The stress paths can be related to the proposed preloading, which allows to constrain if the core samples suffered a normal consolidation path or if they are overconsolidated. The data show that four experiments indicate normal consolidation in agreement with their known overburden. K005 is characteristic of underconsolidation, as it displays underconsolidated conditions already for the second pressure step at 640 kPa, while the core sample was recovered from 91 m depth (Fig.

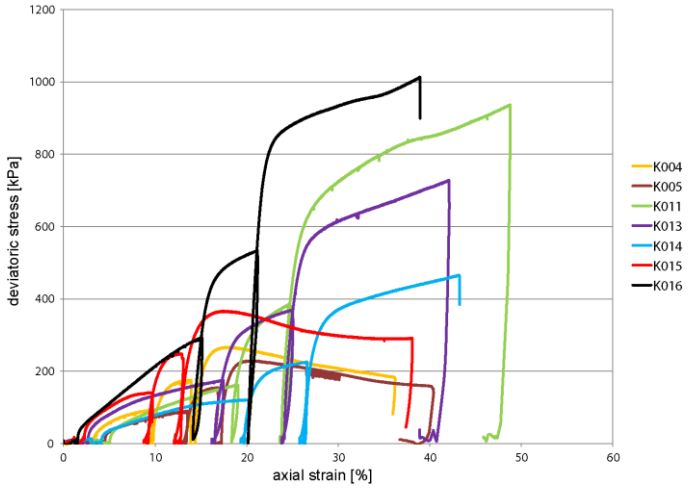

Fig. 3: Stress/strain-records of pressure stepping experiments at confining pressures of 400, ~640 and ~1000 kPa and constant displacement rate of 0.1 mm/min; sample numbers are indicated.

Pressure stepping experiments (Fig. 3) can be used to determine the effective shear parameters cohesion (C) and angle of internal friction (ϕ). For experiments K004, K005 and K015 the maximum $\sigma1/\sigma3$ could be determined from the three pressure steps and the Mohr-Coulomb condition could be plotted (Fig. 4). For the other four pressure stepping experiments a peak strength could not be reached, but the stress-strain records display continuously increasing trends. Therefore, we defined the criterion maximum $\sigma1/\sigma3$ at or extrapolated to 10% axial strain from which the Mohr-Coulomb condition was plotted for the experiments K011, K013, K014 and K016 (Fig. 4). The resulting C- and ϕ-values from the Mohr-Coulomb plots are summarized in Table 1. Experiments K004, K005, K014 and K015 show cohesion values of 25-50 kPa and angles of internal friction of 24.6 - 28.7° in accordance to clay or silty clay. K013 agrees in the cohesion (29 kPa), but has a slightly too high internal friction angle of 32°. Internal friction angles of experiments K011 and K016 are much too high for the sample material (> 35°) and the cohesion of these two samples is low (12 and 4 kPa, respectively).

The detected stress paths of the experiments can be used to determine the state of sample consolidation, i.e. if the sample is under- or overconsolidated at the given deformation conditions. The sample material suffered different compaction when solely taking the original depths of the cores into account and neglecting any higher

5). In contrast, K011 and K016 (~63 m depth, from the same core) imply overconsolidation, because all of their stress paths are indicative of overconsolidated conditions (Fig. 5).

Discussion

The structurally strong samples tend to be overconsolidated and are all from the drill holes at the toe of the accretionary prism, while the weak and preferentially underconsolidated samples are from the hanging wall of the Megasplay fault (Fig. 6). This geomechanical characterization corresponds to the tectonic disposition of more distributed deformation and folding at the prism toe and strong faulting and localized deformation in the Megasplay zone. Hence, we postulate that brittle faulting of the structurally weak sediments of the Megasplay zone in response to a large seismic event is capable of producing surface breaks generating tsunamis. In contrast, the structurally strong sediments from the accretionary prism toe are more amenable to slow, stable slip and distributed deformation (folding) within large volumes. The observed difference in rheological behavior is therefore a key for understanding strain concentration and brittle faulting within the rather uniform silty and clayey sedimentary sequence of the Nankai accretionary prism.

Experiment	K004	K005	K011	K013	K014	K015	K016
core number and section	C0004C -8H-2	C0001E -11H-1	C0007C -7X-1	C0006E -20X-2	C0008A -9H-3	C0008C -7H-8	C0007C -7X-1
depth [mbsf]	65,26	91	62,89	127,975	76,06	60,96	62,89
cohesion [kPa]	25,7	24,9	12,1	29,3	34,1	49,7	4,2
angle of friction	27,1°	24,6°	35,8°	32°	28,7°	25,3°	40,4°

Table 1

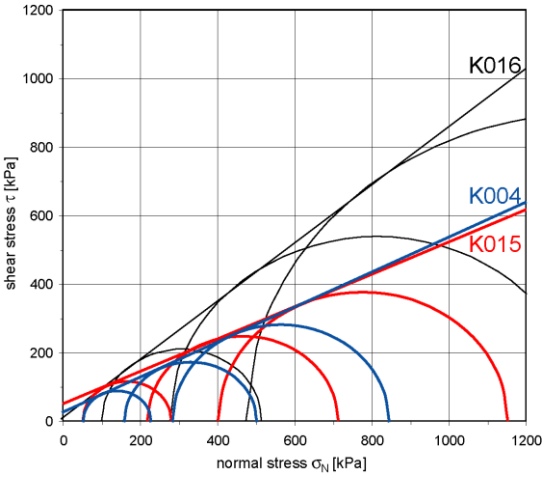

Fig. 4: Mohr-Coloumb diagrams from the experiments K004, K015, K016.

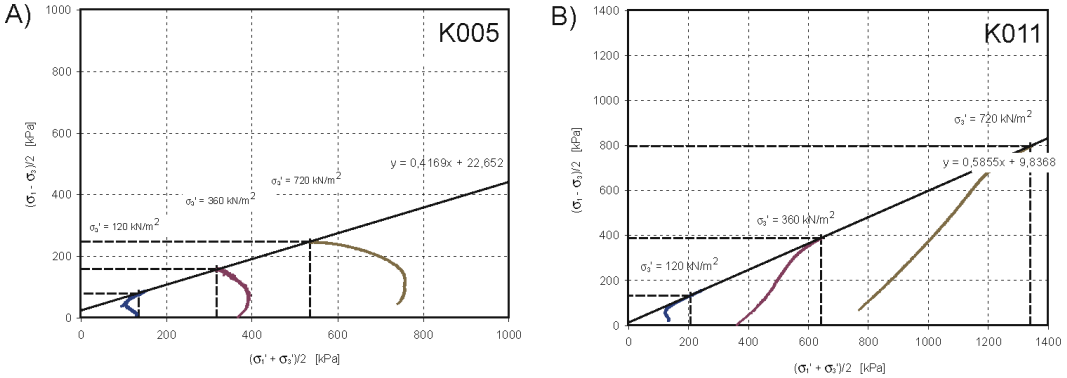

Fig. 5: Stress path diagrams of the pressure stepping tests with examples of (A) underconsolidation (K005; 91 mbsf), and (B) overconsolidation (K011; 63 mbsf).

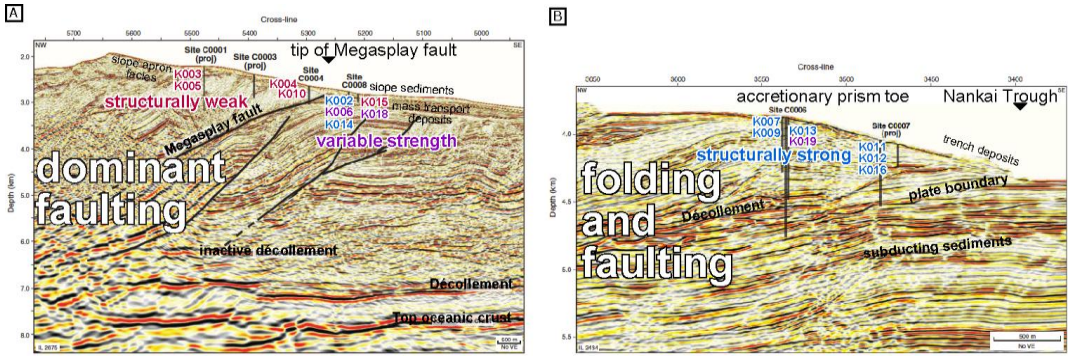

Fig. 6: Distribution of structurally weak and strong samples in the in the zone of the Megasplay fault and at the toe of the accretionary prism. In the footwall of the Megasplay fault, where the upper sedimentary cover is dominated by slope sediments and mass transport deposits, the samples show both, weak and strong behavior.

References:
Dixon, T.H. & Moore J.C., 2007. The seismogenic zone of subduction thrust faults. Columbia University Press, New York 665 pp.
Kinoshita, M., Tobin, H., Ashi, J., Kimura, G., Lallemant, S., Screaton, E.J., Curewitz, D., Masago, H., Moe, K.T., and the Expedition 314/315/316 Scientists, 2009. Proc. IODP, 314/315/316: Washington, DC (Integrated Ocean Drilling Program Management International, Inc.). doi:10.2204/iodp.proc.314315316.2009
Moore, G.F., Park, J.-O., Bangs, N.L., Gulick, S.P., Tobin, H.J., Nakamura, Y., Sato, S., Tsuji, T., Yoro, T., Tanaka, H., Uraki, S., Kido, Y., Sanada, Y., Kuramoto, S., and Taira, A., 2009. Structural and seismic stratigraphic framework of the NanTroSEIZE Stage 1 transect. In Kinoshita, M., Tobin, H., Ashi, J., Kimura, G., Lallement, S., Screaton, E.J., Curewitz, D., Masago, H., Moe, K.T., and the Expedition 314/315/316 Scientists, Proc. IODP, 314/315/316: Washington, DC (Integrated Ocean Drilling Program Management International, Inc.).Okino, K., Shimakawa, Y., and Nagaoka, S., 1994. Evolution of the Shikoku Basin. J. Geomagn. Geoelectr., 46(6):463–479
Park, J.-O., Tsuru, T., Kodaira, S., Cummins, P.R., and Kaneda, Y., 2002. Splay Fault Branching Along the Nankai Subduction Zone. Science 297, 1157-1160.
Sultan, N., Cochonat, P., Canals, M., Cattaneo, A., Dennielou, B., Haflidason, H., Laberg, J.S., Long, D., Mienert, J., Trincardi, F., Urgeles, R., Vorren, T.O. & Wilson, C., 2004. Triggering mechanisms of slope instability processes and sediment failures on continental margins; a geotechnical approach. In: COSTA, continental slope stability; a contribution to the Energy, Environment and Sustainable Development Programme FP5 of the European Commission, number EVK3-CT-1999-00006, Elsevier, Amsterdam, pp. 291-321.

ICDP

Structural, volcanic, temporal, compositional and environmental evolution of explosive volcanism of Nemrut and Süphan volcanic systems, sources for the tephra framework of Lake Van sediments (Anatolia)

M. SUMITA[1], H.-U. SCHMINCKE[1]

[1] Leibniz-Institute for Marine Science, IFM-GEOMAR, Wischhofstr. 1, 24148 Kiel, Germany

Goals

Primary fallout and pyroclastic flow tephra deposits - some of large volume - reflect the volcanic, temporal and compositional evolution of explosive volcanism of Nemrut and Süphan volcanoes, terrestrial climate conditions, short-term climate/environmental impact of large-magnitude eruptions and the structural evolution of the Lake Van basin over the past ca. 250 ka. The importance of tephra layers for the Paleovan drilling project lies in (a) their enormous stratigraphic value in (1) correlating widely spaced outcrops on land allowing to infer erupted magma volumes and reconstruct paleowind directions and (2) correlating sediments between holes and sites – several hundred tephra layers having been cored – , (b) temporal framework ($^{40}Ar/^{39}Ar$ ages of alkali feldspars) and (c) supply of elements from the unstable glass to the lake water.

Results

Structural aspects

Tectonism is arguably the dominant factor in generating Lake Van basin. During fieldwork in 2010, we found further impressive evidence for synvolcanic faulting along two dominant directions, strengthening the findings of our preceding field campaigns and establishing the presence of broad synvolcanic fault zones tens of m wide and major uplift of Lake Van sediments.

The N-S direction

The most impressive evidence for the regional dominance of N-S fractures is the ca. 5 km-long Incekaya eruptive fissure system that propagated from south to north, visible evidence ending at the shore of Lake Van where sustained phreatomagmatic eruptions representing a colossal phreatomagmatic underwater eruption generated large Incekaya hyaloclastite cone, a prominent landmark along the southern shore of Lake Van, high eruption columns having produced a widespread hyaloclastite marker bed traceable at least as far as Tatvan, 15 km to the west. About 5 km due north, a 100 m-wide zone of complex intense faulting including a number of small-scale (meters to tens of meters) horst-and-graben structures cuts the western part of Halepkalesi peninsula, the dominant direction of faulting also being roughly N-S. Several tens of meters of ***uplifted carbonaceous lake sediments interlayered with tephra deposits*** both locally complexly deformed, are well exposed along the southwestern cliffs of the peninsula. This zone appears to represent a locally uplifted segment of a major N-S trending fault zone. We cannot exclude that the origin of the faulted complex developed over an intrusion but the overall control of a roughly N-S aligned lineament approximately in line with the Incekaya fracture would hold either way.

Between the town of Ovakişıa close to Lake Nazik and the canyon of deeply incised river Suçıkan, a tributary to river Karmis that drains Ahlat basin and embouches into Lake Van, a major fault zone also several tens of meters wide cuts the tephra sequences parts of which we were able to correlate to widespread tephra deposits in the Ahlat-Tatvan area. We speculate that the anomalous local thickness of ignimbrites coupled with their high elevation – compared to other areas – might reflect another major broad zone of deformation characterized by faulting and possibly phases of subsidence and uplift along the periphery of the major load of Nemrut volcanic edifice.

The E-W direction

North and northeast of Ahlat, a thick tephra sequence, probably chiefly sourced in Nemrut volcano, directly overlies thick coarse Miocene continental red beds abruptly abutting along a fault contact against altered early Cretaceous submarine lavas and sediments. Basement and tephra deposits have subsided along a series of roughly ENE-WSW striking step-faults towards the shore of Lake Van, possibly part of a major fault zone bordering the basin to the north as also suggested by submarine seismic evidence (Krastel, Cukur pers. comm.). Faults cutting the tephra deposits appear to be of several ages and some maybe nearly contemporaneous with major eruptions.

Both fault directions appear to reflect the complex stress field of the broad graben zone that includes Lake Van and that continues to the present as reflected in the N-S fracture of the historic rhyolite and basalt eruptions on the high shoulders of Nemrut volcano as well as the dominant direction of documented earthquake hypocenters in the area.

Tatvan Hole

The origin of a major subcircular depression in the western part of the lake, ca 20 km across and 150 m deeper than the surrounding lake floor, informally called Tatvan Hole, is enigmatic. We here tentatively suggest a volcano-tectonic origin. The center of this hole is about 40 km E of the center of Nemrut caldera. Caldera-like subsidence of many tens of meters caused by subterranean magma drainage erupting 10 km or more elsewhere are well known. For example, during the largest eruption in the 20th century in July 1912, Katmai caldera subsided by > 10 m

while eruption took place 10 km to the west in Novarupta. During the minor eruption of Miyakejima eruption (Japan) in 2000, a piston some 600 m in diameter subsided by > 2 km (!) in the center of the edifice, magma apparently being siphoned off along lithospheric fractures. We cannot exclude that Tatvan Hole and Nemrut volcano represent a similarly coupled system but a purely tectonic origin of Tatvan Hole cannot be excluded in view of the two dominant directions of faulting discussed above.

Environmental effects

Detection of significant short-term eruption-induced environmental, especially climatic impacts of the ca. 10 major explosive eruptions of Nemrut during the past ca. 250 ka on the environment has been a major goal of our project. Tephra deposits several m thick sealing thousands of km^2 around Lake Van for a long time will significantly impact the vegetation. Evidence at hand such as incomplete soil development between tephra units and dominant wind erosion and reworking of unconsolidated tephra suggests pervasive dry conditions prevailing through much of at least the past ca. 220 ka, and thus an environment highly susceptible to external forcing. However, locally severe and rapid erosion of the thickest fallout deposit (AP1, ca. 220 ka, likely erupted magma volume > 50 km^3) and thus apparently by far the largest explosive eruption of Nemrut Volcano, lacking signs of weathering or „normal" erosional channels might have resulted from lasting massive precipitation immediately following the eruption resulting from stratospheric aerosol veils. Massive precipitation is well know to last for weeks to months following major volcanic eruptions such as Laki (Iceland) (1783) or has been inferred by us for Laacher See eruption (12.900 BP).

Major fallout fans east of Tatvan reflect westerly, contrasted with dominant SW wind directions for tephra layers in the Ahlat area.

Evidence for temporal wet conditions and specific biological reactions is provided by a fossil swamp deposit in a small intramontane basin ca 25 km southeast of Nemrut Volcano. Here, up to 8 tephra layers within a 1.5 m section of black organic-rich swamp deposits are interlayered with *diatomites* likely reflecting diatom blooms most probably triggered by release of silica from the glass of tephra deposits laid down under water. This suggests close coupling between diatomite blooms and abundance of glass shards of subaqueous tephra layers likely to be found in the cored sediments as well.

Regional stratigraphy, volcanology and temporal evolution

We have extended the basic tephrostratigraphy of Nemrut and Süphan deposits established in the central Tatvan-Ahlat area into several directions with emphasis on the stratigraphy below megatephra AP1 (ca. 220 ka in age). Several fallout units, at least one characteristic ignimbrite and one lava flow were deposited below AP1 and some of the sub-AP1 stratigraphy has been correlated over at least 10 km. Clarification and physically dating of this stratigraphic interval is especially important to allow dating of the lower part of the cored sediments drilled in 2010. The lack of dense vegetation in the area is a bonus while the lack of deeper erosional channels necessitates the search for distant small outcrops over a wide area.

Some 12 major and many tens of minor fall and flow deposits were identified on land in a large area (>1500 km^2) between Van-Bitlis-Muş-Tatvan-Lake Nazik-Ahlat and Ercis erupted over the past ca. 250 ka. Magma volumes of some of these eruptions must have amounted to several tens of km^3, in the range of some of the larger Plinian eruptions known worldwide. Debris avalanche deposits on the lower slopes of Nemrut and especially common at Süphan, must have entered the lake and probably generated tsunamis when impacting water and massive deposits on the lake floor.

Based on the framework of the Ahlat tephrostratigraphy, we have begun to take a closer look at Süphan tephras that are interlayered with tephras interpreted by us to be Nemrut-derived based on their composition. The Süphan volcanic system differs fundamentally from the Nemrut system not only petrologically (see below). The volcano (4058 m asl) is basically more youthful, its steep – as contrasted with the gentle Nemrut – slopes towering 2400 m above lake level and 1100 above Nemrut volcano. Its surface morphology is dominated by domes, some cones and collapse scars. At least one young huge debris avalanche deposits that carpets the land with an impressive hummocky deposit of complex juxtaposed blocks of an extreme variety of volcanic rocks extends over a distance of more than 20 km. Several older debris avalanche deposits were found in the few deep mostly abandoned quarries east of the volcano. We speculate that a multitude of dominantly dacitic to andesitic intrusions have triggered repeated sector collapses over an extended period of time. On the other hand, widespread large volume ignimbrite and fallout sheets correlatable over large distances have not yet been found but petrographic, mineralogical and chemical analyses have just started.

The reporting of many new age $^{40}Ar/^{39}Ar$ dates of feldspar phenocrysts underway since early 2010 is delayed because of temporary instrumental breakdown but might be available by Mid-March and will be discussed together with results from ongoing analytical work.

Compositional aspects

Continued EMP analyses of glass, feldspar, pyroxene, olivine and biotite phenocrysts and whole rock analyses of > 80 tephra units on land and core catcher samples, the first comprehensive database for tephra from Nemrut and Süphan volcanoes, have confirmed the major conclusions reported earlier. In short, Nemrut tephra compositions are dominantly alkaline to peralkaline but range to andesitc in composition. Fractionating phases are chiefly alkali feldspar (dominantly anorthoclase), hedenbergitic clinopyroxene, fayalitic olivine, minor phases being aenigmatite, chevkinite and zirkon apart from the ubiquituous iron titanium oxides and apatite. Ignimbrite deposits commonly show highly complex compositions with strongly corroded plagioclase phenocrysts and a broader range of mafic phenocrysts. OH^- bearing phases (biotite and amphibole) are generally lacking.

Contrasting with the dominantly equilibrium assemblages in the Nemrut fallout sheets (but not most ignimbrites) are the Süphan tephras that are characterized by extraordinarily complex clinopyroxene/hypersthene/olivine/strongly zoned plagioclase disequilibrium assemblages reflecting common magma mixing. Moreover, amphibole and/or biotite are common but not ubiquituous evidence for the H_2O-rich Süphan as contrasted with the volatile (H_2O-)-poor Nemrut magmas. These characteristics suggest small and short-lived high level magma reservoirs within Süphan edifice,

episodically emptied in small-volume eruptions associated with dome collapse events as reflected in the common presence of glassy nonvesicular tephra components interpreted as derived from domes.

All geochemical characteristics at hand suggest a major contrast between the subduction-type Süphan and the mildly alkalic intraplate Nemrut systems indicating that their local tectonic setting, magmatic sources and pathways are fundamentally different, Nemrut having developed inside a graben and Süphan above a subducted slab.

Basaltic eruptive centers

Several small local basaltic eruptive centers, bordering western Lake Van between Tatvan and Ahlat, likely represent the common eruption of dense mafic magmas at the foot of more evolved large volcanic edifices, the large erupted volume of the huge basaltic Incekaya system being an exception. We thus suggest that *sublacustrine* basaltic eruptions may have been common during the evolution of the Nemrut and possibly Süphan systems since their flanks extend downwards beyond the shores of the lake. Basaltic eruptions may also occur at the top of Nemrut volcano, however, as shown by the historic basalt/rhyolite eruption at ca. 2800 m asl. Compositionally, the basalts sofar analyzed are mildly alkalic and thus likely parent magmas to the moderately to strongly evolved erupted Nemrut volcanics. However, the basalts are generally moderately evolved, more primitive basaltic magmas having not yet found. Small basaltic cones of the Süphan system have not been studied sofar, emphasis being on the evolved tephra deposits.

Tephra in the Lake Van cores drilled

Tephra recovered and suggested interpretation of major intervals of several meters without recovery will be discussed once rules of early presentation of drilling results have been established. As to be expected from the land evidence – and as predicted – tephra is a major component of Lake Van sediments and is represented by hundreds of layers – and non-recovered intervals.

IODP

Biomarker evidence for intense aerobic methane oxidation during sapropel transitions

H.M. TALBOT[1*], L. HANDLEY[1], G. DE LANGE[2], T. WAGNER[1]

[1] School of Civil Engineering and Geosciences, Newcastle University, Newcastle upon Tyne, NE1 7RU, UK. (h.m.talbot@ncl.ac.uk; luke.handley@ncl.ac.uk; thomas.wagner@ncl.ac.uk)
[2] Geosciences - Utrecht University Budapestlaan 4, 3584 CD Utrecht, The Netherlands. (gdelange@geo.uu.nl)

Methane (CH_4) is an important greenhouse gas and understanding its cycling through the ocean-atmosphere system is crucial. Bacteriohopanepolyols (BHPs) are membrane lipids produced by a variety of bacteria and 35-aminobacteriohopane-30,31,32,33,34-pentol (aminopentol) is a highly specific biomarker for aerobic methane oxidation, known only from Type I methanotrophs [1]. This compound, together with related structures, has previously been reported from the oxic/anoxic transition zone of the Black Sea water column [2, 3] as well as a range of lacustrine sediments [4, 5, 6], terrestrial environments and sediments from the Congo and Amazon deep sea fans up to an age of 1.2 Ma [7]. Aminopentol concentrations in marine sediments can therefore potentially be used to identify periods of methane emission and oxidation in the geological record and the possible links between the poorly constrained process of aerobic methane oxidation and water column redox conditions.

Here, we investigate the potential role of aerobic methane oxidation during the rapid redox transitions that occur at the onset and recovery from Sapropel conditions. . We report for the first time the observation of bacteriohopanepolyol (BHP) biomarkers, including aminoBHPs indicative of aerobic methane oxidising bacteria, in sapropel units S1 from the Eastern Mediteranean (Core MS66PC; location 33N1.9'; 31E47.9'; waterdepth 1630 m) off the River Nile. Aminopentol, was the most abundant aminoBHP in both units investigated. We also observe aminopentol directly above and below 2 successive sapropel intervals in Mediterranean Pliocene sediments (ODP Site 967B). In this setting, we hypothesise that the change in redox conditions that occurs during the lead into and out of sapropels is directly linked to the intensity of aerobic methane oxidation.

By analogy with their occurrence in the Black Sea water column we hypothesise that the target biomarkers are focused to periods of increasing or decreasing deoxygenation in the run-up or recovery from sapropel conditions, however, more detailed knowledge of the exact timing of these first biomarker observations is vital. Comparison with other geochemical evidence on productivity (e.g. Ba) and redox conditions (trace elements) is ongoing to support the biomarker interpretation.

References:
[1] Talbot et al., (2001) J. Chrom A. 921, 175-185.
[2] Blumenberg et al. (2007) Org. Geochem. 38, 84-91.
[3] Wakeham et al. (2007) Org. Geochem. 38, 2070-2097.
[4] Talbot et al., (2003) Org. Geochem. 34 , 1353-1371.
[5] Talbot & Farrimond (2007) Org. Geochem. 34 , 1212-1225.
[6] Coolen et al. (2008) Env. Microbiol. 10, 1789-1803.
[7] Talbot et al. unpublished data.

IODP

Plio-Pleistocene evolution of Arctic-Atlantic water mass exchange and erosional input in the Fram Strait

C.TESCHNER[1], M. FRANK[1], B.A. HALEY[2]

[1] Leibniz Institut für Meereswissenschaften IFM-GEOMAR, Wischhofstrasse 1-3, 24148 Kiel, Germany
[2] COAS, College of Oceanic and Atmospheric Sciences, Oregon State University, Corvallis, OR 97331-5503

We determined the isotopic composition of neodymium (Nd) and lead (Pb) of past seawater to reconstruct water mass exchange and erosional input between the Arctic Ocean and the Norwegian-Greenland Seas over the past 5 Myr. For this purpose, sediments of ODP site 911 (leg 151) located at 900 m water depth on the Yermak Plateau in the Fram Strait were used. The paleo-seawater variability of Nd and Pb isotopes was extracted from the sea water-derived metal oxide coatings on the sediment particles following the leaching method of Gutjahr et al. (2007). All radiogenic isotope data were acquired by Multi-Collector (MC) ICP-MS. The site 911 stratigraphy of Knies et al. (2009) was applied.

Surface sediment Sr and Nd isotope data, as well as downcore Sr isotope data obtained on the same leaches are close to seawater and confirm the seawater origin of the Nd and Pb isotope signatures. The deep water Nd isotope composition extracted from site 911 was in general more radiogenic (εNd = -4.3 to -10) than present day deep water (-10.1 to -11.8) in the area of the Fram Strait (Andersson et al., 2008) and does not show a systematic long-term trend over time. In contrast, the radiogenic isotope composition of Pb evolved from $^{206}Pb/^{204}Pb$ ratios around 18.55 to more radiogenic values around 19.15 between 2 Ma and today.

Over the past 5 million years the data indicate that overall mixing of water masses from the Arctic Ocean and the Norwegian-Greenland Seas have controlled the Nd isotope signatures on the Yermak Plateau. Prior to 1.7 Ma the Nd isotope signatures were somewhat less radiogenic than waters from approximately the same depth in the central Arctic Ocean (Haley et al., 2008) pointing to a greater influence of inflowing waters from the Norwegian-Greenland Seas. After 1.7 Ma intermediate waters in the central Arctic and on Yermak Plateau have varied around similar values indicating general water mass mixing conditions similar to today.

In contrast, the Pb isotopic composition increased after 2.2 Ma, which resembles the Pb isotope evolution of the deep Arctic Ocean as recorded by sedimentary ferromanganese micronodules (Winter et al., 1997) and the Pb isotope evolution of North Atlantic Deep water in the North Atlantic recorded by ferromanganese crusts (Burton et al., 1997; Reynolds et al., 1999). This indicates that the Pb isotope composition of deep waters in the Fram Strait was strongly influenced by Pb inputs resulting from incongruent weathering and preferential release of radiogenic Pb originating from glacially weathering old continental landmasses, such as Northern Canada, Greenland, or parts of Svalbard over the past 2 Ma.

References:

Andersson, P.S., Porcelli, D., Frank, M., Björk, G., Dahlqvist, R. and Gustafsson, Ö. (2008): Neodymium isotopes in seawater from the Barents Sea and Fram Strait Arctic-Atlantic gateways. Geochim. Cosmochim. Acta 72, 2854-2867

Burton, K., Ling, H.F. and H.L. O'Nions (1997) Closure of the Central American Isthmus and its effect on deepwater formation in the North Atlantic. Nature, 386, 382-385

Gutjahr, M., Frank, M., Stirling, C.H., Klemm, V., van de Flierdt, T. and Halliday, A.N. (2007): Reliable extraction of a deepwater trace metal isotope signal from Fe-Mn oxyhydroxide coatings of marine sediments. Chemical Geology 242, 351-370

Haley B. A., M. Frank, R.F. Spielhagen and A. Eisenhauer (2008): Influence of brine formation on Arctic Ocean circulation over the past 15 million years. Nat. Geosci. 1, 68–72

Knies, J., J. Matthiessen, C. Vogt, J.S. Laberg, B.O. Hjelstuen, M.Smelror, E. Larsen, K. Andreassen, T. Eidvin and T.O. Vorren (2009): The Plio-Pleistocene glaciation of the Barents Sea–Svalbard region: a new model based on revised chronostratigraphy. Quaternary Science Reviews 28, 9-10, 812-829

Reynolds, B., M. Frank and R.K., O'Nions (1999) Nd- and Pb-isotope time series from Atlantic ferromanganese crusts: implications for changes in provenance and paleocirculation over the last 8 Myr. Earth and Planetary Science Letters, 173, 381-396.

Winter, B.L., C.M. Johnson and D.L. Clark (1997): Strontium, neodymium, and lead isotope variations of authigenic and silicate sediment components from the Late Cenozoic Arctic Ocean: Implications for sediment provenance and the source of trace metals in seawater. Science 61, 4181-4200

IODP

Reconstructing water mass exchange and climate variability in the northernmost Atlantic and Arctic oceans during the beginning of the Quaternary

C.TESCHNER[1], M. FRANK[1], B.A. HALEY[2]

[1]Leibniz Institut für Meereswissenschaften IFM-GEOMAR, Wischhofstrasse 1-3, 24148 Kiel, Germany
[2]COAS, College of Oceanic and Atmospheric Sciences, Oregon State University, Corvallis, OR 97331-5503
[1]Leibniz Institut für Meereswissenschaften IFM-GEOMAR, Wischhofstrasse 1-3, 24148 Kiel, Germany

During the first 16 months of the project surface sediments of the proposed ODP/IODP cores and from nearby locations (Fig. 1) were sampled. The leaching method to extract the seawater derived radiogenic Nd and Pb isotope signatures from the early diagenetic ferromanganese coatings of the sediments (Gutjahr et al., 2007) was extensively tested and, where necessary, improved for the different core locations by comparison of core top data to the modern dissolved bottom water Nd isotope signatures in the same areas (Lacan and Jeandel, 2004; Andersson et al., 2008). These test results for sediments in the N-Atlantic (at or near Site 984), the Norwegian-Greenland Seas (near Site 907) and on the Yermak-Plateau in the Fram Strait (Site 911) (Fig. 2) showed that the data of ODP Site 911 gave Nd isotope signatures closest to the modern ocean bottom water signatures, which was supported by Sr isotope signatures very close to seawater in the same leachates. The Nd isotope results of Sites 907 were slightly too radiogenic and those of Site 984 were significantly too radiogenic compared with expected values from deep water data although it has to be stated that there are no direct deepwater data available for Sites 907 and 984. We suspect that small amounts of basaltic ash with highly radiogenic Nd isotope signatures originating from Iceland were dissolved and responsible for the positive offset. This was further tested by extracting and analyzing the seawater Nd isotope data from the carbonate shells of planktonic and benthic foraminifera, which yielded more negative and in

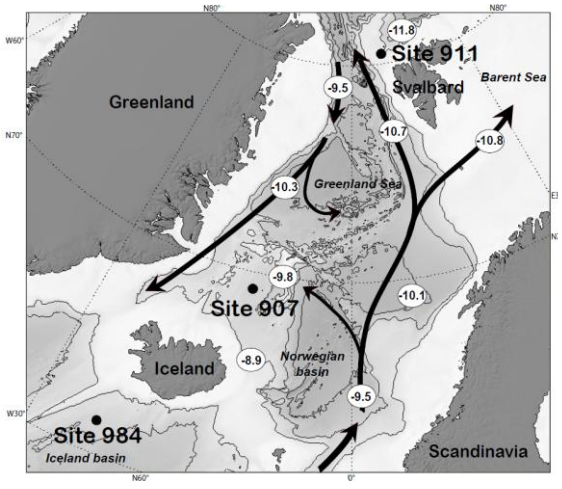

Figure 1: Study area with ODP Sites 911, 907 and 984. Black arrows indicate intermediate deep circulation in the Nordic Seas. Ellipses mark εNd in the deep waters of different basins (Lacan and Jeandel, 2004; Anderssson et al., 2008).

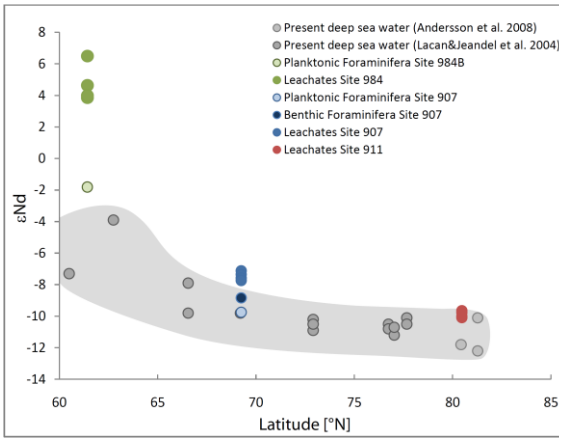

Figure 2: Comparison of Nd isotope data obtained from sediment leachates, foraminifera and nearby deep waters for Sites 911, 907 and 984.

the case of site 907 fully realistic numbers, whereas for site 984 the numbers still seem slightly too positive.

Based on these results downcore samples covering the proposed time period of the past 5 million years were obtained at the IODP-Core Repository in Bremen and the first Nd and Pb isotope data set was produced for ODP Site 911 (900 m water depth). It is located NW of Svalbard on the southeastern slope of the Yermak Plateau in the Fram Strait. The core has been intensively studied (Knies et al., 2002, 2009) and the stratigraphy of Knies et al. (2009) was applied. Further improvements of the stratigraphy in the older part of the core using 10Be/9Be dating are currently being carried out in the frame of a separate collaborative project with Jochen Knies, funded by the Geological Survey of Norway.

Today the location of Site 911 is strongly influenced by the inflow of Atlantic water from the Norwegian-Greenland Seas (NGS). The western inflow branch from the NGS along the west coast of Svalbard has an εNd of -10.7 (Piepgras & Wasserburg, 1987) and shows somewhat less radiogenic values of -11.8 ± 0.4 north of Svalbard although these data are from shallower water depths (Andersson et al., 2008) (Fig. 1). The deep waters flowing from the Arctic Ocean into the NGS through the western Fram Strait are characterized by εNd values of -9.5 (Andersson et al., 2008). The core location is thus well suited to study the variability of the water mass exchange between the Arctic Ocean and the NGS and to reconstruct erosional inputs over the past 5 Ma. After leaching the samples following a modified leaching protocol of Gutjahr et al. (2007) the isotopic compositions of neodymium (Nd) and lead (Pb) were measured by Multi-Collector (MC) ICP-MS.

The deep water Nd isotope data extracted from site 911 were in general more radiogenic (εNd = -4.3 to -10) than present day deep water (-10.1 to -11.8) over the past 5 million years and do not show a systematic trend over time (Fig. 3). The Sr isotope data obtained on the same leaches are close to seawater and confirm the seawater origin of the Nd, as well as the Pb isotope signatures discussed below. There is considerable Nd isotope variability on millennial time scales but no systematic correlation to glacial and interglacial stages marked by changes in IRD abundance is observed, which will have to be verified by additional high resolution data of particular glacial/interglacial intervals in this core. The least radiogenic signature occurred at 1.2 Ma whereas at 2.7 Ma and 0.65 Ma shifts to highly radiogenic Nd isotope compositions of εNd = -4.8 and -4.3, respectively, were found. Both radiogenic peaks occurred during pronounced glaciations (G7-G9 (2.74-2.67 Ma) and MIS 16 (0.688-0.62-Ma)) and indicate major inflow of waters from highly radiogenic source areas, either from Iceland in the south or the Siberian Putorana flood basalts in the Kara Sea region. In case the latter was the source region, brine-water production resulting from increased sea-ice formation at the edges of ice sheets grounding on large areas of the Arctic Kara Sea and Novaya Zemlya shelves was the most likely mechanism (Haley et al., 2008a). Both peaks were accompanied by more positive Nd isotope signatures of the detrital sediment particles indicating a contemporaneously enhanced sediment supply from the above Siberian shelf regions. The shift at 2.7 Ma occurred precisely at the onset and major intensification of Northern Hemisphere Glaciation and documents that this event was accompanied by a major but, in contrast to records from the deep Arctic Basin and the western North Atlantic, unexpectedly transient change in weathering inputs and/or high latitude ocean circulation. This will have to be verified by further analyses for this time window from central Arctic Ocean Site 302 and the GNS locations.

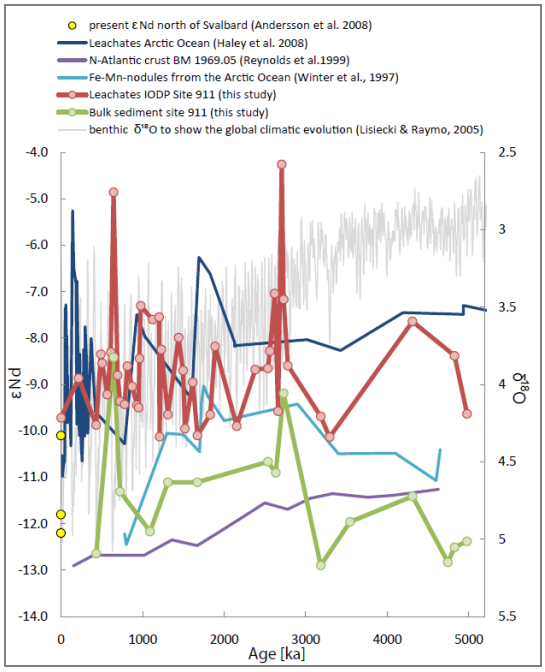

Figure 3: Comparison of the new Nd isotope data of Site 911 with Leg 302 and other paleo environmental records. The red curve shows the newly acquired deep water Nd isotope data leached from the sediments of Site 911 and the green curve shows the Site 911 εNd data of the bulk sediments. Dark blue curve: central Arctic Leg 302 (Haley et al., 2008a); yellow symbols: Nd isotopic composition of waters from different depths north of Svalbard (Andersson et al., 2008); violet curve: western North Atlantic (Reynolds et al., 1999), grey curve in the background: global oxygen isotope stacked of Lisiecki and Raymo (2005).

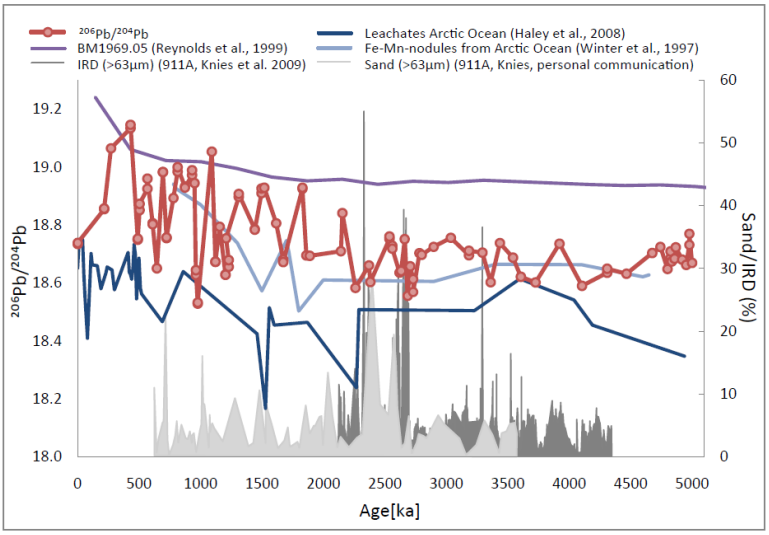

Figure 4: Comparison of the new Pb isotope data of Site 911 with other paleoenvironmental records.
The red curve shows the newly acquired deep water Pb-isotope data leached from the sediments of Site 911. The dark blue curve shows the results from central Arctic Leg 302 (Haley et al., 2008a) and the light blue curve illustrates Fe-Mn-micronodules from the Alpha ridge (Winter et al., 1997). The violet curve represents a location in the western North Atlantic bathed in NADW (Reynolds et al., 1999) and the grey areas mark the sand/IRD content in % of total weight.

Over the past 5 million years the data indicate that overall mixing of water masses from the Arctic Ocean and the Norwegian-Greenland Seas have controlled the Nd isotope signatures on the Yermak Plateau. Prior to 1.7 Ma the Nd isotope signatures were somewhat less radiogenic than waters from approximately the same depth in the central Arctic Ocean (Haley et al., 2008) pointing to a greater influence of inflowing waters from the Norwegian-Greenland Seas. After 1.7 Ma intermediate waters in the central Arctic and on Yermak Plateau have varied around similar values indicating general water mass mixing conditions similar to today.

The radiogenic Pb isotope compositions at Site 911 evolved from $^{206}Pb/^{204}Pb$ ratios between 18.55 and 18.75 prior to 2.2 Ma to generally more radiogenic values between 18.5 and 19.15 thereafter (Fig. 4). Similar to the Nd isotopes the pronounced higher resolution variability, which was particularly pronounced after 2.2 Ma does not seem to systematically correlate with changes in IRD inputs and thus changes in glacial/interglacial ice sheet extent and ocean circulation, which will have to verified at higher resolution for selected intervals. The general increase after 2.2 Ma closely resembles the Pb isotope evolution of the deep Arctic Ocean as recorded by sedimentary ferromanganese micronodules (Winter et al., 1997) and the Pb isotope evolution of North Atlantic Deep water in the North Atlantic recorded by ferromanganese crusts (Burton et al., 1997; Reynolds et al., 1999). In contrast to the central Arctic Ocean record from the Lomonosov Ridge, which has been under the influence of weathering inputs from Siberia over the past 5 million years (Haley et al., 2008b), this indicates that the Pb isotope composition of deep waters in the Fram Strait has been increasingly dominated by highly radiogenic Pb resulting from incongruent weathering and preferential release of radiogenic Pb originating from glacially weathering old continental landmasses, such as Northern Canada, Greenland, or parts of Svalbard over the past 2 Ma.

References:

Andersson, P., D. Porcelli, M. Frank et al. (2008) Neodymium isotopes in seawater from the Barents Sea and Fram Strait Arctic-Atlantic gateways. Geochim. Cosmochim. Acta, 72, 2854-2867.

Burton K.W., H.-F. Ling and R.K. O'Nions (1997) Closure of the Central American Isthmus and its effect on deepwater formation in the North Atlantic. Nature, 386, 382-385.

Gutjahr, M., M. Frank, C. H. Stirling et al. (2007) Reliable extraction of a deepwater trace metal isotope signal from Fe-Mn oxyhydroxide coatings of marine sediments. Chem. Geol., 242, 351– 370.

Haley B. A., M. Frank, R.F. Spielhagen and A. Eisenhauer (2008a) Influence of brine formation on Arctic Ocean circulation over the past 15 million years. Nat. Geosci. 1, 68–72.

Haley B.A., M. Frank, R.F. Spielhagen and J. Fietzke (2008b) Radiogenic isotope record of Arctic Ocean circulation and weathering inputs of the past 15 million years. Paleoc., 23, PA1S13, doi:10,29/2007PA001486.

Knies, J., J. Matthiessen, A. Mackensen et al. (2007) Effects of Arctic freshwater forcing on thermohaline circulation during the Pleistocene. Geology, 35, 1075-1078.

Knies, J., J. Matthiessen, C. Vogt et al. (2002) Evidence of 'Mid-Pliocene (~3 Ma) global warmth' in the eastern Arctic Ocean and Implications for the Svalbard/Barents Sea ice sheet during the late Pliocene and early Pleistocene (~3 – 1.7 Ma). Boreas, 31, 82-93.

Knies, J., J. Matthiessen, C. Vogt et al. (2009) The Plio-Pleistocene glaciation of the Barent Sea-Svalbard region: a new model based on revised chronostratigraphy. Quat. Sci. Rev., 28, 812-829.

Lacan, F. and C. Jeandel (2004a) Denmark Strait water circulation traced by heterogeneity in neodymium isotopic compositions. Deep-Sea Res. I, 51, 71–82.

Lisiecki, L.E., and M.E. Raymo (2005) A Pliocene-Pleistocene stack of 57 globally distributed benthic δ18O records. Paleocean., 20, doi: 10.1029/2004PA001071.

Piepgras, D.J. and G.J. Wasserburg (1987) Rare earth element transport in the western North Atlantic inferred from Nd isotopic observations. Geochim. Cosmochim. Acta, 51, 1257-1271.

Reynolds, B.C., M. Frank and R.K. O'Nions (1999) Nd- and Pb-isotope time series from Atlantic ferromanganese crusts: Implications for changes in provenance and paleocirculation over the last 8 Myr. Earth. Planet. Sci. Lett., 173, 381-396.

Winter, B., C. M. Johnson, and D. L. Clark (1997) Strontium, neodymium and lead isotope variations of authigenic silicate sediment components from the late Cenozoic Arctic Ocean: Implications for sediment provenance and the source of trace metals in sea water. Geochim. Cosmochim. Acta, 61, 4181– 4200.

IODP

Origin of the modern deep-sea macrobenthos: insights from Cretaceous bathyal echinoderms from the subtropical N-Atlantic (ODP Leg 171B)

B. THUY[1], A.S. GALE[2], M. REICH[1,3], L.D. NUMBERGER-THUY[1,4], S. STÖHR[5], M. KUCERA[6]

[1]: Geoscience Centre, University of Göttingen, Department of Geobiology, Goldschmidtstrasse 3, D-37077 Göttingen, Germany; E-mail: nebyuht@yahoo.com
[2]: School of Earth & Environmental Sciences, University of Portsmouth, Burnaby Building, Burnaby Road, Portsmouth, PO1 3QL, Great Britain. E-mail: Andy.Gale@port.ac.uk
[3]: Geoscience Centre, University of Göttingen, Museum, Collections & Geopark, Goldschmidtstraße 1-5, D-37077 Göttingen, Germany. E-mail: mreich@gwdg.de
[4]: E-mail: lnumber@gwdg.de
[5]: Swedish Museum of Natural History, Department of Invertebrate Zoology, Box 50007, 10405 Stockholm, Sweden; E-mail: sabine.stohr@nrm.se
[6]: Institute of Geosciences, University of Tuebingen, Sigwartstrasse 10, D-72076 Tübingen, Germany; E-mail: michal.kucera@uni-tuebingen.de

The origin and possible antiquity of the modern deep-sea fauna have been controversially debated since the beginning of deep-sea research in the nineteenth century. Hypotheses have thus far mostly argued on the basis of biogeographic distribution patterns and molecular clock estimates, and have predominantly suggested a latest Mesozoic or Cenozoic origin. Deep-sea anoxic/dysoxic events and the mid-Cenozoic cooling of deep water masses have generally been considered to have eradicated previous deep-sea communities which were then replaced by the modern fauna. However, in the near absence of direct fossil evidence, considerations on the origin of the modern deep-sea fauna are highly speculative. Here, we report on well preserved fossils of a Lower Cretaceous echinoderm assemblage from deep-sea sediments of the NE-Atlantic, consisting of diagnostic disarticulated skeletal parts of all five extant groups of echinoderms. The composition of the assemblage on family and, in some cases, genus level is similar to modern deep-sea echinoderm communities. Our findings suggest that at least a significant part of the modern deep-sea fauna is considerably older than previously assumed. They force a thorough reappraisal of the impact on deep-sea biodiversity of major palaeoceanographic events, such as oceanic anoxia/dysoxia, as well as of faunal exchange processes with shallow marine communities.

ICDP

Dreikomponentige Magnetfeldmessungen in der Outokumpu-Bohrung (Finnland)

C. VIRGIL[1], A. HÖRDT[1], S. EHMANN[1], M. LEVEN[2], E. STEVELING[2], J. KÜCK[3]

[1] Institut für Geophysik und extraterrestrische Physik, Technische Universität Braunschweig
[2] Institut für Geophysik, Georg-August-Universität Göttingen
[3] Helmholtz-Zentrum Potsdam Deutsches GeoForschungsZentrum GFZ, Potsdam

Einleitung

Die Messungen des Magnetfeldes entlang von Bohrlöchern wird schon seit langer Zeit genutzt, um Aufschluss über die Struktur des umgebenen Gesteins zu erlangen. Die bisher üblichen Verfahren nutzen hierzu jedoch nur das Totalfeld oder aber das Vertikal- und Horizontalfeld. Dass aber der vollständige Vektor des Magnetfeldes weit mehr Informationen enthält und somit zuverlässigere Vorhersagen ermöglicht, ist schon in vielen theoretischen Arbeiten erkannt worden.

So werden die Vektorinformationen genutzt, um Störkörper eindeutiger zu charakterisieren (z.B. Hattula und Paarma, 1981; Silva und Hohmann, 1981) oder zusammen mit Oberflächenmessungen eine gemeinsame Interpretation durchzuführen (Li und Oldenburg, 2000). Eine weitere Anwendung besteht in der Modellierung von Schichtungen, die von der Bohrung durchdrungen werden (Bosum et al., 1988; Gallet und Courtillot, 1989). Aus dreikomponentigen Magnetfelddaten lassen sich in diesem Fall zusätzlich zur Amplitude auch die Richtung der Magnetisierung der Schichten berechnen. Diese vektoriell bestimmten Magnetisierungen liefern wichtige Informationen für paläomagnetische Polbestimmungen (Bosum und Scott, 1988) und geben Aufschluss über die tektonische Entwicklung der Region. Weiterhin können Bohrkerne durch Vergleich der „In-Situ“ bestimmten und der im Labor am Kern gemessenen remanenten Magnetisierung reorientiert werden.

Um diesen starken theoretischen Hintergrund nutzen zu können, wird eine Bohrlochsonde benötigt, welche das Magnetfeld in drei Komponenten, sowie die Orientierung in Bezug auf ein geographisches Referenzsystem aufzeichnet. Die Schwierigkeit hierbei liegt in der exakten Orientierungsbestimmung. In Levanto et al. (1959) wird eine Sonde vorgestellt, die mit Hilfe einer pendelgesteuerten Lageregelung den Vektor des Magnetfeldes relativ zu dem Bohrloch messen konnte. Dies setzt aber genaue Kenntniss über den räumlichen Verlauf der Bohrung, sowie ein geneigtes Bohrloch voraus. Bosum et al. (1988) entwickelten eine Bohrlochsonde, die mit Hilfe von Inklinometern und einem mechanischen Kreisel die Lage der Sonde aufzeichnete. Allerdings erwies sich der Kreisel als zu ungenau, um eine kontinuierliche Vektormessung durchzuführen.

Unsere Sonde, das „Göttinger Bohrlochmagnetometer“ (GBM) verfügt als Orientierungssystem über drei orthogonal zueinander angebrachte, optische Faserkreisel (Fibre Optic Gyro, FOG). Diese zeichnen sich durch eine hohe Auflösung von $9 \cdot 10^{-5}$ ° und durch eine geringe Drift von weniger als 2 °/h aus. Zusammen mit einem Förstersonden Tripel ist es uns so möglich, das Magnetfeld kontinuierlich in drei Komponenten zu messen und in das

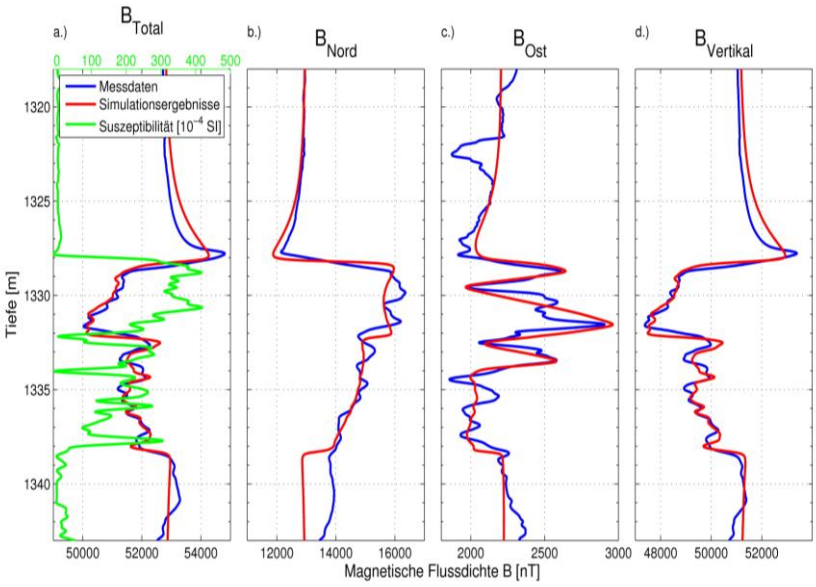

Abbildung 1: Vergleich von GBM-Messdaten (blau) mit Simulationsergebnis (rot), Ausschnitt. Magnetisierbare Schichten im Bereich hoher Suszeptibilität (grün). a.) Totalkomponente der magnetischen Flussdichte (berechnet aus B_N, B_O, B_V) und Suszeptibilität, b.) Nordkomponente, c.) Ostkomponente, d) Vertikalkomponente der magenetischen Flussdichte.

geographische Referenzsystem Nord, Ost und Vertikal (abwärts) zu übertragen. Die erreichte Genauigkeit dieser Reorientierung ergibt sich zu 0.14 ° in der Inklination und 1.4 ° in der Deklination. Mit dieser Sonde wurde im September 2008 eine Messreihe in der Tiefbohrung Outokumpu OKU R2500 (Finnland) (Kukkonen, 2007) durchgeführt. Das Ziel dieser Messungen war die Bestimmung der Magnetfeldanomalie in drei Komponenten. Mit diesen Daten wurde die Magnetisierung der durchbohrten Gesteinsschichten mittels numerischen Simulationen berechnet, um Aufschluss über die geologische Entwicklung der so genannten „Outokumpu-Formation“ und den Entstehungsprozess der darin enthaltenen Erzlagerstätten zu erhalten. Innerhalb der heterogenen Formation lassen sich drei Teufenbereiche identifizieren, die unterschiedliche Vorzugsrichtungen in der Magnetisierung aufweisen. Dies steht vermutlich mit einer unterschiedlichen tektonischen Entwicklung im Zusammenhang. Außerdem wurden die langwelligeren Anteile der magnetischen Anomalie verwendet, um in Kombination mit seismischen Daten die die Bohrung umgebenen Gesteinsformationen zu charakterisieren.

Vorbereitung und Datenverarbeitung

Eine Voraussetzung für die Bestimmung der Gesteinsmagnetisierung war die Optimierung der Messprozedur und der Weiterentwicklung der Datenverarbeitung. Dazu sind zunächst umfangreiche Kalibriermessungen durchgeführt worden. So wurden unter anderem die Offsets, die Skalenfaktoren und die Schiefstellung der Magnetfeldsensoren untereinander in dem magnetischen Laboratorium „Magnetsrode“ mittels des dort vorhandenen Braunbekspulensystems bestimmt. Mit dem Braunbekspulensystem war es auch möglich, die kombinierte Übertragungsfunktion der Magnetfeldsensoren und der verbauten Tiefpassfilter der Sonde zu bestimmen.

Ein weiterer wichtiger Schritt bei der Kalibrierung der Sonde betrifft die Faserkreisel. Diese weisen eine temperaturabhängige Drift auf, die einer tatsächlich auftretenden Rotation überlagert ist, und die vor der Reorientierung von den Messdaten abgezogen werden muss. Es zeigte sich außerdem, dass die Kreisel nicht exakt senkrecht aufeinander stehen, sondern eine Winkelabweichung von 0.19° zwischen x- und z-Kreisel, bzw. 0.02 ° zwischen y- und z-Kreisel aufweisen. Um die in den Kalibriermessungen ermittelten Eigenschaften der Magnetfeldsensoren und Faserkreisel auf die Messdaten anwenden zu können, mussten die bestehenden Programme zur Datenauswertung angepasst, bzw. ergänzt werden. So wurde zum Beispiel die Berechnung der Rotation der Sonde mittels einer „Direct Cosine Matrix“ durchgeführt, welche eine kontinuierliche Drehung beschreibt.

Eine weitere Verbesserung in der Reorientierungsgenauigkeit wurde durch das „Einnorden“ der Sonde erreicht. Zu Beginn und am Ende einer jeden Messung wurde die Sonde über der Bohrung hängend mit Hilfe einer neu entwickelten Zieleinrichtung auf eine feste Marke ausgerichtet. Die Genauigkeit hierbei beträgt 0.05 ° (Virgil et al., 2010). Mit der Kenntnis der genauen Lage der Sonde im Raum kann man den Einfluss der Erdrotation auf die Faserkreisel sehr präzise berechnen. Ein weiterer Vorteil liegt darin, dass man die aus den Faserkreiseldaten berechnete Ausrichtung der Sonde zu diesen beiden Zeitpunkten vergleichen kann. Aus diesen Daten lassen sich zusätzliche Driftkorrekturen für die Kreisel berechnen. Ein Vergleich zwischen den reorientierten Magnetfelddaten im geographischen Referenzsystem Nord, Ost, Vertikal (abwärts gerichtet) unter den einzelnen Messungen ermöglicht eine Abschätzung der erreichten Genauigkeit zu RMS_{Nord}=330 nT, RMS_{Ost}=10 nT and $RMS_{VertiKal}$=170 nT. Dies entspricht einer Genauigkeit 1.4 ° in der Inklination und 0.14 ° in der Deklination.

Auswertung

Um das Verständnis über die geologische Entwicklung der Region um Outokumpu (Finnland) zu erweitern, ist es nötig, ein Modell der die Bohrung umgebenen, magnetisierten Schichten zu erstellen. Ein erster Ansatz zur Berechnung der Magnetisierungen der Gesteinsschichten in der Outokumpu-Formation mit unendlich ausgedehnten,

horizontal geschichteten Hohlzylindern hat sich als nicht ausreichend herausgestellt. Die berechneten Magnetisierungen hängen bei dieser Methode sehr stark von der Wahl des Hintergrundfeldes ab. Außerdem zeigt sich in den Übergangsbereichen von magnetisierten zu unmagnetisierten Schichten ein starker Einfluss der räumlichen Ausdehnung der simulierten Schicht, welcher in diesem Modell nicht berücksichtigt wird.

Um das bestehende Modell durch komplexere Geometrien zu verbessern, war es zunächst nötig heraus zu finden, welche Parameter einen starken Einfluss auf eine Bohrlochmagnetikmessung haben und somit in dem Modell berücksichtigt werden müssen. Dazu wurden numerische Simulationen mit dem Programm Comsol Multiphysics mit homogen magnetisierten, elliptischen Zylinderscheiben durchgeführt. Es wurden folgende Parameter untersucht: Länge der Halbachsen, Orientierung der langen Halbachse zur Magnetisierungsrichtung, Durchmesser der Bohrung im Zentrum des Zylinders, Dezentralisierung der Sonde in der Bohrung und Neigung der Schicht zur horizontalen Ebene. Es hat sich heraus gestellt, dass die wichtigsten Parameter die Länge der beiden Halbachsen und die Orientierung zur Magnetisierungsrichtung sind. Aufgrund dieser Untersuchungen wurde ein neues Modell zur Berechnung der Magnetisierungen der durchbohrten Gesteinsschichten verwendet. Mit dem Programm Comsol Multiphysics werden nun die magnetischen Anomalien von horizontal geschichteten elliptischen Zylindern berechnet. Die Dicke der Zylinder wird durch Teufenabschnitte mit ähnlicher Suszeptibilität (Abb. 2a.) vorgegeben, welche durch eine Sonde der Operational Support Group des GFZ in der Bohrung gemessen wurde. Zur Berechnung der induzierten Magnetisierung wird das Hintergrundfeld aus der unmittelbaren Umgebung der Schichten bestimmt und mit der gemessenen Suszeptibilität multipliziert. Die verbleibenden freien Parameter sind damit die große und kleine Halbachse des Zylinders und deren Orientierung zu Nord, sowie die remanente Magnetisierung in drei Komponenten. Diese Parameter werden durch gezieltes Probieren variiert, bis die Simulationsergebnisse mit den gemessenen Feldern hinreichend gut übereinstimmen. In Abbildung 2 sind die Simulationsergebnisse (rot) und die gemessenen magnetischen Flussdichten (blau) beispielhaft für die erste magnetisierte Sektion in der Outokumpu-Formation aufgetragen. Für die anderen beiden magnetisierten Sektionen wurde der Vektor der remanenten Magnetisierung analog bestimmt.

Aus diesen Vektorinformationen über die remanente Magnetisierung der Gesteinschichten in der Outokumpu-Formation werden die Inklination und Deklination berechnet. Es zeigt sich, dass die Inklination in allen drei Sektionen sehr ähnlich ist. Vergleicht man den Mittelwert von 20° mit der Inklination des paleomagnetischen Feldes vor 1.88 Ga von 31.6° (Pesonen et al. 2003), zeigt sich eine Abweichung von 11.6 °. Die Deklinationen zeigen jedoch mit -8° in der ersten, 170° in der zweiten und 30° in der dritte Sektion eine starke Variation sowohl untereinander, als auch zur Deklination des paleomagnetischen Feldes von -19.6° (Pesonen et al. 2003). Diese Variationen könnten auf Faltungsprozesse nach der magnetischen Prägung des Gesteins hinweisen.

Eine weitere Anwendung für die vom GBM gemessenen Vektoren des Magnetfeldes ist die Interpretation der langwelligen Anomalien durch Störkörper in der Umgebung der Bohrung. Hierbei werden seismische Messungen (Heikkinen et al., 2007) genutzt, um aus den Bereichen hoher Reflektivität ein Startmodell für die geometrische Ausdehnung der magnetisierten Gesteine zu bestimmen. Dieser Ansatz wurde verfolgt, da es eine Hypothese gab, die die Bereiche mit hoher Reflektivität ähnliche magnetische Eigenschaften zuschrieb (I. Kukkonen, *pers comm.*). In Abbildung 2 ist ein Common Mid Point Profil abgebildet, welches sich von Nordwest nach Südost verläuft und die Bohrung schneidet. Die Rechtecke geben die geometrische Ausdehnung der simulierten Quader wieder. Aufgrund von weiteren seismischen Messungen konnte die Streichrichtung der Objekte zu Nordost bestimmt werden. In der Simulation wurde die Länge zu 6 km angenommen. Da somit die geometrischen Parameter eingegrenzt sind, müssen noch die magnetischen Eigenschaften durch gezieltes Probieren bestimmt werden. Im Unterschied zu den durchbohrten Schichten stehen hier jedoch keine Suszeptibilitätsmessungen zur Verfügung, so dass eine eindeutige Trennung zwischen induzierter und remanenter Magnetisierung nicht möglich ist. Zur Charakterisierung der Schichten wurde deshalb die scheinbare Suszeptibilität berechnet, die aufgrund von feldparallelen remanenten Magnetisierungsanteilen von der eigentlichen abweichen kann. In Abbildung 2 ist die berechnete, scheinbare Suszeptibilität durch die Einfärbung der Quader aufgezeigt.

Aus der gemeinsamen Interpretation der magnetischen und seismischen Eigenschaften lassen sich neue Erkenntnisse über den strukturellen Aufbau der betrachteten Region erlangen. So zeigt sich, dass die Schichten zwischen 65 m und 275 m, bzw. 960 m und 1040 m nur sehr schwache Magnetisierbarkeiten im Vergleich zu den restlichen Schichten aufweisen. Dies führt zu dem Schluss, dass diese Gesteinsformationen eine andere geologische Zusammensetzung aufweisen. Während die starken Anomalien auf in Serpentinit eingelagertem Magnetit und Pyrrhotin zurückzuführen sind, bestehen die schwach magnetisierten Einheiten sehr wahrscheinlich aus dünnen Lagen Schwarzschiefer.

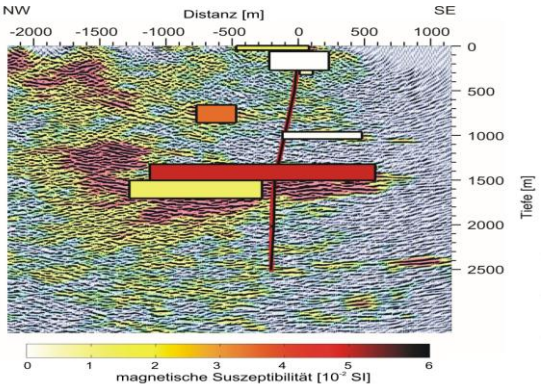

Abbildung 2: Seismisches CMP-Profil durch die Outokumpu Tief-bohrung. Rosa Färbung entspricht hoher Reflektivität. Quader repräsentieren simulierte Einheiten.

Danksagung

Wir danken vielmals Ilmo Kukkuonen (GTK Finland) für die Ermöglichung der Messungen und die

organisatorische Unterstützung; Martin Töpfer und Christian Carnein (Operational Support Group OSG/ICDP, GFZ) für den logistischen und technischen Beitrag; Meri-Liisas Airo (GTK Finland) und Frank Dietze (KIT) für die Bereitstellung zusätzlicher Bornkerndaten, sowie Johannes Stoll (Metronix) für die Hilfe bei der Verbesserung des Reorientierungsalgorithmus. Dieses Projekt wird von der DFG unterstützt (DFG, Ho 1506/16-1, LE 1293/1-1).

References:

Bosum, W., Eberle, D. und Rehli, H.-J. 1988. A Gyro-orientated 3-component Borehole Magnetometer for Mineral Prospecting, with Examples of its Application. Geophysical Prospecting 36, 933-961

Bosum, W. und Scott, J. H. 1988. Interpretation of Magnetic Logs in Basalt, Hole 418A. Proceedings of the Ocean Drilling Program, Scientific Results, Vol. 102

Gallet, Y. und Courtillot, V. 1989. Modeling magetostratigraphy in a borehole. Geophysics 54, No. 8, 973-983

Hattula, H. und Paarma, H. 1981. Equipments used in Borehole Magnetometry at Rautaruukki Oy. In: Interprtation of Boreholemagnetic Data and some special Problems of Magnetometry, Department of Geophysics, University of Oulo, Report Nr. 1

Heikkinen, P. J., Koivisto, E. und Kukkonen, I. 2007. FIRE High Resolution Seismic Survey in Outokumpu. In: Kukkonen I.T., (Editor), 2007. Outokumpu Deep Drilling Project, Sec. International Workshop, May 21-22, 2007, Espoo, Finland. Programme and Extended Abstracts. Geological Survey of Finland, Report Q10.2/2007/29, 17-20.

Kukkonen, I. T. 2007. Outokumpu Deep Drilling Project, Second International Workshop. Programme and Extended Abstracts, siehe: http://www.gsf.fi/projects/o_k_deepdrilling/

Levanto, A. E. 1959. A three component magnetometer for small drillholes and its use in ore prospecting. Geophysical Prospecting, Vol. 7, Issue 2, 183-195.

Li, Y. und Oldenburg, D. W. 2000. Joint inversion of surface and three-component borehole magnetic data. Geophysics 65, No. 2, 540-552

Pesonen, L. J., Elming,S.-A., Mertanen, S., Pisarevsky, S., D'Agrella-Filho, M. S., Meert, J. G., Schmidt, P. W., Abrahamsen, N. und Bylund, G. 2003. Paleomagentic configuration of continents during the Proterozoic, Tectonophysics, Volume 375, Issues 1-4, 289-324.

Silva, J. B. C. und Hohmann, G. W. 1981. Interpretation of three-component borehole magnetometer data. Geophysics 46, No. 12, 1721-1731

Virgil, C., Hördt, A., Klein, T., Kück, J., Leven, M. und Steveling, E. 2010. High precision orientation of three-component magnetic downhole logs. Scientific Drilling, No. 9, 37-40

ICDP

Paleoenvironments, Evolution, and Geomicrobiology in a Tropical Pacific Lake: The Lake Towuti Drilling Project (TOWUTI)

H. VOGEL[1,2], J.M. RUSSELL[3], S. BIJAKSANA[4], S.Y. CAHYARINI[5], D. FOWLE[6], D. HAFFNER[7], Y. HUANG[3], S. IDRIYANTI[8], J. KING[9], M. MELLES[1], A. NOREN[10], D. OPPO[11], T. VON RINTELEN[12], N. WATTRUS[13]

[1] University of Cologne, Institute of Geology and Mineralogy, Zülpicher Str 49a, D-50674 Köln, Germany, e-mail to: vogelh@uni-koeln.de
[2] Umeå University, Climate Impacts Research Centre (CIRC), SE-98107 Abisko, Sweden
[3] Brown University, Department of Geological Sciences, Providence (RI), USA
[4] Institut Teknologi Bandung, Bandung, Indonesia
[5] Indonesian Institute of Sciences (LIPI), Centre for Geotechnology, Bandung, Indonesia
[6] University of Kansas, Geology Department, Lawrence, USA
[7] University of Windsor, Great Lakes Institute of Environmental Research (GLIER), Windsor, Canada
[8] University of Indonesia, Bandung, Indonesia
[9] University of Rhode Island, Graduate School of Oceanography, Providence (RI), USA
[10] University of Minnesota, National Lacustrine Core Repository (Lacore), Minneapolis, USA
[11] Woods Hole Oceanographic Institution (WHOI), Woods Hole (MA), USA
[12] Museum für Naturkunde Berlin, Berlin, Germany
[13] University of Minnesota Duluth, Large Lakes Observatory (LLO), Duluth, USA

Lake Towuti (2.5°S, 121°E) is a, 560 km^2, 200-m deep tectonic lake at the downstream end of the Malili lake system, a set of five, ancient (1-2 MYr) tectonic lakes in central Sulawesi, Indonesia. Lake Towuti's location in central Indonesia provides a unique opportunity to reconstruct long-term paleoclimate change in a crucially important yet understudied region- the tropical Western Pacific warm pool, heart of the El Niño-Southern Oscillation. The Malili Lakes have extraordinarily high rates of floral and faunal endemism, and the lakes are surrounded by one of the most diverse tropical forests on Earth. Drilling in Lake Towuti will identify the age and origin of the lake and the environmental and climatic context that shaped the evolution of this unique lacustrine and terrestrial ecosystem. The ultramafic (ophiolitic) rocks and lateritic soils surrounding Lake Towuti provide metal substrates that feed a diverse, exotic microbial community, analogous to the microbial ecosystems that operated in the Archean Oceans. Drill core will provide unique insight into long-term changes in this ecosystem, as well as microbial processes operating at depth in the sediment column.

While the Malili Lakes have long been considered high-priority drilling sites, only now do we have the requisite site survey information to propose the development of ICDP's first lake drilling target in the tropical western Pacific. High-resolution seismic reflection data (CHIRP and airgun) combined with numerous long sediment piston cores collected from 2007-2010 demonstrate the enormous promise of Lake Towuti for an ICDP drilling campaign. Well-stratified sequences of up to 150 m thickness, uninterrupted by unconformities or erosional truncation, are present in multiple sub-basins

within Towuti, providing ideal sites for long-term environmental, climatic, and limnological reconstructions. Multiproxy analyses of our piston cores document a continuous and detailed record of moisture balance variations in Lake Towuti during the past 60 kyr BP, highlighted by arid conditions during northern hemisphere stadials and the last glacial maximum, followed by a dry early and wet late Holocene. This history suggests that climate in central Indonesia responds most strongly to high-latitude climate forcing, despite Indonesia's remote location, and secondarily to southern hemisphere insolation forcing, a hypothesis we aim to test across multiple glacial-interglacial cycles through scientific drilling. Indeed, numerous high-amplitude reflectors in the upper 150 m of lacustrine fill suggest repeated cycles of moisture-balance variations in the tropical Pacific.
The principal objectives of our proposed ICDP deep drilling initiative are to:

(1) Document the timing, frequency, and amplitude of orbital- to millennial-scale changes in surface hydrology and terrestrial temperature in the Indo-Pacific Warm Pool across multiple glacial-interglacial cycles;
(2) Understand how variations in terrestrial hydrology and temperature in central Indonesia respond to changes in the mean state of the ENSO system, the monsoons, high-latitude forcing, and insolation;
(3) Analyze the long-term stability and resilience of rainforest vegetation to changes in climate, greenhouse gases, and fire frequency;
(4) Study the extent, biogeography, and metabolism of microbial life in the sediments of a non-sulfidic, ferrginous basin, and their relationships to carbon cycling, redox metal deposition, and the concentration of metal ore minerals;
(5) Study the effects of climate-driven changes in the aquatic environment on both lacustrine microbial populations, and the geobiosphere within the lake's sediment;
(6) Determine the age of Lake Towuti, and the ensuing rates of speciation of Towuti's endemic fauna and flora;
(7) Identify the timing of past lake level fluctuations in Towuti, changes in hydrological connections among the Malili Lakes, and how these influenced biological colonization events, habitat stability, and modes of speciation (sympatric, allopatric).

As an important milestone towards deep drilling an ICDP workshop proposal has been submitted by the core group of principal investigators (see authors) led by JM Russell in January 2011. If granted the ICDP workshop shall take place in Bandung/Indonesia in fall 2011 with the main goals to establish an international science team, review data from the ongoing pre-site survey, select primary drill sites, and formulate/extend the principal objectives for a future deep drilling and ICDP full proposal.

ICDP

The sediment record of Lake Ohrid (Albania/Macedonia) – a valuable archive of past climate and ecosystem dynamics

H. VOGEL[1,2], B. WAGNER[1], C. ALBRECHT[3], W. FINSINGER[4], M.J. LENG[5], A.F. LOTTER[6], J. REED[7], S. SCHOUTEN[8], R. SULPIZIO[9], V. VALSECCHI[4], G. ZANCHETTA[10,11], AND THE SCOPSCO SCIENCE TEAM

[1] University of Cologne, Institute of Geology and Mineralogy, Zülpicher Str 49a, D-50674 Köln, Germany
[2] Umeå University, Climate Impacts Research Centre (CIRC), SE-98107 Abisko, Sweden
[3] Department of Animal Ecology & Systematics, Justus Liebig University Giessen, Heinrich-Buff-Ring 26–32 (IFZ), 35392 Giessen, Germany
[4] University of Montpellier 2, Institute of Botany, Rue A. Broussonnet 163, F-34090 Montpellier, France
[5] NERC Isotope Geosciences Laboratory (NIGL), British Geological Survey, Nottingham, UK
[6] Utrecht University, Institute of Environmental Biology, Budapestlaan 4, NL-3584 CD Utrecht, The Netherlands
[7] University of Hull, Department of Geography, Cottingham Rd., Hull HU6 7RX, UK
[8] Royal Netherlands Institute for Sea Research (NIOZ), Landsdiep 4, NL-1797 SZ 't Horntje (Texel), The Netherlands
[9] University of Bari, CIRISIVU, c/o Dipartimento Geomineralogico, via Orabona 4, I-70125, Bari, Italy
[10] University of Pisa, Dipartimento di Scienze della Terra, via S. Maria 53, I-56126, Pisa, Italy
[11] INGV sez. Pisa, via della Faggiola 4, I-56100, Pisa, Italy

Lake Ohrid is a transboundary lake with approximately two thirds of its surface area belonging to the Former Yugoslav Republic of Macedonia and about one third belonging to the Republic of Albania (Fig. 1). With more than 210 endemic species described, the lake is a unique aquatic ecosystem and a hotspot of biodiversity. This importance was emphasized, when the lake was declared a UNESCO World Heritage Site in 1979, and included as a target area of the International Continental Scientific Drilling Program (ICDP) already in 1993. Though the lake is considered to be the oldest, continuously existing lake in Europe, the age and the origin of Lake Ohrid are not completely unraveled to date. Age estimations vary between one and ten million years and concentrate around two to five million years, and both marine and limnic origin is proposed.

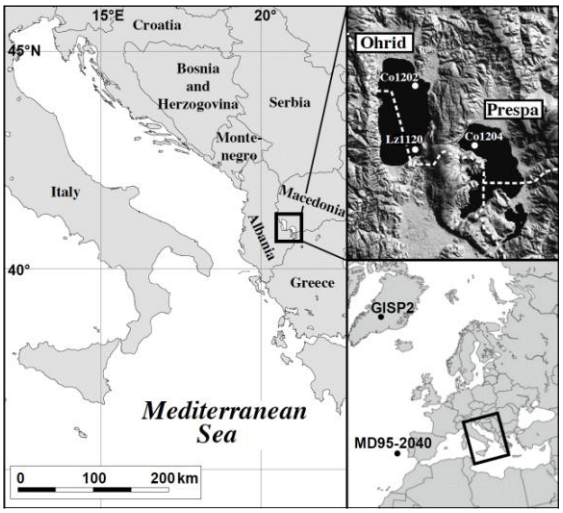

Fig. 1. Map of the northern Mediterranean region showing the location of lakes Ohrid and Prespa. White dots indicate coring locations Lz1120 and Co1202 in the southeastern and northeastern part of Lake Ohrid, and coring location Co1204 in the northwestern part of Lake Prespa. Dashed white line indicates the border between Albania, Macedonia and Greece. The insert at the right (bottom) shows the locations of the marine sediment core MD95-2040 from the western Iberian margin and the GISP2 ice core from Greenland.

In order to provide a better understanding of Lake Ohrid as a system and its response to climatic and environmental change on longer time scales a comprehensive pre-site survey was set up in pursuit of the **S**cientific **C**ollaboration **O**n **P**ast **S**peciation **C**onditions in Lake **O**hrid (SCOPSCO) ICDP deep drilling initiative. Since 2004 numerous surface sediment samples and several sediment successions have been recovered from Lake Ohrid and its hydrological connected sister lake Lake Prespa. The longest records from these lakes cover the last glacial-interglacial cycle and reach back to MIS 6. These existing sediment records from Lakes Ohrid and Prespa allow a better understanding of modern sedimentation processes (Vogel et al. 2010a), insights on local responses of the environment and biota to climate changes on long and short time scales (Wagner et al. 2009, 2010; Albrecht et al. 2010; Holtvoeth et al. 2010; Leng et al. 2010; Lindhorst et al. 2010; Reed et al. 2010; Vogel et al. 2010b; Wilke et al. 2010) and also, due to Lake Ohrid's position at the border of (sub)tropical and mid-latitudinal atmospheric circulation systems, on regional and extra-regional climate dynamics.

As the setting and catchment characteristics differ from lake to lake and in order to employ lacustrine sediment records as archives of climatic and environmental change, a thorough knowledge of modern processes and factors controlling sedimentation in each particular lake is required. Modern sedimentation in Lake Ohrid is controlled by a complex interaction of multiple processes. Analysis of biogeochemical bulk parameters, selected metals, pigment concentrations as well as grain size distributions revealed a significant spatial heterogeneity in surface sediment composition. It implies that modern sedimentation in Lake Ohrid is controlled by an interaction of multiple natural and anthropogenic factors and processes. Major factors controlling surface sediment composition are related to differences in geological catchment characteristics, anthropogenic land use, and a counterclockwise rotating surface water current (Vogel et al. 2010a). Despite these distinct spatial differences, Lake Ohrid appears to have reacted uniformly to climatic forcing on changes in catchment configuration, limnology and hydrology in the past as evidenced by contemporaneous changes in sediment composition and proxy data in long sediment successions from different parts of the lake basin (Wagner et al. 2009; 2010; Holtvoeth et al. 2010; Leng et al. 2010; Reed et al. 2010; Vogel et al. 2010b).

Due to the hydrologic connection of Lake Ohrid via karst aquifers with upstream Lake Prespa a combined investigation of sediment records from both lakes allowing insight on contemporaneous changes of their hydrology, chemistry, and trophic state is crucial for the interpretation of climatic and environmental change recorded in sediments of Lake Ohrid. As an important prerequisite for such a comparative study, a regional tephrostratigraphic framework including tephra layers found in both lakes and marine records in the closer vicinity was established (Sulpizio et al. 2010). This tephrostratigraphic framework allows an absolute correlation of important stratigraphic intervals in records from both lakes. During the last ca. 48 ka, there is no indication for distinctly lower lake levels of Lake Prespa compared to today, although the relatively low volume and low water depth make the lake very sensitive to changes in precipitation and evaporation (Wagner et al. 2010). The Pleistocene records from lakes Prespa and Ohrid indicate relatively stable sedimentation conditions. At least partial ice-cover on the lakes during winter, a well-mixed water column and oligotrophic conditions with a marginal increase of lake productivity at the end of MIS 3 characterize the lakes. Coldest conditions during MIS 2 are documented by the lowest organic matter content in both lakes and the highest abundance of concretionary horizons in Prespa, thus indicating a well mixed water column. The Pleistocene/ Holocene transition in both lakes is relatively sharp and delayed compared to other climate records from the region. The Holocene sediments are characterized by high organic matter, particularly in Lake Prespa, and high carbonate, particularly in Lake Ohrid. The differences between both lakes indicate that Lake Prespa was under mesotrophic conditions during this period, since the lake water warms up faster in spring and summer. Lake Ohrid in contrast, with a larger volume and water depth, remained oligotrophic during the Holocene (Wagner et al. 2009; 2010; Vogel et al. 2010b). Short-term events are well documented during the Pleistocene and the Holocene. The most prominent short-term events during the Pleistocene are tentatively correlated with Heinrich events, which are characterized by increased aeolian activity, lower temperatures and/or increased aridity in the Balkan region. During the Holocene, the 8.2 ka event and the 4.2 ka event are well recorded in both lakes, but indicate different environmental change, with cool and dry conditions characterizing the 8.2 event and rather dry conditions characterizing the 4.2 ka event. Anthropogenic impact is superimposed on the climatic and environmental change during the past ca. 2500 yr BP (Wagner et al. 2010).

Early human occupation and environmental impacts resulting thereof from the early-mid Holocene to the present day often limit qualitative and quantitative reconstructions from terrestrial paleorecords to preceding periods in the Mediterranean. In order to study climate and

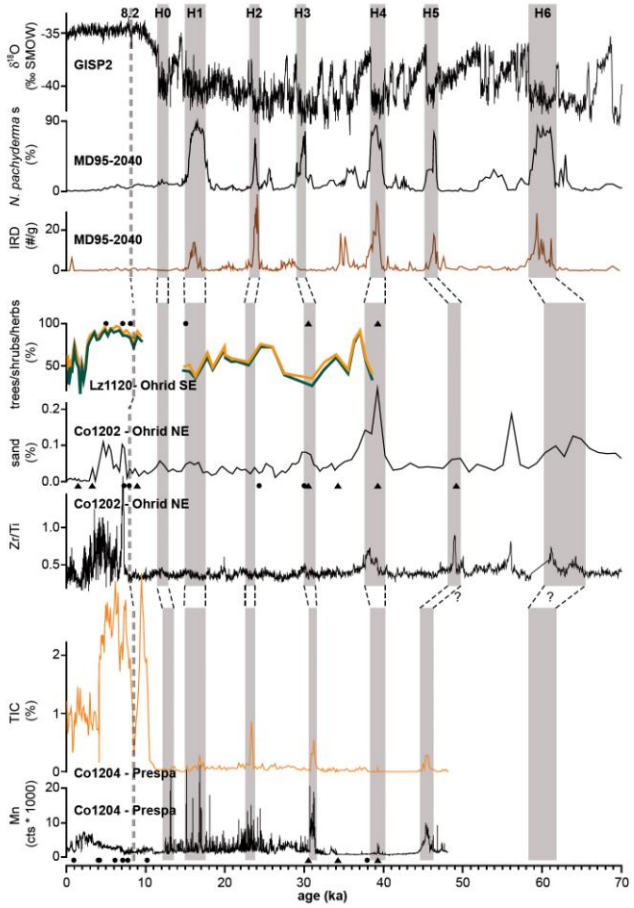

Fig. 2. Paleoenvironmental records from Lake Prespa (core Co1204; Wagner et al. 2010) and Lake Ohrid (cores Lz1120 and Co1202; Wagner et al., 2009; Vogel et al., 2010b) compared with the number of IRD grains and the cold water thriving foraminifera *N. pachyderma s.* from the western Iberian margin (Fig. 1; MD95-2040; de Abreu et al., 2003) and with the $\delta^{18}O$ record from the GISP2 ice core (Grootes et al., 1993). Black dots and triangles in the cores from lakes Prespa and Ohrid indicate horizons, which were used for radiocarbon dating and tephrochronology. The timing and thickness of Heinrich events H1–H6 is according to de Abreu et al. (2003).

environmental change and their underlying dynamics under comparable conditions as today anthropogenically unbiased records allowing qualitative and quantitative reconstructions from former interglacials are required. One such record (Core Co1202; Fig. 1) covering the last peak interglacial (MIS 5e) as well as preceding and subsequent periods has become available from Lake Ohrid. Chronological control for the core section covering the MIS 6/5 transition and MIS 5 is given by three geochemically correlated and independently dated tephra layers centered at 131 (P-11), 108.4 (X-6), and 101.2 ka (X-5) (Vogel et al. 2010c; Fig. 3).

A multiproxy study was set up to study climatic variability and its impact on Lake Ohrid's ecosystem, hydrology, and catchment dynamics during the MIS 6/5 transition and the Last Interglacial. This approach combines novel molecular and established sedimentological, geochemical, and paleoecological tools. Palynological, sedimentological, and diatom data imply that the Last Interglacial at Lake Ohrid was preceded by a relatively warm interstadial period between c. 136 and 132 ka (Fig. 3). This interstadial was followed by a cold reversal/stadial centered at c. 131 ka, characterized by a marked vegetation shift towards more steppic element taxa (Fig. 3f), a decrease in productivity as indicated by diatom assemblage changes (Fig. 3k), and stronger erosion of the lake's catchment recorded through increases in sand content (Fig. 3e) at site Co1202. From c. 129 ka a gradual increase in arboreal taxa (Fig. 3h) in concert with gradually increasing in-lake productivity (Fig. 3i, k, l, m, o) probably marks the beginning of full interglacial climate conditions at Lake Ohrid. From c. 124 ka in-lake productivity indicators show a gradual decline, which points to steadily decreasing lake water temperatures and/or restricted nutrient availability. Interestingly arboreal pollen taxa show a gradual increase during the same period, potentially as an effect of proceeding soil formation and stabilization in the steep terrain surrounding the lake fostering the establishment of a dense vegetation cover. A sudden drop in in-lake productivity indicators starting at about 116 ka probably marks the end of last interglacial climate conditions at Lake Ohrid.

In order to provide a better understanding of climate dynamics and the impact of external and internal forcings on the highly vulnerable Mediterranean region quantitative information on temperature and precipitation back in time is required. As today these crucial datasets exist only sparsely at a representative spatial and temporal resolution in the Mediterranean region. In case of Lake Ohrid we applied newly developed molecular tools (TEX_{86}, MBT/CBT) in combination with established pollen based transfer functions to achieve quantitative estimates on temperature and precipitation evolution in course of the last glacial-interglacial cycle back to MIS 6. Initial results appear very promising and imply c. 5-6°C lower temperatures in the glacial compared with the interglacial periods and c. 2°C higher temperatures during the Last Interglacial if compared to the Holocene. The reconstructed glacial and interglacial temperatures from Lake Ohrid correspond relatively well with temperature anomalies derived from SST reconstructions in the marine and pollen-based temperature reconstructions in the terrestrial vicinity. The origin of the TEX_{86} and MBT/CBT signatures in lacustrine environments is, however, not completely decoded. To shed more light on the origin and seasonal distribution of compounds influencing the TEX_{86} and MBT/CBT signatures a comprehensive seasonal water-sampling program was performed in 2010. Investigations of water samples and organic compounds contained are still ongoing but might yield important information for a better understanding of these novel molecular tools in lacustrine environments.

Rapid and/or severe climate changes are likely to have a strong impact on the biotic inventory of lakes. To test the response of Lake Ohrid's biota to climate changes over longer time scales fossil records of different taxa have been analysed (Albrecht et al. 2010; Reed et al. 2010; Wagner et al. 2009). As one example the discovery of a fossil gastropod and bivalve record from the Last Interglacial period enabled the comparison of modern and fossil assemblages. Comparison of the fossil faunal composition with recent mollusc associations in Lake Ohrid revealed a

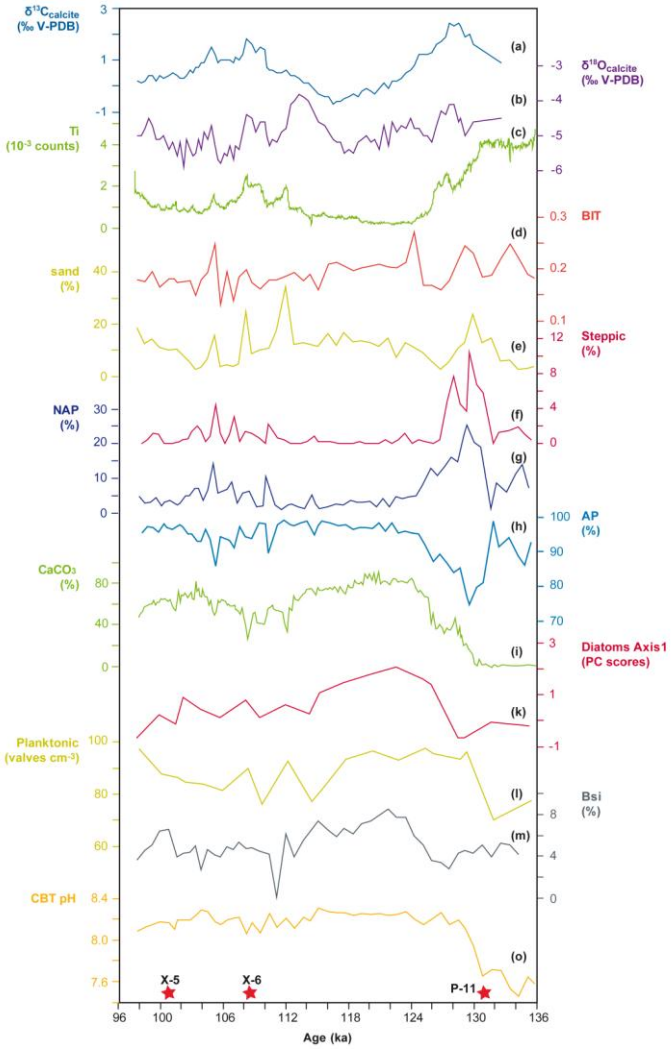

Fig. 3. Lake Ohrid (core Co1202) proxy data. (a) δ13C measured on authigenic calcite (Leng et al. 2010). (b) δ18O measured on authigenic calcite (Leng et al. 2010). (c) Titanium (Ti) counts (Vogel et al. 2010b). (d) Branched and isoprenoid tetraether (BIT) index. (e) sand content (Vogel et al. 2010b). (f) Concentration of steppic pollen taxa. (g) Concentration of non arboreal (NAP) pollen taxa. (h) Concentration of arboreal (AP) pollen taxa. (i) CaCO3 concentrations (Vogel et al. 2010b). (k) Diatom PCA axis 1 scores (Reed et al. 2010). (l) Concentration of planktonic diatom taxa (Reed et al. 2010). (m) biogenic silica (BSi) concentrations (Vogel et al. 2010b). (o) Cyclisation ratio of branched tetraethers (CBT) inferred "lake water" pH using the Weijers et al. (2007) calibration.

total of 13 mollusc species (9 gastropod and 4 bivalve species), which exclusively included species also found in the present fauna. This implies that no mollusc extinctions occurred since the Last Interglacial despite rapid and severe climatic and environmental changes in course of the last glacial-interglacial cycle (Albrecht et al. 2010).

Results of the pre-site survey indicate the high sensitivity of Lake Ohrid to climatic and environmental change and thus not only emphasize it as a world class site for paleoclimate research but also as one of the few sites worldwide where the impact of geological/climatic events on the lake's biota can be investigated in detail. The existing records are, however, too short to provide information about the age and origin of the lake and to unravel the mechanisms controlling the evolutionary development leading to the extraordinary high degree of endemism. High-resolution hydroacoustic profiles (INNOMAR SES-96 light and INNOMAR SES-2000 compact) and multichannel seismic (Mini-GI-Gun) studies demonstrate well the interplay between sedimentation and active tectonics and impressively prove the potential of Lake Ohrid for an ICDP drilling campaign. The maximum sediment thickness is ˜680 m in the central basin, where unconformities or erosional features are absent. Thus the complete history of the lake is likely recorded. A deep drilling in Lake Ohrid would help

(i) to obtain more precise information about the age and origin of the lake,
(ii) to unravel the seismotectonic history of the lake area including effects of major earthquakes and associated mass wasting events,
(iii) to obtain a continuous record containing information on volcanic activities and climate changes in the central northern Mediterranean region, and
(iv) to better understand the impact of major geological/environmental events on general evolutionary patterns and shaping an extraordinary degree of endemic biodiversity as a matter of global significance.

For this purpose, five primary drill sites were selected based on the results obtained from sedimentological studies, tectonic mapping in the catchment and detailed seismic surveys conducted. For the recovery of up to ca. 680 m long sediment sequences at water depths of more than 260 m a newly developed platform operated by DOSECC shall be used. Important milestones concerning the operational and logistical planning of the deep drilling have been achieved through joint efforts by the scientific community represented by the PI´s, local authorities in Macedonia and Albania, ICDP and DOSECC. The ICDP project will commence in summer 2011 with shallow drilling operations and will be pursued in spring-summer 2012 with the deep drilling operations .

References:

Albrecht A, Vogel H, Hauffe T, Wilke T (2010) Sediment core fossils in ancient Lake Ohrid: testing for faunal change since the Last Interglacial. Biogeosciences, 7, 3435-3446.

de Abreu L, Shackleton NJ, Schönfeld J, Hall MA, Chapman MR (2003) Millenial-scale oceanic climate variability off the Western Iberian margin during the last two glacial periods. Marine Geology, 196, 1–20.

Grootes PM, Stuiver M, White JWC, Johnsen SJ, Jouzel J (1993) Comparison of oxygen isotope records from the GISP2 and GRIP Greenland ice cores. Nature, 366, 552–554.

Holtvoeth J, Vogel H, Wagner B, Wolff GA (2010) Lipid biomarkers in Holocene and glacial sediments from ancient Lake Ohrid (Macedonia, Albania). Biogeosciences, 7, 3473-3489..

Leng M, Baneschi I, Zanchetta G, Jex CN, Wagner B, Vogel H (2010) Late Quaternary palaeoenvironmental reconstruction from Lakes Ohrid and Prespa (Macedonia/Albania border) using stable isotopes. Biogeosciences, 7, 3109-3122.

Lindhorst K, Vogel H, Hilgers A, Zander A, Krastel S, Wagner B, Wessels M, Daut G (2010) Stratigraphic analysis of lake level fluctuations in Lake Ohrid: an integration of high resolution hydro-acoustic data and sediment cores. Biogeosciences, 7, 3531-3548.

Reed JM, Cvetkoska A, Levkov Z, Vogel H, Wagner B (2010) The last glacial-interglacial cycle in Lake Ohrid (Macedonia/Albania): testing diatom response to climate. Biogeosciences, 7, 3083-3094.

Sulpizio R, Zanchetta G, D´Orazio, Vogel H, Wagner B (2010) Tephrostratigraphy and tephrochronology of lakes Ohrid and Prespa, Balkans. Biogeosciences, 7, 3273-3288.

Vogel H, Wessels M, Albrecht C, Stich H-B, Wagner B (2010a) Spatial variability of recent sedimentation in Lake Ohrid (Albania/Macedonia). Biogeosciences, 7, 3333-3342.

Vogel H, Wagner B, Zanchetta G, Sulpizio R, Rosén P (2010b) A paleoclimate record with tephrochronological age control for the last glacial-interglacial cycle from Lake Ohrid, Albania and Macedonia. Journal of Paleolimnology, 44, 295-310.

Vogel H, Zanchetta G, Sulpizio R, Wagner B, Nowaczyk N (2010c) A tephrostratigraphic record for the last glacial-interglacial cycle from Lake Ohrid, Albania and Macedonia. Journal of Quaternary Science. 25, 320-338.

Wagner B, Lotter AF, Nowaczyk N, Reed JM, Schwalb A, Sulpizio R, Valsecchi V, Wessels M, and Zanchetta G (2009) A 40,000-year record of environmental change from ancient Lake Ohrid (Albania and Macedonia), Journal of Paleolimnology, 41, 407-430.

Wagner B, Vogel H, Zanchetta G, Sulpizio R (2010) Environmental change within the Balkan region during the past ca. 50 ka recorded in the sediments from lakes Prespa and Ohrid. Biogeosciences, 7, 3187-3198.

Wilke T, Schultheiß R, Albrecht C, Bornmann N, Trajanovski S, Kevrekidis T (2010) Native Dreissena freshwater mussels in the Balkans: in and out of ancient lakes. BiogeoscieCnes, 7, 3051-3065.

Weijers JWH, Schouten S, van den Donker JC, Hopmans EC, Sinninghe Damsté JS (2007) Environmental controls on bacterial tetraether membrane lipid distribution in soils. Geochimica et Cosmochimica Acta, 71, 703-713.

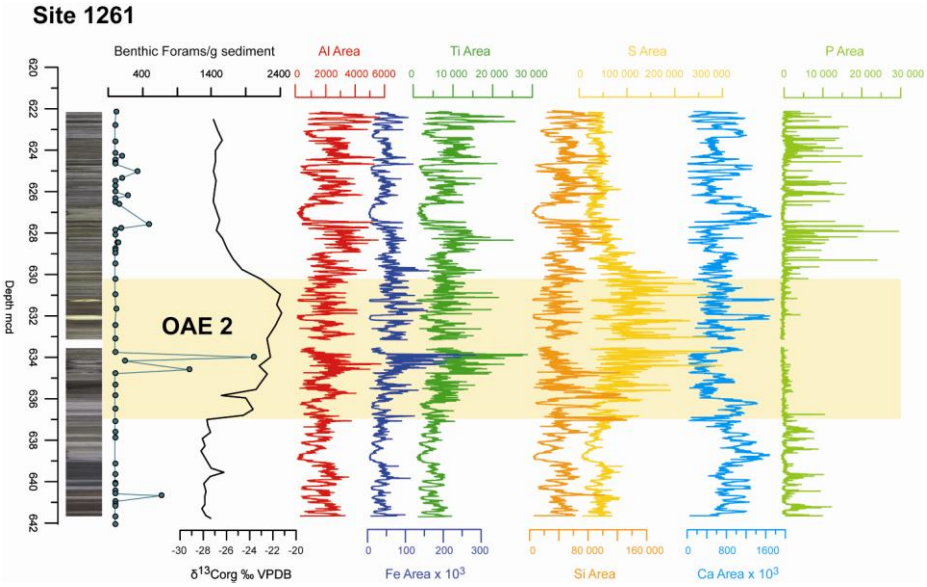

Figure 1: Relative variations of element concentrations at Site 1261 recorded by XRF core scanning.

IODP

Orbitally forced feedbacks of Oceanic Anoxic Event 2 – pulses of climate cooling and ocean ventilation in the tropical Atlantic and temperate shelf sea of Europe

S. VOIGT[1], D. BRÜSCH[1], O. FRIEDRICH[1], H. PÄLIKE[1,2]

[1] Goethe -University Frankfurt, Altenhöferallee 1, 60439 Frankfurt, Germany
[2] NOC Southampton, European Way, Southampton, SO143ZH, UK

The Cenomanian – Turonian OAE 2 is reflected by one of the most extreme carbon cycle perturbations in Earth's history possibly triggered by massive volcanic CO2 degassing during the emplacement of large igneous provinces (LIPs). Severe climatic, oceanographic and biotic feedbacks are reported from different depositional settings ranging from coastal and shallow environments to the open ocean. The nature of these changes as well as their spatial and temporal dimension is still not well understood to date. Many authors recorded overall-warming while others suggested intervals of climatic cooling. The ocean circulation was considered to have been sluggish with a well stratified water-column or intensified with increased productivity and enhanced organic carbon burial flux. The formation of oceanic anoxia was widespread but not contemporaneously at different oceanic settings and mainly controlled by local conditions.

The main difficulty to integrate these different observations lies in the insufficient resolution of available timescales. Although regional orbital age models exist at shelf settings from both sides of the Atlantic Ocean, their correlation to the open ocean is not unequivocal. This study presents results of spectral analysis of relative changes in XRF-element concentrations derived from two sites, the oceanic ODP-Site 1261 (Demerara Rise, tropical Western Atlantic) and the shelf-sea locality at Wunstorf (Northern Germany).

Site 1261 is the shallowest site of Leg 207 situated close to the continental margin. The investigated succession comprises 20 m of cyclic bedded planktic foraminiferal packstones and organic-rich mudstones whereby the OAE 2 interval, a horizon of elevated TOC values, is about 7 m thick (Erbacher et al. 2005, Nederbragt et al. 2006). A short-lived period of surface-water cooling and bottom-water oxygenation is indicated by TEX86 data and the repopulation of the seafloor with benthic foraminifera in the lower third of the OAE 2 interval (Forster et al. 2007, Friedrich et al. 2008).

At Wunstorf, the OAE 2 succession was deposited in

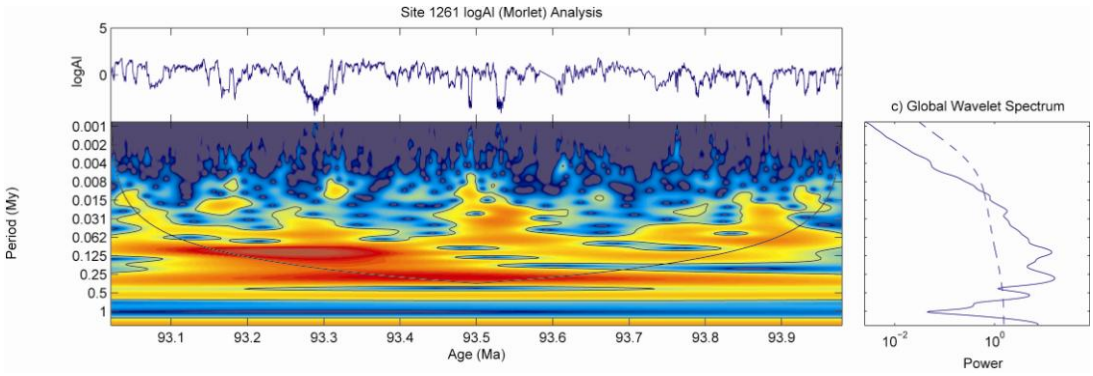

Figure 2: Wavelet analysis of the logAl time series in the time domain shows a strong spectral power at the frequeny of short eccentricity and a weaker signal in the precession band.

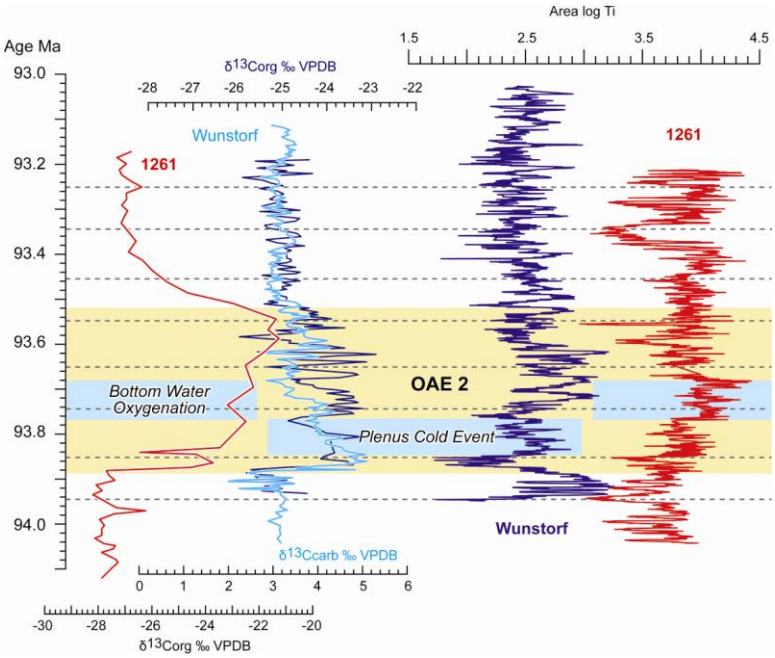

Figure 3: Correlation of carbon isotope records and relative changes in Ti concentrations at Wunstorf and ODP Site 1210B based on the cyclostratigraphic age models developed for each site. Dotted lines mark the short eccentricity cyclicity. According to this age model the two oxygenation events are not identical but are offset by about 100 kyr.

an intra-shelf basin. Sediments consist of rhythmically bedded laminated black shales, dark marls and marly limestones. Hierarchical bundling of sedimentary cycles as well as spectral analysis and Gaussian filtering of dominant frequencies detected from Ti element concentrations reveal cycle frequency ratios characteristic for short eccentricity modulated precession (Voigt et al. 2008). Typically, the short eccentricity cycles commence with distinct black shales or black shale-marl alternations that evolve into limestones or limestone-marl couplets. One exception is a short eccentricity cycle within the lower third of the OAE 2 interval that is free of black shales indicating a short-lived oxygenation event. This horizon corresponds to the "Plenus Cold Event", a migration pulse characterised by the south spread of boreal species.

The time series generated by high-resolution XRF-core scanning at Site 1261 shows a distinct cyclicity for elements that reflect relative changes of detrital input as Al, Ti, or Fe (Figure 1). Results of evolutionary spectral analysis (wavelet analysis) in the depth domain show a prominent cycle frequency at 1-2 m that represents the short eccentricity cycle by using the age model of Hardas and Mutterlose (2006) (Figure 2).

At both localities, Wunstorf and Site 1261, the OAE 2 succession is dominated by the frequency of short eccentricity. According to the orbital age models which are independently derived from the two different sites, the duration of the OAE 2 carbon isotope excursion is almost identical and comprises nearly four short eccentricity cycles. For correlation purposes, the two floating orbital time scales are tied to each other by the most distinct feature of all OAE 2 successions, the first prominent increase of the OAE 2 δ13C anomaly with a magnitude of more than 2 ‰ (Figure 3).

The sedimentary cycles within OAE 2 are correlative between the two depositional systems in the intra-shelf basin of Europe and at the continental margin of the tropical Atlantic. However, the "Bottom water oxygenation" event at Demera Rise and the "Plenus Cold Event" in Europe are not coeval. Although tropical and midlatitude shelf-sea cooling are orbitally forced feedbacks of OAE 2 related to the frequency of short eccentricity, the SST cooling pulse in the equatorial Atlantic delays the „Plenus Cold Event" by about 100 kyrs. These results show that the climatic response to OAE 2 as the increased sequestration of atmospheric CO2 are not related to a single events as supposed by Damsté et al. (2010) but instead was strongly mediated by regional boundary conditions and orbitally forced lead-lag relationships.

References:

Damste, J.S.S., van Bentum, E.C., Reichart, G.J., Pross, J., and Schouten, S., 2010, A CO_2 decrease-driven cooling and increased latitudinal temperature gradient during the mid-Cretaceous Oceanic Anoxic Event 2: Earth and Planetary Science Letters, v. 293, p. 97-103.

Erbacher, J., Friedrich, O., Wilson, P.A., Birch, H., and Mutterlose, J., 2005, Stable organic carbon isotope stratigraphy across Oceanic Anoxic Event 2 of Demerara Rise, western tropical Atlantic: Geochemistry Geophysics Geosystems, v. 6.

Forster, A., Schouten, S., Moriya, K., Wilson, P.A., and Sinninghe Damst,, J.S., 2007, Tropical warming and intermittent cooling during the Cenomanian/Turonian oceanic anoxic event 2: Sea surface temperature records from the equatorial Atlantic: Paleoceanography, v. 22, p. PA 1219, doi:10.1029/2006PA001349.

Friedrich, O., Erbacher, J., and Mutterlose, J., 2006, Paleoenvironmental changes across the Cenomanian/Turonian Boundary Event (Oceanic Anoxic Event 2) as indicated by benthic foraminifera from the Demerara Rise (ODP Leg 207): Revue de Micropaléontologie, v. 49, p. 121-139.

Hardas, P., and Mutterlose, J., 2007, Calcareous nannofossil assemblages of Oceanic Anoxic Event 2 in the equatorial Atlantic: Evidence of an eutrophication event: Marine Micropaleontology, v. 66, p. 52-69.

Nederbragt, A.J., Thurow, J., and Pearce, R., 2007. Sediment composition and cyclicity in the mid-Cretaceous at Demerara Rise, ODP Leg 207. In Mosher, D.C., Erbacher, J., and Malone, M.J. (Eds.), Proc. ODP, Sci. Results, 207: College Station, TX (Ocean Drilling Program), 1–31. doi:10.2973/odp.proc.sr.207.103.2007

Voigt, S., Erbacher, J., Mutterlose, J., Weiss, W., Westerhold, T., Wiese, F., Wilmsen, M., and Wonik, T., 2008, The Cenomanian-Turonian of the Wunstorf section (North Germany): global stratigraphic reference section and new orbital time scale for Oceanic Anoxic Event 2: Newsletters on Stratigraphy, v. 43, p. 65-89.

IODP

Melt-rock reaction processes in peridotites from IODP Leg 304/305 (Atlantis Massif, 30°N, Mid-Atlantic ridge)

A. VON DER HANDT[1, 2, 3], E. HELLEBRAND[2]

[1] Max-Planck Institute for Chemistry, Department of Geochemistry, J.-J. Becher Weg 24, 55128 Mainz
[2] SOEST, University of Hawaii at Manoa, 1680 East-West Road, 96822 Honolulu
[3] University of Freiburg, Institute of Geoscience, Albertstrasse 23B, 79104 Freiburg

Very olivine-rich plutonic lithologies (> 70% olivine), in the following referred to as olivine-rich troctolites (ORT), have now been identified at several locations dominantly along slow-spreading mid-ocean ridges. Their compositions (high Mg#, Cr-rich cpx) and textures (rounded olivine enclosed by poikilitic plagioclase and less abundant clinopyroxene) are consistent with the conventional definition of a primitive cumulate produced by crystallization of MORB-type parental melts.

Particularly well preserved ORT were recovered at Atlantis Massif, 30°N, Mid-Atlantic Ridge, an oceanic core complex drilled during IODP Legs 304/305. In both drill holes at Site U1309, ORT comprise around 50 m of core length that is otherwise dominantly composed of gabbroic lithologies. Several studies on ORT from Atlantis Massif concluded that they instead represent reactively overprinted residual mantle peridotites, transformed in several steps by large melt influx at shallow levels (1;2;3;4). Common to all models is an early stage of dunitization and disaggregation of mantle peridotite that occurs at high melt-rock ratios followed by concomitant precipitation of plagioclase and clinopyroxene in the pore space.

We performed a detailed petrologic investigation of mantle peridotites drilled at Atlantis Massif. Mantle peridotites represent a subordinate lithology in IODP drill holes U1309B and D (<0.5%) and occur as screens surrounded by troctolites and olivine gabbros. The unmodified protolith at Atlantis Massif is probably best represented by a highly depleted harzburgite (cpx: Na_2O 0.04 wt%, TiO_2 0.05 wt%; forsterite 0.91, NiO 0.39 wt%) that occurs in an interval farthest away from any magmatic contacts. All other peridotite samples show replacive mineral textures and compositional variation in agreement with prolonged melt-rock reaction. We interpret these mineral changes as a glimpse into the early stages in the formation of ORT and use our observations to amend existing models of ORT formation.

In general, all peridotite units contain samples that allow us to trace the evolution of a residual protolith to the ORT compositional field. Contrary to existing models, we discern a first stage of opx to cpx transformation followed by the subsequent formation of several generations of cpx that result in a texturally and compositionally distinct cpx that is similar to ORT cpx. During this process, textural features such as poikilitic cpx enclosing olivines also start to develop. Our model reduces the need for high melt-rock ratios early in the transformation process as well as influx by compositionally different melts but rather reflects limited infiltration and evolution in a quasi-closed system at shallow levels.

References:
(1) Drouin, M., et al. (2009), Chem. Geol., 264 (1-4), 71–88;
(2) Drouin, M., et al. (2010). Geochemistry Geophysics Geosystems 11(6): doi:10.1029/2009GC002995;
(3) Godard, M., et al. (2009). Earth and Planetary Science Letters 279(1-2): 110-122;
(4) Suhr, G., et al. (2008). Geochemistry Geophysics Geosystems 9(10): doi:10.1029/2008GC002012.

ICDP

Phylogenetic and lipid biomarker analysis indicating the viability of methanogenic communities within Holocene and Late Pleistocene permafrost deposits in the Lena Delta, Siberia

D. WAGNER[1], J. GRIESS[1,2], K. MANGELSDORF[2]

[1] Alfred Wegener Institute for Polar and Marine Research, Research Unit Potsdam, Telegrafenberg A45, 14473 Potsdam, Germany
[2] Helmholtz Centre Potsdam, GFZ German Research Centre for Geosciences, Telegrafenberg B423, 14473 Potsdam, Germany

Permafrost environments of the Northern hemisphere are suspected to be strongly affected by the currently observed and predicted global temperature rise (IPCC, 2007). Given that about one third of global soil carbon is preserved in high Arctic environments, a degradation of permafrost due to potential future increases of atmospheric and soil temperatures might lead to an increased bioavailability of recent as well as ancient carbon. Thus, an intensified microbial turnover of these particular carbon pools, driven by substrate availability and temperature, might cause the release of large amounts of greenhouse gases such as methane.

To predict the risk for the future climate and estimate the global atmospheric carbon budget, it is important to understand the microbial driven methane dynamics of the Siberian Arctic and their response to climate changes in the past. Therefore, a combination of quantitative and qualitative analyses of recent and fossil methanogenic communities were performed to reveal variations in permafrost deposits of the Siberian Arctic.

The El'gygygtgyn permafrost core and lake sediments of 142 m and 517 m length, respectively, were recovered within the ICDP project “Scientific Drilling in El’gygytgyn Crater Lake” from November 2008 to May 2009. In addition to that, a 23 m long permafrost core drilled in 2002 on Kurungnakh Island, Lena-Delta, Siberia, was examined. Permafrost environments can be quite different. Whereas the terrestrial core from El'gygytgyn represent a dry and TOC poor habitat, the permafrost core drilled on Kurungnakh Island was TOC rich. These two sites will be compared. However, in the current abstract we will focus on the results of the permafrost deposits from Kurungnakh Island.

The studied permafrost sequence is characterized by strong vertical variations of the total organic carbon (TOC) and in-situ methane content. The TOC content varies from 2 to 27%, whereas the methane concentrations range from 2 to 2300 ppm in certain layers. Generally, in-situ methane contents reflect the TOC profile with depth. In this context important questions are: Is this methane produced by recently active methanogenic communities in the permanently frozen ground or was the methane produced

and trapped during times of sediment deposition and permafrost progression, thus originate from fossil communities?

Lipid biomarkers and amplifiable DNA were successfully recovered throughout the whole Kurungnakh permafrost sequence with an age of up to 42 ka. Analysis on the abundance and distribution of branched and isoprenoidal glycerol dialkyl glycerol tetraether (GDGT) core lipids (being indicators for bacteria and archaea, respectively) revealed variations within the vertical profile following the trends outlined by the TOC and methane contents. At 17 m soil depth an interesting interval is indicated by a pronounced occurrence of archaeal GDGTs. Additionally, a variety of intact phospholipid esters indicate the presence of a viable microbial community at this depth. Furthermore, the respective interval is characterized by comparably low abundance of methane, but high amounts of archaeol and a high diversity of methanogenic archaea, as shown by genetic fingerprints obtained from denaturing gradient gel electrophoresis (DGGE). This suggests the possibility of recent methanogenesis in permanently frozen ground, whereas methane might have diffused through the soil and has been trapped in overlaying TOC-rich layers. Phylogenetic analysis on the basis of clone libraries of the respective methanogenic communities show changes in composition and dominance of the different genera with depth. This observation is discussed as an adaption of microorganisms to substrate quality and quantity of soil organic matter or sedimentation conditions during times of sediment deposition.

References:

Intergovernmental Panel on Climate Change (IPCC) 2007. Climate Change 2007: Contribution of Working Group I to the Fourth Assessment Report of the Intergovernmental Panel on Climate Change, The Physical Basis of Climate Change: http://www.ipcc-wg2.org/index.htl .

IODP

PANGAEA® - a data management component in IODP

H.-J. WALLRABE-ADAMS[1], M. DIEPENBROEK[1], H. GROBE[2], R. HUBER[1], U. SCHINDLER[1]

[1]MARUM, Centre for Marine Environmental Sciences, University of Bremen, 28359 Bremen, Germany
[2]Alfred Wegener Institute for Polar and Marine Research, Columbusstrasse, 27568 Bremerhaven, Germany

Data management in scientific drilling programs such as the Integrated Ocean Drilling Program (IODP) performs two functions: firstly, the capture of drilling and scientific data during an expedition and secondly, the long-term storage and dissemination of these data. The capture of data for IODP-Mission Specific Platform (MSP) expeditions is separated into two phases.

1. Drilling, curation, logging, and basic scientific data need to be collected at the drill site during the drilling phase (offshore phase).
2. Additional data are then captured post-drilling after the cores have been transported to the Bremen Core Repository (onshore phase - "Onshore Science Party"). This latter phase captures detailed measurements, descriptions, images and log data for the split cores.

For the *European Consortium for Ocean Research Drilling* (ECORD) – specifically for the *ECORD Science Operator* (ESO), which organizes and operates Mission Specific Platform (MSP) expeditions on behalf of the Integrated Ocean Drilling Program - PANGAEA® is responsible for the long term archiving of expedition as well as post-cruise data. At the end of the moratorium of each expedition – one year after the Onshore Science Party - all data are publicly available via PANGAEA's search engine, via a specific MSP Data Portal, and via the IODP Scientific Earth Drilling Information Service.

Besides being the ESO long-term data archiving facility, PANGAEA® is the lead developer of the *Scientific Earth Drilling Information Service* (SEDIS)), which provides access to the data of the three *Implementing Organisations* (IOs) of IODP: ECORD, the United States (IODP-USIO) and Japan (CDEX). SEDIS was planned to be implemented within three phases. Phases one and two are finished; at the moment phase three is in progress in cooperation with INSTAAR (Inst. of Arctic & Alpine Research, Univ. of Colorado, Boulder). The SEDIS portal comprises information about data sets, publications and expeditions supported by a search thesaurus. The final SEDIS portal will include an advanced data search and download functionality. Visualization and analysis tools (e.g. GIS, GeoMapApp, CoreWall) and mapping tools (Internet Mapping Service, GoogleTM Earth) will be implemented. Additionally a data submission application is planned.

To date no mechanism is implemented in IODP to systematically search, collect and archive post-cruise data. PANGAEA® has therefore initiated a project on behalf of IODP-MI to harvest and archive published data produced either on samples derived from expeditions, or on samples requested from archived core by post-cruise researchers. Main tasks are:

1. Identifying all current and legacy post-cruise publications related to DSDP, ODP or IODP from major reference databases (e.g.Georef, ScienceDirect etc.),
2. Extracting data tables and publishing these data in a publicly available archive accessible to the IODP SEDIS system (i.e. in Pangaea).

Since the beginning of this project (2007) about 35 journals have been processed with more than 1300 DSDP/ODP/IODP publications. In ~700 publications >3000 data sets were found in tables/appendices/supplements and were made available in machine readable form through PANGAEA® and SEDIS.

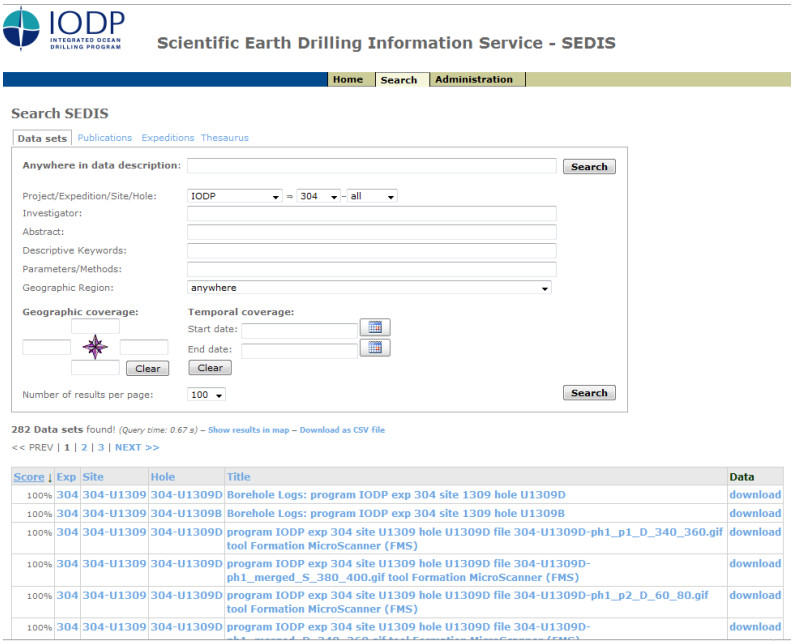

Figure 1. SEDIS portal component 'Data Search'. The geographical position of data sets and expeditions can be visualized on a map. **www.sedis.iodp.org**

IODP

Antarctic Ice Sheet Retreat since the LGM – Relation to Southern Hemisphere Temperature And Global Sea-Level Rise

M. E. WEBER[1], G. KUHN[2], P. U. CLARK[3], D. SPRENK[1]

[1] Institute of Geology and Mineralogy, Zuelpicher Str. 49a, 50935 Cologne, Germany, michael.weber@uni-koeln.de
[2] Alfred-Wegener-Institute for Polar and Marine Research, Am Alten Hafen 26, 27568 Bremerhaven, Germany
[3] Oregon State University, 104 Wilkinson Hall, Corvallis, OR 97331-5506, USA.

Reconstruction of the last global sea level rise faces uncertainties because only a few robust results are available for Antarctic ice sheets. Modeling studies reconstruct a late ice-sheet retreat starting around 12 ka BP and ending around 7 ka BP with a large impact of an unstable West Antarctic Ice Sheet (WAIS) and a small impact of a stable East Antarctic Ice Sheet (EAIS). However, two regions in the Atlantic sector of the Southern Ocean provide evidence that Antarctica responded much earlier and possibly provided a significant contribution to the last sea-level rise.

On the continental slope of the southeastern Weddell Sea, varved sediment preserverd during the Last Glacial Maximum (LGM), indicative for intense, seasonally variable bottom-water production, presumably caused by brine injection in polynias and shelf-ice plowing in front of the ice shelf, which had advanced toward the shelf edge. The following postglacial bioturbated mud favors at least partially open surface water and occasionally intensified iceberg calving. The termination of varvation marked the retreat of the EAIS from the shelf edge around 19 ka BP. The timing coincides with Meltwater Pulse 19 ka from the Northern Hemisphere (NH) and with the initiation of the temperature increase over East Antarctica. After a short ice re-advance, a second retreat occurred around 16 ka – also a time of enhanced global sea-level rise and a period when glaciers rapidly retreated in Patagonia.

Sediments from the central Scotia Sea are located in the prolongation of the "iceberg alley", where icebergs exit the Weddell Sea to the north. Accordingly, this is an excellent location to trace ice-sheet dynamics. Sites MD07-3134 and MD07-3133 document four phases of enhanced iceberg activity as indicated by the amount of small ice-rafted debris (IRD) at 19.5, 16.5,14.5, and 12 ka. The first two are most likely related to the two ice-sheet retreat signals documented by the Weddell Sea sites. The third phase relates to Meltwater Pulse 1A; the fourth phase falls roughly into period of the Younger Dryas.

Since all four phases manifested at times when atmospheric temperature rise over East Antarctica accelerated, we interpret all phases as ice-sheet retreat signals. Since models can only produce a fraction of the required global meltwater from NH ice sheets, and most phases relate to prominent global meltwater pulses, there is also indication that Antarctica contributed a substantial amount of meltwater to global sea-level rise during the four phases, with the EAIS as a major contributor during the first three phases, and the WAIS contributing mainly to the last phase when the Antarctic Cold Reversal had ended. In any case, our study shows that the oceanic record in the Weddell and Scotia Seas, the atmospheric temperature development over East Antarctica, and global sea-level rise are closely related, with possibly severe impacts on future climate and ice-sheet modeling studies.

IODP

Reconstruction of the early diagenetic history of deep subseafloor sediments at Site U1341 on Bowers Ridge (Bering Sea, IODP Exp. 323)

L.M. WEHRMANN[1], C. MÄRZ[2], P. MEISTER[1], T.G. FERDELMAN[1], B. BRUNNER[1]

[1] Biogeochemistry Department, Max Planck Institute for Marine Microbiology, Celsiusstrasse 1, D-28359 Bremen, Germany
[2] Geosciences, School of Civil Engineering and Geosciences, Drummond Building, Newcastle University, Newcastle upon Tyne, NE1 7RU, United Kingdom

Deep subseafloor sediments at Bering Sea Site U1341 drilled during IODP Expedition 323 show large down-core variability in the distribution of geochemical paleoproxies, e.g., Ba/Al and Si/Al ratios. These results are evidence of prominent changes in opal productivity over the last 4.3 Ma at this site located at 2177 m water depth on Bowers Ridge. Concomitantly, geochemical signatures of microbially mediated early diagenetic processes in the pore-water show non-steady state distributions that reflect variability in the extent of organic carbon respiration in the subseafloor sediment at this site over time. Present-day microbial activity associated with organic carbon mineralization is comparably low as evidenced in low concentrations of dissolved inorganic carbon (DIC), alkalinity (both ~12 mM), and ammonium (5.1 mM), and a minor decrease in pore-water sulfate concentration in the top 50 meters below seafloor (mbsf). Pore-water sulfate concentrations, however, decrease further below 140 mbsf to minimum values <12 mM at around 450 mbsf before increasing again below. The depth of minimum sulfate concentration overlaps with a zone characterized by strongly ^{34}S-enriched pyrite values and depletion of barium to detrital background. These results indicate that the extent of microbial sulfate reduction was higher at Site U1341 during the deposition time of this sediment interval (corresponding to ~2.0 and 3.4 Ma) which drove sulfate to depletion and resulted in the dissolution of biogenic barite. Most likely this facilitated the onset of methanogenesis, anaerobic oxidation of methane (AOM) and the installation of a sulfate-methane transition zone (SMTZ) in the sediment. In accordance with this hypothesis, the stable sulfur isotope composition of pore-water sulfate mirrors the sulfate concentration profile and shows strong ^{34}S-enrichement at the depth of minimum sulfate concentration.

Our data indicate that pore-water sulfate concentration and stable sulfur isotope profiles are still strongly imprinted by this pronounced zone of past high microbial activity. In contrast, the distribution of multiple ^{13}C-depleted diagenetic dolomite layers (-14.2 to –17.2 ‰) throughout the sediment column between 150 and 600 mbsf suggest that this may not have been the only time period where a SMTZ was present at Site U1341 in the past. Our study shows that non-steady pore-water sulfate profiles help to reconstruct past events of low and high microbial activity in the deep subsurface, they nonetheless do not replace a careful assessment of the diagenetic mineral phases archived in the sedimentary record to resolve the diagenetic history of a study site in greater detail.

IODP

The Eocene/Oligocene Transition – a cyclostratigraphic perspective

T. WESTERHOLD[1], U. RÖHL[1]

[1] MARUM - Center for Marine Environmental Sciences, University of Bremen, Leobener Strasse, Bremen, 28359, Germany

The Eocene/Oligocene transition ~34 million years ago was a critical turning point in Earth's climatic history. A warm, high-diversity greenhouse world of the early Eocene ceded to the glacial, icehouse conditions of the early Oligocene. At this transition the calcite compensation depth (CCD) deepened by ~1.2 km marking the most pronounced perturbation during the past ~150 Myr. Coincidence with a rapid stepwise increase in benthic oxygen stable isotope ratios was interpreted to reflect a combination of Antarctic ice sheet growth and decrease in deepwater temperatures. In contrast, up to today the extent and stability of land ice in the "doubthouse" world of the middle and late Eocene remain uncertain. This interval in Earth's history is critical to test climatic and evolutionary hypotheses about the Eocene deterioration. Here, it is important to note that the stratigraphy of the Eocene/Oligocene transition events, the relationship between them and the stability of the precursor late Eocene climate remain subjects of debate.

Key records for the breakthrough in reconstructing the late Eocene and Oligocene epochs were those recovered by Ocean Drilling Program (ODP) Leg 199, Site 1218 in particular. Data from Site 1218 allowed astronomical time calibration of the entire Oligocene, but the lack of carbonate in the uppermost Eocene at this site made the detailed time control as available for the Oligocene much less certain for the late Eocene. Although the paleomagnetic record during these times was of high quality, global stratigraphic correlation is hindered by the lower mass accumulation rate, the absence of a detailed isotope stratigraphy, and sparser biostratigraphic control. In order to facilitate the development of an integrated magneto- and biostratigraphic framework with a stable isotope stratigraphy (necessary to enable global correlation), the recovery of carbonate sediment with a high quality magnetostratigraphy was targeted and successfully retrieved during IODP Expedition 320 (Pacific Equatorial Age Transect I – PEAT I). The integration of these new records with Leg 199 data has the potential to substantially improve the existing geological timescales and even extend the astronomically calibrated time scale far back into the Eocene.

The sections recovered during Integrated Ocean Drilling Program (IODP) Exp. 320 provide an excellent way to assess competing interpretations of the E/O transition across a depth transect of sites with excellent age control from the world's largest ocean. So far the most complete Eocene/Oligocene boundary section recovered from the equatorial Pacific has been Site 1218 on 42 Ma old crust; however, it is far from being pristine. The recently recovered sediments from IODP Exp. 320 provide

a new depth transect for several Cenozoic key horizons, such as the Eocene/Oligocene transition at Sites U1331-U1334.

Here we present preliminary results from our new project. The main scientific goal is to substantially contribute to our understanding of the variability of the Paleogene climate with focus on the Eocene/Oligocene transition. Fundamental interaction of the carbon cycle, solar forcing, and glacial events has been documented for the Oligocene suggesting that the climate system responses to complex orbital variations via expansion and contraction of biosphere productivity. We apply high resolution datasets to investigate and test if orbital forcing is imprinted upon paleoclimatic records through an influence on the carbon cycle in the middle to late Eocene climate in the equatorial Pacific. Reconstruction of the CCD will address how and why the acidity of the oceans changed in association with shifts in global climate (e.g. Carbonate Accumulation Events, Middle Eocene Climate Optimum). Stable isotopic composition of bulk sediment and microfossils will further assist in reconstructing the carbon cycle dynamics in the Eocene climate system at high-resolution.

We will show: (1) examples of post-cruise refinements of the shipboard composite depth scales and composite records of IODP Expedition 320 Sites U1331, U1332, U1333, U1334 as well as ODP Leg 199 Sites 1218, 1219 and 1220 based on high resolution XRF core scanning data, physical property data, and stratigraphic data; aim is to define a complete high-resolution time series for the middle to late Eocene and earliest Oligocene interval (magnetic polarity chrons C12n to C20n). (2) Examples of detailed time series analysis of the integrated Leg 199 and Exp. 320 sites and a preliminary cyclostratigraphy based on the identification of the stable long eccentricity cycle (405 kyr). (3) First results to calibrate the XRF core scanning intensities with data for discrete samples acquired by the Portable Energy Dispersive Polarization X-ray Fluorescence analyzer (EDP-XRF) at MARUM and crosscheck with other geochemical data available (incl. shipboard $CaCO_3$). (4) First results toward a new high-resolution bulk stable isotope record across the Eocene/Oligocene transition.

ICDP

Drilling into the Campi Flegrei Caldera to characterize the deep fluid regime in time and space (CFDDP)

T. WIERSBERG, J. ERZINGER

Helmholtz-Zentrum Potsdam, Deutsches GeoForschungsZentrum, Telegrafenberg, 14473 Potsdam

The basic idea of Campi Flegrei Caldera Deep Drilling Project (CFDDP) is to drill one shallow hole (500 m) and one deep hole (4 – 5 km total depth) inside the Campi Flegrei caldera close to the caldera rim to improve our understanding on volcanism associated to large calderas, to study the geothermal potential of the area for energy exploitation of this and similar volcanic areas, and to develop new technologies for volcano monitoring and environmental control.

The scientific objective of CFDDP is to study in detail the substructure of the Campi Flegrei Caldera to understand the link between magmatic and geothermal systems in the generation of seismic unrest and eruptions. This includes the determination of the composition, rheology and degree of gas/brine/water saturation at shallower depth and to answer important questions linked to the mechanism of generation of static deformation and seismicity.

The shallow well will be assembled with instrumentation for long-term geophysical monitoring, and will also provide access to fluids and gases at bottom hole temperatures of about 200° C. The deep hole will approach and possible penetrate the fragile-ductile transition at temperatures of 350°- 400° C which may act as a barrier, separating an upper convective aquifer zone from a lower, supercritical zone that host gases from the degassing magma chamber underneath. Drilling of the shallow well was originally planed for 2010, but is postponed to early 2011 due to problems encountered in obtaining legal

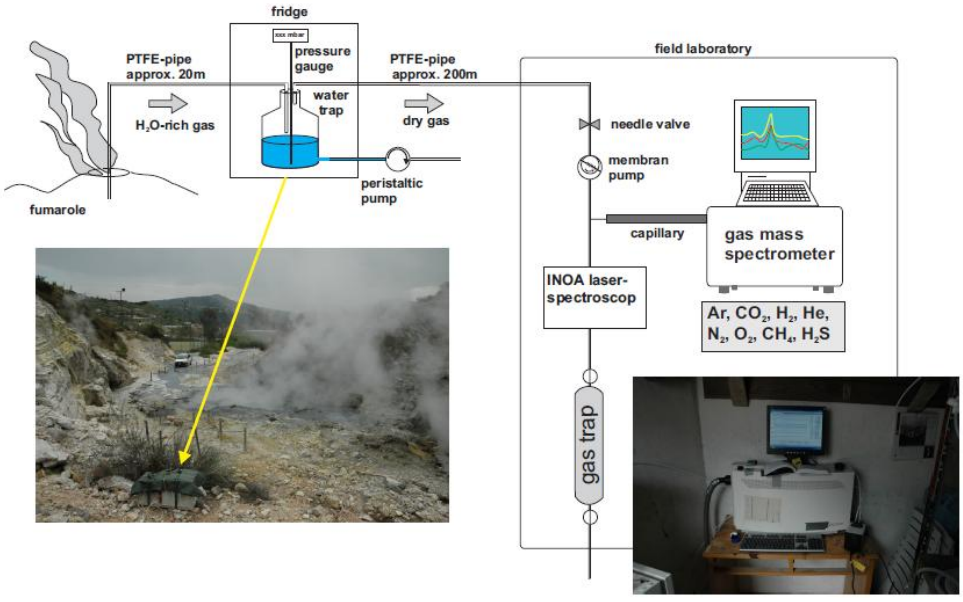

Set up of the gas monitoring station at the Pisciarelli fumarole field.

permissions. Thus, drilling of the main hole will probably not be conducted before 2012.

We plan to perform geochemical monitoring of volcanic gas emissions to assess the input of shallow and deep fluids to the fluid regime and to characterize migration processes of fluids from depth to the surface. We would like to sample and monitor fluids and gases from the shallow well to identify short- and long-term variation in the fluid and gas composition in time to improve our understanding of the temporal evolution of the Campi Flegrei magmatic system. Realtime montoring of drilling mud gas during dring of the deep hole will be performed to reveal information on the molecular composition and distribution of gases versus depth. Results from this experiment will help characterizing the Campi Flegrei fluid regime in space. Stable isotope and noble gas isotope analysis will be conducted on gas samples from all individual experiments.

Since 2009 we are conducting a preliminary study on the chemistry of vent gases in Campi Flegrei which comprises on-line monitoring of volcanic gas from a vent in the fumarole field of Pisciarelli at the eastern outer flank of the Solfatara. Intermittently, the station is analyzing continuously the composition of gases on a minute base by means of a quadrupole mass spectrometer. Volcanic gas is continuously pumped from the vent through 200 m Teflon© in to a small field laboratory, where the gas phase is analysed for H_2, H_2S, CH_4, N_2, O_2, Ar, He, and CO_2 and, in addition, with a tuneable diode laser spectrometer for CO_2. Prior to gas analysis, gaseous water is condensed in a cooling device close to the fumarole. In average the water-free gas phase is composed of CO_2 (98.5 vol.-%), N_2 (1.0 vol.-%), H_2S (0.24 vol.-%), H_2 (0.11 vol.-%), CH_4 (60 ppmv), Ar (20 ppmv) and He (10 ppmv). Diurnal variations that are most likely related to tidal effects have been observed.

ICDP

First comparison between core catcher and composite pollen profiles of the ICDP lake drilling project at Laguna Potrok Aike, Argentina

M. WILLE[1], F. SCHÄBITZ[1], THE PASADO SCIENCE TEAM[2]

[1] University of Cologne, Seminar for Geography and Education, Gronewaldstr. 2, 50931 Cologne

[2] http://dc-app1-02.gfz-potsdam.de/site/contacts/contacts-search-all?select=3&term=pasado

Laguna Potrok Aike is a maar lake situated in the Argentinean part of the Pali Aike Volcanic field on the southern South American mainland. In the framework of the multinational ICDP deep drilling project PASADO first pollen analytical results of the basal section (8000-10350 cm) of the composite core 5022-2CP can be compared with a previous study of the core catcher samples of coring site 2C.

A robust time control of the presented core section is not available as according to sedimentological results most of the shown composite profile is disturbed. However, the core interval might cover the time between ca. 48,000 and 51,000 years before present.

Both profiles are dominated by pollen taxa of a cold steppe vegetation. Background noise of pollen from *Nothofagus* (Andean Forest) is always present but somewhat higher amounts start around 9800 cm. In the middle part of the profile increasing *Nassauvia* values indicate cooler and/or drier conditions than before or at the top of the profile. *Botryococcus* and *Pediastrum kawraiskyi* algae seem to indicate different ecological conditions in the lake.

Basic dynamics in the core catcher and the composite profiles are comparable (e.g. decreasing Poaceae and Asteraceae values, increase in *Pediastrum* algae). Therefore the core catcher profile represents a good pilot pollen study for the composite profile.

In 30 cm resolution pollen analysis is not suited to identify disturbance in the composite core. Therefore, a comparison with sedimentology is necessary.

A comparison with the coming diatom record will probably shed light on the different ecological conditions that caused the contrasting algae signal.

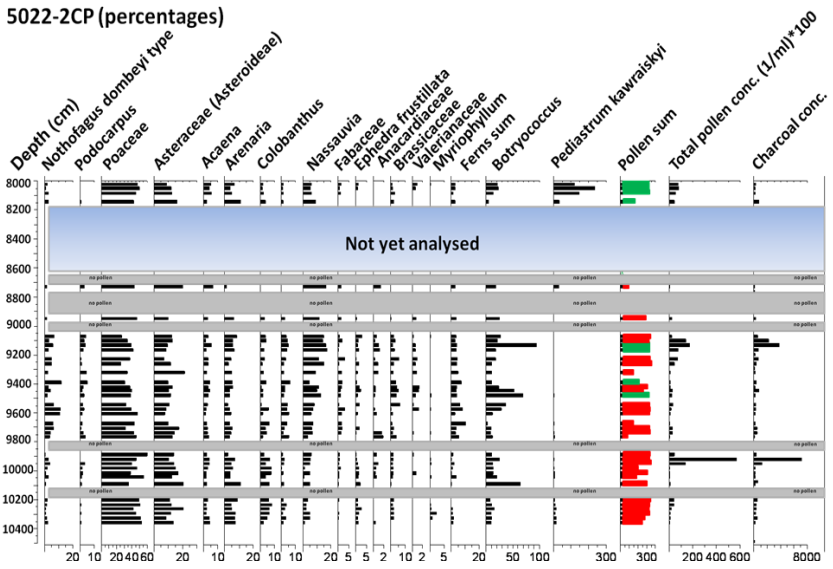

Fig. 1: Selected pollen proxies of composite profile: 5022-2CP. Red samples are disturbed, green are undisturbed.

This study shows the significantly increased quality of multi-proxy in comparison to single proxy studies.

As the project continues for another year, a pollen study of the complete composite core will soon be available

IODP

Assessing Arctic Submarine Slope Stability by Scientific Ocean Drilling

D. WINKELMANN[1], W. GEISSLER[2]

[1] Leibniz Institute for Marine Science (IFM-GEOMAR), Wischhofstr. 1-3, 24148 Kiel, Germany
[2] Alfred Wegener Institute for Polar and Marine Research, Am Alten Hafen 26, 27568 Bremerhaven, Germany

Submarine landsliding represents a major natural hazard to infrastructure at coasts and seafloor. It also dangers coastal communities by tsunami generation and the associated socio-economic consequences. Thus, understanding of submarine landslides, their conditions and trigger mechanisms, recurrence rates and potential impact remains an important task for the evaluation of risks in coastal management and offshore industrial activities. In the light of a changing globe with warming oceans and rising sea-level accompanied by increasing human population along coasts and enhanced near- and offshore activities, slope stability issues gain more importance than ever before.

The Arctic exhibits the most rapid and drastic changes following global warming and is predicted to change even faster. Rising air temperatures and enhanced inflow of less-cooled Atlantic water into the Arctic Ocean reduces sea-ice cover (positive feedback through decreasing albedo) and in consequence warms the surroundings. Therefore, submarine slope stability may be challenged considering large areas of permafrost and hydrates.

The Hinlopen/Yermak Megaslide (HYM; Cherkis et al., 1999, Vanneste et al., 2006, Winkelmann et al., 2006, 2008) north of Svalbard is the first and so far only reported large-scale submarine landslide in the Arctic Ocean. The HYM exhibits the highest headwalls that have been found on siliciclastic margins. With more than 10.000 km² areal extent and app. 2.400 km³ of involved sedimentary material, it is one of the largest exposed submarine slides worldwide. It probably caused a tsunami with circum-Arctic impact. Its geometrical configuration and timing is different from submarine slides on other glaciated continental margins. Thus, it raises the question whether slope stability within the Arctic Ocean is governed by processes specific to this environment. The extraordinary thick slabs (up to 1800 m) that were moved translationally during sliding raise the question on the nature of the weak layers associated with this process. Theories involving higher pore pressure are being challenged by this observation, because either extreme pore pressures or alternative explanations have to be considered. To assess the actual submarine slope stability and failure potential in the Arctic Ocean, we suggest to investigate the HYM in great detail.

We propose to drill and recover weak layer material of the HYM from the adjacent, intact strata by scientific ocean drilling. We further propose to drill into the adjacent deforming slope to identify material properties of detachments and monitor their deformation in-hole.

References:

Cherkis, N.Z., Max, M.D., Vogt, P.R., Crane, K., Midthassel, A., Sundvor, E., 1999, Large-scale mass wasting on the north Spitsbergen continental margin, Arctic Ocean. Geo-Marine Letters 19, 131-142.

Vanneste, M., Mienert, J., Bünz, S., 2006, The Hinlopen Slide: A giant, submarine slope failure on the northern Svalbard Margin, Arctic Ocean. Earth Planetary Science Letters 245, 373-388.

Winkelmann, D., Jokat, W., Stein, R., Winkler, A., 2006, Age and extent of the Yermak Slide north of Spitsbergen, Arctic Ocean, Geochemistry, Geophysics, Geosystems 7 (6), doi:10.1029/2005GC001130.

Winkelmann, D., Geissler, W., Schneider, J., Stein, R., 2008a, Dynamic and timing of the Hinlopen/Yermak Megaslide north of Spitsbergen, Arctic Ocean, Marine Geology 250, 34-50.

ICDP

Carbon and nitrogen isotope composition of bulk sedimentary organic matter from Laguna Potrok Aike during the last Glacial and the Holocene

J. ZHU[1], A. LÜCKE[1], H. WISSEL[1], C. MAYR[2,3], M. OEHLERICH[2], C. OHLENDORF[4], B. ZOLITSCHKA[4] AND PASADO SCIENCE TEAM (J.ZHU@FZ-JUELICH.DE)

[1] Institute of Bio- and Geosciences, IBG-3: Agrosphere, Forschungszentrum Jülich, D-52428 Jülich
[2] Dept. of Earth and Environmental Sciences, University of Munich, D-80333 Munich, Germany
[3] Institute of Geography, University of Erlangen-Nürnberg, D-91054 Erlangen, Germany
[4] GEOPOLAR, Institute of Geography, University of Bremen, D-28359 Bremen, Germany

The 106 m long Site 2 composite profile 5022-2CP from the ICDP expedition PASADO to Laguna Potrok Aike offers a record of environmental variability during the last 54,000 years BP (according to age model V.1 (Kliem et al., unpublished)) in southern Patagonia, Argentina. During the initial phase of the project we have investigated the organic carbon and nitrogen isotopic composition of bulk sediment and plant debris of core catcher samples. The carbon and nitrogen content of the core catcher fine sediment fraction (<200 µm) is low to very low (around 1 % and 0.1 %, respectively). The carbon isotope composition shows comparably little variation around a value of -26.0 ‰. The positive values of the Holocene and the Late Glacial are only sporadically reached down core. Compared to this, separated moss debris is remarkably 13C depleted with a minimum at 31.5 ‰. The nitrogen isotope ratios of glacial Laguna Potrok Aike sediments are lower than those of the younger part of the record. In comparison to the composite profile 5022-2CP discussed in the following, data patterns revealed by the core catcher samplers can give first insights but not fully retrieve the general picture. In parts, core catcher data may even underestimate parameter relations severely. Nevertheless, they are an adequate tool to gain fast insights into long sediment profiles.

	$\delta^{15}N$ VS TN	$\delta^{13}C$ VS TOC	$\delta^{15}N$ VS $\delta^{13}C$	$\delta^{15}N$ VS C/N	$\delta^{13}C$ VS C/N
Entire composite profile	-0,17	0,59	-0,15	-0,09	0,66
7500-0 cal. BP	-0,53	0,57	-0,49	-0,53	0,43
16,223-7500 cal. BP	-0,51	0,58	-0.79	-0,54	0,63
53,210-16,223 cal. BP	-0,22	0,53	-0,04	-0,14	0,41

Tab.1: Correlation coefficients for the entire composite profile 5022-2CP and three selected periods (7500-0 cal. BP; 16,223-7500 cal. BP; 53,210-16,223 cal. BP) between variables measured in this study.

Here we report on carbon and nitrogen isotope investigations of bulk sedimentary organic matter. For the transition period from the Last Glacial to the early Holocene (ca. 24,000 – 8,400 cal. BP) investigations were carried out with high temporal resolution (2 cm). For the other periods, the time resolution is still lower (8 cm for carbon and 16 cm for nitrogen). We have analysed the disturbed as well as the undisturbed lacustrine facies to learn more about effects of lake internal re-deposition.

Our data suggest three major units along the composite profile (Fig.1). The glacial part is characterized by very low TOC and TN contents. C/N ratio is almost completely below 10. Carbon isotope composition shows more or less constant values at around -26 ‰, although in certain periods larger variations are observed. Similar to carbon, the nitrogen isotope composition shows no clear trend during the Glacial. Around 16,223 cal. BP an abrupt shift occurs for all data interpreted as imprint of the onset of the last deglaciation. TOC and TN content increased dramatically and C/N ratio rose to above 10, occasionally above 15. The carbon isotope composition is more positive with values of around -23‰. Contrary to carbon, the nitrogen isotope composition has decreased by ca. 1‰ with deglaciation and reached the highest value of the profile during the early Holocene. According to our data and the applied age-depth model, this abrupt shift from the Glacial to the Late Glacial occurred within only ca. 70 years. Within the complete profile the carbon isotope composition correlates well with the TOC content and the C/N ratio. A clear negative correlation exists between carbon and nitrogen isotopes during the late Glacial and the early Holocene (Tab.1).

Previous studies of Holocene and Late Glacial sediments from Laguna Potrok Aike have indicated that palaeoproductivity dynamics of the lake and organic matter input from the catchment area can be tracked in carbon and nitrogen isotope signatures of bulk organic matter (Mayr et al. 2009). With an interdisciplinary multi-proxy approach and in accord with other terrestrial and marine records, the investigated carbon and nitrogen isotope data in this study will contribute to our understanding of the environmental development in southernmost Patagonia.

References

Mayr, C., Lücke, A., Maidana, N., Wille, M., Haberzettl, T., Corbella, H., Ohlendorf, C., Schäbitz, F., Fey, M., Janssen, S., Zolitschka, B. (2009): Isotopic and geochemical fingerprints of environmental changes during the last 16,000 years on lacustrine organic matter from Laguna Potrok Aike (southern Patagonia, Argentina). - Journal of Paleolimnology, 42:81-102.

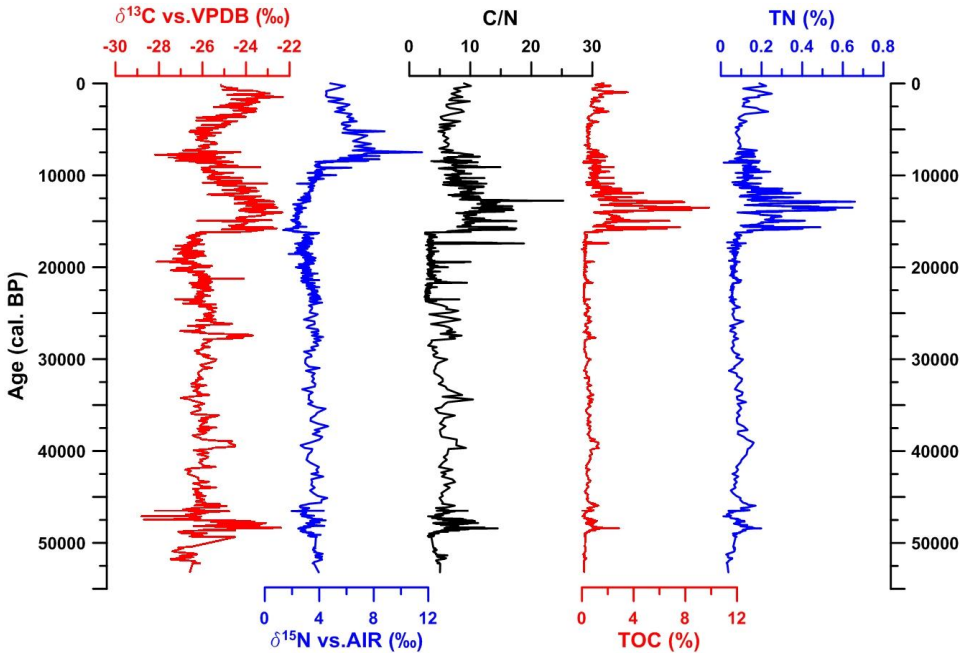

Fig. 1: Downcore changes in carbon and nitrogen isotope composition, C/N ratio, TOC and TN content for core 5022-2CP from the ICDP site Laguna Potrok Aike according to the age model V.1. Here only samples from undisturbed sediments (<200µm) were used.